Molecular tectonics based on porphyrin, dipyrrins, and heterocyclic amines functionalized by nucleobases

Elsa Tufenkjian

UNIVERSITÉ DE STRASBOURG

ÉCOLE DOCTORALE DES SCIENCES CHIMIQUES

UMR 7140

THÈSE présentée par :

Elsa Tufenkjian

soutenue le : **14 décembre 2018**

pour obtenir le grade de : **Docteur de l'université de Strasbourg**

Discipline/ Spécialité : Sciences Chimiques

Tectonique Moléculaire à base de Porphyrines, de Dipyrrines, et d'hétérocycles azotés fonctionnalisés par des Nucléobases

THÈSE dirigée par :
M. HOSSEINI Mir Wais Professeur, Université de Strasbourg
Mme. BULACH Véronique Professeur, Université de Strasbourg

RAPPORTEURS :
M. GROS Claude Professeur, Université de Bourgogne
M. VINCENT Stéphane Professeur, Université de Namur

AUTRES MEMBRES DU JURY :
M. MAHY Jean-Pierre Professeur, Université Paris-Sud
M. KUBIK Stefan Professeur, Université de Kaiserslautern

To my family,

Acknowledgements

I would like to express my gratitude to the members of the jury: Pr. Claude Gros, Pr. Stéphane Vincent, Pr. Jean-Pierre Mahy and Pr. Stefan Kubik for accepting to evaluate my PhD thesis.

My following thanks go to my thesis supervisors: Pr. Véronique Bulach and Pr. Mir Wais Hosseini. I would like to thank Pr. Véronique for her guidance in chemistry, for our long discussions and all the advices during the past three years. I thank her for the support not only in science but also in my extra-curricular and social activities, and for being a great role model. I would like to thank Pr. Mir Wais Hosseini for giving me the opportunity to work in his laboratory, for all his wise advices and motivation throughout my thesis.

I would like to express my appreciation to Dr. Abdelaziz Jouaiti and Dr. Stéphane Baudron for their scientific guidance and for their help in my project. I thank them for always keeping their door open for discussion and for answering my questions. I would like also to thank Audrey Fluck for everything; from helping me in the lab to the fun chats that often switch to her discovering something "unsafe" in the lab and giving me advices. I would like to thank Nathalie Kyritsakas for all the X-Ray analysis, all the shared coffee breaks and the laughs. Thanks to Pr. Sylvie Ferlay and Dr. Aurélie Guenet for all the counseling and advices. Thanks to Valerie Rey for all the administrative help and for her welcoming smile and loving attitude. Furthermore, I would like to thank all the PDI and Idex team for my scholarship and for the caring and loving environment.

I would like to thank all my laboratory colleagues, who made this three years journey not only an interesting experience, but most importantly, a memorable one. Thanks to Berangere, Donata, and Romain for being great friends and for the time we spend together inside and outside the lab. Thanks to Cyril, Damien, Fan, Ivan, Julien, Katia, Keven, Maxim, Sacha and Titia for the friendly atmosphere in the lab. I would like to thank my friends in Strasbourg: Antoine, Najwa, Mariane, Farouk, Garen, Filipa, Lamis, Bechara, Shree, Youssef, Rogeria, Sayali, Stefanos, Fragiska, Mariebelle and many more I missed to note for making me feel at home and for all the fun we had together during the past years. I would like to dedicate a huge thanks to my friends back home for their support, motivation and love, especially my best friends: Joy, Melanie, Taline and Rania. I thank my boyfriend, George, for his love, patience, support, motivation and his help in this journey. Last but not least, I would like to thank my parents, my grandfather, my brother, my aunt and the rest of my family for their endless support, blind trust, motivation and love.

Table of Contents

Acknowledgments

Table of Contents

List of Abbreviations

French Summary

General Introduction

Introduction..... 1

I. Supramolecular chemistry.....3

II. Molecular Tectonics.....4

II. 1. Molecular tectons.....5

II. 1. a) Endo- and Exo-receptors.....5

II. 1. b) Complementary and self-complementary tectons.....6

II. 2. Intermolecular interactions.....7

II. 2. a) van der Waals interactions.....7

II. 2. b) π-π interactions.....8

II. 2. c) Hydrogen bonds.....8

II. 2. d) Electrostatic interactions.....9

II. 2. e) Coordination bonds.....9

II. 3. Molecular networks.....9

II. 3. a) Dimensionality and geometry of molecular networks.....10

II. 3. b) Coordination networks.....12

II. 3. b) 1) Metallic centers.....12

II. 3. b) 2) Organic tectons bearing coordinating sites.....13

II. 3. b) 3) Metal-Organic-Frameworks (MOFs) 18

II. 3. c) Hydrogen bonded networks.....21

II. 3. c) 1) Hydrogen bonding patterns.....22

II. 3. c) 2) Examples of hydrogen bonded networks.....24

II. 3. c) 3) Hydrogen bonded Organic-Frameworks (HOFs) 27

III. Nucleobases.....30

III. 1. pKa values of nucleobases.....32

III. 2. Tautomerism of nucleobases……...33
III. 3. Nucleobase interactions……..34
III. 4. Nucleobases self-assemblies……...37
III. 4. a) Guanine……...37
III. 4. b) Cytosine……..39
III. 4. c) Adenine……...40
III. 4. d) Thymine and Uracil……40
III. 5. Supramolecular assemblies based on NB……42
III. 5. a) Nucleobase duplex systems……....43
III. 5. b) Nucleobase based polymers……...45
III. 5. c) Nucleobase based networks ……...47
IV. Aim of the project…….....52
V. References……..…….....53

Chapter I: Porphyrin bearing Nucleobases…….58

I. Porphyrin…….....60
I. 1. Structure and nomenclature…….....60
I. 2. Synthesis…….....61
I. 2. a) A_4…….....61
I. 2. b) *Trans*-A_2B_2…….....62
I. 3. Characterization…….....64
I. 3. a) ^{1}H-NMR…….....64
I. 3. b) UV-Visible spectroscopy…….....65
I. 4. Complexation and Geometry…….....66
II. Porphyrin bearing nucleobases…….....67
II. 1. Examples of porphyrin bearing nucleobases (NB) ……..68
II. 2. Aim of the project…….....78
II. 3. Porphyrin bearing NB *via* C-C bond……79
II. 3. a) Synthesis of Zn(II)[5,15-di(trimethylsilylethynyl)-10,20-dipentylporphyrin]…….81
II. 3. b) Protection of 5-iodouracil……....82
II. 3. c) Synthesis of Zn(II)[5,15 di(N_1-(benzylhydry)uracil)-10,20-dipentylporphyrin](**T1**)..83

II. 3. d) Deprotection of **T1**…….....84
II. 3. e) Iodination and alkylation of NBs…….85
II. 3. e) 1) Alkylation of 5-iodouracil……...85
II. 3. e) 2) Iodination and alkylation of cytosine……..…86
II. 3. e) 3) Iodination and alkylation of adenine……86
II. 3. f) Synthesis of Zn(II) [5,15 -di(N1-hexyluracil)- 10,20-dipentylporphyrin] (**T3**)……87
II. 3. g) Cross coupling reaction of I-Cy-C6 and **Zn-Po1**……88
II. 4. Porphyrin bearing NB *via* C-N bond…….90
II. 4. a) Synthesis of 5,15-di(4-(bromomethyl)phenyl)-10,20-diphenylporphyrin (**Po2**)…….92
II. 4. b) Substitution of **Po2** mixture…….92
II. 4. c) Synthesis of 5,15-di(4-(bromomethyl)phenyl)-10,20-dimesitylporphyrin (**Po3**)…….93
II. 4. d) Synthesis of 5,15-di(N_1-methylphenylthymine)-10,20-dimesitylporphyrin (**T5**)…...94
II. 4. e) Synthesis of 5,15-di(N_9-methylphenyladenine)-10,20-dimesitylporphyrin (**T6**)……95
II. 4. f) Synthesis of 5,15-di(N_1-methylphenylcytosine)-10,20-dimesitylporphyrin (**T7**)……96
II. 4. g) Synthesis of 5,15-di(N_9-methylphenylguanine)-10,20-dimesitylporphyrin (**T9**)……97
II. 4. h) Synthesis of 5,10,15,20-tetrakis(4-(bromomethyl)phenyl)porphyrin (**Po4**)……98
II. 4. i) Synthesis of 5,10,15,20-tetrakis(N_1-methylphenylthymine)porphyrin (**T10**)……...99
II. 4. j) Substitution of **Po4** with adenine and cytosine……100
III. Conclusion and Perspectives…….....100
IV. References……..…….....102

Chapter II: Dipyrrins bearing Nucleobases…….105

I. Dipyrrins…….....107
I. 1. Structure and nomenclature…….107
I. 2. Synthesis……..108
I. 3. BODIPY……..110
I. 4. Dipyrrin complexes……..111
I. 5. Dipyrrin complexes in hydrogen bonded networks……117
II. Dipyrrins bearing nucleobases……..119
II. 1. Some examples of dipyrrins functionalized by NBs……..120
II. 2. Aim of the project……...121

II. 3. Synthesis of dipyrrins bearing NBs……122
II. 3. a) 1,3,7,9-tetramethyl-5-(N_1-methylphenylthymine)-dipyrrin (T-dipyrrin) (**T11**)……124
II. 3. b) 1,3,7,9-tetramethyl-5-(N_9-methylphenyladenine)-dipyrrin (A-dipyrrin) (**T12**)…….124
II. 3. c) 1,3,7,9-tetramethyl-5-(N_1-methylphenylcytosine)-dipyrrin (C-dipyrrin) (**T13**)……125
II. 3. d) 1,3,7,9-tetramethyl-5-(N_9-methylphenylguanine)-dipyrrin (G-dipyrrin) (**T15**)……126
III. H-bonded network based on Zn(II)(T-dipyrrin)$_2$ ……128
IV. Conclusion and perspectives……131
V. References……...133

Chapter III: Pyridine and Terpyridine bearing Nucleobases…….137

I. Heterocyclic amines……139
I. 1. Pyridines……..139
I. 2. Terpyridines……140
I. 2. a) Terpyridine-Metal complexes……140
I. 2. b) Synthesis of terpyridine ligands……..143
II. Heterocyclic amines functionalized by NBs……145
II. 1. Examples of heterocyclic amines functionalized by NBs……...145
II. 2. Aim of the project……...155
II. 3. Pyridine bearing NBs……..158
II. 3. a) Synthesis of 4-(N_1-methylthymine)pyridine (**T-Py**) (**T16**) ……...159
II. 3. b) Synthesis of 4-(N_9-methyladenine)pyridine (**A-Py**) (**T17**)……160
II. 3. c) Synthesis of 4-(N1-methylcytosine)pyridine (**C-Py**) (**T18**)……..162
II. 3. d) Synthesis of 4-(N_9-methylguanine)pyridine (**G-Py**) (**T20**)……..164
II. 4. Coordination networks based on **Ad-Py** (**T17**)……...165
II. 4. a) **A-Py-Cd(II)** network……165
II. 4. b) **A-Py-Hg(II)** network……167
II. 5. Coordination networks based on **C-Py** (**T18**) ……169
II. 5. a) **C-Py-Zn(II)** network……170
II. 5. b) **C-Py-Cd(II)** network……....171
II. 6. Terpyridine bearing NBs……172
II. 6. a) Synthesis of 4'-(4-bromomethylphenyl)-2,2':6',2"-terpyridine (**Br-terPy**)……..173

II. 6. b) Synthesis of 4'-(N_1-methylphenylthymine)-2,2':6',2"-terpyridine (**T-terPy**) (**T21**).173
II. 6. c) Synthesis of 4'-(N_9-methylphenyladenine)-2,2':6',2"-terpyridine (**A-terPy**) (**T22**).174
II. 6. d) Synthesis of 4'-(N_1-methylphenylcytosine)-2,2':6',2"-terpyridine(**C-terPy**) (**T23**).175
II. 6. e) Synthesis of 4'-(N_9-methylphenylguanine)-2,2':6',2"-terpyridine (**G-terPy**) (**T25**).175
II. 7. Structural characterization of complexes based on **T-terPy** (**T21**)……176
II. 7. a) **T-TerPy-Cu(II)** network……...176
II. 7. b) **T-TerPy-Cd(II)** network……..177
III. Conclusion and perspective…….....179
IV. References.....……...181
Conclusion and Perspectives……..185
I. Conclusion……...186
II. Perspectives……188
Experimental Part…….…….190
Crystallographic data…….247
Annex……...277
List of Tectons…….326

List of Abbreviations

Å: Ångström
ACN: acetonitrile
acac: acetylacetonate
A: adenine
aq.: aqueous
BODIPY: boron dipyrromethene
C: cytosine
DCM: dichloromethane
DDQ: 2,3-dichloro-5,6-dicyano-1,4-benzoquinone
DMF: dimethylformamide
DMSO: dimethylsulfoxide
DNA: deoxyribonucleic acid
DPM: dipyrromethane
Eq.: equivalent
G: Guanine
HOF: Hydrogen bonded Organic Framework
hrs: hours
HRMS: high resolution mass spectroscopy
Hz: Hertz
IR: infrared spectroscopy
J: coupling constant
MOF: Metal-Organic-Framework
MS: mass spectroscopy
OAc: acetate
P: 2-amino-6-chloropurine
pKa: acidity constant
Py: Pyridine
terPy: terpyridine
RT: room temperature
SBU: Secondary Building Units
STP: Standard Temperature and Pressure
T: thymine
TFA: trifluoroacetic acid
THF: tetrahydrofuran
TLC: Thin Layer Chromatography
UV: ultraviolet
Φ: quantum yield
λ: wavelength
ε: molar absorption coefficient

Résumé

1) Introduction

La tectonique moléculaire est une partie de la chimie supramoléculaire traitant de la formation d'architectures périodiques mono-, bi- et tridimensionnelles.[1, 2] Ces assemblages, décrits tels des réseaux moléculaires sont générés *via* l'auto-assemblage de briques moléculaires complémentaires nommées tectons. Ces derniers possèdent des sites de reconnaissance basés sur des interactions non-covalentes et réversibles. La dimensionnalité de l'assemblage généré est fonction du nombre, de la position, et de l'orientation des sites de reconnaissance localisés à la périphérie des tectons. L'itération du processus de reconnaissance entre les tectons conduit ainsi à la formation d'architectures moléculaires de géométries et dimensionnalités variées, la reconnaissance entre les briques s'effectuant *via* des interactions supramoléculaires réversibles. Cette réversibilité est primordiale au processus puisqu'elle conduit ainsi à la formation d'architectures ordonnées thermodynamiquement stables. Le processus de reconnaissance entre les tectons peut faire intervenir un seul type d'interactions supramoléculaires mais il est également possible de générer des réseaux moléculaires *via* des interactions supramoléculaires de plusieurs types. Un grand nombre d'architectures périodiques utilisent des interactions directionnelles telles que la liaison de coordination ou la liaison hydrogène, l'avantage étant de permettre ainsi une certaine maitrise de la topologie de l'assemblage final formé.

Les réseaux de coordination sont obtenus par assemblage de tectons possédant des sites de coordination et des cations métalliques. Ces interactions sont sélectives, directionnelles et d'énergie relativement fortes (*ca* 50-100 kJ/mol) sur l'échelle des interactions supramoléculaires.[3] Des ligands tels que porphyrines ou de dipyrrines ont été largement utilisés pour la formation de réseaux de coordination et ce grâce à leur stabilité mais également leur capacité à complexer un grand nombre de cations métalliques. Outre leur capacité à complexer des cations métalliques dans leur cavité centrale, les porphyrines peuvent également proposer des sites coordinants en position méso et/ou β pyrroliques.[4] Une dipyrrine est schématiquement comparable à une demi-porphyrine et possède donc les propriétés associées. Des tectons à base de pyridines ou de terpyridines ont également été largement utilisés pour la formation de polymères de coordination de topologie et géométries variées.

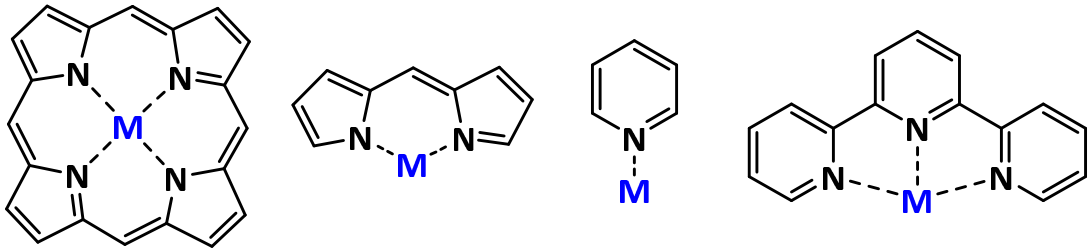

Figure 1: Structure de ligands coordinants: porphyrine, dipyrrine, pyridine, terpyridine (de gauche à droite).

Les liaisons Hydrogène ou liaisons H (D-H···A) sont de interactions directionnelles se produisant entre un site donneur, D-H (D étant un atome électronégatif)) et un site accepteur, A. La polarisation de la liaison D-H associée à la présence de doublets non liants sur le site A conduisent à une interaction D-H---A dont l'énergie reste relativement forte (*ca* 4 to 60 kJ/mol). Cette interaction est directionnelle, réversible et aisément modulable par différents stimuli externes tels que la température, le pH, la nature du solvant, ou encore la concentration.[5,6] Ainsi, de multiples réseaux moléculaires à base de liaisons hydrogène ont été décrits dans la littérature. Les liaisons H ont également été utilisées comme interactions secondaires dans les réseaux de coordination.[7] La liaison hydrogène est une interaction largement utilisée pour stabiliser les édifices dans les organismes vivants. Ainsi, ce sont les liaisons hydrogène entre bases nucléiques (NBs) complémentaires qui conduit à la double hélice d'ADN et d'ARN (Figure 2).

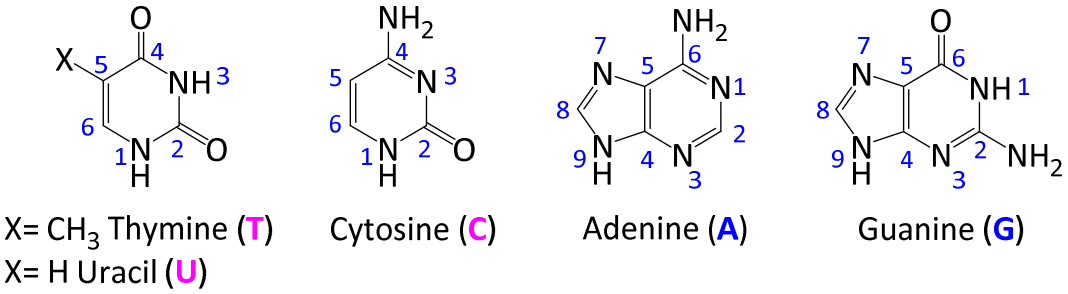

Figure 2: Les NBs présentes dans l'ADN ou l'ARN .

Les NBs se classent en deux catégories: les pyrimidines : Cytosine (**C**), Thymine (**T**) and Uracil (**U**) et les purines : Adenine (**A**) and Guanine (**G**).[8] Le processus d'appariement des brins d'ADN est basé sur la complémentarité des NBs au travers d'interactions dites de Watson-Crick , du nom des chercheurs les ayant mises en évidence (figure 3).[9] Cette complémentarité s'effectue grâce à la formation de 2 ou 3 liaisons hydrogène entre les purines et les pyrimidines complémentaires.

Ainsi, les paires **A-T** et **A-U** sont générées (K_a *ca.* 10^2 M^{-1}) *via* la formation de deux liaisons hydrogène entre l'Adénine (**A**) et ses purines complémentaires : la Thymine **T** (X=CH_3) ou l'Uracile **U** (X=H) respectivement.[10] De même, la Guanine **G** est complémentaire à la Cytosine **C** *via* la formation de 3 liaisons hydrogène conduisant ainsi à la formation de la paire **G-C** avec une constante d'association K_a de l'ordre de 10^5 M^{-1} et donc bien supérieure aux paires précédentes.[11]

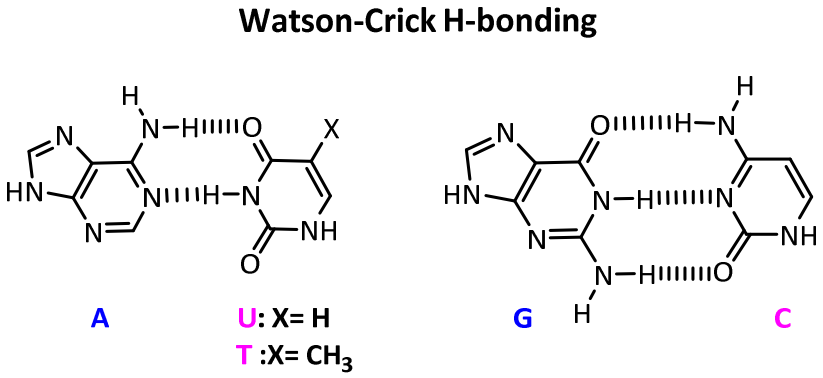

Figure 3: les appariements dits de Watson-Crick : **A**-**T** et **G**-**C**

Les appariements de Watson-Crick sont les plus connus, mais il existe de nombreuses autres possibilités d'appariements des NBs. Ainsi près de 30 combinaisons ont été identifiées, ceci incluant les auto-appariements puisque les 5 NBs sont auto-complémentaires.[12] Ces propriétés ont suscité un grand intérêt pour les NBs et notamment dans le design de réseaux moléculaires à base de liaisons H.[13] Outre leur capacité à interagir au travers de la formation de liaison H, les NBs peuvent également interagir avec des cations métalliques *via* les doublets non liants présents sur les azote ou les oxygène. Des systèmes à base de NBs judicieusement fonctionnalisées ont ainsi trouvé de nombreuses applications telles que par exemple le transfert d'énergie, le transfert d'électrons, la formation de gels, les récepteurs biologiques, ou l'administration de médicaments.[14]

L'un des buts de la tectonique moléculaire est une meilleure compréhension des mécanismes conduisant à la formation de réseaux moléculaires, mais aussi la possibilité de prédire la topologie des assemblages formés. Il s'agit également d'optimiser les processus de synthèse afin de générer des assemblages ciblés à partir de briques moléculaires pré-programmées. Le but ultime est de pouvoir non seulement maitriser la topologie mais aussi les propriétés des architectures formées.

Ainsi, la formation de tectons fonctionnalisés par des NBs est un sujet d'intérêt dans le champ de la tectonique moléculaire. Le but de ce travail de doctorat vise la synthèse d'une librairie de tectons de géométries variées substitués par des NBs et possédant également des sites coordinants (Figure 4). De telles briques moléculaires devraient permettre de générer des assemblages infinis dans lesquels les liaisons de coordination et les liaisons H seraient impliquées dans le processus de reconnaissance. Ces interactions sont toutes deux directionnelles, permettant ainsi en principe une certaine prédiction quant aux assemblages possibles en fonction de conditions données. De plus, on peut s'attendre à la formation de réseaux moléculaires de coordination stabilisés par la présence de multiples liaisons H additionnelles. Pour le site coordinant nous avons ciblé le macrocycle porphyrinique, la dipyrrine, la terpyridine et la pyridine.

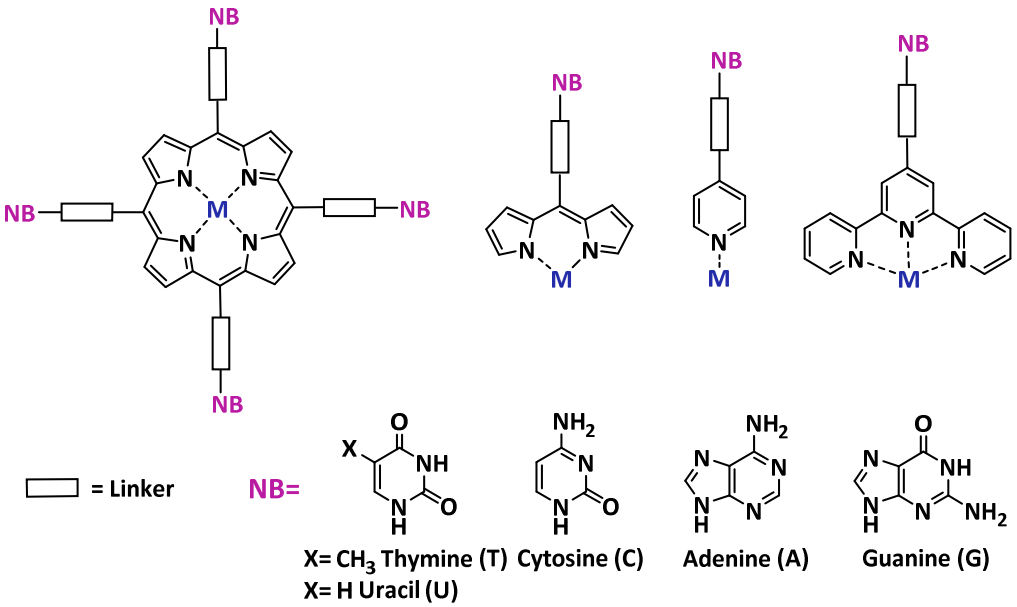

Figure 4: Représentation des tectons ciblés.

2) Résultats et Discussion

Le macrocycle porphyrinique est d'un grand intérêt en chimie supramoléculaire et plus particulièrement en tectonique moléculaire.[15] Il peut accepter de nombreux cations métalliques dans sa cavité centrale. De plus, il peut être fonctionnalisé à sa périphérie par des sites additionnels (sites coordinants, et/ou donneurs ou accepteurs de liaisons H), et son caractère aromatique permet la formation d'interactions additionnelles de type π-π stacking. La première partie de ce travail de thèse traite de la synthèse de porphyrines fonctionnalisées par 2 ou 4 NBs et de leur cristallisation

en présence ou non de cations métalliques additionnels afin de générer des réseaux moléculaires à l'état cristallin. En fonction du nombre et de la nature des NBs positionnées à la périphérie de la porphyrine, il est possible d'envisager la formation de différents types de réseaux moléculaires. La formation de tectons porphyriniques possédant deux NBs en position *trans* peut s'envisager selon plusieurs stratégies. Nous en avons principalement étudié deux (Figure 5). La première est basée sur la formation d'une liaison C-C entre la porphyrine et la NBs *via* une réaction de couplage pallado-catalysée (figure 5, réaction de Suzuki et réaction de Sonogashira). Dans un second temps, nous avons mis à profit une réaction d'alkylation impliquant les différentes NBs et une porphyrine judicieusement substituée (figure 5, bas).

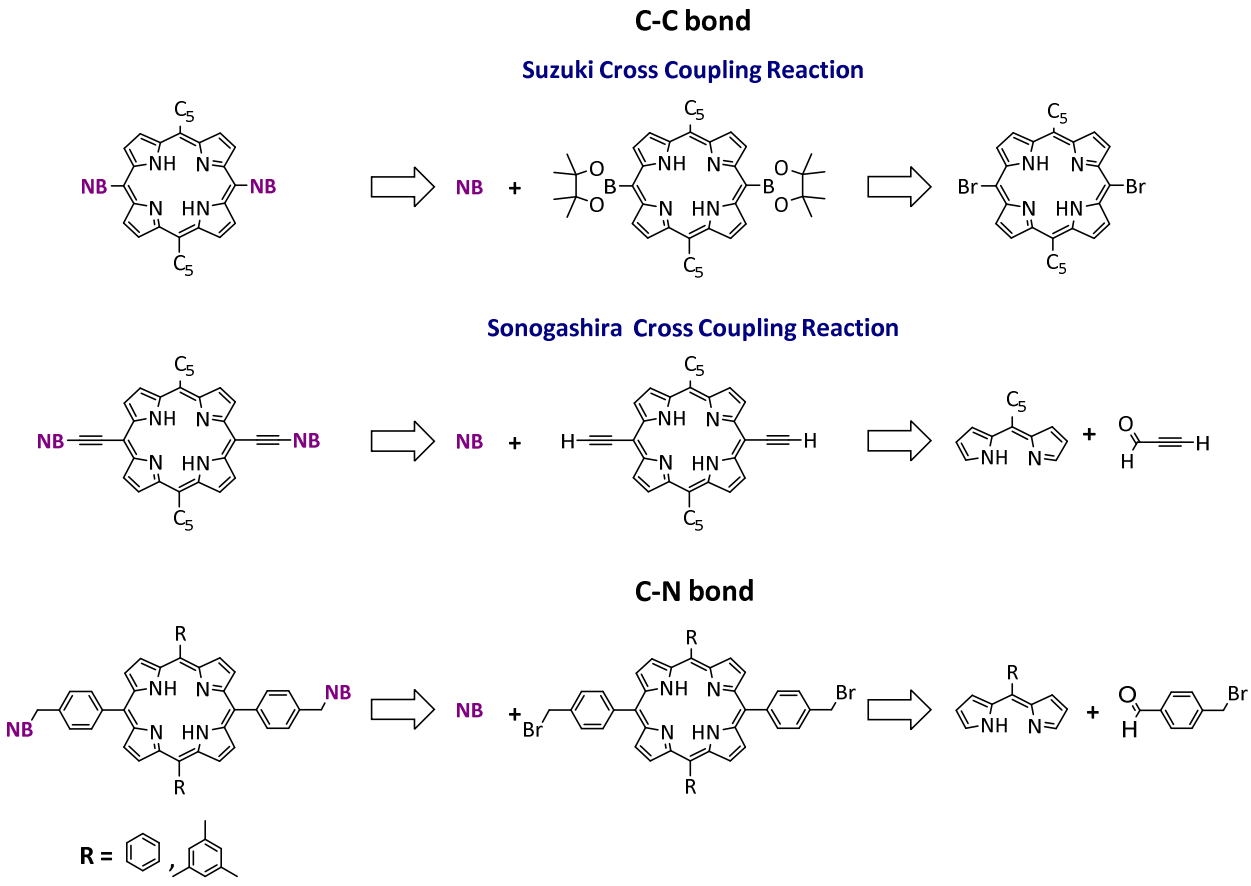

Figure 5: Schéma rétrosynthétique envisagé pour former des porphyrines *trans* substituées par de 2 NBs.

Dans un premier temps, nous avons étudié la connexion de NBs à la porphyrine *via* un couplage de Suzuki (Figure 5). La 10,20-dipentyl-porphyrine a été synthétisée, dibromée en position trans. La réaction de cette dernière avec le 4,4,5,5-tétraméthyl-1,3,2-dioxaborolane conduit à la formation d'un mélange de porphyrines mono et di- « boronée ».[16] Un premier essai de couplage

a été effectué avec le 5-bromouracile (**Br-U**) préalablement protégé par un groupement benzylhydryle en suivant une procédure décrite .[17] La réaction de Suzuki entre ce bromouracile protégé et la porphyrine « boronée » conduit invariablement à la formation de la 10,20-dipentyle-porphyrine et non au produit ciblé.

Nous avons ensuite étudié le couplage de Sonogashira selon une procédure one-pot entre des NBs et une porphyrine substituée en position méso *trans* par des groupements éthynyles protégés. (Figure 6). Le complexe porphyrinique de départ, la 5,15-dipentyl-10,20-(triméthylsilyléthynyle)porphyrine de zinc (**ZnPo1**) est obtenue *via* une réaction dite 2+2 entre le dipyrrylméthane (**C5-DPM**) et le (triméthylsilyle)propionaldéhyde en présence de $BF_3.Et_2O$ dans le $CHCl_3$ suivi de la métallation de la cavité porphyrinique par du Zn(II) (Figure 6). [18]

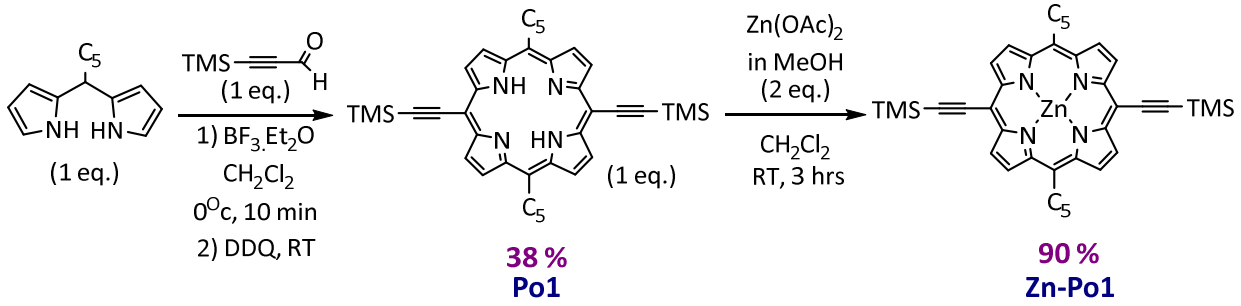

Figure 6: Synthèse de **Po1** and **Zn-Po1**.

Le 6-iodouracile est protégé par un groupe benzylhydryle selon une procédure décrite conduisant à la formation du N1-hydryl-6-iodouracile (**I-U-Ph₂**) (Figure 7(a)).[17] La réaction de la porphyrine **Zn-Po1** avec le **I-U-Ph₂** selon un couplage de Sonogashira conduit, après purification, à la formation du tecton ciblé, **T1**, avec un rendement de 88 % (Figure 7(b)). La déprotection de l'uracile est effectuée par traitement de **T1** par une solution d'acide triflique (10%) dans le TFA[17] Ceci conduit à la formation d'un précipité vert de 5,15-diuracil-10,20-dipentylporphyrin (**T2**) avec un rendement de 80 % (Figure 7(c)). **T2** est très faiblement soluble dans la plupart des solvants organiques et sa caractérisation s'est avérée délicate. Cette faible solubilité peut être expliquée par l'auto-assemblage de **T2** en solution du fait de l'auto-complémentarité du tecton formé *via* la formation de liaisons H entre les uraciles de porphyrines adjacentes. Aucun essai de cristallisation n'a à ce jour conduit à la formation de monocristaux.

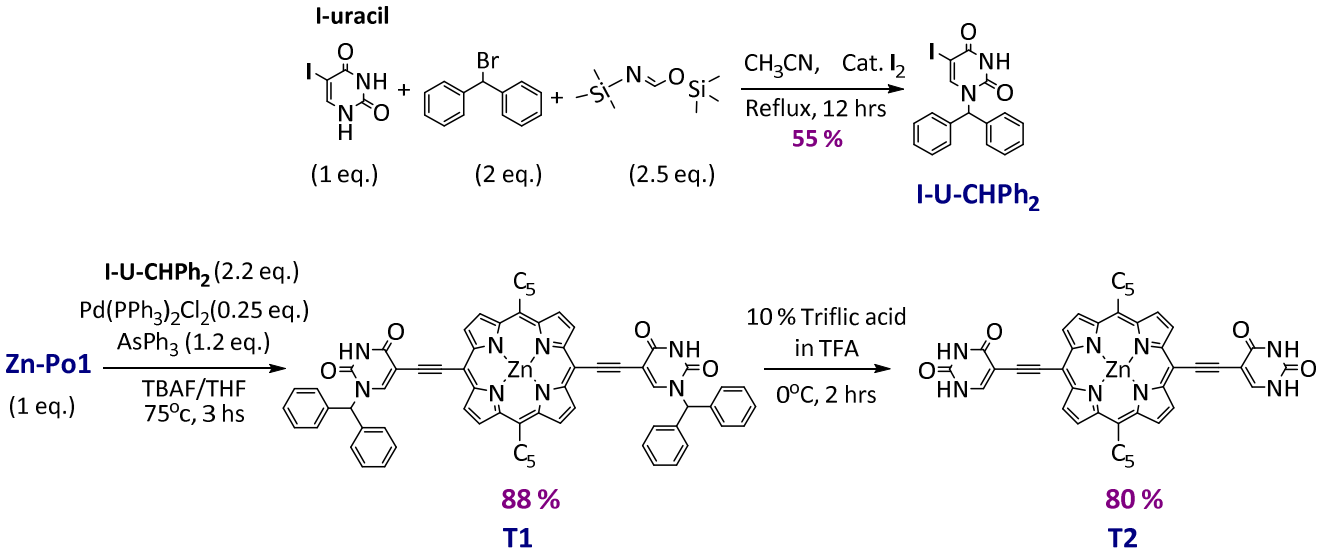

Figure 7: Synthèse de **T1** and **T2**.

Afin d'optimiser la solubilité du tecton final, nous avons voulu remplacer le groupement benzylhydryle par une chaine alkyle en C6. L'alkylation de l'uracile est effectuée en faisant réagir 2 équivalents de iodouracile avec 1.3 équivalent de Cs_2CO_3 et 1 équivalent de1-bromohexane dans la DMF anhydre. L'uracile alkylé, **I-U-C$_6$**, est obtenu avec un rendement de 94%. Il est mis à réagir avec **Zn-Po1** dans des conditions similaires à celles utilisées pour la synthèse de **T1**, ce qui conduit à la formation de Zn(II)[5,15-di(N_1-hexyluracil)-10,20-dipentylpoprhyrine, **T3**, avec un rendement de 80 % (figure 8). **T3** a été caractérisé par RMN, UV-Vis, IR, and HRMS. Des cristaux de **T3** ont également été obtenus mais leur qualité n'était pas suffisante pour permettre une caractérisation par diffraction des rayons X (DRX).

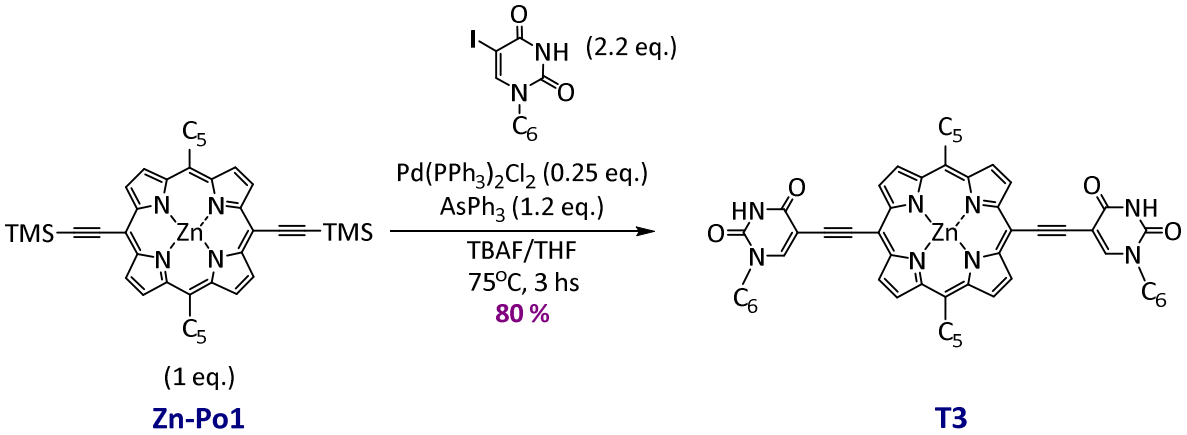

Figure 8: Synthèse de **T3**.

Nous avons tenté de reproduire la même réaction entre **Zn-Po1** et la 8-iodo-adenine ou la 6-iodo-cytosine préalablement alkylées, mais n'avons pu isoler les tectons ciblés.
Nous avons donc exploré une deuxième stratégie qui consistait à connecter les NBs à la périphérie de la porphyrine *via* des liaison C-N impliquant les sites NH des NBs.
La substitution des sites N1 des pyrimidines et N9 des purines avec des chaines alkyles ont été décrites.[19, 20, 21] Nous l'avons-nous-même mise précédemment à profit pour synthétiser **I-U-C6**. Cette stratégie appliquée à une porphyrine substituée en position *méso* par 2 ou 4 p-bromométhylphényle devrait conduire à des tectons fonctionnalisés par 2 ou 4 NBs respectivement.

Nous avons dans un premier temps ciblé la porphyrine précuseur : la 5,15-di(4-bromomethylphényl)-10,20-di(phényl)porphyrine. Pour ce faire nous avons fait réagir le 4-(bromométhyl)benzaldéhyde (**Ald-Br**) avec le phényl-dipyrrométhane (**Ph-DPM**) (figure 9), en visant ainsi la formation exclusive de la porphyrine *trans*-A_2B_2 ciblée. Malheureusement, ces conditions conduisent à la formation d'un mélange de porphyrines, pouvant être expliqué par le phénomène de scrambling. Nous avons néanmoins tenté de séparer les différents constituants du mélange par chromatographie sur colonne. La porphyrine symétrique A_4, ou méso-tétraphénylporphyrine (TPP) a ainsi pu être isolée. Par contre les porphyrines A_2B_2 (*cis* and *trans*) A_3B, et AB_3 ont été beaucoup plus délicates à purifier du fait de leur polarité très proche. Nous avons tenté de faire réagir ce mélange avec un excès de thymine dans le but de fonctionnaliser l'ensemble des porphyrines et ainsi générer des tectons de différence de polarité plus marquée. Le mélange de porphyrines **Po2** (figure 9) est mis à réagir avec un excès de thymine en présence de K_2CO_3 dans la DMF. Le mélange obtenu est purifié sur colonne. La porphyrine A_3B, 5-(N_1-méthylphénylthymine)-10,15,20-triphenylporphyrin (**T4**), a ainsi pu être isolée. Malheureusement les autres constituants du mélange n'ont pas pu être purifiés.

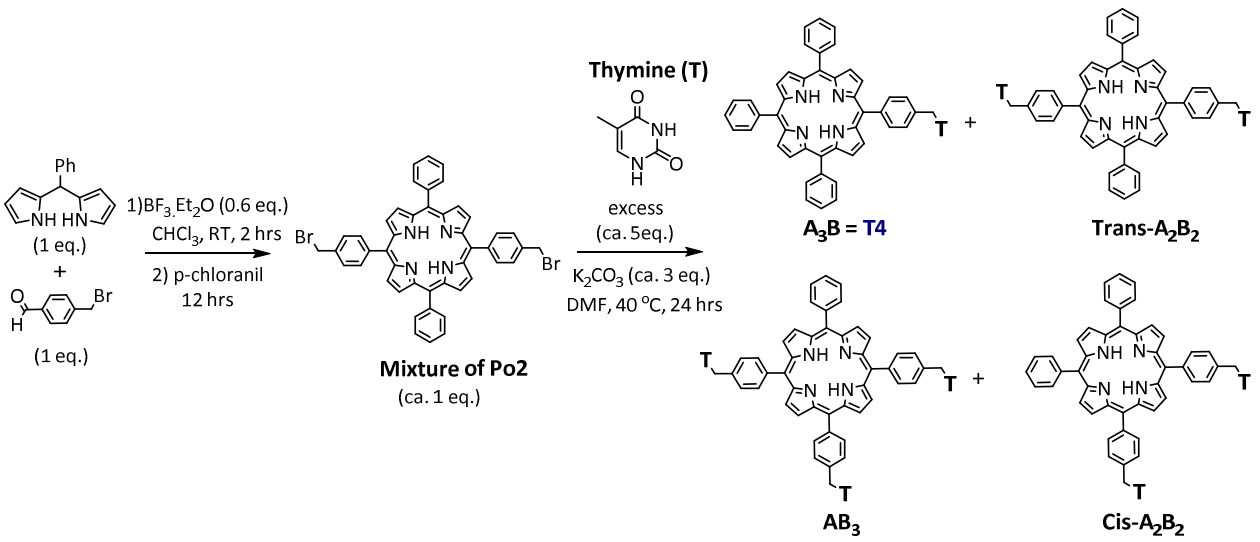

Figure 9: Synthèse de **T4.**

Afin de diminuer les possibilités de scrambling, nous avons remplacé Ph-DPM par le mésityl-DPM. En effet, il a été montré que l'utilisation d'un DPM encombré pouvait limiter le scrambling lors de la réaction. Nous avons également modifié le catalyseur et utilisé le TFA plutôt que $BF_3.Et_2O$. Ainsi, **Ald-Br** réagit avec le **mésityl-DPM** en présence de TFA suivant un protocole décrit pour des composes similaires.[38(a)] La 5,15-di(4-(bromométhylphényl)-10,20 dimésitylporphyrin (**Po3**) a ainsi pu être isolée avec un rendement de 15%. (Figure 10).

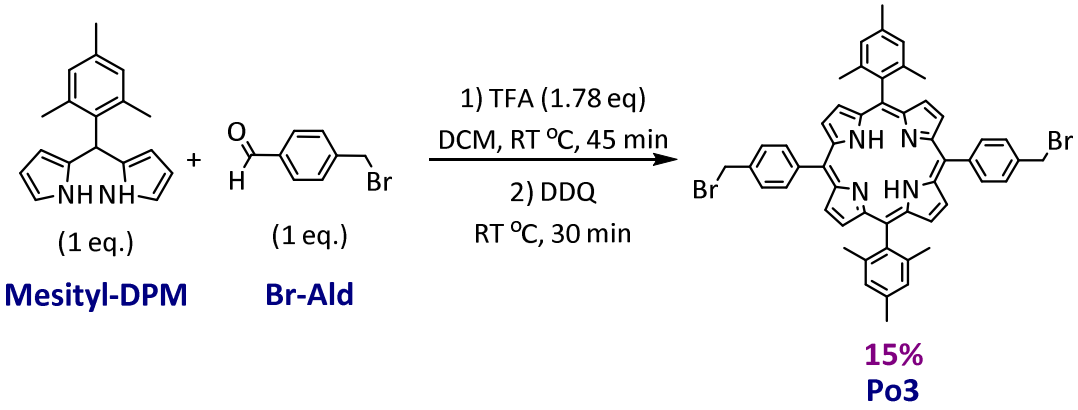

Figure 10: Synthèse de **Po3**.

Po3 réagit avec la thymine et avec l'adénine en présence de K_2CO_3 dans la DMF pour former respectivement la 5,15-di(N_1-méthylphénylthymine)-10,20-dimésitylporphyrin (**T5**) et la 5,15-di(N_1-méthylphenyladénine)-10,20-dimésityl porphyrin (**T6**) avec un rendement de 72 % et 54 % (Figure 11).

L'utilisation d'une base plus forte, NaH, a été necessaire avec la cytosine [9(b)] et a permis d'isoler le tecton **T7** avec un rendement de 37% (Figure 11).

Pour le tecton **T9** nous avons procédé en deux étapes du fait de la faible solubilité de la guanine. Ainsi, nous avons fait réagir la 2-amino-6-chloropurine **P** avec **Po3** en présence de K_2CO_3 dans le DMF. **T8** est isolé avec un rendement de 88% . L'hydrolyse de **T8** par une solution aqueuse de HCl conduit à la formation de **T9** possédant deux guanines en position méso *trans* avec un rendement de 98%. (Figure 11).

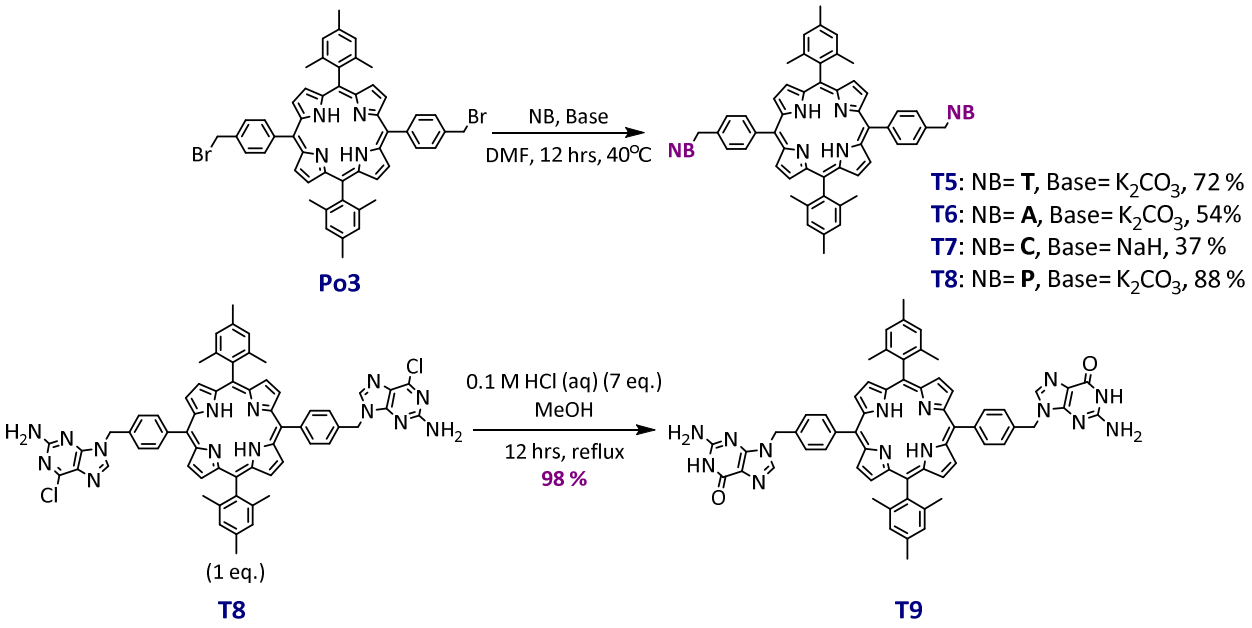

Figure 11: The synthesis of **T5**-**T9**.

Nous avons également voulu introduire 4 NBs à la périphérie de la porphyrine. La porphyrine de départ, la 5,10,15,20-tétrakis(4-(bromométhyl)phényl)porphyrin (**Po4**) est synthétisée en faisant réagir du pyrrole et du 4-(bromométhyl)benzaldehyde selon une procédure décrite.[11] (**Po4**) réagit avec un excès de thymine en présence de K_2CO_3 et conduit à la formation de la porphyrine tétrasubstituée par 4 thymines, **T8**, avec un rendement de 70%. Nous avons effectué le même type de réaction à partir de **Po4** et de la cytosine ou de l'adénine. Malheureusement dans ces deux cas, seules des espèces fortement insolubles sont formées.

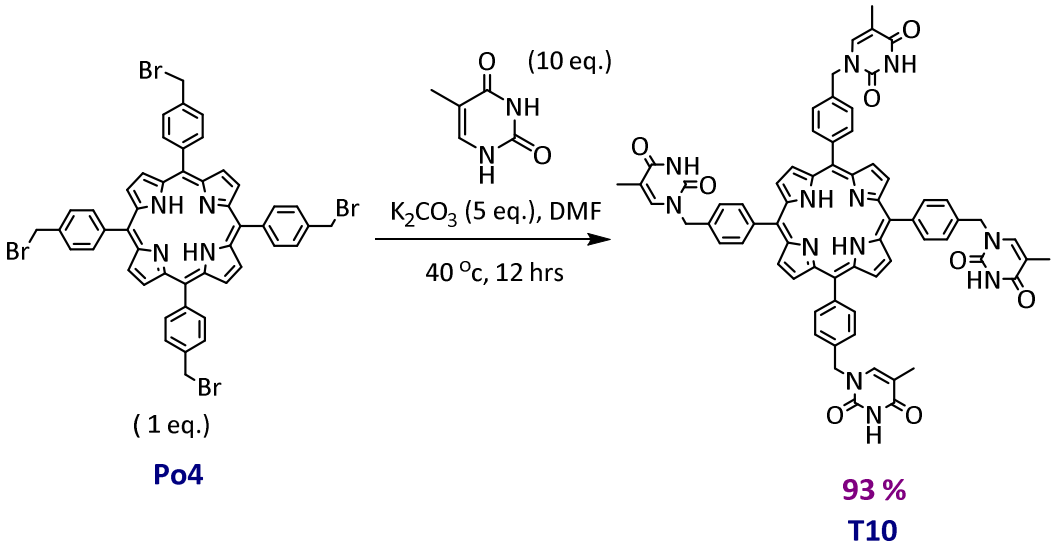

Figure 12: Synthèse de **T10**.

Nous avons ainsi mis au point la synthèse de 10 nouveaux tectons porphyriniques contenant des NBs. Ces tectons ont tous été caractérisés par RMN, UV-Vis, IR et HRMS. De nombreux essais de cristallisation, en présence et absence de cations métalliques additionnels ont été effectués afin de caractériser les assemblages obtenus par DRX. A ce jour aucune caractérisation structurale n'a abouti, mais de nombreux essais de cristallisation sont toujours en cours. Nous avons également tenté de générer des assemblage de tectons complémentaires tels que par exemple **T5** avec **T6** ou **T7** avec **T9**. Ces essais sont également toujours en cours.

Dans un deuxième temps, nous avons voulu étendre cette stratégie à d'autres sites coordinants et notamment les dipyrrines. Dans un premier temps nous avons utilisé une stratégie similaire à celle utilisée pour les porphyrines, en faisant réagir les NBs avec un dipyrrine substitué en position 5 par un 4-bromométhyphényl. La première étape consistait à faire réagir du pyrrole avec du 4-bromomethylbenzaldéhyde selon les conditions classiques d'obtention des dipyrrines. Malheureusement, aucun des essais effectués n'a conduit au dipyrrine ciblé. Nous avons donc utilisé une stratégie différente, détaillée figure 13 qui consistait à synthétiser dans une première étape un aldéhyde fonctionnalisé par une NB puis à le faire réagir avec le 2,4-diméthylpyrrole. Le 4-(bromométhyl)benzaldéhyde est mis à réagir avec l'une des 4 NBs dans le DMF en présence de K_2CO_3 pour **T**, **A** and **P** et en présence de NaH pour **C** conduisant respectivement à la formation de **T-Ald**, **A-Ald**, **P-Ald** et **C-Ald** (Figure 13). Ces 4 aldéhydes réagissent séparément avec le

2,4-diméthylpyrrole, et après oxydation au DDQ, 4 nouveaux tectons à base de dipyrrines (**T11**, **T12**, **T13**, **T14**) ont été isolés. L'hydrolyse de **T14** conduit au tecton **T15** (Figure 13). Ces 5 tectons ont été caractérisés par RMN, UV-Visible, IR and HRMS.

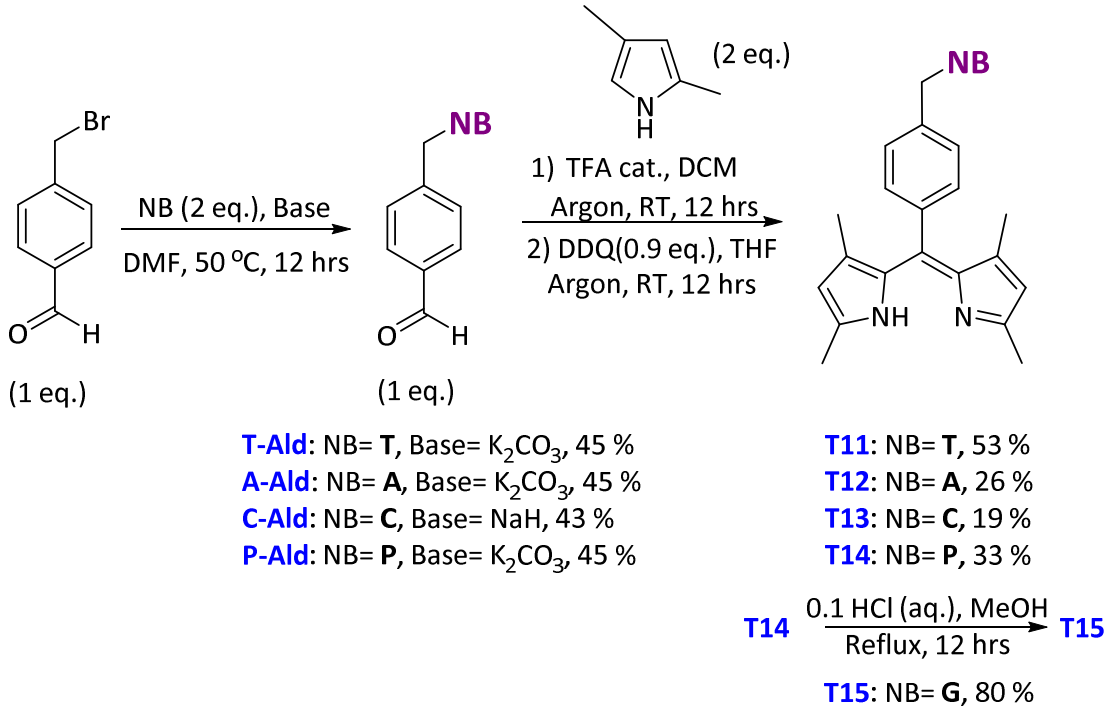

Figure 13: Synthèse de **T11**-**T15**.

De nombreux essais de cristallisation de **T11-T15** avec ou sans cations métalliques additionnels ont été effectués afin de permettre une caractérisation des assemblages formés par diffraction des RX. Nous avons obtenu des monocristaux de **T11 (T-dipyrrin)** en présence de $Zn(OAc)_2.2H_2O$. La résolution structurale par DRX montre que la dipyrrine a été métallée durant le processus de cristallisation conduisant à la formation d'un complexe bis-dipyrrine de zinc, **T-dipyrrin-Zn(II)**, qui s'auto-assemble pour conduire à un réseau moléculaire à base de liaisons H (figure 14). L'ion Zn(II) est tétracoordiné par 2 dipyrrines et l'unité asymétrique contient 4 complexes bis-dipyrrine de zinc non équivalents (**I**, **II**, **III**, **IV**). Ces 4 complexes sont connectés *via* des liaisons H entre les thymines formant ainsi un tétramère (**I-II-III-IV**). Chaque tétramère est en interaction avec 2 autres tétramères *via* des interactions CH---O impliquant le CH d'une thymine (position C125) du complexe **III** et le carbonyle d'une thymine du complexe **IV** conduisant ainsi à la formation d'un ruban monodimensionnel.

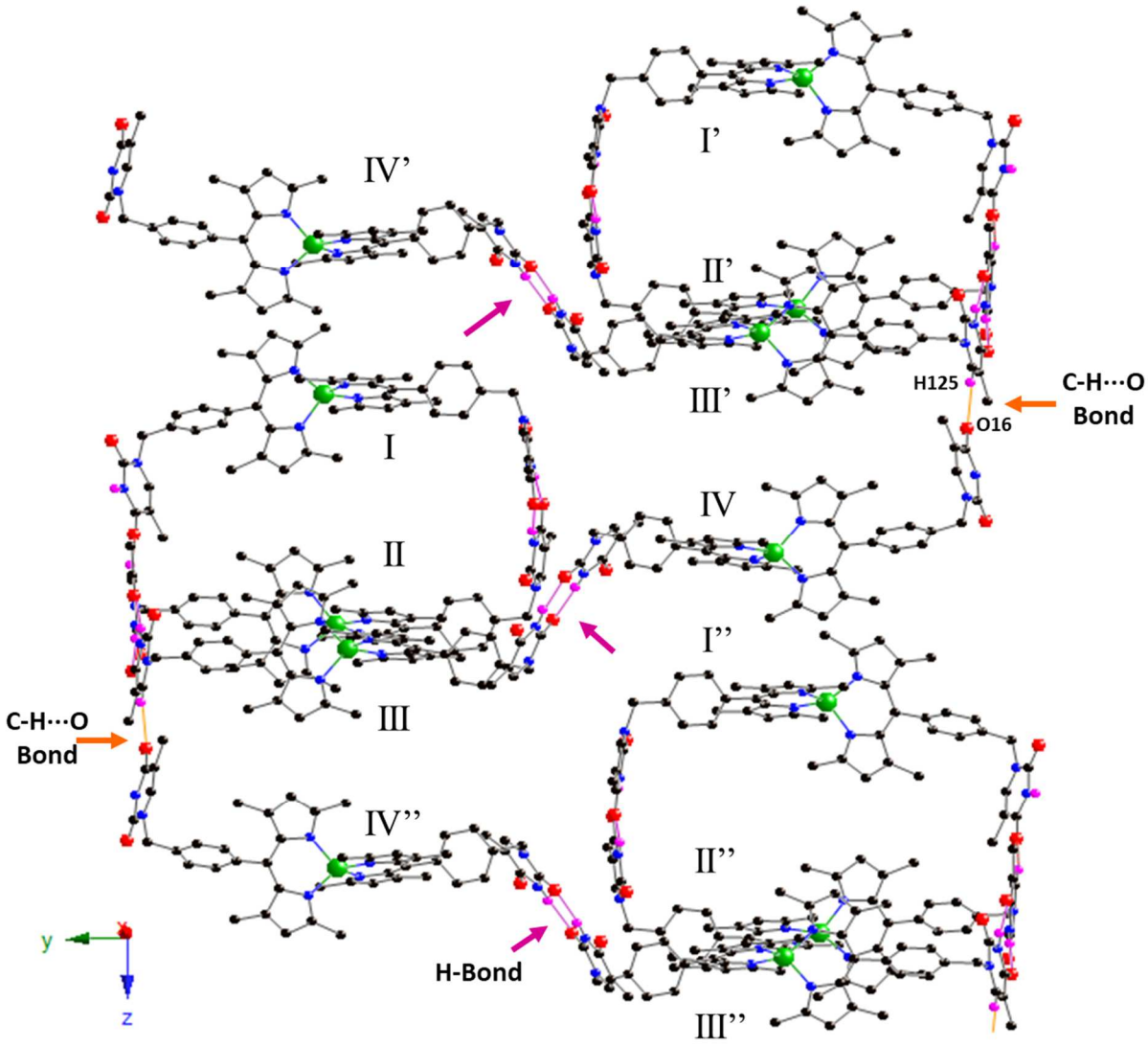

Figure 14: Une portion du réseau 1D obtenu par auto-assemblage de **T**-dipyrrin-Zn(II) (**T11**).

Dans une dernière partie, nous nous sommes intéressés à l'introduction de NBs à la périphérie de pyridine et de terpyridine *via* la stratégie concluante utilisée pour les porphyrines et les dipyrrines. Ainsi, la 4-bromométhylpyridine est mise à réagir avec la thymine, l'adénine, la cytosine, ou la 4-chloro-2-aminopurine selon les conditions exposées précédemment. Ceci conduit à la formation de 4 nouveaux tectons, **T-Py**, **A-Py**, **C-Py** et **P-Py** (**T16**-**T19)** avec des rendements de 45%, 53 %, 30 % and 30 % respectivement (Figure 15). **P-Py** est hydrolysé par une solution aqueuse de HCl (0.1 M) pour conduire à **G-Py** (**T20**) avec un rendement de 96% (Figure 15).

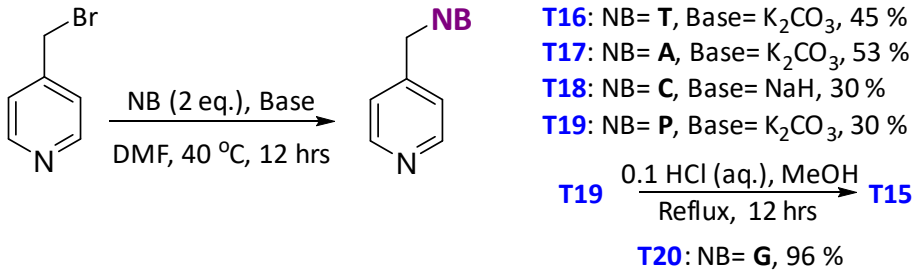

Figure 15: Synthèse de **T16**-**T20.**

Ces briques moléculaires ont été caractérisées par RMN, UV-Visible, IR and HRMS. De nombreux essais de cristallisation ont été effectués en présence et en absence de cations métalliques additionnels. Des monocristaux de **T-Py**, **A-Py** and **C-Py** ont été obtenus et analysés par diffraction des RX. **T-Py** (**T16**) s'auto-assemble *via* des liaisons H (NH—N_{py}) impliquant le NH de la thymine et l'azote de la pyridine d'un tecton adjacent, le tout conduisant à la formation d'un réseau 1D en zigzag. Ces chaines 1D adoptent un empilement anti-parallèle *via* des interactions π-π additionnelles (Figure 16 (a)). L'auto-assemblage de **A-Py** conduit à la formation de dimères grâce à la formation de deux liaisons H entre adénine de tectons adjacents (Figure 16 (b)). On note également la présence d'interactions supplémentaires de type π-π stacking entre les cycles des adénines mais également entre les cycles des pyridines. Enfin, **C-Py** s'organise à l'état solide *via* la formation de liaisons H entre cytosines pour ainsi former un réseau monodimensionnel. Chaque cytosine est en interaction avec 3 cytosines adjacentes *via* la formation de 4 liaisons H (Figure 16 (c)). De plus, les chaines adjacentes sont en interaction de type π-π stacking impliquant les cycles de cytosines.

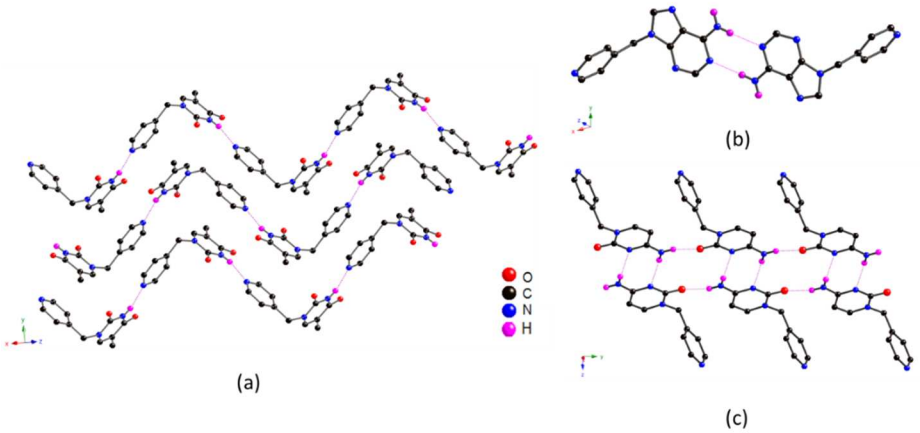

Figure 16: Portions des structures cristallines de (a) **T-Py**, (b) **A-Py** and (c) **C-Py**.

Des essais de cristallisation ont été effectués avec de nombreux cations métalliques notamment des sels Co(II), Cd(II), Ag(II), Cu(II), Pd(II), Ni(II), Zn(II). Des monocristaux de **A-Py** ont été obtenus en présence de $Cd(NO_3)_2.2H_2O$ et en présence de $HgCl_2$. Dans les deux cas, l'analyse par DRX montre que la pyridine est liée au cation métallique et que l'adénine est impliquée dans la formation du réseau soit au travers de liaisons de coordination et de liaisons H dans **A-Py-Cd(II)** soit uniquement au travers de liaisons de coordination dans **A-Py-Hg(II)**.

Le complexe **A-Py-Cd(II)** s'organise en une architecture infinie impliquant deux types d'interactions: des liaisons de coordination et des liaisons H (Figure 17). Le Cd(II) hexacordiné, 4 tectons **A-Py** occupant le plan équatorial et deux nitrates occupant les deux positions apicales. Le plan équatorial est occupé par deux pyridines en *trans*, les deux autres positions étant occupées par 2 adénines liées au cation métallique par l'azote N3 (figure 17). Chaque tecton joue ainsi le rôle de ligand bidentate pontant entre deux Cd(II), ce qui conduit à la formation d'un réseau monodimensionnel de type ruban dont la stœchiométrie est de 2 **A**-Py pour 1 Cd(II). Des interactions additionnelles de type liaisons H entre les adénines de rubans adjacents (figure 17) conduisent au réseau 2D final (Figure 17).

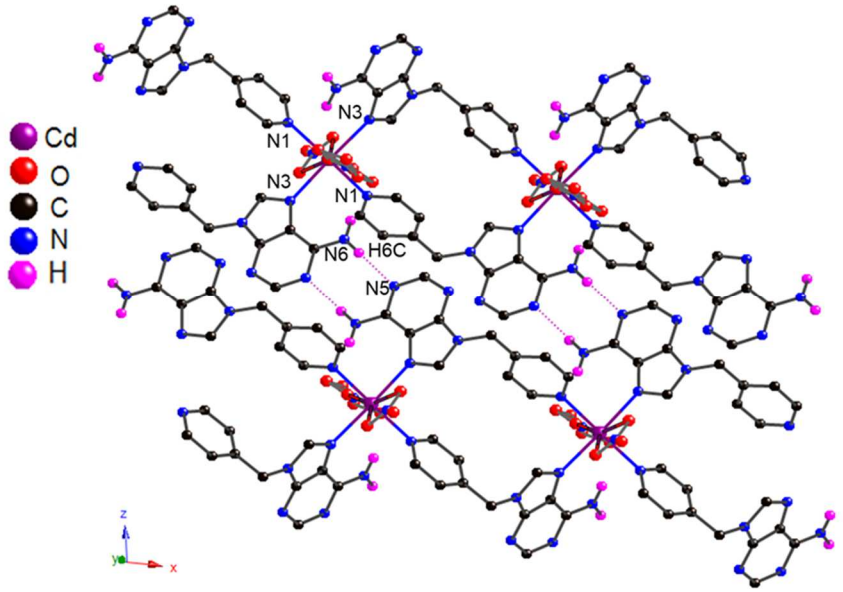

Figure 17: Une portion de la structure de **A-Py** en présence de **Cd(II).**

En présence de Hg(II), **A-Py** forme une structure en hélice pour laquelle la stœchiométrie ligand/Hg1 est de 1/1(figure 18 haut). Un deuxième cation Hg2, non équivalent à Hg1, est présent

dans la maille. La stœchiométrie finale est différente à celle obtenue avec le Cd(II) puisqu'elle est ici de 1 **A**-Py pour 2 Hg(II). Hg1 est tétracoordiné et adopte une géométrie tétraédrique déformée. Sa sphère de coordination est formée de deux chlorures et de deux ligands **A-Py**, l'un coordiné via la pyridine et le deuxième via l'azote N5 de l'adénine. Ainsi, dans la structure obtenue, **A-Py** joue à nouveau le rôle de ligand bidentate pontant entre deux Hg1, conduisant ainsi à la formation d'une hélice (figure 18 haut). Hg2 est en interaction avec l'azote N3 de chaque adénine ainsi qu'avec 3 chlorures dont l'un, Cl1, fait office de ligand pontant entre Hg1 et Hg2 (Figure 18 bas). Ainsi, dans cette structure, l'adénine présente est uniquement impliquée dans des liaisons de coordination, et le ligand **A-Py** forme 3 liaisons de coordination : 2 avec un Hg1 et une avec Hg2

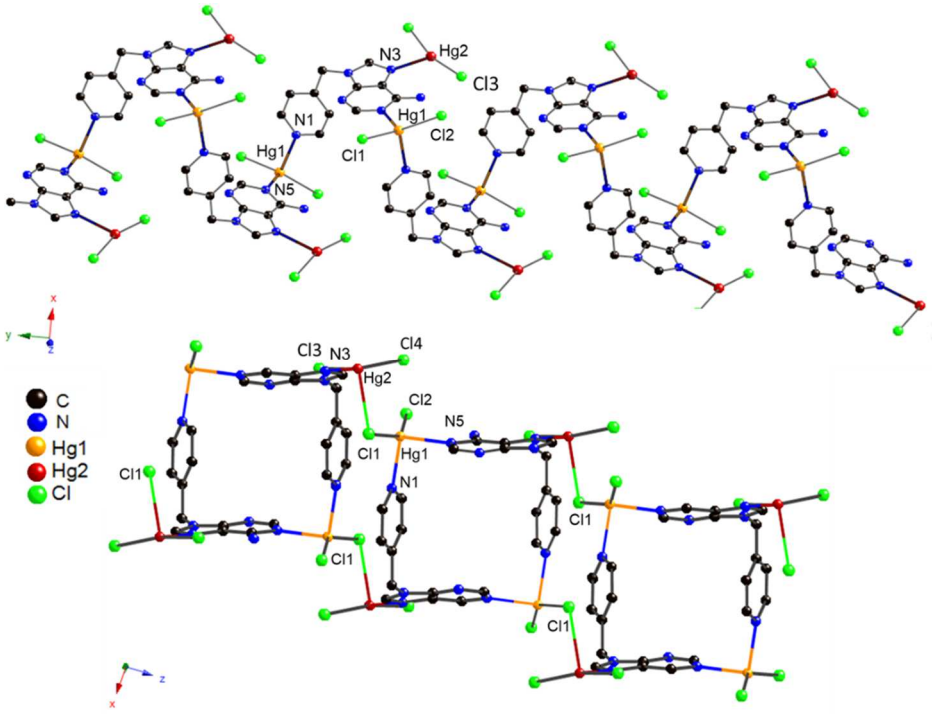

Figure 18: Une portion de la structure obtenue pour **A-Py** en présence de **Hg(II).**

Nous avons également pu isoler des monocristaux de **C-Py** en présence de $Zn(NO_3)_2.6H_2O$ et de $Cd(NO_3)_2.4H_2O$. Dans les deux cas, le cation métallique est présent dans la structure avec une stœchiométrie M(II) / **C-Py** égale à 1 / 1. Deux **C-Py** sont connectés à deux cations métalliques, Zn(II) ou Cd(II), de façon convergente, ce qui conduit à la formation de dimères, M_2(**C-Py**)$_2$ (figure 19, gauche). Dans le cas du Zn(II), chaque **C-Py** fait office de ligand bidentate pontant. Ainsi chaque Zn(II) est coordiné par une pyridine et une cytosine, deux nitrates venant compléter la

sphère de coordination du cation métallique. Les cytosines sont impliquées dans des liaisons H additionnelles, impliquant les oxygènes des carbonyles et les groupements NH_2 (figure 19) , ainsi chaque ligand est impliqué dans deux liaisons de coordination et deux liaisons H

En présence de Cd(II), **C-Py** forme un dimère comparable *via* la coordination pontante de **C-Py** à deux Cd(II). De plus, la cytosine chélate le Cd(II) en occupant deux positions en *cis* du cation métallique hexacoordiné (figure 19 droite). Enfin, la sphère de coordination du Cd(II) est complétée par 3 nitrates bidentates, l'un étant chélatant et les deux autres étant pontants entre deux dimères.

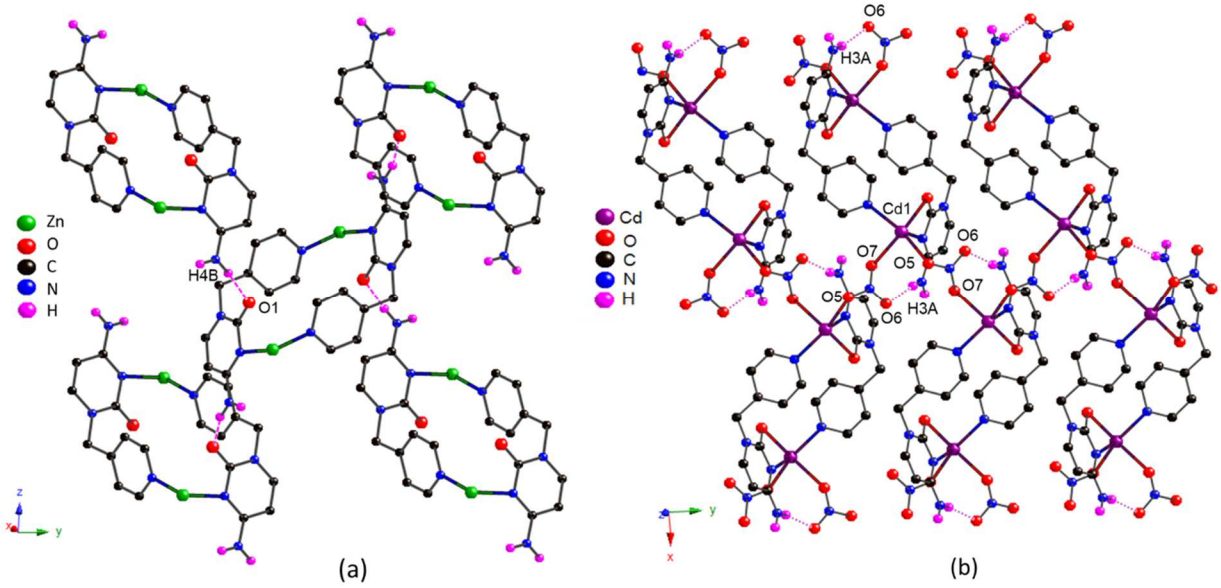

Figure 19: Une portion de la structure obtenue à partir de **C-Py** en présence de (a) Zn(II) (les anions ont été omis par souci de clarté) et (b) Cd(II)

Dans un dernier temps, nous avons ciblé la formation de tectons à base de terpyridine. Ainsi **T**,**A**, **C** ou **P** réagissent avec la 4'-(4-(bromométhyl)phényl)terpyridine (**terPy**) dans la DMF en présence de base (Figure 20). **T-terPy**, **A-terPy**, **C-terPy** and **P-terPy** (**T21**-**T24)** sont formés avec des rendements de 40 % , 54 %, 79% et 43% respectivement. L'hydrolyse de **T24** conduit au tecton **G-Terpy** (**T25**) (Figure 20) avec un rendement de 98%.

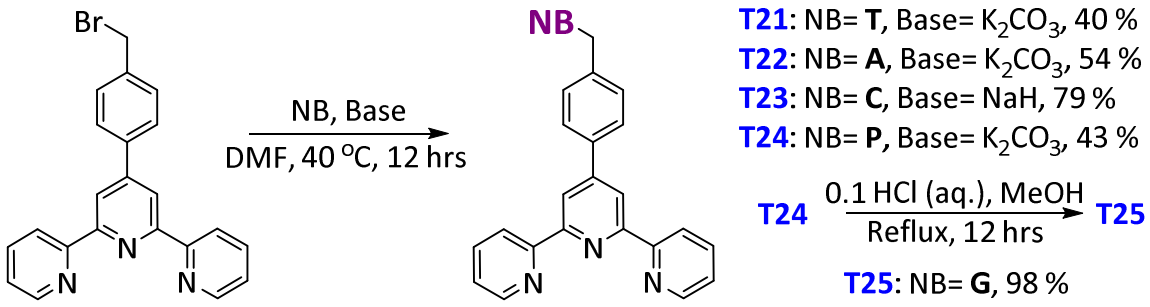

0 Synthèse de **T21**-**T25**.

Ces 5 nouveaux tectons (**T21-T25**) ont été caractérisés par RMN, UV-Visible, IR and HRMS. De nombreux essais de cristallisation ont été effectués en présence et en absence de cations métalliques additionnels. Des monocristaux ont été obtenus pour **T-terPy** en présence de $Cu(OAc)_2$ ou de $Cd(NO_3)_2.4H_2O$. Leur analyse par DRX a montré la formation de complexes **T-terPy-Cu(II)** et **T-terPy-Cd(II)** (Figure 21). Dans les deux structures, le ligand terpyridine agit comme un ligand tridentate pour le cation Cu(II) ou Cd(II). Le complexe **T-terPy-Cu(II)** s'auto-assemble en un dimère *via* la formation de deux liaisons H impliquant les thymines. Chaque dimère interagit avec deux dimères adjacents grâce à des interactions de type π-π stacking entre les terpyridines (Figure 21(a)). Dans la structure avec Cd(II), chaque complexe **T-terPy-Cd(II)** est en interaction H avec deux complexes adjacents (Figure 21(b)) impliquant les thymines. On observe également des interactions de type π-π entre les terpyridines.

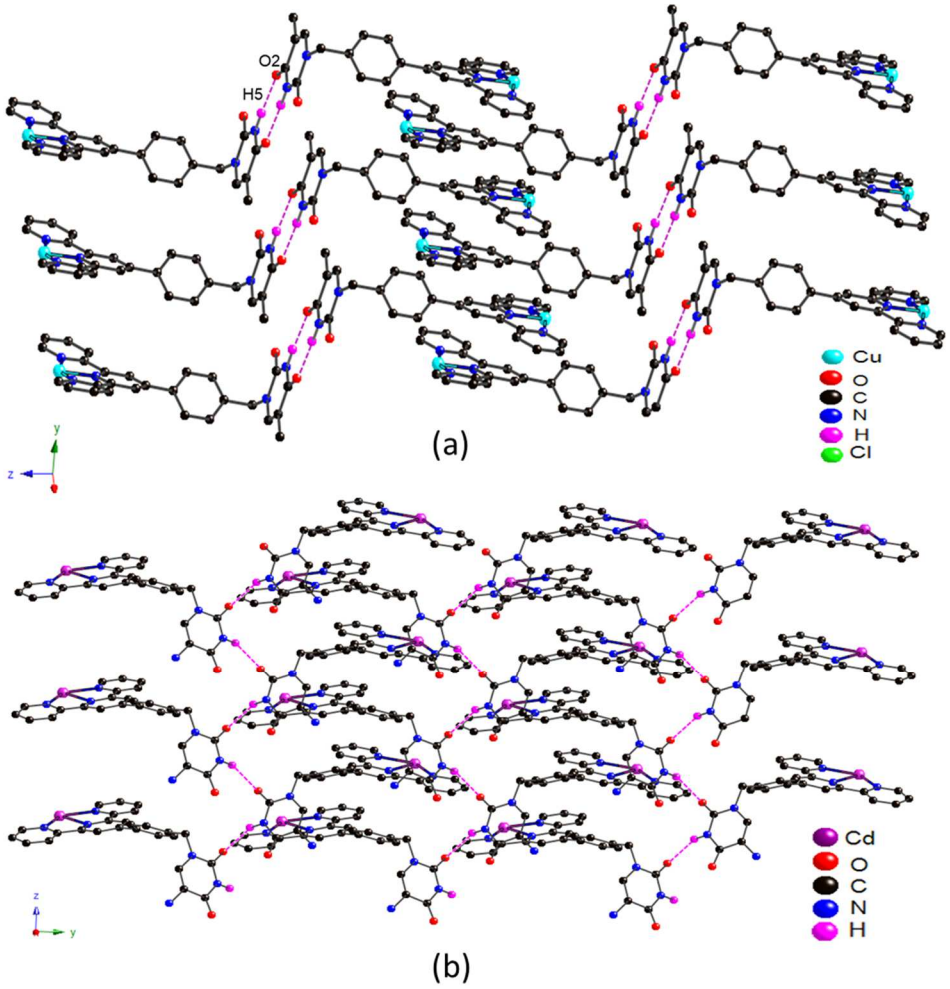

Figure 20: Une portion de la structure de (a) **T-terPy-Cu(II)** et de **T-terPy-Cd(II)** (dans les deux cas, les anions en interaction avec le cation métallique ont été omis par souci de clarté)

3) Conclusion générale

Une librairie de 25 nouveaux tectons à base de porphyrines, dipyrrines, terpyridines ou pyridines substituées par des NBs a été constituée. Trois tectons porphyriniques (**T1**, **T2** et **T3**) ont été obtenus *via* un couplage de Sonogashira entre une porphyrine substituée en position méso *trans* par des groupements éthynyles (**Po1**) et **I-U-Ph2** ou **I-U-C6**. Malheureusement la même stratégie étendue à l'adénine ou à la cytosine n'a pas conduit aux tectons ciblés. Nous avons alors visé la substitution de porphyrines *via* la formation de liaisons C-N utilisant le site N1 des pyrimidines ou N_9 des purines. Nous avons fait réagir **T**, **A**, **C**, **P** et **G** avec la 5,15-di(4-(bromométhylphényl)-10,20 dimésitylporphyrine et généré 5 nouveaux tectons : **T5** -**T9** (Figure 22). Cette même stratégie nous a également permis d'isoler le tecton **T10**, tétrasubstitué par 4 thymines en position méso. Cette stratégie a également été fructueuse avec les dipyrrines et permis de générer les tectons **T11-T16** ainsi qu'avec les pyridines et les terpyridines, **T17**-**T25** (Figure 22).

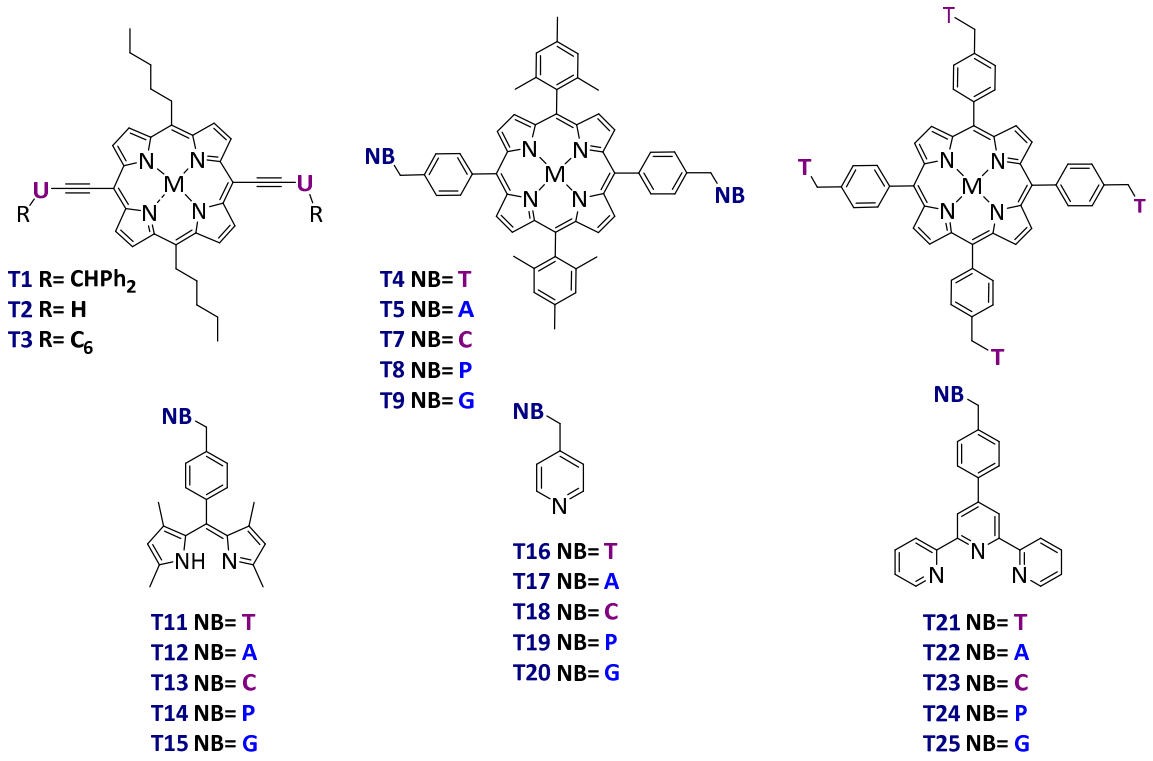

Figure 21: Représentation de la librairie des 25 tectons synthétisés.

L'ensemble de ces tectons ont été caractérisés par RMN, UV-Visible, IR and HRMS et de nombreux essais de cristallisation ont été effectués en présence et en absence de cations métalliques additionnels. L'analyse DRX a été effectuée pour **T16**-**T18**. Les tectons à base de pyridine et d'adénine (**T17**) et de cytosine (**T18**) s'assemblent *via* la formation de liaisons H entre les NBs. Le tecton **T16** forme également un réseau moléculaire à base de liaisons H mais dans ce cas la pyridine et la thymine sont toutes les deux impliquées dans la connectivité.

En présence de Zn(II), le tecton **T11** à base de dipyrrine et de thymine forme un réseau complexe de (**T11**)$_2$Zn impliquant 4 complexes bis-dipyrrines non équivalents en interaction *via* des liaisons H entre les thymines présentes à leur périphérie.

Des réseaux de coordination sont formés à partir de **T17** en présence de Cd(II) ou de Hg(II) ainsi qu'à partir de **T18** en présence de Zn(II) et Cd(II). Les pyridines sont impliquées dans des liaisons de coordination avec les cations métalliques présents. Les NBs font office de ligands coordinants (**T17**-Hg(II)) ou ligands coordinants et en interaction H (**T17**-Cd(II), and **T18**-Cd(II) et **T18**-Zn(II)). Enfin, le complexe à base de terpyridine M(II)-**T21** (M=Cu(II) ou Cd(II)) s'assemble à l'état solide par formation de liaisons H entre les thymines conduisant soit la formation de dimères (avec Cu(II)), soit à la formation d'un réseau moléculaire à base de liaisons H (avec Cd(II)).

Ce travail est toujours en cours, notamment au travers des nombreux essais de cristallisation en cours, et il sera poursuivi par des essais de cristallisation supplémentaires. En effet, de multiples combinaisons sont possibles à partir de cette bibliothèque de 25 tectons permettant d'envisager des assemblages homoleptiques mais aussi hétéroleptiques, ajouter à un vaste choix des cations additionnels potentiels et à de nombreuses possibilités d'interactions additionnelles par liaison H. Il conviendra également de poursuivre l'effort de synthèse visant des tectons plus rigides à base de dipyrrines, ou de terpyridines, tels que cela avait été envisagé en début de thèse avec les porphyrines. De plus, la synthèse de complexes de type BODIPY ou d'hélicates à partir des dipyrrines **T11**-**T16** serait un challenge particulièrement intéressant pouvant conduire à des assemblages aux propriétés originales.

Références

1) (a) M. W. Hosseini, *Acc. Chem. Res*., **2005**, *38*, 313-23. (b) M. W. Hosseini, *CrystEngComm*, **2004**, *6*, 318-322.

2) S. Mann, *Nature*, **1993**, *365*, 499-505.

3) (a) B.F. Abrahams, B. F. Hoskins, R. Robson*, J. Am. Chem. Soc*., **1991**, *113*, 36063607. (b) M. W. Hosseini, *Acc. Chem. Res*., **2005**, *38,* 313-323.

4) (a) L. R. Milgrom, The Colors of of Life: An Introductions to the chemistry of Porphyrins and Related Compounds, Ed. Oxford, **1997.** (b) Y. Wi Y. –W. Lin, J. Wang, *J. Inorg. Biochem.*, **2013**, *129*, 162-171. (c) Y. W. Lin, *Biochim. Biophys. Acta.,* **2015**, *1854*, 844-859.

5) S. K. Yang, S. C. Zimmerman, *Isr. J. Chem.* **2013**, *53*, 511-520.

6) J. B. Asbury, T. Steinel, M. D. Fayer, *J. Phys. Chem. B*., **2004**, *108*, 6544-6554.

7) (a) M. Simard, D. Su, J. D. Wuest, *J. Am. Chem. Soc.* **1991**, *113*, 4696-4698. (b) Sargsyan, A. A. Schatz, J. Kubella, M. Balaz, *Chem. Commun*., **2013**, *49*, 1020-1022.

8) W. Saenger, Principles of Nucleic acids structure, *Springer*, New York, **1984.**

9) J. D. Watson, F. H. Crick, *Nature,* **1953**, *171*, 737-737.

10) (a) Y. Kyogoku, R. C. Lord and A. Rich, *Proc. Nat. Acad. Sci. USA*, **1967**, *57*, 250-257. (b) Y. Kyogoku, R. C. Lord and A. Rich, *Proc. Biochim. Biophys. Acta*, **1969**, *179,* 10-17.

11) (a) S. C. Zimmerman and P. S. Corbin, *Struct. Bond*., **2000,** *96*, 63-94. (b) T. J. Murray and S. C. Zimmerman, *J. Am. Chem. Soc*., **1992**, *114,* 4010-4011. (b) J. Pranata, S. G. Wierschke and W. L. Jorgensen*, J. Am. Chem. Soc*., **1991**, *113*, 2810-2819. (c) J. Sartorius, H.J. Schneider, *Chem. Eur. J.,* **1996**, *2*, 1446-1452.

12) (a) W. Saenger, Principles of Nucleic Acid Structures, *Springer-Verlag, New York,***1983**. (b) K. Hoogsteen, *Acta Cryst.*, **1963**, *16*, 907-915. (c) R. E. A. Kelly, L. N. Kantorovich, *J. Mater. Chem.,* **2016**, *16*, 1894-1905. (d) Ciesielski, M. El Garah, S. Masiero, P. Samori, *Small*, **2016**, *12*, 83-95.

13 (a) J. L. Sessler, J. Jayawickramarajah, *Chem. Comm.*, **2005**, 1939-1949. (b) S. Sivakova, S. J. Rowan, *Chem. Soc. Rev*., **2005**, *34*, 9-21. (b) J. L. Sessler, C. M. Lawrence, J. Jayawickramarajah, *Chem. Soc. Rev*., **2007**, *36*, 314-325. (c) J. Hamblin, S. P. Argent, A. J. Blake, C. Wilson, N. R. Champness, *CrystEngComm*, **2008**, *10*, 17821789. (d) S. Kyung, S. C. Zimmerman, Isr. J. Chem.,

2013, 53, 511-520. (e) L. Qi, L. L. Gundersen, C. H. Gorbitz, *CrystEngComm*, **2018**, *20*, 1179-1184.

14) (a) J. L. Sessler, M. Sathiosatham, C. T. Brown, T. A. Rhodes, G. Wiederrecht, *J. Am. Chem. Soc.,* **2001**, *123*, 23655-3660. (b) A. Lopez, J. Liu, *ChemNanoMat*, **2017**, *3*, 670-684. (c) N. Sreenivasachary, J.-M. Lehn, *PNAS*, **2005**, *102*, 5938-5943. (d) G. Sargsyan, B. M. Leonard, J. Kubelka, M. Balaz, *Chem. Eur. J.*, **2014**, *20*, 1878-1892.

15) I. Goldberg, *CrystEngComm*, **2008**, *10*, 637-645. (b) O. K. Farha, A. M. Shultz, A. A. Sarjeant, S. T. Nguyen, J. T. Hupp, *J. Am. Chem. Soc.*, **2011**, *133*, 5652-5655. (c) E. Khun, V. Bulach, M. W. Hosseini, *Chem. Commun.*, **2005**, 3906-3908.

16) (a) M. A. Bakar, N. N. Sergeeva, T. Juillard, M. O. Senge, *Organometallics*, **2011**, *30*, 3225-3228. (b) N. Aratani, A. Ouska, *Chem. Commun*., **2008**, 4067-4069.

17) F. Wu, M. G. Buhendwa, D. F. Weaver, *J. Org. chem*., **2004**, *69*, 9307-9309.

18) (a) C. H. Lee, J. S. Lindsey, *Tetrahedron*, **1994,** *50***,** 11427-11440. (b) S. Rucareanu, O. Mongin, A. Schuwey, N. Hoyler, A. Gossauer, Journal , *J. Org. Chem.* **2001,** *66,* 4973-4988.

19) (a) F. Wu, M. G. Buhendwa, D. F. Weaver*, J. Org. Chem.,* **2004**, *69*, 9307-9309. (b) N. Bilbao, V. Vazquez-Gonzalez, M. T. Aranda, D. Gonzalez- Rodriguez, *Eur. J. Org. Chem.*, **2015**, 7160-7175.

20) (a) C.M. White, M. F. Gonzalez, D. A. Bardwell, L. H. Rees, J. C. Jeffery, M. D. Ward, N. Armaroli, G. Calogero, F. Barigelleti, *J.Chem.Soc, Dalton Trans*, **1997**, 727-735. (b) N. Armaroli,,F. Barigelleti, G. Calogero, L. Flamigni, C.M. White, *Chem Commun*.,**1997**, 2181-2182.(c) S. Ellipilli, K. N. Ganesh, *J. Org. Chem*., **2015**, *80*, 9185-9191.

21) (a) S. Ellipilli, K. N. Ganesh, *J. Org. Chem*., **2015**, *80*, 9185-9191. (b) A. Kiviniemi, M. Murtola, O. Ingman, P. Virta, *J. Org. Chem.*, **2013**, *78*, 5153-5159. (c) K. Pomeisl, A. Holy, R. Pohl, *Tetrahedron Letters*, **2007**, *48*, 3065-307.

‘‘The human mind adjusts itself to a certain point of view, and those who have regarded nature from one angle, during a portion of their life, can adopt new ideas with difficulty ’’

Antoine Lavoisier

Science is the study of the structure and the behavior of the natural world through a series of hypotheses, observation and experiments. The constant source of inspiration provided by nature challenges scientists to keep on projecting new theories, developing new methods, and designing new materials. In the early years, chemists aimed to study the structural and the physical properties of natural elements. Observing nature’s complex architectures, inspired construction methods and engineering designs. Nowadays, chemists and engineers aim to mimic nature’s complex structures relying on two different approaches to construct new products, the “top-down” and the “bottom-up” approach.

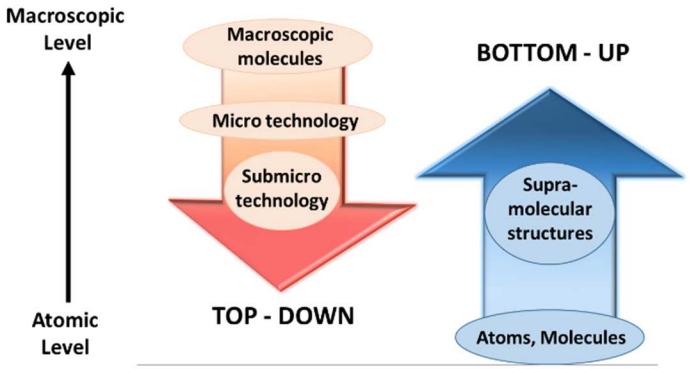

Figure 1: Top-down and bottom-up approach

The top-down approach, as shown in Figure 1, is based on the decomposition of larger materials into smaller ones going from the macroscopic level to the microscopic level using tools to cut, shape, and break down materials into the desired shape and size. This approach is limited to physical methods. However, the bottom-up approach uses the chemical properties of single molecules to build larger molecular architectures thus going from the atomic level to the macroscopic level. Chemists use this approach through different methods. The first technique deals with classical organic or inorganic molecular synthesis, and it is used for synthesizing medication for pharmaceutical and biological applications. The second method, to build large scaled materials, is covalent polymerization. Polymerization is famous in polymer industry to manufacture plastics,

caoutchouc, latex and others. This procedure is based on the formation of covalent bonds through chain reactions between monomers resulting in long polymers of different chain length and molecular weight. The third method is molecular self-assembly, which relies on the principles of supramolecular chemistry. This process assembles building blocks into large architectures *via* weak and reversible interactions.

In general, the first step to produce large scaled architectures is to synthesize monomers or building blocks, using the concept of covalent molecular synthesis. The second step is to polymerize monomers into large-scale polymer materials, or to self-assemble building blocks into supramolecular architectures. The second strategy is the main objective of this thesis, which deals with supramolecular chemistry and molecular tectonics.

Introduction

Table of Contents

I. Supramolecular Chemistry……3
II. Molecular Tectonics……..4
II. 1. Molecular tectons……...5
II. 1. a) Endo- and Exo-receptors……5
II. 1. b) Complementary and self-complementary tectons……..6
II. 2. Intermolecular interactions……7
II. 2. a) van der Waals interactions……7
II. 2. b) π-π interactions……..8
II. 2. c) Hydrogen bonds……8
II. 2. d) Electrostatic interactions……9
II. 2. e) Coordination bonds……9
II. 3. Molecular networks……9
II. 3. a) Dimensionality and geometry of molecular networks……10
II. 3. b) Coordination networks……12
II. 3. b) 1) Metallic centers……...12
II. 3. b) 2) Organic tectons bearing coordinating sites……..13
II. 3. b) 3) Metal bonded Organic-Frameworks (MOFs) ……18
II. 3. c) Hydrogen bonded networks……21
II. 3. c) 1) Hydrogen bonding patterns……..22
II. 3. c) 2) Examples of hydrogen bonded networks……24
II. 3. c) 3) Hydrogen-Organic-Frameworks (HOFs) ……27
III. Nucleobases…….....30
III. 1. pKa values of nucleobases……..32
III. 2. Tautomerism of nucleobases……...33
III. 3. Nucleobase interactions……..34
III. 4. Nucleobases self-assemblies……...37
III. 4. a) Guanine……...37
III. 4. b) Cytosine……..39
III. 4. c) Adenine……...40
III. 4. d) Thymine and Uracil……40
III. 5. Supramolecular assemblies based on NB……42
III. 5. a) Nucleobase duplex systems……....43
III. 5. b) Nucleobase based polymers……...45
III. 5. c) Nucleobase based networks ……...47
IV. Aim of the project…….....52
V. References…….....53

I. Supramolecular chemistry

The curiosity of chemists was not simply satisfied by the study of the behavior of atoms and molecules. Therefore, investigations started to extend beyond the atomic and molecular level into the supramolecular level.

Principles of supramolecular chemistry were first introduced by Johannes Diderik van der Waals in 1873 and by Hermann Emil Fischer, who developed the concept of molecular recognition and host-guest chemistry in 1894. In the late 20th century, the Nobel Prize winners Donald J. Cram, Jean-Marie Lehn and Charles J. Pedersen elaborated the principles of host-guest chemistry through "their development and use of molecules with structure-specific interaction of high selectivity."

Professor Jean-Marie Lehn, who introduced the concept of supramolecular chemistry in 1978, stated, "Just as there is a field of molecular chemistry based on covalent bond, there is a field of supramolecular chemistry, the chemistry of molecular assemblies and of the intermolecular bonds".[1] He also defined supramolecular chemistry as "chemistry beyond the molecule".[2]

From these descriptions, several important points could be deduced. First, molecular synthesis generates molecules by covalent bonds *via* chemical reactions. However, supramolecular chemistry generates molecular architectures by non-covalent intermolecular bonds *via* the self-assembly of building blocks. Second, the properties of supramolecular bonds differ from covalent bonds because of their reversible nature. Third, supramolecular chemistry is a combination of both: molecular synthesis (synthesis of building blocks) and molecular recognition.[3]

The inspiration of supramolecular chemistry is related to biological components and processes. DNA, ribosomes, hemoglobin and millions of other biological and natural beings are organized, structured and function through interactions similar to those discussed in supramolecular chemistry. Even if, biological systems are still far more sophisticated than artificial systems, the concept of supramolecular chemistry has increased the level of understanding of chemical constructions of biological,[4] organic, and inorganic materials with promising applications in gas storage,[5] catalysis,[6] photoactivity [7] and others.

II. Molecular Tectonics

Molecular tectonics is a field of supramolecular chemistry dealing with the formation of one, two and three-dimensional periodic architectures. The term was proposed by Professor Stephan Mann in 1993.[8] The general concept is to self-assemble **molecular tectons** or building blocks *via* **intermolecular interactions** into periodic architectures referred to as **molecular networks** (Figure 1).[9]

Tectons offer complementary interaction sites leading to a recognition pattern through non-covalent and reversible interactions, allowing the component to have the ability to self-repair into the most thermodynamically stable architecture. The iteration (repetition) of these interactions lead to the translation of the recognition pattern in space generating molecular architectures of different geometries and dimensionality. The role of supramolecular chemists is to control the self-assembly processes by controlling the design of tectons through classical molecular synthesis, which should in principle allow the prediction of the topology and geometry of the final assembly.

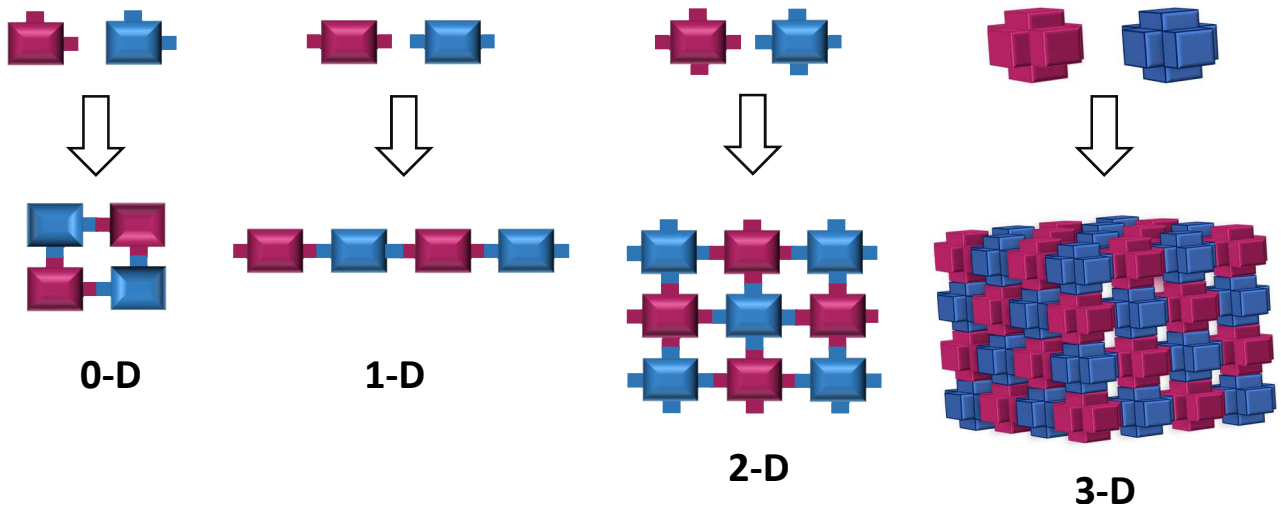

Figure 1: Schematic representation of the dimensionality of networks.

II. 1. Molecular tectons

Tecton comes from the word "tekton" from classical Greek, which means builder. In supramolecular chemistry, the word tecton is used to describe the building blocks or active molecular construction units designed by using classical molecular synthesis. These tectons bear recognition sites (chemical functionalities) which are able to generate certain recognition patterns formed by intermolecular interactions. The geometry and dimensionality of the final molecular network depends on the position, the orientation, the type and the number of the recognition sites of a tecton. Considering those parameters tectons could be classified into different groups.

II. 1. a) Endo- and Exo-receptors

Depending on the position and orientation of their recognition sites, tectons can be classified into two groups: the endo- and exo- receptors.

The endo-receptors (Figure 2) possess interaction sites located in a convergent manner thus forming discrete architectures. Endo-receptors act as host molecules, and with a suitable substrate (guest molecule) they form host-guest complexes called inclusion complexes. Examples of such receptors are: crown ethers,[10] cryptands[11] and cages[12].

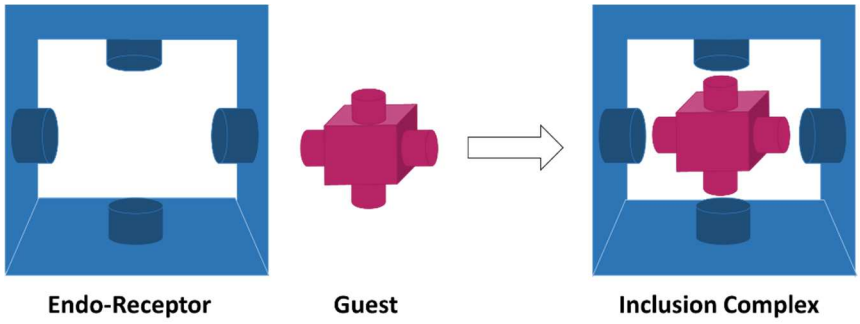

Figure 2: Schematic representation of endo-receptors.

The exo-receptors (Figure 3) display interaction sites with divergent orientation. If exo-receptors have one recognition site and are joined with stopper building blocks, they form discrete complexes. On the other hand, if exo-receptors have more than one connecting site and are joined

with connector building blocks, they form infinite complexes called molecular networks, which will be further discussed.

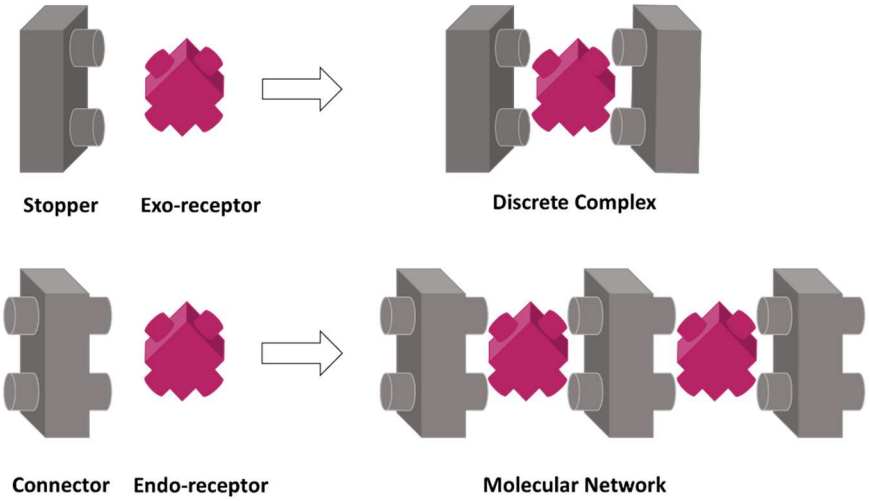

Figure 3: Schematic representation of endo-receptors.

II. 1. b) Complementary and self-complementary tectons

Considering the nature of interaction sites, two families of tectons may be distinguished. Tectons bearing complementary interaction sites are referred to as self-complementary tectons. Such tectons have the ability to self-assemble into a network on their own. Complementary tectons have un-complementary interaction sites and need a complementary partner to assemble into a molecular network (Figure 4).

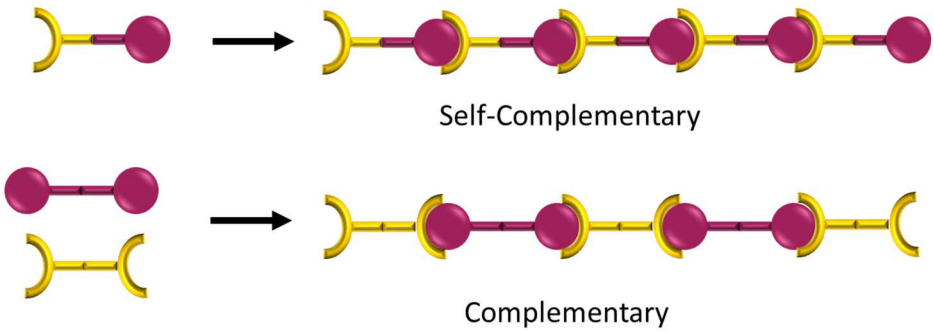

Figure 4: Schematic representation of self-complementary and complementary tectons.

Last but not least, the chemical nature and the number of recognition sites of tectons dictate the type of intermolecular interactions and the dimensionality of the final molecular network respectively, which is further elaborated in the following paragraphs.

II. 2. Intermolecular interactions

As mentioned previously, building supramolecular architectures requires the periodic organization of tectons through non-covalent intermolecular interactions, which direct the assembly processes by their strength, directionality and specificity. Those interactions are described as supramolecular interactions rather than bonds, because compared to covalent bonds they are weak and reversible. The use of weak and reversible interaction is an essential key to build a thermodynamically stable architecture, since it permits self-repairing processes to take place during the construction event. Several interactions, which vary in strength from 0.5 kJ/mol to 400 kJ/mol, offer these characteristics (Figure 5). In some cases, tectons assemble into molecular network *via* one type of intermolecular interactions. However, tectons with different interaction sites can assemble into networks *via* more than one intermolecular interaction.

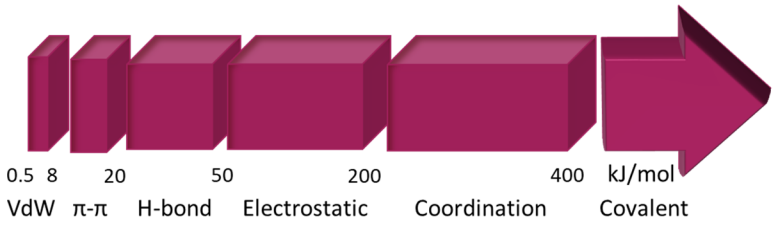

Figure 5: Energy scale of molecular interactions used for building supramolecular assemblies.

II. 2. a) van der Waals interactions

van der Waals interactions are weak attractive forces (0.4-4 kJ/mol) based on electrostatic interactions resulting from induced or permanent dipoles in molecules. There are three types of van der Waals interactions:

1) Debye forces: are dipole-induced dipole interactions that take place between a permanent dipolar molecule and a polarizable molecule.

2) Keesom forces: are dipole-dipole interactions that take place between two permanent dipolar molecules.
3) London forces: are induced dipole-induced dipole interactions that take place between two molecules with spontaneous dipoles.

All of these interactions are non-directional, nor highly selective and only effective in a short range. Therefore, they only lead to macroscopic effect when combined in large numbers.

II. 2. b) π-π interactions

π-π interactions are attractive non-directional interactions slightly stronger (5-12 kJ/mol) than van der Waals interactions. They take place between aromatic molecules arranged in parallel fashion (π stacking) or in an edge-to-face orientation. Usually, one of the aromatic ring is more electron rich while the other is more electron poor. Those types of interactions are famous in molecular tectonics since they stack aromatic molecules in an optimal way to minimize repulsive interactions and to maximize attraction leading to a more stable network.

II. 2. c) Hydrogen bonds

Hydrogen bonds (D-H···A) are attractive and directional interactions that take place between hydrogen donors (D-H) and a hydrogen acceptor (A). Hydrogen donors (D-H) are based on electronegative atoms bearing a labile hydrogen for example: alcohols (-OH), primary amines (-NH) and amides ((CO)-NH) functions. Hydrogen acceptors are electronegative functions such as ethers (-O-), carbonyls (-C=O) and tertiary amines (=N-). The interaction between a proton donor and a proton acceptor is referred to as hydrogen bond since a proton is shared creating a local bond between D and A. The average distance between D-A varies from 2.5 Å to 3.2 Å and the angle D-H···A falls in a range of 120° to 180°. The energies of H-bonds can vary from 4 to 60 kJ/mol and more making them relatively strong supramolecular interactions. H-bonds are observed frequently in natural architectures for example, the assembly of DNA through Watson-Crick hydrogen bonds between nucleobases. The latter is used in designing molecular networks through the assembly of H-bonding complementary tectons bearing nucleobases, which is the main concept of this thesis.

II. 2. d) Electrostatic interactions

Electrostatic interactions are also known as charge-charge interactions. They are electric forces between molecules with the opposite or same charges (δ^+ and δ^-). Attractive electrostatic interactions exist between closely packed opposite charged molecules. Whereas, repulsive electrostatic interactions are present between molecules with the same charge.

II. 2. e) Coordination bonds

Coordination bonds are formed between coordinating sites of organic ligands and metal cations. These bonds are selective, directional and the strongest among supramolecular interactions (50-100 kJ/mol). An organic ligand acts as Lewis base offering a lone electron pair to the metal cation, which acts as Lewis acid forming electrostatic attraction between the negatively polarized or charged donor atom of the ligand and the positively charged metal ion. Coordination bonds are the most popular interactions used in supramolecular engineering, due to their strength and their directionality, which enable them to replace multiple weak interactions.

II. 3. Molecular networks

For molecular tectonics, designing and synthesizing complementary or self-complementary tectons is followed by the self-assembly processes of the tectons in the crystalline phase. Playing on the orientation of recognition sites of tectons can lead to discrete (convergent orientation) or infinite (divergent orientation) architectures. As mentioned before, the approach of building infinite architectures is named molecular tectonics and the term molecular networks is given to these architectures. Molecular networks are produced by the iteration of the interaction processes between tectons that leads to the translation of the recognition patterns in space. Several factors can control the dimensionality and geometry of molecular networks, two of them being the number of interaction sites of a tecton and the directions of the translation process of the recognition pattern in space.

II. 3. a) Dimensionality and geometry of molecular networks

1-D networks

One-dimensional networks form the simplest category since the iteration process of the recognition pattern between tectons is translated into only one direction in space. Normally, 1-D networks are the result of the assembly of complementary tectons or self-complementary tectons possessing two divergent recognition sites. In literature, several examples of 1-D molecular networks are known, and they usual adopt a linear chain,[13] zigzag chain,[14] wavy[15] or helical geometries[16] (Figure 6).

Figure 6: Schematic representation of geometries adopted by 1D networks.

2-D networks

Two-dimensional networks are generated when the iteration process of a recognition pattern between tectons is translated into two directions of space. 2-D networks consist of complementary tectons or self-complementary tectons offering at least three divergent recognitions sites forming recognition patterns translated in two directions in space. 2-D networks are represented as sheets or planes of different geometries such as planar[17], sine wave[18], or zigzag[19] (Figure 7).

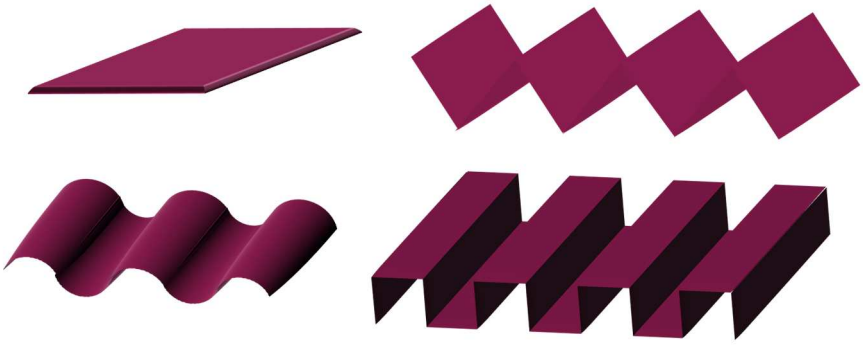

Figure 7: Schematic representation of possible 2D sheets.

Depending on the number and orientation of recognition sites, 2D networks can display different motifs. For example, three recognition sites can result in a honeycomb[20] arrangement while four recognition sites can result in a square-grid[21] or a rectangular-grid[22] arrangement depending on the orientation of the sites (Figure 8).

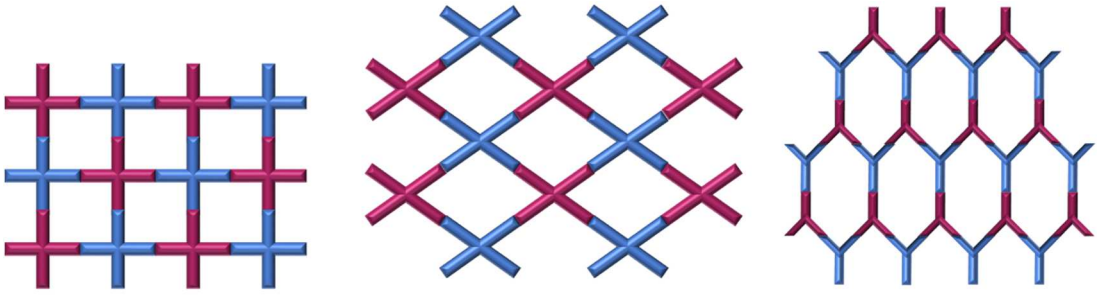

Figure 8: Schematic representation of possible 2D motifs.

3-D networks

Three-dimensional networks are more complex architectures than 1-D and 2-D networks and it is more difficult to predict the final topology of such networks. 3-D networks are generated by complementary or self-complementary tectons having at least four divergent recognition sites, which allow the formation of recognition patterns translated into three non-coplanar directions in space. The most famous 3-D networks geometries are the cubic[23] and the diamondoid[24] (Figure 9).

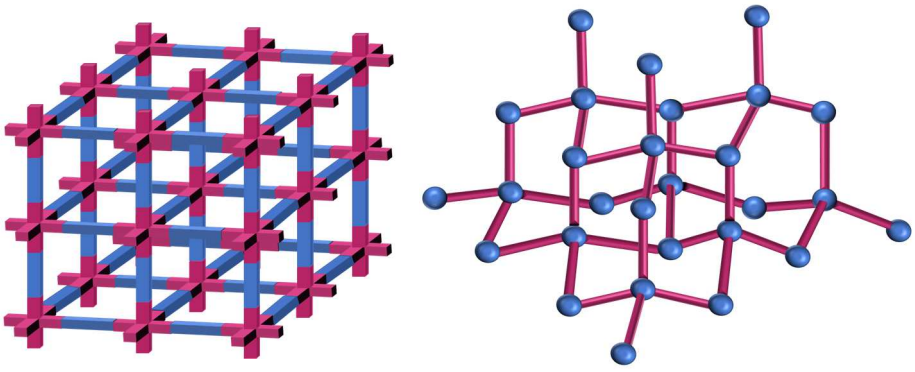

Figure 9: Schematic representation of 3D geometries.

In principle, all intermolecular interactions could be used to generate molecular networks (Figure 5). The chemical function of the sites dictates which type of intermolecular interactions would assemble the tectons. Thus, designing molecular tectons and the chemical functions of their sites provide the ability to control the type of interactions between the tectons. The most used intermolecular interactions are coordination and hydrogen bonds because of their reversibility, directionality and relatively higher strength leading to the formation of **Coordination Networks** and **Hydrogen Bonded Networks** respectively. van der Waals and π-π interactions are also widely used in molecular tectonics, but they usually act as secondary interactions.

II. 3. b) Coordination networks

Coordination networks are generated through coordination bonds between organic tectons bearing coordinating sites and metallic centers. Tectons should possess at least two divergent interaction sites able to coordinate to the metal center, which interconnects in its turn consecutive organic tectons. Coordination networks are referred to as Coordination Polymers since they are "repeating coordination entities in 1, 2 or 3 dimensions".[25] They include pure inorganic networks and hybrid organic-inorganic networks or frameworks.
The topology of coordination networks relies on the geometry of the metallic centers or complexes and the denticity and geometry of the organic tectons.

II. 3. b) 1) Metallic centers

For Coordination networks, metal centers act as bridges between organic tectons and form connecting nodes that are translated in space. The periodic table offers a variety of metals that can be used in building coordination networks. A metal cation can have all its coordination sites vacant and available to coordinate tectons or can have some of its sites vacant and others blocked by better coordinating ligands. Figure 10 shows the multiple geometries of metal centers. The choice of the metal cation is a primary factor in determining the geometry of the final assembly. Frequently used metallic centers are the d-block metals, due to their well-understood and predictable geometries and diverse properties.[26] The f-block metals are also interesting due to their high coordination

number (up to 8 or 10) and their photophysical properties.[27] Coordination networks may be based on one or more metal cations thus offering homo or heterometallic periodic architectures.

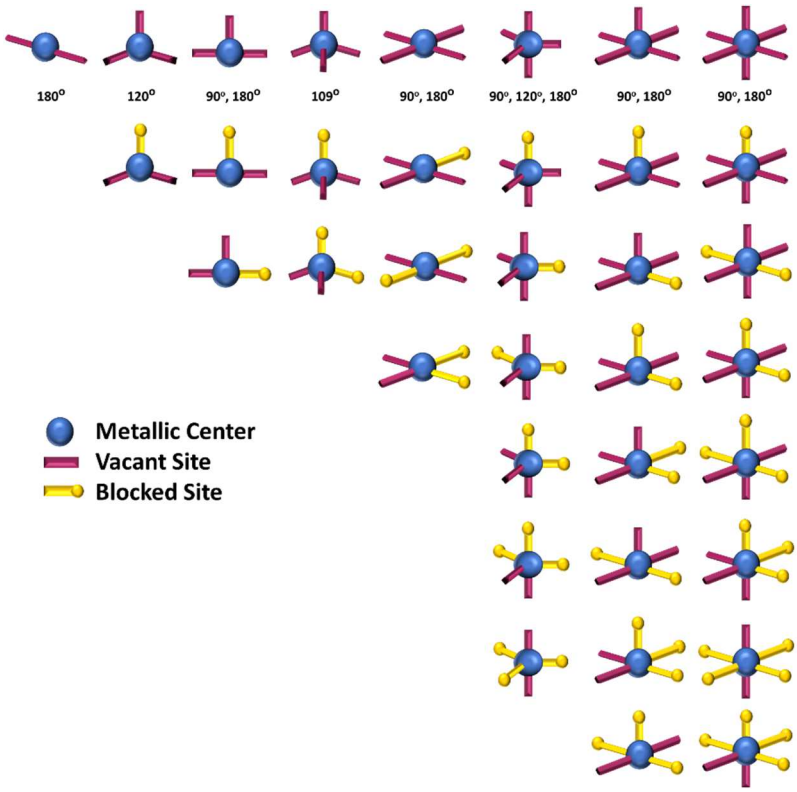

Figure 10: Schematic representations of the geometries around a metallic center.

II. 3. b) 2) Organic tectons bearing coordinating sites

Organic coordinating tectons have the ability to coordinate various metallic cations *via* their coordinating atoms, primarily oxygen and nitrogen atoms of chemical functions such as carboxylates, alcohol or amine. The number and the orientation of the coordinating sites of the tecton control the dimensionality of the final network. As mentioned previously, organic tectons should have at least two divergent coordinating sites to generate an infinite architecture. The spatial orientation of those sites can differ from one tecton to the other resulting in different coordination networks. To describe the number of the sites, the term denticity is used. Figure 11 shows the different denticity of coordinating tectons. Monodendate, bidentate, tridentate and tetradentate tectons have one, two, three and four divergent coordinating sites respectively. Tectons with convergent coordinating sites are called chelate.

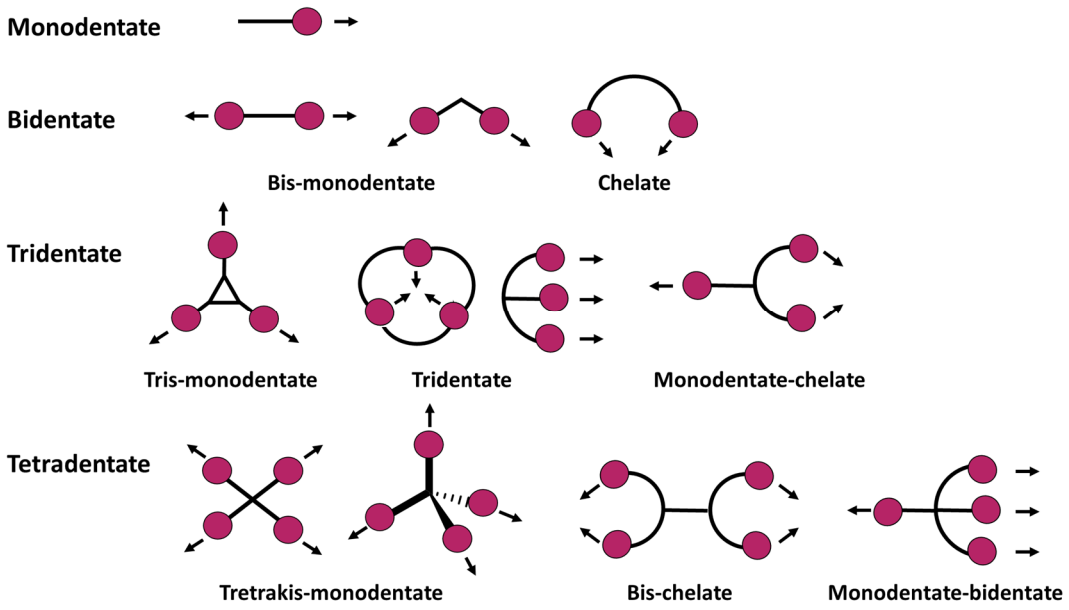

Figure 11: Schematic representations of possible denticity of organic coordinating tectons.

The huge variety of possible combinations between organic tectons and metal cations results in infinite numbers of coordination networks with various features. Among widely used organic tectons are porphyrins because of their unique electronic structure and stable macrocyclic square planar geometry.[28] Furthermore, they are perfect candidates for constructing 1D, 2D and 3D coordination networks due to their tetraaza core that has the ability to coordinate various metal cations, and their *meso* and β-pyrrolic positions that could be functionalized by peripheral coordinating substituents.

An example of a tecton based on a porphyrin is the (5,10,15,20-tetrakis(4-carboxyphenyl)porphyrin),[29] TCPP, which assembles into a 2D coordination polymer upon complexation with $Zn(NO_3).2H_2O$. The Zn^{2+} ions are incorporated into the central core of the porphyrin and result in the formation of ZnTCPP repeating units linked by paddle-wheel Zinc-dimers (Zn_2(carboxylate)$_4$) acting as a secondary building units (SBU) and leading to the formation of square grids. The Zn-TCPP-Zn flat 2D network is stabilized by the completion of the Zn^{2+} coordination sphere by water molecules, one binding the axial site of the central Zn^{2+} ion of ZnTCPP and the other two binding the two axial positions of $Zn_2(COO)_4$. The 2D sheets are stacked along the *c* axis, however no strong binding interactions are observed between the layers (Figure 12).

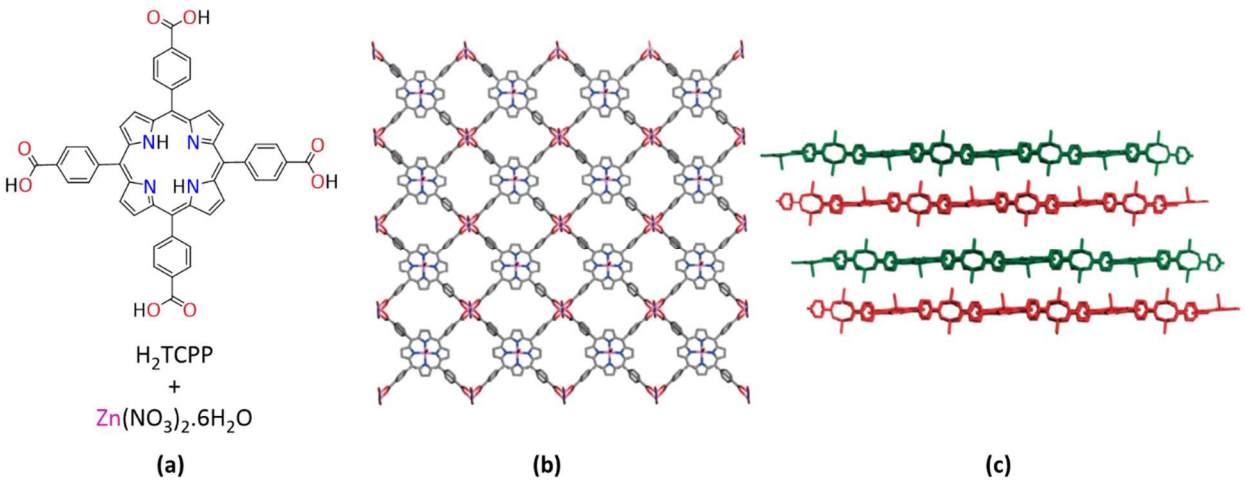

Figure 12: (a): The chemical structure of H_2TCPP (b) 2D coordination network of ZnTCPP-connected by Zn dimers. (c) Successive layers along the *c* axis. Figure taken from reference 29.

Another attractive molecular motif to build coordination polymers is the dipyrrin scaffold. Dipyrrin ligands are half porphyrin-like coordinating tectons with similar properties. They can interact with various metallic cations and they are easily substituted by peripheral coordinating sites. Therefore, they are suitable tecton to build 1D, 2D and 3D coordination networks.

An example of a 1D coordination network based on dipyrrin tectons is the one obtained from bis(dipyrrinato)Zn(II) complex (Figure 13), which self-assembles into a 1D polymeric chains *via* the coordination of the Zn(II) center.[30]

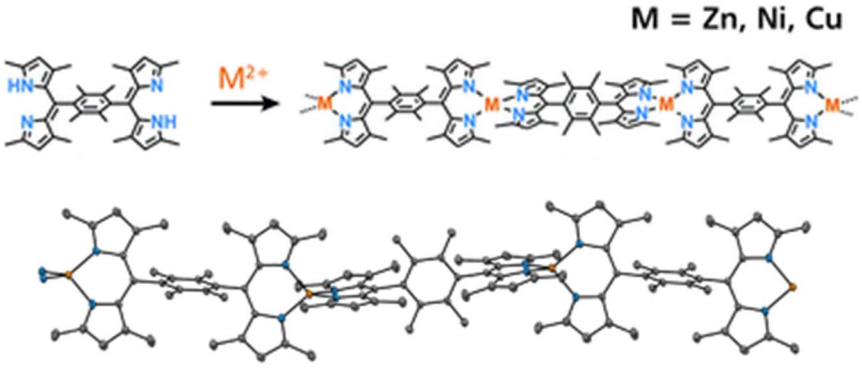

Figure 13: (Top) The formation of the 1D network based on bis(dipyrrinato)Zn(II) complex (Bottom) Crystal Structure of the 1D chain. Figure modified from reference 30.

Pyridine based tectons are often used along with their bipyridine derivatives and the terpyridine analogues. Numerous coordination networks have been generated through the coordination of pyridine based tectons to a wide range of metallic centers.

An interesting example of such networks is the 3-dimensional polymeric network described by C. S. Hawes *et al* [31] based on ligand (L): α,α-p-xylylenebis (1-(4-pyridylmethylene)-piper-4-azine). The coordinating tecton (L) is an unusual long and highly flexible divergent ligand bearing two *trans* pyridine. (L) assembles into a coordination network in the presence of cadmium nitrate and terephthalic acid (H_2TPA). The cadmium ions are coordinated by two pyridine groups of L molecules and two carboxylate groups of H_2TPA, both acting as bridges between two metal centers. Bridging through (L) and TPA linkages leads to a 3-dimensionnal distorted diamondoid topology with an 8-fold interpenetration forming a densely packed structure stabilized by various van der Waals contacts and C-H···π interactions (Figure 14).

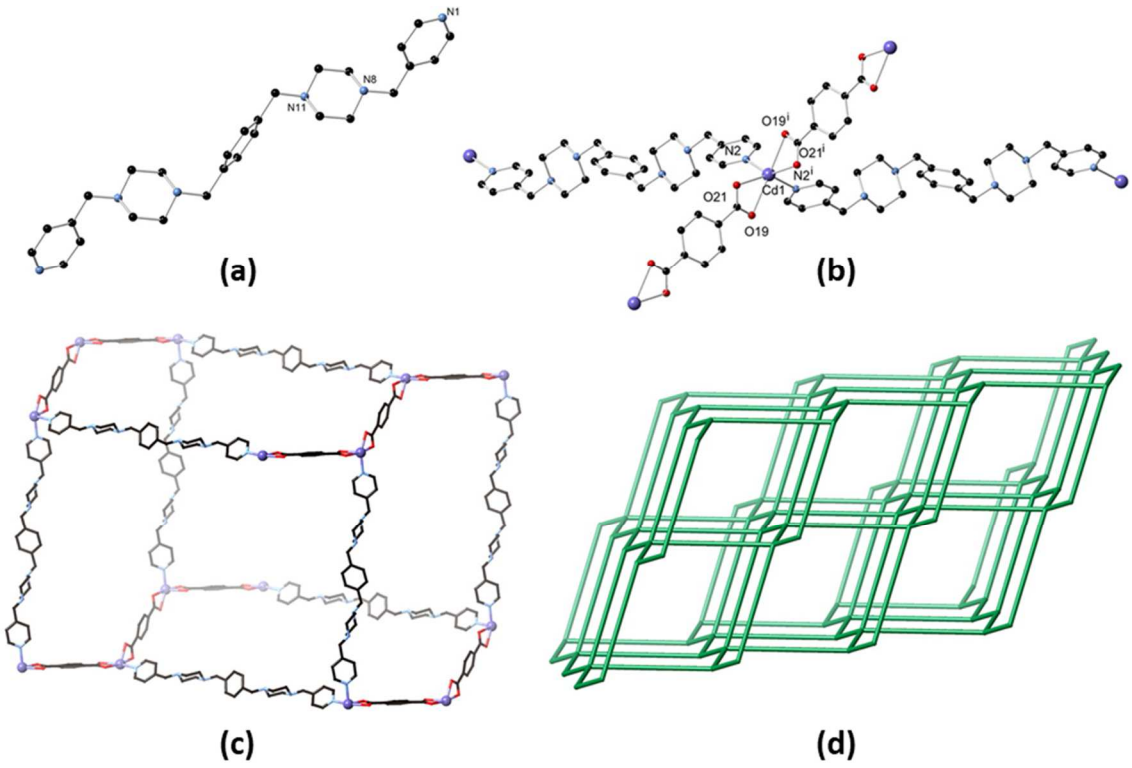

Figure 14: (a) The crystal structure of (L). (b) The coordination environment of Cd(II) ions. (c) The single adamantoid cage within extended structure of (L)-Cd (c and d) Representation of a single 3D-diamondoid network. Figure modified from reference 31.

Moreover, organic tectons can have different coordination sites. For example, tecton bearing both pyridine (**Py**) and terpyridine (**terPy**) was previously described.[32] The **Py-terPy** entity illustrated in Figure 15 is a divergent monodentate-tridentate tecton that generated a 1-D coordination polymer in the presence of $CoCl_2.6H_2O$. The Co(II) center is four-coordinated with the pyridine unit of one tecton and the terpyridine unit of another tecton forming a connecting node along the 1D chain. The directional 1D chains are positioned in a parallel manner but oriented in opposite direction, thus leading to an overall non-directional system.

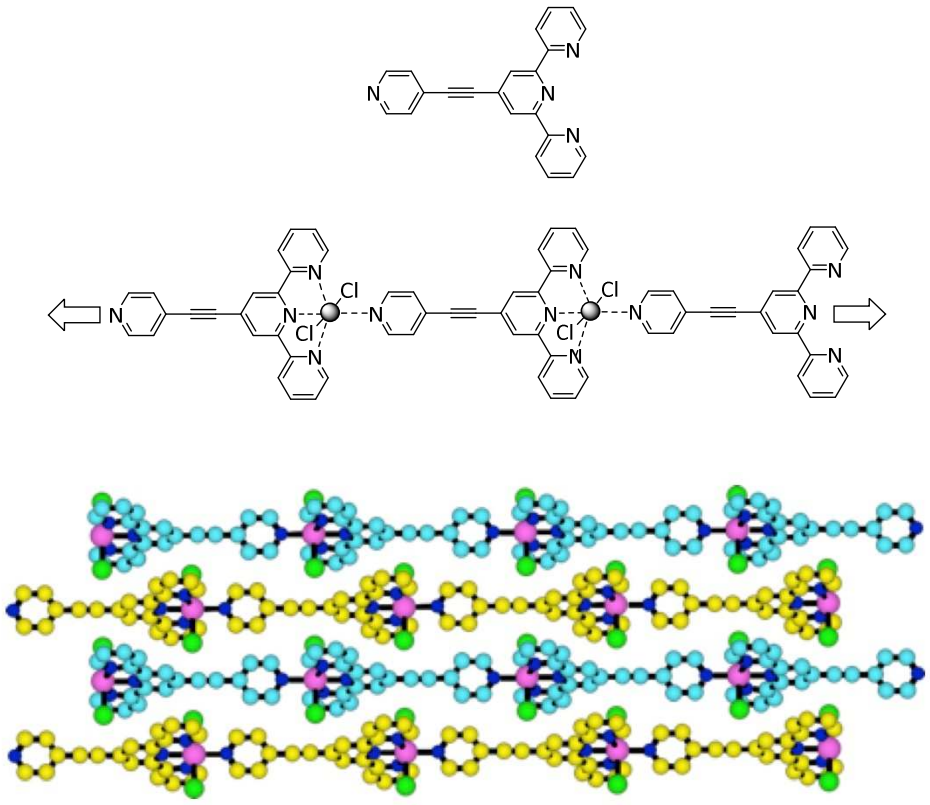

Figure 15: (Top) The chemical structure of the **Py-terPy** tecton (Center) molecular representation of the directional coordination polymer (Bottom). A portion of the X-ray crystal structure of the 1-D network.[32]

Furthermore, a more recent example published by M. W. Hosseini and P. Samori describes a Nickel (II) metalloporphyrin based tecton bearing pyridine and terpyridine coordination sites.[33] Periodic arrays of monometallic and heterobimetallic coordination polymers were generated on a highly oriented pyrolytic graphite surface (HOPG). A monometallic 1-dimensional Co(II) coordination network is formed though coordination of Co(II) by **Py** and **terPy** sites of adjacent

porphyrin tectons. Similarly, a heterobimetallic 1-D network is obtained starting from the Ni(II) metalloporphyrin in the presence of external Co(II). Figure 16 shows a schematic representation of the homometallic and heterobimetallic porphyrins and the 1-D directional coordination networks (Figure 16). The formation of directional networks with syn-packing were observed by STM.[33]

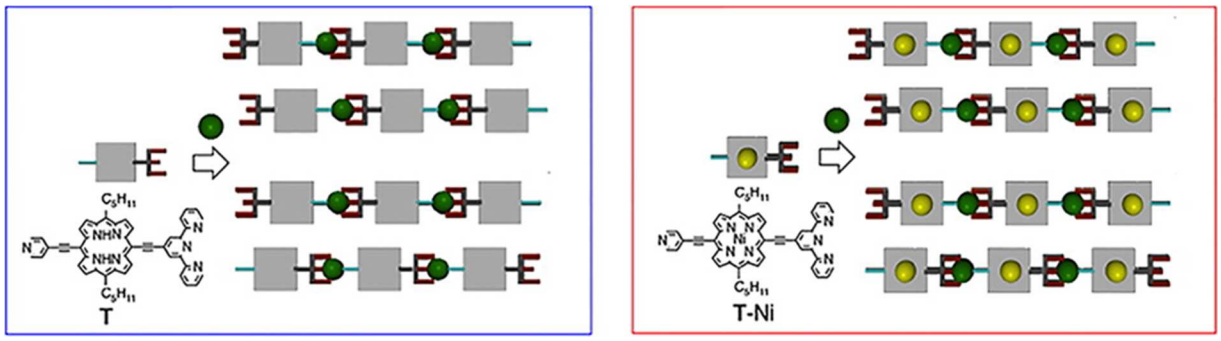

Figure 16: The schematic representations of the homometallic (Left) and heterobimetallic (Right) Ni(II) porphyrin based tectons, and the 1-D directional Co(II) coordination networks in *syn*-orientation (top) and *anti*-orientation (Bottom). Figure modified from reference 33.

II. 3. b) 3) Metal-Organic Frameworks (MOFs)

The most famous hybrid organic-inorganic network is the Metal-Organic Frameworks or MOFs.[34] They are crystalline materials assembled *via* coordination bonds between multidentate organic tectons and transition metal cations. Their structures are characterized by an open framework that can be porous, therefore they are also referred to as porous coordination polymers (PCPs). In some cases, the MOFs are stable after eliminating the solvent and could host guest molecules making them interesting for gas storage, gas adsorption and separation, catalysis, sensing application and others. MOFs became a subject of interest for chemists after the work of R. Robson in 1989 and 1990.[35] One of the first examples is MOF-5, which is based on 1,4-benzenedicarboxylate (BDC) as an organic coordinating tecton and Zn (II) as a metal center.[36] The structure of MOF-5 is a simple cubic six-coordinated net build of Zn_4O-tetrahedra that are capped on each edge with a carboxylate group resulting in a $Zn_4(O)(BDC)_3$ clusters, which represent the vertices of the cube (Figure 17). These clusters are linked by 1,4-benzenedicraboxylate units acting as the edges of the cube and forming a 3-D intersecting channel system.

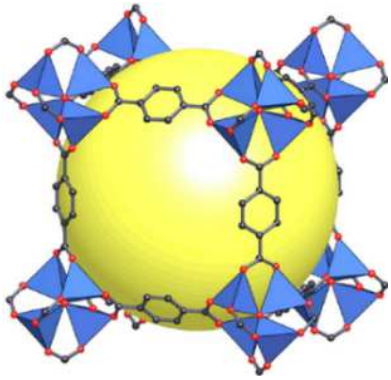

Figure 17: Representation of one cavity of MOF-5 as a yellow ball.[36]

After MOF-5, numerous monometallic MOFs with stable pores were described and applied in different fields. Furthermore, heterometallic MOFs became the center of attraction and assembling metallatecton into M^1M^2OF dominated the literature. An example of a heterometallic MOF is the Cu (II)-Cd(II) imidazole-appended dipyrrin MOF reported by our group.[37] This M^1M^2OF was built in two steps. Step one was the formation of the metallatecton by coordination of an imidazole-appended dipyrrin ligand with Cu(II) forming a bisdipyrrin complex with two imidazole coordinating sites. Step two was to combine this Cu(II) complex with Cd(II) which lead to a 2D grid-type MOF offering 1D porous channels upon parallel stacking (Figure 18).

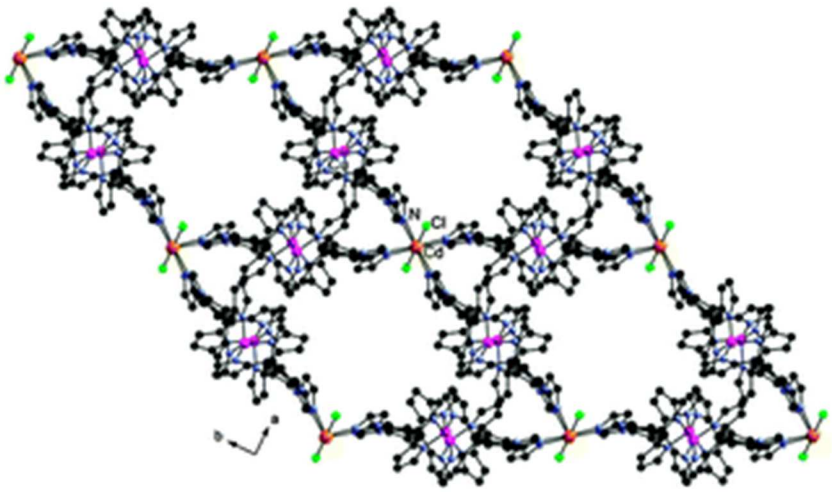

Figure 18: The X-Ray structure of the 1D channels. Figure modified from reference 37.

A metal organic framework based on tectons bearing different coordination sites than the examples above is the La-PhBTTc MOF, recently described by S. Kitagawa.[38] The La-PhBTTc MOF is

assembled by coordination of 1,4-phenylene-benzen-1,3,5-tris(2-thiophene-5-carboxylate) ligand (PhBTTc) to La(III) metallic cation resulting in 1D hexagonal channels with the lewis acid sites aligned within the channel, making this MOF a good Lewis Acid catalyst (Figure 19).

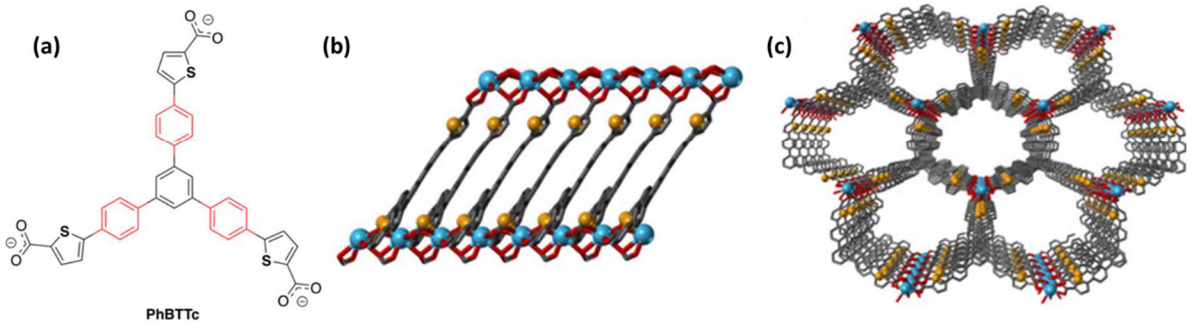

Figure 19: (a) The molecular structure of PhBTTc. (b) La-PhBTTc X-Ray structure viewed along the *b* axis. (c) The framework structure of La-PhBTTc. Figure modified from reference 38.

Coordination sites based on pyrrolic and pyridyl rings are perfect candidates to build coordination networks, due to their stable structures and affinity to various metal centers. Therefore, the work of this thesis focuses on these coordination sites. Our aim is to synthesize a library of new tectons and assemble them into H-bonded coordination networks using porphyrin, dipyrrins, pyridines and terpyridines as coordination sites. A more detailed explanation of their properties will be discussed in their respective chapters. (Figure 20)

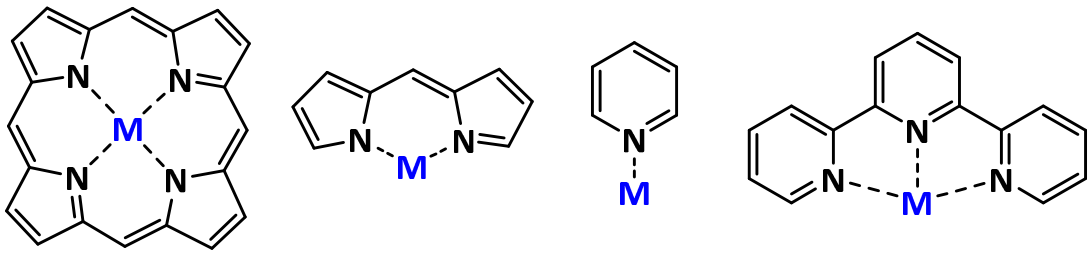

Figure 20: A general representation of the coordination sites of the coming chapters: porphyrin, dipyrrins. pyridine, terpyridine (From left to right).

II. 3. c) Hydrogen bonded networks

Nature uses non-covalent interactions to maintain well-defined 3-D biological macromolecules such as DNA, RNA, and proteins. Their discrete structures and biological functions are based on hydrogen bonds between their building blocks (nucleobase H-bonds for DNA and RNA, and peptide bonds for proteins) (Figure 21). Inspired by nature, chemists and engineers designed molecules bearing functional sites based on electronegative and labile hydrogen atoms behaving as proton donors (D-H), or based on electropositive atoms behaving as proton attractors (A). Moreover, supramolecular chemists used these molecules to generate patterns and networks aiming to imitate the naturally occurring hydrogen bonds in order to explore, understand and decode H-bonding architectures. Hydrogen bonds showed several advantages over other non-covalent interactions such as, directionality and reversibility, and being synthetically accessible and responsive to external stimuli (temperature, pH, solvent, concentration etc.) making them the center of attraction of recent studies. [39, 40]

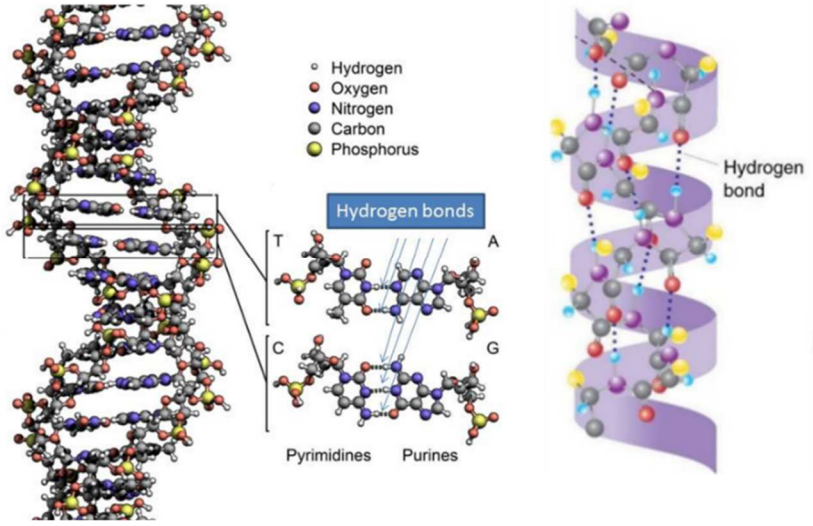

Figure 21: (Left) The DNA helix structure assembled *via* H-bonds between nucleobases, (Right) the secondary α-helix bonded by H-bonds between amide functions.

To form infinite H-bonded structures, tectons should have two or more divergent sites. Self-complementary tectons bearing both proton donor sites (D-H) and proton attractor sites (A) can self-assemble into homopolymers *via* hydrogen bonds of the self-complementary sites. Moreover, heteropolymers are generated through the assembly of two, three or more building blocks bearing

complementary recognition sites leading to di-block, tri-block or multi-block hydrogen bonded polymers respectively.[39] More complex 2D and 3D networks are generated by self-complementary or complementary tectons bearing three or more recognition sites generating patterns oriented in two and three directions in space. Such structures are usually further stabilized by weak interactions such as, van der Waal, π-π stacking and electrostatic interactions.

II. 3. c) 1) Hydrogen bonding patterns

Hydrogen bonded networks are composed of tectons with sterically accessible hydrogen bonding moieties where the hydrogen bond interactions are perturbed minimally by competing steric or ionic interactions. Different functional groups show clear preferences for specific hydrogen bond interactions forming defined patterns throughout the network. Numerous patterns could be obtained leading either to finite assemblies or to infinite networks. Some examples are shown in the figure below.[41]

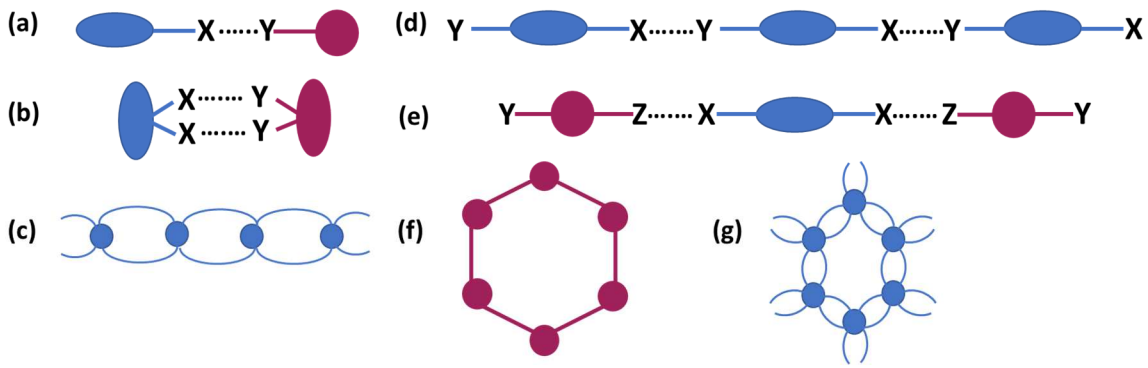

Figure 22: Examples of H-bonded patterns leading to finite assemblies (a, b and f) or infinite networks (c, d , e, g).[41]

Tectons with one hydrogen bond donor or/and acceptor sites can form dimers *via* 1 H-Bond, with an average energy of 12.3 kJ/mol, as in example (a) of Figure 22. Moreover, tectons can assemble *via* 2 H-bonds forming a ring geometry as in Figure 22 (b).[41] The energy of the interaction of two tectons can vary from 4 to 63 kJ/mol according to the number of hydrogen bonds that take place between the two recognition sites. As the number of the H-bonds increases, the interaction is enhanced leading to more stable arrangements. In the above representations (Figure 22), single or

double H-bonds are considered, but triple, quadruple and even sextuple hydrogen bonds can be formed between two partners.

Examples of Figure 22 (a) and (b) result in discrete structures since the recognition sites are oriented in a convergent manner. However, the location of the recognition sites in divergent positions could lead to infinite structures (Figure 22 (c), (d) and (e)). In Figure 22 (d), the tecton is self-complementary bearing a proton donor and a proton acceptor thus it self-assembles *via* H-bonds between its complementary sites. In example (e), two tectons form a network where one bears (X = DH) proton donor sites and the other has attractor sites (Y & Z = A1 & A2). In this case, the H-bond formed is selective and occurs only between the best proton donor and the best donor acceptor (Z or A1). Many other patterns are found in the literature for example, the cyclic pattern (Figure 22 (f)) and the hexagonal pattern (Figure 22 (g)).[41]

In addition to the number of H-bonding sites, the alternation of donor (D) and acceptor (A) groups also affect the strength and stability of the bond. Studies showed that AAD-DDA systems in DNA are significantly more stable than ADA-DAD systems, because of additional secondary electrostatic attractive forces present between the opposite partially charged sites of the AAD-DDA motif [42] (Figure 23). Moreover, AAA-DDD hydrogen bonding motifs, formed by a tecton with only proton attractor sites and a tecton with only proton donor sites, exhibits a very high association constant, due to the three cumulative electrostatic attractive forces between the AAA-DDD sites. Therefore, by avoiding alternation of donor and acceptor groups the stability of the H-bonds can increase.[39,43]

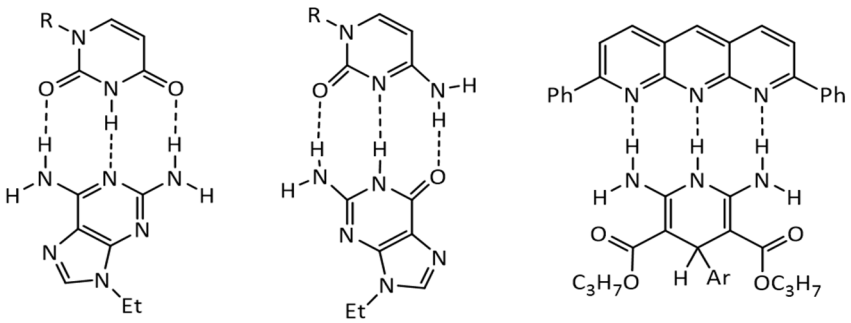

Figure 23: H-bonding pairs with three hydrogen bonds.[39]

II. 3. c) 2) Examples of hydrogen bonded networks

Numerous examples of hydrogen bonded 1-D chain networks or polymers assembled *via* hydrogen bonds are known in the literature. For example, Hawker and Meijer[44] groups reported a supramolecular chain-end-functionalized polymers containing multiple hydrogen-bonding groups (ADD or DAA), which can assemble *via* triple hydrogen bonds. They synthesized a poly(benzylmethacrylate) polymer functionalized at its end chain with 2-ureido-4[1*H*]-pyrimidinone (UPy) leading to a ADD tecton, and a poly(butyl acrylate) polymer, functionalized by a diamido-1,8-naphthyridine (NaPy) moiety, giving the complementary DAA tecton. The UPy-NaPy triple hydrogen bonding resulted in the formation of supramolecular diblock polymers *via* 3 H-bonds (Figure 24).

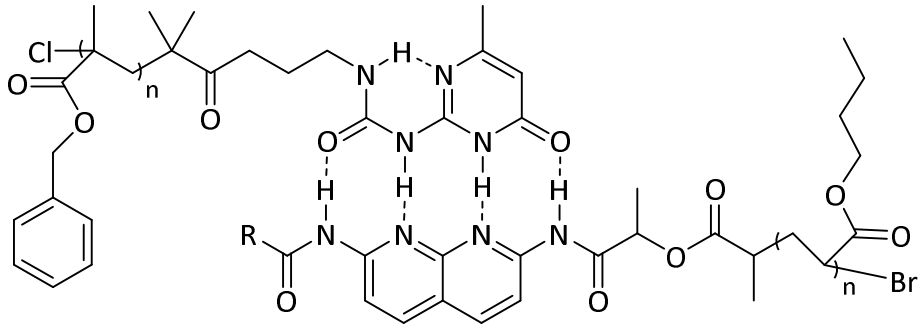

Figure 24: Supramolecular polymer assembled via UPy-Napy quadruple H-bonds. Figure modified from reference 44.

As mentioned previously, supramolecular chemists were interested in designing helix systems to imitate DNA's 3D helical structure, aiming to explore and understand the patterns found in such a complex network. An example of a helix structure was designed by the group of M. W. Hosseini.[45] This network is assembled through the H-bond of two tectons: a calix[4]arene based tecton bearing four pyridine proton acceptor sites and 4,4'-diphenol molecule which possesses two H-bond donors oriented in a divergent way. The two tectons form a single stranded helical structure by mutual bridging *via* the H bonds between the pyridine sites and the OH sites. The repeating unit of the helix, which extends along the *z*-axis, is composed of 4 calixarene tectons, 4 diphenol tectons and 4 $MeNO_2$ solvent molecules. Two pyridine sites located in *trans* positions of the calix backbone are hydrogen bonded to the OH groups of the diphenol tectons, and the other two

remaining pyridine sites participate in H-bonding with solvent $MeNO_2$ molecules resulting in a single stranded helical network (Figure 25).

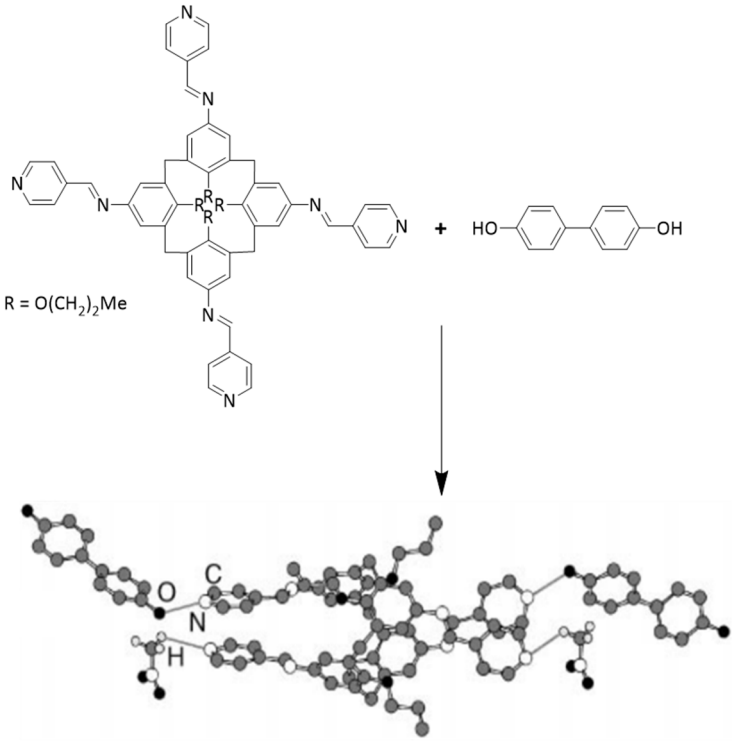

Figure 25: The X-ray structure of a portion of the hydrogen bonded network formed *via* the H-bonds between the 4,4'-biphenol and the two *trans* pyridines sites of the calix[4]arene based tecton. The other pyridine *trans* pair are H-bonded to $MeNO_2$ solvent molecules. Figure taken from the reference 45.

Interestingly, the 1-D helical strands are associated to each other in a helical fashion leading to quintuple helical braids, due to van der Waals and edge-to-edge interactions between the pyridine rings and phenyl groups (Figure 26). Finally, the quintuple helices associate laterally into compacted solids as shown in the figure below.

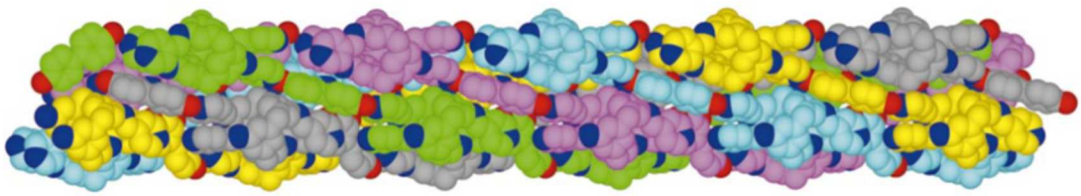

Figure 26: X-ray structure showing the formation of quintuple helical arrangement comprised of five right handed helical strands represented in different colors. Figure taken form reference 49.

In addition to helixes, H-bonded networks can have different geometries such as cyclic hexagonal structures. For example, Figure 27 shows a hexagonally closed packed 2-D hydrogen bonded network composed of a macrocyclic tecton bearing 6 phenolic groups.[46] The self-assembly of the macrocycle *via* 6 H-bonds between the exterior OH groups results in a one-dimensional arrangement forming single layered motifs. The structure is stacked with each layer consisting of sheets of macrocycles H-bonded to one another forming a 2-D close packed structure. The stacking mode of the network is further stabilized by van der Waals and electrostatic interactions between aromatic rings in adjacent layers (Figure 27).

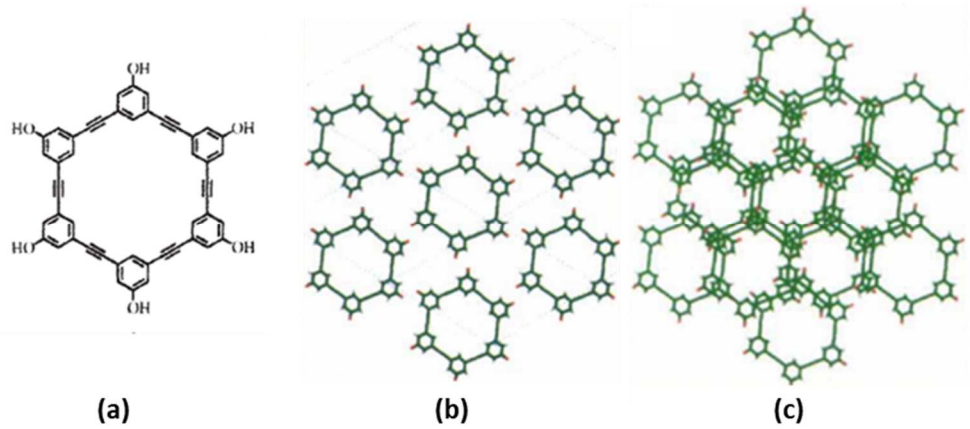

Figure 27: (a) The molecular structure of the macrocycle bearing OH groups (b) The X-Ray structure of single layer motif (c) X-Ray structure of the packing of three layers. Figure modified from reference 46.

Another recent example is based on catechol moieties.[47] The H-bonded network is obtained by the self-assembly of an adamantane-based bis catechol tecton (Figure 28).

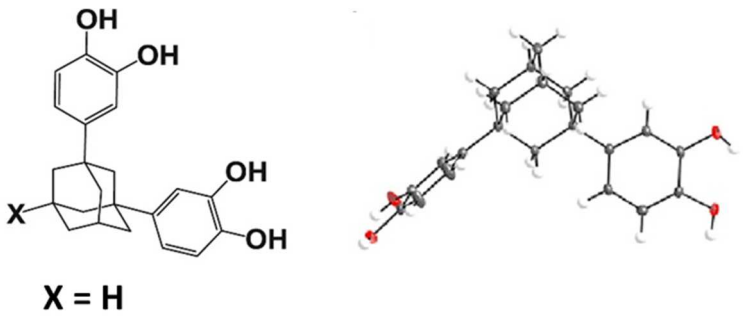

Figure 28: Molecular structure of adamantane-based catechol tecton. Picture modified from reference 47.

In the presence of ethyl acetate, the tecton crystallizes into cyclic frameworks forming channels in the crystalline lattice filled with solvent molecules (Figure 29). The cyclic structures are constructed from two adamantane-catechol molecules linked by H-bonds between the OH groups. Each cyclic structure is bonded to the adjacent one through H-bonds between the hydroxyl groups of catechol moieties forming a 1D structure. The 1D polymers are directed into layers resulting in channels filled with ethyl acetate. The layers are stacked *via* CH-π interactions between the catechol rings and the adamantane parts.

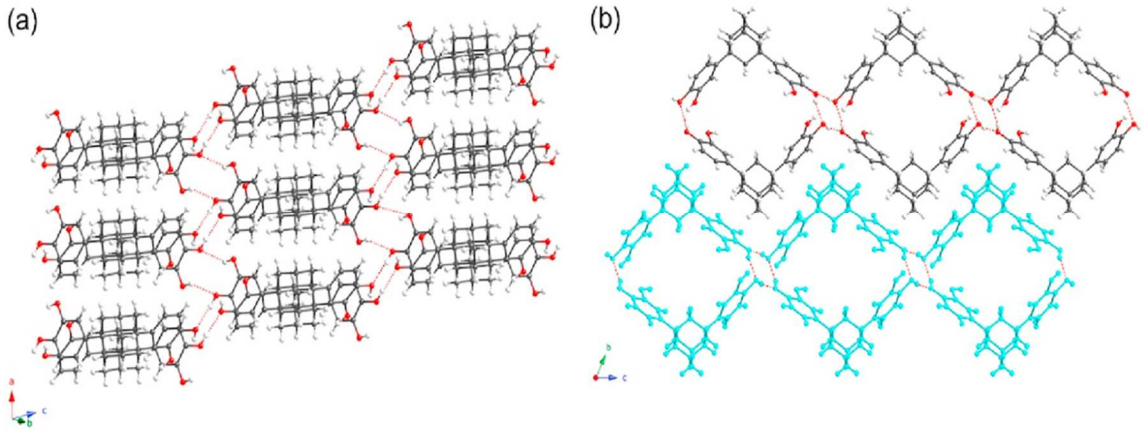

Figure 29: (a) side and (b) top views of the H-bonded structure. Figure modified from reference 47.

As in the example above, H-bonded tectons can assemble into networks forming porous channels that are filled with solvent molecules. In some cases, removing the solvent molecules result in the collapse of the structure. Recently however, hydrogen bonded frameworks (HOFs) with permanent porosity have been described and explored for their different applications.

II. 3. c) 3) Hydrogen bonded Organic Frameworks (HOFs)

Hydrogen bonded organic frameworks (HOFs) are self-assembled through hydrogen bonding interactions between pure organic building blocks. Compared to MOFs, they are more fragile and difficult to stabilize because of their weaker interactions. Although, HOFs were proposed as potential porous materials about two decades ago, no example of frameworks with permanent porosity were described until recently. The H-bonding within HOFs resulted in a weak structurally

porous framework that usually collapsed upon removal of the solvent guest molecules after thermal and vacuum activation.[48] However, HOFs are easily synthesized, purified, characterized and regenerated by simple recrystallization. Therefore, they attracted attention as potential porous materials for several applications especially gas storage, gas separation and molecular recognition.[49] The first HOF reported with high selectivity for C_2H_2/C_2H_4 separation is the HOF-1.[48]

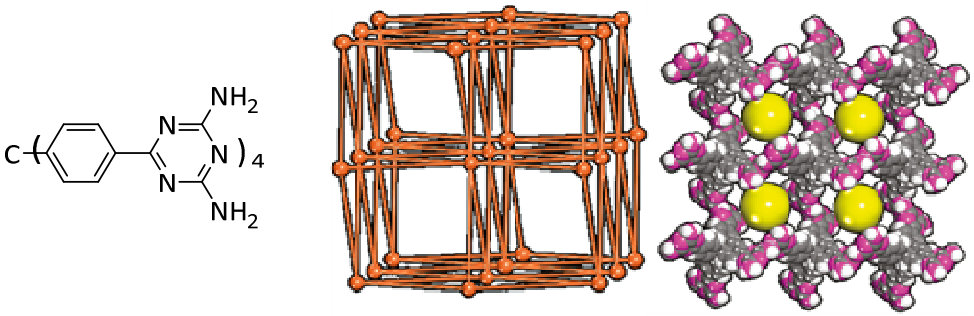

Figure 30: (Left) The DAT organic building block, (Center) the 3-D body centered cubic network, (Right) and the 1-D channels along the *c* axis represented by the yellow balls. Figure modified from reference 48.

HOF-1 is a three-dimensional porous network assembled through H-bonds between the organic tecton bearing four 2,4-diaminotriazine (DAT) groups (Figure 30). Each tecton is connected to four neighboring ones by eight strong hydrogen bonds resulting in 8-connected nodes that form a three-dimensional body-centered cubic network with one-dimensional porous channel along the *c* axis. The framework is further stabilized by multiple aromatic π-π interactions among the organic building blocks. One of the amine groups within the 2,4-diaminotriazine moieties is not involved in the hydrogen bonding, and thus is exposed on the pore surfaces for potential interactions with gas molecules. The permanent porosity of HOF-1, activated under high vacuum at room temperature and then at 100 °C, was evaluated by CO_2 gas adsorption, which proved the macro-porous characteristic of this framework. In addition, the C_2H_2/C_2H_4 gas separation capacity of HOF-1 was examined. The studies showed that HOF-1 takes up a much larger amount of C_2H_2 than C_2H_4, indicating that it is a very promising microporous material for the C_2H_2/C_2H_4 separation at an ambient temperature. At 273 K, HOF-1 can absorb acetylene up to 63.2 $cm^3.g^{-1}$ (STP), which corresponds to 2.1 mol of C_2H_2 absorbed per mole of HOF-1. On the other hand, HOF-1 can adsorb only 8.3 $cm^3.g^{-1}$ (STP) of C_2H_4. The C_2H_2/C_2H_4 molar ratio separation selectivity of HOF-1 is

equivalent to 7.6, which is higher than average values of previously reported MOFs. The collaborative size exclusive effect confined by the small narrow pores and the preferential stronger interactions of C_2H_2 with the basic amine groups of the host framework enable HOF-1 to act as an extraordinarily highly selective microporous material for the C_2H_2/C_2H_4 separation at ambient temperature.

A more recent hydrogen-organic-framework is the HOF-7[50], which is assembled from 2,4-diaminotriazinyl (DAT) of a functionalized ZnTDPP porphyrin compound (5,10,15,20-tetrakis(4-(2,4-diaminotriazinyl)phenyl)porphyrinato zinc). ZnTDPP molecules self-assembled through H-bonds involving their 4 DTA moieties generating two-dimensional supramolecular layers. The layers are further packed into a 3D framework *via* π–π interactions between the ZnTDPP molecules, thus generating a microporous structure (Figure 31). The permanent porosity and gas separation properties of the desolvated HOF-7 were examined. The studies proved the microporous nature of HOF-7 and demonstrated its CO_2 gas adsorption ability along with moderately selectivity for CO_2/N_2 separation.

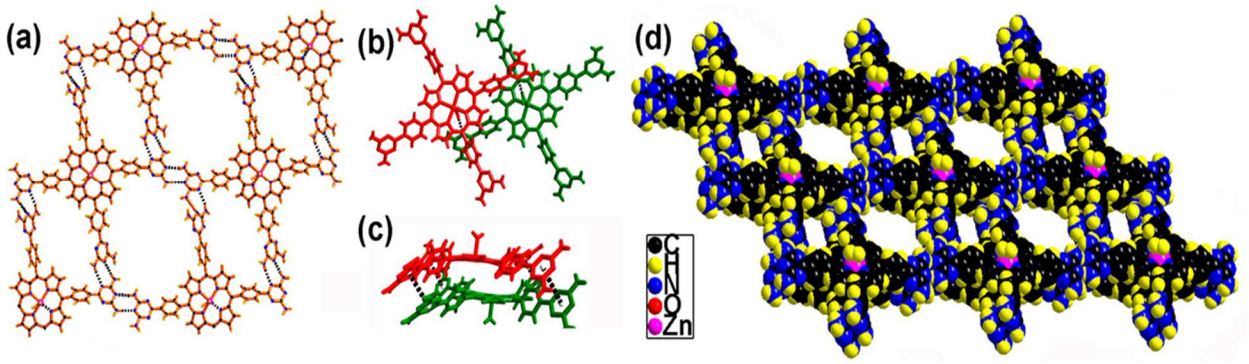

Figure 31: (a and b) The X-Ray structure of HOF-7 showing the H-bonds interactions, (c) Intermolecular π-π interaction in HOF-7, (d) 3D packing framework of HOF-7 along the *a* axis. Figure modified from reference 50.

When it comes to hydrogen bonding interactions, predicting and controlling the final topology of the network can be a challenge, due to their high reversibility and flexibility. Nature has provided nucleobases (NBs) as hydrogen bonding moieties, which are stable, reliable and predictable. Our goal is to build molecular networks assembled by coordination and hydrogen bonding interactions.

Therefore, we chose to focus on nucleobases as H-bonding motifs and to introduce them at the periphery of ligands such as porphyrins, dipyrrins, pyridines and terpyridines.

III. Nucleobase

Nucleobases (NBs) are heterocyclic nitrogenous bases found in the repeating units of DNA (deoxyribonucleic acid) and RNA (ribonucleic acid), which are referred to as nucleotides. The latter consist of three molecules: sugar, heterocycle and phosphate. The sugar, ribose or deoxyribose, is in a cyclic furanoside form and is connected by β-glycosyl linkage to the nucleobases to produce the four normal nucleosides: adenosine, guanosine, cytidine, thymidine in DNA and uridine in RNA.[51] The pairing of DNA complementary strands is due to the unique molecular recognition of the natural nucleobases *via* Watson-Crick hydrogen bonding interactions.[52] In addition, the formation of the duplex DNA structure is a result of intermolecular forces including π-π stacking, van der Waals interactions, and hydrophobic effects.[53] (Figure 32)

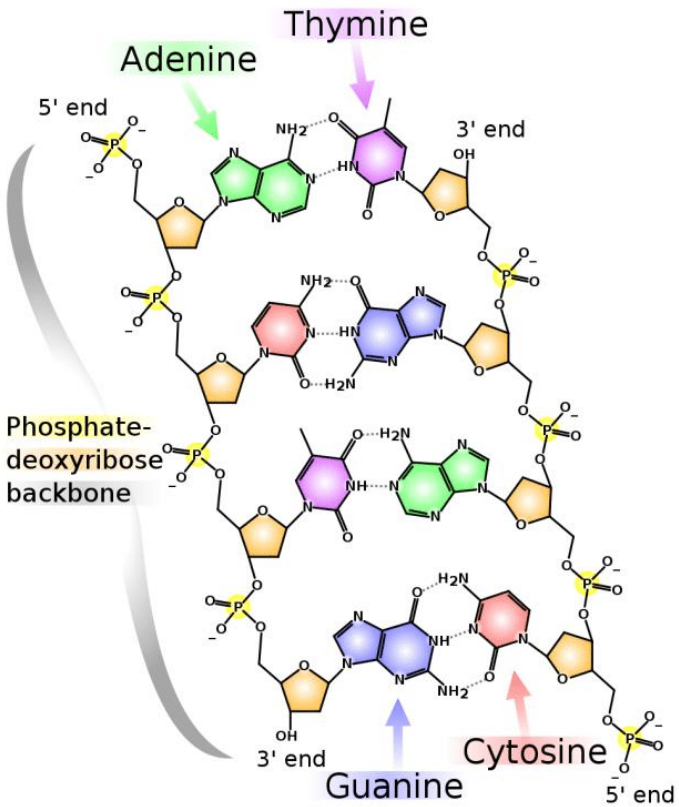

Figure 32: The chemical structure of DNA.

The five natural nucleobases are divided into two groups: the monocyclic pyrimidines and the dicyclic purines. The pyrimidines consist of Thymine (**T**) in DNA, Uracil (**U**) in RNA, and Cytosine (**C**). Moreover, the purines consist of Adenine (**A**) and Guanine (**G**) (Figure 33).

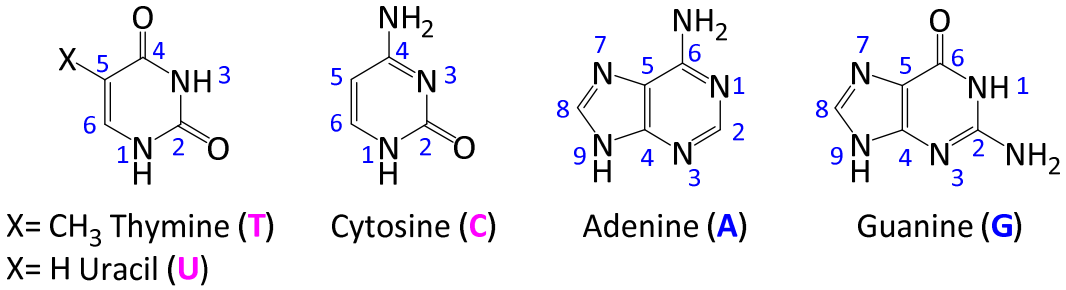

Figure 33: DNA nucleobases

DNA base pairing takes place between complementary pyrimidines and purines through 2 or 3 hydrogen bonds (Figure 34). Adenine is complementary to Thymine or Uracil (X = CH_3 for T, X = H for U) *via* two hydrogen bonds forming the **A**-**T** or **A**-**U** pairs (K_a *ca.* 10^2 M^{-1}).[54] Guanine is complementary to Cytosine *via* three hydrogen bonds forming the **G**-**C** pair (K_a *ca.* 10^5 M^{-1}).[55]

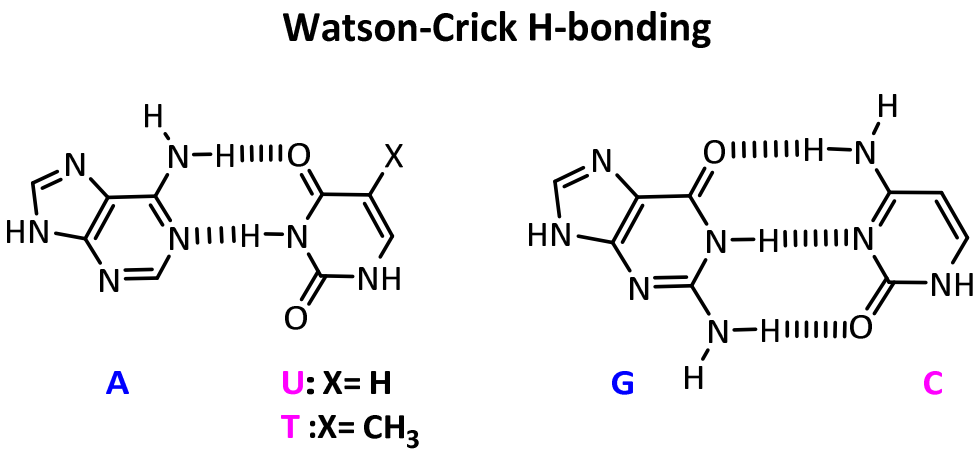

Figure 34: **A**-**T** and **G**-**C** Watson-Crick Hydrogen pairing.

III. 1. pKa values of nucleobases

The protonation and deprotonation of nucleobases occur within a 3.5 pH shift from neutrality (from 3.5 to 10.5). At a pH 10.5, the deprotonation occurs at the N1 position of pyrimidines (**T** and **C**) and at N9 of purines (**A** and **G**). A higher alkaline media will deprotonate the N3 and N1 of thymine and guanine respectively. At slightly acidic (pH *ca.* 4-5), protonation of N1 of adenine and N3 of cytosine is observed. More acidic conditions (pH<2) will protonate N7 of guanine and adenine. At sufficiently lower pH, adenine is doubly protonated at N1 and N7 positions and thymine is protonated at O4.[57] pKa values of these protonation and deprotonation are represented in Figure 35.[56]

In all of the mentioned cases, ring nitrogen atoms are protonated rather than the amino nitrogen atoms (N6 of A, N4 of C, and N2 of G). This is in agreement with calculated charge densities. The electrostatic isopotential curves calculated for the approach of a proton or a nucleophilic agent demonstrate that the attack is primary at the ring nitrogen atoms and at the keto oxygen atoms, and not at the amino groups.[57]

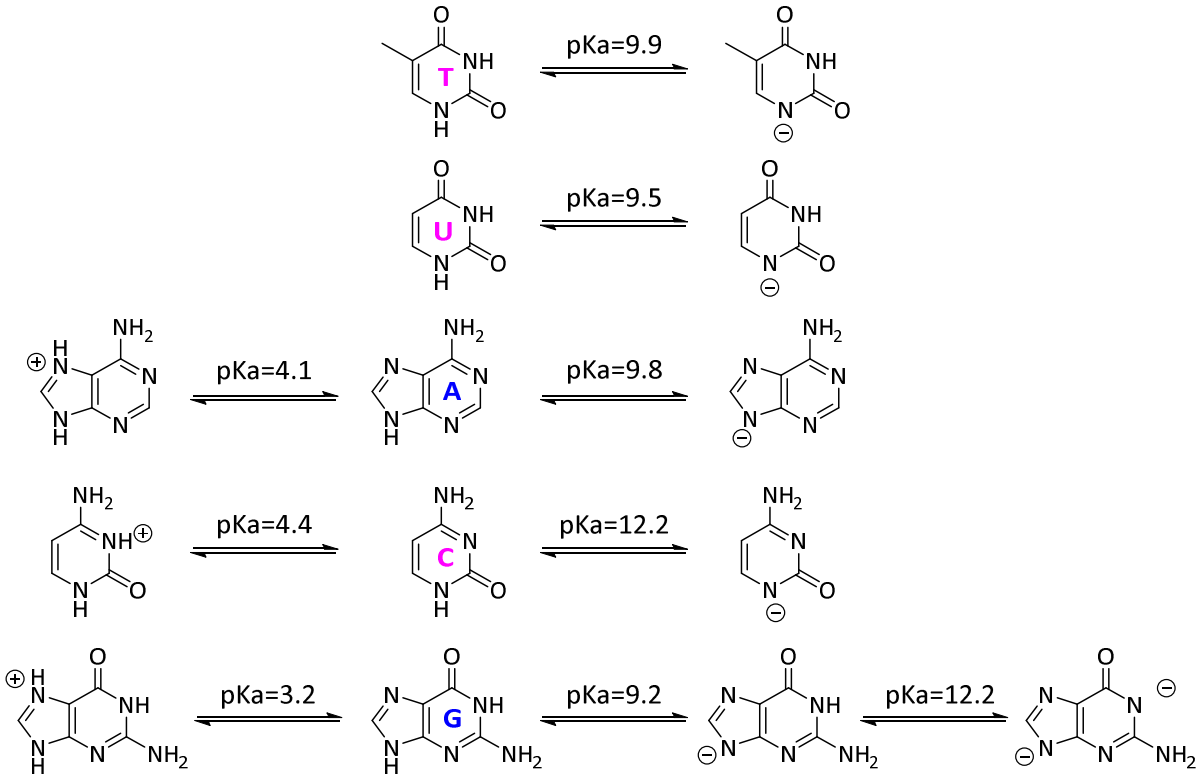

Figure 35: pKa values of nucleobases.[56]

III. 2. Tautomerism of nucleobases

In solution, heterocyclic molecules tend to yield a mixture of species (tautomers) in equilibrium (Figure 36).[52, 58] Tautomerism depends on the pKa of the respective heteroatoms and on the nature of the solvent.

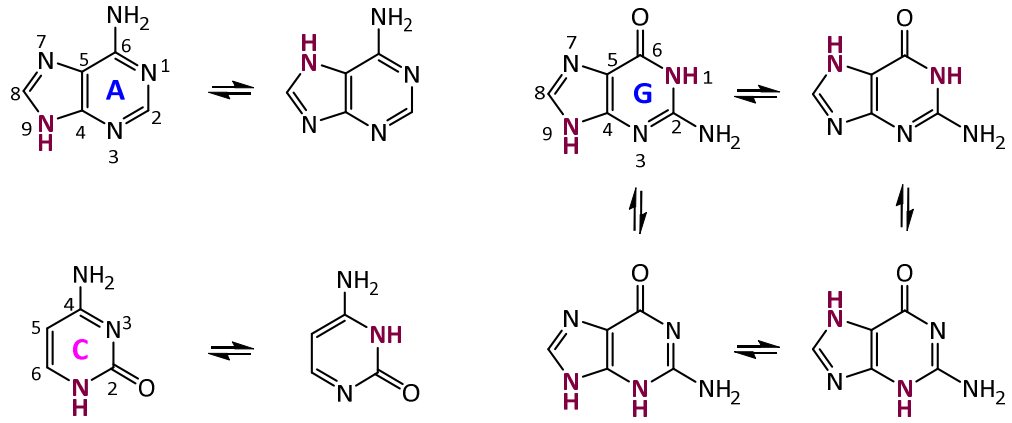

Figure 36: Prototropic tautomerism in unsubstituted adenine (**A**), cytosine (**C**), and guanine (**G**).

These tautomeric processes in NBs change the positions of proton atoms, thus leading to new hydrogen bonding patterns. For example, a keto group with acceptor properties is transformed into a donor enol group. Similarly, a donating amino group becomes an imino group with accepting properties.

The enol tautomeric forms of uracil or guanine have the same binding patterns than cytosine and adenine in their normal amino form respectively. Moreover, the imino form of cytosine or adenine can substitute the uracil and guanine respectively (Figure 37). Thus, tautomerism could be disastrous for base pairing and the self-replicating systems in DNA and RNA. Several studies (UV, IR, NMR, X-Ray) were conducted to study the possible tautomers and their stability. They concluded that for adenine and thymine (or uracil) the naturally occurring bases (amino and keto form) are dominant, with less than a 0.01 % for all other tautomers. For guanine and cytosine, less than 15 % of tautomeric forms are present in nature, where the keto and amino form dominates the base-paring motifs. In general, NBs in their major tautomeric form are found in DNA and RNA, and this is controlled by the different factors (sugar moieties, phosphate groups, medium in the

cell….) therefore the NBs are always suitable for their biological tasks except in the case of mutation.[51,52,58]

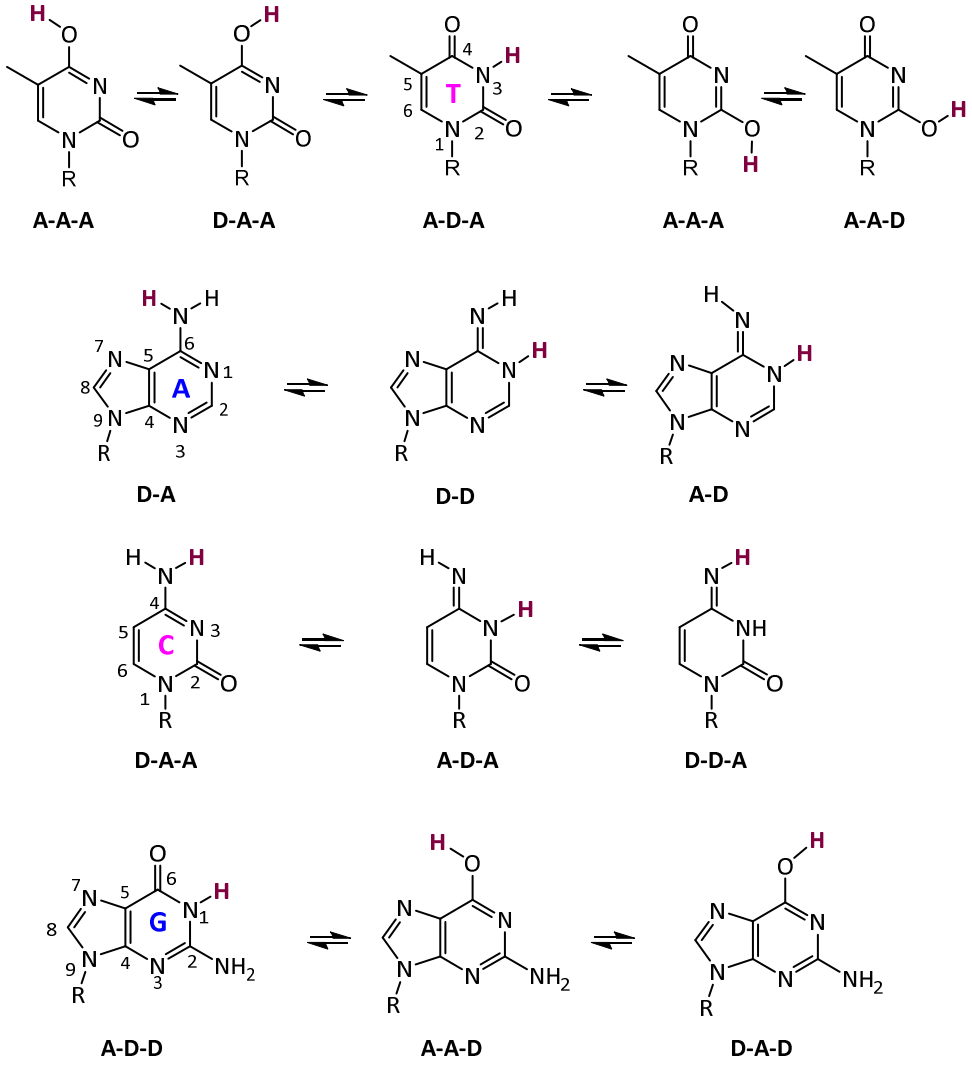

Figure 37: Keto-enol and amino-imino tautomerism in NBs. Note that uracil have the same tautomers as thymine. Donor sites are denoted as D and Acceptor sites as A. enol G (DA) = A (DA), enol T (DAA) = C (DAA), imino A (AD)= T (AD) or G (AD), imino C (ADD) = T (ADD)

III. 3. Nucleobase interactions

Complementary nucleobases interact with each other through Watson-Crick hydrogen bonding resulting in the most stable and dominate **G**-**C** and **A**-**T** pairs (*E* (**G**-**C**) = -70.25 kJ/mol, *E* (**A**-**T**) = -29.29 kJ/mol).[51] However, many alternative pairing patterns are possible.[51,54,55,58] For instance, the Hoogsteen[59] interactions between adenine and thymine is another mode of bonding that occurs

on the opposite site of the purine nucleobases (E(**A**-**T**)$_{Hoogsteen}$ = -27.6 kJ/mol). Along with Hoogsteen interactions, other non-traditional base pairs are present in DNA, RNA and protein-DNA interactions. They include the reverse Watson-Crick H-bonding (E(**A**-**T**)$_{Reverse\ W.C}$ = -29.2 kJ/mol), reverse Hoogsteen H-bonding (E (**A**-**T**) $_{Reverse\ Hoogsteen}$ = -28.6 kJ/mol), Wobble or the mismatch form (E(**G**-**A**)$_{Wooble}$ = -39.3 kJ/mol, E(**G**-**T**)$_{Wooble}$ = -32.5 Kcal/mol).[51] The reverse modes are defined by a *trans* or *cis* conformation of the two sugar moieties or any substituent 'R' on N_1 of pyrimidines and N_9 of purines (Figure 38).

Nucleobase interactions can be divided into two groups: homo pairing and hetero pairing. Examples of the hetero pairing are the interactions discussed previously. In addition to hetero pairing, homo pairing is also possible, since each NB heterocycle possesses an alternation of proton donor and proton acceptors sites, making them self-complementary. There are multiple potential homo pairs of nucleobases, for example 15 possible pairs for guanine, 11 for cytosine, 21 for adenine and 10 for thymine or uracil.[60] Not all of these homo pairing lead to stable dimers. The most stable homo pairing are represented in Figure 38 with interaction energy of -67.1 kJ/mol for **G**-**G**, -44.9 kJ/mol for **C**-**C**, -23.4 kJ/mol for **A**-**A** and -22.7 kJ/mol for **T**-**T**.[51]

After several studies (DFT calculations, UV, IR, NMR, X-Ray…), potential base pairs were narrowed down to the most stable 28 base-pairing motifs. These 28 pairs are formed *via* at least two hydrogen bonds and include homo and hetero pairing of pyrimidines and purines assembled into symmetrical and non-symmetrical motifs.[60] The most stable pairing is Watson-Crick **G**-**C** base pairing followed by the self-assembly of guanine **G**-**G** and **C**-**C**. The Watson-Crick **A-T** base paring is less stable than the **G-C** however it is more favorable than the self-assembly of **A-A** and **T-T**. The order of base pair interactions from the most stable base pair to the least stable is as follows: **G**-**C**> **G**-**G**> **C**-**C**> **A**-**T**> **A**-**A**> **T**-**T**.[51-55, 60]

Furthermore, purines A and G can form larger aggregates due to the presence of two binding sites. Besides being able to form 1:1 complexes through either of their two faces, A and G can form 2:1 aggregates with an appropriate partner, for instance the T–A–T and the G–G–C triplets. Such complexes are involved in the formation of triple DNA helix.[61] Moreover, there exists a unique pairing formed between C^+–G–C base-triplet. The N_3 of the cytosine needs to be protonated to allow the donation of a hydrogen bond to N_7 of guanine (Figure 38).

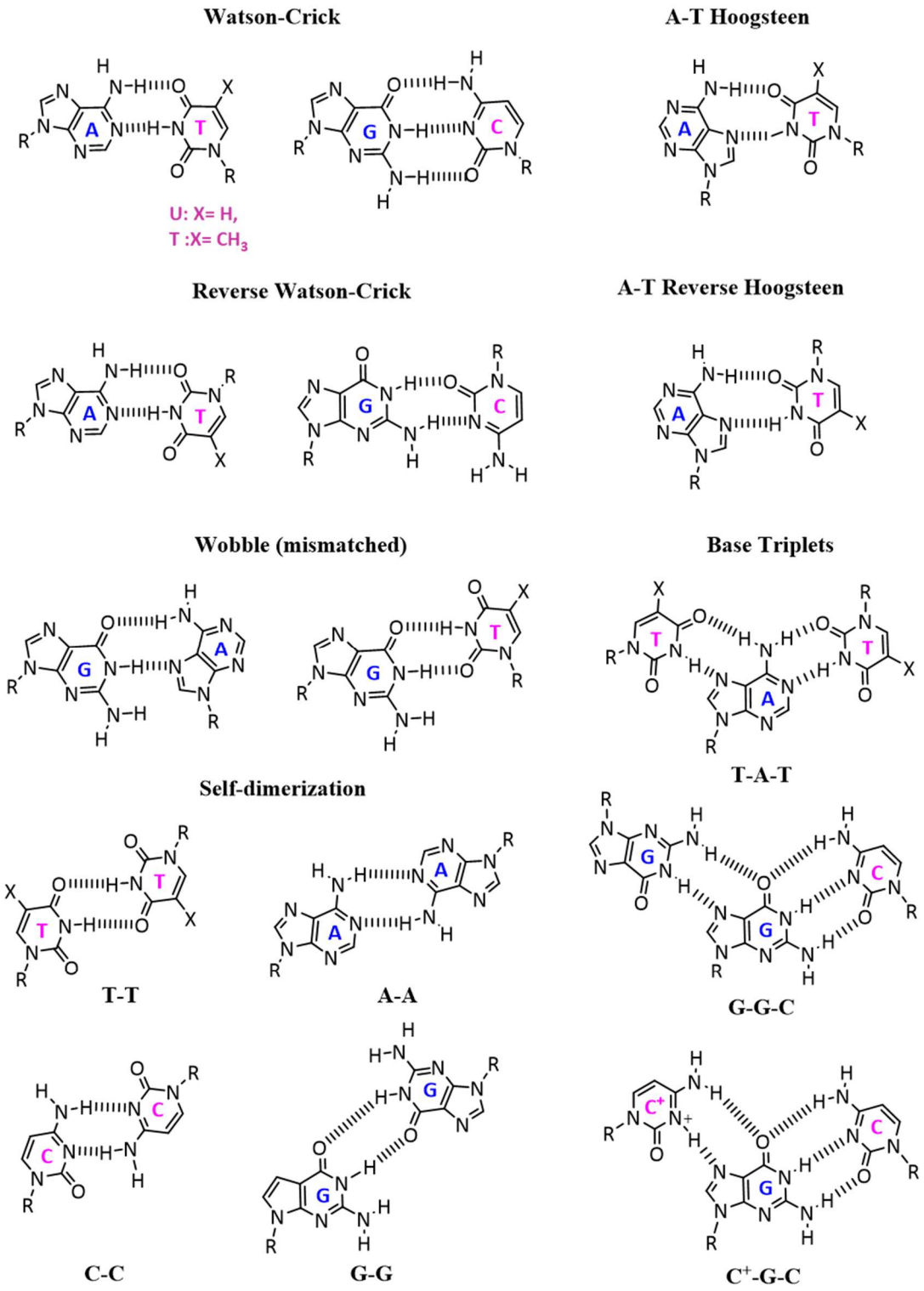

Figure 38: Watson-Crick base-pairing, as well as Reverse Watson-Crick, A-T Hoogsteen and Reverse Hoogsteen, G-A and G-T Wobble (mismatch) paring, example of homo pairing, and T-A-T, G-G-C, and C^+-G-C Base Triplets (Hoogsteen and Watson-Crick).

In protic solvent, nucleobases pairing is decreased, due to competition with the solvent. They tend to stack in columns rather than self-assemble through H-bonding.[62] Moreover, because of their aromatic structure, NB can self-assemble *via* π-π interactions. In addition, the presence of accessible coordinating sites in NBs, such as nitrogen and oxygen lone pairs, provide them the ability to bind to several metal cations (Figure 39).[51,52,63]

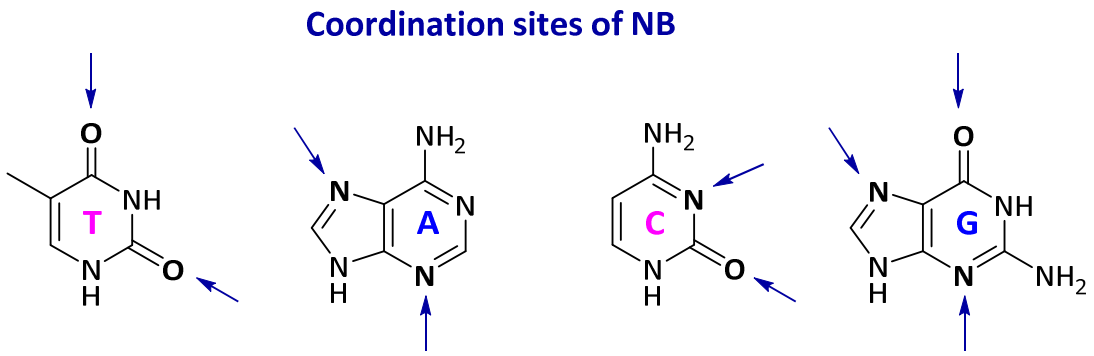

Figure 39: Schematic representation of the coordination sites of the nucleobases.[63]

III. 4. Nucleobases self-assemblies

The four nucleobases possess several interaction sites oriented in a divergent manner, which open the possibility to self-assemble into different one, two or three-dimensional architectures. Therefore, numerous solid-state crystallographic and scanning tunneling microscope (STM) studies have been performed to explore the self-assembly of nucleobases from the most stable and complex guanine architectures to the weakest thymine assemblies.[63,64]

III. 4. a) Guanine

All nucleobases have the ability to self-assemble into dimers. However, guanine homooligomers are the most interesting. Guanine possesses two complementary arrays, a donor/donor site at positions N(1)–H and N(2)–H_2 and an acceptor/acceptor site at positions O6 and N7. The aromatic surface of guanine and the complementarity of its sites, allow it to self-assemble *via* strong hydrogen bonds (K_{GG} *ca.* 10^2-10^4 M^{-1} in $CDCl_3$) into a variety of supramolecular architectures. Depending on the experimental conditions, guanine can self-assemble into linear tapes (ribbons) or macrocycles (G-quartets) (Figure 40).[63-65]

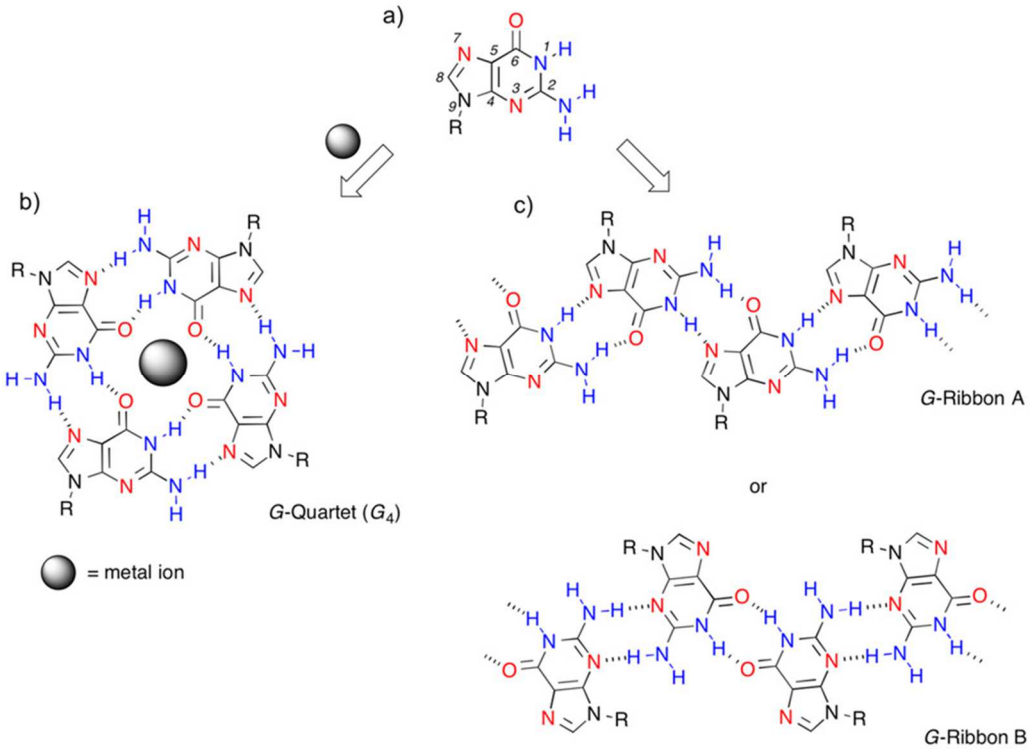

Figure 40: Different guanine architectures. Figure taken from reference 64.

In the presence of a metal cation such as K^+, Na^+, Cs^+ or Ba^{2+}, guanine molecules can form G-quartet (**G**4) based architectures such as octamers or columnar polymeric aggregates. These architecture are stabilized by metals cations and by cyclic H-bonds formed between N(2)–H···N(7) and N(1)–H···O(6) of neighboring guanine molecules. In the absence of metal templating center, guanine can self-assemble *via* H-bonds into ribbon-like structures in the solid state and in solution. Two ribbon structures with different H-bond patterns can be formed. Ribbon-A is assembled though cyclic N(2)–H···O(6) and N(1)–H···N(7) H-bonds. G-ribbon A is thermodynamically more stable in the solid state but in solution it slowly undergoes a structural transition toward a more thermodynamically stable G-ribbon B, which is characterized by N(1)–H···O(6) and N(2)–H···N(3) intermolecular cyclic H-bonds (Figure 40).[65]

In addition to G-quartets and ribbon architectures, other assemblies were studied by scanning tunneling microscopy (STM) upon the deposition of guanine molecules on inert surfaces. Single-molecular-scale STM images revealed that guanines can form ordered one- and/or two-dimensional unique structures. For example, a 1 D guanine based chain was reported on Cu (111)

substrate at a low-temperature (*ca.* 80 K).[66] This assembly is composed of guanine molecules linked to each other by two H-bonds on their Watson-Crick sites and two H-bonds on their Hoogsteen sites.[60] Moreover, guanine molecules were deposited onto an inert Au (111)[67] substrate at room temperature, which resulted in a heterochiral phase corresponding to two enantiomerically pure homochiral **G**4 based 2D networks (R and L) (Figure 41). Within the **G**4 based architecture, the molecules interact *via* two H-bonds: N(2)–H···N(7) and N(1)–H···O(6). The presence of N(9)–H and N(3) sites at the exterior of the quartets made it possible to form a third binding motif. N(9)–H···N(7) H-bonds take place between the quartets, thus resulting in a 2D network.[64]

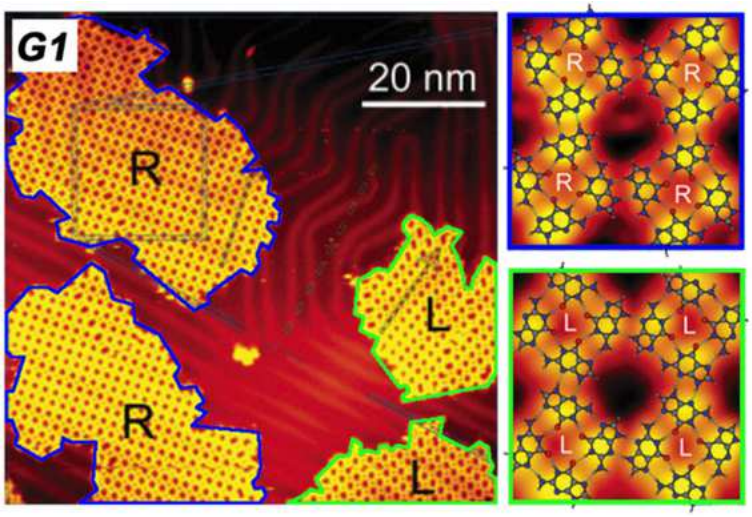

Figure 41: STM image containing mirror phases of enantiomerically pure R (right-handed) and L (left-handed) **G4** - based 2D network self-assembled on Au(111) surfaces under UHV. Figure modified from reference 64.

III. 4. b) Cytosine

Cytosine possesses a unique chemical structure with two proton donors (D) and two proton acceptors (A), which can result in a D-A-A-D recognition pattern. Similar to guanine studies, the cytosine self-assembly was studied by scanning tunneling microscopy (STM) upon deposition on inert surfaces. Early studies demonstrated that cytosine self-assembles into a one-dimensional chain when deposited on Cu (111) surface. Neighboring cytosine molecules in *trans* conformation made it possible for the two D-A sites to fall in a suitable arrangement, thus extending into a 1 D chain through 2 H-bonds between each cytosine ring.[60,66]

Moreover, recent studies showed that cytosine can self-assemble into glass like structures with ribbon-like or hexameric macrocyclic geometries. Among various patterns are two ribbon assemblies that take place *via* two H-bonds: N(4)–H···O(2) and N(1)–H···N(3) or N(4)–H···N(3) and N(1)–H···O(2). In addition, the hexameric macrocyclic arrangement assembles *via* 3 H-bonds N(4)–H···O(2), N(1)–H···N(3) and C(5)–H···N(3). The homo-pairing pattern of cytosine molecules is dependent on the nature of surface coverage. An example of the glassy state of cytosine obtained on Au(111) substrate is represented in Figure 42 (b).[64]

III. 4. c) Adenine

The self-assembly of adenine can be extremely complex. As mentioned previously, 21 possible dimers can be formed.[60] Therefore, several one-dimensional chains can be proposed, but the most stable arrangement was studied by STM upon depositing adenine on a Cu (111) surface.[60,66] The chain is formed through an alternation of Watson-Crick and Hoogsteen H-bonding between neighboring adenine molecules.

In addition to 1D chains, a 2 dimensional hexagonal adenine network was observed by STM studies on several substrate such as Cu(110)[68], graphite[69] and other[70]. Moreover, at a much lower deposition rate, a double chain adenine based structure was observed.[71] Therefore, adenine can assemble into several competing structures. Nonetheless, it has been recently shown that, when deposited on Au(111) substrate, adenine molecules form highly ordered 2-dimensional supramolecular networks stabilized by N(9)–H···N(3), N(6)–H···N(7) and N(6)–H···N(1) hydrogen bonds (Figure 42 (c)). [72]

III. 4. d) Thymine and Uracil

Thymine and uracil share similar bonding sites as all the other nucleobases. However, early STM studies showed that they randomly aggregate into small clusters upon depositing them on inert surfaces. [66] Moreover, one of the few reported assemblies of thymine deposited on Au(111) surface is a 1 D filament stabilized by two different pairing motifs A and B.[68] Motif A assembles *via* three H bonds N(3)–H···O(2), N(3)–H···O(4), and C(6)–H···O(4). Motif B assembles through two H-bonds N(3)–H···O(2) and N(1)–H···O(4).[64] In addition, the self-assembly of uracil was also studied by STM on several surfaces. Uracil molecules adsorbed on Ag(111) formed close-packed 2D islands, which was driven by the formation of H-bonded dimers characterized by N(3)–

H···O(4) pairing. Furthermore, upon depositing uracil molecules on Cu(111), deprotonation at the N(3) site occurs, thus leading to the formation of tiara-like structures (Figure 42 (e)). [64,67]

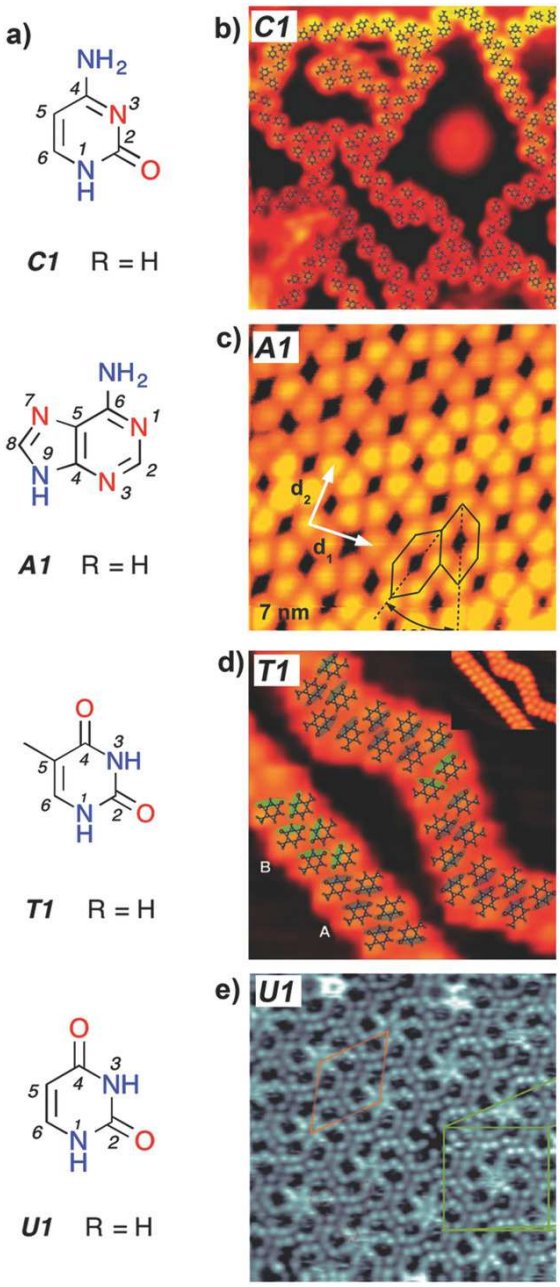

Figure 42: (a) The chemical structures of cytosine (C1), adenine (A1), thymine (T1), and uracil (U1), H-bonding donor and acceptor sites are indicated in blue and red respectively. The reference of NBs are kept as found in the publication (ref 64). b) STM image of a "glassy state" of **C1** on Au(111). c) Self-assembled architectures of **A1** molecules on Au(111). d) Ribbon-like assembly of **T1** molecules on Au(111). e) STM image of sub-monolayer coverage of **U1** on Cu(111) showing a domain of the tiara-like structure. Figure taken from reference 64.

III. 5. Supramolecular assemblies based on NB

Nucleobases are a targeted motif in supramolecular chemistry due to their multiple possibility of non-covalent interactions. Using common NBs offered the advantage of exploiting different building units (T, U, A, C, G).[62,73] However, the solubility of nucleobases in normal aprotic solvents is a limiting factor for synthetic chemistry. In addition to their low solubility, tautomerism and non Watson-Crick binding modes resulted in many complications in terms of prediction and controlling the final topology of the assemblies.[63,73]

Biological systems have overcome these problems due to the sugar and phosphate molecules linked to NBs. Inspired from nature, supramolecular chemists resolved these complications using different strategies. For example, Watson-Crick H-bonding could be favored by introducing bulky groups close or directly on certain unwanted H-bonding sites. In addition, steric hindrance with regard to the ribose unit can also pre-organize a certain type of assembly over others. Moreover, the choice of the solvent and the solute concentration can minimize the formation of non-discrete aggregates. The first two strategies lead to the synthesis of alkylated or substituted purines and pyrimidines with lipophilic tails or sugar residues functionalized with solubilizing protecting groups without changing the characteristics of the H-bonding sites of the nucleobases. Such modification resulted in interesting soluble nucleobase motifs for supramolecular chemistry.

Furthermore, extension of NB interaction sites, by introducing additional H-bonding functions on the parent nucleobase, resulted in more stable paring motifs and more complex architectures.[63,73]

Last but not least, supramolecular and synthetic chemistry based on nucleobases helped in implementing an artificially expanded genetic information system (AEGIS)[74], where the number of nucleobases increased from 4 to 12 nucleobases. AEGIS is now used in clinic to monitor the load of several viruses.[75]

Example of such NBs derivatives are presented in Figure 43. The modified NB (1) [76] is a guanine derivative than can self-assemble into a G-quartet without the presence of metal templating cations. Molecule (2) is a synthetic thymine derivative that results in the formation of gels.[77] NB (3) has an extended H-bonded function on the Hoogsteen site of guanine moieties. This synthetic modified nucleobase can bind to guanine by four H-bonds forming a stronger G-G motif.[78] Molecules (4) and (5) are example of the AEGIS nucleobase system (Figure 43).[74]

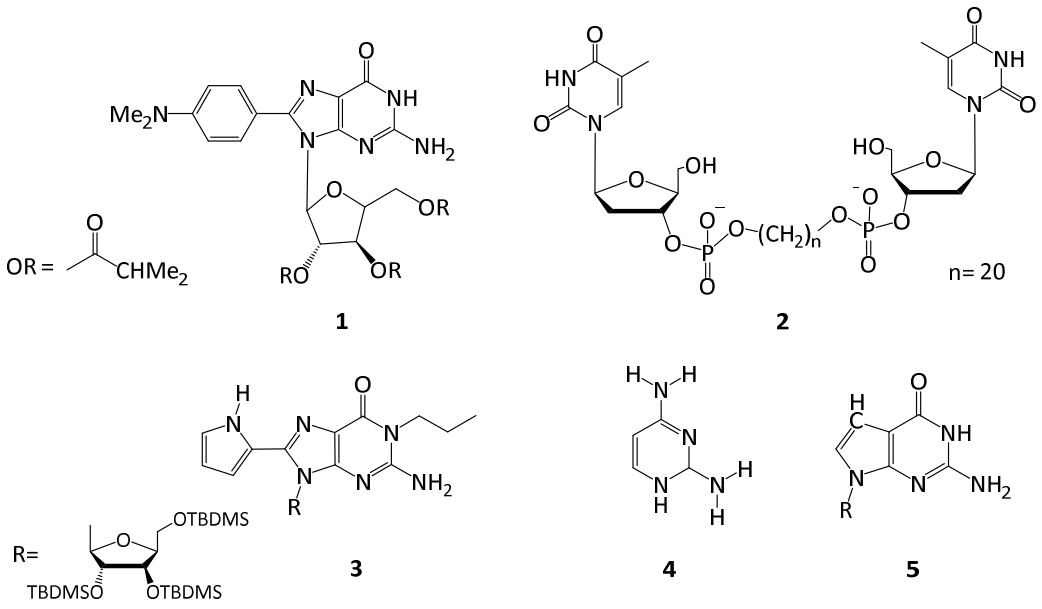

Figure 43: Examples of modified nucleobases.

III. 5. a) Nucleobase Duplex Systems

A large library of NB based dimeric systems is found in the literature. Example of such structures are the four duplex systems (I), (II), (III) and (IV) by J. L. Sessler and coworkers (Figure 44). (I) is based on the **T**-**A** complementary pair linked by a diethynyl-anthracene spacer, *via* their C9 and C5 position respectively, resulting in a discrete duplex. To enhance the solubility of the **T**-A pair, their respective N9 and N1 positions are substituted by functionalized ribose moieties. Moreover, (II) is a poly(ethylene glycol) functionalized amide linked to guanine from one end and to a complementary cytosine from the other end. The **G**-**C** pairs are linked by their N7 and N1 positions respectively, thus increasing the solubility of G and C and favoring the Watson-Crick H-bonding patterns. However, the assembly of this molecule was relatively weak due to the flexibility of the linker.[73,79] The ridged G-G structure (III) is held together by four hydrogen bonds between four modified guanine moieties. This structure is very stable and stayed in its dimeric form in all solution phase conditions (temperature, concentration).[80] Last but not least, a unique guanine based structure (V) assembles into a G4-quartet without the presence of the templating cation *via* Watson-Crick and Hoogsteen G-G interactions. In addition to these duplex systems, a molecular

box based on adenine and thymine interactions was described by Gokel and colleagues.[81] The assembly (V) is stabilized by Hoogsteen interactions and one N–H···O hydrogen bond.

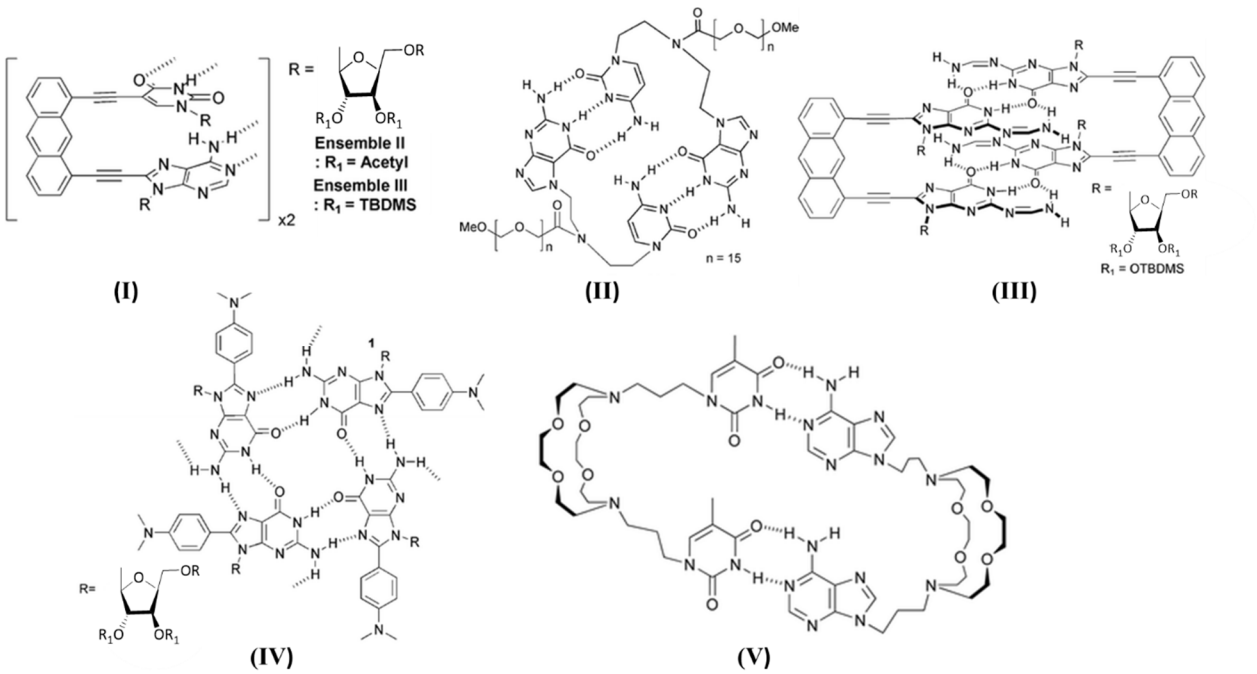

Figure 44: Structural representation of (I), (II), (III), (IV), and (V). Figure modified from reference 73.

Moreover, as mentioned previously, the presence of accessible nitrogen and oxygen lone pairs in the aromatic heterocyclic NBs structure provides the possibility to participate in different kind of interactions other than hydrogen bonds. Therefore, NBs can act as metal-binding motif in the presence of suitable metal cations, and can stack *via* π-π interactions. Loeb *et al.* [82] designed a molecular receptor that uses the diversity of nucleobase interactions. The receptor is based on a metallo-thiocyclophane molecule that binds adenine through three simultaneous interactions. The first interaction is a metal-adenine coordination bond between Pd (II) metal center and the amino function at the N(3) position. In addition, adenine interacts with the receptor by two H-bonds between its N(6) position and the ethylene glycol O atom. The structure is further stabilized by a third interaction, which is π-π stacking between the electron poor aromatic rings of the adenines and the electron rich aromatic rings of the receptor (Figure 45).

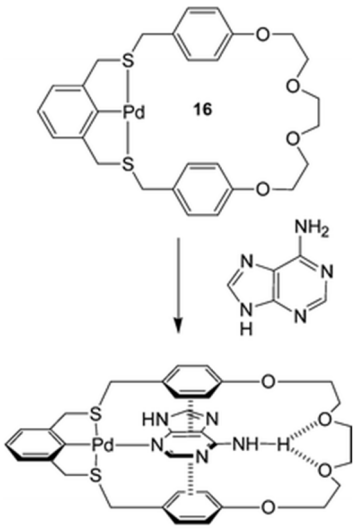

Figure 45:Thiocyclophane metallo-receptor bonded to Adenine through π-π stacking, H-bonds and coordination interactions. Figure modified from reference 63.

As mentioned previously, the diversity and the structure of nucleobase interaction sites make it an interesting building block to be used in designing polymers and supramolecular networks.

III. 5. b) Nucleobase based polymers

One of the extension of nucleobase hydrogen interactions involves the generation of supramolecular H-bonded polymers. NBs chain-end or side-chain functionalization of polymers helps the organization of polymeric assemblies into fibers, film and gels. An example of such polymeric systems is the cytosine bi-functional polymer which was obtained by attaching a functionalized cytosine to an amine terminated poly(ethyleneglycol) (Figure 46). The cytosine based polymer formed dimeric assemblies through four hydrogen bonds.[83]

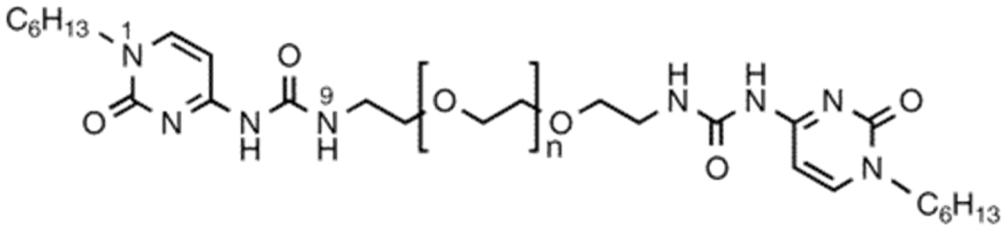

Figure 46: Cytosine based polymer. Figure modified from reference 83.

Other end chain polymers are the alkyl di-amides polymers bridging adenine and thymine molecules (Figure 47). These polymers resulted in different final arrangements. The bis-thymine polymer produced double helical ropes, while the complementary bis-adenine resulted in only microcrystalline solids. Moreover, the mixed adenine–thymine structure formed supramolecular fibers *via* Watson-Crick **T**-**A** H-bonds.[84]

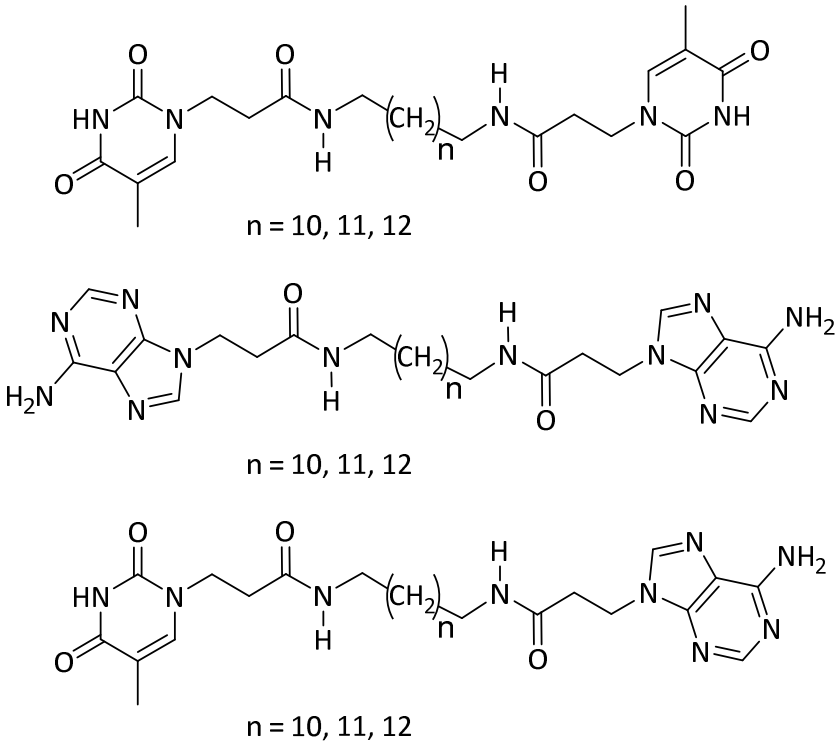

Figure 47: The thymine and adenine based di-amide polymers.[73]

In addition to H-bonded polymeric assemblies, nucleobases can generate coordination systems if joined with a metal salts. NBs can act as a chelate or as a bidentate ligands bridging metallic centers thus generating polymeric assemblies. An interesting example is the Pt(II)-cytosine polymer obtained by reacting *cis*-$[PtCl_2(NH_3)_2]$ salt and sodium cytosinate (Na^+ Cytosine$^-$) in the presence of $AgNO_3$.[85] In this polymer, the Ag^+ coordinates to the available N3 site of the cytosine, while the cis-$[Pt(NH_3)_2]_2^+$ moiety coordinates *via* the N1 position, leading to the formation of a hetero bi-metallic chain with the cytosine ligands in a head-to-tail orientation. The coordination sphere of silver ions is completed by a water molecule and intramolecular interactions with the O2 atoms of the cytosine base (Figure 48).

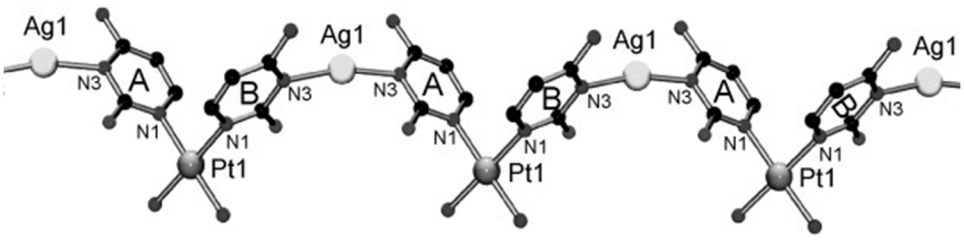

Figure 48: Cytosine-Pt-Ag polymers, the counter ions are removed for clarity. Figure taken from reference 85.

Adenine has several potential coordination sites, however the Hoogsteen sites are the most favored to coordinate to metallic cation.[86]An example of such coordination pattern is the Cd(II) polymeric chains of chelate-tethered adenine derivative (ethylenediamine-N9-ethyladenine, A-Et-en).[87] The structure of $[Cd_2Br_6(A\text{-}Et\text{-}en)_2]$ shows the metal center in two different coordination environments. The first metal center is an octahedral Cd(II) coordinated to four bridging halides and two adenines coordinated in *trans* position *via* N7. The second Cd(II) is in distorted-octahedral geometry coordinated to two of bridging halides, to one terminal halide, to the nitrogen atoms of the diamine group, and to N3 of adenine (Figure 49).

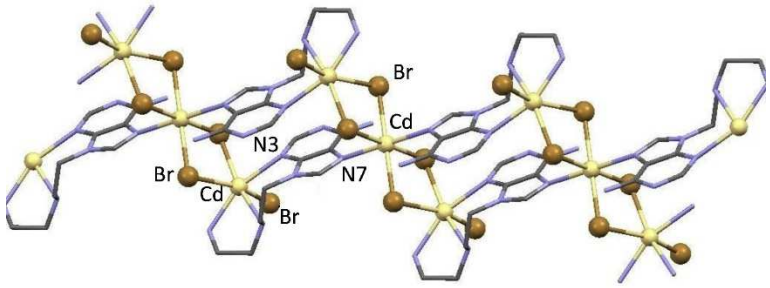

Figure 49: The X-Ray structure of the polymeric chaine of $[Cd_2Br_6(A\text{-}Et\text{-}en)_2]$. Figure taken from 86.

III. 5. c) Nucleobase based networks

Nucleobases ability to self-assemble *via* H-bonds, to coordinate metal centers, and to interact by π-π stacking provide all the means to act as interesting tectons in generating molecular networks. Over the past decade, nucleobase based networks became the center of attraction in the field of molecular tectonics, and several architectures assembled *via* NBs interactions were described.

Example of such networks is the system based on thymine reported by N. R. Champness and coworkers.[88] Di-(N_1-benzoyl)thymine and tri-(N_1-benzoyl)thymine were synthesized by condensation reactions of thymine with 1,4-bis-(bromomethyl)benzene and 1,3,5-tri(bromomethyl)-2,4,6-trimehtylbenzene respectively (Figure 50).

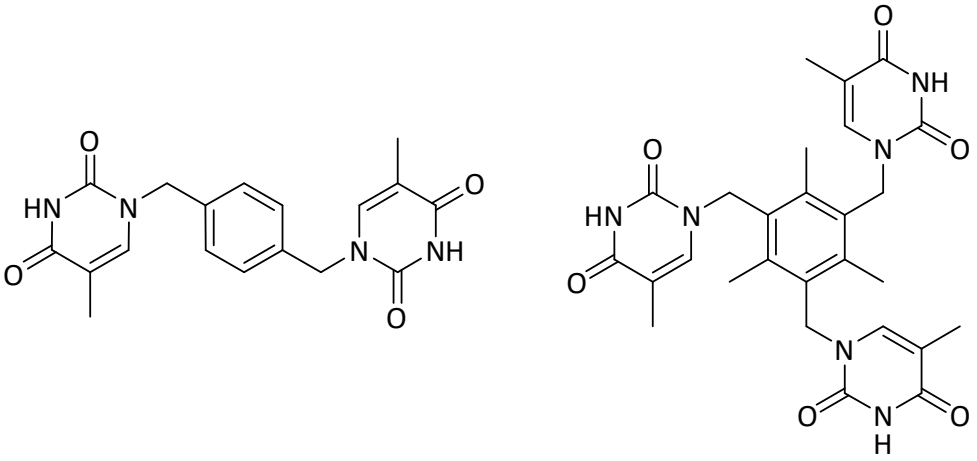

Figure 50: The molecular structure of the two tectons bearing thymine moieties.[88]

Di-(N_1-benzoyl)thymine tecton self-assembles into one dimensional chains through double H-bonds between the thymine moieties. The imide carbonyl is not involved in the H-bond paring and makes a close contact with the hydrogen of methylene groups of the neighboring chains. The *zig-zag* chains are stacked *via* π-π interactions into infinite columns running throughout the structure (Figure 51).

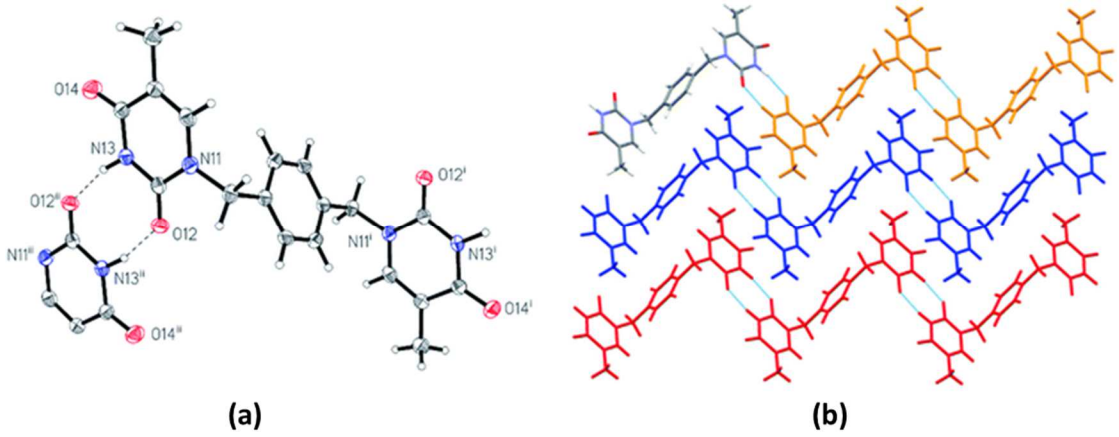

Figure 51: (a) The X-Ray structure of di-(N_1-benzoyl) thymine. (b) The X-Ray structure of the 1-D H-bonded zigzag chains stacked above each other. Figure modified from reference 88.

Tri-(N_1-benzoyl)thymine forms a one dimensional molecular ladder with all three thymine moieties binding to other thymine sites in adjacent molecules *via* double hydrogen bonds. The ladder structure is propagated along its length by interactions of independent thymine moieties with the 'rungs' being formed by a homo-dimer between the third moiety. Two crystallographically identical benzene molecules occupy the space between the thymine-dimer 'rungs' resulting in an infinite stack of molecules running along the ladder (Figure 52).

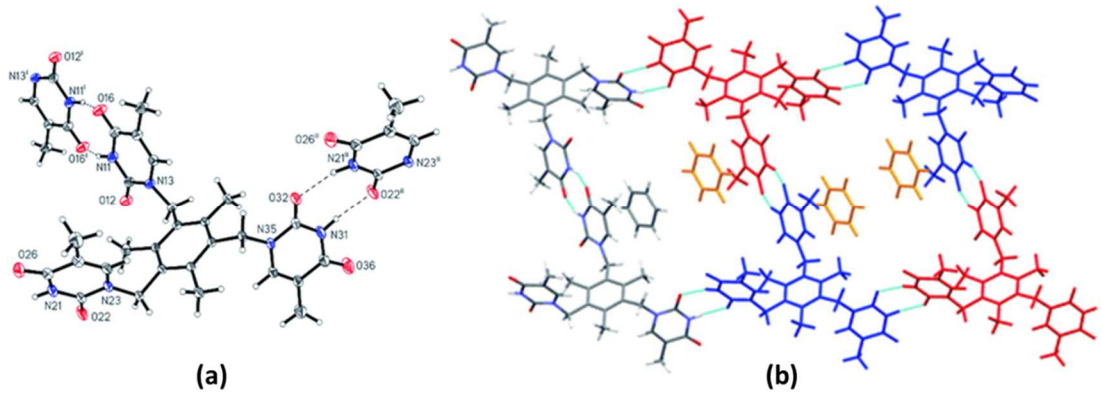

Figure 52: (a) The X-Ray structure of tri-(N_1-benzoyl) thymine. (b) The X-Ray structure of the molecular ladder. Figure modified from reference 88.

Another example of a tecton bearing thymine (**T**) molecules is the 4-tmpm (tetrakis(4-(thyminemethyl)phenyl)methane.[89] The X-Ray structure of 4-tmpm shows that three out of the four thyminylmethylphenyl arms (T2–4) display pseudo three-fold rotation symmetry (Figure 53).

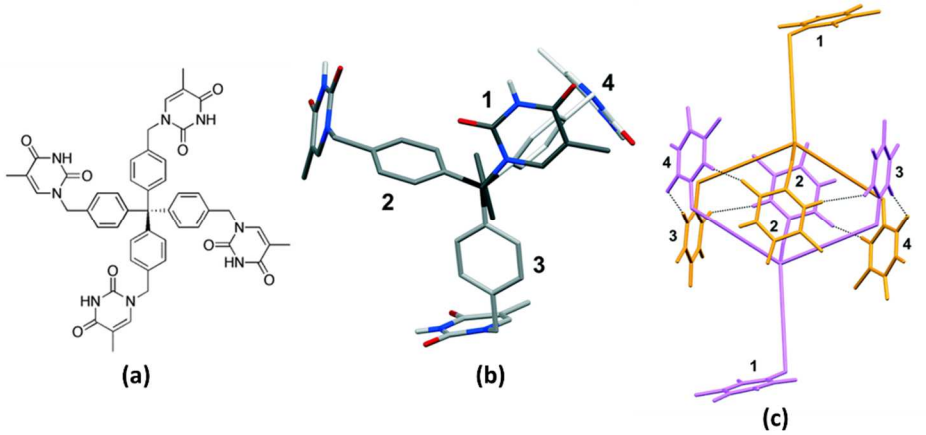

Figure 53: (a) The molecular structure of 4-tmpm. (b) The X-Ray structure of 4-tmpm showing its three-fold rotation symmetry. (c) X-Ray structure of a hydrogen bonded dimer, one molecule is in orange and the other is in light purple. Figure modified from reference 89.

Two molecules of 4-tmpm form a dimer joined by six strong C–H···O hydrogen bonds between the thymine carbonyl groups (*ortho*) of one molecule and the thymine CH sites of the second molecule as shown in Figure 54 (right). The 4-tmpm dimer is formed thought the H-bonds between their T2, T3 and T4 thymine moieties leaving the T1 moieties free and perpendicular to the plane of the dimer. Each T2, T3 and T4 are involved in two C–H···O bonds resulting in the six H-bonds forming the dimers. All of these interactions involve only the *ortho* carbonyl groups, thus the N–H sites and the *para* carbonyl groups of the thymine moieties are free to form interactions with adjacent dimers. In the dimer, the T3 rings form intermolecular H-bonds between their *para* carbonyl and NH groups. This is represented in the Figure below in the yellow zone. The dimers are linked to each other by two different hydrogen-bonding interactions. The first interaction is the double H-bonds between the T1 moieties belonging to one dimer and the T4 moieties belonging to the neighboring dimer. The second interaction is between the T2 rings of one dimer and the T1 of the other dimer *via* one H-bond between the NH sites of T2 and the carbonyl sites of T1, which are not hydrogen bonded to T4. Therefore, T1 is not involved in the dimer formation. However, it links the dimers to each other by three N–H···O bonds, 2 H-bonds with T4 and one H-bond with T2 (Figure 54).

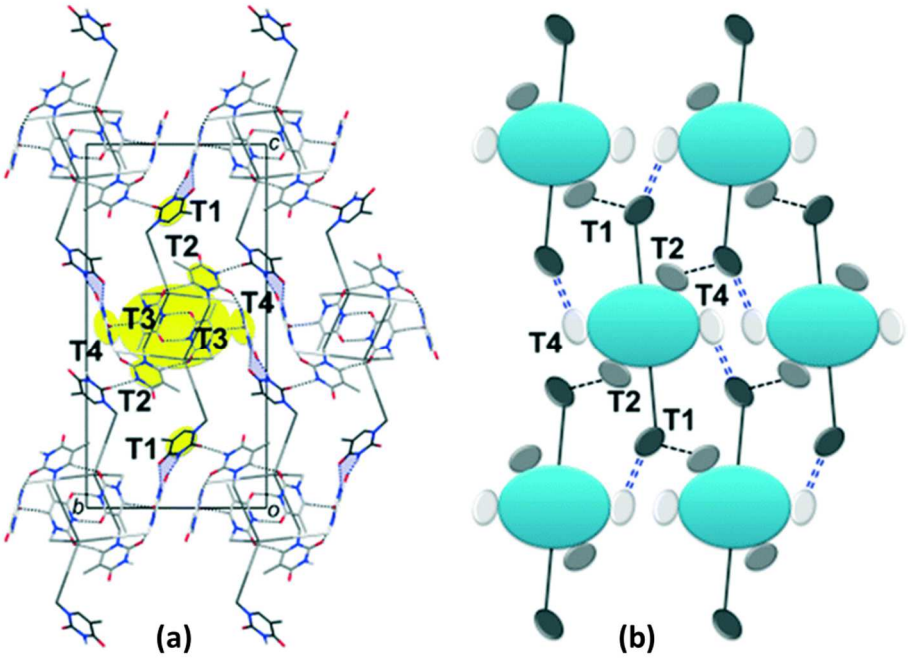

Figure 54: (a) The crystal packing of 4-tpmp molecules. Phenol groups are represented as sticks. The yellow balls represent the T3 interactions and the central core of the dimer. (b) Schematic representation of the packed structure through H-bonds between the dimers. Figure taken from reference 89.

In designing molecular networks based on nucleobase pairing, thymine is the most used one because of its higher solubility and least isomeric forms among the other nucleobases. However, several examples of networks with other NBs have been reported. For instance, the synthesis of 9,9'-diadenine (A2A) tecton and its assembly into H-bonded network was reported.[90] A2A is soluble only in DMSO and in HFIP solvent (1,1,1,3,3,3-hexafluoro-2-propanol), which was used to co-crystalize A2A molecules. The network based on A2A is self-assembled through hydrogen bonds between the adenine moieties into tapes decorated on both sides by HFIP molecules. Each A2A molecule is H-bonded to four different HFIP molecules *via* H-bonds between the NH or N sites of the adenines and the OH group of HFIP molecules as seen in the figure below (Figure 55 and 56).

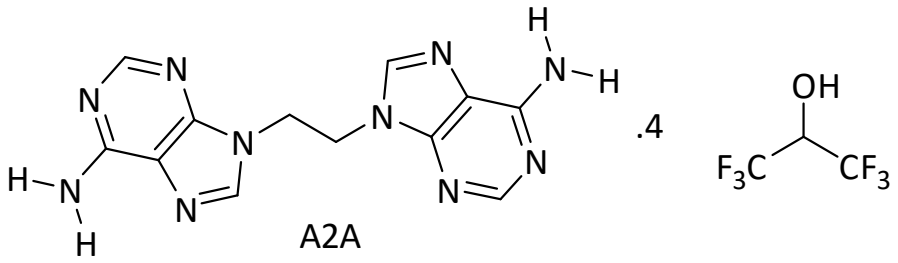

Figure 55: The molecular structure of the adenine based tecton A2A and HFIP solvent.

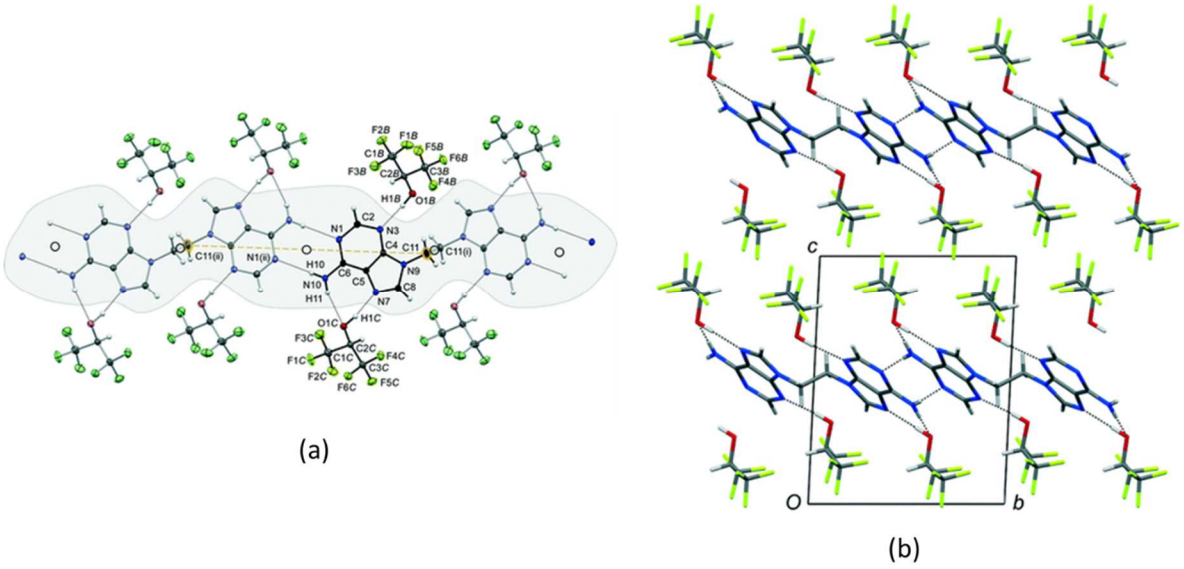

Figure 56: (a) The X-Ray structure of A2A tectons assembled with HFIP solvent molecules. (b) Molecular packing of A2A structure viewed from a-axis. Figure modified from reference 90.

IV. Aim of the Project

Synthetically modified or substituted nucleobases provide various applications when linked to suitable substituents. Electron and energy transfer, DNA binding, biological receptors, gel formation, drug delivery and other applications were reported for nucleobase containing systems.[81,91] In addition, the field of molecular tectonics provides the essential tools to improve and master the design of extended supramolecular architectures. Therefore, building nucleobase systems for fundamental and applied studies using the concept of molecular tectonics is of wide interest. Similarly, we envisioned the design of NBs based architectures using different coordinating sites aiming to generate hydrogen bonded coordinated networks. The coordination sites we choose to work with are porphyrin, dipyrrin, terpyridine and pyridine. The choice of these ligands is based on their properties and will be presented in the corresponding chapter of this manuscript. Furthermore, the choice of the metal cations used to generate the metallatectons and H-bonded coordinated networks is according to the geometry that the metal center can adapt and its counter ions. Our aim is to synthesize a library of novel tectons of various geometry bearing four nucleobases (Figure 57), and to study their assembly into molecular networks.

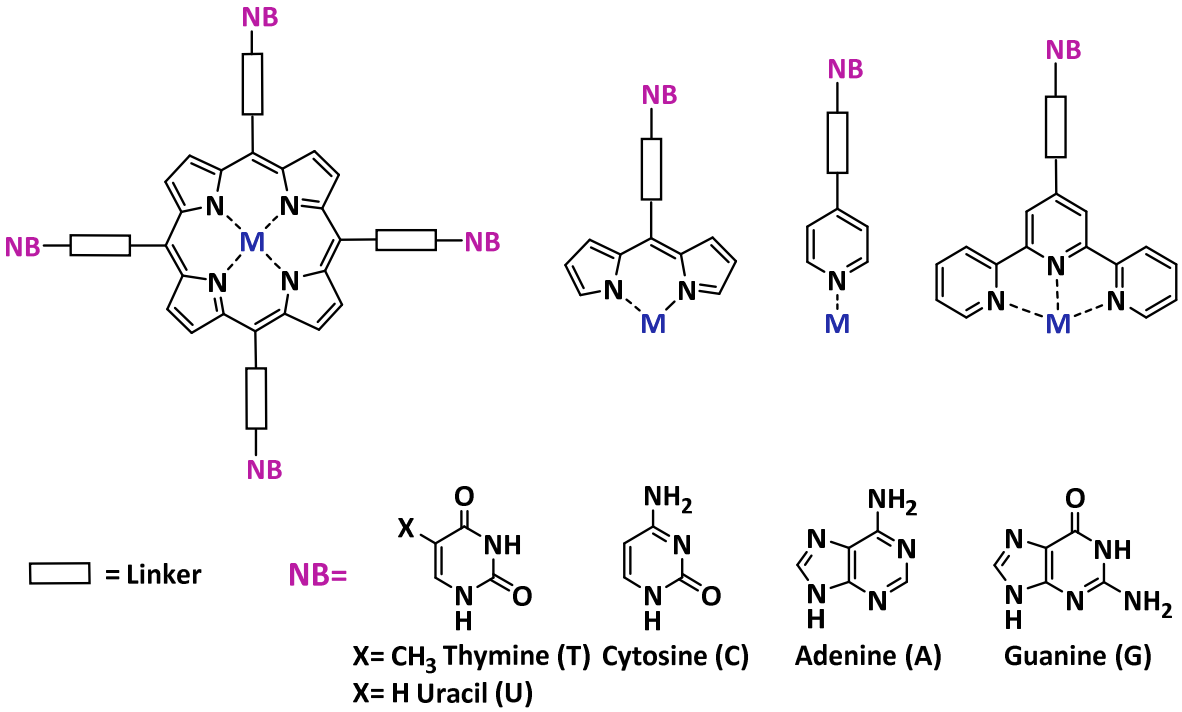

Figure 57: Schematic representation of targeted tectons.

V. References

1) J. M. Lehn, *Pure Appl. Chem*., **1978**, *50*, 871-892.

2) J. M. Lehn, *Angew. Chem. Int. Ed. Engl.,* **1988**, *27*, 89-112.

3) J. M. Lehn, Supramolecular Chemistry, Concepts and Perspectives, *VCH, Weinheim,* **1995.**

4) P. Horcajada, R. Gref, T. Baati, P. K. Allan, G. Maurin, P. Couvreur, G. Frey, R. E, Morris, C. Serre, *Chem. Rev.,* **2012**, *112*, 1232-1268.

5) H. Seunghee, M. Oh, M. Park. J. W. Joon, J. S. Chang, M.S. Lah, *Chem. Commun.,* **2009**, 5394-5396.

6) (a) P. Bhattacharya, S. H. Kim, P.Chen, Ran Chen, A. M. Spuches, J. M. Brown, M. H. Lamm, P. C. Ke, *J. Phys. Chem*., **2012**, 116, 15775-15781, (b) D. R. Gabdrakhmanov, F. G. Valeeva, V. E. Semenov, D. A. Samarkina, A. S. Mikhailov, V. S. Reznik, L. Y. Zakharova, *Macroheterocycles, **2016***, *9*, 29-33.

7) (a) M. Haider, Z. Pikeramenou, *Chem. Soc. Rev.*, **2005**, *34*, 120-132. (b) M. D. Allendorf, C. A. Bauer, R. K. Bhakta, R. J. T. Houk, *Chem. Soc. Rev.,* **2009**, *38*, 1330-1352.

8) S. Mann, *Nature*, **1993**, *365*, 499-505.

9) (a) M. W. Hosseini, *Acc. Chem. Res*., **2005**, *38*, 313-23. (b) M. W. Hosseini, *CrystEngComm*, **2004**, *6*, 318-322.

10) C. J. Pederson, *J. Am. Chem. Soc.,* **1967**, 89, 7017-7036.

11) B. Dietrich, J. M. Lehn, J. P. Sauvage, *Tetrahedron Lett*, **1969**, *10*, 2889-2892.

12) L. R. MacGillivray, J. L. Atwood, Angew. *Chem. Int. Ed.,* **1999**, *38*, 1018-1033.

13) S. Ferlay, A. Jouaiti, M. Loi, M. W. Hosseini, A. De. Cian, P. Turek, *New J. Chem.,* **2003**, *27*, 1801-1805.

14) E. Deiters, V. Bulach, N. Kyritsakas, M. W. Hosseini, *New J. Chem.,* **2005**, *29*, 1508-1513.

15) M. A. Beswick, C. Lopez-Casideo, M. A. Paver, P. R. Raithby, C. A. Russell, A. Steiner, D. S. Wright, *Chem Comm*., **1997**, 109-110.

16) P. Grosshans, A. Jouaiti, V. Bulach, J. M. Planeix, M. W. Hosseini, J. F. Nicoud, *CrystEngComm*, **2003**, *5*, 414-416.

17) K. Biradha, Y. Hong, M. Fujita, *Angew. Chem. Int. Ed.,* **2000**, *39*, 3843-3845.

18) B. F. Abrahams, T. A. Hudson, R. Robson, *J. Mol. Struct.,* **2006**, *795*, 2-8.

19) J. T. Brewer, S. Parkin, R. B. Grossman, *Cryst Growth Des.*, **2004**, *4*, 591-594.

20) M. L. Tong, S. L. Zheng, X. M. Chen, *Chem. Comm.,* **1999**, 561-562.

21) T. Kajiwara, H. Higashimura, M. Higuchi, S. Kitagawa, *ChemNanoMat,* **2018**, *4*, 103-111.

22) K. Biradha, M. Fujita, *J. Chem. Soc. Dalton Trans.,* **2000**, 3805-3810.

23) A. L. Mackay, *Nature*, **1958**, *314*, 604-606.

24) R. Mondal, M. K. Bhunia, K. Dhara, *CrystEngComm*, **2008**, *10*, 1167-1174.

25) S. R. Batten, N. R. Champness, X. M. Chen, J. Garcia-Martinez, S. Kitagawa, L. Ohrstrom, M. O' Keeffe, M. P. Suh, J. Reedijk, *Pure and Applied Chemistry*, **2013**, *85*, 1715-1724.

26) (a) Farruseng, D. Metal-Organic Frameworks: Applications from Catalysis to Gas Storage; *John Wiley & Sons: Weinheim,* **2011**. (b) S. R. Batten, S. M. Neville, D. R. Turner, Coordination Polymers: Design, Analysis and Application; *Royal Society of Chemistry: Cambridge*, **2009**.

27) (a) H. Z hang, D. Chen, H. Ma, P. Cheng, *Chem. Eur. J.*, **2015**, *21,*15854-15859. (b) L. V. Meyer, F. Schönfeld, K. Müller-Buschbaum, *Chem. Commun.,* **2014**, *50*, 8093-8108. (c) G. Tobin, S. Comby, N. Zhu, R. Clérac, T. Gunnlaugsson, W. Schmitt, *Chem. Commun.,* **2015**, *51*, 13313-13316.

28) (a) S. J. Lee, J. T. Hupp, *Coord. Chem. Rev.*, **2006**, *250*, 1710-1723. (b) I. Goldberg, *Chem. Commun*., **2005**, 1243-1254. (d) K. S. Suslick, P. Bhyrappa, J.-H. Chou, M. E. Kosal, S. Nakagaki, D. W. Smithenry, S. R. Wilson, *Acc. Chem. Res.,* **2005**, *38*, 283-291.

29) R. Makiura, R. Usui, E. Pohl, K. Prassides, *Chem. Lett.,* **2014**, *43*, 1161-1163.

30) R. Matsuoka, R. Toyoda, R. Sakamoto, M. Tsuchiya, K. Hoshiko, T. Nagayama, Y. Nonoguchi, K. Sugimoto, E. Nishibori, T. Kawaib, H. Nishihara, *Chem. Sci*., **2015**, *6*, 2853-2858.

31) C. S. Hawes, S. E. Hamilton, J. Hicks, G. P. Knowles, A. L. Chaffee, D. R. Turner, S. R. Batten, *Inorg. Chem.,* **2016**, *55*, 6692-6702.

32) A. Jouaiti, V. Jullien, M. W. Hosseini, J. M. Planeix, A. D. Cian, *Chem. Commun.*, **2001**, 114-115.

33) M. El Garah, N. Marets, M. Mauro, A. Aliprandi, S. Bonacchi, L. De Cola, A. Ciesielski, V. Bulach, M. W. Hosseini, P. Samorì, *J. Am. Chem. Soc.*, **2015**, *137*, 8450-8459.

34) O. M. Yaghi, M. O'Keeffe, N. W. Ockwig, H. K. Chae, M. Eddaoudi, J. Kim, *Nature*, **2003**, *423*, 705-714.

35) B. F. Abrahams, B.F. Hoskins, R. Robson, *J. Am. Chem. Soc*., **1991**, *113*, 3606-3607.

36) H. Li, M. Eddaoudi, M. O'Keeffe, O. M. Yaghi, *Nature*, **1999**, *402*, 276-229.

37) A. Beziau, S. A. Baudron, D. Pogozhev, A. Fluck, M. W. Hosseini, *Chem. Comm.,* **2012**, *48*, 10313-10315.

38) T. Kajiwara, H. Higashimura, M. Higuchi, S. Kitagawa, *ChemNanoMat,* **2018**, *4*, 103-111.

39) S. K. Yang, S. C. Zimmerman, *Isr. J. Chem.* **2013**, *53*, 511-520.

40) J. B. Asbury, T. Steinel, M. D. Fayer, *J. Phys. Chem. B*., **2004**, *108*, 6544-6554.

41) (a) C. Etter, J. C. MacDoland, J. Bernstein, *Acta Cryst*., **1990**, *B46*, 256-262. (b) M. C. Etter , *Acc. Chem. Res.*, **1990**, *23*, 120-126, (c) M. C. Etter, *The Journal of Physical Chemistry.,* **1991**, *12*, 4610-4618.

42) W. L. Jorgensen, J. Oranta, *J. Am. Chem. Soc*., **1990**, *112*, 2008-2010.

43) T. J. Murray, S. C. Zimmerman*, J. Am. Chem. Soc*., **1992**, *114*, 4010-4011.

44) K. E. Feldman, M. J. Kade, T. F. A. De Greef, E.W. Meijer, E. J. Kramer, C. J. Hawker, *Macromolecules,* **2008**, *41*, 4694-4700.

45) W. Jaunky, M. W. Hosseini, J. M. Planeix, A. D. Cisn, N. Kyritsakas, J. Fischer, *Chem. Comm.,* **1999**, 2313-2314.

46) D. Venkataraman, S. Lee, J. Zhang, J. S. Moore, *Nature*, **1994**, *371*, 591-593.

47) M. Kawahata, M. Matsuura, M. Tominaga, K. Katagiri, K. Yamaguchi, *Journal of Molecular Structure*, **2018**, *1164*, 116-122.

48) Y. He, S. Xiang, B. Chen, *J. Am. Chem. Soc.,* **2011**, *133,* 14570-14573.

49) (a) P. Li, Y. He, Y. Zhao, L. Weng, H. Wang, R. Krishna, H. Wu, W. Zhou, M. O'Keeffe, Y. Han, B. Chen, *Angew. Chem., Int. Ed.*, **2015**, *54*, 574-577. (b) P. Li, Y. He, H. D. Arman, R. Krishna, H. Wang, L. Weng, B. Chen, *Chem. Commun*., **2014**, *50*, 13081-13084. (c) P. Li, Y. He, J. Guang, L. Weng, J. C-G. Zhao, S. Xiang, B. Chen, *J. Am. Chem. Soc*., **2014**, *136,* 547-549.

50) W. Yang, Bin L. H. Wang, O. Alduhaish, Khalid Alfooty, M. A. Zayed, P. Li, H. D. Arman, B. Chen, *Cryst. Growth Des.,* **2015**, *15*, 2000-2004.

51) W. Saenger, Principles of Nucleic acids structure, *Springer*, New York, **1984.**

52) J. D. Watson, F. H. Crick, *Nature,* **1953**, *171*, 737-737.

53) G. A. Jeffery and W. Saenger, Hydrogen bonding in Biological structures, *Springer*, Berlin, **1991.**

54) (a) Y. Kyogoku, R. C. Lord and A. Rich, *Proc. Nat. Acad. Sci. USA*, **1967**, *57*, 250-257. (b) Y. Kyogoku, R. C. Lord and A. Rich, *Proc. Biochim. Biophys. Acta*, **1969**, *179,* 10-17.

55) (a) S. C. Zimmerman and P. S. Corbin, *Struct. Bond*., **2000,** *96*, 63-94. (b) T. J. Murray and S. C. Zimmerman, *J. Am. Chem. Soc*., **1992**, *114,* 4010-4011. (b) J. Pranata, S. G. Wierschke and W. L. Jorgensen*, J. Am. Chem. Soc*., **1991**, *113*, 2810-2819. (c) J. Sartorius, H.J. Schneider, *Chem. Eur. J.,* **1996**, *2*, 1446-1452.

56) (a) J. Clauwaert, J. Stockx, Interactions of polynucleotides and their components, Chapter I Dissosciation constants of the bases and their derivatives, *Z. Naturforsch. B,* **1968**, *23*, 25-30. (b) G. D. Fasman, Handbook of Biochemistry and Molecular Biology, Vol I Nucleic acids, *Chem. Rubber. Co. Cleveland, Ohio.,* **1975**, 76-206. (c) R. Krishnamurthy, *Acc. Chem. Res.,* **2012**, *45*, 2035-2044, (d) V. Verdolino, R. Cammi, B. H. Munk, H. B. Schlegel, *J. Phys. Chem. B.,* **2008,** *112,* 16860-16873.

57) B. Pullman, *J. Chem. Soc.,* **1959**, 1621-1623.

58) (a) N. B. Leontis, J. Stombaugh and E. Westhof, *Nucleic Acid Res.,* **2002**, *30*, 3497-34531. (b) M. G. M. Purwanto and K. Weisz, *Curr. Org. Chem*., **2003**, *7*, 427-446.

59) K. Hoogsteen, *Acta. Cryst*., **1963**, *16*, 907-916.

60) R. E. A. Kelly, L. N. Kantorovich*, J. Matter. Chem.,* **2006,** *16*, 1894-1905.

61) V. N. Soyfer, V. N. Potaman, Triple-Helical Nucleic Acids, *Springer*, New York, **1995.**

62) J. L. Sessler, J. Jayawickramarajah, *Chem. Comm.,* **2005**, 1939-1949.

63) S. Sivakova, S. J. Rowan, *Chem. Soc. Rev*., **2005**, *34*, 9-21.

64) A. Ciesielski, M. El Garah, S. Masiero, P. Samori, *Small*, **2016**, *12*, 83-95.

65) J. T. Davis, *Angew. Chem. Int. Ed.* **2004**, *43*, 668-698.

66) M. Furukawa, H. Tanaka and T. Kawai, *J. Chem. Phys.*, **2001**, *115*, 3419-3423.

67 W. Xu , R. E. A. Kelly , H. Gersen, E. Laegsgaard, I. Stensgaard, L. N. Kantorovich, F. Besenbacher, *Small,* **2009**, *5*, 1952-1956.

68) W. Xu, R. E. A. Kelly, R. Otero, M. Schock, E. Laegsgaard, I. Stensgaard, L. N. Kantorovich, F. Besenbacher, *Small,* **2007**, *3*, 2011-2014.

69) M. Edelwirth, J. Freund, S. J. Sowerby, W. M. Heckl, *Surf. Sci.*, **1998**, *417*, 201-209.

70) S. J. Sowerby, W. M. Heckl, G. B. Petersen, *J. Mol. Evol.,* **1996**, *43*, 419-424.

71) M. Furukawa, H. Tanaka, T. Kawai, *Surf. Sci.,* **2000**, *445,* 1-10.

72) M. Lukas, R. E. A. Kelly, L. N. Kantorovich, R. Otero, W. Xu, E. Laegsgaard, I. Stensgaard, F. Besenbacher, *J. Chem. Phys*, **2009**, *130*, 24705-24711.

73) J. L. Sessler, C. M. Lawrence, J. Jayawickramarajah, *Chem. Soc. Rev*., **2007**, *36*, 314-325.

74) C. R. Geyer, T. R. Battersby, S. A. Benner, *Rules for designing artificial genetic systems, The nucleobases, Structures,* **2003***, 11,*1485-1498.

75) S. A. Benner, *Acc. Chem. Res.*, **2004**, *37*, 784-797.

76) J. L. Sessler, M. Sathiosatham, K. Doerr, V. Lynch, K. A. Abboud, *Angew. Chem. Int. Ed.*, **2000**, *39*, 1300-1303.

77) R. Iwaura, K. Yoshida, M. Masuda, K. Yase, T. Shimizu, *Chem. Mater.,* **2002**, *14*, 3047-3053.

78) J. L. Sessler, J. Jayawickramarajah, C. L. Sherman , J. S. Brodbelt, *J. Am. Chem. Soc.,* **2004**, *126*, 11460-11461.

79) J. L. Sessler, R. Wang, *J. Am. Chem. Soc.,* **1996**, *118*, 9808-9809.

80) J. L. Sessler and R. Wang, *Angew.* Chem. *Int. Ed. Engl.,* **1998**, *37*, 1726-1729.

81) O. F. Schall and G. W. Gokel, *J. Am. Chem. Soc.,* **1994**, *116*, 6089-6100.

82) J. E. Kickham, S. J. Loeb and S. L. Murphy, *Chem. Eur. J.,* **1997**, *3*, 1203-1213.

83) V. G. H. Lafitte, A. E. Aliev, P. N. Horton, M. B. Hursthouse, K. Bala, P. Golding and H. C. Hailes, *J. Am. Chem. Soc.*, **2006**, *128*, 6544-6545.

84) T. Shimizu, R. Iwaura, M. Masuda, T. Hanada and K. Yase, *J. Am. Chem. Soc.*, **2001**, *123*, 5947-5955.

85) P. Amo-Ochoa, O. Castillo, C.J. Gómez-García, K. Hassanein, S. Verma, J. Kumar, F. Zamora, *Inorg. Chem.,* **2013**, *52*, 11428-11437.

86) P. Amo-Ochoa, F. Zamora, *Coord. Chem. Rev.,* **2014,** *276*, 34-58.

87) D. Amantia, M.A. Shipman, C. Price, M.R.J. Elsegood, W. Clegg, A. Houlton, *Inorg. Chim. Acta.*, **2006**, *359*, 3515-3520.

88) J. Hamblin, S. P. Argent, A. J. Blake, C.Wilson, N. R. Champness, *CrystEngComm*, **2008**, *10*, 1782-1789.

89) L. Qi, L. L. Gundersen, C. H. Gorbitz, *CrystEngComm*, **2018**, *20*, 1179-1184.

90) L. Qi, L. L. Gundersen, C. H. Gorbitz, *CrystEngComm*, **2016**, *18*, 6352-6357.

91) (a) J. L. Sessler, M. SAthiosatham, C. T. Brown, T. A. Rhodes, G. Wiederrecht, *J. Am. Chem. Soc.,* **2001**, *123*, 23655-3660. (b) A. Lopez, J. Liu, *ChemNanoMat*, **2017**, *3*, 670-684. (c) N. Sreenivasachary, J.-M. Lehn, *PNAS*, **2005**, *102*, 5938-5943. (d) G. Sargsyan, B. M. Leonard, J. Kubelka, M. Balaz, *Chem. Eur. J.*, **2014**, *20*, 1878-1892.

Chapter I: Porphyrins bearing Nucleobases

Table of Contents

I. Porphyrin……60
I. 1. Structure and nomenclature……60
I. 2. Synthesis……61
I. 2. a) A_4……61
I. 2. b) *Trans*-A_2B_2……62
I. 3. Characterization……64
I. 3. a) ^{1}H-NMR……64
I. 3. b) UV-Visible spectroscopy……65
I. 4. Complexation and geometry……66
II. Porphyrin bearing nucleobases……67
II. 1. Examples of porphyrin bearing nucleobases (NB) ……68
II. 2. Aim of the project……78
II. 3. Porphyrin bearing NB *via* C-C bond……79
II. 3. a) Synthesis of Zn(II)[5,15-di(trimethylsilylethynyl)-10,20-dipentylporphyrin]……81
II. 3. b) Protection of 5-iodouracil……82
II. 3. c) Synthesis of Zn(II)[5,15 di(N_1-(benzylhydry)uracil)-10,20-dipentylporphyrin](**T1**)..83
II. 3. d) Deprotection of **T1**……84
II. 3. e) Iodination and alkylation of NBs……85
II. 3. e) 1) Alkylation of 5-iodouracil……85
II. 3. e) 2) Iodination and alkylation of cytosine……86
II. 3. e) 3) Iodination and alkylation of adenine……86
II. 3. f) Synthesis of Zn(II) [5,15 -di(N1-hexyluracil)- 10,20-dipentylporphyrin] (**T3**)……87
II. 3. g) Cross coupling reaction of I-Cy-C6 and **Zn-Po1**……88
II. 4. Porphyrin bearing NB *via* C-N bond……90
II. 4. a) Synthesis of 5,15-di(4-(bromomethyl)phenyl)-10,20-diphenylporphyrin (**Po2**)……92
II. 4. b) Substitution of **Po2** mixture……92
II. 4. c) Synthesis of 5,15-di(4-(bromomethyl)phenyl)-10,20-dimesitylporphyrin (**Po3**)……93
II. 4. d) Synthesis of 5,15-di(N_1-methylphenylthymine)-10,20-dimesitylporphyrin (**T5**)…...94
II. 4. e) Synthesis of 5,15-di(N_9-methylphenyladenine)-10,20-dimesitylporphyrin (**T6**)……95
II. 4. f) Synthesis of 5,15-di(N_1-methylphenylcytosine)-10,20-dimesitylporphyrin (**T7**)……96
II. 4. g) Synthesis of 5,15-di(N_9-methylphenylguanine)-10,20-dimesitylporphyrin (**T9**)……97
II. 4. h) Synthesis of 5,10,15,20-tetrakis(4-(bromomethyl)phenyl)porphyrin (**Po4**)……98
II. 4. i) Synthesis of 5,10,15,20-tetrakis(N_1-methylphenylthymine)porphyrin (**T10**)……...99
II. 4. j) Substitution of **Po4** with adenine and cytosine……100
III. Conclusion and Perspectives……100
IV. References……102

I. Porphyrin

Porphyrins are one of the tetra-pyrrolic macrocyclic molecules found in biological systems.[1] For example, porphyrin iron complexes are found in the Heme, the red pigment in red blood cells and the cofactor of Hemoglobin. Porphyrin scaffolds present in hemoglobin and myoglobin are involved in the transport and storage of oxygen. Porphyrin's unique chemical and physical features and biological applications made them one of the most studied molecules in history. Moreover, investigations to ameliorate the synthesis of porphyrin and to functionalize them into molecules with applications in different fields (Catalysis[2], Photovoltaic[3], molecular materials[4], molecular tectonics[5]…) are still of current interest.

I. 1. Structure and nomenclature

Porphyrins consist of four pyrrole rings linked by four methylene bridges with a principal plan (P_{24}) composed of 20 carbon atoms (8 beta, 4 *meso*, and 8 alpha) and four nitrogen atoms (Figure 1). Following the IUPAC nomenclature, the macrocycle is numbered from 1 till 20 and the four pyrrole rings are labeled from A to D. Porphyrin has 12 positions (8 β-pyrrolic and 4 *meso*) that may be functionalized, an aromatic structure with 18 π electrons, and a tetraaza core able to coordinate various metal centers.

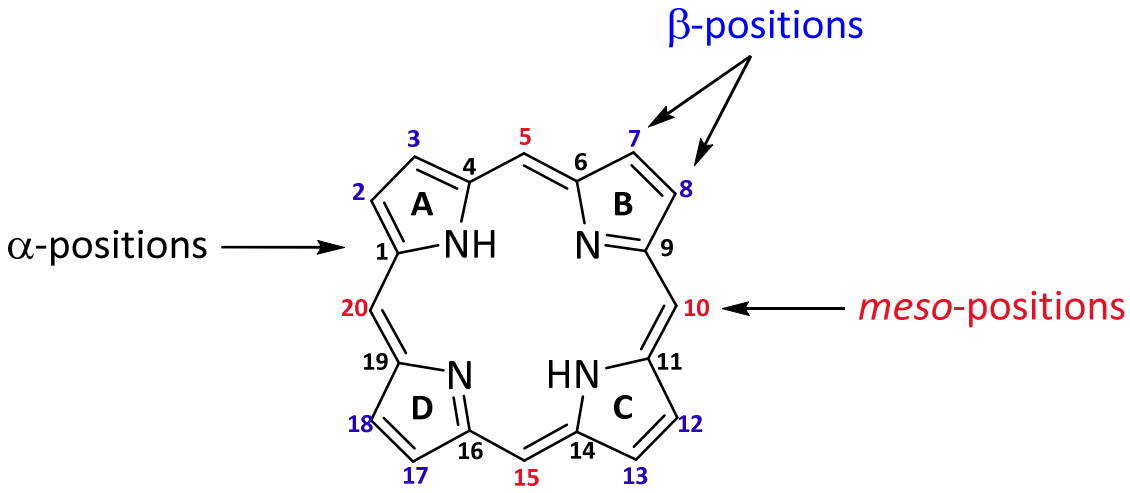

Figure 1: The chemical structure and nomenclature of porphyrin.

I. 2. Synthesis

The first method to synthesize a porphyrin started in the 1930 by Fischer[6] and Rothemund.[7] As previously mentioned, a porphyrin possesses four *meso* and eight β-pyrrolic positions that can be functionalized. In our case we are interested in functionalizing the *meso* positions, more precisely A_4 and *trans*-A_2B_2 porphyrins (Figure 2).

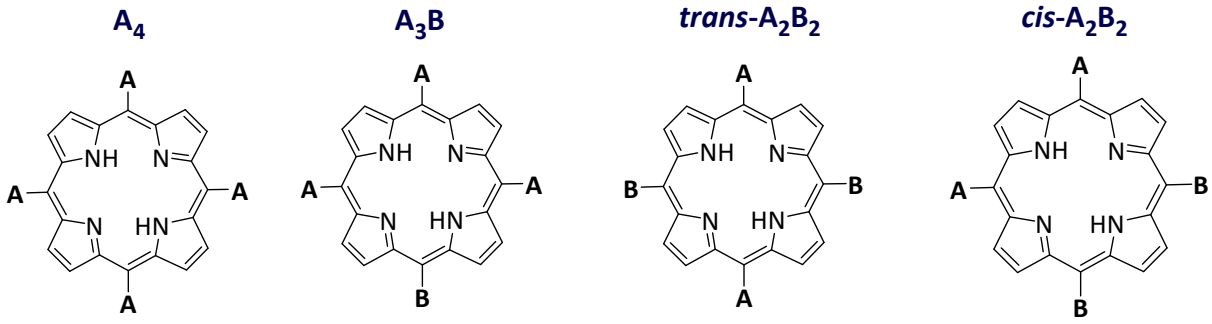

Figure 2: Representation of *meso* substituted porphyrins.

I. 2. a) A_4

The A_4 type porphyrin possesses the same substituents in the four *meso* positions, a famous example is the tetraphenylporphyrin (TPP). TPP was synthesized under harsh conditions with low yields, by reacting pyrrole and benzyladehyde at 220 °C for 48 hours in air, which acts as an oxidizing agent (Figure 3).[7]

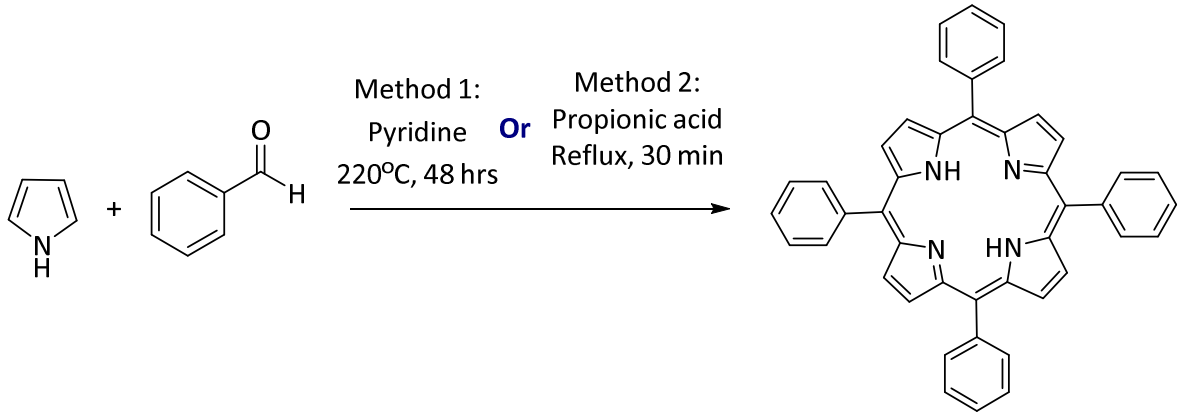

Figure 3: Synthesis of TPP.

Later in 1967, Adler and Long ameliorated the synthesis of TTP. [8] They developed a new method using propionic acid as a solvent and refluxing pyrrole with benzaldehyde for 30 minutes (Figure 3). TPP was obtained in a shorter time and higher yields compared to the Rothemund method. However, the use of an acidic medium at high temperature, limited the nature of aldehydes that could be used.

Lindsey *et al.* [9] then developed a new strategy using milder conditions, in which the ring closure of the tetrapyrrole and the oxidation of the porphyrinogen are two separate steps (Figure 4). In this method, the pyrrole and the aldehyde are reacting at room temperature in chloroform or dichloromethane in the presence of an acid catalyst: boron trifluoride etherate ($BF_3.Et_2O$) or trifluoroacetic acid (TFA). This step leads to the formation of the porphyrinogen, which is subsequently oxidized into the porphyrin by the addition of an oxidizing agent, such as 2,3-dichloro-5,6-dicyano-1,4-benzoquinone (DDQ) and p-chloranil.

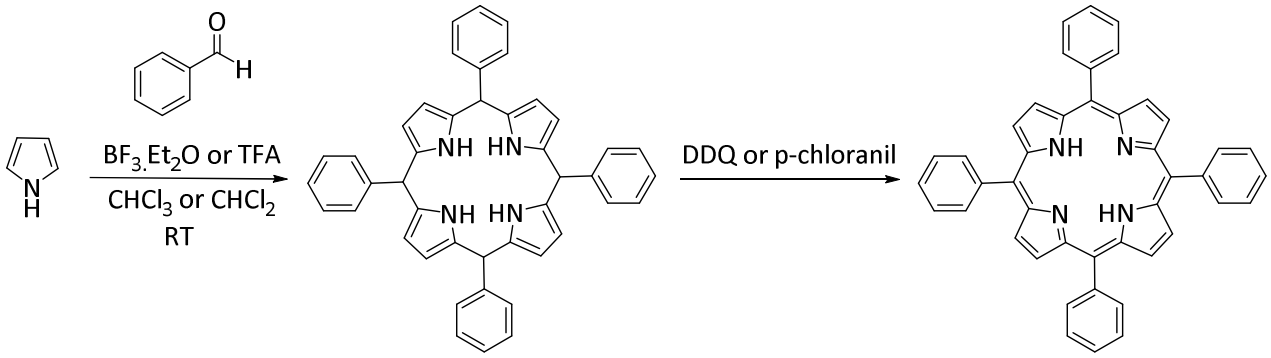

Figure 4: The two-step reaction to synthesize TPP.

I. 2. b) *Trans*-A_2B_2

Trans-A_2B_2 type porphyrin bears two different substituents in *trans meso* positions. The first attempts to synthesize such porphyrins were developed by Little *et al*[10], who adapted the Adler and Longo's method based on refluxing pyrrole in propionic acid as a solvent in the presence of two different aldehydes. This method was named "the mixed aldehyde method", and it produces six different porphyrins (Figure 5). The separation of the six porphyrins is difficult and time consuming.

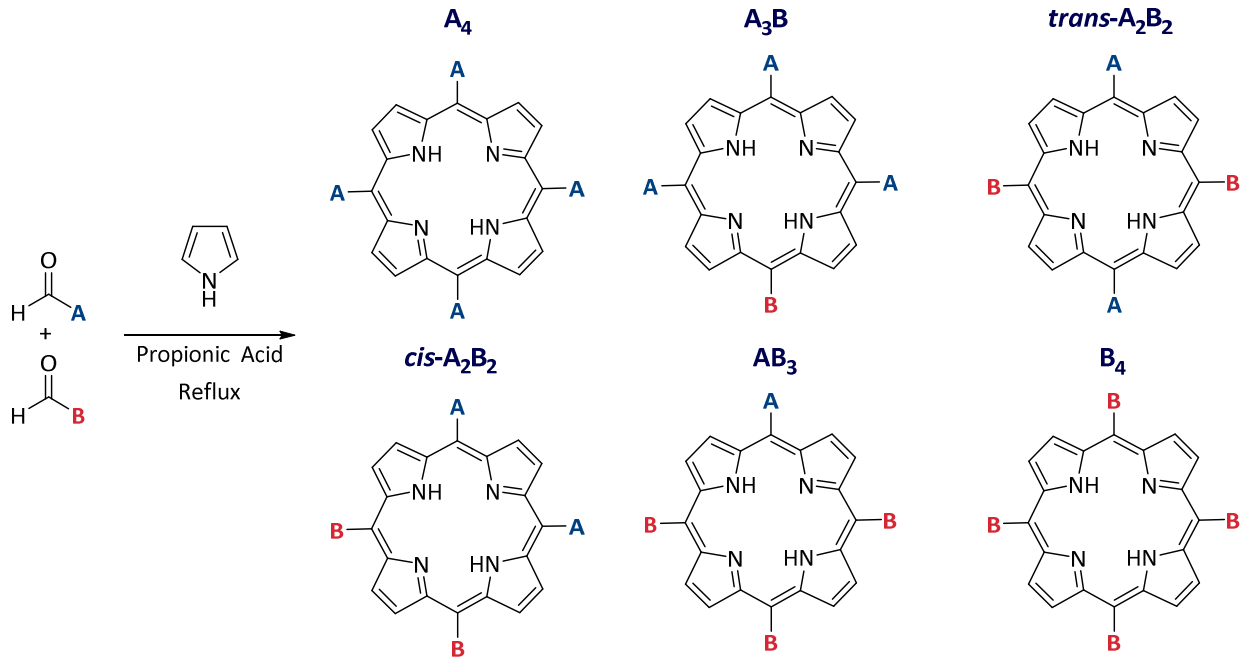

Figure 5: Mixture of porphyrins generated by the "mixed aldehyde method".

MacDonald *et al.* [11]developed a more selective method for the synthesis of porphyrins using a two-step procedure. The first step consists of synthesizing a dipyrromethane (DPM) derivative from one aldehyde (A-CHO) and an excess of pyrrole in the presence of an acid catalyst. The second step is a [2+2] condensation reaction between the DPM and the second aldehyde (B-CHO) in the presence of an acidic catalyst followed by an oxidation reaction (Figure 6).

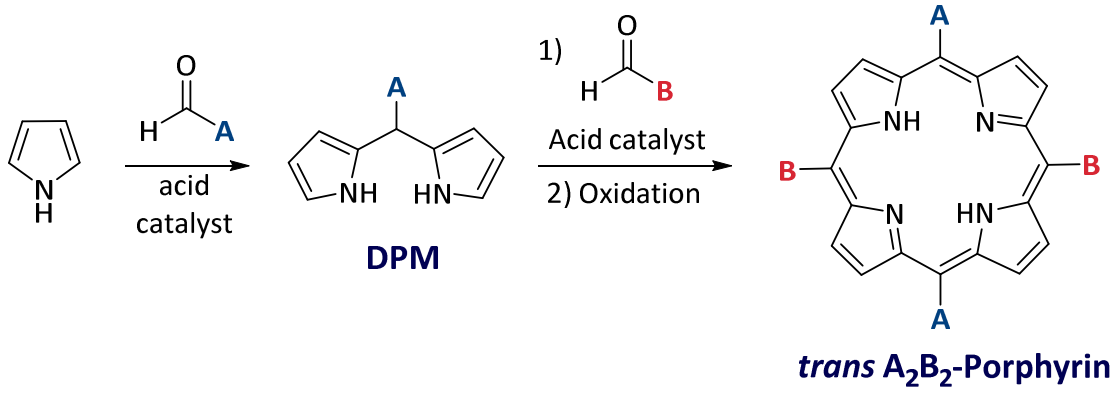

Figure 6: Synthesis of *trans*-A_2B_2 porphyrin by [2+2] condensation reaction.

Moreover, A_2B_2 porphyrins could also be obtained following the Adler method, by reacting the DPM with a second aldehyde in propionic acid under reflux.[12] Both methods are feasible, however the choice depends on the nature of the aldehyde and the stability of the DPM.

The disadvantage of the [2+2] condensation reaction is related to a phenomenon called "scrambling". DPM in acidic media can undergo fragmentation and recombination with unconsumed starting material leading to the formation of a mixture of six porphyrins. The mixture is usually hard to separate, and could be avoided by playing on the concentration of the reactants and the nature of DPM used. Lindsey *et al*[13] reported that low concentration (10Mm) and the use of a sterically hindered DPM usually lower the degree of scrambling.

Another approach to synthesize *meso*-substituted porphyrins was inspired by the developments in metal-mediated cross-coupling reactions.[14] This method consists of using a halogenated *meso* porphyrin in metal catalyzed cross-coupling reactions. To synthesize A_2B_2 porphyrins, four steps are followed. The first two steps are the synthesis of the porphyrinogen and its oxidation into a porphyrin bearing two substituents in *trans meso*-positions, following the [2+2] condensation method. The third step is to halogenate the porphyrin, in the other two *trans* positions, using halogenating agents such as N-Bromosuccinimide (NBS). This step results in a porphyrin bearing two *meso*-halogenated sites that could be used as a starting material in Suzuki, Sonogashira, Stille or other cross coupling reactions. Examples of such coupling reactions will be further explained later in this chapter.

I. 3. Characterization

The aromatic structure of porphyrins provides unique properties that can be characterized by different techniques such as ^{1}H-NMR and UV-Vis.

I. 3. a) ^{1}H-NMR

The cyclic conjugated π-electron system of porphyrins causes a large magnetic anisotropy. The external magnetic field going through the aromatic rings sets up a current of mobile π-electrons that gives rise to a secondary magnetic field coming from the center of the macrocycle with strong anisotropic effect, thus leading to the shielding of the protons inside the ring and the deshielding

of the protons located outside the ring. Therefore, the 2 NH protons located in the cavity of the porphyrin appear highly shielded (around -2 ppm) and as a large broad peak. Conversely, the 8 β-pyrrolic protons appear downfield shifted, usually between 8 and 10 ppm, and their multiplicity being representative of the symmetry of the porphyrin.

I. 3. b) UV-Visible Spectroscopy

Porphyrins have distinctive UV-Vis absorption spectra due to π-π* transitions. The absorption spectra shows two different bands located in different zones. The first zone is located around 420 nm and corresponds to the Soret band, a very intense band ($\varepsilon \sim 10^5$ L. $mol^{-1}.cm^{-1}$), due to the transition between the fundamental state S_o and the singlet excited state S_2. The second zone is located between 500 and 700 nm and corresponds to the Q bands (Figure 7). Those bands are of lower intensity ($\varepsilon \sim 10^3 - 10^4$ L. $mol^{-1}.cm^{-1}$) and are due to the transition between the fundamental state S_o and the singlet excited state S_1. The Q bands are responsible for the color of the porphyrin and are affected by its symmetry and by the geometry of its core. A free base porphyrin with a D_2h symmetry shows four Q bands, while only two Q bands are observed for a metallated porphyrin with a D_4h symmetry.

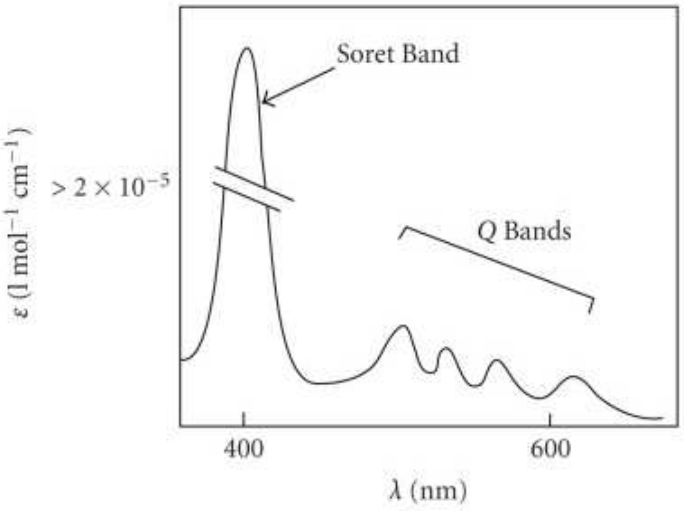

Figure 7: UV-Vis spectrum of a free base *meso*-substituted porphyrin.

I. 4. Complexation and geometry

The porphyrin core acts as a tetradentate ligand, which coordinates various metal cations after the deprotonation of the two inner NH groups. Porphyrin's central cavity has an ideal size to accommodate first row transition metals, while the metal cations with higher volume are located out of the cavity often causing deformation of the porphyrin core (Figure 8). Moreover, metal cations can have additional ligands coordinated in the axial positions to complete their coordination sphere.

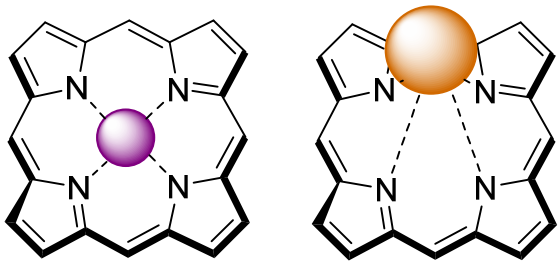

Figure 8: Schematic representation of the position of the metal center with respect to its size.

The macrocyclic structure of porphyrins can be distorted, depending on the nature of the substituents on the *meso* and β-positions, and depending on the metal cation present in the porphyrin cavity. In the solid-state, several conformations were identified as shown in Figure 9.

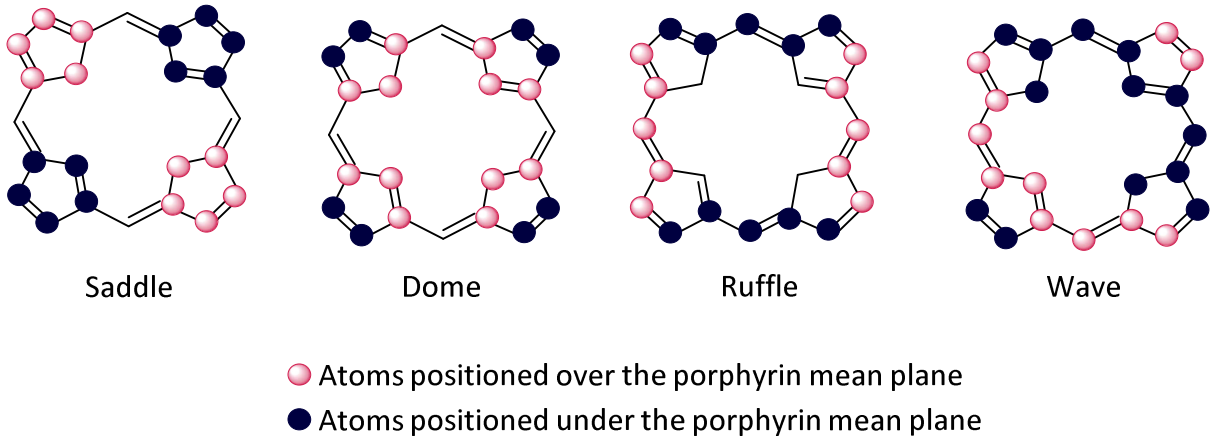

Figure 9: Schematic representations of porphyrin deformation.

Due to their aromatic systems, porphyrins can self-assemble *via* π-π interactions leading to two assemblies in the solid state: the H or J aggregates. The H aggregate consists of porphyrin molecules stacked vertically one over the other through face-to-face π-π interactions, and the J aggregates corresponds to porphyrins stacked in a shifted manner above each other (Figure 10).

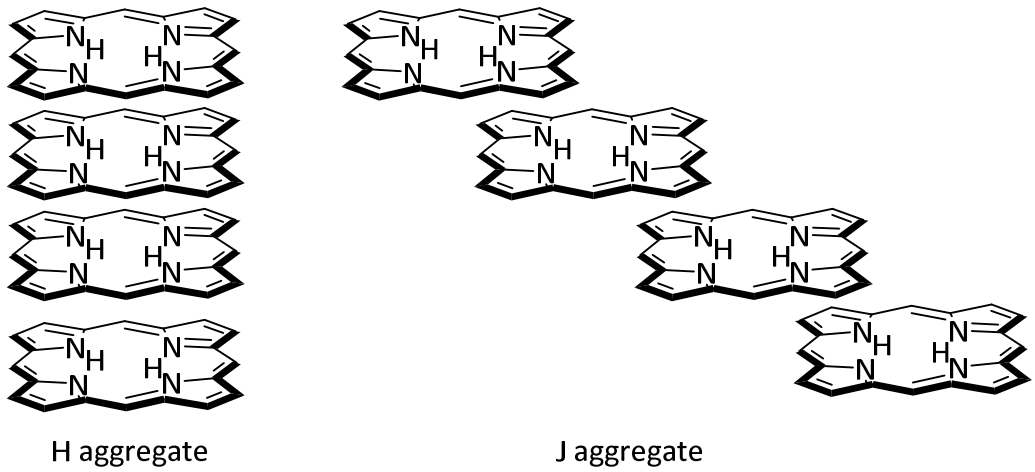

Figure 10: Schematic representations of H and J aggregates.

II. Porphyrin Bearing Nucleobases

The porphyrin backbone is of high interest in supramolecular chemistry and molecular tectonics, [5]especially for the formation of coordination networks. It can be functionalized by a wide range of coordinating groups and can accept numerous metal cations in its cavity. Moreover, it may self-assemble through π-π interactions. An additional interesting feature of porphyrins is the possibility to introduce H-bonding recognition sites at the periphery of the macrocycle, in order to design tectons that assemble into stable architectures *via* hydrogen, coordination and π-π interactions. Nucleobases are the most famous H-bonding moieties due to their biological importance and their strong and selective propensity to form H-bonds. Both porphyrins and nucleobases are naturally occurring molecules, and linked together they should lead to supra-molecules with a wide range of properties and applications.

II. 1. Examples of Porphyrin Bearing Nucleobases (NB)

J. S. Sessler *et al.*[15] described several dimeric assemblies based on guanine and cytosine bearing porphyrin scaffolds forming photo antennas for photo-induced energy transfer. The three systems shown in the Figure 11 are examples of NB-porphyrin based assemblies *via* Watson-Crick H-bonds between guanine and cytosine, leading to an energy transfer from the Zn-porphyrin to the free base porphyrin.

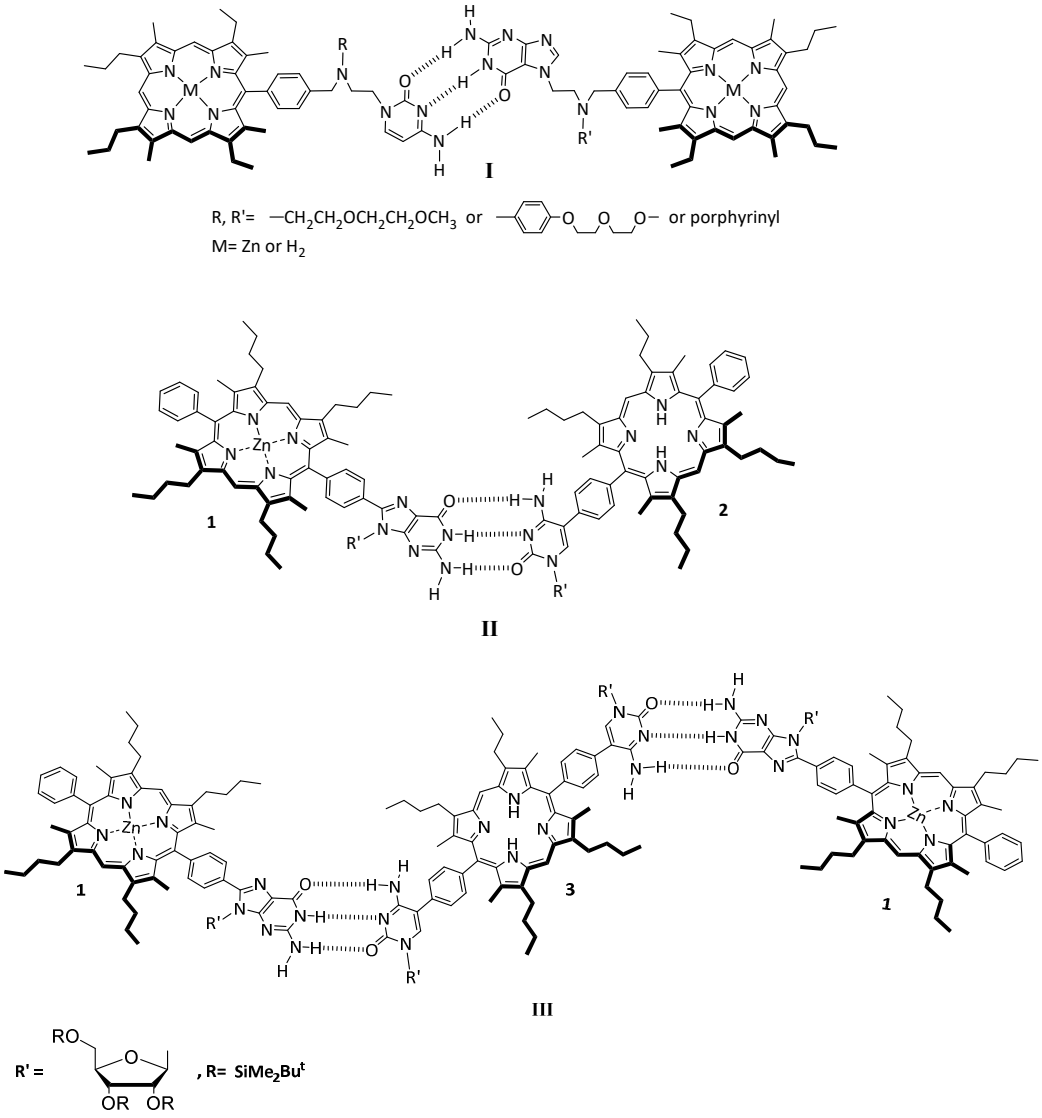

Figure 11: Representation of dimeric and trimeric **G-C** Watson-Crick H-bonded energy transfer systems based on zinc-porphyrin donors and porphyrin acceptors.[15, 16]

The porphyrins present in the assembly I [16] were prepared by alkylation of a nucleobase derivative with an electrophilic porphyrin to provide the targeted molecules that assembled into dimeric systems through Watson-Crick hydrogen bonding. Following the irradiation of the dimeric assembly, only photoinduced triplet-triplet energy transfer was observed. Unfortunately, no singlet-singlet energy transfer occurred, due to the flexibly of the linkage between the porphyrins and the NBs. To overcome this limitation, more rigid molecules were synthesized (Figure 12 and 13). The dimeric assembly II is composed of a Zn(II) guanine-porphyrin that serves as the energy donor, and of a free base cytosine-porphyrin acting as the energy acceptor. The two porphyrins are arranged side by side linked through the three H-bonds between **G** and **C** (Figure 11). Assembly III, is a trimeric assembly composed of a central free base porphyrin bearing two cytosine in trans *meso* positions linked by H-bonding to two Zn (II) guanine based porphyrins (Figure 11). The zinc porphyrins funnel energy into the central free base porphyrin which serves as an energy trap.

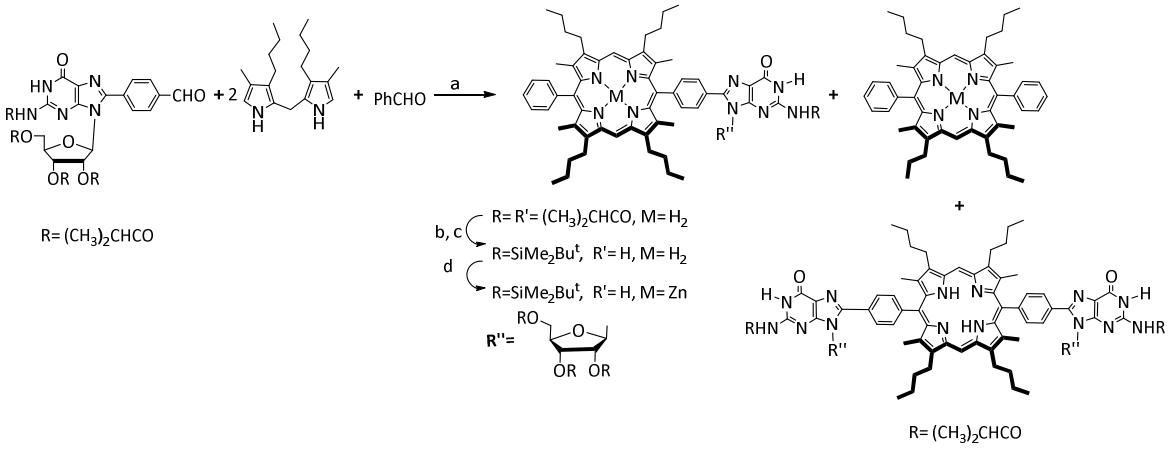

Figure 12: Synthesis of porphyrins bearing guanine for assemblies II and III, (a) (i) TFA, CH_2Cl_2, argon, room temperature, 4 h; (ii) NaOAc, 30 min; (iii) p-chloranil, room temperature, 6 h. (b) NH_3/MeOH, room temperature, 36 h. (c) TBDMS-C1, imidazole, DMF, room temperature, overnight, (d) $Zn(OAc)_2$, MeOH, reflux, 30 min.[16]

The porphyrins assembly II and III were synthesized by condensation of a mixture of 1 equivalent of nucleobase-benzaldehyde and 1 equivalent of benzaldehyde with 2 equivalents of 4,4-dimethyl-3,3'-dibutyldipyrrylmethane. The guanine and cytosine aldehydes were obtained by Stille cross-coupling reactions that involved the Pd-catalyzed coupling between an organostannyl benzaldehyde derivatives and halogenated nucleobases. The reaction lead to a mixture of three porphyrins composed by the mono-substituted porphyrin, the di-substituted porphyrin, and 5,15-

diphenylporphyrin (Figure 12 and 13). Subsequent deprotection of the NBs and the selective reprotection of the sugar moieties gave rise to the unmasked cytosine and guanine porphyrins. The latter compounds were converted into their corresponding zinc porphyrins.[17]

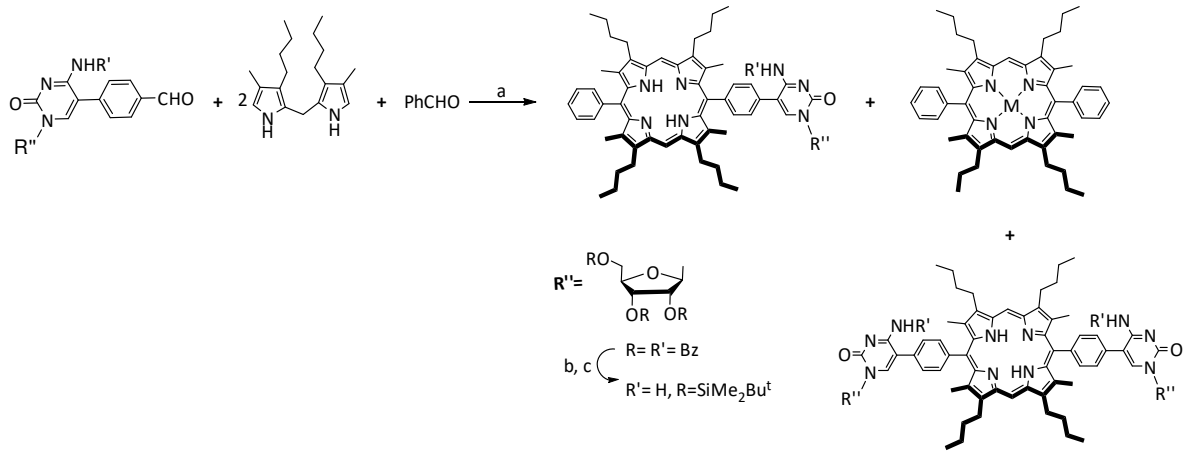

Figure 13: Synthesis of porphyrin bearing cytosine for assemblies II and III, (a) (i) TFA, CH_2Cl_2, argon, room temperature, 7 h; (ii) NaOAc, 1 h; (iii) p-chloranil, room temperature, overnight, (b) NH_3/MeOH, room temperature, 36 h. (c) TBDMS-C1, imidazole, DMF, room temperature, overnight.[16]

Uracil-functionalized porphyrins were described by C. M. Drain *et al.*[18] The primary objective was to synthesize porphyrin building blocks bearing complementary triple hydrogen bonding moieties represented in Figure 14. One of the porphyrins was functionalized by alkylated uracil moieties and the other by a pyridine derivative that binds uracil *via* 3 H-bonds. The functionalized porphyrins were prepared following the Adler[19] synthesis by reacting two different aldehydes with pyrrole that resulted in a mixture of 6 different porphyrins (Figure 15). This method was used because the five compounds bearing the H-bonding moieties are interesting building blocks to design potential self-assembled arrays.

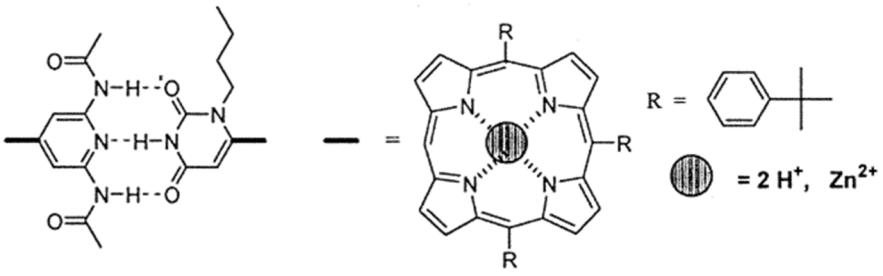

Figure 14: Schematic representation of potential assemblies of porphyrin building blocks *via* complementary H-bonding substituents. Figure modified from reference 18.

The targeted uracil-aldehyde, 1-butyl-6-formyluracil, was obtained by the protection of the aldehyde function of 6-formyluracil, followed by an alkylation of the N1 site with n-butylbromide, and then the deprotection of the aldehyde function. 1-butyl-6-formyluracil was reacted with 4-tert-butylbenzaldehyde and pyrrole in a mixture of nitrobenzene and acetic acid in the presence of zinc acetate (Figure15). This reaction resulted in six different porphyrins, which were separated by column chromatography. To increase the yield of the four porphyrins bearing **U**, the number of equivalent of 1-butyl-6-formyluracil was increased, the concentration of the mixture was decreased, and 4-tert-butylbenzaldehyde was added 10 minutes after adding the uracil aldehyde to pyrrole.

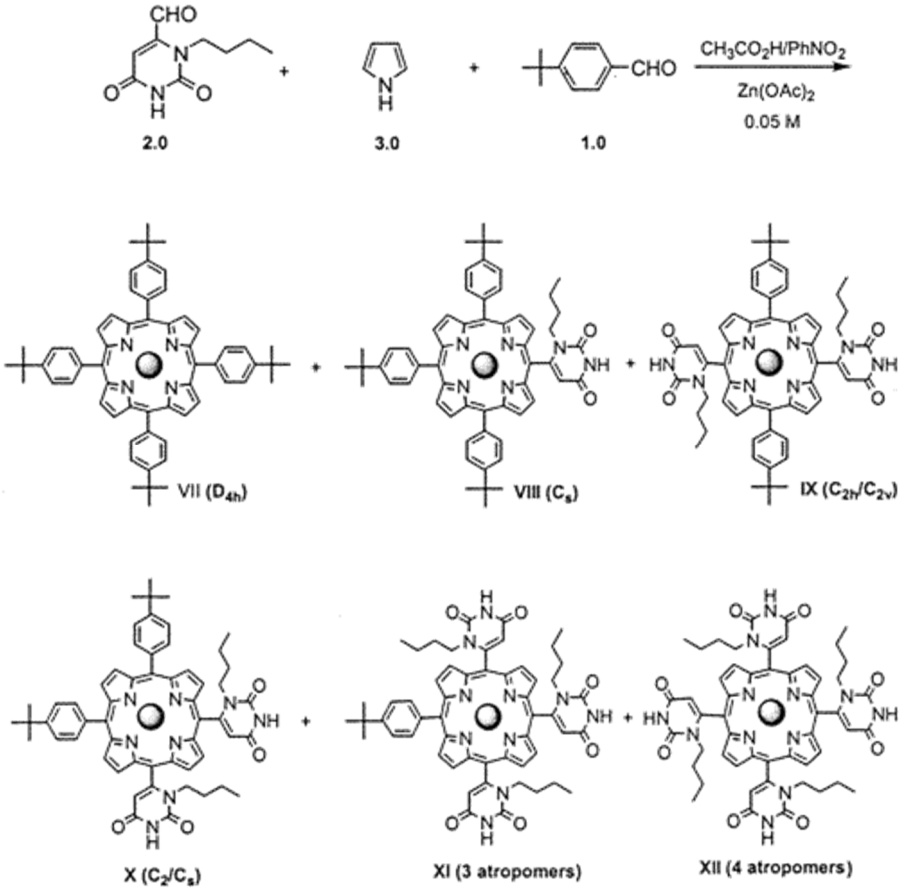

Figure 15: Reaction scheme for porphyrin bearing uracil. Figure taken from reference 18.

The solubility of the *cis* disubstituted porphyrin is expected to be less than that of the *trans* isomers due its greater polarity. However, the disubstitued *cis* uracil-porphyrin was found to be more

soluble than the *trans* isomer. This could be due to the self-complementary H-bonded assembly of linear polymeric tapes formed between the *trans* isomers *vs* the closed tetrameric squares assembly of the *cis* isomers. The *cis* isomer bearing complementary hydrogen bonding sites forms a tetrameric square assembly proven by ^{1}H-NMR and ESI-MS analysis. Moreover, these studies showed that the complementary interactions between the uracil and pyridyl moieties are stronger than their self-complementary interactions (Figure 16).

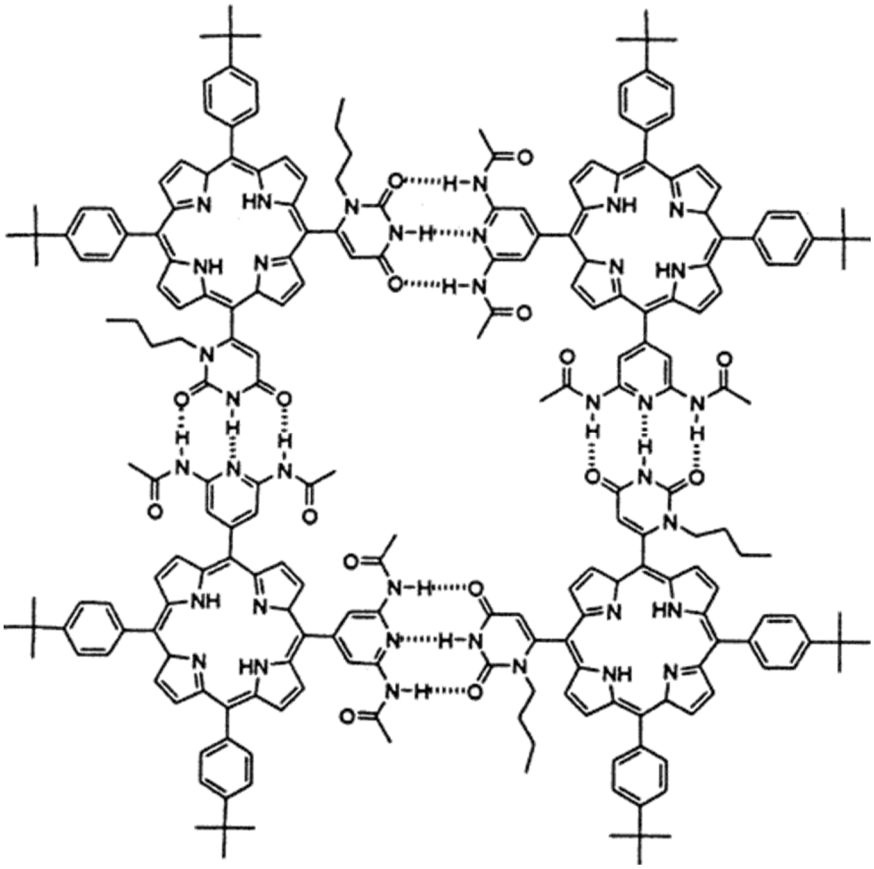

Figure 16: The tetrameric square assembly formed from the *cis* isomers. Figure taken from reference 18.

Other strategies such as Pd-catalyzed cross coupling reactions have been used to introduce nucleobases into the *meso* positions of porphyrins. An example reported by J. L. Sessler[20] described the Sonogoshira cross coupling reaction between a porphyrin bearing a triple bond and an iodinated cytosine derivative. 5-iodocytidine (a cytosine substituted by a sugar moiety at the N_1 position) and 5-(4-ethynylphenyl)-10,15,20-triphenylporphyrin were reacted with palladium tetra-triphenyl phosphine ($Pd(PPh_3)_4$) and copper iodide (CuI) in toluene in the presence of

trimethylamine (Et_3N) at 50 °C, resulting in the targeted cytosine functionalized porphyrin. The latter was used to generate a dyad, with a guanine functionalized fullerene C60, that undergoes photoinduced electron transfer (PET) (Figure 17). The dyad was assembled *via* three H-bonding between **C** and **G**, where the electron transfer takes place from the zinc porphyrin to the fullerene through the **G**-**C** Watson Crick H-bonding.

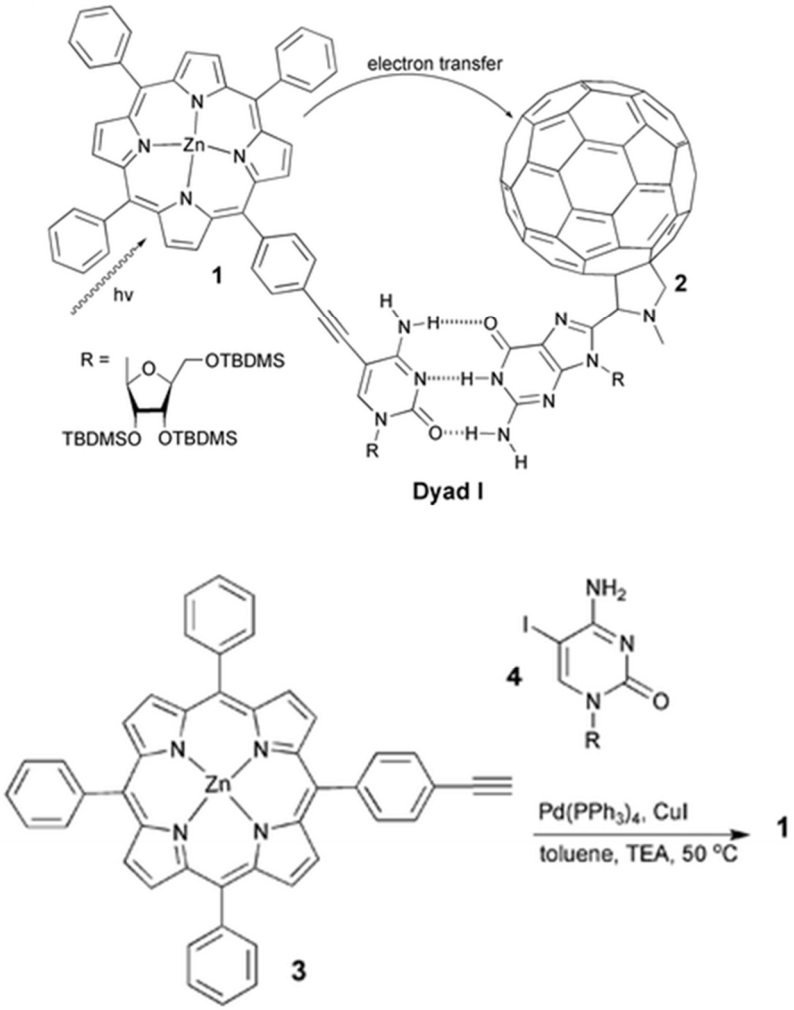

Figure 17: (Top) The self-assembly of the dyad through G-C interaction. (Bottom) The reaction Scheme of the porphyrin synthesis. Figure taken from reference 20.

Another pathway could be followed to introduce nucleobases into the *meso* positions of porphyrins, *via* Sonogashira coupling, which is to react a halogenated porphyrin with a nucleobase bearing a triple bond. This procedure was used by M. Balaz[21] in order to synthesize DNA-

templated porphyrin nanoassemblies.[22] The porphyrin functionalized by 2,6-diaminopurine (**DAP**), an adenine derivative, which has an extra amine function on position 2, interacts with thymine *via* 3 H-bonds instead of the 2 H-bonds between **T**-**A** (Figure 18).

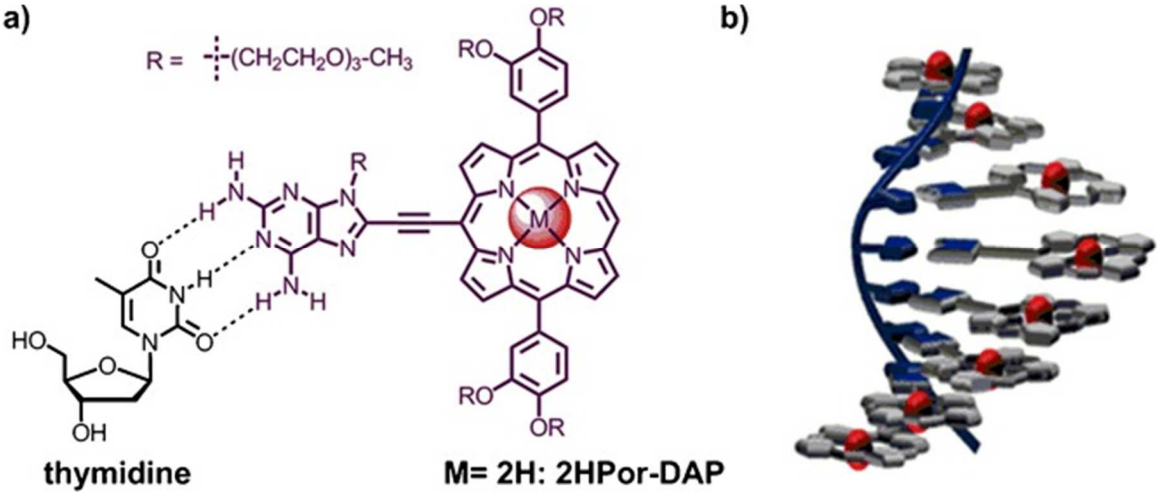

Figure 18: a) Hydrogen bonding between porphyrin–diaminopurine conjugate (2HPor-DAP) and thymidine. (b) representation of right-handed DNA-templated multiporphyrin nanoassembly. Figure taken from reference 21.

The 12-steps synthetic pathway is depicted in Figure 19. The first step is to protect the N9 position of **DAP** in order to avoid any by-products and to increase its solubility. The **DAP** was deprotonated by NaH and reacted with triethylene glycol monomethyl ether tosylate to produce N-triethyleneglycol–**DAP**, which was then brominated by N-bromosuccinimide (NBS) in the C8 position. The brominated **DAP** was reacted with mono(trihexylsilane)acetylene under Sonogashira cross-coupling conditions ($Pd_2(dba)_3$, PPh_3, and CuI in piperidine) to yield the trihexylsilane-diaminopurine– acetylene conjugates. In parallel, the Zn (II) porphyrin was prepared by Lindsey's acid-catalyzed condensation of dipyrromethane with substituted 3,4-dihydroxy-benzaldehyde, followed by a metalation with zinc acetate. The bromination of the porphyrin was performed using NBS. The trihexylsilane protection group on the **DAP** was removed with TBAF to give the diaminopurine–acetylene that was coupled with the bromoporphyrin, under Sonogashira cross-coupling conditions, resulting in the diaminopurine-porphyrin conjugate ZnPor-DAP. The 2HPor-**DAP** was obtained after demetallation of ZnPor-**DAP** using TFA.

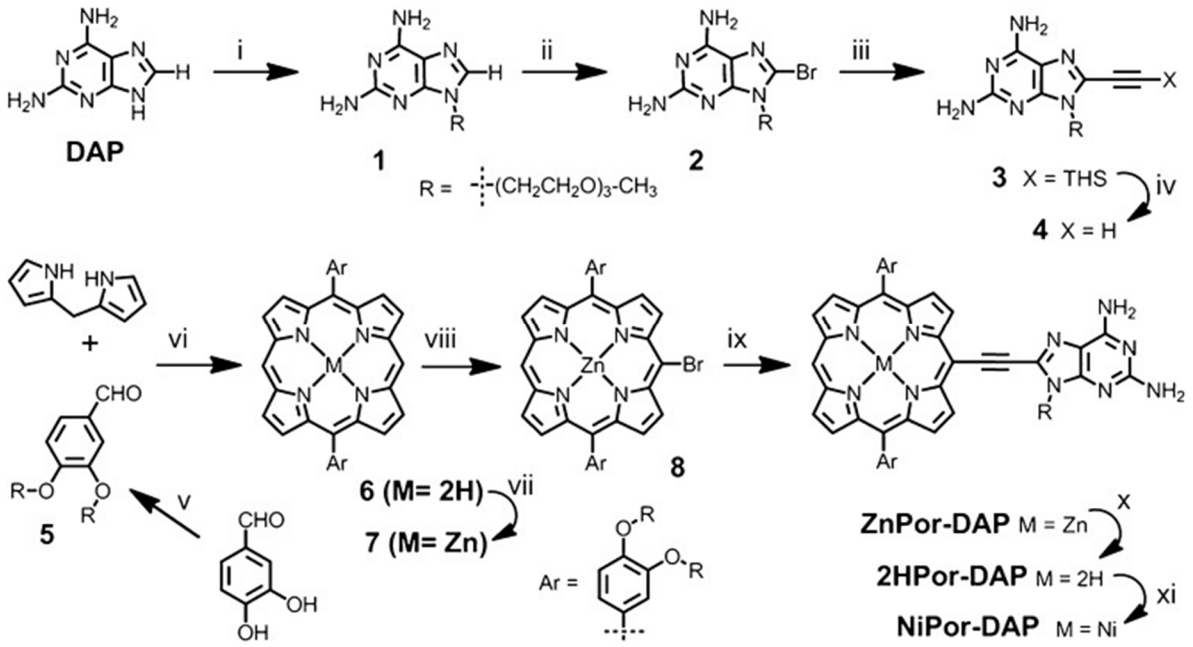

Figure 19: Synthesis of porphyrin–diaminopurine conjugates. (i) 1) NaH, DMF, 60 °C, 2 h, 2) 2-(2-(2-methoxyethoxy)ethoxy)ethyl 4-methylbenzenesulfonate, 0 °C, 7 h. (ii) N-bromosuccinimide (NBS), CH_3CN, RT, 1.5 h. (iii) $Pd_2(dba)_3$, Ph_3P, ethynyltrihexylsilane , CuI, piperidine, 40 °C, 4 h. (iv) tetra-n-butylammoniumfluoride (TBAF), CH_2Cl_2, RT, 30 min. (v) triethylene glycol monomethyl ether tosylate, K_2CO_3, CH_3CN. (vi) trifluoroacetic acid (TFA), then 2,3-dichloro-5,6-dicyano-1,4-benzoquinone (DDQ); (vii) $Zn(OAc)_2 \cdot 2H_2O$, $CHCl_3$, CH_3OH, RT. (viii) NBS, $CHCl_3$, C_5H_5N.(ix) **4**, $Pd_2(dba)_3$, PPh_3, CuI, DMF, triethylamine (TEA), 40 °C, 15 h. (x) TFA, CH_2Cl_2, RT, 4 h. (xi) $Ni(OAc)_2 \cdot 4H_2O$, DMF, 120 °C, 4 h. Figure taken from reference 21.

N. R. Champness et *al* [23] have reported the synthesis and the surface based assembly of thymine functionalized porphyrin tecton. The targeted tectons is a tetra-(phenylthymine)porphyrin (tetra-TP) for surface-based self-assembly studies, and a mono-thymine-tri-(3,5-di-*tert*-butylphenyl) porphyrin (mono-TP) was used as a model compound to probe the nature of intermolecular interactions in solution.

The tetra-TP was synthesized by reacting a protected thymine derivative, 1-formylphenyl-3-benzoyl-thymine, with a large excess of pyrrole using TFA to initiate the reaction, followed by an oxidation with DDQ. The deprotection [24] of the thymine moieties was performed using NH_4OH in THF to yield the targeted tecton (Figure 20).

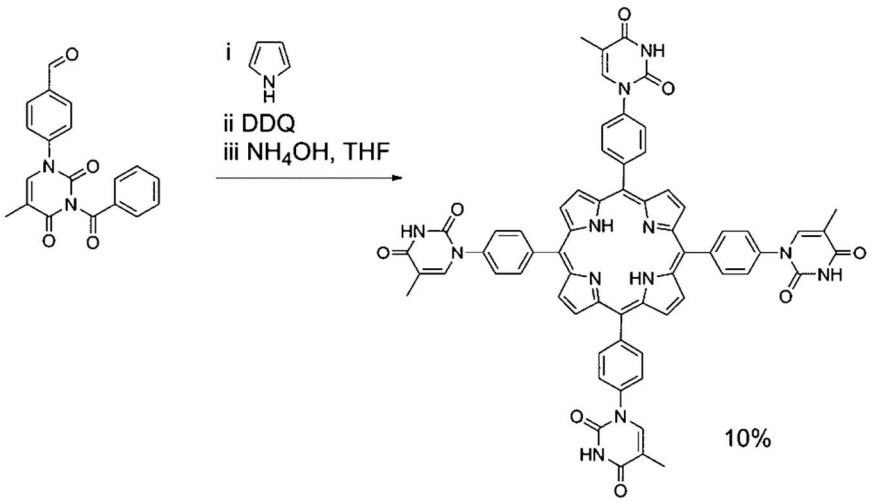

Figure 20: Synthetic route used for the preparation of tetra-TP. Figure taken from reference 23.

The thymine moieties were linked to the porphyrin core by phenyl groups so that the porphyrin and the thymine could be co-planar and parallel to the surface, on which the molecules will be deposited. A small quantity of saturated solution of tetra-TP was deposited onto a HOPG substrate. STM images showed the self-assembly of tetra-TP molecules displaying square-grid like networks stabilized by inter-thymine H-bonds (Figure 21).

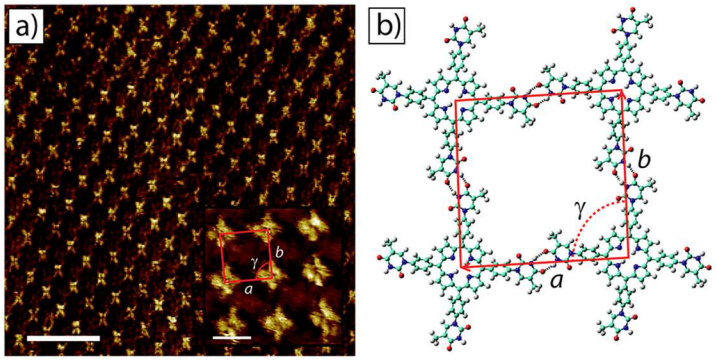

Figure 21: (a) 2D tetra-TP self-assembled network at the TCB–HOPG liquid–solid interface. (b) Large scale STM image of tetra-TP network. Figure taken from reference 23.

Mono-TP was synthesized in two steps (Figure 22). The first step involved the reaction of 1-formylphenyl-3-benzoyl-thymine (protected thymine) with a large excess of pyrrole in the presence of $InCl_3$, and afforded the desired dipyrromethane. The latter was reacted with a suitable

tert-butyl functionalized carbinol species, using Lindsey's approach,[25] in the presence of TFA, and then oxidized by DDQ. A subsequent deprotection of the benzoyl-protected thymine was achieved using NH_4OH. The *tert*-butyl functionalized appendages increases the porphyrin's solubility and allow studies in solution. (Figure 22)

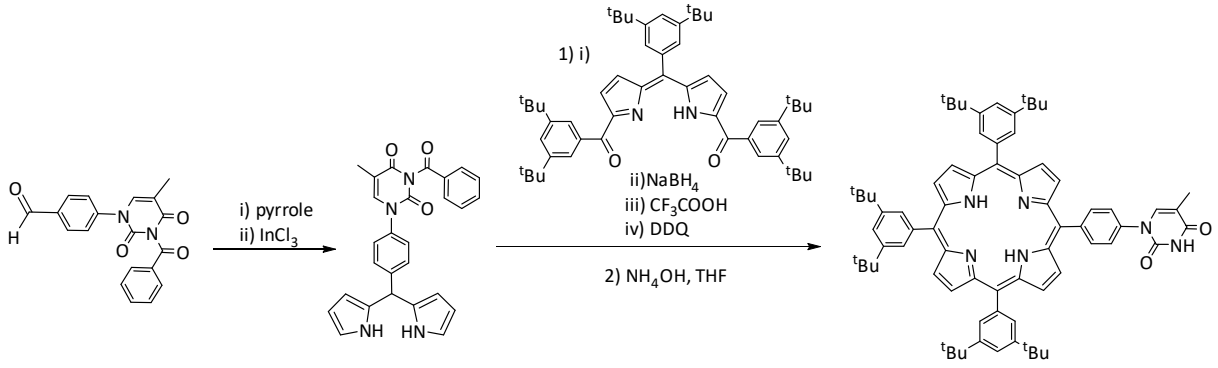

Figure 22: Synthesis of Mono-TP.

The crystal structure of the mono-TP (Figure 23) shows the nature of the intermolecular interactions between thymine-substituted porphyrins. A double hydrogen-bonding interaction is observed between thymine moieties of adjacent molecules. The thymine approaches in a coplanar fashion the porphyrin core. As for the phenyl ring between the porphyrin and the thymine, it adopts an orientation that approaches in an orthogonal mode the porphyrin plane. Moreover, adjacent molecules pack *via* π–π interactions between a thymine moiety of one molecule and a pyrrole of an adjacent molecule.

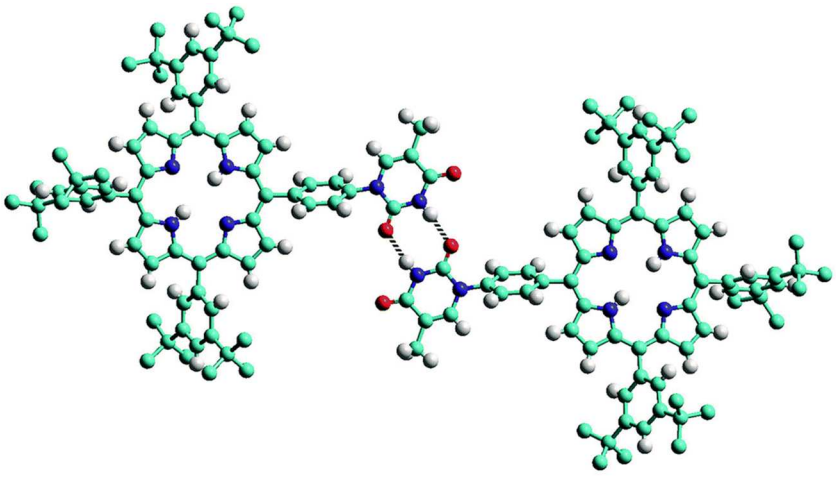

Figure 23: The single crystal X-ray structure of mono-TP illustrating the formation of the thymine double hydrogen-bonding interaction. Figure taken from reference 23.

II. 2. Aim of the Project

The aim of the project is to synthesize a library of new di or tetra-functionalized NB porphyrin based tectons (Figure 24). As discussed previously, several strategies could be followed to prepare porphyrin bearing nucleobases. We focused on two strategies based on Pd-catalyzed cross coupling reactions and alkylation reactions between appropriate starting materials, linking the porphyrin and the nucleobases through C-C or C-N bond respectively.

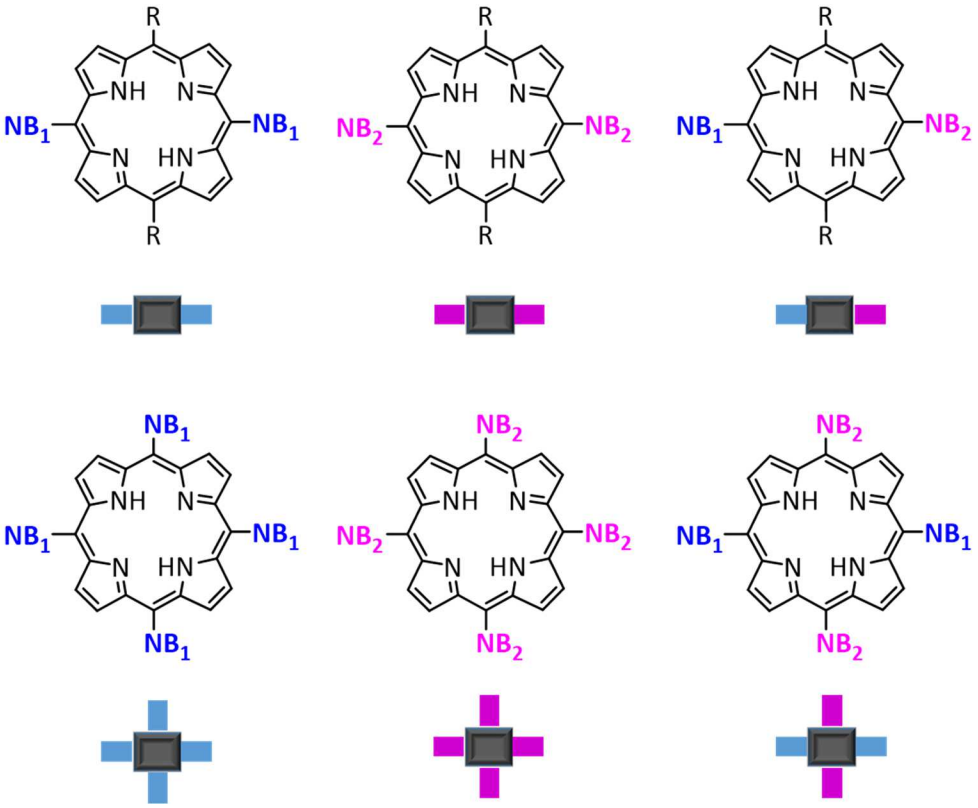

Figure 24: Schematic representation of the targeted tectons. NB_1 and NB_2 are complementary nucleobases and R is a solubilizing substituent.

Nucleobases are known for their complementary base pairing property and their self-assembly into polymeric architectures. Playing on the nature and the number of NBs on a porphyrin scaffold can result in several potential molecular networks. Introducing NBs in two *trans* positions could lead to 1D polymeric assemblies, and introducing them into the four *meso* positions could even lead to 2D architectures formed by NB H-bonding (Figure 25). NBs have low solubility in aprotic solvent, therefore some solubilizing substituents (represented by R) are used to increase the solubility of the final targeted porphyrin tectons.

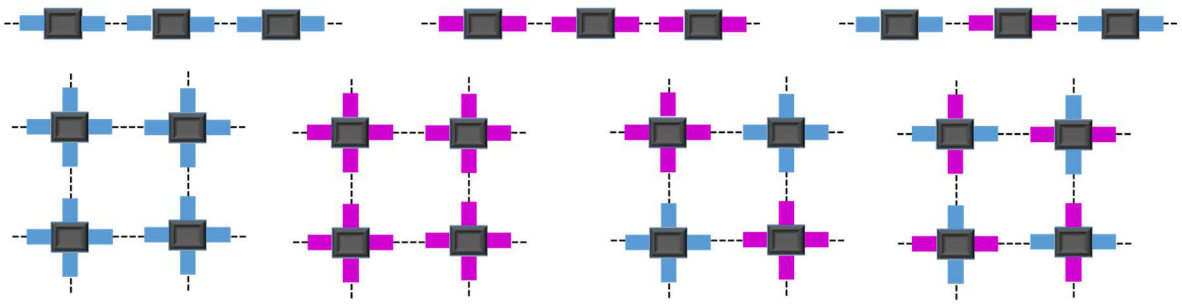

Figure 25: Schematic representations of 1D (top) and 2D (bottom) H-bonded networks using the targeted tectons.

Moreover, metallation of the porphyrin scaffold can assist in the formation of more complex networks of higher dimensionality, by introducing for example bidentate coordinating ligand in the apical position of the metallic center.

II. 3. Porphyrin Bearing NB *via* C-C bond

To synthesize the targeted tectons, we focused on strategies involving Pd-catalyzed cross coupling reactions (either Suzuki or Sonogashira) as key steps, thus leading to the formation of a C-C linkage between the NBs and the porphyrin scaffolds. A three-part procedure was considered to generate the *trans* A_2B_2 final tectons (Figure 26). The first part consists in the synthesis of the corresponding *meso*-substituted starting porphyrins: either a porphyrin bearing two boron moieties in *trans* positions or a *trans meso*-bisethynylporphyrin for Suzuki and Sonogashira cross coupling reactions respectively. In both cases, the two remaining *trans* positions were occupied by C5 alkyl chains in order to increase the solubility of the final porphyrin. The second part deals with the halogenation of the nucleobase and the protection of the N1 position of pyrimidines and the N9 position of purines to increase their solubility in aprotic solvents, and to avoid secondary reactions. The third and last part is the coupling of the porphyrins and the nucleobase derivatives under Suzuki or Sonogashira conditions.

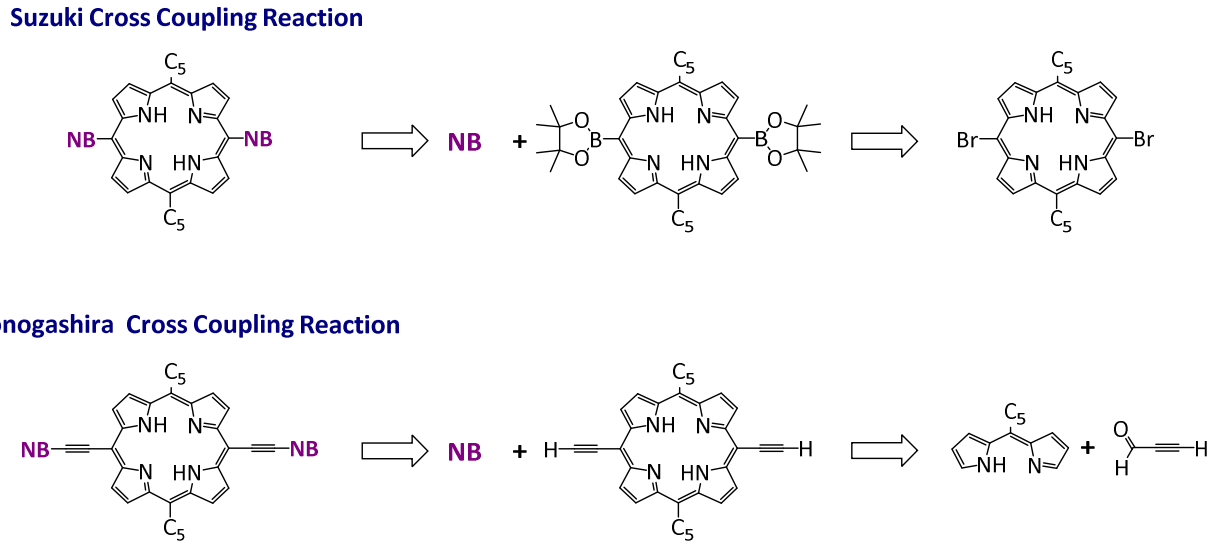

Figure 26: Retrosynthesis of *trans*-A_2B_2 porphyrin bearing NBs following Suzuki and Sonogashira C-C coupling.

First we attempted to connect NB to porphyrins *via* Suzuki Coupling (Figure 26). 10,20-dipentyl-porphyrin was synthesized, then brominated and reacted with 4,4,5,5-tetramethyl-1,3,2-dioxaborolane leading to a mixture of mono-boronated and diboronated porphyrins (Figure 27).[26] The first attempt was made by using the commercially available 5-bromouracil (**Br-U**). The latter was protected by a benzylhydryl group following a known procedure, which will be discussed later in detail.[32] The Suzuki cross coupling reaction between the protected **Br-U** and the mono-boronated porphyrin was performed under different conditions. For example, $Pd(PPh_3)_4$ and $Pd(OAc)_4$ catalysts were used in DMF, dioxane or in a mixture of THF: MeOH: H_2O in the presence of a base, such as K_2CO_3, KOAc or Cs_2CO_3. Unfortunately, the coupling was never successful. By following the reactions by TLC, we could observe in all cases the deboronation of the porphyrin instead of the formation of a new product.

Since Suzuki cross coupling reaction was not successful, we focused on the coupling of porphyrins bearing ethynyl substituents in *meso* positions with NB derivatives under Sonogashira cross coupling conditions (Figure 26). TMS protected ethynyl porphyrins were synthetized and reacted with NB under a one-pot procedure.

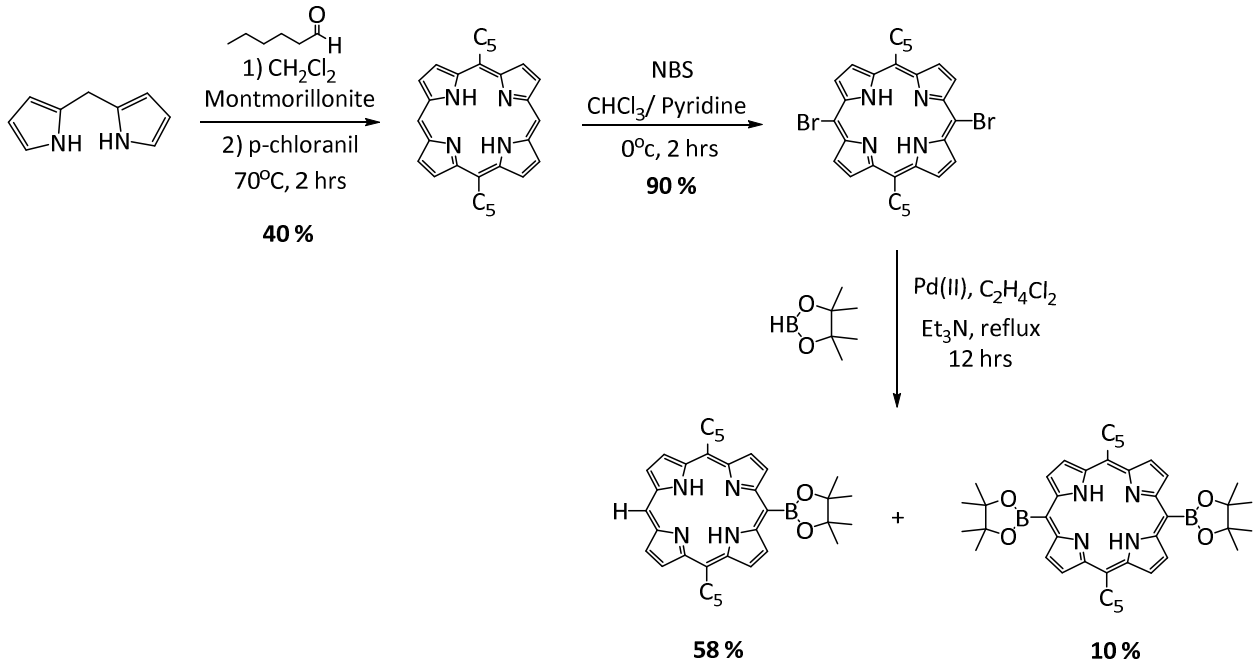

Figure 27*:* Synthesis and boronation of 10,20-dipentyl-porphyrin.

II. 3. a) Synthesis of Zn(II)[5,15-di(trimethylsilylethynyl)-10,20-dipentylporphyrin](Zn-Po1)

The synthesis of the targeted porphyrin following the Macdonald[27] [2+2] condensation was performed following a procedure described for similar diethynyl-porphyrins.[28] The starting 5-pentyl-dipyrromethane (C5-DPM) was synthesized following the procedure described by J. S. Lindsey.[29] Hexanal was reacted with an excess of pyrrole in the presence of TFA under argon at room temperature to yield 47 % of C5-DPM. The latter was reacted with ethynyltrimethylsilane and $BF_3.Et_2O$ in dichloromethane (DCM) then oxidized with DDQ leading to 5,15-dipentyl-10,20-(trimethylsilylethynyl)porphyrin (**Po1**) in 38 % yield. The metallation of the porphyrin was performed in 90% yield, upon addition of zinc acetate in methanol to a solution of **Po1**-leading to the Zn(II) [5,15-di(trimethylsilylethynyl)-10,20-dipentylporphyrin] (**Zn-Po1**) (Figure 28).

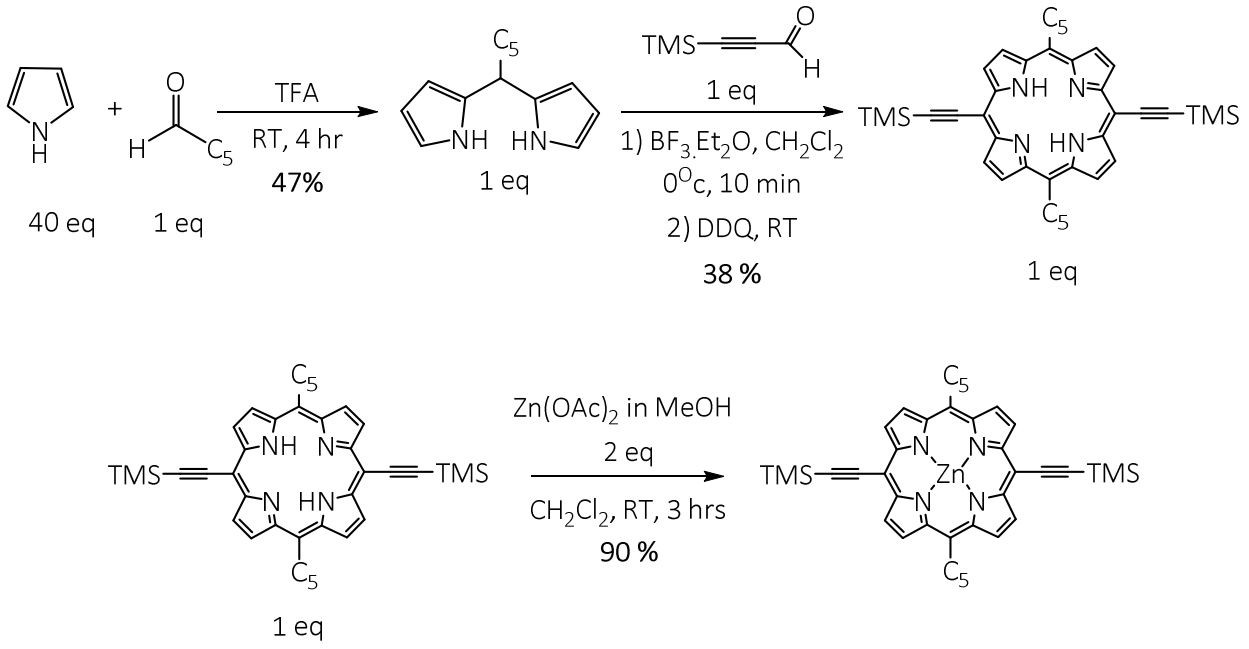

Figure 28: Synthetic scheme of **Zn-Po1**.

II. 3. b) Protection of 5-iodoUracil

Commercially available 5-iodouracil (**I-U**) is insoluble in usual organic media. Moreover, the tautomeric forms and the low solubility of uracil might affect the yield of the final cross coupling reaction.[30] Therefore, the insertion of a solubilizing protecting group in the N1 position is necessary in order to increase the solubility of the halogenated NB. Direct substitution of uracil could lead to a mixture of monosubstituted and disubstituted products, which blocks the Watson-Crick H bonding sites.[29, 31] Hence, the choice of the protecting group should fit certain criteria, such as a regioselective insertion on the targeted N1 site that is not involved in the Watson-Crick H-bonding and mild conditions for the protection and deprotection steps. The protection of 5-iodouracil with benzylhydryl group, described by D. F. Weaver et *al.*[32] fits these criteria. The substitution of benzylhydryl group is selective to the most active and least hindered amine site, which is in our case the targeted N1 site. In acidic medium, the deprotection is quantitative and fast without any effects on the functional groups of the uracil analogue. Therefore, we proceeded with the protection of uracil by benzylhydryl group (Figure 29).

I-U was reacted with bis(trimethylsilyl)actamide (BSA) in acetonitrile, followed by the treatment with benzylhydryl bromide in the presence of a catalytic amount of I_2 to yield 55 % of N1-(benzylhydryl)-5-iodouracil (**I-U-Ph$_2$**) which was characterized by ^{1}H-NMR and ^{13}C-NMR.

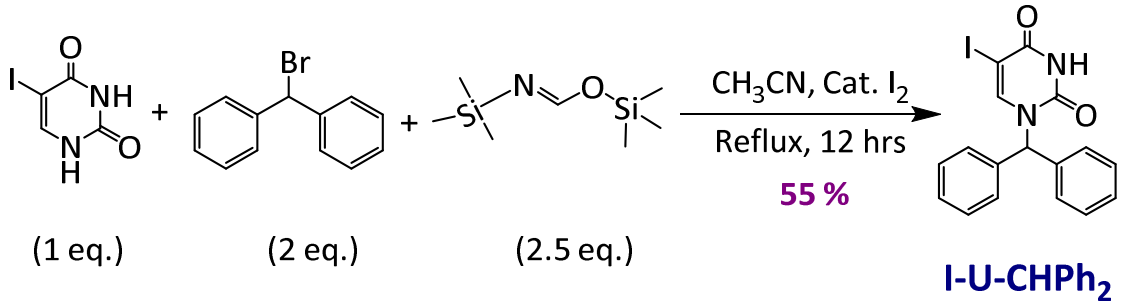

Figure 29: Synthesis of **I-U-Ph$_2$**.

II. 3. c) Synthesis of Zn(II) [5,15 -di(N$_1$-(benzylhydry)uracil)- 10,20-dipentylporphyrin] (T1)

Sonogashira cross coupling is based on a Pd-catalyzed reaction in the presence of a base and CuI. However, other conditions were proven to be as effective as the classical conditions.[33] To synthesize the targeted porphyrin bearing uracil tecton, we first followed a modified version of the one pot Sonogashira coupling reactions.[34] $Pd(PPh)_2Cl_2$ was used as a catalyst and $AsPh_3$ as a co catalyst instead of CuI, to avoid any metallation of the porphyrin core. One equivalent of **Zn-Po1** and 2.2 equivalent of **I-U-Ph$_2$** were treated with 1 M TBAF solution in THF. The deprotection of the TMS functions proceeded instantly and was confirmed by TLC. Then $AsPh_3$ (1.2 eq.) and a catalytic amount of $Pd(PPh)_2Cl_2$ (0.25 eq.) were added under argon to the mixture (Figure 30). The targeted porphyrin **T1** is formed after 3 hours under reflux and isolated in 88% yield. **T1** was characterized by different means such as NMR, UV, IR, HRMS. Moreover, many attempts to crystalize **T1** aiming to grow single crystals suitable for X-Ray diffraction were performed using different conditions. Unfortunately, single crystals suitable for X-Ray analysis were not obtained.

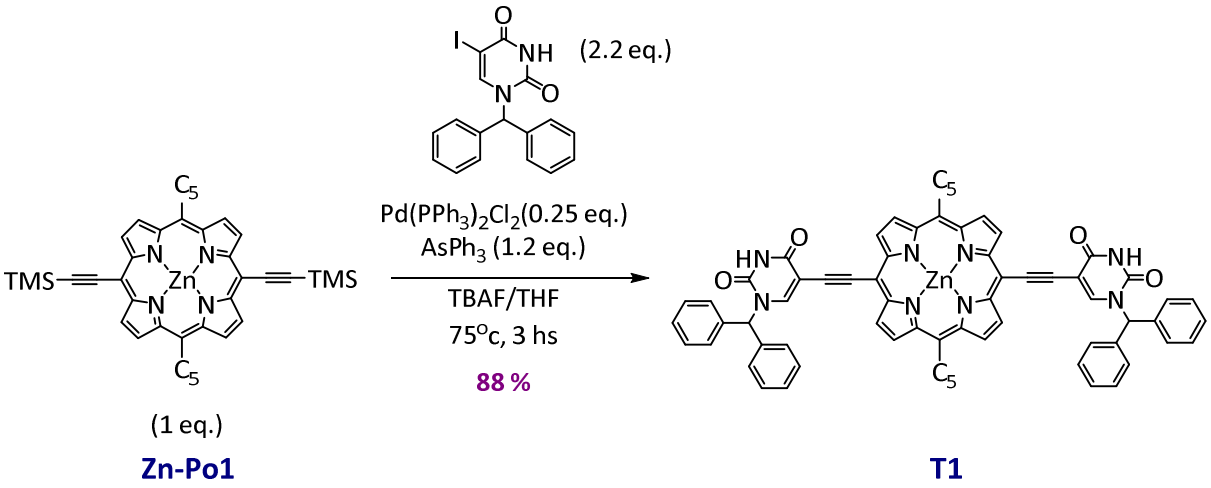

Figure 30: Synthesis of **T1**.

II. 3. d) Deprotection of T1

Then, we proceeded in deprotecting the uracil moieties targeting a less hindered tecton that can self-assemble into H-bonded networks (Figure 31).

Following a procedure reported to deprotect uracil, **T1** was treated with 10 % of triflic acid in TFA solution at 0 °C for 2 hours.[31] Upon adding ice to the reaction, a green precipitate of 5,15-diuracil-10,20-dipentylporphyrin (**T2**) was formed with a yield of 80 %.

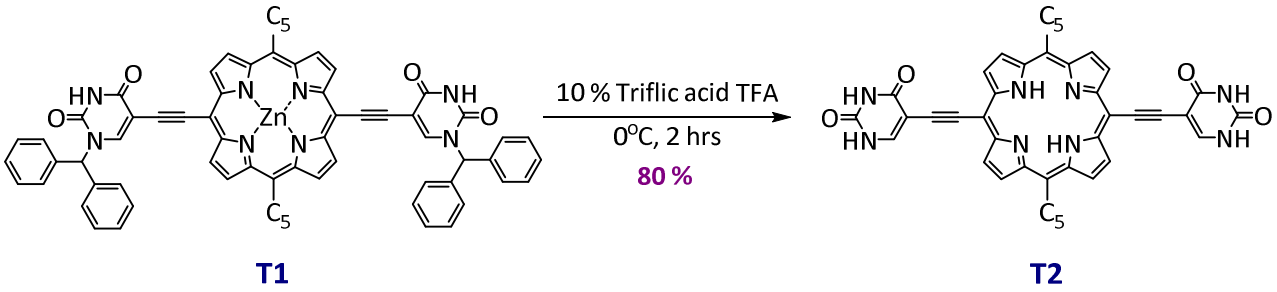

Figure 31: Deprotection of the Uracil moieties of **T1**, and formation of **T2**.

Due to the strong acidic conditions, demetallation of the porphyrin cavity occurs during the course of the reaction, leading the free base porphyrin **T2**. The UV-Vis spectrum of **T2** compared to **T1** is shown in Figure 32. Moreover, upon addition of HCl vapor to a solution of **T2**, its UV-Vis spectrum shifts verifying that **T2** is a neutral free base porphyrin.

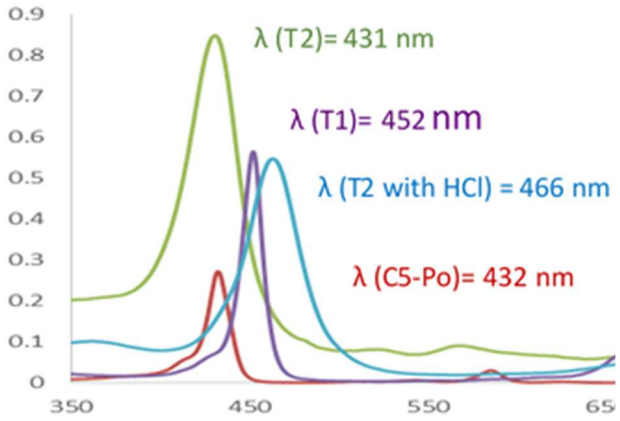

Figure 32: UV-Vis analysis of **Po1**, **T1**, and **T2**

The poor solubility of **T2** in $CDCl_3$ and d6-DMSO made it impossible to acquire a clear NMR spectrum. However, **T2** was successfully characterized by HRMS, IR and UV-Vis. Due to its poor solubility, all the attempts to grow single-crystals of **T2** failed.

II. 3. e) Iodination and Alkylation of NBs

To functionalize a porphyrin with cytosine and adenine, the iodination of the nucleobases was performed using described procedures.[31] Moreover, the benzylhydryl group used to protect the N1 site of uracil was replaced by a C6 alkyl chain, in order to decrease the steric hindrance around the NBs H-bonding sites and also to increase the solubility of the targeted tectons. Alkylation reaction of the nucleobases was accomplished using reported conditions with the highest yields.[31]

II. 3. e) 1) Alkylation of 5-iodouracil

The reported procedure is to react one equivalent of 5-iodouracil with 1.2 equivalent of 1-iodohexane (I-C_6) with Cs_2CO_3 in dry DMF resulting in the formation of the N1-alkylated uracil in 16% yield.[31] In order to increase the reported yield, we tried to modify the described procedure. First, Br-C_6 was used instead of I-C6 following the reported conditions. The reaction resulted in a mixture of mono-substituted and di-substituted products that were separated by column chromatography to yield 21 % of N1-hexyluracil and 48 % of N1, N3-dihexyluracil. Second, 5-iodouracil was used in excess and bromohexane was used as limiting reagent. Two equivalents of

iodouracil was reacted with 1.3 equivalent of Cs_2CO_3 and 1 equivalent of 1-bromohexane in dry DMF at 40 °C to yield 94 % of the targeted product **I-U-C$_6$** (Figure 33).

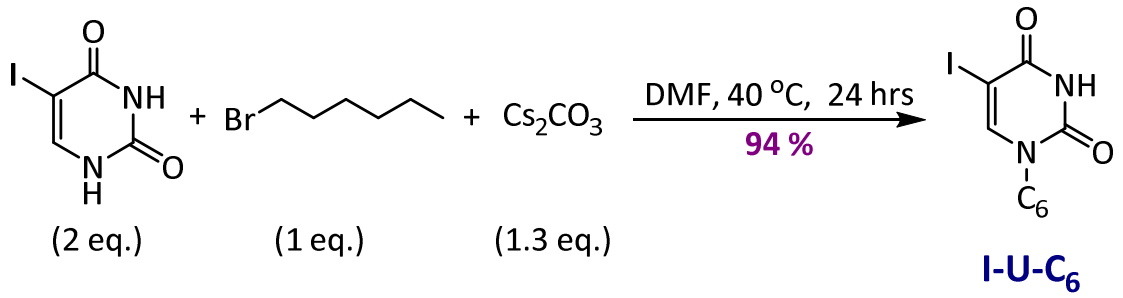

Figure 33: Synthesis of **I-U-C$_6$**.

II. 3. e) 2) Iodination and alkylation of cytosine

To synthesize 5-iodo-N_1-hexylcytosine (**I-C-C$_6$**), we reproduced the described two-step procedure.[31] Cytosine was treated with 1.5 equivalent of iodine and 1.4 equivalent of iodic acid in acetic acid to result in 94 % of 5-iodo-cytosine (Figure 34). The latter was reacted with bromohexane in DMF in the presence of K_2CO_3 to yield 40 % of the targeted **I-C-C$_6$**. The yields obtained are similar to those reported.

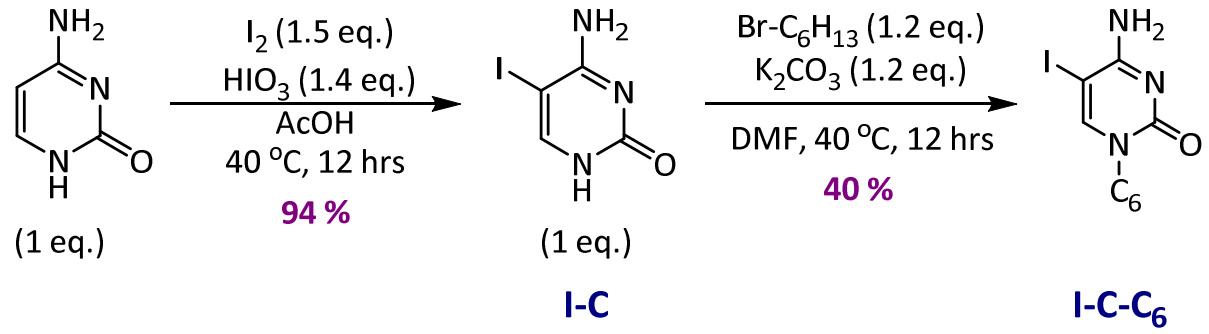

Figure 34: Synthesis of **I-C-C$_6$**.

II. 3. e) 3) Iodination and alkylation of Adenine

The alkylation of adenine followed by its iodination was reported to be more effective and resulted in a higher yields.[31] Therefore, to synthesize N_9-hexyl-8-iodoadenine (**I-A-C$_6$**), we followed the described two-step procedure reported for the alkylation and iodination of similar compounds (**I-**

A-C$_2$ and **I-A-C$_{10}$**). Adenine was first reacted with one equivalent of 1-bromohexane in the presence of 1.2 equivalent of K_2CO_3 in dry DMF to yield 90 % of N_9-hexyladenine. The alkylated adenine was then treated with one equivalent of periodic acid (H_5IO_6) and catalytic amount (0.38 eq.) of I_2 in dry DMF to result 60 % of the final targeted **I-A-C$_6$** (Figure 35).

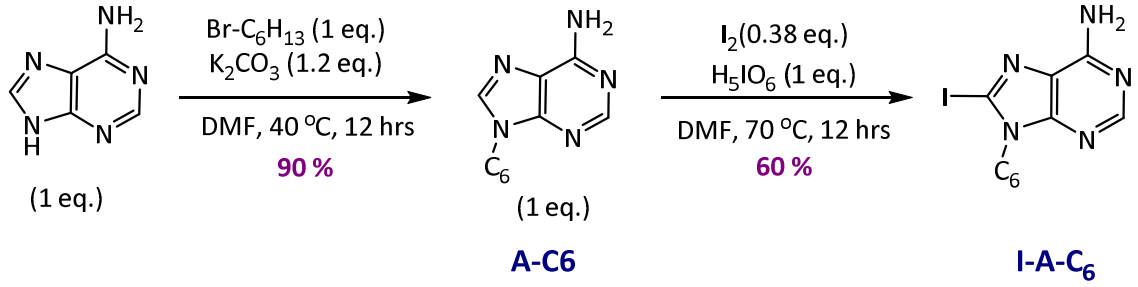

Figure 35: Synthesis of **I-A-C$_6$**.

II. 3. f) Synthesis of Zn(II) [5,15 -di(N_1-hexyluracil)- 10,20-dipentylporphyrin] (T3)

Zn(II)[5,15-di(N_1-hexyluracil)-10,20-dipentylpoprhyrin (**T3**) was synthesized following the same one-pot procedure used to synthesize **T1**. **Zn-Po1** was reacted with **I-U-C$_6$**, $Pd(PPh_3)_2Cl_2$ and $AsPh_3$ in 1 M TBAF solution in THF under argon for 3 hours heated under reflux (Figure 36). After purification by column chromatography and on bio-beads, **T3** was isolated in 80 % yield.

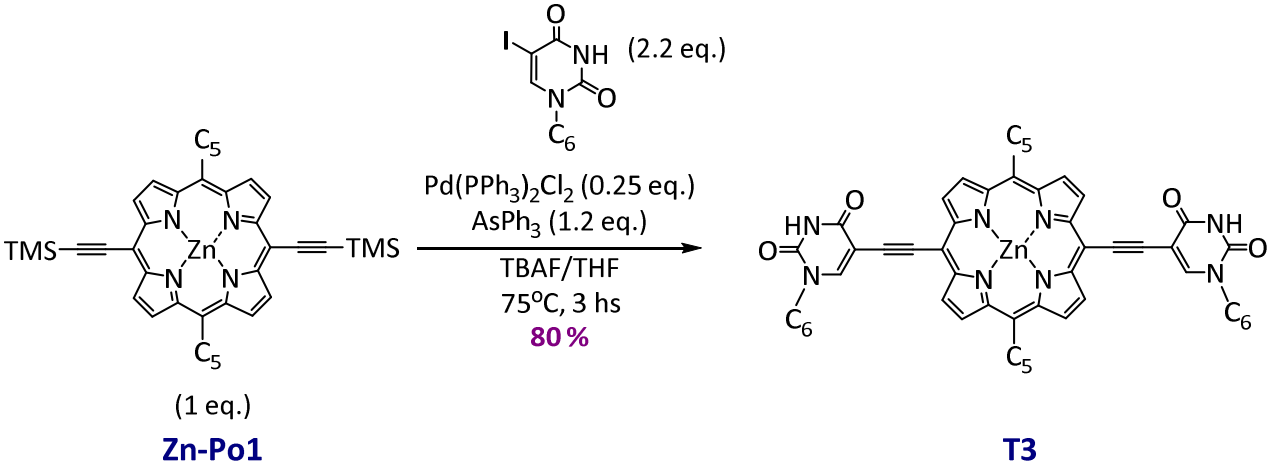

Figure 36: Synthesis of **T3**.

T3 was characterized by NMR, UV-Vis, IR, and HRMS. Due to the poor quality of the crystals, we did not obtain the crystal structure of **T3** by X-Ray diffraction. Unfortunately, we faced a

problem in reproducing the cross coupling reaction between **Zn-Po1** and **I-U-C$_6$** because of the high reactivity of **Zn-Po1**, which undergoes side reactions. During trails to reproduce **T3,** the reaction was followed by TLC, which showed the gradual disappearance of the starting material (**Zn-Po1**) and the appearance of a dark polar product with a large different polarity than the targeted **T3** porphyrin.

II. 3. g) Cross coupling reaction of I-C-C$_6$ and Zn-Po1

We proceeded to introduce the second pyrimidine, cytosine, to the *meso* position of porphyrin by reacting **I-C-C$_6$** with **Zn-Po1** following the same conditions used for **T1** and **T3** (Figure 37). The reaction was followed by TLC, which showed the disappearance of the spot corresponding to **Zn-Po1**. After 3 hours, several dark polar spots were observed by TLC. The reaction was stopped and treated following the same procedure as for **T1** and **T3**. The crude was then purified by column chromatography using polar solvents to give several fractions. The ^{1}H-NMR spectrum of the fractions revealed that the targeted product was not produced. Instead, the NMR showed peaks attributed to the porphyrin with unprotected triple bonds and other porphyrins that we were not able to identified. Moreover, unreacted **I-C-C$_6$** was observed in one of the fractions. Therefore, we deduced that the cross coupling reaction of **I-C-C$_6$** and **Zn-Po1** was not successful under these conditions.

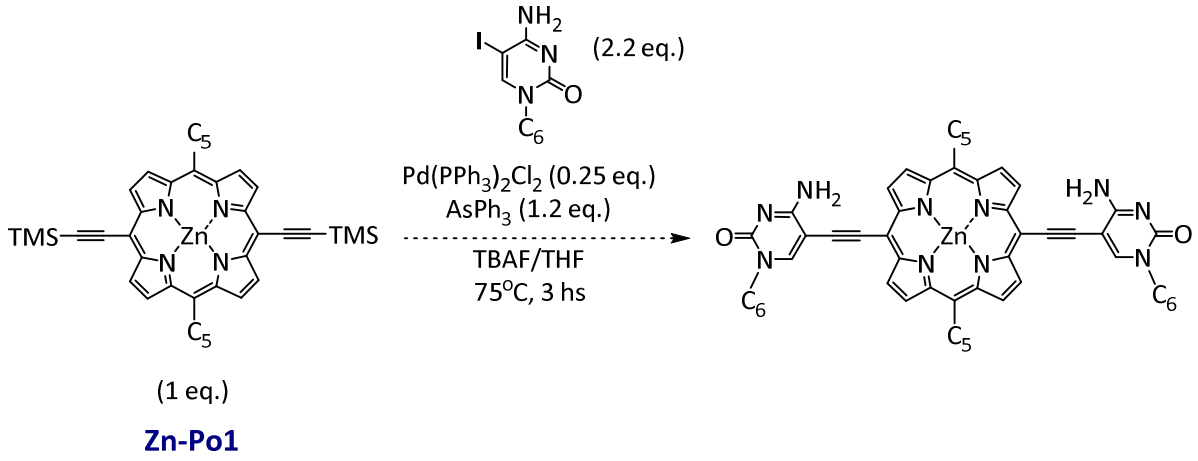

Figure 37: Synthetic strategy to introduce cytosine to **Zn- Po1**.

We thus run a test reaction using similar procedure, but replacing the **Zn-Po1** by a cheaper reactant with the similar reactivity: ((4-methoxyphenyl)ethynyl)trimethylsilane (CH_3O-Ph-TMS). The first step was to verify that the deprotection of the triple bond using TBAF in THF was effective. Therefore, the deprotection and the coupling reactions were achieved in two separate steps. The reaction of CH_3O-Ph-TMS with TBAF leads to the formation of the unprotected product: CH_3O-Ph treated in almost quantitative yield, as proven by the complete disappearance of the peak attributed for the TMS protecting group in the ^{1}H-NMR spectrum. In order to optimize the coupling reaction and test other conditions, we reacted CH_3O-Ph with **I-C-C$_6$** in the presence of $Pd(OAc)_2$ /PPh_3 (Figure 38). Under those conditions, the targeted molecule was obtained in 30 % yield. The low yield could be explained by the interaction of the Pd catalyst with cytosine, thus decreasing its ability to catalyze the coupling reaction and modifying the reactivity of **I-C-C$_6$**.

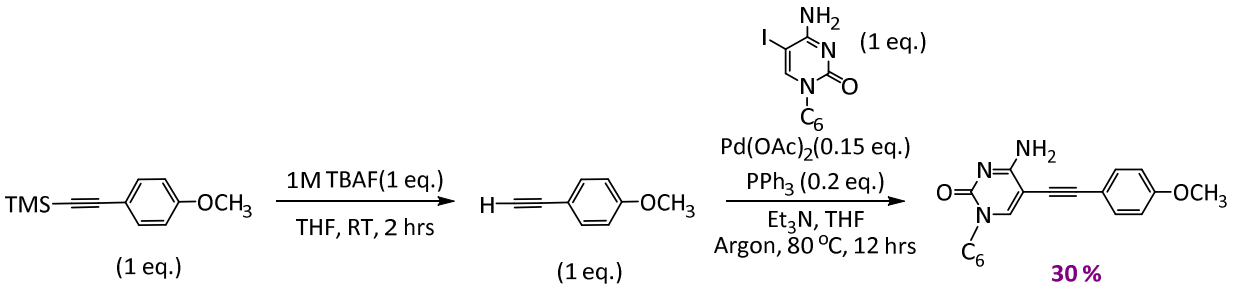

Figure 38: Test reaction for Sonogashira coupling with **I-C-C$_6$.**

We applied the same conditions to **Zn-Po1** and **I-C-C$_6$**. Unfortunately, we obtained a mixture of porphyrins that appeared to be difficult to purify. Moreover, the ^{1}H-NMR spectrum of the mixture did not show any peaks that could correspond to the presence of **I-C-C$_6$** at the periphery of the porphyrin. One explanation can be that the deprotection of the triple bond leads to a highly reactive porphyrin, which undergoes side reactions.

Since Sonogashira couplings between **Zn-Po1** and the **I-U-C$_6$** or **I-C-C$_6$** was not as efficient as expected, we tried to reverse the reactive sites, by introducing the triple bonds on the NBs, instead of introducing it on the porphyrin, and then to couple them with a 5,15-dibromoporphyrin (Figure 39). Following the known procedure for introducing a triple bond on **DAP** reported by M. Balaz (Figure 18 and 19),[21] we tried to react 8-Iodo-N$_9$-hexyladenin with trimethylsilylacetylene (TMSA) in the presence of CuI and $Pd_2(dba)_3$ in piperidine for 24 hours (Figure 39). The reaction was followed by TLC, which showed the synthesis of a new product. Unfortunately, ^{1}H-NMR and

MS showed that the new product is not the targeted adenine derivative; instead, it was the N_9-hexyladenine. Other conditions were used to obtain the targeted product, for example **I-A-C6** (1eq) was reacted with TMSA (2 eq.) in the presence of $Pd(PPh_3)_2Cl_2$ (0.1 eq.) and CuI (0.2 eq.) in a mixture of THF: Et_3N (4:1) at 40 °C for 24 hours. Unfortunately, under these conditions, the de-iodination took place as well.

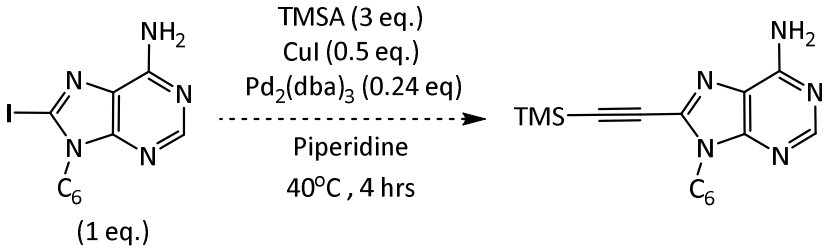

Figure 39: Reaction between **I-A-C6** and TMSA.

Since the Pd-catalyzed cross coupling reaction was not successful, we focused on more straightforward strategies to introduce nucleobases in the periphery of porphyrins and explore the possibility to link NBs to porphyrin *via* a C-N bond.

II. 4. Porphyrin Bearing NB via C-N bond

The substitution of N1 sites of pyrimidines and N9 sites of purine with different alkyl substituents were reported by various laboratories.[35] Moreover, the success we encountered in alkylating thymine, cytosine, and adenine inspired us to explore a new strategy, based on connecting the NBs at the periphery of porphyrins *via* C-N bonds. We first checked the procedure by reacting thymine with bromomethylbenzene (Figure 40). The latter was reacted in stoichiometric amount in the presence of K_2CO_3 in DMF resulting the targeted product with a yield of 60 %.

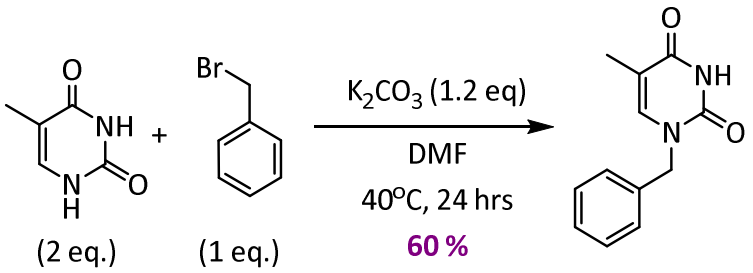

Figure 40: Test reaction of thymine substitution.

The test reaction proved that the substitution of thymine with an aromatic reagent bearing a bromine site can be successful. Therefore, we aimed to introduce either 2 or 4 NBs to a porphyrin bearing 2 or 4 *meso* (p-bromomethylphenyl) following the same strategy (Figure 41).

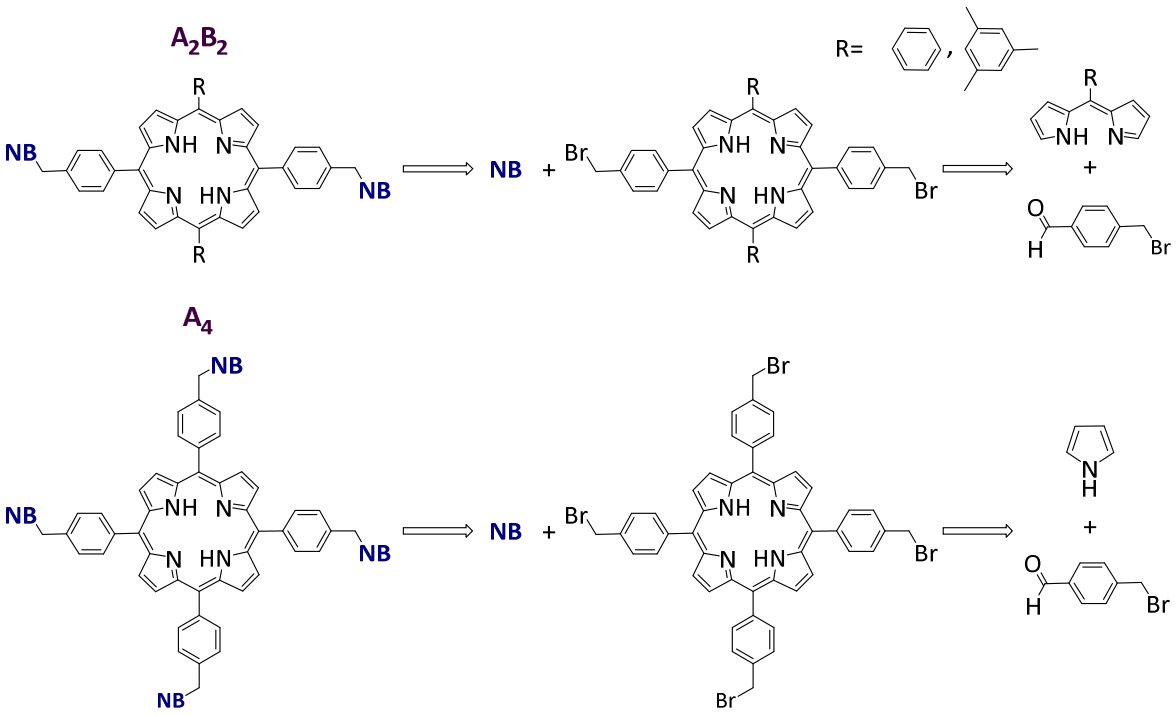

Figure 41: Retrosynthesis of the targeted tectons.

To synthesize porphyrins with *meso*-bromobenzyl groups, 4-(bromomethyl)benzaldehyde (**Ald-Br**) was reacted with phenyl-dipyrromethane (**Ph-DPM**) or pyrrole to produce di or tetra substituted porphyrins respectively. **Ph-DPM** was synthesized following known procedures,[36] and **Ald-Br** was obtained upon reduction of the commercially available 4-(bromomethyl)benzonitrile by DIBAL-H (Figure 42). [37]

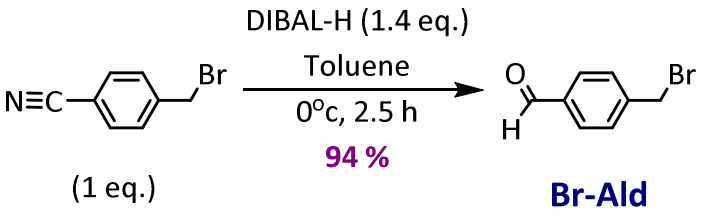

Figure 42: Synthesis of **Ald-Br**.

II. 4. a) Synthesis of 5,15-di(4-(bromomethyl)phenyl)-10,20-diphenylporphyrin (Po2)

5,15-di(4-(bromomethyl)phenyl)-10,20-diphenylporphyrin (**Po2**) was synthesized by reacting stoichiometric amount of **Ph-DPM** and **Ald-Br** in the presence of $BF_3.Et_2O$ in chloroform at room temperature, then oxidized by *p*-chloranil (Figure 43). Unfortunately, these conditions led to the formation of a mixture of porphyrins due to scrambling. The mixture was purified on column chromatography, however only A4, the tetraphenylporphyrin (TPP), could be isolated as pure compound. The *cis* and *trans* A_2B_2, A_3B, and AB_3 porphyrins have close polarity and their separation was difficult. We thus reacted the mixture with excess of thymine, aiming to synthesize thymine functionalized porphyrins with different polarities, and thus facilitating their separation.

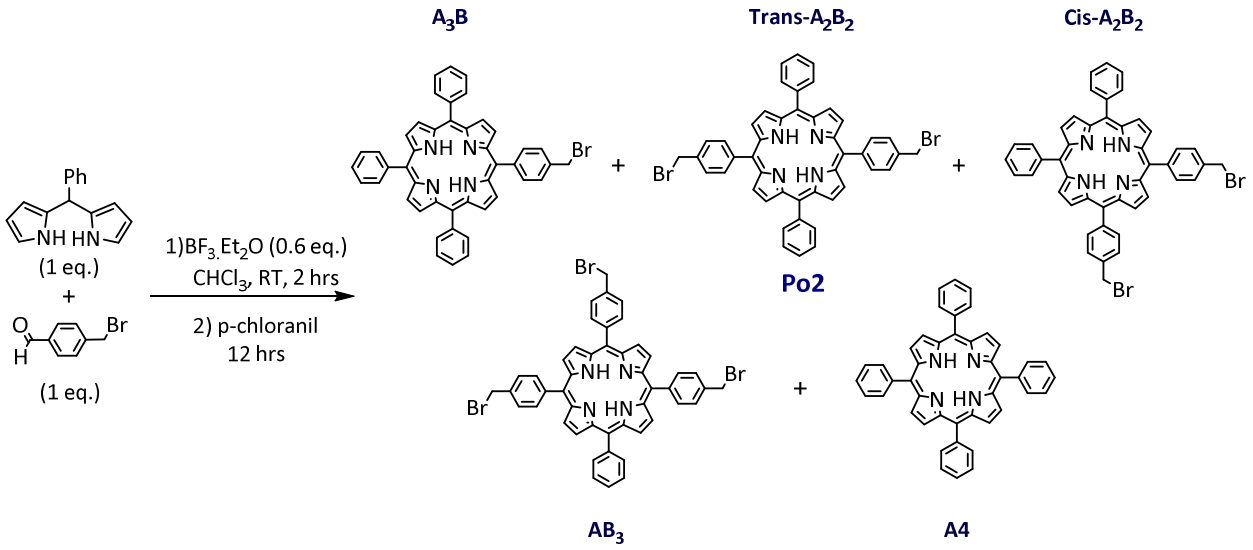

Figure 43: Synthesis of **Po2**.

II. 4. b) Substitution of Po2 mixture

The mixture of porphyrins **Po2** was reacted with an excess of thymine in the presence of K_2CO_3 in DMF to give a mixture of thymine substituted porphyrins (Figure 44). The crude was separated by column chromatography using a gradient of eluents. The A_3B porphyrin, 5-(N_1-methylphenylthymine)-10,15,20-triphenylporphyrin (**T4**), was successfully isolated and characterized by NMR, IR, HRMS and UV. Unfortunately, the separation of *cis*-A_2B_2, *trans*-A_2B_2, and AB_3 porphyrins was not successful.

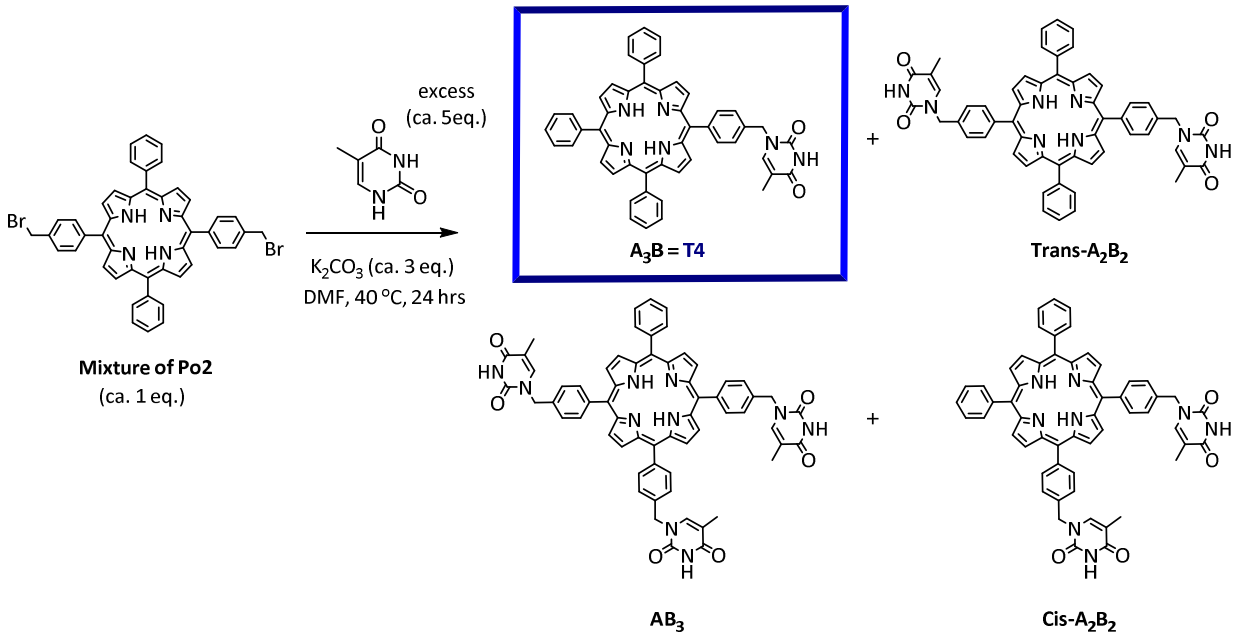

Figure 44: Synthesis and Isolation of **T4**.

II. 4. c) Synthesis of 5,15-di(4-(bromomethyl)phenyl)-10,20-dimesitylporphyrin (Po3)

To decrease the degree of scrambling, we followed the conditions described by Lindsey *et al.*[38] that consist of: increasing the steric hindrance of the *meso*-substituent on the DPM, using an acid with a lower Lewis acidity, and decreasing the concentration of the reactants. Therefore, we focused on reacting **Ald-Br** with **mesityl-DPM** in the presence of TFA instead of $BF_3.Et_2O$ following an optimized procedure described for similar products (Figure 45).[38 (a)]

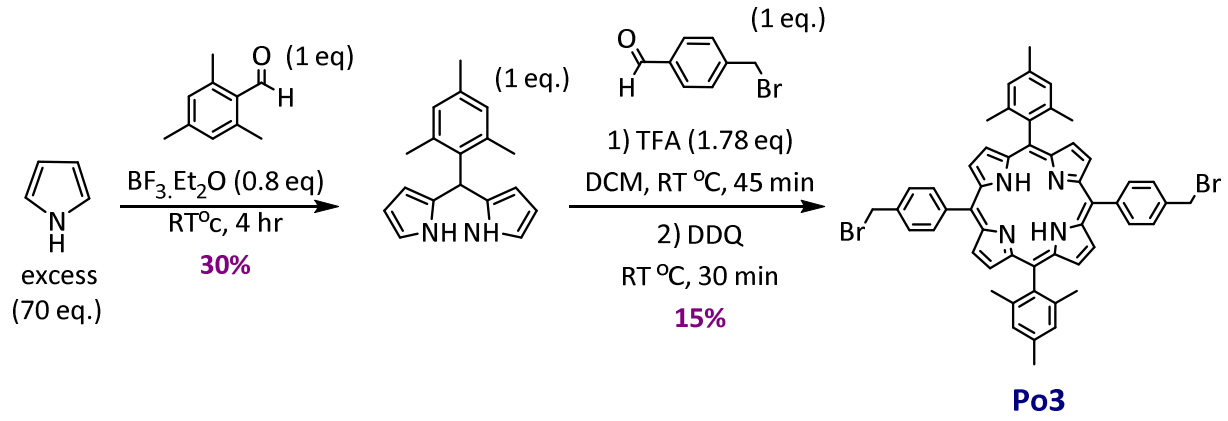

Figure 45: Synthesis of **Po3**.

Mesityl-DPM was obtained in 30% yield following a reported procedure.[39] Then **Ald-Br** was reacted with **Mesityl-DPM** in the presence of TFA to produce 5,15-di(4-(bromomethyl)phenyl)-10,20 dimesitylporphyrin (**Po3**) in 15 % yield without any scrambling. We thus reacted **Po3** with the 4 different NBs in order to generate four new *trans*-A_2B_2 tectons.

II. 4. d) Synthesis of 5,15-di(N_1-methylphenylthymine)-10,20-dimesitylporphyrin (T5)

Po3 was reacted with an excess of thymine in the presence of K_2CO_3 in dry DMF at 40 °C. The reaction was followed by TLC to verify the disappearance of the starting material. After 24h, one major product is formed together with other minor products. The crude was extracted, and then purified by column chromatography to yield 72 % of the targeted **T5** tecton bearing thymines in the *trans meso*-positions (Figure 46).

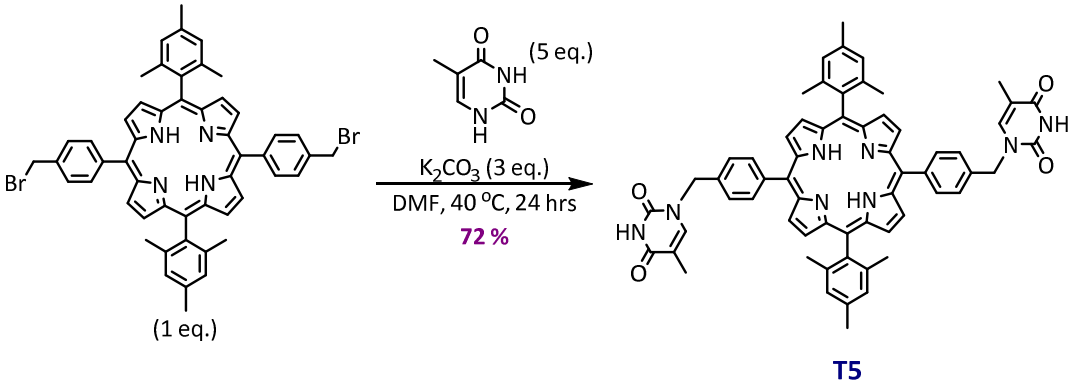

Figure 46: Synthesis of **T5**.

T5 was characterized by NMR, HRMS, IR, and UV-Vis. The ^{1}H-NMR spectrum of **T5** showed that the peaks corresponding to the CH_2 protons are affected by the nature of the deuterated solvent used. In $CDCl_3$, the signals of the CH_2 functions appear as two peaks, each corresponding to 2H with a $\Delta\delta$ = 0.25 ppm. Upon the addition of CD_3OD, the peaks shift close to each other and $\Delta\delta$ decreases to 0.07 ppm. In d_6-DMSO, the signal corresponding to the CH_2 function appears as one singlet integrating for 4 protons. We can deduce that, in chloroform hydrogen bonding interactions take place between the molecules that result in a dissymmetric porphyrin, where the CH_2 functions are not equivalent. Upon addition of methanol, the H-bonding between the thymine moieties is

interrupted, thus the CH_2 are almost equivalent. DMSO is able to destroy all the H-bonding between the tectons, therefore in d_6-DMSO the porphyrin is symmetrical and the CH_2 functions are equivalent.

II. 4. e) Synthesis of 5,15-di(N_9-methylphenyladenine)-10,20-dimesitylporphyrin (T6)

The same procedure was followed to synthesize **T6**. **Po3** was reacted with an excess of adenine and K_2CO_3 in dry DMF leading to the targeted **T6** tecton in 54 % yield. In addition, a minor by-product **T6'** was isolated with a yield of 5 % (Figure 47).

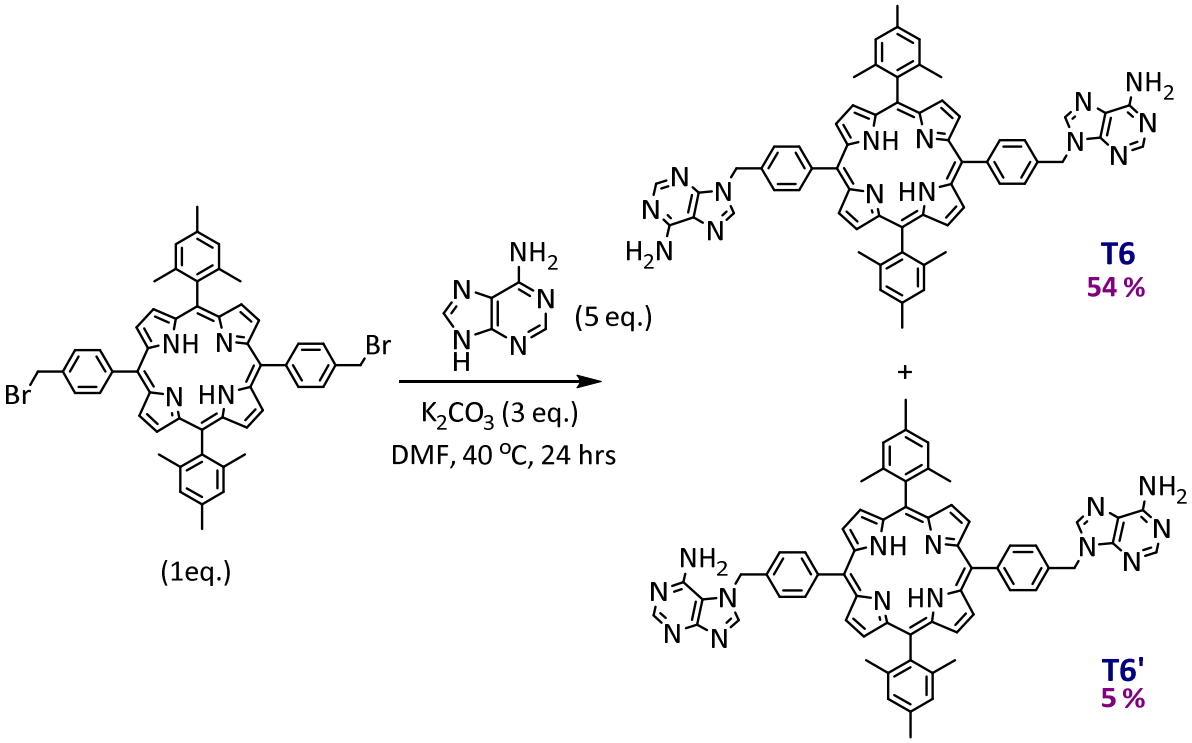

Figure 47: Synthesis of **T6** and **T6'**.

NMR, HRMS, IR and UV-Vis characterization confirmed the structure of **T6** bearing 2 adenine connected in *trans*-positions *via* their N_9 amine sites. The MS of the byproduct **T6'** showed the same mass as **T6**, however its ^{1}H-NMR and the ^{13}C-NMR spectra were different. The ^{1}H-NMR of **T6'** showed: two peaks for the CH_2, two different peaks for the protons at the C_7 position of the adenine (each integrating for 1 H), more peaks for the *meso*-phenyl protons proving that they are

not equivalent, and more peaks corresponding to the β-pyrrolic hydrogens, thus indicating a lower symmetry for **T6'** when compared to **T6**. We conclude that the by-product is a porphyrin bearing two adenines, one *via* its N_9 site (similar to the its isomer **T6**) and the other *via* its N7 site, which is possible because of the tautomeric forms of adenine. Moreover, **T6'** is more soluble and less polar than **T6** since H-bonding between adenines in **T6'**are less favored.

II. 4. f) Synthesis of 5,15-di(N_1-methylphenylcytosine)-10,20-dimesitylporphyrin (T7)

To introduce cytosine to the *meso* position of a porphyrin, **Po3** was reacted with cytosine in the presence of K_2CO_3 following the previous reaction conditions. However, the yield was very low. Cytosine's pKa is higher than adenine's and thymine's,[30] therefore we decided to use a stronger base to deprotonate the N_1 site of the cytosine. **Po3** was reacted with an excess of cytosine and NaH leading to the formation of **T7** in 37% yield (Figure 48). The yield is lower than that of the previous substitution reactions because of the low solubility and high polarity of **T7** that affected the purification of the crude material.

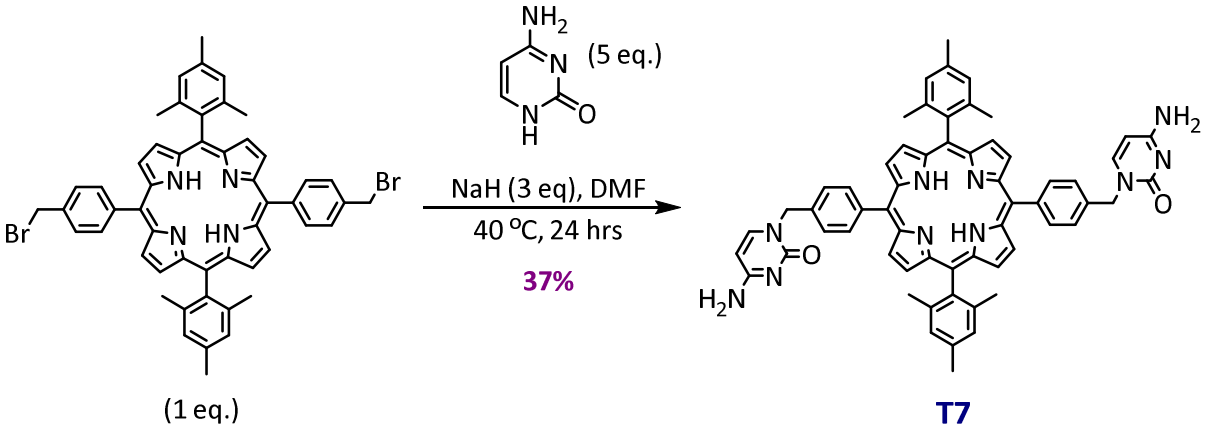

Figure 48: Synthesis of **T7**.

T7 was characterized by NMR, UV-Vis, IR and HRMS. The ^{1}H-NMR spectrum of **T7** showed two broad peaks integrating 2 H each that corresponds to the two non-equivalent NH of the two cytosine moieties. This is a characteristic of the tautomeric form of the cytosine moieties of **T7** in solution.

II. 4. g) Synthesis of 5,15-di(N9-methylphenylguanine)-10,20-dimesitylporphyrin (T9)

The fourth nucleobase, guanine, was reacted with **Po3** in the presence of K_2CO_3 following the same conditions used for **T5** and **T6**. Unfortunately, the reaction did not produce the targeted tecton. We were able to deduce from the TLC analysis that only highly polar products were obtained and their isolation was difficult. Moreover, the NMR and MS of the crude did not show the peaks corresponding to the presence of guanine in the periphery of the porphyrin.

We decided to use 2-amino-6-chloropurine (**P**) as a precursor of guanine (**G**) since it is more soluble, and it is described in the literature as more reactive than guanine. Moreover, **P** can be transformed into **G** by a hydrolysis under acidic conditions.[31] Therefore, we reacted an excess of **P** with of **Po3** and K_2CO_3. The reaction was followed by TLC that showed the formation of two products. The crude was extracted and purified by column chromatography to yield 80 % of 5,15-di(N1-methylphenyl-2-amino-6-chloropurine)-10,20-dimesitylporphyrin **(T8)** as a major product and a minor product **T8'** with a yield of 8%. **T8** and **T8'** have the same MS but differ by NMR. **T8** is the desired tecton, while **T8'** is its isomer bearing two non-equivalent **P** connected in *trans meso*-positions of the porphyrins, one *via* its N_9 site and another *via* its N_7 site (Figure 49).

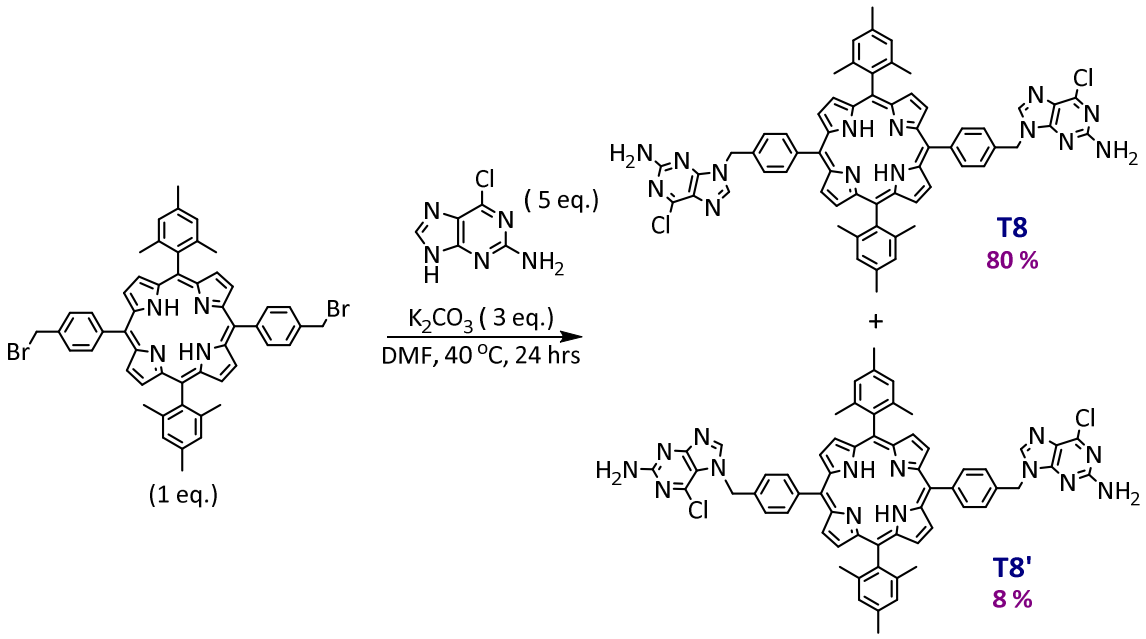

Figure 49: Synthesis of **T8** and **T8'**.

T8 was then hydrolyzed using HCl aqueous solution to yield **T9**, a porphyrin bearing two guanines in its two *meso* positions (Figure 50). The hydrolysis reaction was followed by TLC that indicated a large difference in polarity between **T8** and **T9**. When the oxidation was over, the crude was treated with a basic solution leading to the formation of a precipitate of **T9** in 98 % yield.

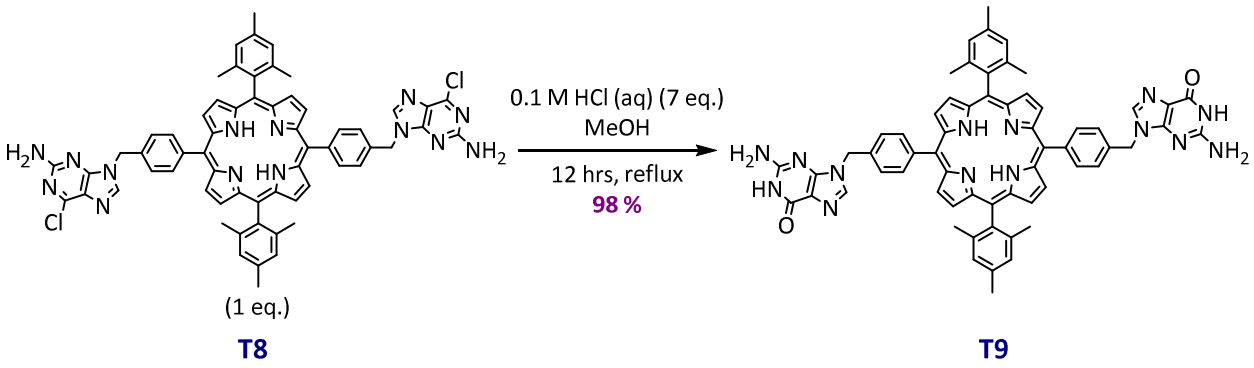

Figure 50: Oxidation of **T8** into **T9**.

T8 and **T9** were characterized by NMR, HRMS, IR and UV. We were able to verify the success of the oxidation by comparing the MS of **T8** and **T9**. In addition, the IR spectra of **T8** and **T9** were compared to the IR of guanine and 2-amino-6-chloropurine. The IR of **P** and **T8** shows a signal at 1628 cm^{-1} that corresponds to the C=N stretching. However, a signal found at a higher value equivalent to 1682 cm^{-1} is present in the IR spectrum of **G** and **T9**, which corresponds to the C=O stretching. Moreover, the appearance of a broad peak in the ^{1}H-NMR of **T9** corresponding to the NH function of **G**, which is absent in **T8**, was an additional proof of a successful oxidation.

II. 4. h) Synthesis of 5,10,15,20-tetrakis(4-(bromomethyl)phenyl)porphyrin (Po4)

To introduce four NBs, 5,10,15,20-tetrakis(4-(bromomethyl)phenyl)porphyrin (**Po4**) was synthesized following a known procedure yielding the targeted **Po4** in 70 % yield [40] (Figure 51).

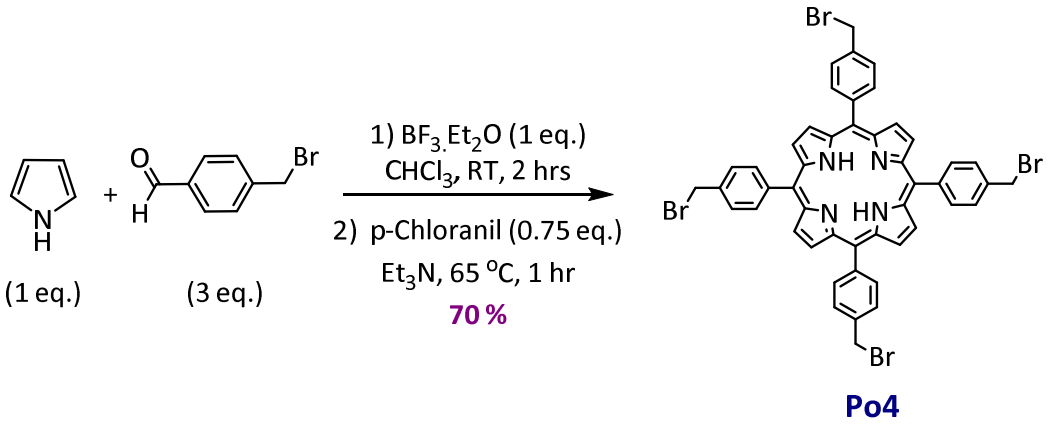

Figure 51: Synthesis of **Po4**.

II. 4. i) Synthesis of 5,10,15,20-tetrakis(N_1-methylphenylthymine)porphyrin (T10)

To introduce thymine in the 4 *meso* positions, **Po4** was reacted with an excess of thymine in the presence of K_2CO_3. The reaction was stired overnight and was followed by TLC to verify the disappearance of **Po4**. When the reaction was completed, the crude was dried, then triturated with water. The precipitate was filtered and dried to yield 93 % of the targeted **T10** (Figure 52). NMR, UV-Vis, IR and HRMS were performed to characterize and confirm the structure of **T10**.

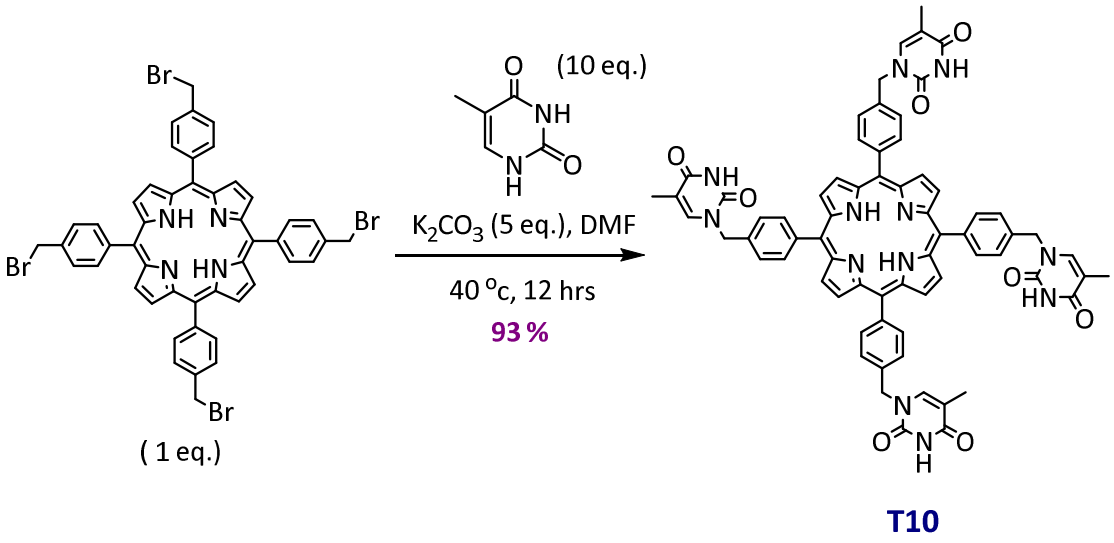

Figure 52: Synthesis of **T10**.

II. 4. j) Substitution of Po4 with Adenine and Cytosine

Aiming to introduce cytosine and adenine to the porphyrin backbone, **Po4** was reacted in DMF with an excess of **A** and **C** in the presence of K_2CO_3 and NaH respectively (Figure 53). Unfortunately, in both cases, precipitates were formed in the reaction media, and the crudes were insoluble in all organic solvents. Characterization of the products by NMR was limited by their low solubility. MS analysis showed that the substitution of the four sites was not complete. Therefore, we deduced that substituting the four *meso* positions by **A** and **C** will lead to insoluble products, due to the strong self-assembly processes between the porphyrins *via* H-bonds oriented in different directions.

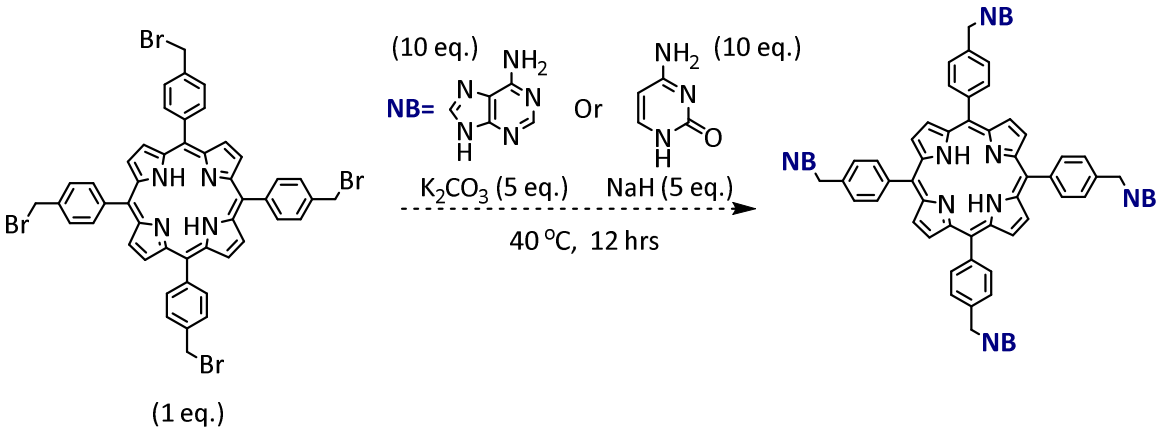

Figure 53: Substitution reaction between **Po4** and **A** or **C**.

III. Conclusion and Perspective

Our objective was to generate H-bonded networks based on porphyrins bearing nucleobases. In order to synthesize the building units, two strategies were studied. The first strategy is based on the connection of NBs to a porphyrin backbone *via* C-C bonds. Suzuki and Sonogashira cross coupling reactions were tested to connect NBs moieties to the corresponding porphyrin derivatives. Unfortunately, the Suzuki cross coupling reaction between a boronated porphyrin and a halogenated uracil was not successful. Therefore, we focused on Sonogashira cross coupling reactions between **Po1** and uracil derivatives, **I-U-Ph2** and **I-U-C6**, to produce **T1** and **T3** respectively. The uracil of the **T1** tecton was deprotonated resulting in **T3.** Moreover, a cross coupling reaction between **Po3** and **I-C-C6** was performed under both, different and similar

conditions. Unfortunately, the coupling was not successful, and the synthesis of **T1** was not reproducible. The complications of the cross coupling reactions shifted our attention to another strategy that proved to be more effective.

The second strategy is based on connecting NBs to porphyrins by C-N bonds *via* their NH sites. Substitution of the N1 site of pyrimidines and N9 site of purines with aromatic substituents bearing reactive bromine sites was successful in the presence of a base. Using this strategy, we were able to introduce **T**, **A**, **C**, **P** and **G** in the periphery of the porphyrin macrocycle generating five new *trans*-A_2B_2 porphyrin based tectons **T5**-**T9**. Moreover, the tetra-functionalized **Po4** porphyrin was successfully substituted with thymine to yield **T10**. However, the substitution of cytosine and adenine produced insoluble products that could not be isolated nor characterized.

As a conclusion, 10 new porphyrin based tectons bearing H-bonding NBs sites were synthesized and fully characterized (Figure 54). Our main perspective is to study the self-assembly of each tecton by X-Ray diffraction. Furthermore, we aim to design molecular networks based on the assembly of complementary tectons, such as **T5** and **T6** or **T7** and **T9**. Unfortunately, no single crystals suitable for X-ray analysis are yet obtained. Therefore, the attempt to crystalize the tectons using different combinations is still under investigation. Moreover, metal cations can be introduced in the azacore of the porphyrins, which could result in the formation of H-bonded metalla-porphyrin networks. Moreover, the introduction of an additional coordinating bidentate ligand, such as 4,4'-bipyridine, during the diffusion process could lead to an increase of the dimensionality of the final network by the coordination of the bidentate ligand in the axial position of the metal present in the porphyrin cavity.

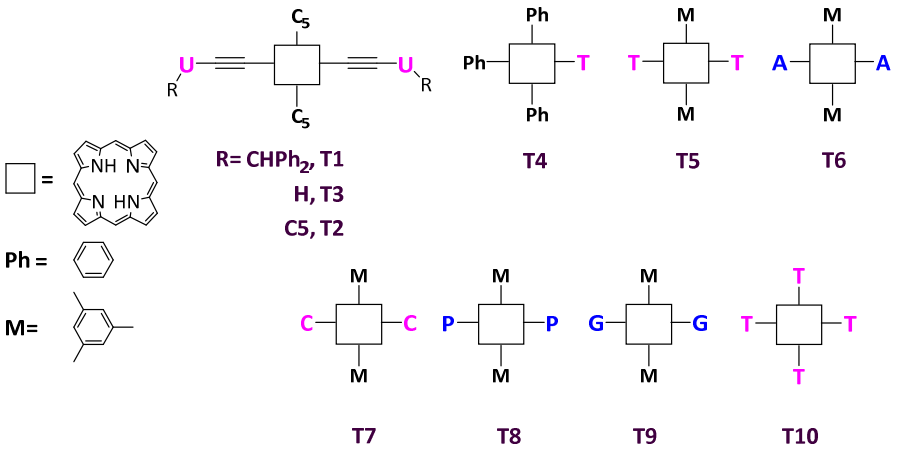

Figure 54: Schematic representation of all tectons **T1**-**T10**.

IV. References

1) (a) L. R. Milgrom, The Colors of of Life: An Introductions to the chemistry of Porphyrins and Related Compounds, Ed. Oxford, **1997.** (b) Y. Wi Y. –W. Lin, J. Wang, *J. Inorg. Biochem.*, **2013**, *129*, 162-171. (c) Y. W. Lin, *Biochim. Biophys. Acta.,* **2015**, *1854*, 844-859.

2) (a) J. E. Jones, J. V. Ruppel, G.-Y. Gao, T. M. Moore, X. P. Zhang, *J. Org. Chem.*, **2008**, *73*, 7260-765. (b) X.-L. Yang, M. –H. Xie, C. Zou, Y. He, B. Chen, M. O' Keeffe, C. D. Wu, *J. Am. Chem. Soc.*, **2012**, *134*, 10638-10645.

3) (a) C. Jiao, N. Zu, K. W. Huang, P. Wang, J. Wu, *Org. Lett.*, **2011**, *13*, 3652-3655. (b) L. Li, Y. Hang, J. Peng, Y. Cao, X. Peng, *Org. Electron.*, **2013**, *112*, 515-521.

4) (a) N. Marets, V. Bulach, M. W. Hosseini, *New J. Chem.*, **2013**, *37*, 3549-3558. (b) W. Y. Gao, M. Chrzanowski, S. Ma, *Chem. Soc. Rev*., **2014**, *43*, 5841-5866.

5) I. Goldberg, *CrystEngComm*, **2008**, *10*, 637-645. (b) O. K. Farha, A. M. Shultz, A. A. Sarjeant, S. T. Nguyen, J. T. Hupp, *J. Am. Chem. Soc.*, **2011**, *133*, 5652-5655. (c) E. Khun, V. Bulach, M. W. Hosseini, *Chem. Commun.*, **2005**, 3906-3908.

6) H. Fischer, H. Orth, *Die Chemie Des Pyrrols: Pyrrol farbstoffe*, Johnson Reprint, **1968**.

7) P. Rothermund, *J. Am. Chem. Soc.*, **1935**, *57*, 2010-2011.

8) A. D. Adler, F. R. Longo, J. D. Finarelli, J. Goldmacher, J. Assour, L. Korsakoff, *J. Org. Chem*., **1967**, *32*, 476-476.

9) J. S. Lindsey, I. C. Schreiman, H. C. Hsu, P. C. Kearney, A. M. Marguerettaz, *J. Org. Chem*., **1987**, *52*, 827-836.

10) R. G. Little, J. A. Anton, P. A. Loach, J. A. Ibers, *J. Heterocycl. Chem.,* **1975**, *12*, 343-349.

11) G. P. Arsenault, E. Bullock, S. F. MacDonald, *J. Am. Soc*., **1960**, *82*, 4384-4389.

12) S. J. Lee, R. A. Jensen, C. D. Malliakas, M. G. Kanatzidis, J. T. Hupp, S. T. Nguyen, *J. Mater. Chem*., **2008**, *18*, 3640-3642.

13) B. J. Littler, Y. Ciringh, J. S. Lindsey, *J. Org. Chem.*, **1999**, *64*, 2864-2872.

14) (a) S. G. DiMango, V. S.Y. Lin, M. J. Therien, *J. Org. Chem. Soc*., **1993**, *115*, 2513-2515. (b) S. G. DiMango, V. S.Y. Lin, M. J. Therien, *J. Am. Chem. Soc.*, **1993**, *115*, 2513-2515.

15) (a) A. Harriman, Y. Kubo, J. L. Sessler, *J. Am. Chem. Soc.*, **1992**, *114*, 388-390. (b) J. L. Sessler, B. Wang, A. Harriman, *J. Am. Chem. Soc.*, **1993**, *115*,10418-10419.

16) A. Harriman, D. J. Magda, J. L. Sessler, *J. Phys. Chem.*, **1991**, *95*, 1530-1532.

17) J. L. Sessler, B. Wang, A. Harriman, *J. Am. Chem. Soc.*, **1995**, *117*, 704-714.

18) A. Shi, K. M. Barkigia, J. Fajer, C. M. Drain, *J. Org. Chem.,* **2001**, *66*, 6513-6522.

19) A. DA dler, F. R. Longo, J. D. Finarelli, J. Goldmacher, J. Assour, L. Korsakoff, *J. Org. Chem*., **1967**, *32*, 476-480.

20) J. L. Sessler, J. Jayawickramarajah, A.Gouloumis, T. Torres, D. M. Guldi, S. Maldonado, K.J. Stevenson, *Chem. Commun.*, **2005**, 1892-1894.

21) G. Sargsyan, B. M. Leonard, J. Kubelka, M. Balaz, *Chem. Eur. J.*, **2014**, *20*, 1878-1892.

22) G. Sargsyan, A. A. Schatz, J. Kubelka, M. Balaz, *Chem. Commun.*, **2013**, *49*, 1020-1022.

23) A. G. Slater, Y. Hu, L. Yang, S. P. Argent, W. Lewis, M. O. Blunt, N. R. Champness, *Chem. Sci.*, **2015**, *6*, 1562-1569.

24) Y. Choi, C. George, M. J. Comin, J. J. Barchi Jr, H. S. Kim, K. A. Jacobson, J. Balzarini, H. Mitsuya, P. L. Boyer, S. H. Hughes, V. E. Marquez, *J. Med. Chem.*, **2003**, *46*, 3292-3299.

25) (a) C.-H. Lee, F. Li, K. Iwamoto, J. Dadok, A. A. Bothner-By, J. S. Lindsey, *Tetrahedron*, **1995**, *51*, 11645-11672. (b) P. D. Rao, S. Dhanalekshmi, B. J. Littler, J. S. Lindsey, *J. Org. Chem.*, **2000,** *65*, 7323-7344.

26) (a) M. A. Bakar, N. N. Sergeeva, T. Juillard, M. O. Senge, *Organometallics*, **2011**, *30*, 3225-3228. (b) N. Aratani, A. Ouska, *Chem. Commun*., **2008**, 4067-4069.

27) G. P. Arsenault, E. Bullock, S. F. Macdonald, *J. Am. Soc*., **1960**, *82*, 4384-4389.

28) W. G. Scott, H. L. Anderson, *Synlett*, **1996**, *11*, 1039-1040.

29) C. H. Lee, J. S. Lindsey, *Tetrahedron*, **1994**, *50***,** 11427-11440.

30) W. Saenger, Principles of Nucleic Acids structure, *Springer*, New York, **1984**

31) N. Biblo, V. Vazque-Gonzalez, M. T. Aranda, D. Gonzalez-Rodriguez, *Eur. J. Org. Chem.*, **2015**, 7160-7175.

32) F. Wu, M. G. Buhendwa, D. F. Weaver, *J. Org. chem*., **2004**, *69*, 9307-9309.

33) (a) K. Sonogashira, Y. Tohda, N. Hagihara, *Tetrahedron Letters.,* **1975**, *50*, 4467-4470. (b) M. Schilz, H. Plenio, *J. Org. Chem.,* **2012**, *77*, 2798-2807. (c) Y. Liang, Y. Xie, J. Li, *J. Org. Chem.*, **2006**, *71*, 379-381.

34) (a) A. Jiblaoui, C. Baudequin, V. Chaleix, G. Ducourthial, F. Louradour, Y .Ramondenc, V.Sol, S. L.-Lhez, *Tetrahedron*, **2013**, *69*, 5098-5103. (b) Y. Liang, Y.-X. Xie, J.-H. Li, *J. Org. Chem.,* **2006**, *71*, 379-381 (c)Y. Liang, Y.-X. Xie, J.-H. Li, *J. Org. Chem.,* **2006**, *71*, 379-381.

35) (a) S. Ellipilli, K. N. Ganesh, *J. Org. Chem*., **2015**, *80*, 9185-9191. (b) A. Kiviniemi, M. Murtola, O. Ingman, P. Virta, *J. Org. Chem.*, **2013**, *78*, 5153-5159. (c) K. Pomeisl, A. Holy, R. Pohl, *Tetrahedron Letters*, **2007**, *48*, 3065-307.

36) J. Laha, S. Dhanalekshmi, M. Taniguchi, A. Ambroise, J. Lindsey, *Organic Process Research & Development*, **2003***, 7*, 799-812.

37) D. A. Roberts, T. W. Schmidt, M. J. Crossley, S. Perrier, *Chem. Eur. J.,* **2013**, *19*, 12759-12770.

38) (a) B. J. Littler, Y. Ciringh, J. S. Lindsey, *J. Org. Chem.,* **1999**, *64*, 2864-2872. (b) G. R. Geier III, B. J. Littler, J. S. Lindsey, *J. Chem. Soc., Perkin Trans. 2*, **2001**, 707-711.

39) (a) C. -H. Lee, J. S. Lindsey, *Tetrahedron*, **1994**, *50*, 11427-11440. (b) P. K. Biswas, S. Saha, Y. Nanaji, A. Rana, M. Schmittel, *Inorg. Chem*., **2017**, *56*, 6662-6670.

40) (a) B. C. Brookser, T. C. Bruce*, J. Am. Chem. Soc.,* **1991,** *11,* 4208-4218. (b) D. A. Roberts, T. W. Schmidt, M. J. Crossley, S. Perrier, *Chem. Eur. J.,* **2013**, *19*, 12759-2770.

Chapter II: Dipyrrins bearing Nucleobases

Table of contents

I. Dipyrrins……......107
I. 1. Structure and nomenclature……...107
I. 2. Synthesis……108
I. 3. BODIPY……110
I. 4. Dipyrrin complexes……111
I. 5. Dipyrrin complexes in hydrogen bonded networks……117
II. Dipyrrins bearing nucleobases……119
II. 1. Some examples of dipyrrins functionalized by NBs……..120
II. 2. Aim of the project……121
II. 3. Synthesis of dipyrrins bearing NBs……..122
II. 3. a) 1,3,7,9-tetramethyl-5-(N_1-methylphenylthymine)-dipyrrin (T-dipyrrin) (**T11**)…...124
II. 3. b) 1,3,7,9-tetramethyl-5-(N_9-methylphenyladenine)-dipyrrin (A-dipyrrin) (**T12**)…...124
II. 3. c) 1,3,7,9-tetramethyl-5-(N_1-methylphenylcytosine)-dipyrrin (C-dipyrrin) (**T13**)…..125
II. 3. d) 1,3,7,9-tetramethyl-5-(N_9-methylphenylguanine)-dipyrrin (G-dipyrrin) (**T15**)…..126
III. H-bonded network based on Zn(II)(T-dipyrrin)$_2$ ……...128
IV. Conclusion and Perspectives……..131
V. References…….....133

I. Dipyrrins

Dipyrrins, known since 1920,[1] have received a wide interest over the past years in supramolecular and coordination chemistry.[2] Under basic conditions, bis-pyrrolic dipyrrins form monoanionic chelating ligands that coordinate to various metal centers. In addition, the dipyrrin backbone can be functionalized to incorporate additional interaction sites, such as coordination and/or H-bonding sites, affording a series of interesting tectons.[3] Therefore, dipyrrin based tectons are used to design 1D, 2D and 3D molecular networks assembled *via* several interactions. Moreover, the dipyrrins are well known for their ability to form helical structures[4] and for their luminescent and fluorescent boron complexes, BODIPY.[5]

I. 1. Structure and nomenclature

The dipyrrin is a bis-pyrrolic molecule, which may be regarded as a half-porphyrin. It is constituted of two conjugated coplanar pyrrole rings linked by a methylene bridge. Dipyrrins are the oxidized form of dipyrromethanes (starting material of porphyrins), that is why they are also known as dipyrromethenes. The nomenclature and numbering system of dipyrrins (IUPAC) is similar to that of porphyrins. The positions 1 and 9 are regarded as α-positions, positions 2, 3, 7 and 8 as β-positions and position 5 as *meso*-position. (Figure 1)

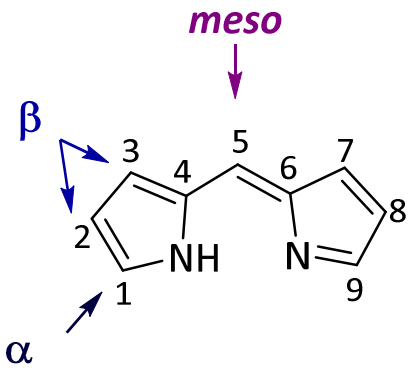

Figure 1: The structure and numbering of dipyrrins

Dipyrrins can exist in three different conformations, according to the rotation of the pyrrole units around the methylene linkage, the E-syn, E-anti and Z-syn (Figure 2 (a)). In addition, under either

acidic or basic conditions, the dipyrrin molecule can exist in the cationic, neutral or anionic states (Figure 2 (b)).

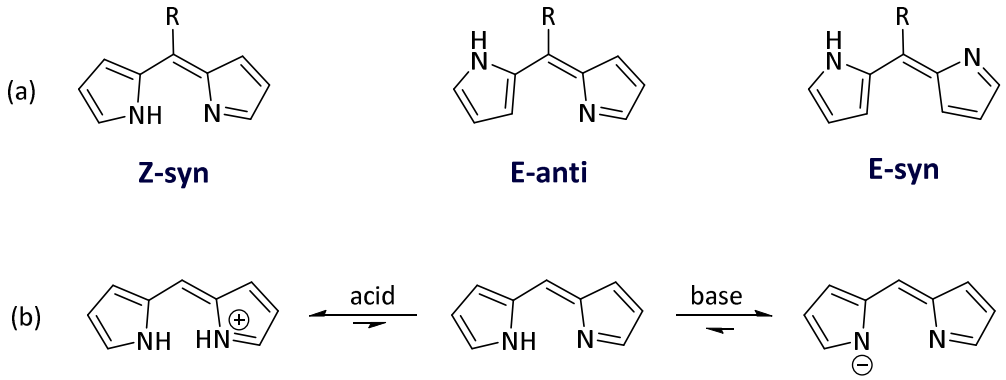

Figure 2: (a) The three conformations of the dipyrrin molecule. (b) The dipyrrin acid-base equilibrium

I. 2. Synthesis

The synthesis of dipyrrins has been first developed by Hans Fischer in 1937.[6] In 1960, the Macdonald coupling reaction was reported for the synthesis of dipyrromethanes as intermediates of porphyrin, in addition to the synthesis of dipyrromethenes (dipyrrins).[7] The Macdonald coupling consisted of a condensation reaction between 2-formylpyrrole and α-unsubstituted pyrrole, in the presence of an acid, such as $POCl_3$ or HBr.[8] This method affords *meso*-unsubstituted dipyrrins, which can be substituted at their α- and β-positions depending on the starting materials. Therefore, symmetrical or non-symmetrical dipyrrins can be synthesized following this method. In addition, the products isolated are dipyrrin salts, which are more stable than free dipyrrins (Figure 3 (a)).

Following the synthetic strategy developed by Dolphin *et al.,* symmetrical *meso*-unsubstituted dipyrrins can be synthesized by reacting two equivalents of pyrrolylester and formic acid.[9] The latter is involved in the release of the leaving group of pyrrolylester, besides being the carbonyl synthon affording the *meso*-unsubstituted dipyrrins. (Figure 3 (b))

Symmetrical *meso*-substituted dipyrrins can be synthesized by reacting 2 equivalents of α-unsubstituted pyrrole with an acyl halide (Figure 3 (c)). In addition, symmetrical dipyrrins can be

synthesized following the two-steps procedure reported by J. S. Lindsey.[10] The α-unsubstituted pyrrole is reacted with an aldehyde in the presence of an acid catalyst, such as TFA or $InCl_3$, affording the dipyrromethane (Figure 3 (d)).[11] The latter is less stable than dipyrrins and sensitive to light, thus the reaction is performed under argon, at room temperature, and always protected from light. The dipyrromethane intermediate is then oxidized into the targeted dipyrrin by DDQ or *p*-chloranil. The symmetrical dipyrrins can be functionalized by a wide range of substituents depending on the aldehyde used. Moreover, this method can be used to synthesize both α- and *meso*-unsubstituted dipyrrins, depending on the used aldehyde and pyrrole (Figure 3(d)).

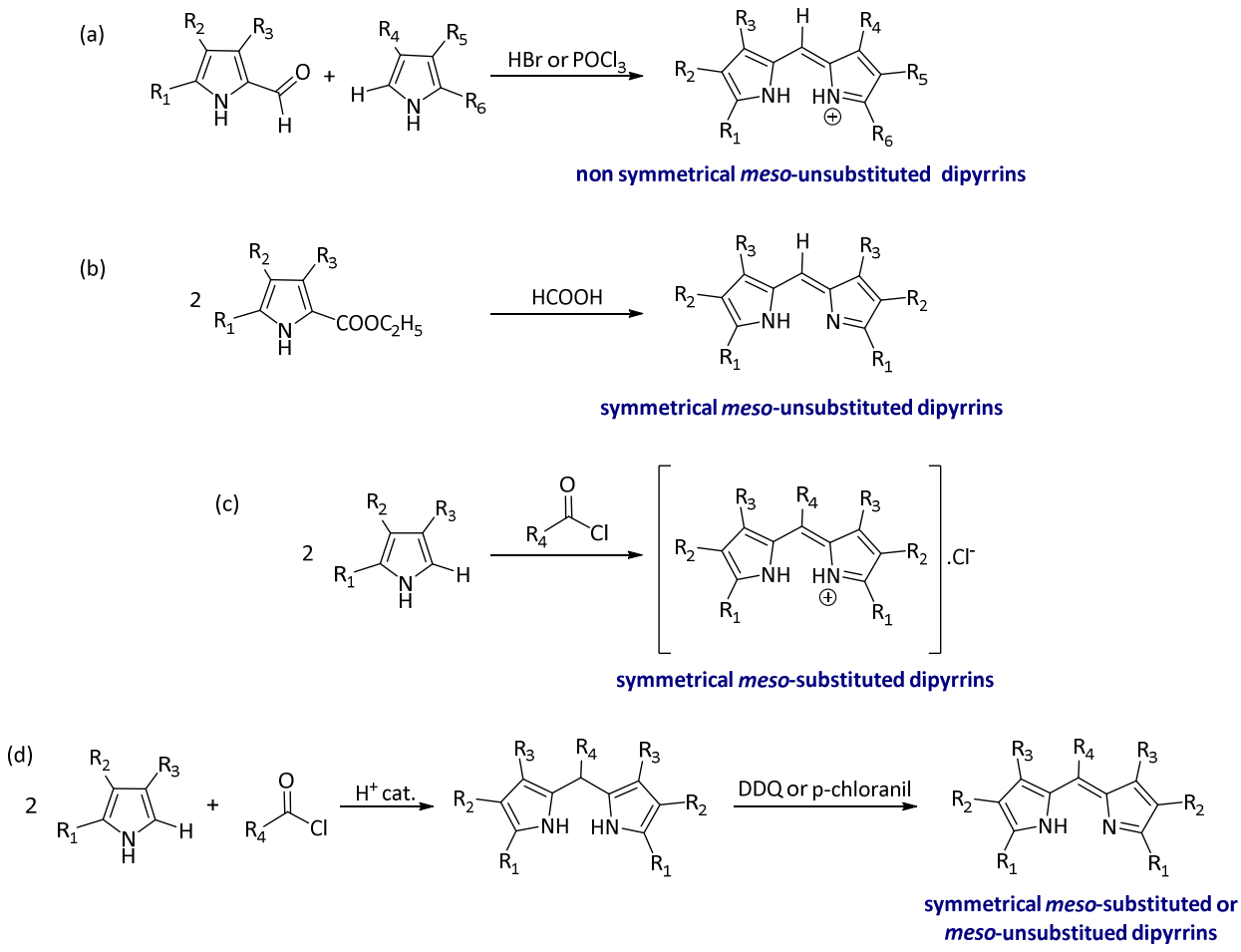

Figure 3: The synthesis of (a) non-symmetrical and (b) symmetrical *meso*-unsubstituted dipyrrins. (c) The synthesis of *meso*-substituted dipyrrins *via* acyl halides. (d) The two-step synthesis of *meso*-substituted or unsubstituted dipyrrins. $R_{1\text{-}6}$ represent any substituent including an H atom (unsubstituted site).

I. 3. BODIPY

Dipyrrins can act as monoanionic chelate ligands under basic conditions, having the ability to form metal complexes. In addition, the dipyrrins have a conjugated π-system, therefore they have an intense absorption band in the visible region of the electromagnetic spectrum.[3(b),4(a)] This leads to complexes with interesting photophysical properties. For instance, the BF_2 complexes BODIPY (4,4-difluoro-4-bora-3a,4a,-diaza-s-indacene, boron dipyrromethene), are well known for their luminescent properties. BODIPY are prominent dyes and are stable luminescent species with high quantum yields and tunable emission wavelength with applications in photodynamic therapy, solar cells, light harvesting and imaging.[12]

The BF_2 complexes and their fluorescent properties were first reported in 1968.[13] The BODIPY's chemical structure is a zwitterion (B^- and N^+) and its numbering system differs from that of dipyrrins (Figure 4).

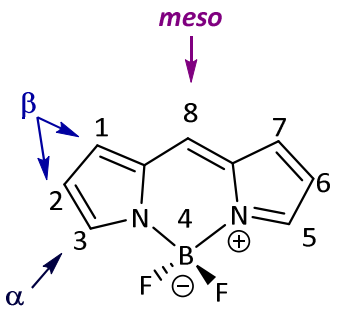

Figure 4: The structure and nomenclature of BODIPY.

BODIPY dyes can be easily functionalized by different substituents, in order to introduce additional recognition sites or to modulate their optical properties. Depending on their peripheral substituents, BODIPYs can act as chemical sensors[14], as transition metal recognition sites[15] and as light harvesting materials[16] (Figure 5).

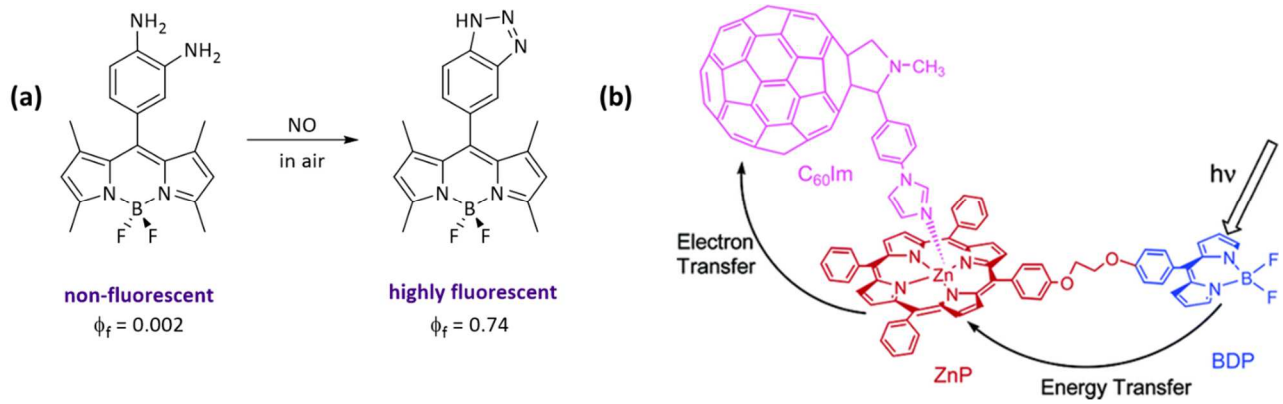

Figure 5: Examples of BODIPY and their applications. (a) The anilino based BODIPY complex acting as a chemical sensor for NO molecules, and its transformation yielding luminescent adducts.[14] (b) The BODIPY photosynthetic combined antenna-reaction center model system.[15]

I. 4. Dipyrrin complexes

Under basic conditions, dipyrrins form mono-anionic chelates that can coordinate to various metal centers including transition metals and semimetals.[3(b), 4(a), 17] Dipyrrins can form homoleptic M(dipyrrin)$_2$ or M(dipyrrin)$_3$ complexes depending on the metallic cation and its oxidation number. (Figure 6)

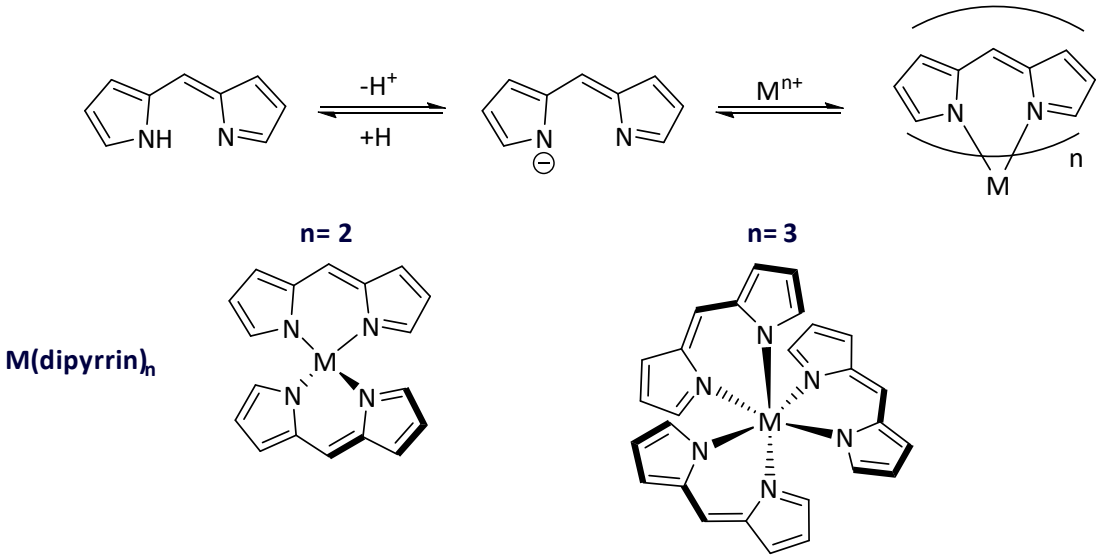

Figure 6: The formation of homoleptic M(II)(dipyrrin)$_2$ and M(III)(dipyrrin)$_3$ complexes.

The M(dipyrrin)$_2$ complex is usually synthesized by reacting 2 equivalents of dipyrrin ligands with one equivalent of metal(II) acetate in methanol. The latter is used as a solvent. Since the formed dipyrrinato complex is not soluble in methanol, the complex can be easily isolated by precipitation and filtration. Metal acetate salts are preferred for the complexation reaction, since acetate counter ions can also act as a base to deprotonate the dipyrrin ligand. Metal cations such as Ni(II)[18], Cu(II)[19], Cd (II)[20], Pd(II)[21] and Zn(II) [22] are used to form M(II)(dipyrrin)$_2$ complexes, which usually adopt a deformed tetrahedral or square planar coordination geometry (Figure 7).

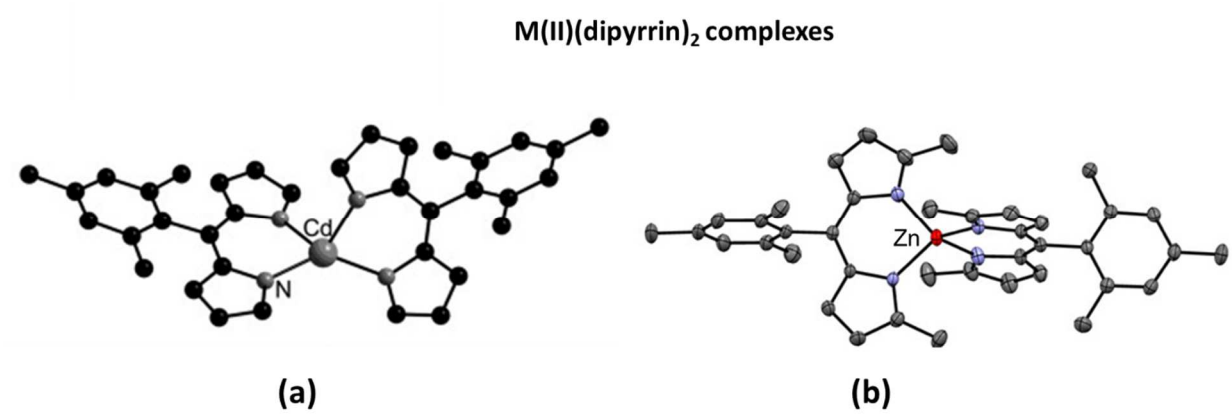

Figure 7: Examples of homoleptic dipyrrinato M(II) complexes. (a) The crystal structure of Cd(II) (5-mesityldipyrrin)$_2$. Figure modified from reference 20. (b) The crystal structure of Zn(II) (1,9-dimethyl-4-mesityldipyrrin)$_2$. Figure modified from reference 22 (b).

The M(dipyrrin)$_3$ complexes are formed by reacting metal cations in +2 oxidation state, which will be oxidized during complexation, or by reacting metal cations in the +3 oxidation state, for example Co(III)[23], Fe(III)[24], In(III)[25] and Ga(III)[26], with three equivalents of a dipyrrin ligand. The metal cation of a tris(dipyrrinato)complex is in an octahedral coordination geometry and the *meso* substituents of three dipyrrin ligands are in a pseudo-3-fold symmetric environment with respect to the metal center. An example of such geometry is shown in Figure 8 (a).

Moreover, neutral dipyrrin molecules can also be regarded as monodentate ligands *via* their imine nitrogen, however few examples of complexes with neutral dipyrrins are described (Figure 8(b)).[27]

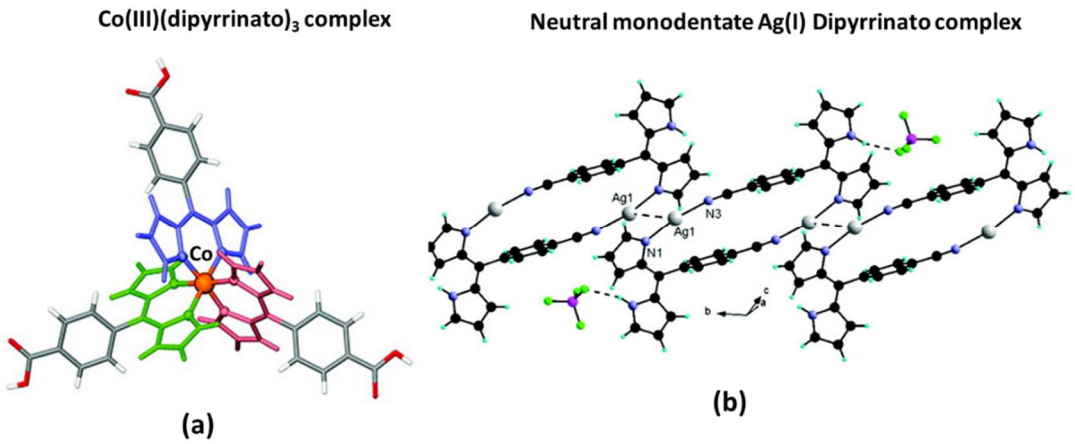

Figure 8: (a) The crystal structure of Co(III)(dipyrrin)$_3$ complex, Figure taken from reference 23 (a). (b) The crystal structure of a neutral monodentate Ag(I) dipyrrinato. Figure taken from reference 27.

The M(II)(dipyrin)$_2$ and M(III)(dipyrin)$_3$ are homoleptic complexes incorporating the same type of ligands around the metal center. In addition, dipyrrin heteroleptic complexes, incorporating at least two different ligands, are also accessible.[28] Such complexes are formed by reacting one equivalent of a dipyrrin ligand with one equivalent of a metal salt. An example of such complexes is the 5-pyridinedipyrrin metallotecton, Cu(II)(Py-dipyrrin)(acac), represented in Figure 9.[29]

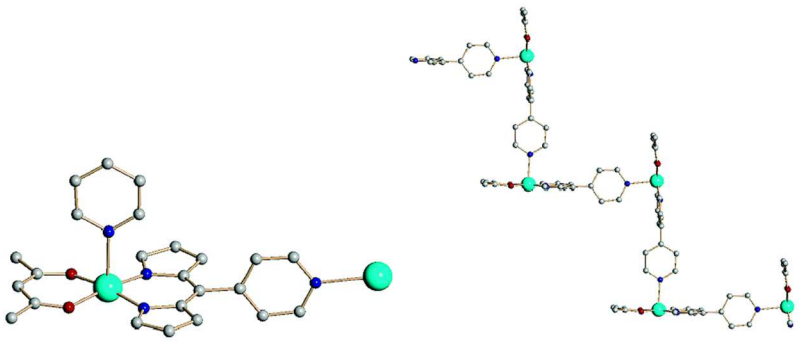

Figure 9: The crystal structure of a heteroleptic Cu(II)(Py-dipyrrin)(acac) complex and its 1-D chain. Figure taken from reference 29.

In addition, the dipyrrin backbone can be functionalized in its periphery by other binding units, affording a dipyrrin metallotecton with secondary coordinating sites (Figure 10).[2] It can self-assemble into homo- or hetero-metallic coordination polymers upon their reaction with the same

or with different metal cations. Figure 10 shows two examples of Zn(II)dipyrrin metallotectons bearing additional coordinating sites. Upon, introducing $CdCl_2$ salt, the metallotecton self-assembles into a 2D grid like network *via* the coordination of the secondary coordination sites (pyridine and imidazole) to the second metal center (Cd(II)).[4(a),30]

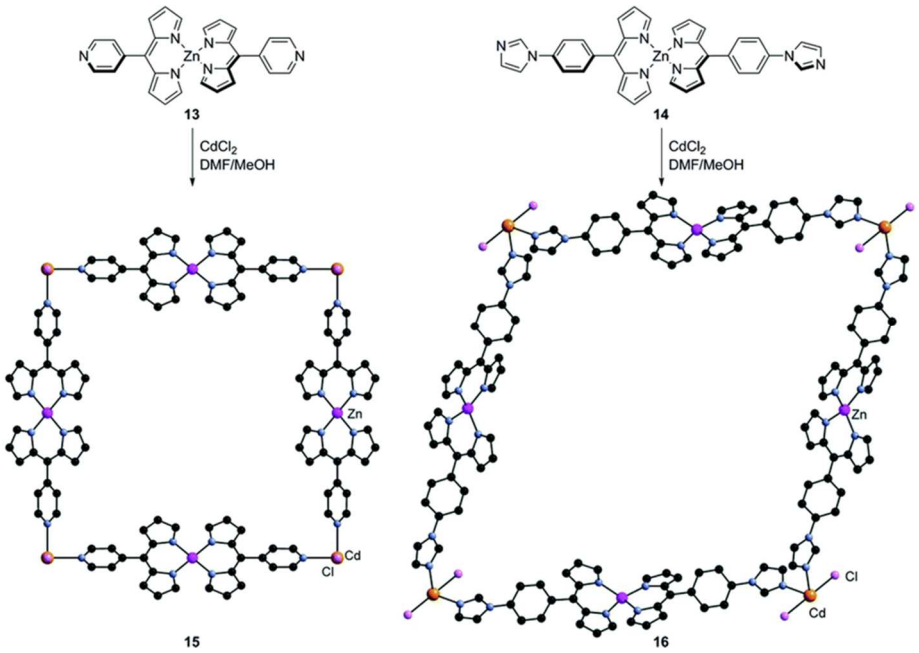

Figure 10: Heterometallic 2D grid type MOFs, obtained by the assembly of Zn(II)dipyrrin complex with $CdCl_2$. Figure modified from reference 4(a).

In addition to *meso-,* α- and β-substituted dipyrrins are also well known.[31] For example, pyridyl moieties were introduced at the β-positions of a BODIPY complex to design rod-like bidentate ligands.[32] The assembly of the pyridyl-BODIPY ligands in the presence of Pd(II) metal center afforded two macrocyclic architectures with triangular and square geometries as represented in Figure 11. The two forms are in equilibrium in solution, and their ratio depends on the solvent. In less polar solvents (dichloromethane and chloroform), both the triangular and square species are present. The use of more polar solvents (acetone, dimethyl sulfoxide and methanol) afforded only the triangular complex, which is entropically favored.

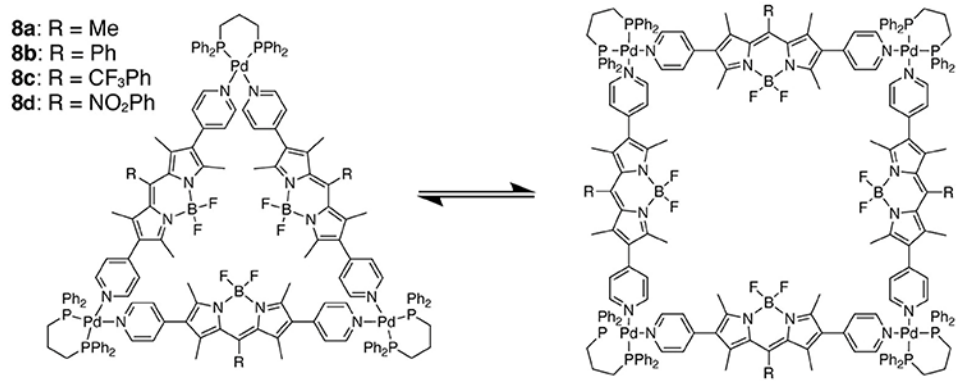

Figure 11: β-substituted dipyrrin and the assembly of its Pd(II) complex in the triangular and square macrocyclic forms. Figure taken from reference 2 (a).

As previously discussed, dipyrrin based tectons are well known for their self-assembly into discrete and infinite supramolecular architectures. In addition, 2,2'-bisdipyrrins possess the ability to form helical arrangements held by coordination bonds.[33] The assembly of bis(dipyrrinato)metal(II) complexes into double-stranded helicates, linked by rigid or flexible spacers, has been reported.[33,34] Examples of such architectures are represented in Figure 12. Furthermore, dipyrrin-based helicates display interesting properties, for instance visible light emission and unique cation-π interactions (Figure 12).[35]

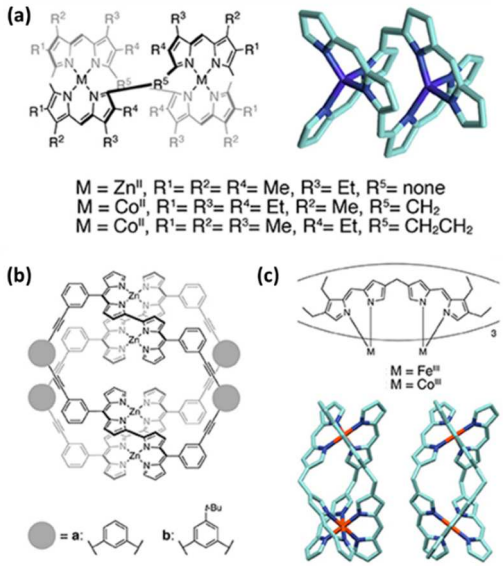

Figure 12: Examples of dipyrrin helical assemblies. (a) The structure of double helicates based on bis-dipyrrin metallotecton connected with flexible alkyl chains.[33] (b) The chemical structure of a double helical complex with rigid aromatic linkers.[34(a)] (c) The structure of triple-stranded M_2L_3 complexes. [34(b)] Figure modified from reference 2(b).

In addition, the assembly of a 2,2'-bisdipyrrin Zn(II) complex bearing peripheral benzonitrile moieties into helical architectures, in the presence of silver salts AgX (X= TfO^-, BF_4^-, SbF_6^-) was reported by our lab.[36] The effect of the solvent and the counter ions used on the final organization of the tectons was discussed. To synthesize the Ni(II) bis-dipyrrin complex (2) shown in Figure 14, the ligand (1) was reacted with $Ni(OAc)_2$. Subsequent oxidation by DDQ followed by demetallation in the presence of HCl afforded the 2,2'-bisdipyrrin ligand (4). The latter was then reacted with $Zn(OAc)_2$ to yield the targeted helical complex, which was studied by X-Ray analysis (Figure 13). The structural investigation showed that the dipyrrin strands are arranged into a double helical structure maintained by the coordination of the Zn(II) to the two bis-dipyrrin, and that the metal cation adopts a distorted tetrahedral geometry (Figure 13).

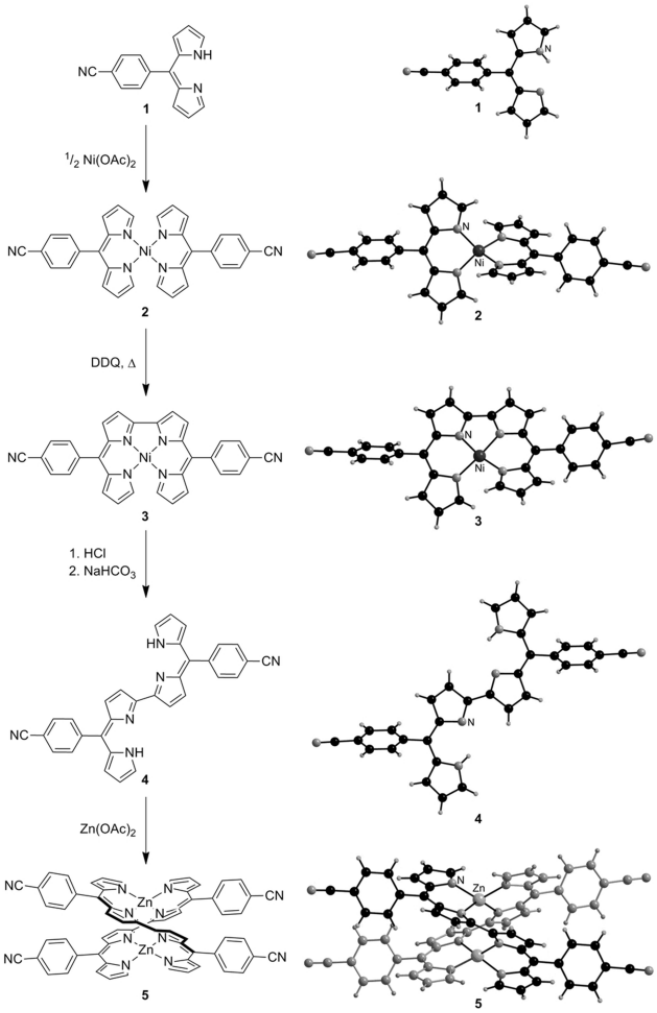

Figure 13: The synthetic pathway of helicate (5) and the crystal structures of compounds (1)-(5). Figure taken from reference 36.

I. 5. Dipyrrin complexes in hydrogen bonded networks

As previously discussed, the dipyrrin backbone can be functionalized by hydrogen bonding sites in addition to the coordination sites. Dipyrrins bearing peripheral hydrogen bonding donor/acceptor sites, for example amides, carboxylic acid and diaminotriazine, have been reported.[37] Such dipyrrins are interesting tectons as they offer two different interaction poles, the coordinating mono-anionic dipyrrin site and the H-bonding site. The former coordinates to metal centers resulting in a bisdipyrrinato complex (metallotecton) (Figure 14 (a)). The latter forms H-bonding interactions between the proton donor and proton acceptor groups, which result in the self-assembly of the metallotecton (Figure 14 (b)). The H-bonding sites can be involved in several H-bonding interactions, and thus forming 2D and 3D H-bonded networks (Figure 14 (c)).[38, 39]

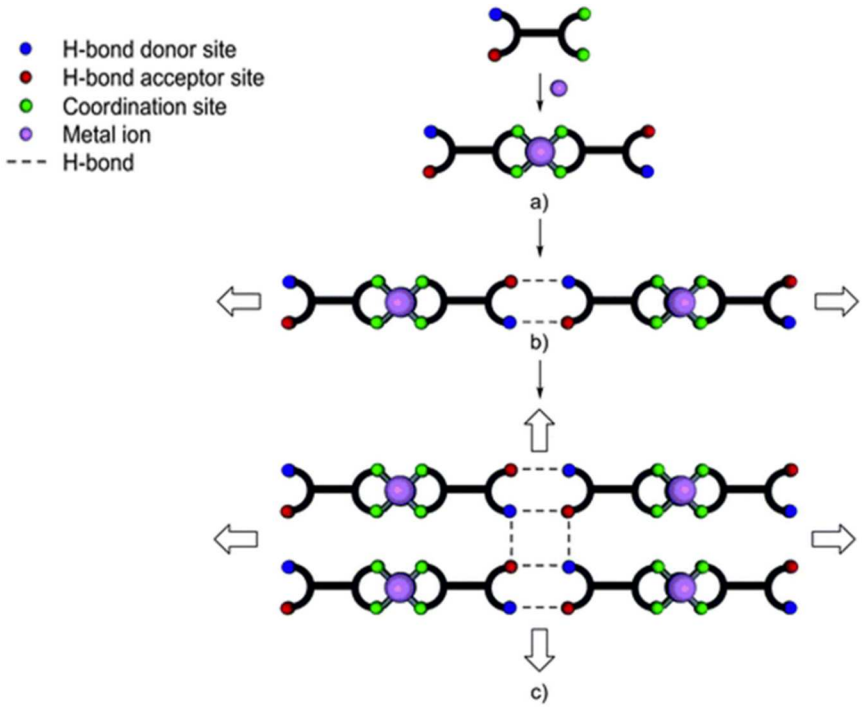

Figure 14: (a) Schematic representations of a dimer formed upon combination of two dipyrrin tectons bearing H-bonding sites with a tetracoordinated metal ion, (b) and its extension into 1D (c) and 2D networks through H-bonds. Figure taken from reference 38.

Examples of such metallotectons are the L1[38] and L2[39] metallotectons represented Figure 15. L1 and L2 are synthesized in a three-step procedure, by reacting the corresponding aldehyde with pyrrole in the presence of a catalytic amount of TFA (acid catalyst), resulting in the

dipyrromethane intermediate, which is then oxidized into the targeted dipyrrin using DDQ. Furthermore, the dipyrrin ligands are mixed with several metal salts ($Ni(OAc)_2$, $Cu(OAc)_2$ and $Zn(OAc)_2$), affording metallotectons bearing H-bonding sites (Figure 15).

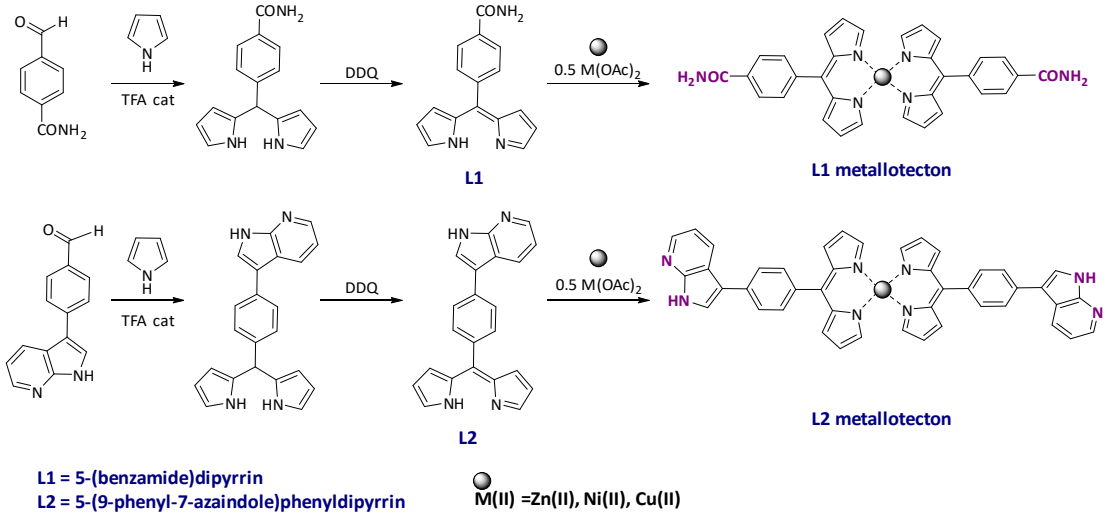

Figure 15: The synthesis of L1[38] and L2[39] metallotectons. The H-bonding sites are represented in purple.

The ligand L1 forms a homoleptic complex in the presence of $Cu(OAc)_2$, which crystallizes in the monoclinic space group *C2/c*. The copper atom, lying on a two-fold axis, is tetra-coordinated and adopts a distorted tetrahedral geometry. L1-Cu(II) complex forms two hydrogen-bonding motifs, thus leading to a 2D hybrid network with a parallel H-bonded ladder-like structure connected by the metal nodes (Figure 16).[38]

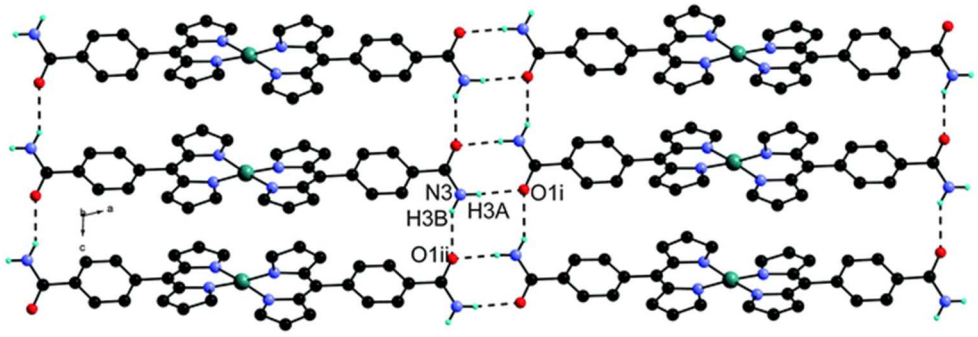

Figure 16: The crystal structure of the 2D network of L1-Cu metallotecton. Only the hydrogen atoms involved in H-bonds are depicted. Figure take form reference 38.

The L2 ligand was mixed with $Ni(OAc)_2$, $Cu(OAc)_2$ and $Zn(OAc)_2$ metal salts, affording three different metallotectons. The Cu(II) and Zn(II) metal centers, coordinate two dipyrrin ligands, and adopt a tetrahedral conformation. However, the Ni(II) metal center adopts a square planar geometry. The three complexes self-assemble into a 1D chain *via* H-bonds between the azaindole sites (Figure 17). However, the formation of a 2D network in this case was not observed, since the azaindole only behaves as a single hydrogen bonding site.[39]

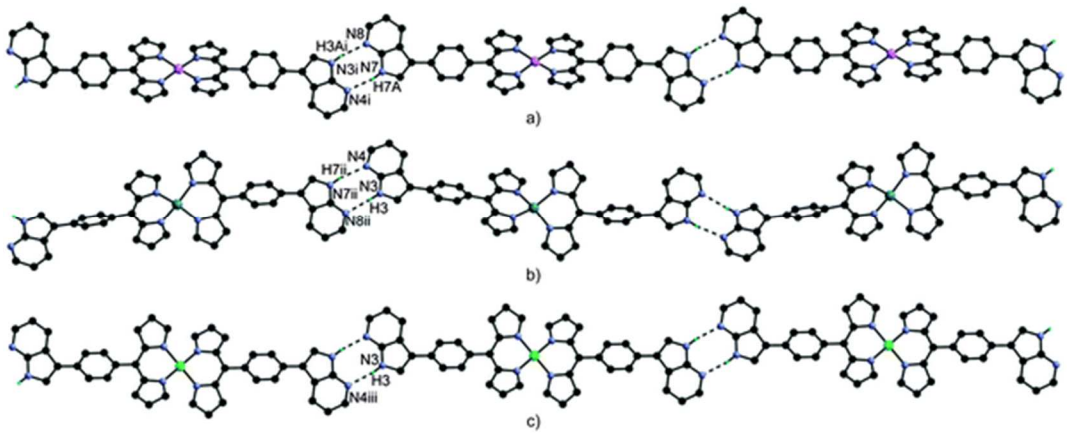

Figure 17: The crystal structure of the 1D hydrogen bonded networks of (a) L2-Zn (II) complex, (b) L2-Cu(II) complex (c) L2-Ni(II) complex. Only the NH hydrogen atoms are shown for clarity. Figure taken form reference 39.

II. Dipyrrins bearing nucleobases

Introducing peripheral coordination or H-bonding sites into the dipyrrin scaffolds results in highly attractive tectons, which may be used to design molecular networks assembled *via* different intermolecular interactions. The dipyrrin ligands can be easily functionalized at the *meso* or α-positions by a wide range of H-bonding moieties, for instance the nucleobases. One must mention that only few examples of dipyrrin bearing nucleobases are known in the literature. However, a wide variety of dipyrrins bearing H-bonding motifs, very similar to the four nucleobases found in DNA, are reported along with their self-assembly.

II. 1. Some examples of dipyrrins functionalized by NBs

A recent example of a BODIPY complex bearing guanine is reported, and its self-assembly into a 2D network is described.[40] The **G**-BODIPY was synthesized by a Sonogashira cross-coupling reaction between iodo-BODIPY and 8-ethynyl guanine (Figure 18) .

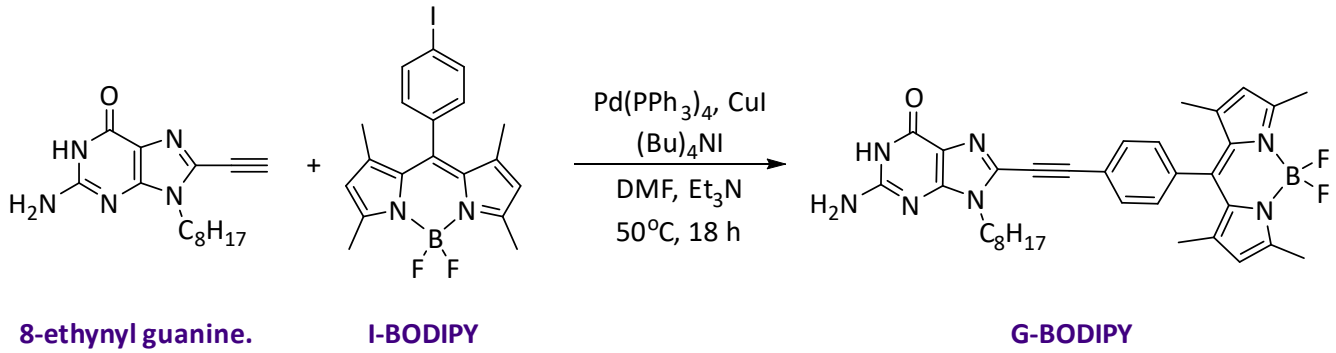

Figure 18: The synthesis of **G**-BODIPY.[40]

The **G**-BODIPY crystalizes in a triclinic space group *P-1*. The guanine sites of two adjacent molecules self-assemble by hydrogen bonding interactions, resulting in a G-ribbon structure with the dipyrrin moieties attached at both sides of the ribbons. The G-ribbons were further packed into a double-layered pattern *via* π-π interactions between two guanine moieties (Figure 19).

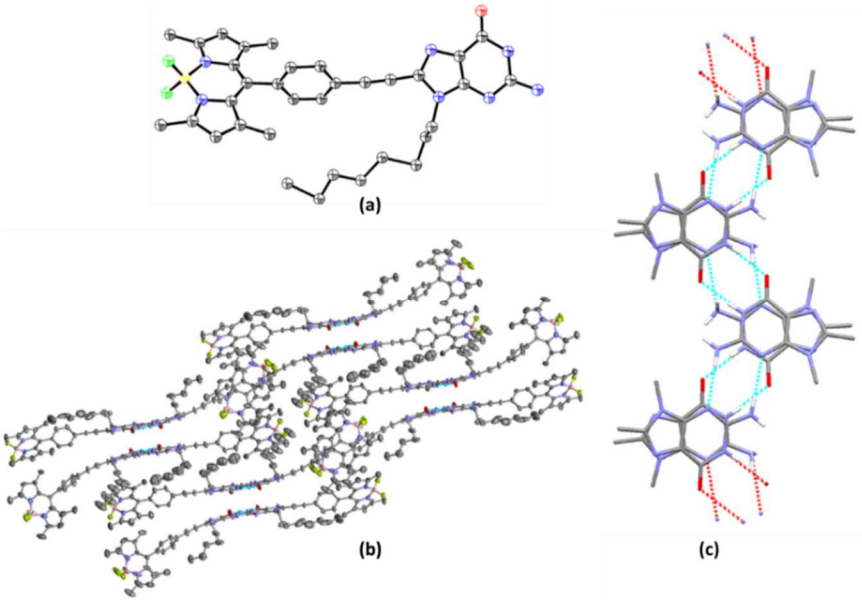

Figure 19: (a) The crystal structure G-BODIPY. (b) The packing of G-BODIPY. (c) The double-layer ribbon-like assembly of G-BODIPY. Figure modified from reference 40.

The diaminotriazinyl (DAT) H-bonding motif has similar H-bonding properties as NBs. A metallotecton bearing three DAT molecules and its assembly into a H-bonded network has been reported.[23(a),41] The complex has a pseudo-octahedral Co(III) core, where the three DAT groups are crystallographically nonequivalent (Figure 20 (b)). Each tecton participates in a total of 10 N-H···N hydrogen bonds, which fall into two categories corresponding to supramolecular synthons I and II in Figure 20 (a). The hydrogen-bonding motif forms S-shaped chains of six DAT groups, which in turn generate an open two-dimensional network (Figure 20 (c)).

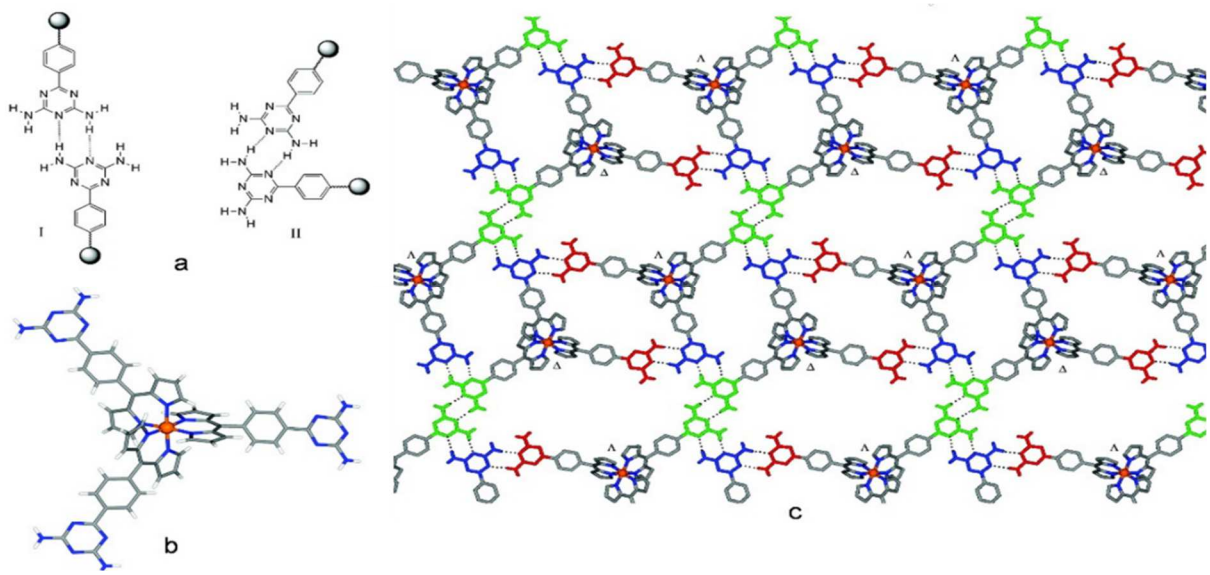

Figure 20: (a) The intermolecular H-bonding between two DAT molecules. (b) The coordination sphere around the Co(III) metal center (c) The 2-D network. The three DAT groups of each tecton are shown in different colors (blue, green, and red). Figure taken from reference 23 (a).

II. 2. Aim of the project

Nucleobases are well known for their H-bonding properties, while dipyrrins have the ability to form either discrete or infinite coordination assemblies. Together, nucleobases and dipyrrins, represent interesting moieties that, when combined, could afford interesting tectons for the formation of novel networks. Therefore, the main objective of this study is to synthesize dipyrrin-based tectons bearing the four nucleobases (**T**, **A**, **C** and **G**), to metallate them with various metal centres and to subsequently design molecular networks assembled *via* NB's H-bonding and dipyrrins' coordination interactions (Figure 21).

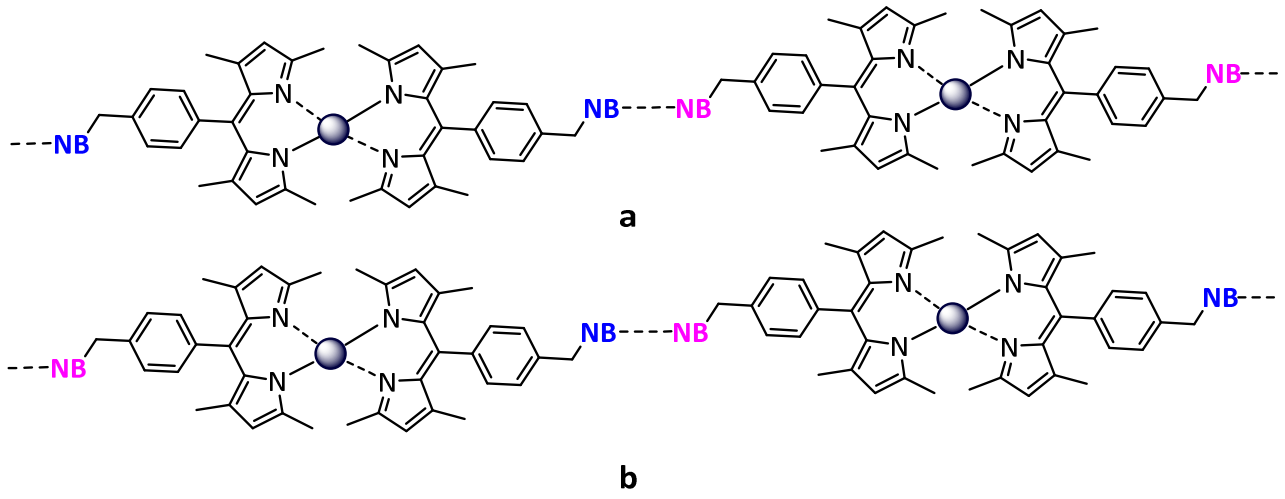

Figure 21: An example of a supramolecular network that could form *via* H-bonding interactions between (a) two complementary homoleptic bisdipyrrin complexes or (b) a heteroleptic self-complementary bisdipyrrin complex.

II. 3. Synthesis of dipyrrins bearing NBs

Dipyrrins are easily functionalized at the *meso* position, by reacting the corresponding aldehyde with pyrrole in the presence of an acid catalyst. We first decided to follow a procedure similar to the one used to introduce NBs at the *meso* position of porphyrins, as described in the previous chapter. The procedure aimed to synthesize a dipyrrin bearing an active bromine site, which will be used a starting material for the substitution reactions with the NBs to afford the targeted tectons (Figure 22).

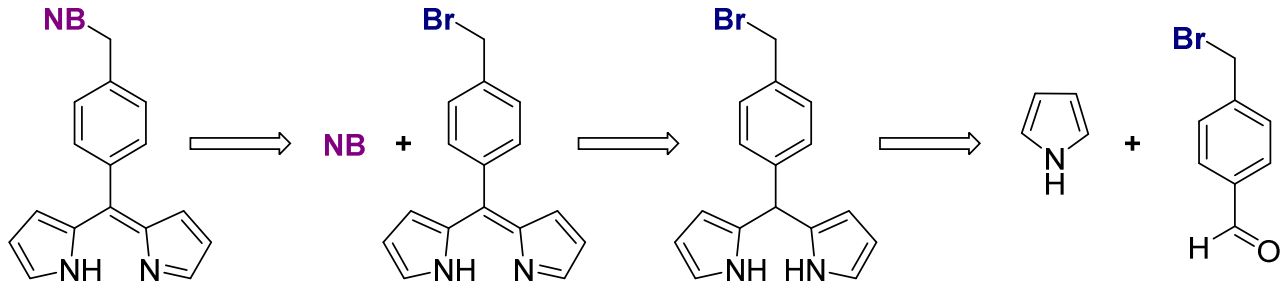

Figure 22: A possible retrosynthetic pathway of the targeted tectons.

Following known procedures for similar compounds,[3(a), 42] an excess of pyrrole (40 eq.) was reacted with an equivalent of 4-(bromomethyl)benzaldehyde (**Ald-Br**) and 2 drops of TFA, in order to synthesize the targeted dipyrromethane bearing an active bromine site. The excess of pyrrole in this case was used to avoid polymerization reactions.[42] The crude was purified by column chromatography, and the product was analyzed by NMR and MS, which proved the formation of a byproduct instead of the targeted dipyrromethane. Indeed, the number of peaks and their integration in the ^{1}H-NMR spectrum did not correspond to the targeted product. In addition, the MS showed a mass of 242.28 $(M+1)^{+1}$ instead of 315.04 $(M+1)^{+1}$, and the isotopic profile is not compatible with the presence of a Br atom in the molecule.

The use of unsubstituted pyrrole might lead to secondary reactions, which form several byproducts. Therefore, pyrrole was replaced with 2,4-dimethylpyrrole aiming to favor the formation of the targeted dipyrrin. Two equivalents of 2,4-dimethylpyrrole were reacted with an equivalent of **Ald-Br** and a catalytic amount of TFA. The dipyrromethane was directly oxidized by DDQ, following known procedures.[2(b), 43] Unfortunately, MS and NMR analysis of the purified product were not compatible with the desired dipyrrin.

The chemical structure of the formed product, in both reactions, was not elucidated. However, it was certain that the bromine group was not present and that it was involved in a secondary reaction. To avoid the loss of the bromine active site, another synthetic strategy was explored (Figure 23). **Br-Ald** was first reacted with the nucleobases in order to synthesize nucleobases bearing an aldehyde function. The latter was then reacted with 2,4-dimethylpyrrole in the presence of TFA to afford the targeted tectons. The 2,4-dimethylpyrrole was used to synthesize the dipyrrin tectons, instead of pyrrole, to increase solubility of the final products and to prevent possible polymerization process.

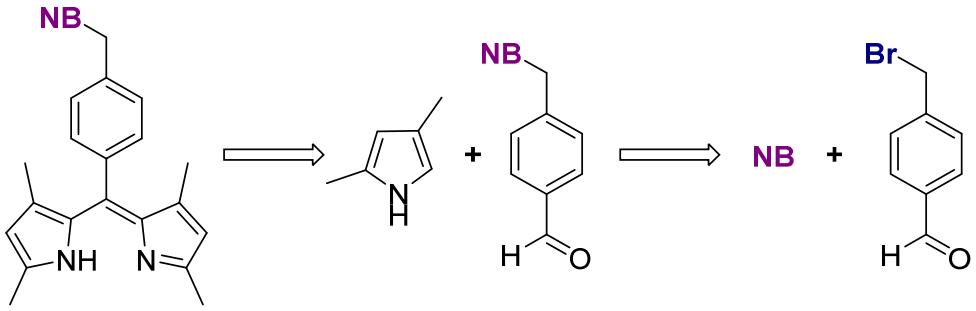

Figure 23: The retrosynthesis of the targeted tectons.

II. 3. a) 1,3,7,9-tetramethyl-5-(N_1-methylphenylthymine)-dipyrrin (T-dipyrrin) (T11)

In order to connect benzaldehyde to thymine (**T**), one equivalent of **Br-Ald** was reacted with 2 equivalents of **T** in the presence of 1.5 equivalents of K_2CO_3.[44,45] The reaction yielded two products, the targeted monosubstituted 4-(N_1-methylthymine)benzaldehyde (**T-Ald**) together with the disubstituted bis-4-(N_1,N_3-methylthymine)benzylaldehyde. The side reaction was expected, since the deprotonation of both amine functions of thymine is possible with K_2CO_3.[45,46] However the conditions used lead to a minimum amount of side product, while making the target one the major compound. The crude was purified by column chromatography to yield 57 % of **T-Ald** and 5% of the di-substituted product (Figure 24).

In a second step **T-Ald** was reacted with pyrrole following procedures described for similar compounds.[2(b), 43] One equivalent of **T-Ald** was reacted with 2 equivalents of 2,4-dimethylpyrrole in the presence of a catalytic amount of TFA (2 drops) in dichloromethane. The formed dipyrromethane was not isolated, and the direct oxidation by DDQ (0.9 eq.) was performed. The crude was purified by column chromatography to yield 53 % of the targeted **T-dipyrrin** (**T11**) (Figure 24). The chemical structure of **T11** was confirmed by NMR and MS analysis. In addition, **T11** was analysed by IR and UV spectroscopies.

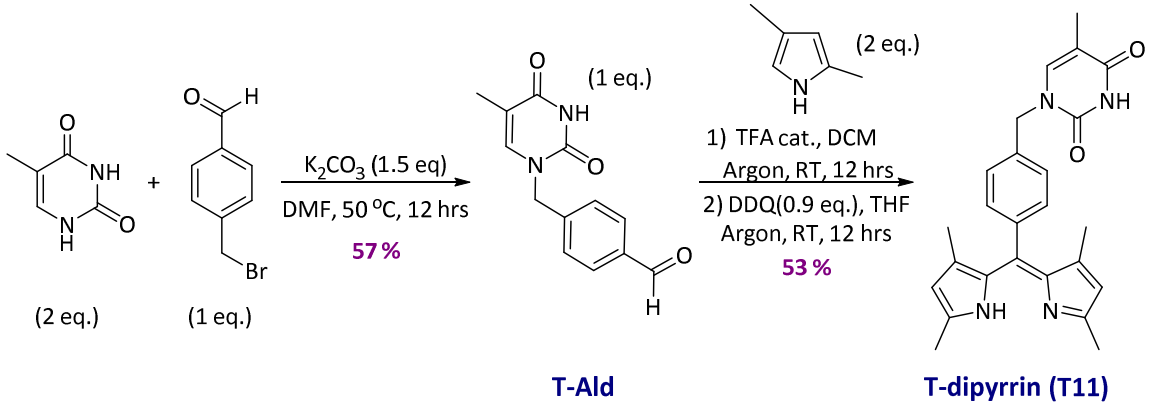

Figure 24: The synthesis of **T-dipyrrin**.

II. 3. b) 1,3,7,9-tetramethyl-5-(N_9-methylphenyladenine)-dipyrrin (A-dipyrrin) (T12)

The same procedure was followed to introduce the second NB, adenine (**A**). **Br-Ald** (1 eq.) was reacted with 2 equivalents of adenine and 1.5 equivalents of K_2CO_3 to afford the targeted **A-Ald** with a yield of 45%. Subsequently, the **A-Ald** was reacted with 2,4-dimethylpyrrole in the

presence of a catalytic amount of TFA in DCM. The crude was oxidized by DDQ (0.9 eq.) to yield 26 % of **A-dipyrrin** (**T12**) (Figure 25).

The low yield, compared to the synthesis of **T11**, can be attributed to the low solubility and high polarity of the formed **A-dipyrrin**, which affected the ease of the purification process. An eluent with higher polarity (5% MeOH and 1% ammonia in DCM) was needed to elute the product. **A-dipyrrin** was characterized by NMR, HRMS, UV and IR, which confirmed the chemical structure of the final tecton.

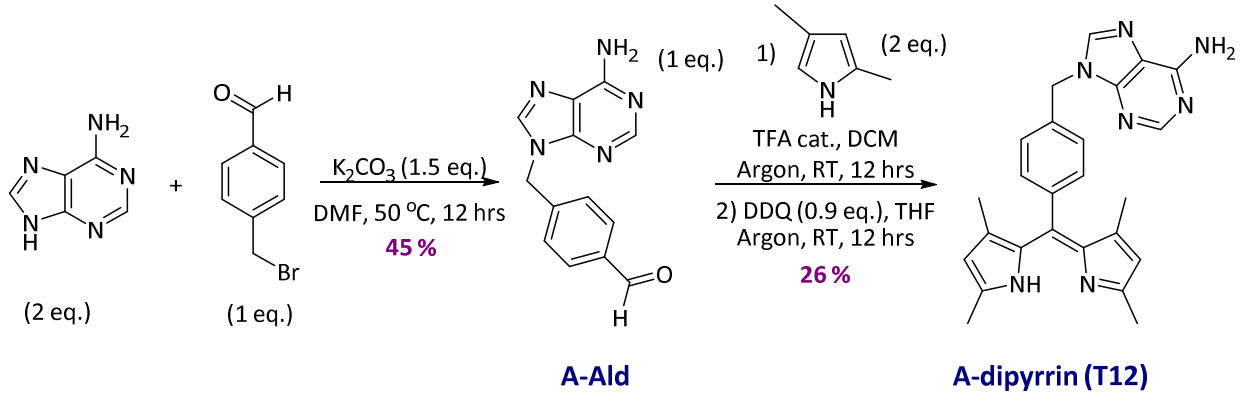

Figure 25: The synthesis of **A-dipyrrin (T12)**

II. 3. c) 1,3,7,9-tetramethyl-5-(N_1-methylphenylcytosine)-dipyrrin (C-dipyrrin) (T13)

To introduce cytosine (**C**) to the dipyrrin backbone, **Br-Ald** (1 eq.) was reacted with 2 equivalents of cytosine and 1.5 equivalents of NaH to afford the targeted **C-Ald** (**T13**) with a yield of 45%. As discussed in chapter I, the deprotonation of the N1 position of cytosine by K_2CO_3 results in a poor yield, thus a stronger base, NaH was used. **C-Ald** was then reacted with 2,4-dimethylpyrrole in the presence of a catalytic amount of TFA in DCM. The obtained crude was oxidized by DDQ (0.9 eq.) to yield 20 % of **C-dipyrrin** (**T13**) (Figure 26). This is the lowest yield obtained out of all the synthesis of the dipyrrins bearing nucleobases. Cytosine is known to form stable dimers *via* 2 H-bonds resulting in its lower solubility and reactivity compared to thymine and adenine.[46] Moreover, an eluent with higher polarity (5% MeOH and 5% ammonia in DCM) was needed to purify **C-dipyyrin**. The synthesis was repeated several times to optimize the yield. Unfortunately, the obtained yields were lower or close to 20% (Figure 26).

C-dipyrrin was characterized by NMR, HRMS, UV and IR analysis, which confirmed the chemical structure of the final tecton. The ^{1}H-NMR of **T13** showed the characteristic peaks of cytosine, with two broad singlets at 7.02 and 7.10 ppm, integrating each for one proton and corresponding to the tautomeric form of cytosine present in solution.

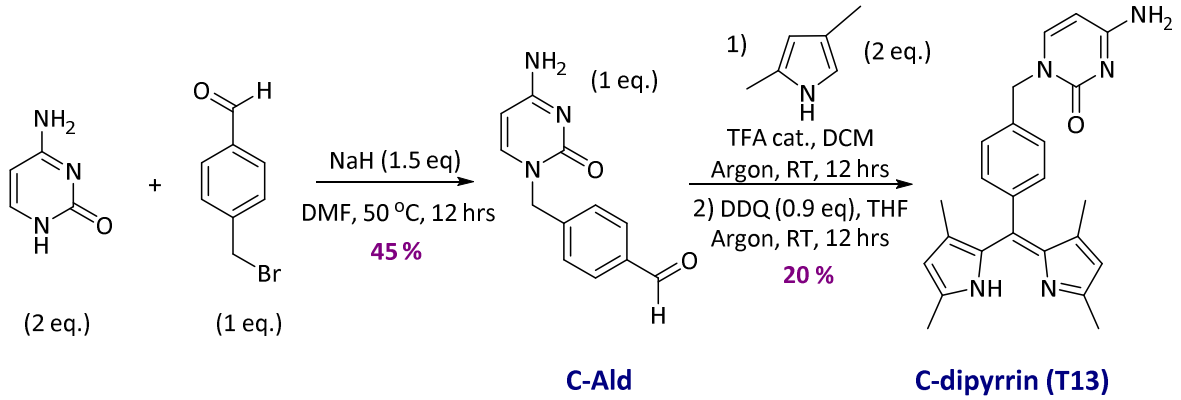

Figure 26: The synthesis of **C-dipyrrin** (**T13**)

II. 3. d) 1,3,7,9-tetramethyl-5-(N$_9$-methylphenylguanine)-dipyrrin (G-dipyrrin) (T15)

The final nucleobase to be introduced to the dipyrrin backbone is guanine (**G**). From the past experiences, reacting guanine will afford a low soluble product, due to the H-bond interactions between guanine moieties. Therefore, 2-amino-6-chloropurine (**P**) was used instead, in order to afford a more soluble dipyrrin intermediate, which can be oxidized to the targeted tecton (**T15**) (Figure 27).

Two equivalents of **P** and one equivalent of **Br-Ald** were reacted in the presence of 1.5 equivalents of K_2CO_3, to afford 43% of the targeted **P-Ald**. The latter was reacted with 2 equivalents of 2,4-dimethylpyrrole and a catalytic amount of TFA. Subsequent oxidation by DDQ was performed, which yielded 33% of **P-dipyrrin** (Figure 27). **T14** was characterized by NMR, IR, UV and HRMS.

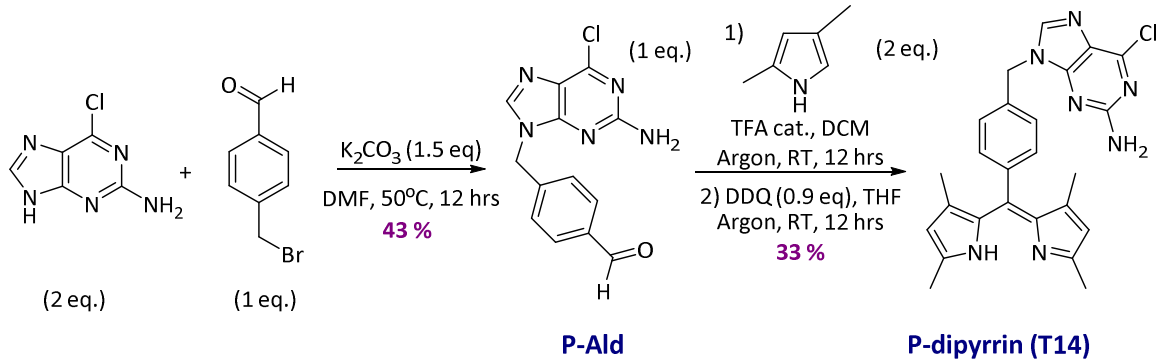

Figure 27: The synthesis of **P-dipyrrin** (**T14**).

A solution of **P-dipyrrin** in methanol was stirred with a 0.1 M HCl aqueous solution. The acid hydrolysis of **P-dipyrrin** afforded **G-dipyrrin** (**T15**) with a yield of 80% (Figure 28).

T15 was characterized by IR and HRMS. Unfortunately, ^{1}H and ^{13}C NMR for **G-dipyrrin** was difficult to perform, due to its low solubility in dichloromethane, chloroform or DMF. In such cases, the NMR is performed in d_6-DMSO, or in a mixture of $CDCl_3$ and MeOD or in deuterated 1,1,1,3,3,3-hexafluoro-2-propanal (HFIP)[47]. Unfortunately, **T15** is also poorly soluble in all these deuterated solvents and no clear NMR spectrum could be obtained.

The success of the acid hydrolysis was proven by the IR and MS analysis. The IR spectrum of **P-dipyrrin** showed a vibration at 1609 cm^{-1} corresponding to the C=N stretching of **P**. In **G-dipyrrin**, this band shifted to 1682 cm^{-1}, which corresponds to the C=O stretching present in **G**. Moreover, the success of the acid hydrolysis was proved by the change of the $[M+1]^{+1}$ peak in MS from 458.18 for **P-dipyrrin** to 440.22 for **G-dipyrin**.

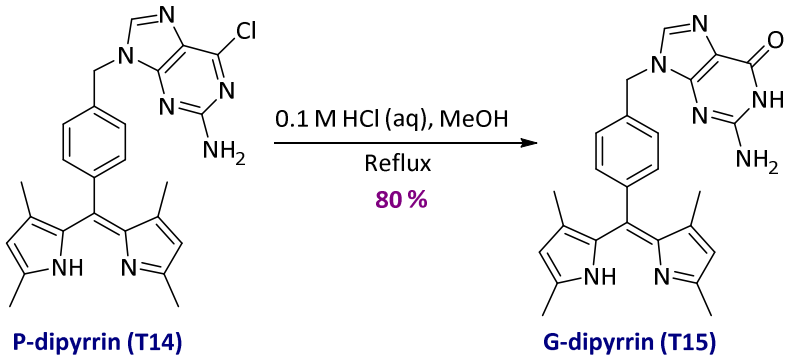

Figure 28: The hydrolysis of **P-dipyrrin** (**T14**) into **G-dipyrrin** (**T15**).

III. H-bonded network based on Zn(II)(T-dipyrrin)$_2$

Numerous attempts to grow single-crystals of these five new dipyrrin ligands (**T11-T15**) , in order to characterize them by X-Ray diffraction, were performed. Different techniques such as liquid diffusion, slow evaporation, or vapour diffusion were explored, but with no success yet. Moreover, we also tried to crystallize the assembly of complementary tectons such as **T-dipyrrin** with **A-dipyrrin** and **G-dipyrrin** with **C-dipyrrin**, but no single crystal has been isolated yet.

The aim of this part is also to generate H-bonded network based on bis-dipyrrin complexes. Thus the tectons were mixed with different metal salts ($M(OAc)_2$, M= Zn (II), Cd (II), Cu(II), Ni(II), Ru(II), Pd(II)). Single crystals were only obtained for **T11 (T-dipyrrin)** in the presence of $Zn(OAc)_2.2H_2O$. The structure obtained revealed that the metallation of the dipyrrin moiety occured, resulting in the formation of a bis-dipyrrin zinc complex, **T-dipyrrin-Zn(II)**, that self-assembled into a complex H-bonded network (Figure 29-31).

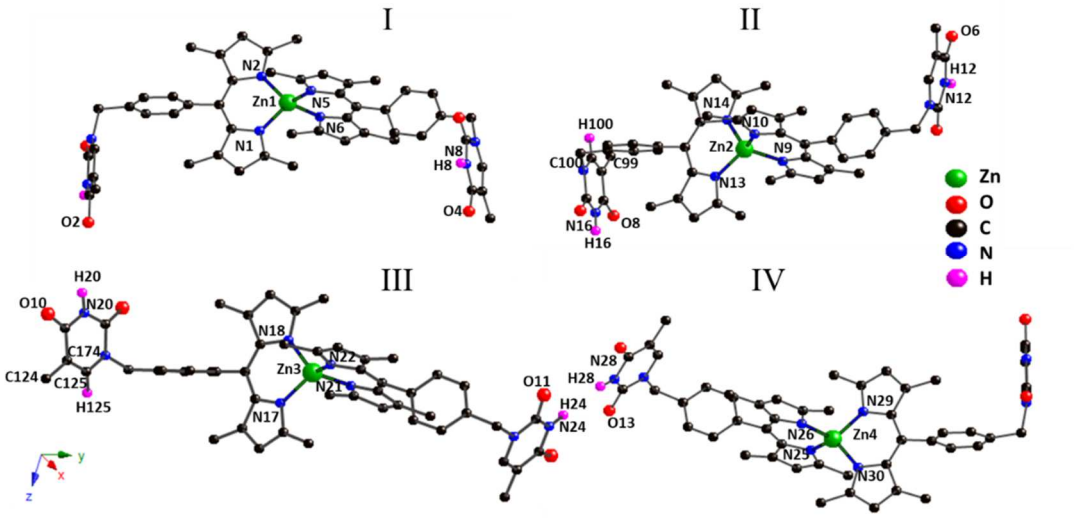

Figure 29: The crystal structure of the 4 complexes (**I**, **II**, **III** and **IV**). For description of **I**, **II**, **III** and **IV** see the text bellow.

T-dipyrrin-Zn(II) crystallizes in the monoclinic $P2_1/n$ space group. Two dipyrrin moieties are coordinated to a zinc ion, forming a H-bonded tetramer involving four nonequivalent bis-dipyrrin complexes (**I**, **II**, **III**, **IV**) (Figure 29 and 30). The zinc cations are all four coordinated, adopting a deformed tetrahedral geometry, with Zn-N distance close to 2.0 Å (Figure 29).

The four complexes differ in the crystal by the orientation of their thymine peripheral sites, which is dictated by the interactions between the thymine moieties. The four complexes are connected *via* H-bonds between the thymine moieties forming a chain (**I-II-III-IV**) (Figure 30).

Complex **I** and **II** are connected by two H-bonds between their thymine moieties with an average distance of 2.90 Å (dO6-N8 and dO4-N12). Moreover, the two complexes are connected *via* a C-H···O interaction between the carbonyl (O2) of the thymine belonging to complex **I** and the π-CH (C100H100) of the thymine belonging to complex **II** with a distance of 3.07 Å (dC100-O2) (according to crystallographic numbering) (Figure 30). In addition to conventional H-bonds (N-H···O), NBs can be involved in weak H-bonds denoted as CH···O. Such interactions are found in biological assemblies, for example between the nucleic acids of DNA and between proteins.[48] Complex **II** and **III** are connected by two H-bonds between the thymines with a distance of 2.82 Å (dN16-O10 and dO8-N20). From the other side, complex **III** is connected to the complex **IV** *via* two H-bonds between the thymines with an average distance close to 2.80 Å (dO11-N28 and dN24-O13) (Figure 30).

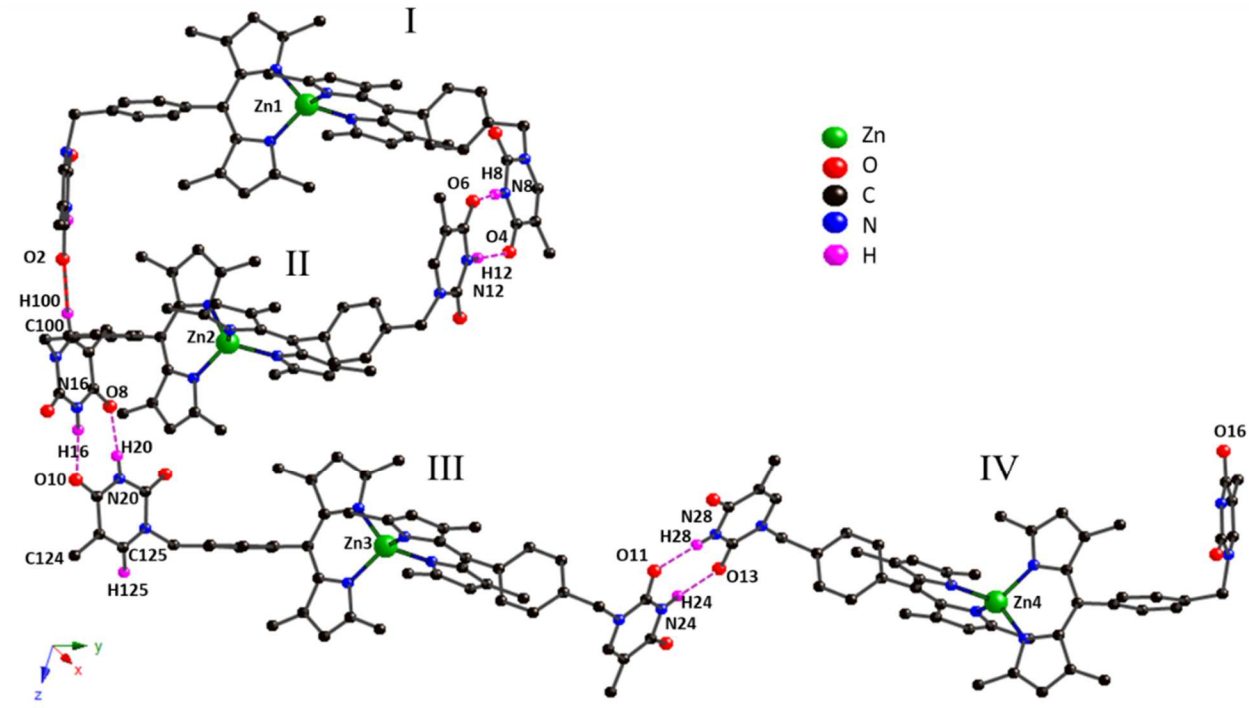

Figure 30: The crystal structure of the H-bonded chain. Hydrogen atoms not included in H-bonding are omitted for clarity.

Each tetramer interacts with two adjacent tetramer through CH---O interaction involving C125 of complex **III** and O16 of complex **IV** of another tetramer, with a C125-O16'' or C125'-O16 distance of 3.196 Å, thus leading to the formation of a 1D H-bonded ribbon (Figure 31).

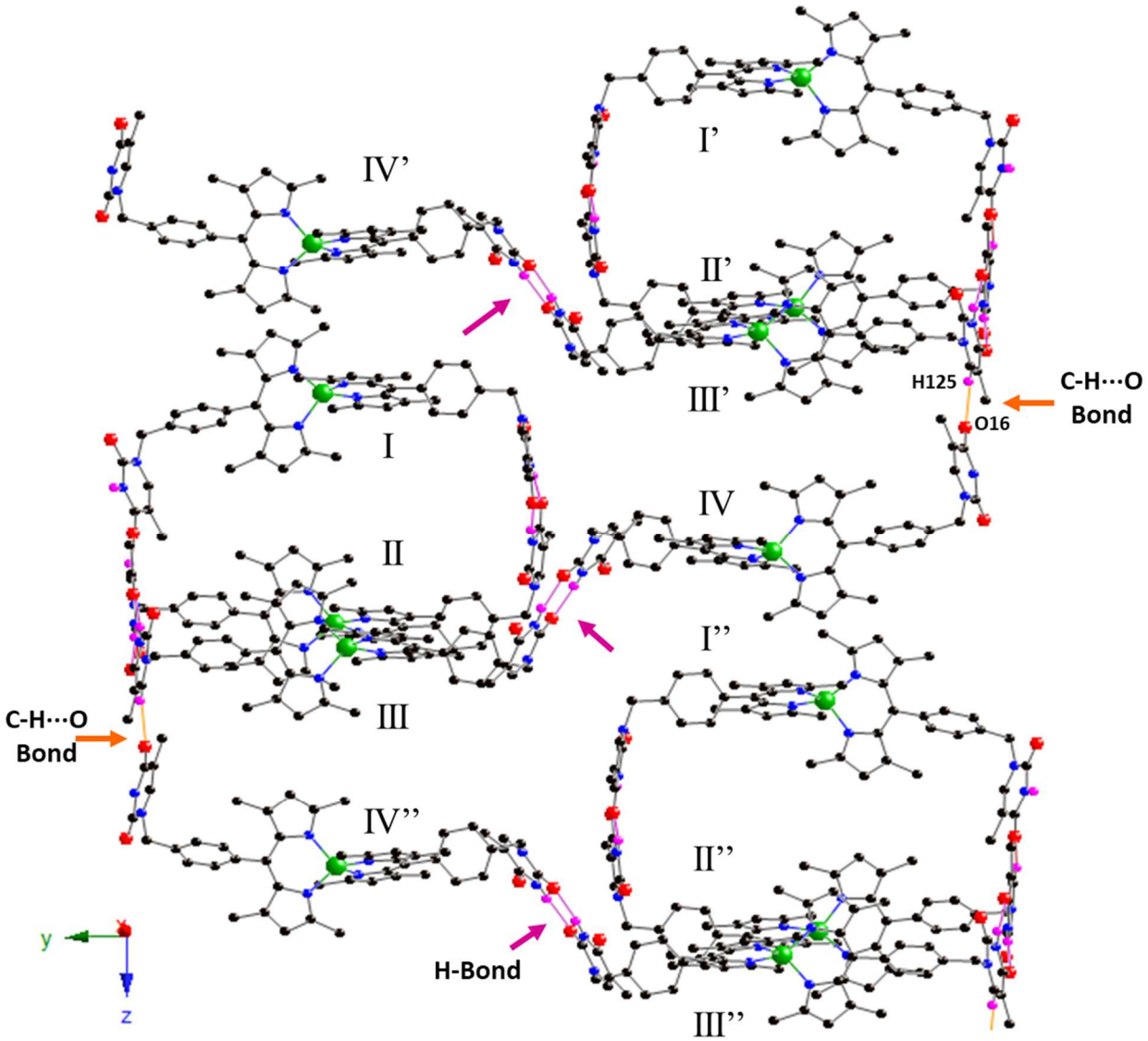

Figure 31: The Crystal Structure of the 1D ribbon.

IV. Conclusion and Perspectives

Introducing H-bonding sites, such as nucleobases, into dipyrrins affords interesting molecular tectons that can self-assemble *via* several intermolecular interactions. The five NBs **T**, **A**, **C**, **P** and **G** were introduced at the *meso*-position of dipyrrins, following a procedure similar to the one used in chapter I for the porphyrins. As a result, five new tectons **T11**-**T15** were synthesized and characterized (Figure 32).

The aim of the project was to design molecular networks assembled *via* Watson-Crick H-bonding between the self-complementary and the complementary tectons. Indeed, the self-assembly of **T11** (**T-dipyrrin**) in the presence of Zn(II) resulted in a 1D network through coordination bonds of the metal center and *via* different **T**-**T** interactions, the Watson-Crick and C-H···O H-bonds (Figure 31).

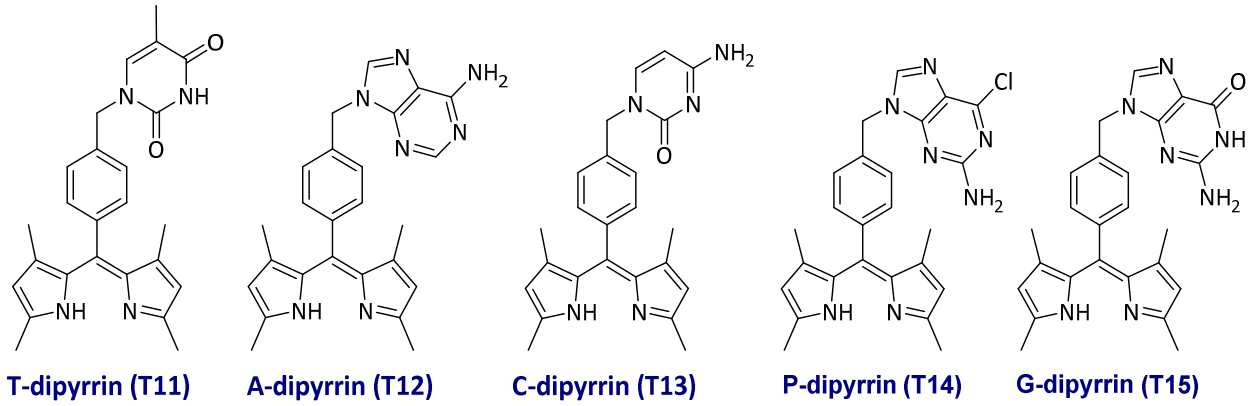

Figure 32: The chemical structure of **T11**-**T15**.

Furthermore, the attempt to design other molecular networks based on the self-assembly of single tecton or by combining complementary tectons, such as **T-dipyrrin** and **A-dipyyrin** or **C-dipyrrin** and **G-dipyrrin**, were performed. Unfortunately, no single crystals suitable for X-ray analysis were obtained yet. Therefore, among many options, the first perspective is to pursue our attempts at crystallizing the tectons with different metal salts. Instead of this one pot procedure, another possibility would be to proceed in a two-step procedure, the first step focusing on the

synthesis and characterization of homo or heteroleptic bis-dipyrrin complex and then to study their assembly in the solid state.

The second perspective is to study the luminescent properties of the **T-dipyrrin-Zn(II)** complex. Moreover, the project can be extended to the synthesis of BODIPY complexes bearing NBs, and the study of their luminescence properties (Figure 33). Last but not least, introducing additional NB in the α-position of the tetramethyl-dipyrrin backbone is possible, by reacting the NB-dipyrrin with the corresponding NB-aldehyde in the presence of *p*-toluenesulfonic acid.[49] This will afford tectons bearing three NBs that have a high potential to form networks *via* 3 H-bonding sites (Figure 33).

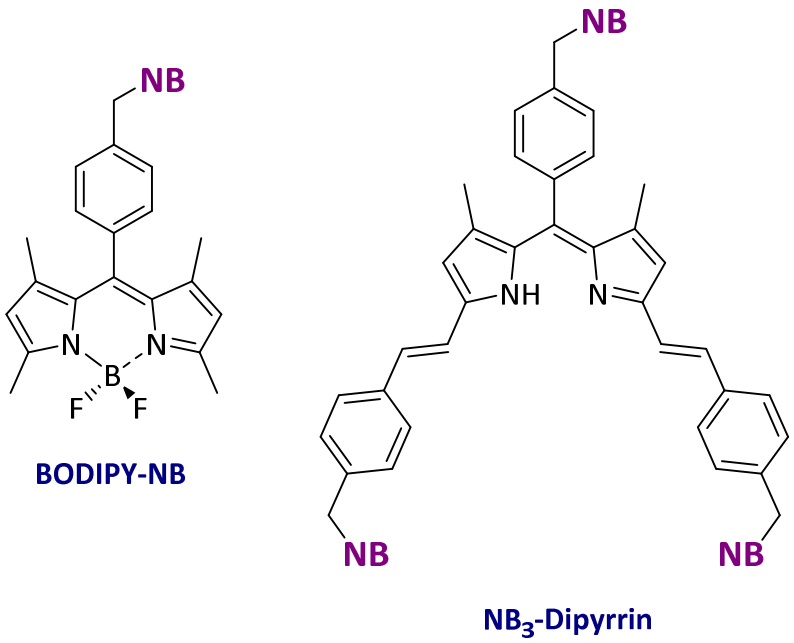

Figure 33: Schematic representation of future tectons.

V. References

1) H. Fischer, M. Schubert, *Ber. Dtsch. Chem. Ges.*, **1924**, *57*, 610-617.

2) (a) R. Matsuoko, T. Nabeshima, *Front. Chem.,* **2018**, *6(349)*, 1-13. (b) S. A. Baudron, *CrystEngComm*, **2010**, *12*, 2288-2295. (c) A. Thompson, S. J. Rettig, D. Dolphin, *Chem. Commun*., **1999**, *3*, 631-632.

3). (a) D. Perl, S. W. Bisset, S. G. Tefler, *Dalton Trans.*, **2016**, *45*, 2440-2443. (b) R. W. Wagner, J. S. Lindsey, *Pure Appl. Chem*., **1996**, *68*, 1373-1380.

4) (a) Y. Zhang, A. Thompson, S. J. Rettig, D. Dolphin, *J. Am. Chem. Soc.*, **1998**, *120*, 13537-13538. (b) M. Bröring, S. Link, C. D. Brandt, E. C. Tejero, *Eur. J. Inorg. Chem.*, **2007**, 1661-1670. (c) G. B. Guseva, L. A. Antina, E. V. Antina, A. I. Vyugin, *Thermochim. Acta.,* **2012**, *544*, 54-56.

5) (a) S. A. Baudron, *CrystEngComm*, **2016**, *18*, 4671-4680. (b) R. Ziessel, G. Ulrich, A. Harriman, *New J. Chem.*, **2007**, *31*, 496-501. (c) R. I. Roacho, A. Metta-Magana, E. Pena-Cabrera, K. Pannell, *Org. Biomol. Chem.*, **2015**, *13*, 995-999.

6) H. Fischer, H. Orth, *Die Chemie des Pyrrols*, Akademische Verlagsgesllscaft, Leipzig, **1937**.

7) G. P. Aresnault, E. Bullock, S. F. Macdonald, *J. Am. Chem. Soc*., **1960**, *82*, 4384-4389.

8) (a) A. Al-Sheikh, K. S. Cameron, T. S. Cameron, K. N. Robertson, A. Thompson, *Org. Lett.*, 2**005**, *7*, 4773-4775. (b) C. W. Wan, A. Burghart, J. Chen, F. Bergstroem, L. B. A. Johansson, M. F. Wolford, T. G. Kim, M. R. Topp, R. M. Hochstrasser, K. Burgess, *Chem. Eur. J.*, **2003**, *9*, 4430-4441.

9) C. Bruckner, V. Karunaratne, S. J. Rettig, D. Dolphin, *Can. J. Chem.,* **1996**, *74*, 2182-2193.

10) C. H. Lee, J. S. Lindsey, *Tetrahedron*, **1994**, *50*, 11427-11440.

11) (a) B. J. Littler, M. A. Miller, C.-H. Hung, R. W. Wagner, D. F. O'Shea, P. D. Boyle, J. S. Lindsey, *J. Org. Chem.*, **1999**, *64*, 1391-1396. (b) J. K. Laha, S. Dhanalekshmi, M. Taniguchi, A. Ambroise, J. S. Lindsey, *Org. Proc. Res. Dev.,* **2003**, *7*, 779-812.

12) (a) N. Boens, V. Leen, W. Dehaen, C*hem. Soc. Rev.*, **2012**, *41*, 1130-1172. (b) A. Bessette, G. S. Hanan, *Chem. Soc. Rev.*, **2014**, *43,* 3342-3405. (c) B. Le Guennic, D. Jacquemin, *Acc. Chem. Res*., **2015**, 48, 530-537. (d) G. Ulrich, R. Ziessel, A. Harriman, *Angew. Chem., Int. Ed*., **2008**, *47*, 1184-1201.

13) A. Terbis, F. H. Kreuzer, Justus Leibigs, *Ann. Chem.*, **1968**, *718*, 208-223.

14) Y. Gabe, Y. Urano, K. Kikuchi,H. Kojima, T. Nagano, *J. Am. Chem. Soc.*, **2004**, *126*, 3357-3367.

15) K. Yamada, Y. Nomura, D. Citterio, N. Iwasawa, K. Suzuki, *J. Am. Chem. Soc.*, **2005**, *127*, 6956-6957.

16) F. D. Souza, P. M. Smith, M. E. Zandler, A. L. MacCarty, M. Itou, Y.Araki, O. Ito, *J. Am. Chem. Soc.*, **2004**, *126*, 7898-7907.

17) T. E. Wood, A. Thompson, *Chem. Rev*., **2007**, *107*, 1831-1861.

18) H. Ruffin, S. A. Baudron, D. Salazar-Mendova, M. W. Hosseini, *Chem. Eur. J*., **2014**, *20*, 2449-2453.

19) L. Do, S. R. Halper, S. M. Cohen, *Chem. Comm.*, **2004**, 2662-2663.

20) A. Beziau, S. A. Baudron, A. Guenet, M. W. Hosseini, *Chem. Eur. J*., **2013**, *19*, 3215-3223.

21) J. D. Hall, T. M. McLean, S. J. Smalley, M. R. Waterland, S. G. Tefler, *Dalton Trans.*, **2010**, *39*,437-445.

22) (a) H. Maeda, T. Hashimmoto, R. Fuji, M. Hasegawa, *J. Nanosci. Nanotechnol.*, **2009**, *9*, 240-248. (b) M. Tsuchiya, R. Sakamoto, M. Shimada, Y. Yamanoi, Y. Hattori, K. Sugimoto, E. Nishibori, H. Nishihara, *Inorg. Chem.*, **2016**, *55*, 5732-5734.

23) (a) S. G. Tefler, J. D. Wuest, *Cryst. Growth Des.*, **2009**, *9*, 1923-1931. (b) S. R. Halper, S. M. Cohen, *Inorg. Chem.,* **2005**, *44*, 486-488.

24) S. M. Cohen, S. R. Halper, *Inorg. Chim. Acta*., **2002**, *341*, 12-16.

25) S. Kusaka, R. Sakamoto, H. Nishihara, *Inorg. Chem.*, **2014**, 53, 3275-3277.

26) J. S. Stork, V. S. Thoi, S. M. Cohen, *Inorg. Chem.,* **2007**, *46*, 11213-11223.

27) D. Pogozhez, S. A. Baudron, M. W. Hosseini, *Dalton Trans*., **2011**, *40*, 437-445.

28) L. Do, S. R. Halper, S. M. Cohen, *Chem. Commun.*, **2004,** 2662-2663.

29) S. R. Halper, M. R. Malachowski, H. M. Delaney, S. M. Cohen, *Inorg. Chem.*, **2004**, *43*,1242-1249.

30) (a) A. Béziau, S. A. Baudron, D. Pogozhev, A. Fluck, M. W. Hosseini, *Chem. Commun.*, **2012**, *48*, 10313-10315. (b) A. Béziau, S. A. Baudron, A. Fluck, M. W. Hosseini, *Inorg. Chem.*, **2013***, 52*, 14439-14448. (c) A. Béziau, S. A. Baudron, D. Rasoloarison, M. W. Hosseini, *CrystEngComm*, **2014**, *16*, 4973-4980. (d) A. Béziau, S. A. Baudron, G. Rogez and M. W. Hosseini, *Inorg. Chem*., **2015**, *54*, 2032-2039 .

31) (a) A. Thompson, S. J. Rettig, D. Dolphin, *Chem. Commun.*, **1999**, *3*, 631-632. (b) N. Sakamoto, C. Ikeda, T. Nabeshima, *Chem. Commun.*, **2010**, *46*, 6732-6734. (c) S. A. Baudron, H. Ruffin, M. W. Hosseini, *Chem. Commun.*, **2015**, *51*, 5906-5909.

32) G. Gupta, A. Das, K. C. Park, A. Tron, H. Kim, J. Min, *Inorg. Chem.*, **2017**, *56*, 4615-4621.

33) (a) Y. Zhang, A. Thompson, S. J. Rettig, D. Dolphin, *J. Am. Chem. Soc.*, **1998**, *120*, 13537-13538. (b) A. Thompson, D. Dolphin, *J. Org. Chem.*, **2000**, *65*, 7870-7877.

34) (a) T. Hashimoto, T. Nishimura, J. M. Lim, D. Kim, H. Maeda, *Chem. Eur. J.*, **2010**, *16*, 11653-11661. (b) Z. Zhang, D. Dolphin, *Chem. Commun.*, **2009**, 6931-6933. (c) T. E. Wood, N. D. Dalgleish, E. D. Power, A. Thompson, X. Chen, Y. Okamoto*, J. Am. Chem. Soc.*, **2005**, *127*, 5740-5741.

35) (a) M. Bröring, S. Link, C. D. Brandt, E. C Tejero, *Eur. J. Inorg. Chem*., **2007**, 1661-1670. (b) E. V. Antina, M. B. Berezin, N. A. Dudina, G. B. Guseva, L. A. Antina, A. I. V'yugin, *Russ. J. Gen. Chem.*, **2010**, *80*, 1216-1218. (c) N. A. Bumagina, E. V. Antina, D. I. Sozonov, *J. Lumin*., **2017**, *183*, 315-321.

36) H. Ruffin, S. A. Baudron, D. Salazar-Mendoza, M. W. Hosseini, *Chem. Eur. J.,* **2014**, *20*, 2449-2453.

37) (a) K. Heinze, A. Reinhart, *Inorg. Chem.*, **2006**, *45*, 2695-2703. (b) S. G. Telfer, J. D. Wuest, *Chem. Commun.*, **2007**, 3166-3168. (*c*) S. G. Telfer, J. D. Wuest, *Cryst. Growth Des.*, **2009**, *9*, 1923-1931. (d) J. C. MacDonald, G. M. Whitesides, *Chem. Rev*., **1994**, *94*, 2383-2420. (e) J. C. MacDonald, G. T. R. Palmorein, *The Amide Linkage: Selected Structural Aspects in Chemistry, Biochemistry and Materials Science* ed., A. Greenberg, C. M. Breneman, J. F. Liebman, *Wiley, New York*, **2000**, 291-336.

38) S. A. Baudron, D. Salazar-Mendoza, M. W. Hosseini, *CrystEngComm*, **2009**, 11, 1245-1254

39) S. A. Baudron, D. Pogozhev, M. W. Hosseini, *CrystEngComm*, **2010**, *12*, 2238-2244.

40) F. Li, Y. Zhang, L. Zhou, X. Zhang, Z.Chen, *J. of Porphyrins and Phthalocyanines*, **2018***, 22*, 944-952.

41) S. G. Tefler, J. D. Wuest, *Chem. Comm.,* **2007**, 3166-3168.

42) G. R Geier III, J. S. Lindsey, *J. Chem. Soc., Perkin Trans. 2,* **2001***, 2*, 677-686.

43) J. S Lindsey, *Acc. Chem. Res*., **2009**, *43*, 300-311.

44) S. Ellipilli, K. N Ganesh, *J. Org. Chem.*, **2015**, *80*, 9185-9191.

45) N. Biblo, V. Vazque-Gonzalez, M. T. Aranda, D. Gonzalez-Rodriguez, *Eur. J. Org. Chem.*, **2015**, 7160-7175.

46) W. Saenger, Principles of Nucleic Acids structure, *Springer*, New York, **1984**.

47) L. Qi, L. -L. Gundersen, E. J. Chamgordani, C. H. Gorbitz, *CrystEngComm*, **2016**, *18*, 6352-6357.

48) S. Horowitz, R. C. Trievel, *J. Biol. Chem.,* **2012**, *287*, 41576-41582.

49) E. Knoevenagel, *Ber. Dtsch. Chem. Ges*., **1898**, *31*, 2596-2619. (b) R. Ziessel, T. Bura, J. H. Olivier, *Synlett*., **2010**, *15*, 2304-2310.

Chapter III: Pyridine and Terpyridine bearing Nucleobases

Table of Contents

I. Heterocyclic amines……..139
I. 1. Pyridines……..139
I. 2. Terpyridines……140
I. 2. a) Terpyridine metal complexes……..140
I. 2. b) Synthesis of terpyridine ligands……..143
II. Heterocyclic Amines functionalized by NBs……145
II. 1. Examples of Heterocyclic Amines functionalized by NBs……145
II. 2. Aim of the project……...155
II. 3. Pyridine bearing NBs……..158
II. 3. a) Synthesis of 4-(N1-methylthymine)pyridine (**T-Py**) (**T16**) ……...159
II. 3. b) Synthesis of 4-(N9-methyladenine)pyridine (**A-Py**) (**T17**)……160
II. 3. c) Synthesis of 4-(N1-methylcytosine)pyridine (**C-Py**) (**T18**)……..162
II. 3. d) Synthesis of 4-(N1-methylguanine)pyridine (**G-Py**) (**T20**)……..164
II. 4. Coordination networks based on **Ad-Py** (**T17**)……..165
II. 4. a) **A-Py-Cd(II)** network……165
II. 4. b) **A-Py-Hg(II)** network……167
II. 5. Coordination networks based on **C-Py** (**T18**) ……169
II. 5. a) **C-Py-Zn(II)** network……170
II. 5. b) **C-Py- Cd(II)** network……....171
II. 6. Terpyridine bearing NBs……172
II. 6. a) Synthesis of 4'-(4-bromomethylphenyl)-2,2':6',2"-terpyridine (**Br-terPy**)……..173
II. 6. b) Synthesis of 4'-(N_1-methylphenylthymine)-2,2':6',2"-terpyridine (**T-terPy**) (**T21**).173
II. 6. c) Synthesis of 4'-(N_9-methylphenyladenine)-2,2':6',2"-terpyridine (**A-terPy**) (**T22**).174
II. 6. d) Synthesis of 4'-(N_1-methylphenylcytosine)-2,2':6',2"-terpyridine(**C-terPy**) (**T23**).175
II. 6. e) Synthesis of 4'-(N_9-methylphenylguanine)-2,2':6',2"-terpyridine (**G-terPy**) (**T25**).175
II. 7. Structural characterization of complexes based on **T-terPy (T21**)……176
II. 7. a) **T-TerPy-Cu(II)** network……...176
II. 7. b) **T-TerPy-Cd(II)** network……...177
III. Conclusion and Perspective…….....179
IV. References.....……...181

I. Heterocyclic amines

Heterocyclic amines (HCAs) are molecules that contain ring moieties with at least one amine function.[1] Furthermore, HCAs are abundant molecules in nature, commonly found in vitamins, agrochemicals, pharmaceuticals and other compounds. Pyrrolic rings along with purines and pyrimidines (NBs), discussed in previous chapters, are examples of HCAs. In addition, the six-membered ring, pyridine, and its derivatives, bipyridines and terpyridines, are HCAs with different chemical and biological applications.[2] They are used in the synthesis of dye and fragrances,[2(c)] pharmaceuticals[2(d)] and agrochemicals[2(c)]. Pyridine based ligands, such as terpyridine, have been extensively used in coordination chemistry and scarcely in molecular tectonics as coordinating building blocks.[3] In this chapter, we will focus on pyridine (**Py**) and terpyridine (**terPy**) derivatives (Figure 1).

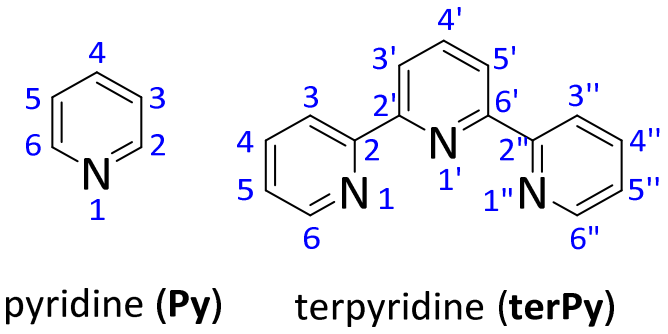

Figure 1: Chemical Structure of pyridine and tepyridine.

I. 1. Pyridines

Pyridines (**Py**) are heterocyclic organic compounds discovered in the 18th century that are used as solvents and reagents in numerous organic synthesis.[4] **Py** are planar molecules with a six π-electrons conjugated system. The electron lone pair of the nitrogen atom of pyridines are not involved in the aromatic ring, thus **Py** is a base with similar chemical properties to those of tertiary amines and a pK_a of *ca* 5.25.[4(a)] Pyridines are relatively electron deficient, due to their electronegative nitrogen atoms. Therefore, they are readily involved in electrophilic aromatic substitution reactions. However, **Py** are more prone to nucleophilic substitutions and metallation of their ring to various metal centers, which makes them widely used in coordination and supramolecular chemistry.[5] In

addition, several synthetic procedures are known for the functionalization of pyridine by other coordinating[6] or hydrogen bonding sites[7]. Moreover, its planar aromatic structure leads often to π-π stacking intyeractions. All of these properties make pyridines attractive tectons for designing molecular networks.[8]

I. 2. Terpyridines

Terpyridines (**terPy**) (2,2';6',2"-terpyridine or 2,6-bis(2-pyridyl)-pyridine) are a heterocyclic compound derived from pyridine. They were first discovered by Morgan and Burstall.[9] The **terPy** are interesting tridentate ligands used in coordination chemistry. [10] The use of **terPy** increased in recent years due to their attractive DNA-binding ability[11], together with their potential photochemical and photophysical properties[12].

I. 2. a) Terpyridine complexes

Terpyridine ligands bind a wide variety of metal centers. They mostly act as tridendate ligands but some bidentate **terPy** complexes [M(CO)(**terPy**)X] (M =Mn (I), X = Br; M = Re (I) X = NO) have been isolated and characterized.[13] Moreover, terpyridine based complexes with Mg(II), Ca(II), Ba(II), Al(III), Sn (II), As and Pb (II) have been reported, but the most popular are with 3d or 4d metal cations such as Fe(II), Zn(II), Cu(II), Ni(II), Ru(II), Pd(II), Co(II), Co(III) and Fe(III). The majority of transition metal complexes incorporate metal ions in the +2 and/or +3 oxidation state in octahedral, or square planar geometries.[14]

Upon coordination to a metallic center, **terPy** based ligands undergo a number of changes. The main difference is the constrained co-planar orientation of the three pyridine cycles with the lone pairs of three nitrogen atoms oriented in a convergent fashion. Moreover, **terPy** ligands in a planar tridentate mode, coordinated to metal centers, exhibit a reduced interannular angle between the central and terminal pyridine rings, and display slight differences in bond length compared to the free ligand (Figure 2).[14]

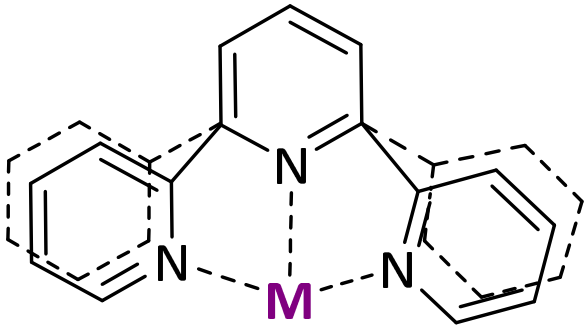

Figure 2: The distortion experienced by a terpyridine ligand upon coordination to a metal ion in a planar tridentate mode.

The **terPy** commonly behave as chelating tridentate ligands, in the majority of complexes exhibiting 1:1 or 1:2 metal:ligand ratio depending mostly on the metal cations and the counter-ions (Figure 3 and Figure 4). The 1:1 mono-terpyridine complexes usually exhibit distorted trigonal-bipyramidal or square-pyramidal geometries. The 1:2 bis-terpyridine complexes are based on an octahedral geometry around the metallic center, and they frequently exhibit a D_{2d} local symmetry. In order to prepare exclusively non symmetrical complexes such as $[M^{n+}(\mathbf{terPy}1)(\mathbf{terPy}2)]^{n+}$, the two ligands are introduced in a two-step procedure (*via* a mono-**terPy** complex intermediate). Suitable metals for this strategy are ruthenium and osmium.[15]

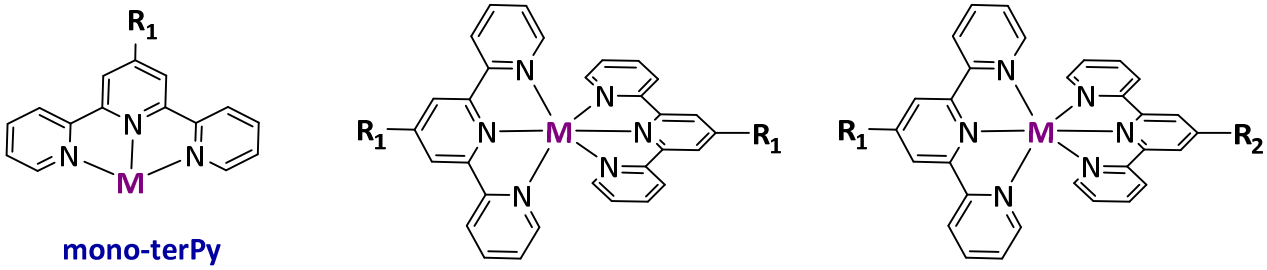

Figure 3: The chemical structure of a 1:1, symmetrical and asymmetrical 1:2 metal: **terPy** complexes. R1 and R2 represent two different substituents and M represents metal centers.

Terpyridines have been widely proposed as analytical reagents for the detection of iron in biological and other materials. The **terPy** are very sensitive to the presence of iron cations and immediately form pinkish complexes. The purple complex cation $[Fe(\mathbf{terPy})_2]^{2+}$ and its blue oxidized product

$[Fe(Terpy)_2]^{3+}$ have been discussed since the first description of **terPy**. In the presence of coordinating counter ions, iron complexes of 1:1 stoichiometry [Fe(**terPy**)X_2] (X = Br, I, or NCS) adopt a trigonal-bipyramidal geometry, with the Fe(II) being five coordinated,. In the presence of more labile ligands, a 1:2 stoichiometry is achieved as shown in the crystal structural analysis of [Fe(**terPy**)$_2$][ClO_4]$_2$.H_2O, with a distorted octahedral geometry around the Fe(II).[16] Terpyridine–ruthenium complexes of the type [Ru(**terPy**)$_2X_2$] (X = Cl^-, ClO_4^-, PF_6^-) are well-known.[17] The Ru (II) metal center in this 1:2 bis-complex is hexacoordinated, and has a distorted octahedral geometry.[18] A main characteristic of such complexes is the strength of the metal–ligand coordination bond, due to the strong metal–ligand (d–π*) back donation. Furthermore, a strong chelate effect is present.[14,15]

In the presence of Cu(II), Zn(II) or Co(II) cations, terpyridine ligands readily forms mono-**terPy** complexes.[19] Such structures adopt usually distorted square-pyramidal or distorted trigonal-bipyramidal geometries. Bis-**terPy** Cu(II) complexes are prepared in the presence excess of terpyridine ligands. In these complexes, the distorted geometry around the metallic center causes the two **terPy** ligands to become nonequivalent.[20] The **terPy** ligands can also coordinate to lanthanides (Ln) forming 1:1, 1:2 or 1:3 complexes. The 1:1 Ln-**terPy** complexes are the most widely investigated, which are nine-coordinate and readily adopt a monocapped square-antiprismatic or nine-coordinate tricapped trigonal-prismatic geometry.[21]

A huge library of terpyridine-based ligands is present in the literature, and their coordination to a large variety of metal cations are described together with potential applications. For example, Ru (II)[22], Ir (III)[23] and Os(II)[24] complexes are known for their luminescent features and photo-physical applications, Fe(III) and Co(II) complexes can act as oxidizing agents,[25] and Cu(II) and Zn(II) complexes are known for their DNA-binding properties.[11, 26]

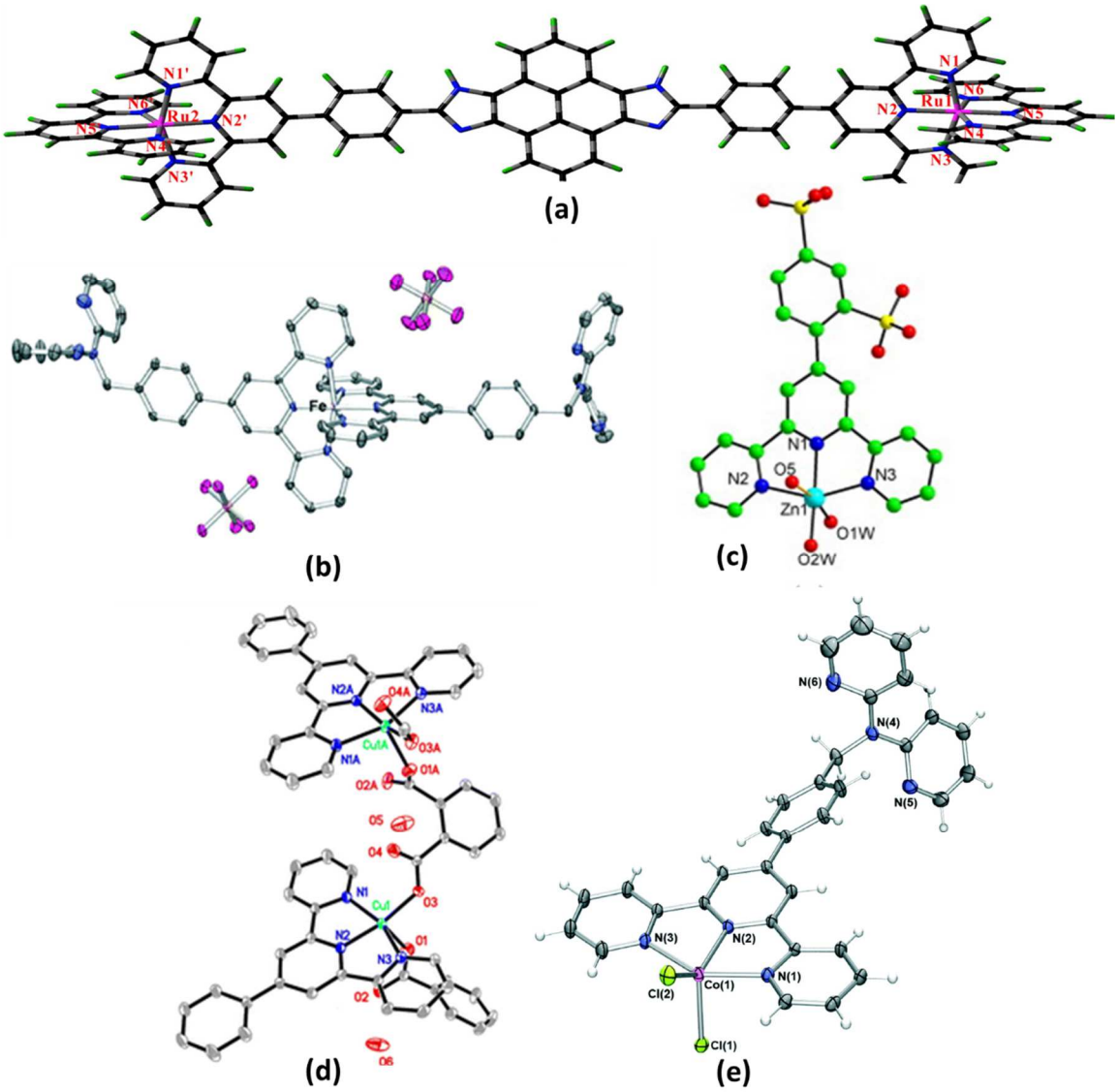

Figure 4: The crystal structure of 1:2 complexes with (a) Ru(II)[17(a)] complex, (b) Fe(II) complex[16(a)] and 1:1 complexes with (c) Zn(II)[19(a)] complex, (d) Cu(II)[19(b)] complex, (e) Co(II)[16(a)] complex.

I. 2. b) Synthesis of terpyridine based ligands

Several methods may be followed to synthesize terpyridine based ligands. For example, 4'-functionalized terpyridines can be synthesized *via* the pyridine and 4'-chloroterpyridine route.[27] The 4'-chloroterpyridine intermediate can then react with alcohols bearing the targeted substituent using a base catalyst, such as KOH. In addition, the cross-coupling of alkynes with bromo-terpyridines is another frequently used method to obtain various functionalized terpyridine ligands (Figure 5). [28]

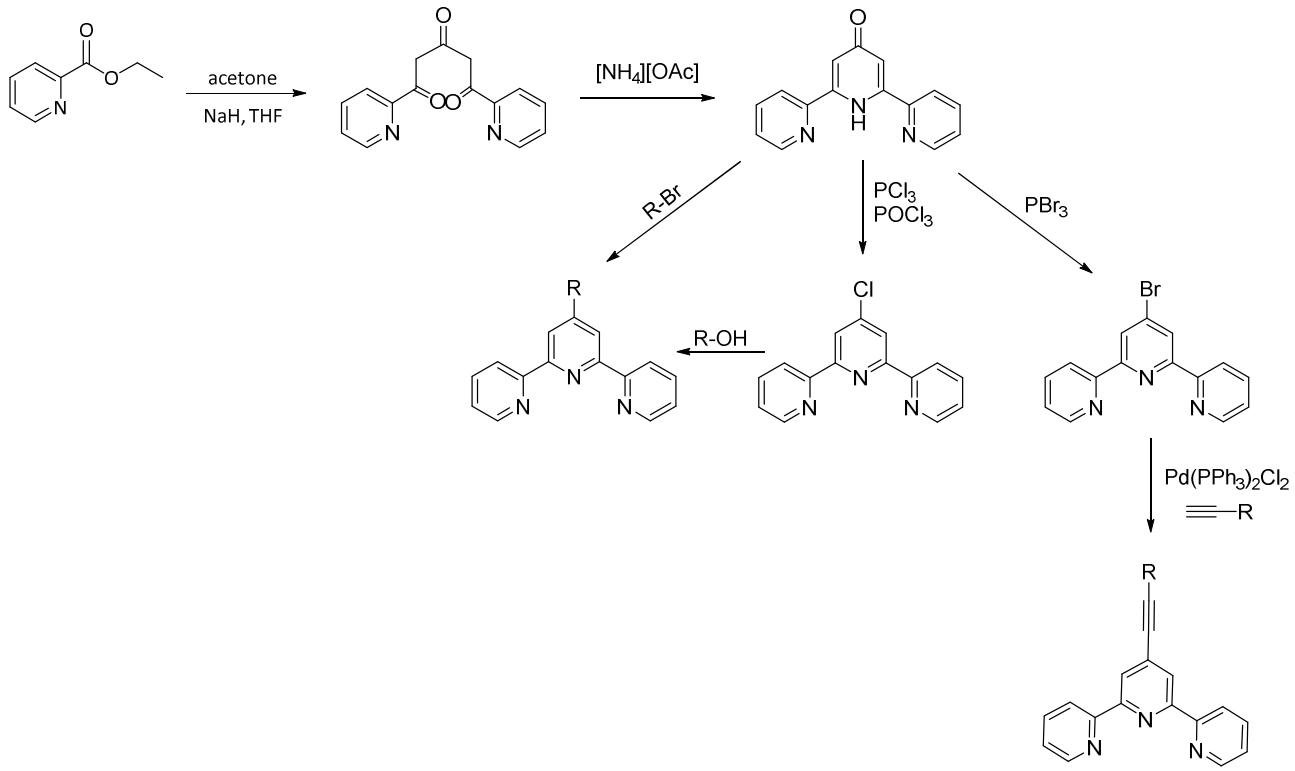

Figure 5: The synthesis of **terPy** ligands *via* the chloro-terpyridine or bromo-terpyridine and Pd-catalyzed cross-coupling reaction.[15]

Moreover, the 4'-functionalized terpyridines are readily obtained by the condensation of benzaldehyde, or by substituted benzaldehyde, with two equivalents of 2-acetylpyridine to give 1,5-diketone.[29] The latter can then be isolated prior to the aza ring closure followed by an oxidative dehydrogenation using ammonium acetate (Figure 6). A second method consists in reacting the starting material in a one-pot synthesis (Figure 6). In our group, the starting material, 4'-(4-tolyl)-2,2':6',2"-terpyridine (4-tolyl-terpy or **tolyl-terPy**) was obtained following the second method.

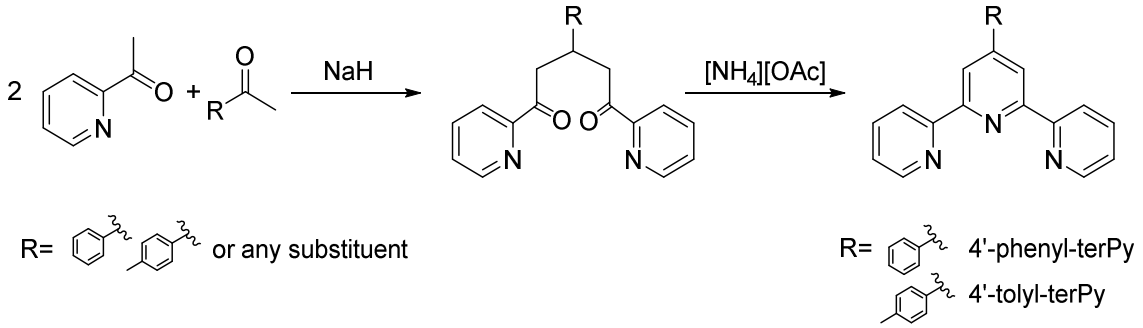

Figure 6: The synthesis of 4'-functionalized terpyridines by condensation of 2-acetylpyridine and an aldehyde.[15]

II. Heterocyclic Amines functionalized by NBs

Pyridine derivatives, as mentioned previously, have the ability to coordinate to various metal centers, and to be functionalized by different substituents. Introducing H-bonded sites to heterocyclic amines (HCA), results in promising molecules for supramolecular chemistry and molecular tectonics. Many pyridine-based molecules functionalized with nucleobases (NBs) are known in the literature, with applications such as DNA binding or photo-activity.[11, 26]

II. 1. Examples of Heterocyclic Amines functionalized by NBs

Numerous examples of building units based on NBs and N-heterocycles have been reported. This part focuses on one typical example of such ligands either with pyridine, bipyridine or terpyridine. The self-assembly of a pyridine ligand bearing isocytosine **iC-Py** and its complex **iC-Py-Pt** were investigated recently at the solid/liquid interface of an HOPG substrate (Figure 7).[30] STM characterization showed that **iC-Py** forms supermolecular ribbon-like motifs, which is in agreement with previous observations of isocytosine substituted compounds.[31] This proves that functionalization of cytosine with a pyridine moiety does not affect its self-assembly propensity.

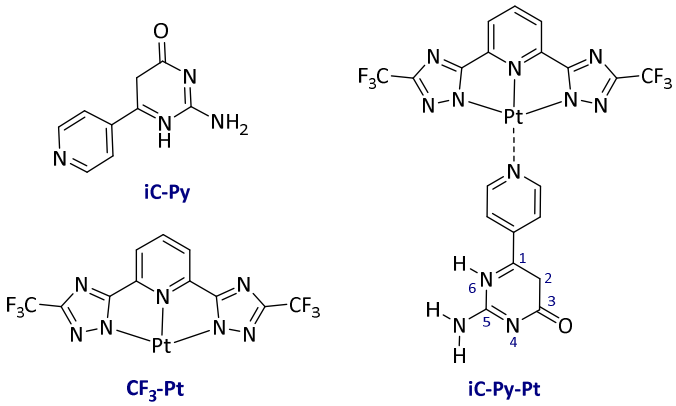

Figure 7: Chemical Structures of **iC-Py**, **CF_3-Pt** and **iC-Py-Pt**.[30]

The self-assembly of **iC-Py-Pt** complex on HOPG substrate changes due to the incorporation of the sterically demanding **CF_3-Pt** moiety. The STM images of the complex reveal the formation of 6 discrete supramolecular cyclic architectures: trimers (iC3), tetramers (iC4), pentamers (iC5), half

of hexamers (1/2 iC6) and hexamers (iC6) (Figure 8). Statistical analysis, DFT calculations, simulated STM images and calculated dissociation energy of the cyclic architectures prove that the six molecular motifs co-exist, and that the most stable and dominant (80 %) are the ½ iC6 and iC6. The latter are formed through hydrogen bonds between the cytosine moieties of type N(6)-H···O(3) and N(5)-H···N(4), and have the highest dissociation energy. iC3, iC4 and iC5 are stabilized by the electrostatic interactions present between isocytosine moieties of adjacent molecules.

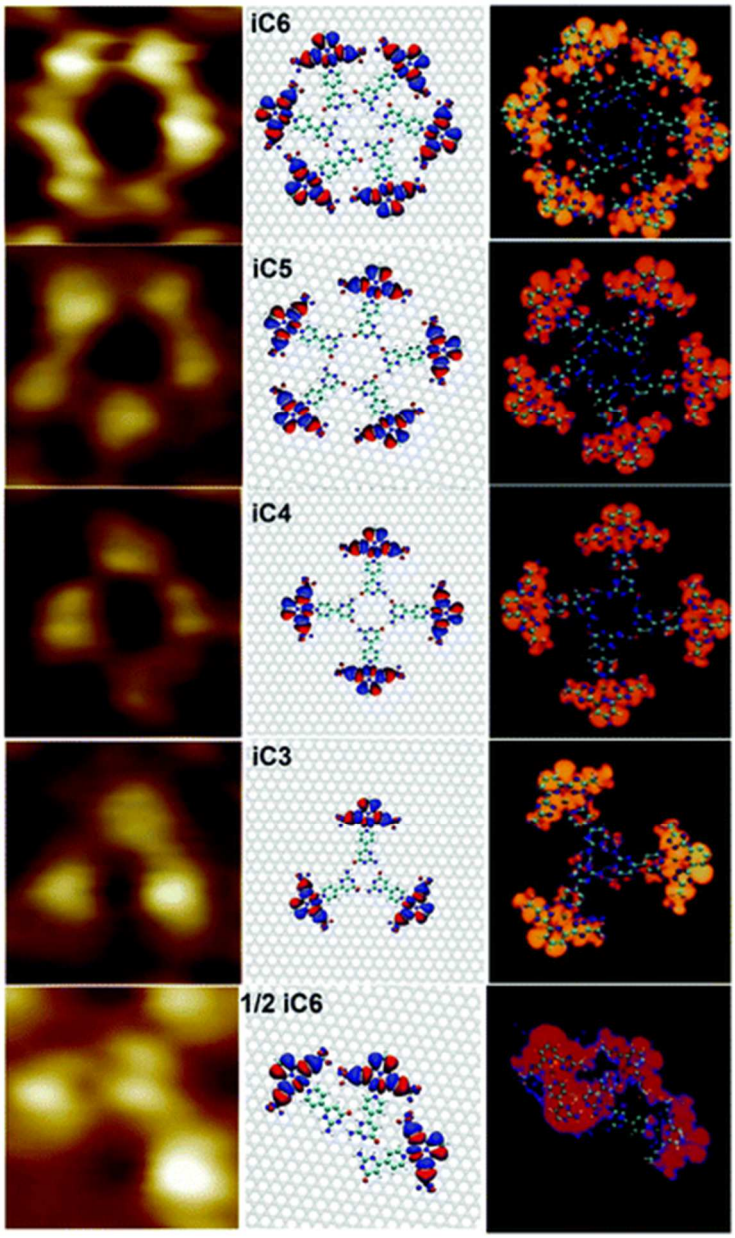

Figure 8: (Left) The STM images of different **iC-Py-Pt-** motifs. (Middle) Simulated structures on graphene. (Right) Simulated STM images of different motifs. Picture taken from reference 30.

Another example of HCAs bearing nucleobases are the described luminophores NB-polypyridyl metal complexes: **A-biPy-Ru**, **T-biPy-Os**, **T-biPy-Re**, **C-biPy-Ru** and **G-biPy-Os**.[32,33] As previously discussed in chapter I and II, functionalization of NBs could be achieved by alkylation of the active NH site. The nucleobase-bipyridine (**biPy**) ligands were synthesized by reacting the respective NB with 5-bromomethyl-2,2'-bipyridine (**Br-biPy**) in the presence of a suitable base (Figure 9). The synthesis of **A-biPy** (N_9-2,2'-bipyridineadenine) was performed by reacting one equivalent of adenine with 2 equivalent of K_2CO_3 and 2.5 equivalents of **Br-biPy,** in the presence of catalytic amount of KI, which yielded 47 % of **A-biPy**. The **T-biPy** (N_1-2,2'-bipyridinethymine) was synthesized by reacting an excess (4 eq.) of thymine, to avoid disubstitution of **T**, with 2 equivalents of K_2CO_3 and 0.8 equivalents of **Br-bipy** in the presence of a catalytic amount of KI to result in 37% the monosubstituted **T-biPy** (Figure 9).[32]

C-biPy (N_1-2,2'-bipyridinecytosine) was obtained by reacting one equivalent of cytosine with 1 equivalent of NaH and 1 equivalent of **Br-biPy** in the presence of a catalytic amount of KI to yield 62 % of the targeted **C-biPy** ligand. To synthesize **G-biPy** (N_9-2,2'-bipyridineguanine), one equivalent of 2-amino-6-chloropurine (**P**) was reacted with 2 equivalents of K_2CO_3 and 1 equivalent of **Br-biPy** in the presence of a catalytic amount of KI to result in 64 % of **P-biPy**. The latter was then oxidized by 0.1 M HCl into the targeted **G-bipy** with a yield of 77% (Figure 9).[33]

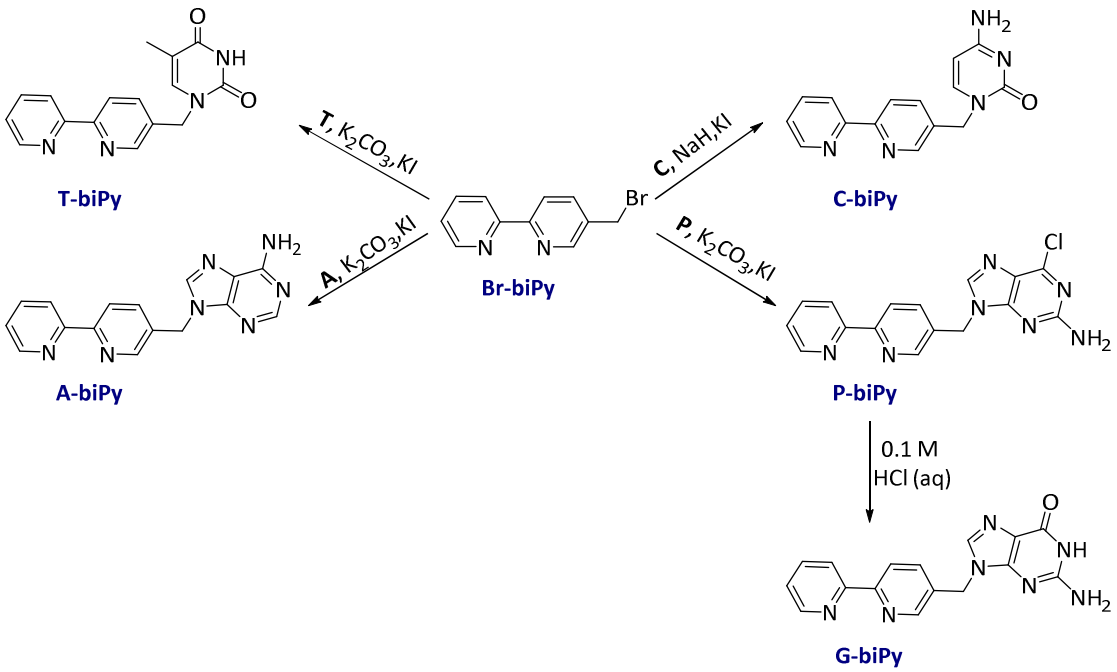

Figure 9: The synthesis of **T-biPy, A-biPy**, **C-biPy**, **P-biPy** and **G-biPy**.[32, 33]

The **A-biPy** ligand was reacted with [Ru(**biPy**)$_2$Cl$_2$] in ethylene glycol and then precipitated by addition of KPF_6 to result in [Ru(**biPy**)$_2$(**A-biPy**)][PF_6]$_2$. The crystal structure of the complex shows its self-association *via* the Watson-Crick H-bonds N(80B)-H···N(76A) between the adenine moieties (Figure 10).[32]

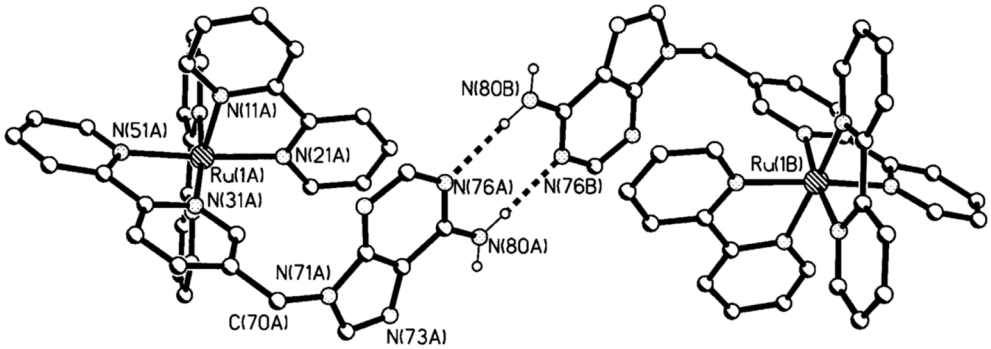

Figure 10: The crystal structure showing the association by H-bonding of two metal complex cations [Ru(**biPy**)$_2$(**A-biPy**)]$^{2+}$. Figure taken from reference 32.

This structure shows that the H-bonds between adenines are the dominant intermolecular interactions between the metal-polypridyl complexes in the solid state. However, in solution this H-bonding interaction makes the complex unsuitable for solution analysis and luminescent studies, because it is only soluble in polar solvents, such as DMF or DMSO. Therefore, the synthesis of a more soluble complex, [Ru(**dbbiPy**)$_2$(**A-biPy**)][PF_6]$_2$ (**A-biPy-Ru**), was performed by the reaction of **A-biPy** with [Ru(**dbbiPy**)$_2$Cl$_2$] bearing solubilizing di-4,4'-tertbutyl-2,2'-dipyridine (**dbbiPy**) ligands (Figure 11).[32]

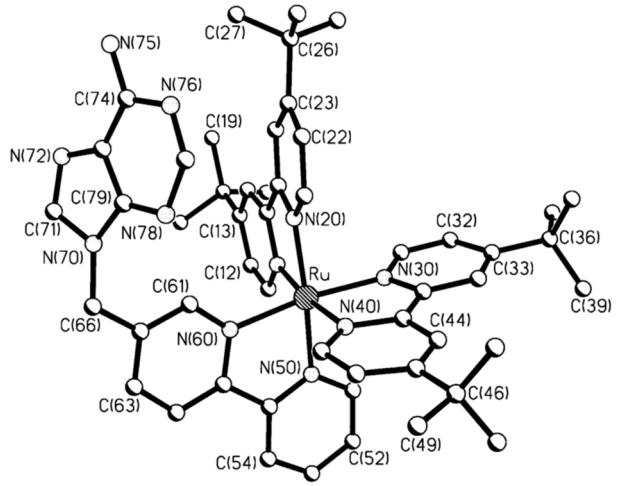

Figure 11: The crystal structure of Ru(**dbbiPy**)$_2$(**A-biPy**) (**A-biPy-Ru**). Figure taken from reference 32.

The **A-biPy-Ru** self-assembles in a different pattern when compared to the previous complex. The adenine moieties are involved in two pairs of hydrogen bonds to two neighboring adenine groups, forming a H-bonded ribbon. The stronger H-bond, N(75B)-H···N(78D), takes place between NH_2 of one adenine and the tertiary amine at position $N_3$of the adjacent adenine. The weaker interaction, C(66D)-H···N(76B), is between the tertiary amine N_1 of adenine and the CH_2 fragment of the adjacent **dbbiPy** molecule. The key factor in forming the ribbon is the hydrogen bonding pattern, since it maximizes the separation between the positively charged metal complex units, which explains why the bipy fragments are disposed alternately above and below the ribbon (Figure 12).[32]

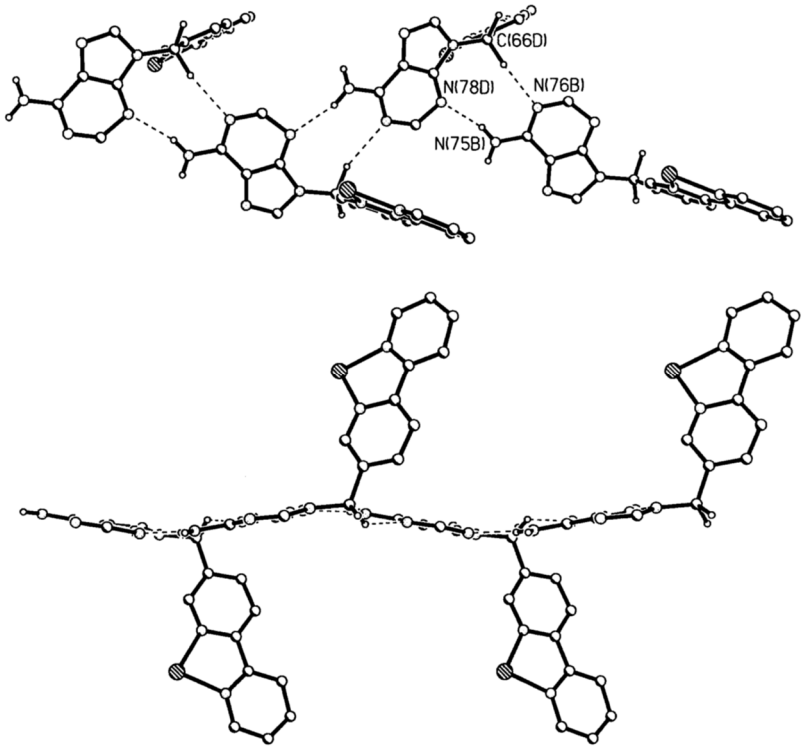

Figure 12: The self-assembly of **A-biPy-Ru** into H-bonding ribbon. Figure taken from reference 32.

The metal-complexes, **T-biPy-Os** and **T-biPy-Re,** were synthesized by reacting **T-biPy** with [Os(**dbbiPy**)$_2$Cl$_2$] and [Re(CO)$_2$Cl] respectively. The reported crystal structure of **T-biPy-Os** reveals the self-association of the complex *via* two H-bonds between the thymine moieties, N(73A)-H···O(74 B) , which is in agreement with the Watson-Crick thymine-thymine interaction (Figure 13).[32]

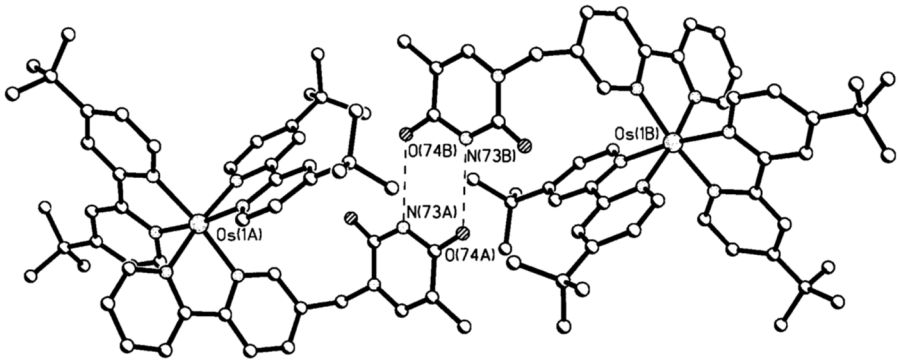

Figure 13: The crystal structure of **T-biPy-Os**. Figure taken from reference 32.

The formation of **Ru-biPy-C**···**G-biPy-Os** association (Figure 14) *via* Watson-Crick H-bonding between cytosine and guanine moieties were demonstrated by comparing the luminescence spectra of a 1:1 mixture of **C-biPy-Ru** and **G-biPy-Os** in CH_2Cl_2 before and after the addition of ethanol. The addition of ethanol causes an increase of the **C-biPy-Ru** luminescence intensity in the **Ru-biPy-C**···**G-biPy-Os** pair. Adding ethanol to a mixture of the **C-biPy-Ru** and **biPy-Os** has no effect on the **C-biPy-Ru** luminescence intensity. This proves that in **Ru-biPy-C**···**G-biPy-Os** pair, the Ru-based emission is quenched. Upon addition of ethanol, the H-bonds between **G** and **C** were interrupted, thus the quenching of the **C-biPy-Ru** luminescence does not take place anymore. In the mixture of **C-biPy-Ru** and **biPy-Os** no H-bonding occurs, therefore no change is observed before and after the addition of ethanol. This implies that an electron exchange takes place from **C-biPy-Ru** complex to **G-biPy-Os** complex *via* the **G-C** Watson-Crick H-bonding.[33]

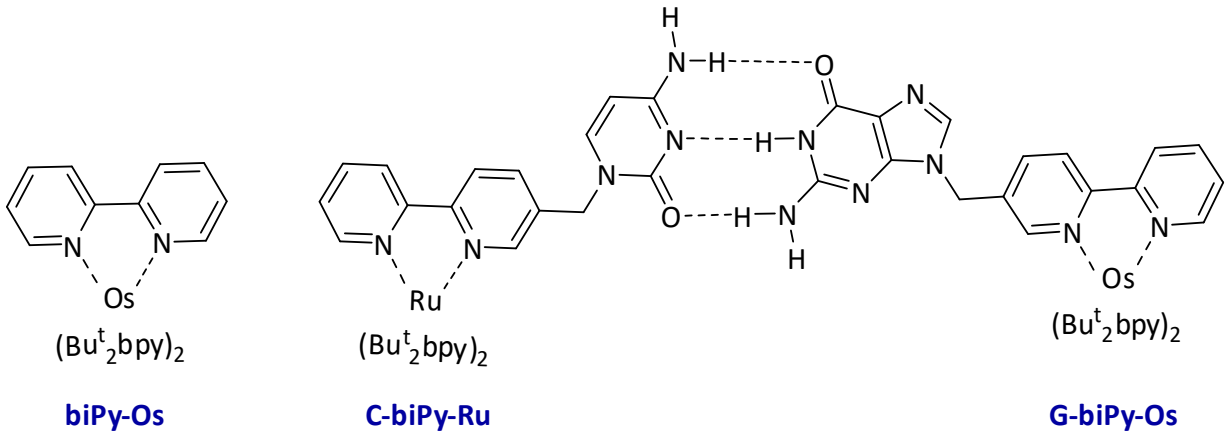

Figure 14: The chemical structure of **biPy-Os** and **Ru-bipy-C**···**G-bipy-Os assembly**.[33]

The synthesis of a terpyridine functionalized with nucleobases, **T-terPy** was performed by reacting **T** with an excess of hexamethyldisilazane to give an intermediate silyl enol ether, which was treated with 4'-(4-bromomethylphenyl)-2,2':6',2"-terpyridine in dichlorethane (Figure 15).[34] The interaction of **T-terPy** with adenosine was investigated by NMR spectroscopy. The NH protons of thymine and adenine are shifted by 3.18 and 4.04 ppm respectively, which proves the H-bonding interaction between the thymine and adenine moieties. In addition, low temperature NMR spectrum clearly shows that the two NH protons of the adenine are not equivalent, indicating that the interaction between **A** and **T** is a Watson-Crick H-binding and not a Hoogsteen interaction. **T-terPy** was coordinated to [$RuCl_3$(**terPy**)] to result in a **T-terPy-Ru(II)** complex, which was mixed with adenosine to probe the H-bonding interaction of a metallated terpyridine (Figure 15). The proton NMR analysis proves that similar behaviors are present between adenine and thymine moieties, since the NH signals shift to lower filed. The calculated stability constant is several orders of magnitude greater than that expected for simple adenosine-thymine interactions (logK = 1.49), proving that H-bonding interactions are enhanced when one of the components is coordinated to a cationic metal center.[34]

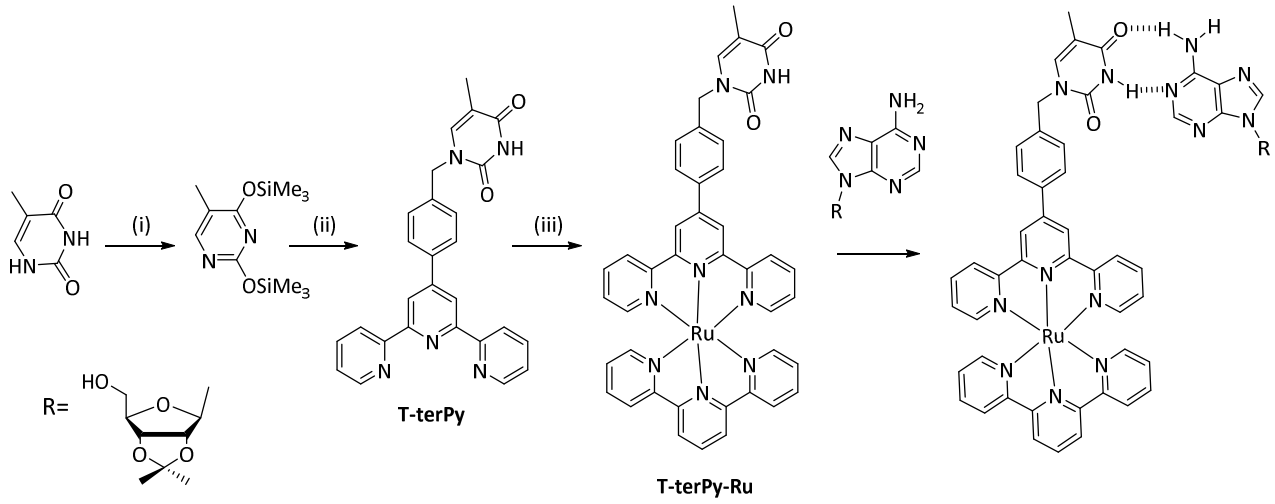

Figure 15: The synthesis of **T-terPy** and **T-terPy-Ru**. (i) hexamethyldisilazane, (ii) 4'-(4-bromomethylphenyl)-2,2':6',2"-terpyridine, $C_2H_4Cl_2$, Bu_4NF, THF, H_2O, (iii) [$RuCl_3$(tpy)], MeOH, N-ethylmorpholine.[34]

Furthermore, bipyridine and terpyridine ligands and their respective complexes with transition metals possess unique electrochemical and photophysical properties, which can be used in luminescent labeling of biomolecules.[35] Moreover, functionalizing these complexes with

nucleobases have been extensively studied as luminescent probes for DNA hybridizations and charge transfer through DNA.[26,36] The synthesis of thymine and cytosine based bipyridine and terpyridine conjugates was reported following Sonogashira and Suzuki cross coupling reactions between appropriate starting materials (Figure 16).[37] The photophysical studies (UV-Vis, Fluorescence…) conducted on these compounds showed that they all possess luminescent properties and in particular, the 5-linked **biPy** derivatives that exert the highest luminescence.

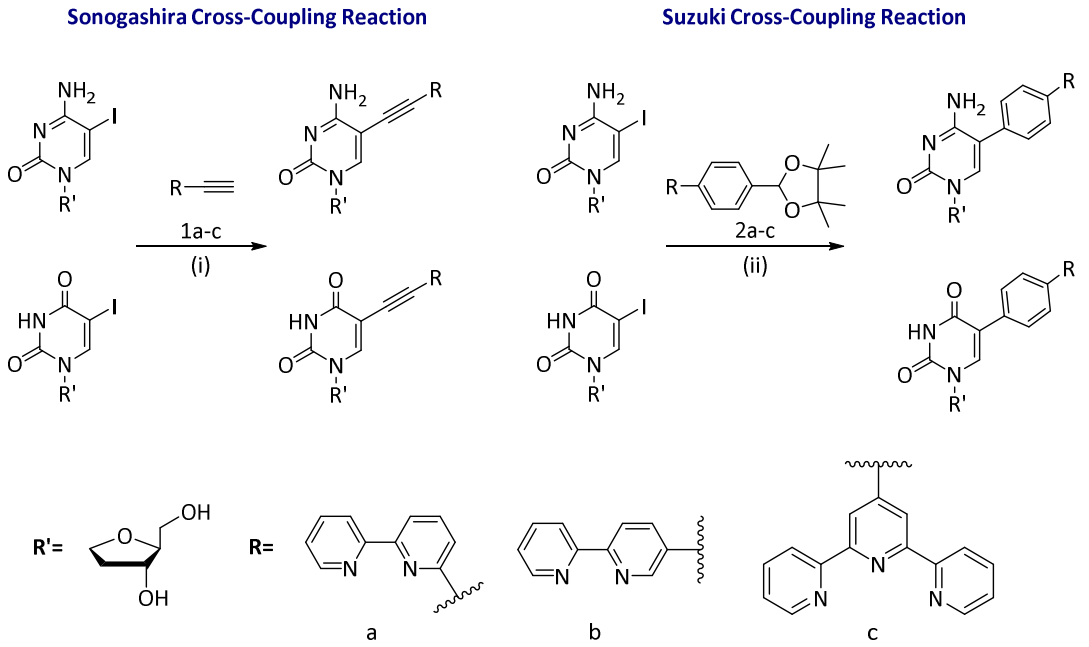

Figure 16: The synthesis of **T** and **C** based **biPy** and **terPy**. (i) $Pd(OAc)_2$, TPPTS, CuI, $(iPr)_2NEt$, DMF, 75°C, 2h. (ii) $Pd(OAc)_2$, TPPTS, Cs_2CO_3, H_2O-MeCN, 90 °C.[37]

In addition, molecules containing both nucleobases and DNA intercalators, as **terPy**, exhibit interesting DNA-binding properties that can be used to promote DNA-drug interactions. Adenine-**terPy** complexes were reported to have DNA-binding abilities.[38, 39] The synthesizes of such complexes were performed by reacting 4'-bromomethylphenyl-2,2':6,2''-terpyridine (**Br-terPy**) and adenine in the presence of a base (NaH or K_2CO_3) to afford the targeted adenine-**terPy** ligand. The latter was reacted with one equivalent of $Cu(NO_3)_2.3H_2O$ and 0.5 equivalents of $Zn(NO_3)_2.6H_2O$ to yield the **A-terPy-Cu**[38] and the **A-terPy-Zn**[39] complexes respectively (Figure 17).

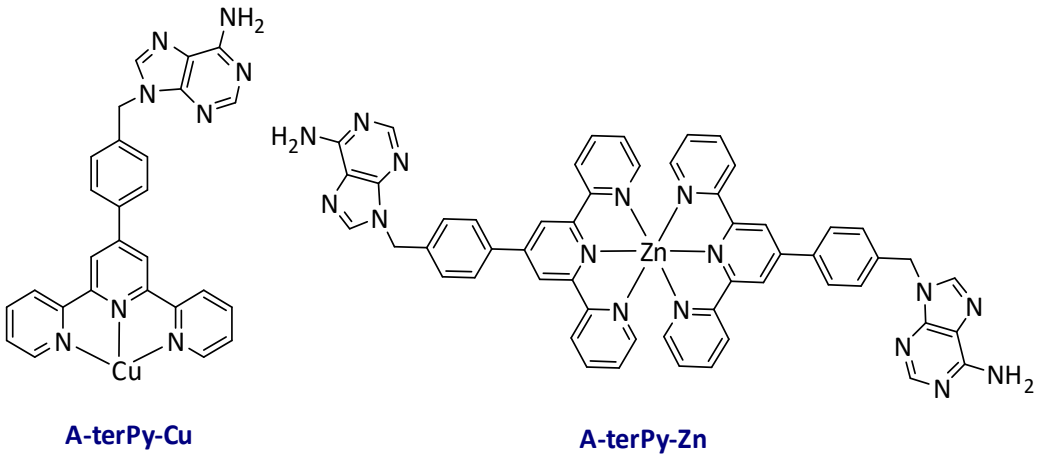

Figure 17: The chemical structure of **A-terPy-Cu**[38] and **A-terPy-Zn.**[39]

The **A-terPy-Cu** complex was characterized by X-Ray diffraction that revealed the self-assembly of the complex *via* Watson-Crick H-bonding between the adenine moieties (Figure 18). The copper center adopted a distorted square pyramidal coordination geometry with one **A-terPy** acting as a tridentate equatorial ligand. The basal plane of the Cu center is occupied by the three nitrogen atoms of **terPy** and an oxygen atom from the nitrate counter ions. In addition, an oxygen atom from water is coordinated to the copper center at its apical position. The phenyl and terpyridine planes are almost coplanar, and the adenine moiety is almost perpendicular to the **terPy** mean plane.[38]

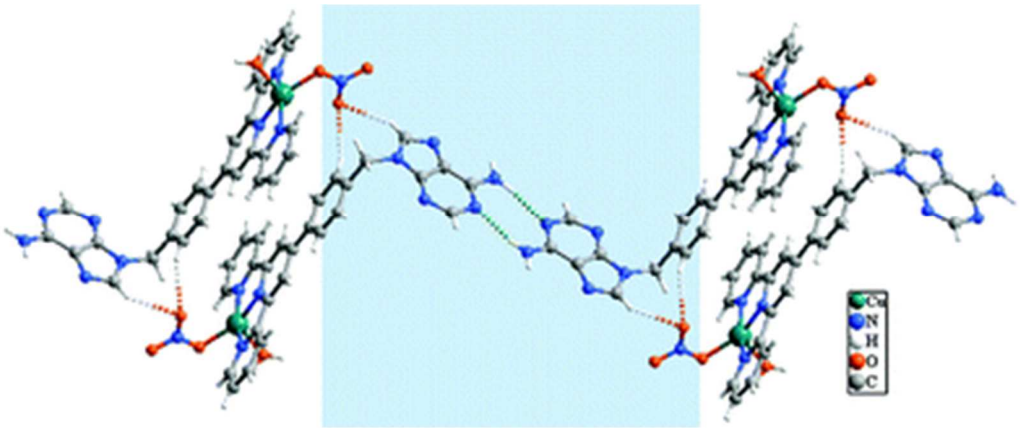

Figure 18: Crystal Structure of **A-terPy-Cu**. Picture taken from reference 38.

To investigate the DNA-binding affinity of the **A-terPy** complexes and the effect of adenine moiety, the studies were compared with those of Cu(II) and Zn(II) with 4'-p-tolyl-2,2':6,2"-terpyridine, (**tolyl-terPy**) complexes, **tolyl-terPy-Cu** and **tolyl-terPy-Zn**.[38, 39]

The intercellular DNA binding of **A-terPy-Cu** and **tolyl-terPy-Cu** were studied by treating human cells with both complexes, and then isolating the DNA from the cells and measuring its concentration. ICP-MS analysis revealed that the copper content in isolated DNA treated with **A-terPy-Cu** was 6 times higher than in those treated with **tolyl-terPy-Cu**, proving that the presence of adenine moiety increases the intercellular DNA-binding of the **terPy** complex. In addition, UV-Vis spectra were used to investigate the DNA binding ability of the complexes. The UV-Vis absorption spectrum of **A-terPy-Cu** exhibits a more pronounced bathochromic shift than that of **tolyl-terPy-Cu,** proving its DNA-binding ability. Several other studies were conducted to prove the affinity of the complexes to DNA, such as CD analysis, influence of DAPI (DNA binding agent) on the **terPy** complexes' affinity, DNA-EB replacement experiment (ethidium bromide, DNA intercalator) and molecular simulations. These analyses revealed that **A-terPy-Cu** and **tolyl-terPy-Cu** complexes bind to DNA simultaneously with other binding agent, and that **A-terPy-Cu** is a better intercalator than **tolyl-terPy-Cu.** Molecular simulations of **A-terPy-Cu** and **tolyl-terPy-Cu** interactions with an oligonucleotide duplex showed that **A-terPy-Cu** binds to the minor groove of the oligonucleotide with the intercalation group parallel to the pseudo dyad axis of the oligonucleotide. The adenine moiety was located in the DNA's major groove due to its large steric effect. However, **tolyl-terPy-Cu** has no preference for the minor groove-binding with its intercalation group being perpendicular to the pseudo dyad axis (Figure 19). The **A-terPy-Cu** complex exhibited more evident intracellular DNA-binding ability than the **tolyl-terPy-Cu** complex.[38]

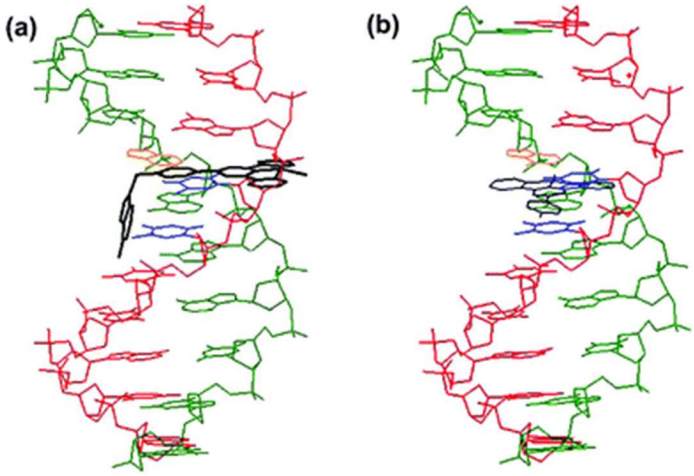

Figure 19: The structures of **A-terPy-Cu** and **tolyl-terPy-Cu** bounded to an oligonucleotide. Figure taken from reference 38.

The DNA binding ability and nuclease activity of **A-terPy-Zn** was also studied and compared to those of **tolyl-terPy-Zn**.[39] The analyses proved that the presence of adenine increased the structural change of DNA and DNA cleavage activity of the terpyridine zinc complex.[39]

II. 2. Aim of the project

Nucleobases (NBs) functionalized with Heterocyclic Amines (HCAs) are interesting building blocks for the design molecular networks assembled *via* coordination bonds and Watson-crick H-bonding. The aim of this chapter is to introduce NBs into pyridine following described procedures for similar products. [32,33,38,39] In addition, we aim to extend the study to terpyridines, and introduce all four NBs on 4'-tolyl-2,2'"6,2"-terpyridine (**tolyl-terPy**). The **NB-Py** and **NB-terPy** tectons are synthesized *via* a substitution reaction between their bromine derivatives, 4-bromomethylpyridine and of 4'-p-bromomethylphenyl-2,2',6',2"-terpyridine (**Br-terPy**) and the nucleobases (Figure 20).

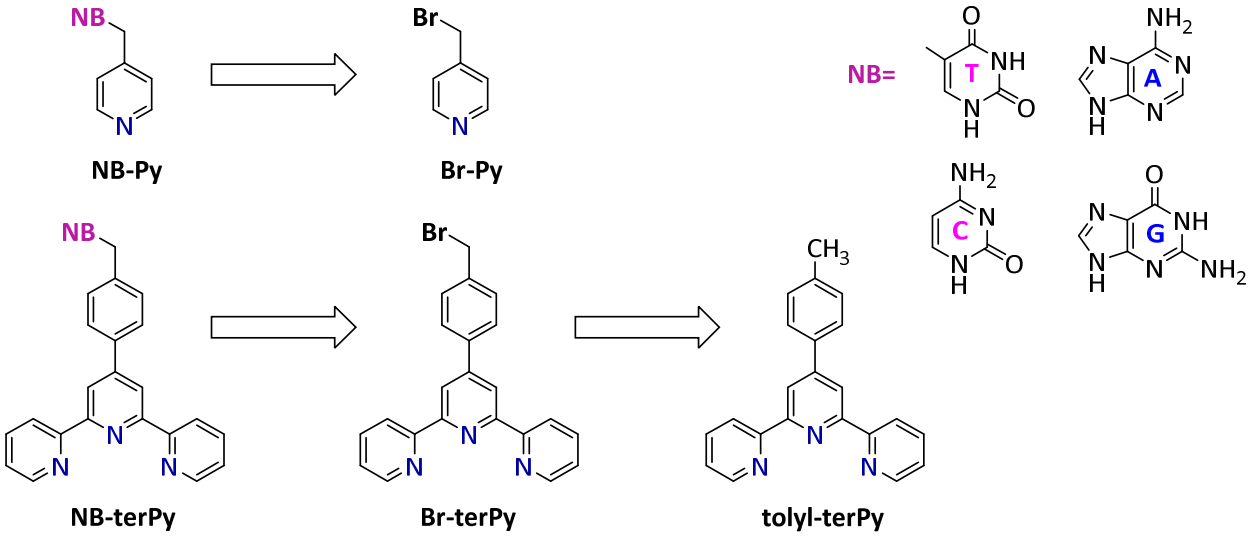

Figure 20: The retrosynthesis of targeted tectons.

The final aim is to assemble theses 8 tectons with various metal salts in order to generate molecular architectures based on NBs H-bonding and **Py** and **terPy** coordination interactions.

Numerous combinations are accessible. For example, pyridine bearing complementary NBs can self-assemble *via* Watson-Crick H-bonding. In addition, NBs are self-complementary, therefore the

self-assembly of the tectons bearing the same NB is also possible.[40] Figure 21 represents possible assembly of **NB-Py** complexes.

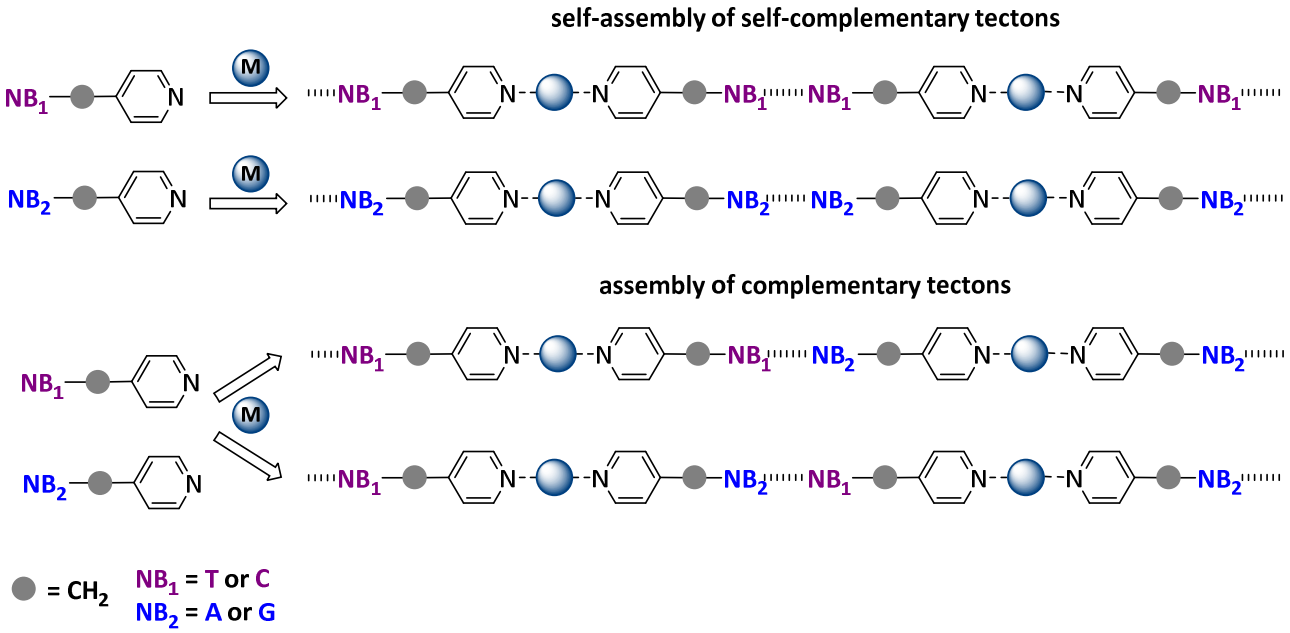

Figure 21: A schematic representation of possible **NB-Py-M** assemblies.

Similarly, **NB-terPy** networks can be assembled *via* self-complementary bis-terpyridine complexes, such as **A-terPy-M$_1$-terPy-T**, or *via* two complementary bis-terpyridine complexes, such as **A-terPy-M$_2$-terPy-A** with **T-terPy-M$_3$-TerPy-T**. Figure 22 shows a schematic representation of possible assemblies. Moreover, similar combinations can be achieved *via* the G-C assembly.

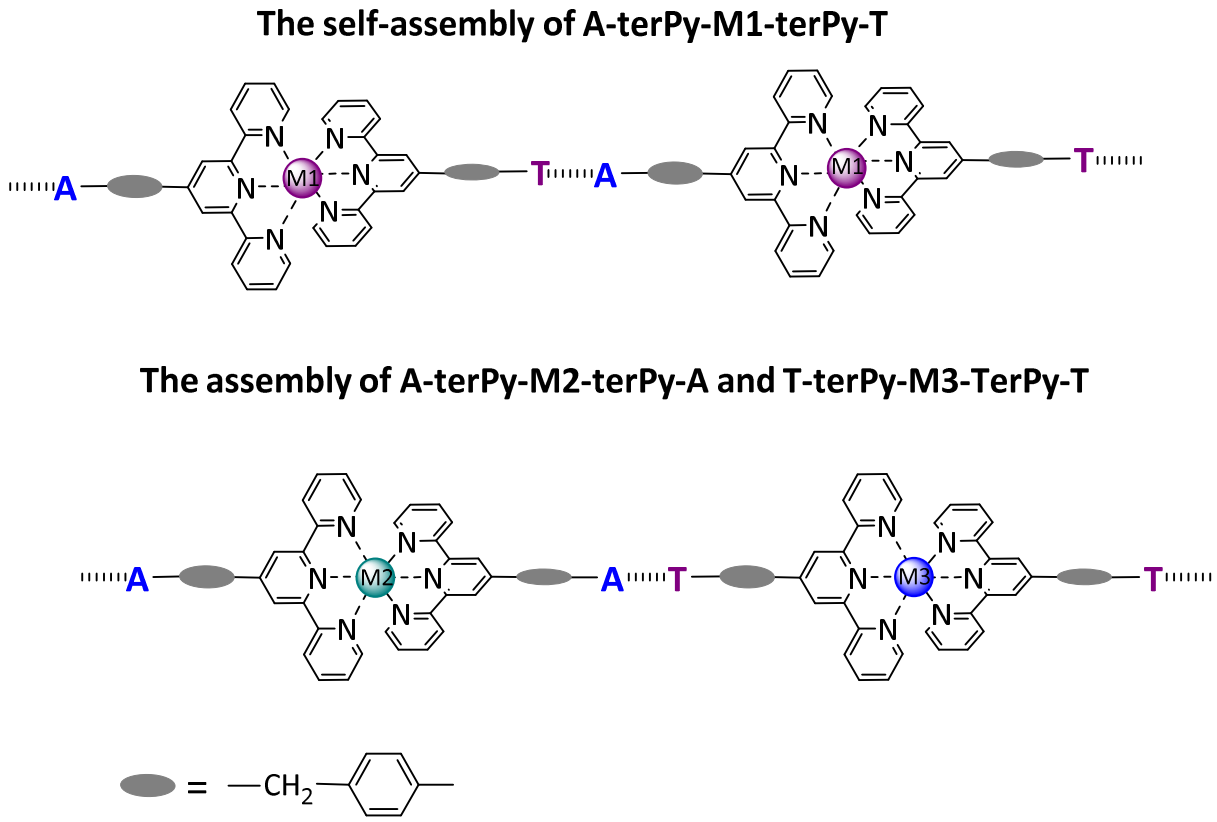

Figure 22: A schematic representation of possible assemblies of **A-terPy-M$_1$-terPy-T**, and **A-terPy-M$_2$-terPy-A** with **T-terPy-M$_3$-terPy-T**.

Furthermore, by changing the metal cation and using both **Py** and **terPy** ligands, it is possible to extend this strategy to networks based on the assembly of heteroleptic complexes, for instance the assembly of self-complementary complexes such as **T-terPy-M$_6$-Py-A**, or the assembly of complementary heteroleptic complexes, for example **A-terPy-M$_4$-Py-A** with **T-terPy-M$_5$-Py-T** (Figure 23).

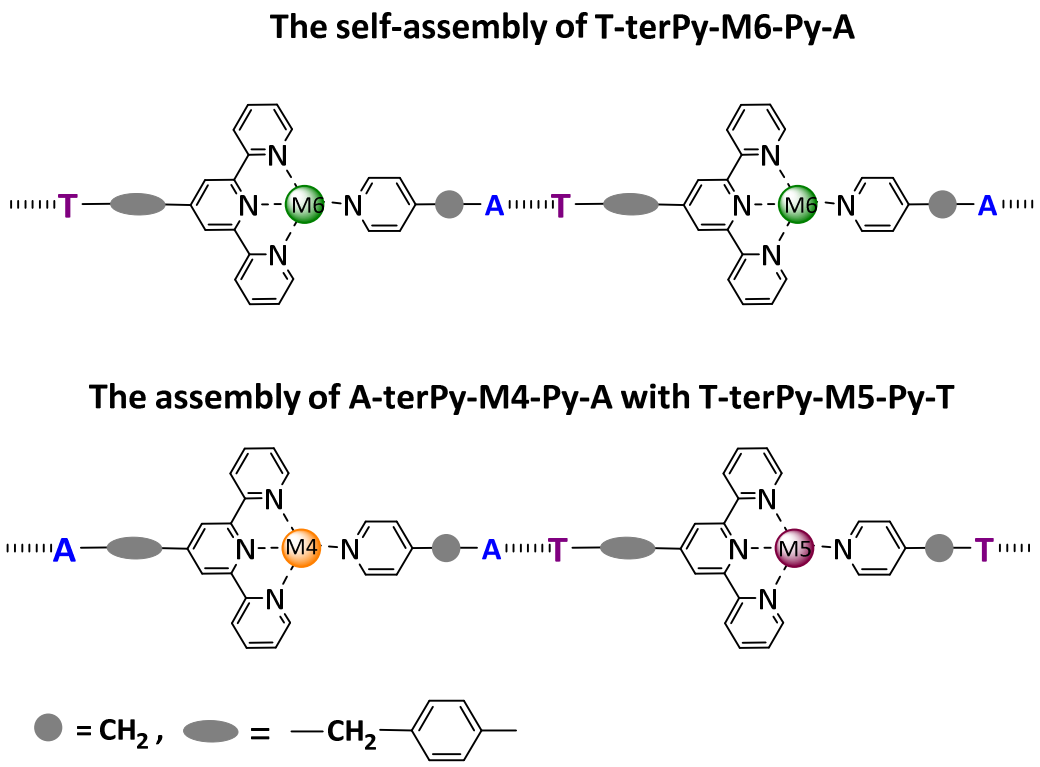

Figure 23: A schematic representation of possible assemblies of heteroleptic complexes **A-terPy-M_4-Py-A** with **T-terPy-M_5-Py-T,** or self-complementary **T-terPy-M_6-Py-A**.

II. 3. Pyridine bearing NBs

To connect a pyridine to the active amine function of the nucleobases (N1 for pyrimidines (**T** and **C**) and N9 for purines (**A** and **G**)), the commercial 4-(bromomethyl)pyridine hydrobromide (**Br-Py**.HBr) was used as a starting material for all the targeted **NB-Py** tectons. **Br-Py**.HBr was reacted with NBs in the presence of a base chosen with respect to the nucleobase used. All reactions were performed in DMF at 40 °C and kept stirring for 12 hours. Increasing the temperature resulted in a faster consumption of the limiting reagent (**Br-Py**), however the obtained product was a mixture of di- and mono substituted pyrimidines or N7- and N9-substituted purines. Thus catalytic amount of KI was added to the reaction media in order to increase the rate of the reaction without increasing the temperature.[32,33] Purification of the crude products was achieved using column chromatography with appropriate eluent gradient. All products were characterized by NMR, HRMS, IR. In addition, single-crystals of **T-Py**, **A-Py**, and **C-Py** were obtained by slow evaporation of a 1:1 dichloromethane: cyclohexane solution and analyzed by X-ray diffraction.

II. 3. a) Synthesis of 4-(N_1-methylthymine)pyridine (T-Py) (T16)

T-Py was obtained by reacting thymine with **Br-Py**.HBr in the presence of 2.5 equivalents K_2CO_3 and a catalytic amount of KI in dry DMF (Figure 24). The base was added to neutralize the hydrobromide present in the starting pyridine and to deprotonate the nucleobase. Thymine can be di-substituted. Therefore, thymine was added in excess (3 eq.) to favor the mono substitution, and decrease the yield of the di-substituted thymine. The reaction yielded the mono-substituted **T-Py** (**T16**) as a major product with a yield of 45% and the di-substituted **T16'** as a minor product (10%), after purification by column chromatography. **T16** is a polar product, therefore part of it might be retained on the column, which affected the yield of the reaction.

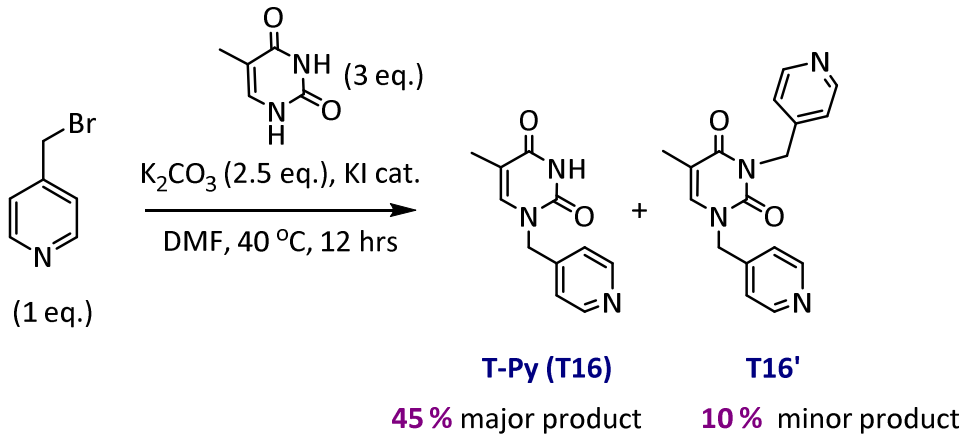

Figure 24: Synthesis of **T-Py** (**T16**).

Single-crystals of **T16** suitable for X-Ray diffraction were obtained and characterized. **T-Py** crystallizes in the monoclinic space group P $2_1/n$. Within the ligand, the pyridine ring is almost perpendicular to the thymine mean plane with an angle of 89°. Tectons self-assemble through a H-bond between the NH of the thymine and the nitrogen of a pyridine of an adjacent tecton with a distance N2-H2···N3 of 2.85 Å, thus leading to a 1D *zig-zag* network (Figure 25 (b)). The *zigzag* chains are stacked into infinite antiparallel rows above each other by π-π stacking forming a two dimensional molecular network. The π-π interaction between pyridine rings display a centroid-centroid separation of 3.50 Å. Moreover, two consecutive and much weaker π-π interactions with a centroid-centroid separation of 4.09 Å are present between the thymine and the pyridine rings (Figure 25 (b)).

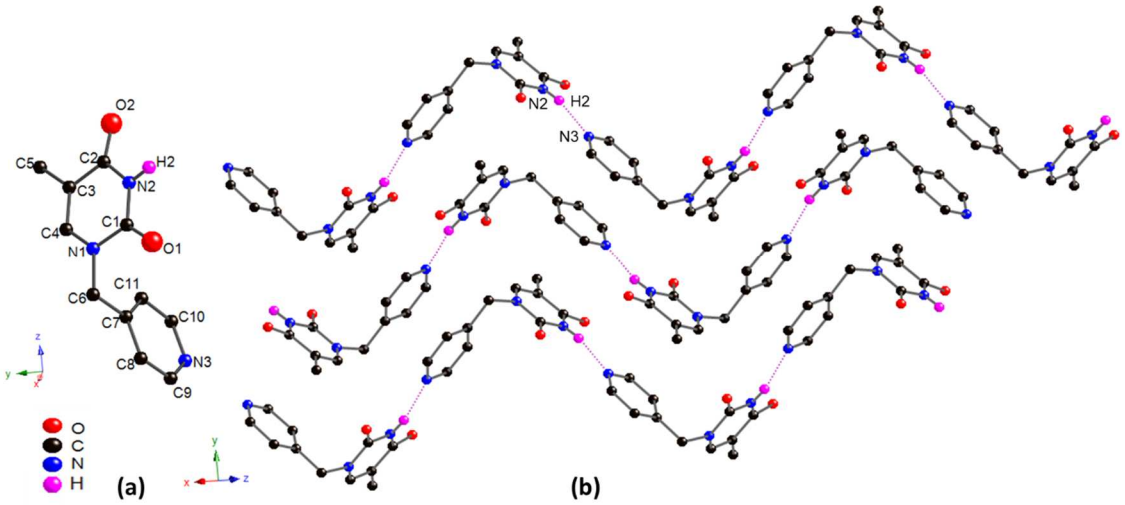

Figure 25: The crystal structure of **T-Py** (a) **T-Py** (b) A portion of the 1D zig-zag chains formed by the H-bond between **Py** and **T** moieties and the π-π stacking between the chains.

II. 3. b) Synthesis of 4-(N9-methyladenine)pyridine (A-Py) (T17)

The synthesis of **A-Py** was achieved following the same conditions used for the synthesis of **T16**. Adenine (2 eq.) was added in excess with respect to the **Br-Py** (1 eq.) in the presence of K_2CO_3 (1.5 eq.). The pyridine was substituted successfully in the targeted amine position (N1 according to the crystallographic numbering, with a yield equal to 53 % of **T17** (Figure 26).

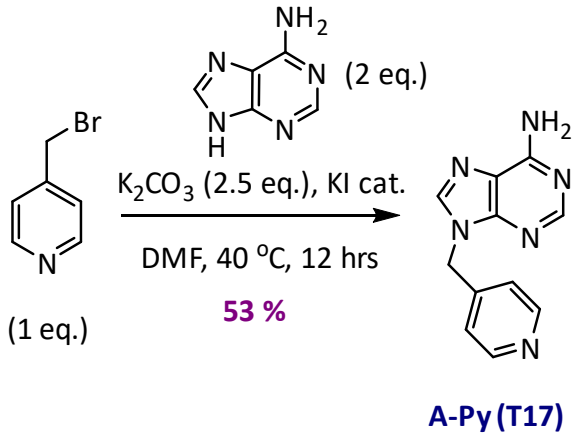

Figure 26: The synthesis of **A-Py** (**T17**).

A-Py was characterized by X-ray diffraction as well. In this case, the predicted Watson-Crick H-bonding[40] was observed between the adenine moieties, and the pyridine is not involved as a

hydrogen bond acceptor. **T17** crystallizes in the monoclinic space group P $2_1/c$. The angle between the pyridine plane and the adenine mean plane is close to 76°. **A-Py** self-assembles into a H-bonded dimer *via* two hydrogen bonds between the adenine moieties with a distance of 3.01 Å (dN3-N5) (Figure 27 (a)). Additional π-π interactions between dimers are present: each adenine are in interactions through π-π interaction between adenine rings of an adjacent dimer (Figure 27 (b)). The centroid-centroid separation is 3.5 Å. Moreover each pyridine interacts with another pyridine of an adjacent dimer, the distance between the centroid of the pyridines is *ca* 3.6 Å (Figure 27 (c)).

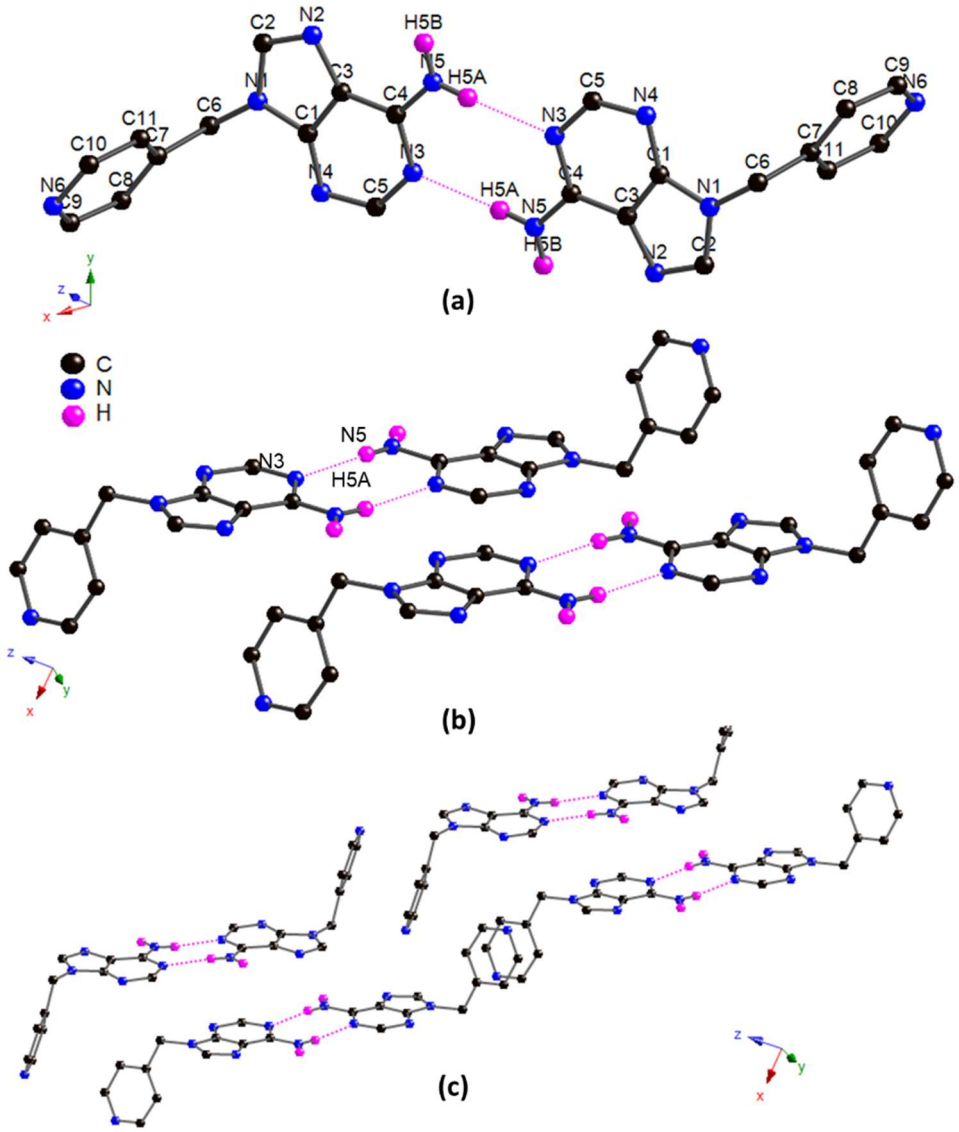

Figure 27: The crystal structure of **A-Py** (a) The structure of dimers formed *via* Watson-Crick H-bonding. (b) The assembly of the dimers *via* by π-π interactions between adenine and (c) between pyridines.

II. 3. c) Synthesis of 4-(N_1-methylcytosine)pyridine (C-Py) (T18)

The reaction between cytosine and **Br-Py** in the presence of K_2CO_3 leads to a very low yield. Thus, deprotonation of **C** at the N1 position was tried by using stronger bases for example, NaH or tBu_4NOH.[41] The best condition to synthesize **C-Py** was to react an excess of cytosine (3 eq.) and **Br-Py** (1 eq.) in the presence of NaH (2.5 eq), and a catalytic amount of KI in dry DMF (Figure 28). The reaction resulted in **C-Py** in a yield of 30 %. The lower yield compared to the previous reactions, can be due to the lower solubility of **C-Py**, and thus a more difficult purification by column chromatography than **A-Py** or **T-Py**.

^{1}H-NMR is in agreement with the tautomeric form of **C-Py** with the presence of the two characteristic NH peaks (instead of NH_2 peak) that appeared as two broad singlets at 7.08 and 7.21 ppm each integrating for one hydrogen.[41]

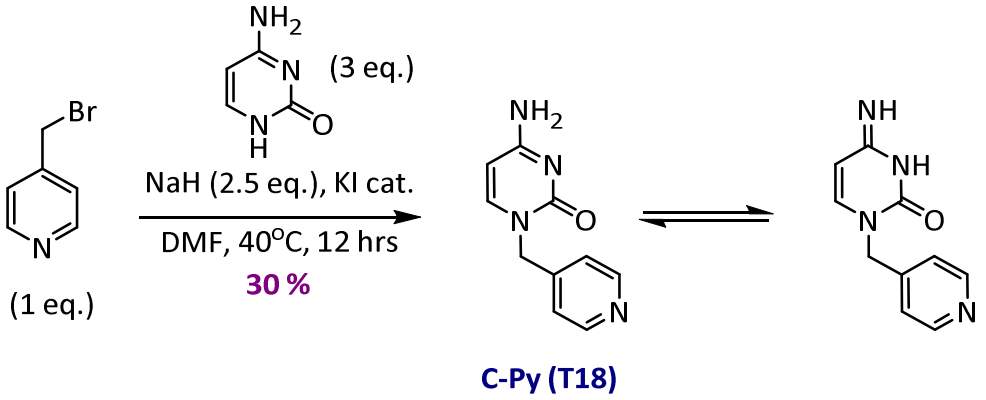

Figure 28: The synthesis of **C-Py** (**T18**).

Monocrystals of **C-Py** suitable for X-Ray diffraction were obtained and characterized. **C-Py** crystallizes in the monoclinic space group P $2_1/c$ (Figure 29 (a)). Within a molecule, the angle between the pyridine and the cytosine mean plane is closed to 85°. The molecules of **T18** are linked as predicted by hydrogen bonds between the cytosine moieties, and organized into a one dimensional chain. The pyridine are not involved in the H-bonded network. Figure 29 (b) shows the H-bonds between the cytosine within the chain. Each cytosine acts as two-H-bond donor (through its NH_2 site) and two-H-bond acceptor (through O1 and N2 lone pairs, and it is in interaction with three adjacent cytosine rings by four different H-bonds. The N3-H3···O1 distance

is equal 2.89 Å (dN3- O1), whereas the N3-H3A···N2 distance is equal to 3.02 Å (dN3- N2) (Figure 29).

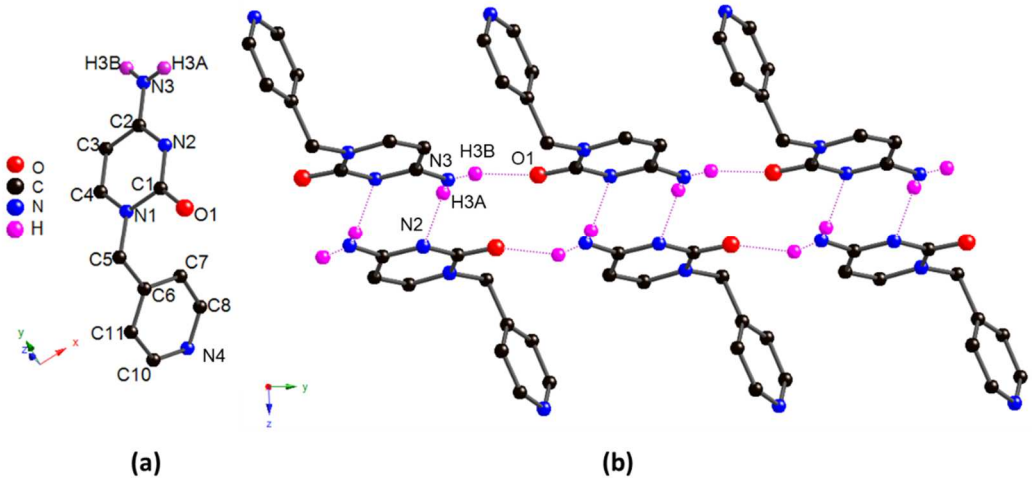

Figure 29: The crystal Structure of **C-Py**. (a) The structure of one molecule. (b) The H-bonding Assembly of the cytosine.

Consecutive chains are stacked *via* π-π interactions between the cytosine rings that are located above each other with a centroid-centroid separation of 3.48 Å. Figure 30 shows a side view of the chain and its translation in space.

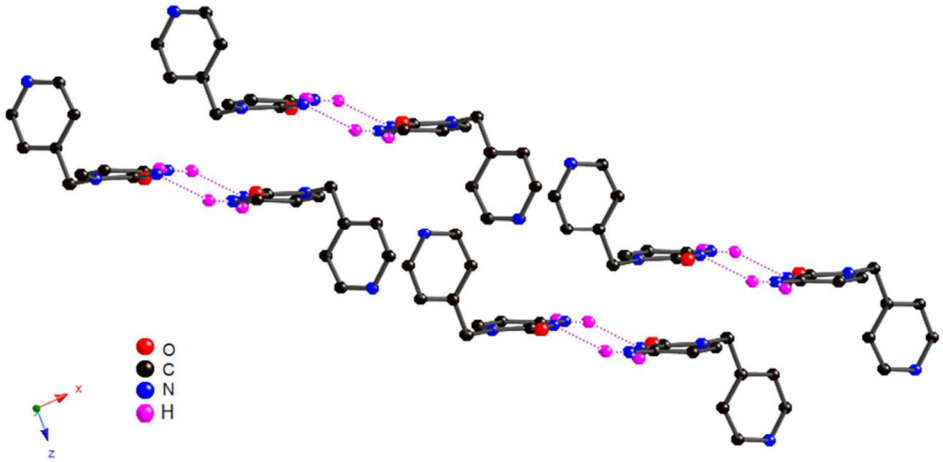

Figure 30: A side view of **Cy-Py**, showing π-π stacking between the cytosine moieties.

II. 3. d) Synthesis of 4-(N9-methylguanine)pyridine (G-Py) (T20)

Initially we tried the direct substitution of guanine with **Br-Py** in the presence of K_2CO_3, however the product was poorly soluble and difficult to purify and the resulting yield was low. Instead, 2-amino-6-chloropurine (**P**) was used as in previous chapters. The synthesis of the last **Py** targeted tecton **(G-Py)** was achieved in two steps. First, **P** was reacted with **Br-Py** in the presence of K_2CO_3, which yielded 30% of **P-Py** (**T19)**. The latter was hydrolyzed by 0.1 M HCl aqueous solution producing the guanine tecton **G-Py** (**T20**) with a yield of 96 % (Figure 31). The success of the acid hydrolysis was proved by the shift of the $[M+1]^{+1}$ peak in MS from 261.07 for **P-Py** to 243.09 for **G-Py**, and by the shift in IR spectrum from 1613 cm^{-1} to 1672 cm^{-1} which represent the C=N stretching of **P-Py** and the C=O stretching of **G-Py** respectively. In addition, the appearance of the broad NH peak of **G-Py** at 10.94 ppm in ^{1}H-NMR, which was not present in ^{1}H-NMR of **P-Py**, proves the hydrolysis of **P-Py** into **G-Py**, and that the substitution took place at position N9.[33, 41]

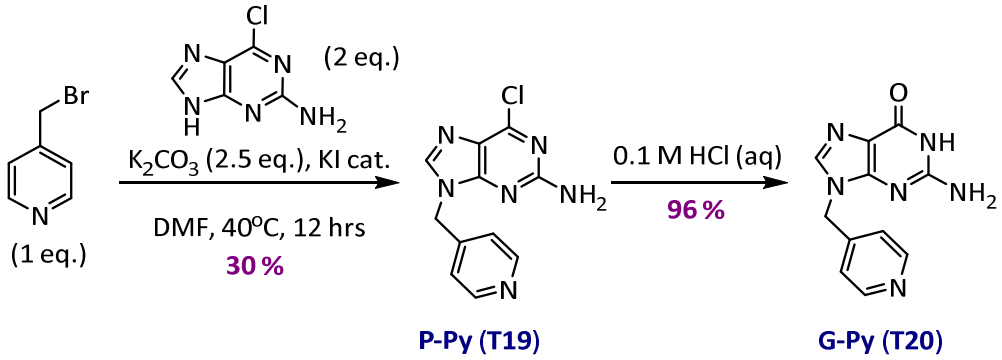

Figure 31: The synthesis of **P-Py** (**T19**) and **G-Py** (**T20**).

Crystallization attempts were made with **G-Py** using different conditions. Unfortunately, all attempts resulted in the formation of amorphous powders, due to the fast precipitation of **G-Py** that exhibited a lower solubility than the other tectons.

Moreover, crystallization of complementary tectons such as **A-Py** with **T-Py** and **C-Py** with **G-Py** was also tried, but no single crystals suitable for X-Ray diffraction analysis was isolated yet. In a second step, crystallization of all the tectons with different metal salts was launched, the aim was to generate stable assemblies based on coordination and H-bonds. The crystallization of **A-Py** and **C-Py** with metal salts resulted in the formation of molecular networks assembled *via* the

coordination of the pyridine **Py** to metal cations, while the NBs are involved in H-bonding or coordination interactions.

II. 4. Coordination networks based on A-Py (T17)

The tecton was crystallized with several metal salts: Co(II), Cd(II), Ag(II), Cu(II), Pd(II), Ni(II), Zn(II) and others. Single crystals were isolated in the presence of Cd(II) and Hg(II) and characterized by X-Ray diffraction. Single crystals of **A-Py-Cd(II)** were obtained by slow diffusion of a solution of $Cd(NO_3)_2.2H_2O$ in acetonitrile into a chloroform solution of **A-Py**. For **A-Py-Hg(II)**, crystals were obtained by slow diffusion of a solution of $HgCl_2$ in ethanol into a chloroform solution of **A-Py**. In both cases, the pyridine coordinates to the metallic cation while the adenine is either involved in H-bonds in of **A-Py-Cd(II)** or is interacting with Hg(II) in **A-Py-Hg(II)** (Figure 32).

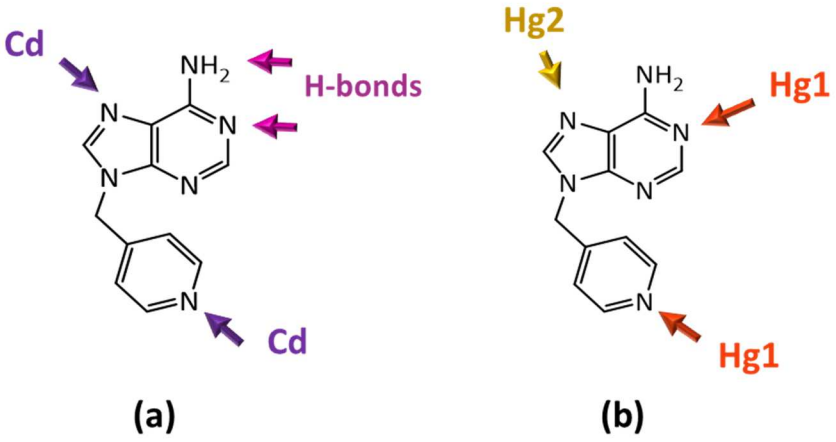

Figure 32: A general view of the different interactions of **T17** with Cd(II) or Hg(II).
(a) in **A-Py-Cd(II)** (b) in **Ad-Py-Hg(II)**.

II. 4. a) A-Py-Cd(II) network

The **A-Py-Cd(II)**, complex crystallizes in the monoclinic *C2/c* space group. The tectons are organized in a periodic architecture linked by two types of interactions: the coordination of Cd(II) metal center to **A-Py**, and the *trans* Watson-Crick hydrogen bonds between the adenine moieties (Figure 33 (b)). Cd(II) is coordinated by four nitrogen atoms, from two pyridine moieties in *trans*

position and two adenine groups in *trans* position, forming a slightly distorted square planar geometry. The two apical positions of Cd(II) are occupied by two nitrates: one acting as a bidentate ligand, while the second being disordered and acting as a monodentate ligand (Figure 33 (a)). The Cd(II) is coordinated in the basal plane to four different **A-Py** ligands. Two *trans* adenine are coordinated to the Cd (II) *via* their N3 nitrogen (according to crystallographic numbering) with a Cd1-N3 distance of 2.40 Å. The other *trans* ligands are coordinated from their pyridine sites with a Cd1-N1distance of 2.32 Å (Figure 33 (a)).

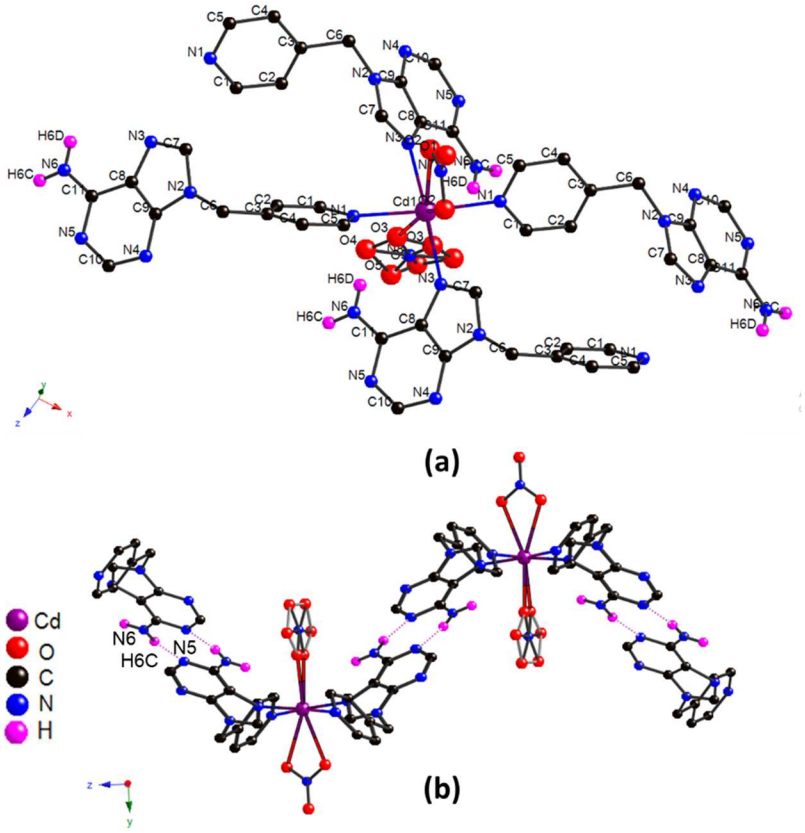

Figure 33: The crystal structure of **A-Py-Cd(II)**. (a) The coordination sphere around Cd(II) center. (b) A side view showing H-bonding between Adenine moieties.

Each **A-Py** tecton acts as a bridging ligand between two adjacent Cd(II) and the angle between the pyridine plane and the adenine mean plane is close to 72°. **A-Py** coordinates a Cd(II) *via* its adenine site (N3) and coordinates a second metallic center from its pyridine site (N1), each Cd(II) being coordinated to four different **A-Py** ligands, resulting in a 1D ribbon-like coordination network with

a 2:1 metal: ligand ratio as represented in Figure 34 (a). The ribbons are linked by hydrogen bonds between the adenine free sites following a *trans* Watson-Crick orientation (Figure 34 (b)) with a distance of 2.98 Å (dN5-N6). The final 2 D H-bonded and coordination network is represented in Figure 34 (b).

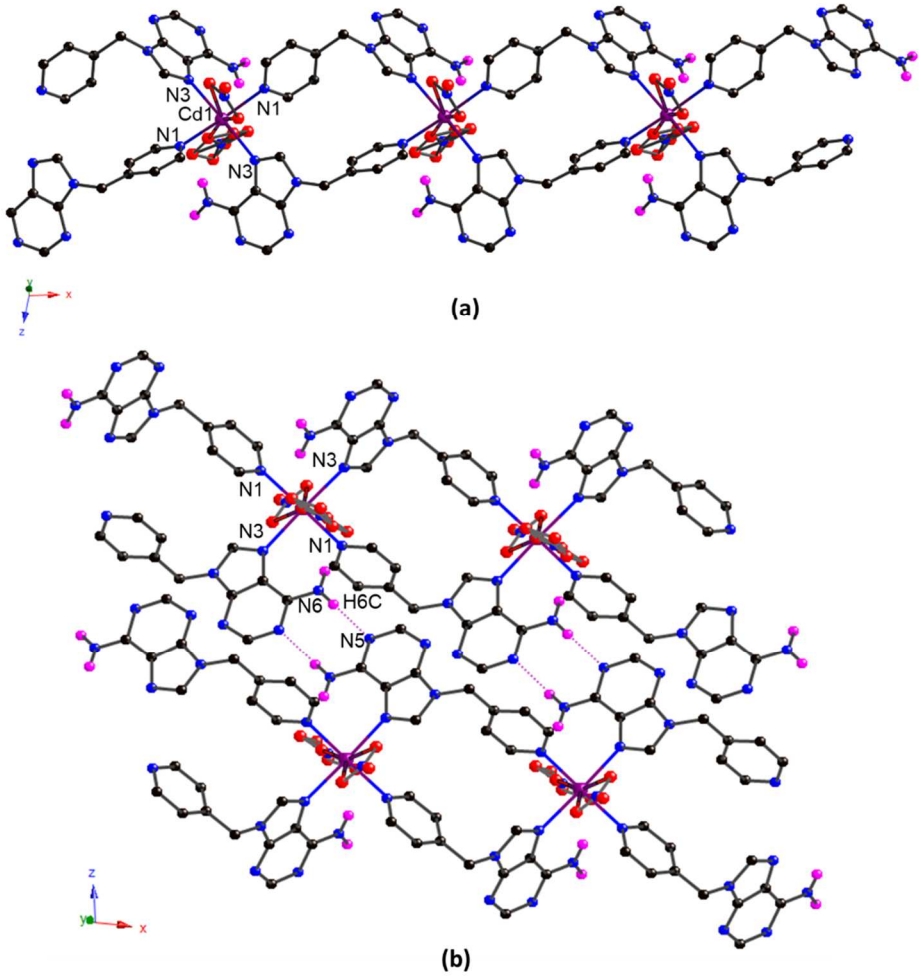

Figure 34: The crystal structure of (a) the 1D ribbon-like coordination network, and (b) the final 2D network of **A-Py-Cd(II).**

II. 4. b) A-Py-Hg(II) network

The **A-Py-Hg(II)** complex crystallizes in the monoclinic space group *P* $2_1/c$ (Figure 35 (a)). The tecton adopts a helix-like structure, as shown in Figure 35 (b) and (c). **A-Py** tectons coordinates two non-equivalent mercury cations: Hg1 and Hg2 (according to crystallographic numbering) (Figure 35 (a)). The connectivity around Hg1 leads to the formation of a helix (Figure 35 (b) and

(c)). Indeed, Hg1 is connected to two nitrogen atoms from two **A-Py** (N1 and N5, according to crystallographic numbering), and two chlorides (Cl1 and Cl2) adopting a distorted tetrahedral geometry around the metallic cation. In the helical structure, **A-Py** is acting as a bidentate ligand involving the coordination of the pyridine (N1) and the adenine (N5) with Hg-N1 and Hg-N5 distances equal to 2.34 Å and 2.38 Å respectively (Figure 35 (a)). The Hg-Cl distances are equal to 2.40 Å. Within a ligand, the angle between the pyridine and the mean plane of the adenine is close 80°.

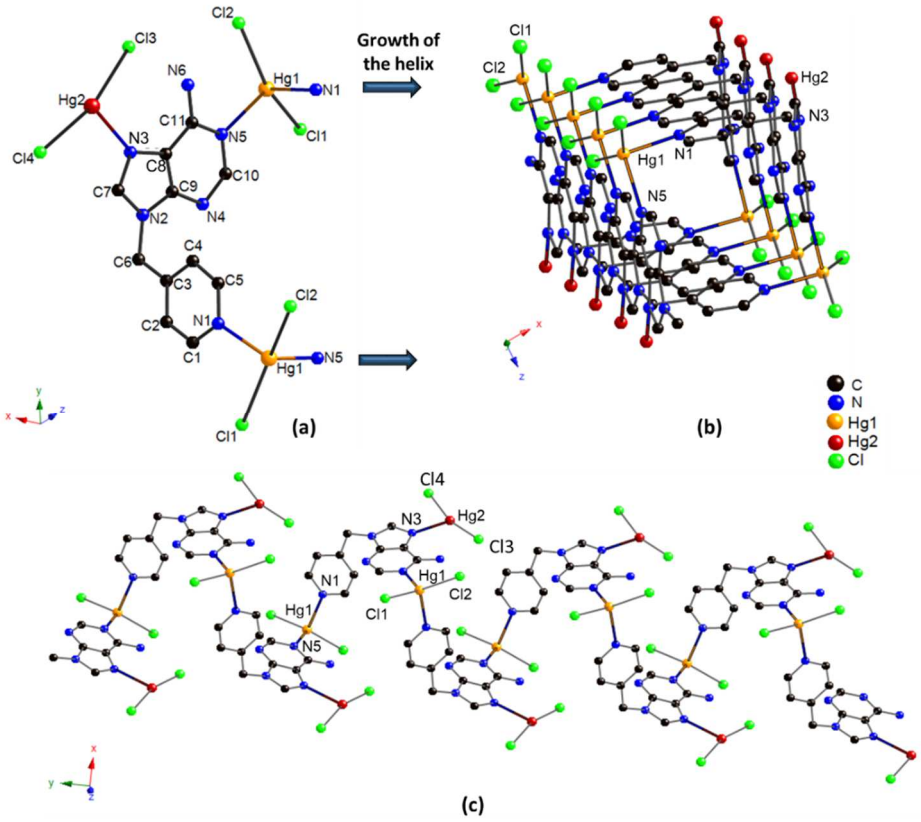

Figure 35: The crystal structure of **A-Py-Hg(II)**. (a) The coordination sphere of Hg1 and Hg2. (b) A side view showing the packed 1D chain. (c) The 1D helix chain.

An additional mercury cation, Hg2, is bonded to the adenine (N3) with a Hg-N3 distance equal to 2.56 Å, leading to a final **A-Py**: Hg stoichiometry of 1:2. Two additional chlorides (Cl3 and Cl4) are connected to Hg2 with a distance of 2.32 Å. To complete its coordination sphere Hg2 interacts with Cl1 of an adjacent helix (Figure 36) with a Hg-Cl distance of 2.88 Å.

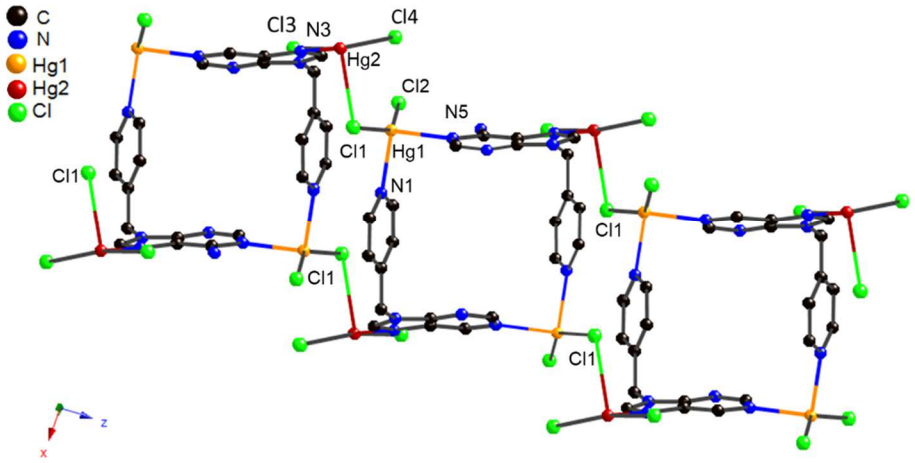

Figure 36: The crystal Structure of the 2 D helix structures linked by a Cl1 atom coordinated to Hg1 of one helix and one Hg2 of the adjacent helix.

II. 5. Coordination networks based on Cy-Py (T18)

Cy-Py was crystallized with many different metal salts: Co(II), Zn(II), Cu(II), Cd(II), Ni(II), Ru(II), and others. Single crystals were obtained by slow diffusion of an acetonitrile solution of $Zn(NO_3)_2.6H_2O$ or $Cd(NO_3)_2.4H_2O$ into a chloroform solution of **Cy-Py** resulting in the formation of **C-Py-Zn(II)** and **C-Py-Cd(II)** based networks respectively. In both cases, the pyridine coordinates to the metallic cation, and the cytosine forms either coordination bonds with Cd(II) or both coordination and H bonds with Zn(II) as depicted in Figure 37.

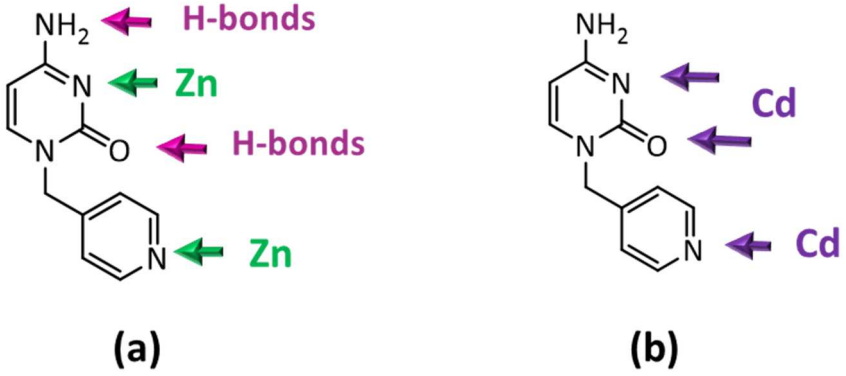

Figure 37: A general view of the interactions of **T18** with Zn(II) and Cd(II).

II. 5. a) C-Py-Zn(II) network

C-Py-Zn(II) crystallizes in the monoclinic space group $P2_1/n$. The Zn(II) cation is four coordinated with two different **C-Py** ligands and two nitrates adopting a deformed tetrahedral geometry (Figure 38 (a)). Zn (II) is coordinated to one **C-Py** from its pyridine site (N1, according to crystallographic numbering) with a distance of 2.01 Å (dZn1-N1) and to a second **C-Py** from its cytosine site (N3) with a distance of 2.04 Å (dZn1-N3). The N1-Zn1-N3 angle is equal to 112.10°. The coordination sphere of the metal cation is completed by two nitrates with Zn-O distances close to 2.0 Å. Two **C-Py** are connected to two Zn^{2+} in a convergent fashion, thus leading to the formation of a Zn_2(**C-Py**)$_2$ dimer and a $Zn^{2+}$to ligand ratio of 1:1 (Figure 38(a)).

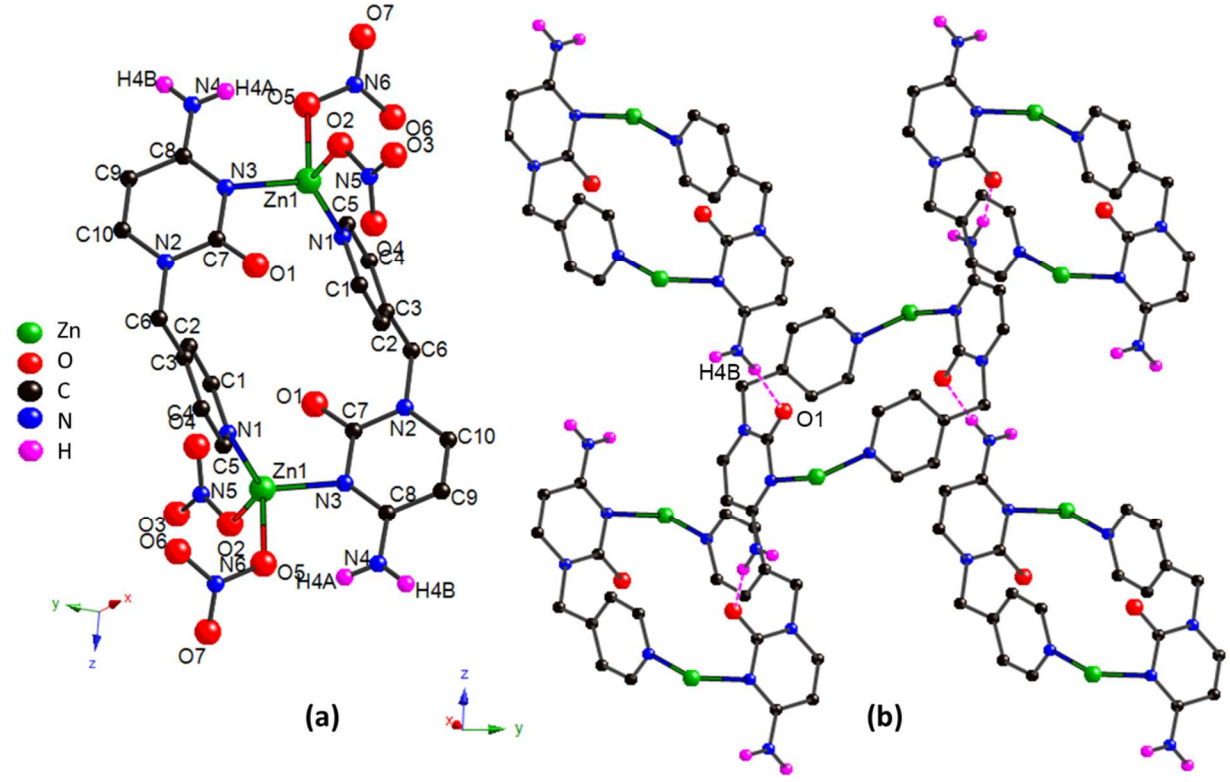

Figure 38: The crystal structure of **Zn(II)-C-Py**. (a) Zn_2(**C-Py**)$_2$ dimer. (b) 2D Network formed by H-bonds between the dimers. Nitrate counter ions are omitted for clarity.

The tertiary amine (N3) of the cytosine is coordinated to the metal cation, consequently it is not involved in H-bonding interactions. However, the carbonyl and NH_2 groups of the cytosine moieties are free to undergo hydrogen bonds with adjacent cytosine rings. Each Zn_2(**C-Py**)$_2$ dimer is

composed of two cytosine rings, and thus a total of two carbonyl groups and two NH_2 groups. These 4 groups are all interacting with 4 adjacent dimers *via* four H-bonds between the O1 of the carbonyl and H4B of the NH_2 functions of the cytosine rings with a distance of 3.01 Å (dO1-N4) as shown in Figure 38 (b). Furthermore, H4A is H-bonded to O5 of a nitrate within a dimer. In this structure, the cytosine sites exhibit coordination interactions and H-bonding, known characteristic for all nucleobases.[40,42]

II. 5. b) C-Py-Cd(II) network

C-Py-Cd(II) crystallizes in the orthorhombic space group *Pbcn*. The organization of the complex is similar to the zinc dimer described above, since it forms a Cd_2(**C-Py**)$_2$ dimer with the pyridine and the cytosine coordinated to the Cd(II) (Figure 39). However, in this structure, cytosine acts as a chelate ligand with N1 and O1 coordinated to the Cd cation. Cd1-N1 and a Cd1-O1 distances are equal to 2.31 Å and 2.51 Å respectively (Figure 39 (a)). Moreover, the geometry around the Cd(II) is different when compared to the Zn dimer. Indeed, Cd(II) is 7-coordinated, since it coordinates to two nitrogen atoms, one from the pyridine site with a Cd1-N4 distance equal to 2.27 Å and the other from the cytosine site (N1), to one oxygen of the cytosine (O1), and to three nitrates, one acting as a chelate ligand with Cd-O distances equal to 2.38 Å and 2.45 Å while the other two nitrates are acting as bridging ligands with two other Cd(II) from two adjacent dimers (Cd1-O5 and Cd1-O7 distances of 2.31 Å and 2.35 Å) (Figure 39 (b)). Within the dimer, the pyridine-Cd-cytosine angles are close to 108 and 84 ° for N4-Cd-N1 and N4-Cd-O1 respectively, while for **C-Py** ligand the angle between the pyridine and the mean plane of cytosine is close to 74°. In the structure, the only hydrogen bond observed is an interaction within a dimer involving hydrogen of N2 (H3A) and an oxygen atom of a bridging nitrate (O6), with a N···O distance of 3.0 Å (Figure 39 (b)).

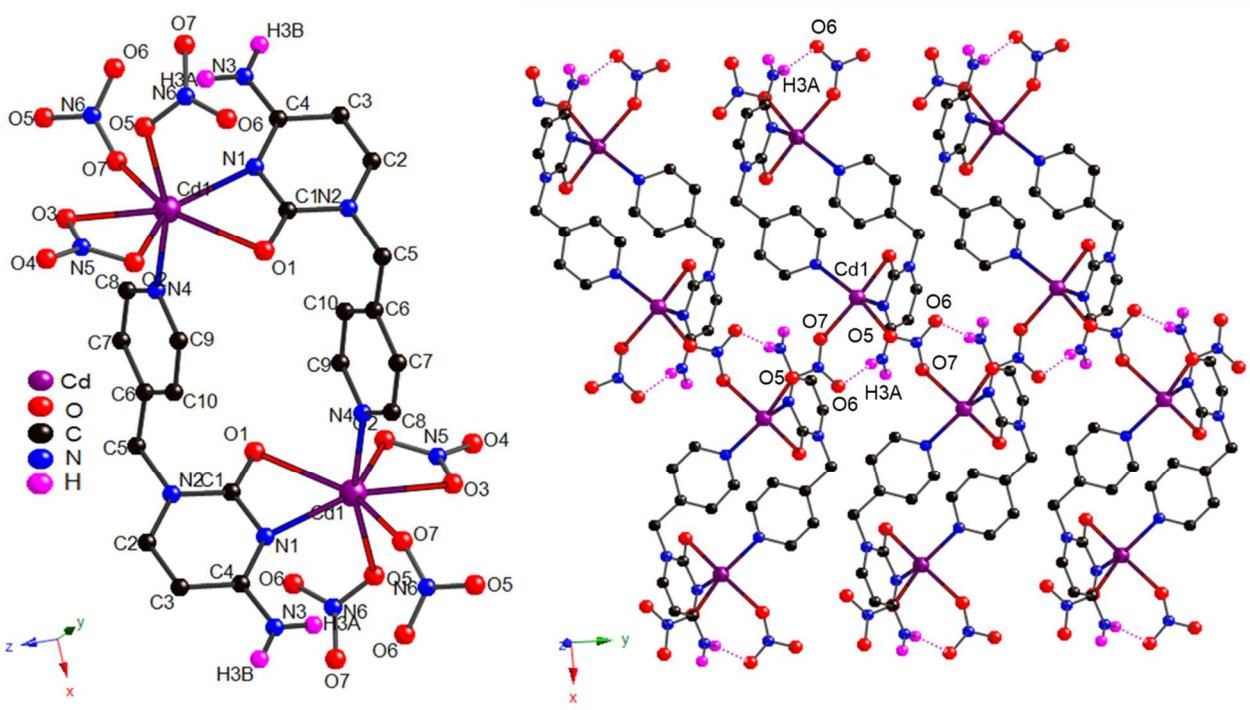

Figure 39: The crystal Structure of **C-Py Cd(II)** (a) Structure of the Cd_2(**C-Py**)$_2$ $(NO_3)_4$ dimer.(b) The coordination network formed through the two nitrate bridging ligands. The chelate NO_3 molecules are omitted for clarity.

II. 6. TerPyridines bearing NBs

As mentioned previously, **terPy** based ligands and complexes are well known compounds. Introducing NBs to **terPy** will result in interesting molecular tectons (**NB-terPy**) bearing one tridentate coordinating site and one H-bonding recognition site. **NB-terPy** may coordinate to a metal center (**M**) forming a **NB-terPy-M** complex that can assemble *via* Watson-Crick H-bonding. Moreover, two equivalents of **NB-terPy** can coordinate around a metal center (**M**) forming a complex bearing two NBs in *trans* positions **NB-terPy-M-terPy-NB,** which can further self-assemble into a network *via* H-bonding interactions (Figure 22). In addition, the aromatic structure of **terPy** will result in π-π interactions that can further stabilize the network and result in 2D or 3D architectures.

The synthesis of **T-terPy** and **A-terPy** was already described.[34,38,39] It was reproduced and extended to the synthesis of **C-terPy** and **G-terPy**. The common strategy to introduce NBs at the 4’ position of **terPy** is to use 4’-(4-bromomethylphenyl)-2,2’:6’,2”-terpyridine (**Br-terPy**) as starting material,

which is obtained from the bromination of 4'-tolyl-2,2':6',2"-terpyridine (**tolyl-terPy**). **Br-terPy** was thus reacted with all NBs in the presence of the suitable base in DMF at 40 °C. We performed reactions with and without KI, but the presence of KI did not increase the yield nor decreased the time. The tectons were characterized by NMR, IR and HRMS. Many attempts to crystallize **NB-terPy** tectons were made either alone or as a mixture of complementary tectons in order to be analyzed in X-Ray diffraction but with no success yet.

II. 6. a) Synthesis of 4'-(4-bromomethylphenyl)-2,2':6',2"-terpyridine (Br-terPy)

Tolyl-terpy was brominated with NBS in benzene under a lamp of 120 Watts to give 60 % of **Br-terPy** (Figure 40).[43]

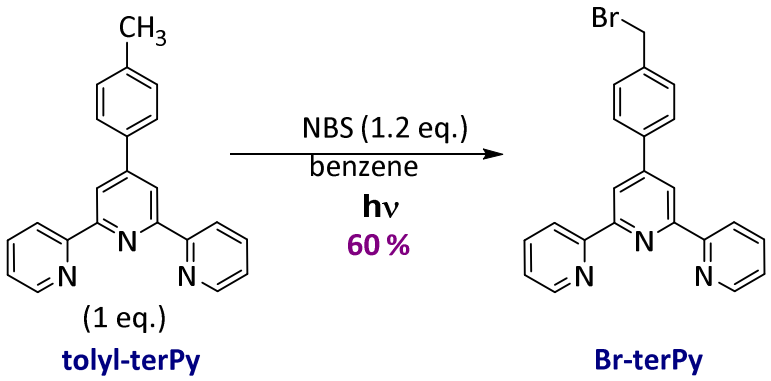

Figure 40: Synthesis of **Br-terPy**.

II. 6. b) Synthesis of 4'-(N1-methylphenylthymine)-2,2':6',2"-terpyridine (T-terPy) (T21)

T-terPy was obtained by reacting an excess of thymine (3 eq.), to prevent di-substitution of thymine, and **Br-terPy** (1 eq.) in the presence of K_2CO_3 (1.5 eq) in dry DMF. The reaction yielded 40% of the targeted **T-terPy** (**T21**) (Figure 41).

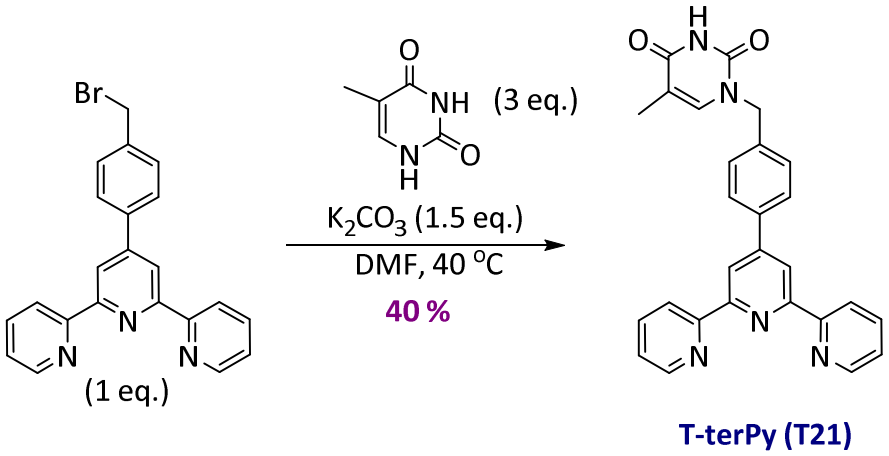

Figure 41: The synthesis of **T-terPy.**

II. 6. c) Synthesis of 4'-(N9-methylphenyladenine)-2,2':6',2"-terpyridine (A-terPy) (T22)

A-terPy was synthesized following the same procedure as for **T-terPy**. Adenine was added in excess (2 eq.) with respect to the **Br-Py** (1 eq.) in the presence of K_2CO_3 (1.5 eq.). **T22** is obtained in 54% yield (Figure 42).

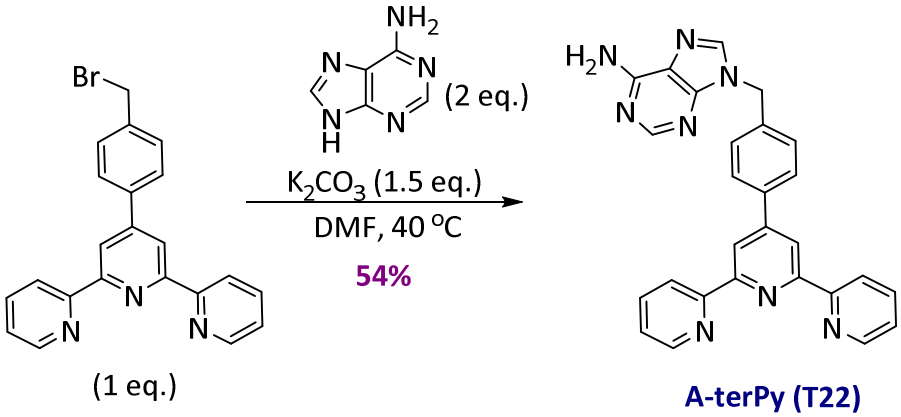

Figure 42: The synthesis of **A-terPy**.

II. 6. d) Synthesis 4'-(N_1-methylphenylcytosine)-2,2':6',2"-terpyridine (C-terPy) (T23)

The substitution reaction between cytosine and **Br-terPy** was performed in the presence of NaH instead of K_2CO_3, which proved to be unsuitable for the deprotonation of **C**. The reaction yielded 79 % of **C-terPy** (**T23**) (Figure 43).

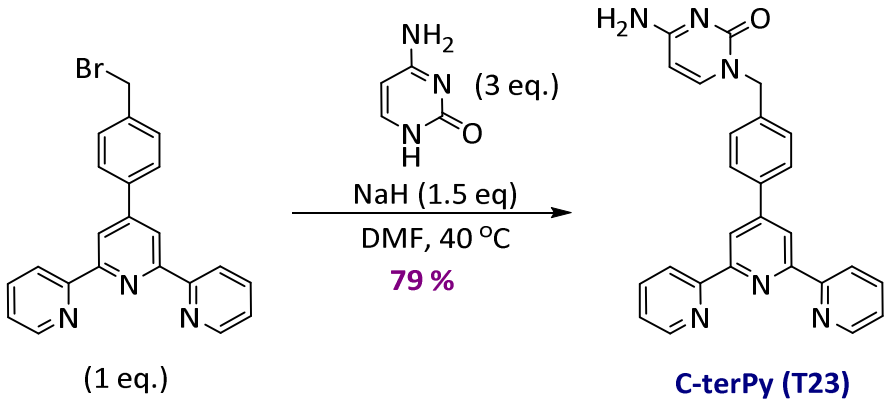

Figure 43: The synthesis of **C-terPy**.

II. 6. e) Synthesis of 4'-(N_9-methylphenylguanine)-2,2':6',2"-terpyridine (G-terPy) (T25)

To introduce guanine in the 4' position of **terPy**, 2-amino-6-chloropurine (**P**) was reacted with **Br-terPy** in the presence of K_2CO_3 to yield 43 % of **P-terPy** (**T24**). The latter was hydrolyzed by 0.1 M HCl aqueous solution producing **G-terPy** (**T25**) with a yield of 96 % (Figure 44). The success of the acid hydrolysis was proved by the shift of the [M+1]+1 peak in MS from 491.15 for **P-terPy** to 473.18 for **G-terPy**, and by the shift in the IR spectrum from 1629 cm^{-1} to 1716 cm^{-1}, which represent the C=N stretching and the C=O of **P-terPy** and **G-terPy** respectively. In addition, the appearance of the broad NH peak of **G-terPy** at 10.68 ppm in ^{1}H-NMR, which was not present for **P-terPy,** confirms the hydrolysis.[33, 41]

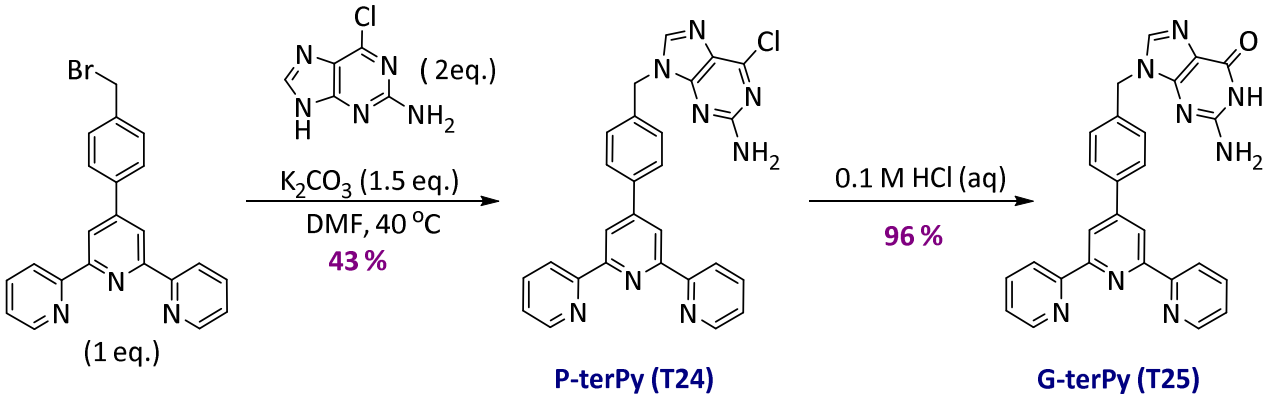

Figure 44: The synthesis of **P-terPy** and **G-terPy**.

II. 7. Structural characterization of complexes based on T-terPy (T21)

The **T21**-**T25** tectons were crystallized with several metal salts, for example Fe (II), Ru(II), Cu(II), Co(II), Ni(II), Pd(II), Cd(II) using 1:1 or 1:2 metal: ligand ratio. Unfortunately, most of the attempts lead to amorphous powder. Nevertheless, monocrystals suitable for X-Ray diffraction were obtained from **T-terPy** with $Cu(OAc)_2$ and **T-terPy** with $Cd(NO_3)_2.4H_2O$ resulting in the formation of mono-**terPy** complexes **T-terPy-Cu(II)** and **T-terPy-Cd(II)**. The crystals were obtained by slow diffusion of a solution of the metal salts in acetonitrile into a solution of **T-terPy** in dichloromethane for **T-terPy-Cu(II)**, and in chloroform for **T-terPy-Cd(II)**. The metallation of the terpyridine occurs during the diffusion process. The characterization by X-Ray diffraction revealed the formation of H-bonds between thymine in both cases. Molecular networks were assembled *via* the coordination of the **terP**y moiety to the metal center (Cu(II) and Cd(II)) and *via* H-bonding of the thymine moieties.

II. 7. a) T-terPy-Cu(II) network

The **T-terPy-Cu(II)** complex crystallizes in the triclinic *P-1* space group. The **terPy** is acting as a tridentate ligand around Cu(II) with a Cu-N distances close to 2.0 Å. One acetate and one chloride (from the dichloromethane) are present in the coordination sphere of the metal cation with Cu1-O3 and Cu1-Cl3 distances equal to 1.93 and 2.53 Å respectively. Furthermore, the second oxygen, O4 (Figure 45 (a)) of the acetate is in close proximity to the Cu(II) with a distance of 2.78 Å. By neglecting this additional Cu-O interaction, the geometry around the Cu(II) is a distorted square

pyramidal geometry with the chloride ion in the apical position. Within the complex, the angle between the mean plane of the terpyridine and the mean plane of the thymine is close to 82°. **T-terPy-Cu(II)** self-assembles into a H-bonded dimer *via* two hydrogen bonds involving the thymine moieties with a distance of 2.84 Å (dN5-O2) (Figure 45 (b)). Each dimer interacts with two other dimers by π-π interactions between the **terPy** moieties with mean plane separation of 3.56 Å (Figure 45 (b)).

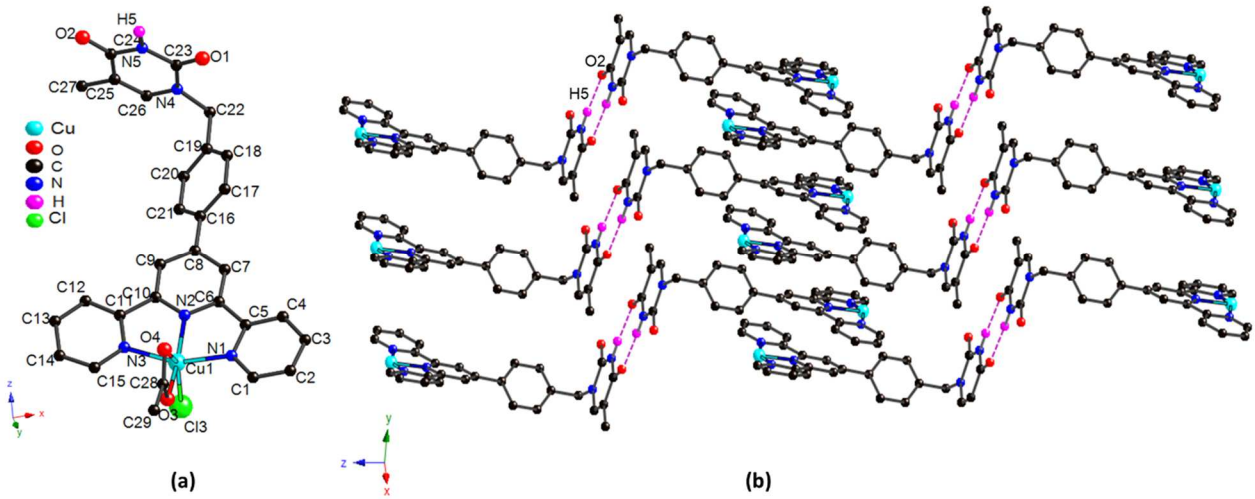

Figure 45: The crystal structure of **T-terPy-Cu(II).** (a) The coordination sphere of Cu(II). (b) A view of H-bonds between **T** and the stacking of the resulting **T-terPy** dimers. Chloride and acetate are omitted for clarity.

II. 7. b) T-terPy-Cd(II) network

The **T-terPy-Cd(II)** complex crystallizes in the monoclinic *Cc* space group. Cd(II) is surrounded by four different ligands, and its coordination sphere is composed of: the terpyridine, two nitrates and a water molecule. The terpyridine is acting as a tridentate ligand with Cd-N distances close to 2.35 Å (Figure 46 (a)). In addition, two nitrates are present, one is a monodentate ligand with a Cd-O distance of 2.40 Å, while the second is located approximately in the same plane of the terpyridine and acts as a bidentate ligand with Cd-O distance of 2.40 and 2.48 Å (Figure 46 (a)). A water molecule occupies the *trans* position of the monodentate nitrate with a Cd1-O12 distance of 2.31 Å (Figure 46 (a)). The angle between the mean plane of the terpyridine and the mean plane of the thymine is close to 62° and 20 ° less than in **T-terPy-Cu(II)**. Each complex is H-bonded to two

adjacent complexes *via* two H-bonds involving the thymine moieties. The thymine moieties are linked to one another by one hydrogen bond between their amine site (N5) and carbonyl site (O1) with a distance of 3.07 Å (dO1-N5) (Figure 46 (b) and (c)). Furthermore, the terpyridine moieties are packed by weak π-π interactions (centroid-centroid separation equals to 3.97 Å).

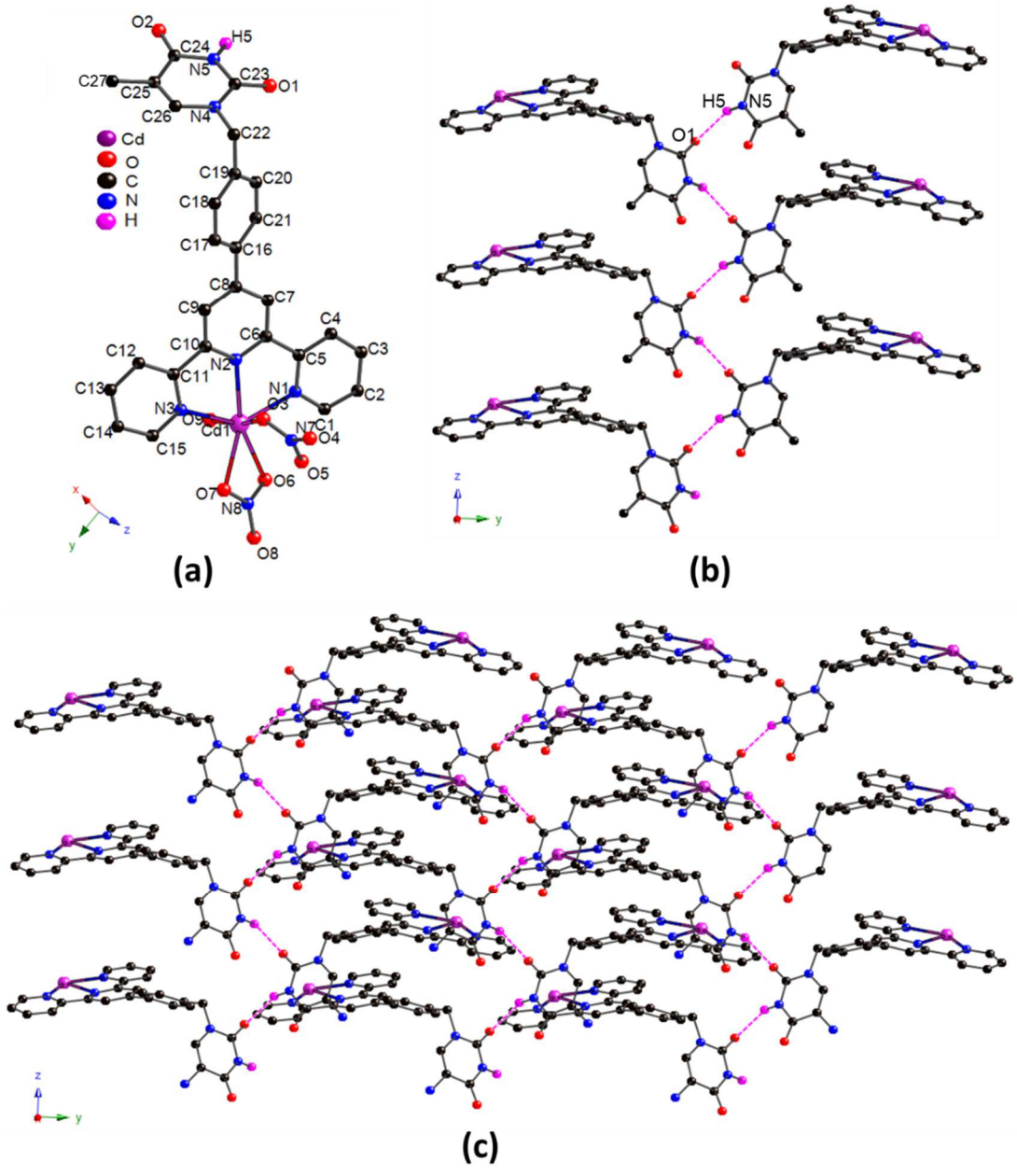

Figure 46: The crystal Structure of (a) **T-terPy-Cd(II)** (b) A view of H-bonds between thymine moieties. (c) View of the network. The counter ions are omitted for clarity.

III. Conclusion and Perspectives

Pyridine and terpyridine molecules are used for different chemical and biological applications. As previously discussed, **Py**-based compounds are used as reagents in production of dyes, agrochemicals and pharmaceuticals.[2] Moreover, the study of the DNA-binding ability of **terPy**-based complexes and their photophysical properties have proved the importance of such complexes in luminescent labeling of biomolecules.[11,12] In addition, **Py** and **terPy** are extensively used in coordination chemistry and in molecular tectonics.[10] Introducing H-bonding sites, such as nucleobases, to **Py** and **terPy** affords interesting molecular tectons that can self-assemble *via* several intermolecular interactions. Therefore, we synthesized a library of **Py** and **terPy** bearing NBs, and our main objective was to study their self-assembly in the presence or absence of additional metal cations. The nucleobases **T**, **A**, **C**, **P** and **G** were introduced in the **Py** and **terPy** backbone generating 10 tectons **T16-T25** (Figure 47). Three of them **T-Py** (**T16**), **A-Py** (**T17**), and **C-Py (T18)** were characterized by X-Ray diffraction. The Watson-Crick H-bonding between the NBs moieties were observed for **A-Py** (**T17**) and **C-Py (T18)**. However, for **T-Py** (**T16)** H-bond interaction between the pyridine and thymine is observed instead of **T**-**T** interactions. Moreover, tectons **A-Py** (**T17**), **C-Py (T18),** and **T-terPy (T21)** formed single crystals suitable for X-Ray analysis with different metal salts, resulting in the **A-Py-Cd(II)**, **A-Py-Hg(II)**, **C-Py-Zn(II), C-Py-Cd(II), T-terPy-Cu(II)** and **T-terPy-Cd(II)** complexes. The metal complexes are formed *via* coordination bonds between the metal cation and **Py** or **terPy** sites, in addition to NBs' H-bonding or coordination interactions that occur in the crystal.

Moreover, crystallization of complementary tectons such as **A-Py** with **T-Py** and **C-Py** with **G-Py** was also tried, but no single crystals suitable for X-Ray diffraction analysis was isolated yet. Similarly, attempts to assemble complementary **NB-terPy** tectons, **T-terPy/A-terPy** and **C-terPy/G-terPy**, were performed. Unfortunately, again single crystals suitable for X-Ray analysis were not obtained yet. Therefore, the future perspective is to combine the complementary tectons and crystalize them with and without metal salts, using different methods, aiming to obtain molecular networks assembled *via* Watson-Crick H-bonding, as shown in Figures 21 and 22. In addition, the second perspective is to combine **NB-Py** and **NB-terPy** tectons with metal salts to generate heteroleptic complexes, which can assemble *via* Watson-Crick H-bonding (Figure 23).

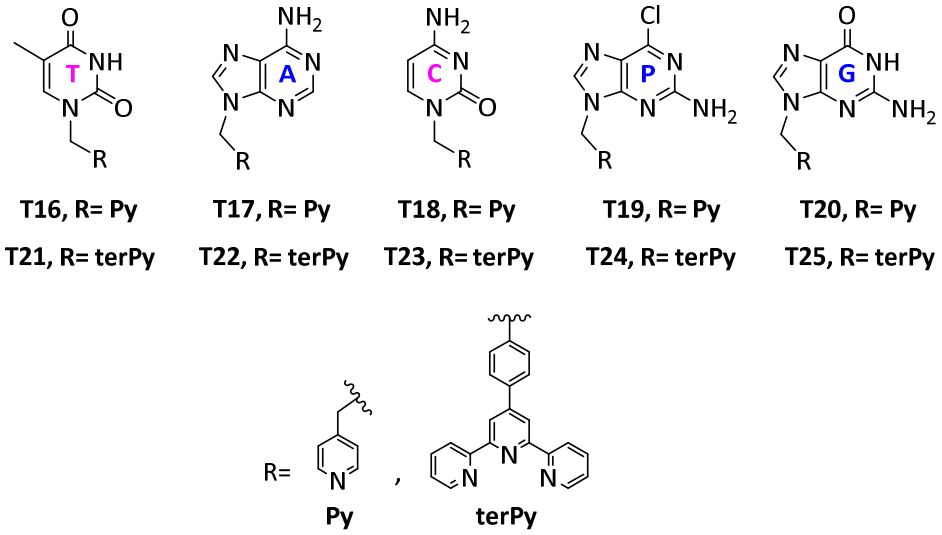

Figure 47: The chemical structure of **T16**-**T25**.

IV. References

1) A. R. Katritzky, C.A. Ramsden, R. J. K. Taylor, *Comprehensive Heterocyclic Chemistry III, Elsevier Science,* **2008**.

2) (a) P. P. Mistry, A. V. Desai, *Heterocyclic Letters*, **2018**, *8*, 145-154. (b) J. H. Weisburger, *Mutation Research*, **2002**, *506-507*, 9-20. (c) H. M. Pinheiro, E. Touraud, O. Thomas, *Dyes and Pigments*, **2004**, *61*, 121-139. (d) E. Vitaku, D. T. Smith, J. T. Njardarson, *J. Med. Chem.,* **2014**, *57*, 10257-10274. (e) G. Trakoontivakorn, K. Nakahara, H. Shinmoto, M. Takenaka, M. O.-Kameyama, H. Ono, M. Yoshida, T. Nagata, T. Tsushida, *J. Agric. Food Chem.*, **2001**, *49*, 3046-3050.

3) (a) M.-J. Lin, A. Jouaiti, D. Pocic, N. Kyritsakas, J. -M. Planeix, M. W. Hosseini, *Chem. Commun.*, **2010**, *46*, 112-114. (b) G. R. Newkome, A. K. Patri, E. Holder, U. S. Schubert, *Eur. J. Org. Chem.*, **2004**, 235-254. (c) D. M. Bassani, J. -M. Lehn, K. Fromm, D. Fenske, *Angew. Chem.*, *Int. Ed.*, **1998**, *37*, 2364-2367.

4) (a) J. A. Joule, K. Mills, *Heterocyclic Chemistry, Chichester: Blackwell Publishing,* **2010**. (b) D. R. Lide, *Handbook of Chemistry and Physics Boca Raton*, **2009**.

5) E. Deiters, V. Bulach, M. W. Hosseini, *New J. Chem.*, **2008**, *32*, 99-10.

6) J. P. Byrne, J. A. Kitchen, T. Gunnlaugsson, *Chem. Soc. Rev.*, **2014**, *43*, 5302-5325.

7) Q.-Y. Zhu, Q.-H. Han, M.-Y. Shao, J. Gu, Z. Shi, J. Dai, *J. Phys. Chem. B.*, **2012**, *116*, 4239-4247.

8) (a) E. Graf, M. W. Hosseini, J.-M. Planeix, N. Kyritsakasa, *New J. Chem.*, **2005**, *29*, 343-346. (b) L. Qin, H.-L. Jia, Z.-J. Guo, H.-G. Zheng, *Cryst. Growth Des.*, **2014**, *14*, 6607-6612.

9) G. T. Morgan, F. H. Burstall, *J. Chem. Soc., Abstr.*, **1932**, 20-30.

10) A. L Gavrilova, B. Bosnich, *Chem. Rev.*, **2004**, *104*, 349-383.

11) (a) K. Chai, Y. Jiang, T. Han, J. Niu, L. Yao, H. Zhang, M. Zeng, L. Zhang, X. Duan, J. Wang, *Polyhedron*, **2019**, *157*, 124-130. (b) D. Mahendiran, R. S. Kumar, V. Viswanathan, D. Velmuruganc, A. K. Rahiman, *Dalton Trans*., **2016**, *45*, 7794-7814. (c) L. A. Levin, C. M. Morgan, K. Ohr, M. E. Williams, *J. Am. Chem. Soc.*, **2005**, *127*, 1674-1680.

12) (a) M. Bar, S. Deb, P. Animesh, S. Baitalik, *Inorg. Chem*., **2018**, *57*, 12010-12024. (b) J. Dietrich, L. Wuensche, G. Anica, R. -G. Markus, H. Ute, H. Katja, *Eur. J. Inorg. Chem.,* **2013**,

17, 3009-3019. (c) W. Leslie, A. S. Batsanov, J. A. K. Howard, J. A. G. Williams, *J. Chem. Soc., Dalton Trans.*, **2004**, 623- 631.

13) (a) I. M. Brown, S. I. Weissman, L. C. Snyder, *J. Chem. Phys*., **1965**, *42*, 1105-1111. (b) C. C. Addison, R. Davis, N. Logan, *J. Chem. Soc.,***1974**, 2071-2075.

14) E. C. Constable, *Adv. Inorg. Chem.*, **1986**, *30*, 69-121.

15) H. Hofmeier, U. S. Schubert, *Chem. Soc. Rev.,* **2004**, *33*, 373-399.

16) (a) D. J. Bray, J. K. Clegg, K. A. Jolliffe, L. F. Lindoy, *CrystEngComm*, **2014**, *16*, 6476-6482. (b) W. M. Reiff, N. E. Erickson, W. A. Baker, *Inorg. Chem.*, **1969**, *8*, 2019-2022.

17) (a) S. Karmakar, D. Maity, S. Mardanya, S. Baitali, *Inorg. Chem*., **2014**, *53*, 12036-12049. (b) H. -J. Park, K. H. Kim, S. Y. Choi, H. -M. Kim, W. I. Lee, Y. K. Kang, Y. K. Chung, *Inorg. Chem.*, **2010**, *49*, 7340-7352. (c) J. P. Sauvage, J. P. Collin, J. C. Chambron, S. Guillerez, C. Coudret,V. Balzani, F. Barigelletti, L. De Cola, L. Flamigni, *Chem. Rev.,* **1994**, *94*, 993-1019. (d) E. C. Constable, M. W. C. Thompson, *New J. Chem.,* **1992**, *16*, 855-876.

18) K. Lashgari, M. Kritikos, R. Norrestam, T. Norrby, *Acta. Crystallogr., Sect. C: Cryst. Struct. Commun.*, **1999**, *55*, 64-67.

19) (a) J. Li, J.-G. Guo, S.-L. Cai, S.-R. Zheng, W.-G. Zhang, Inorg. *Chem. Comm.*, **2016**, *73*, 16-20. (b) W.-W. Fu, S.-Q. Ye, Y. Liu, M. -S. Chen, D.-Z Kuang, *Transition Met Chem*, **2015**, *40*, 227-233.

20) M. I. Arriortua, T. Rojo, J. M Amigo, G. Germain, J. P. Declercq, *Acta Crystallogr*., **1982**, *B38*, 1323-1328.

21) (a) M. Muddassir, X.-J. Song, Y. Chen, F. Cao, R.-M. Wei, Y. Song, *CrystEngComm*, **2013**, *15*, 10541-10549. (b) J. Ketola, L. Jaakkola, J. Hovinen, *Lett. Org. Chem.,* **2008**, *5,* 444-449.

22) D.- C. Jeong, J. Lee, Y. Lee, C. Satheeshkumar, S. Chinnadurai, S. Changsik, *Macromolecules*, **2015**, *48*, 1621-1626.

23) I. M. Dixon, J. P. Collin, J. P. Sauvage, L. Flamigni, S. Encinas, F. Barigelletti, *Chem. Soc. Rev.*, **2000**, *29*, 385-391.

24) J. Fortage, F. Puntoriero, F. Tuyeras, G. Dupeyre, A. Arrigo, I. Ciofini, P. Laine, S. Campagna, *Inorg. Chem.,* **2012**, *51*, 5342-5352.

25) (a) S. Yamaguchi, K. Miyamoto, H. Yahiro, *Catal. Commun.*, **2018**, *116*, 48-51. (b) A. G. Majouga, R. B. Romashkina, A. S. Kashaev, R. D. Rahimov, E. K. Beloglazkina, N. V. Zyk, *Chemistry of Heterocyclic Compounds*, **2010**, *46*, 1076-1083.

26) (a) A. K. F. Maartensson, P. Lincoln, *Dalton Trans.*, **2015**, *44*, 3604-3613. (b) D. R. McMillin, J. J. Moore, *Coord. Chem. Rev.*, **2002**, *229*, 113-121.

27) U. S. Schubert, C. Eschbaumer, O. Hien, P. R. Andres, *Tetrahedron Lett.*, **2001**, *42*, 4705-4707, (b) G. R. Newkome, E. He, *J. Mater. Chem.*, **1997**, *7*, 1237-1244. (c) R.-A. Fallahpour, *Synthesis*, **2003**, 155-184.

28) R. Ziessel, *Synthesis*, **1999**, 1839-1865.

29) (a) E. C. Constable, J. Lewis, M. C. Liptrot, P. R. Raithby, *Inorg. Chim. Acta.*, **1990**, *178*, 47-54. (b) E. C. Constable and M. W. C. Thompson, *New J. Chem.*, **1992**, *16*, 855-876, (c) A. C. Thompson, *Coord. Chem. Rev*., **1997**, *160*, 1-52.

30) M. El Garah, S. Sinn, A. Dianat, A. Santana-Bonilla, R. Gutierrez, L. De Cola. G. Cuniberti, A. Ciesielski, P. Samori, *Chem. Commun.*, **2016**, *52*, 11163-11166.

31) L. M. Toledo, K. Musa, J. W. Lauher, F. W. Fowler, *Chem. Mater.*, **1995**, *7*, 1639-1647. (b) P. R. Lowe, C. H. Schwalbe, G. J. B. Williams, *Acta Crystallogr.,* **1987**, *43*, 330-333. (c) A. Ciesielski, S. Colella, L. Zalewski, B. Bruchmann, P. Samorì, *CrystEngComm*, **2011**, *13*, 5535-5537.

32) C. M. White, M. F. Gonzalez, D. A. Bardwell, L. H. Rees, J. C. Jeffery, M. D. Ward, N. Armaroli, G. Calogero, F. Barigelleti, *J. Chem. Soc, Dalton Trans*, **1997**, 727-735.

33) N. Armaroli, F. Barigelleti, G. Calogero, L. Flamigni, C.M. White, *Chem. Commun*., **1997**, 2181-2182.

34) E. C. Constable, R. A. Fallahpour, *J. Chem. Soc., Dalton Trans*, **1996**, 2389-2390.

35) V. Balzani, A. Juris, M. Venturi, *Chem. Rev.*, **1996**, *96*, 759-833.

36) D. Hurley, Y. Tore, *J. Am. Chem. Soc.*, **2002**, *124*, 13231-12341.

37) L. Kalachova, R. Pohl, M. Kocek, *Synthesis*, **2009**, *1*, 105-112.

38) Q. Jiang, Z. Wu, Y. Zhang, A. C. G. Hotze, M. J. Hannon, Z. Guo, *Dalton Trans.*, **2008**, 3054-3060.

39) Q. Jiang, J. Zhu, Y. Zhang, N. Xiao, Z. Guo, *Biometals*, **2009**, *22*, 297-305.

40) (a) W. Saenger, *Principles of Nucleic acids structure*, *Springer*, New York, **1984**. (b) G. A. Jeffery, W. Saenger, *Hydrogen bonding in Biological structures*, *Springer*, Berlin, **1991**.

41) N. Biblo, V. Vazque-Gonzalez, M. T. Aranda, D. Gonzalez-Rodriguez, *Eur. J. Org. Chem.*, **2015**, 7160-7175.

42) (a) D. Amantia, M. A. Shipman, C. Price, M. R. J. Elsegood, W. Clegg, A. Houlton, *Inorg. Chim. Acta.,* **2006**, *359*, 3515-3520. (b) P. Amo-Ochoa, O. Castillo, C. J. Gómez-García, K.

Hassanein, S. Verma, J. Kumar, F. Zamora, *Inorg. Chem.*, **2013**, *52*, 11428-11437. (c) P. A. Ochoa, F. Zamora, *Coordination Chemistry Reviews*, **2014**, *276*, 34-58. (d) R. Gil-Garcia, M. Ugalde, N. Busto, H. J. Lozano, J. M. Leal, B. Perez, G. Madariga, M. Insausti, L. Lezema, R. Sanz, Lidia M. Gomez, B. Garcia, J. Garcia-Tojal, *Dalton Trans*, **2016**, *45*, 18704-18718. (e) A. Lopez, J. Liu, *ChemNanoMat*, **2017**, *3*, 670-684.

43) J. P. Collin, A. Jouaiti, J. P. Sauvage, J. *Electroanal. Chem., **1990***, *286*, 75-87.

Conclusion and Perspectives

I. Conclusion

Molecular tectonics is a domain of supramolecular chemistry dealing with the formation of one, two and three-dimensional molecular networks. The latter is formed through the self-assembly of tectons bearing complementary interaction sites, which form a recognition pattern *via* specific interactions. In this project, we focused on two types of interactions, the coordination interactions and the hydrogen bonding interactions, more specifically the Watson-Crick H-bonding between nucleobases (NBs).

NBs are found in the main source of life, the DNA, thus making them targeted motifs to be studied in biology and chemistry. Nucleobases have the possibility to form non-covalent interactions, such as the Watson-Crick H-bonding between complementary NBs, self-dimerization interactions and coordination interactions with metal salts. All these properties offer NBs advantages over other motifs when it comes to designing molecular networks assembled *via* non-covalent interactions.

The first objective of this project is to introduce nucleobases to different coordination sites, thus designing molecular tectons with the possibility to self-assemble *via* both coordination and H-bonding interactions. Four coordination scaffolds possessing amine sites were used: porphyrins, dipyrrins, pyridines and terpyridines. Each one of these motifs provides specific properties essential to build molecular networks. Porphyrin has the ability to be functionalized in the 4 *meso* positions along with the 8 β-positions, and to coordinate metal cations *via* its azacore. Similarly, dipyrrins is an anionic bidentate ligand that can be functionalized in the *meso*, β and α positons. In addition, dipyrrins are known to form either homoleptic or heteroleptic metal complexes. Last but not least, pyridines and terpyridines are strong coordinating moieties, which have the ability to form complexes of different stoichiometry and various geometries.

To introduce NBs in the *meso* position of porphyrins, a porphyrin bearing two triple bonds in *trans meso* positions (**Po1**) was synthesized and coupled with **I-U-Ph2** and **I-U-C6**, under Sonogashira conditions, to result in **T1**, **T2** and **T3**. (Figure 1) Unfortunately, complications of the cross coupling reactions prevented the extension of this strategy to other NBs. Therefore, NBs were introduced to porphyrins by C-N bonds *via* their active NH sites, N_1 site of pyrimidines and N_9 site of purines. Using this strategy, we were able to introduce **T**, **A**, **C**, **P** and **G** in the periphery of the porphyrin bearing two *trans* active bromine site, generating 5 porphyrin based tectons **T5**-**T9**. Moreover, a tetra-functionalized porphyrin substituted with 4 thymines (**T10)** was successfully

synthesized. Similarly, the five NBs were introduced in the *meso*-position of dipyrrins bearing a bromine active site, resulting in five novel tectons **T11-T16**. Furthermore, the nucleobases were introduced to pyridine and terpyridine, by reacting each NB with 4-bromopyridine and 4'-(4-bromomethylphenyl) terpyridine resulting **T17**-**T25** (Figure 1).

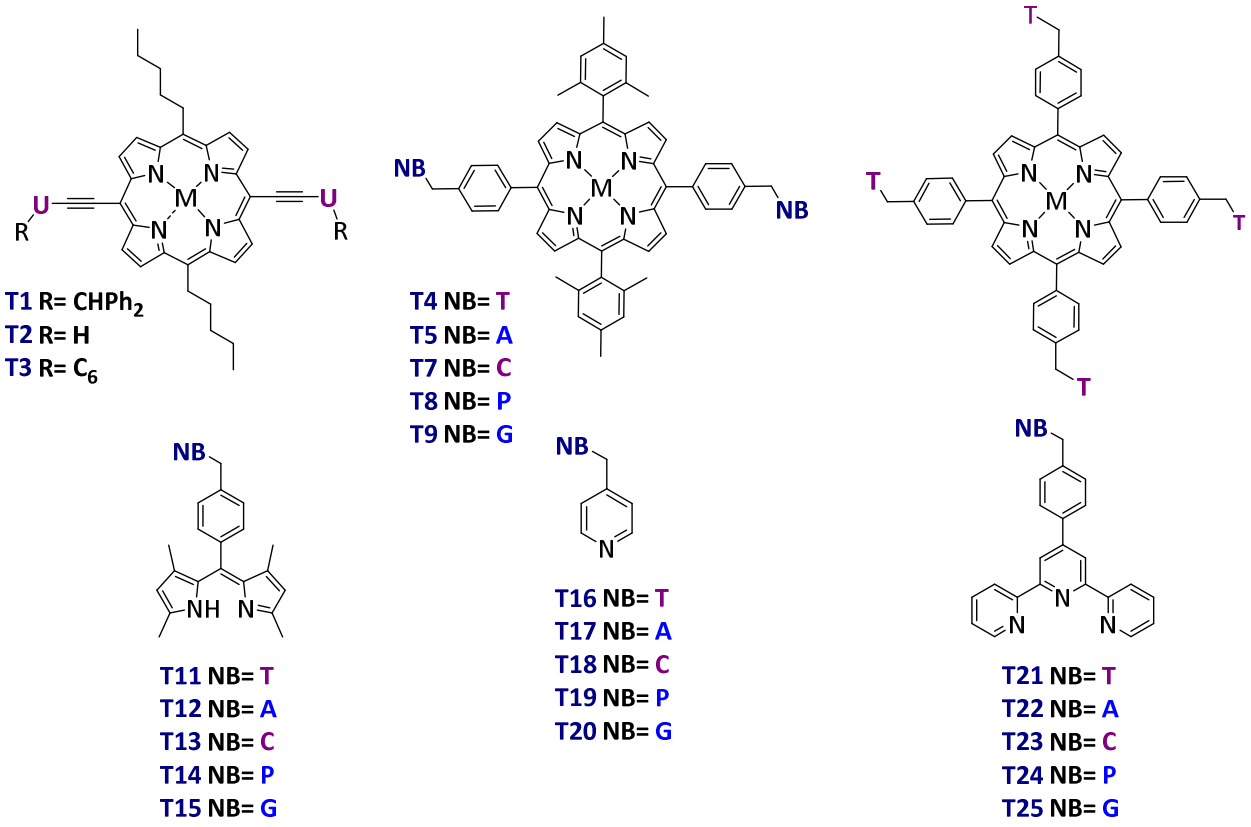

Figure 1: The chemical structure of all synthesized tectons.

The second objective of this PhD project is to generate molecular networks based on the synthesized tectons. To produce molecular networks, the tectons were crystallized by using different methods and under different conditions. In addition to being complementary to their respective base pair partner, nucleobases are self-complementary, thus the self-assembly of each tecton is possible. For that reason, attempts to crystallize each tecton alone with and without metal salts were performed, along with combining complementary tectons. For instance, porphyrin bearing thymine (**T3**) and porphyrin bearing adenine (**T4**) were mixed and crystallized together. The same procedure was done for all complementary tectons. Unfortunately, co-crystals suitable

for X-ray analysis are not yet obtained. However, monocrystals were obtained for several tectons forming networks assembled *via* the H-bonding between the same NB.

The self-assembly of **T11** in the presence of Zn(II) resulted in a molecular network formed *via* the coordination bond of the dipyrrin site to the metal center and *via* **T**-**T** interactions. In addition, the self-assembly of **T16**-**T18** were studied by X-ray analysis. Pyridine bearing adenine (**T17**) and cytosine (**T18**) assembled *via* H-bonding interactions between the adenine and cytosine moieties respectively. However, 4-(N_1-methylthymine)pyridine (**T16**) assembled *via* the H-bond between pyridine and thymine. This proves that, under the conditions used, the H-bonding interaction between **Py** and **T** is thermodynamically more favored than **T**-**T** interactions, which is known to be weaker than the **A**-**A** and **C**-**C** hydrogen bonding. Moreover, the generation of coordination networks was successful for **T17** with Cd(II) and Hg(II) and for **T18** with Zn(II) and Cd(II). Those molecular networks assembled through the coordination interactions of pyridine to the metal center, and through the different interactions of NBs. For example, within the **T17**-Hg(II) and **T18**-Cd(II) networks, the NBs formed coordination interactions with the metal center, and in **T17**-Cd(II) and **T18**-Zn(II), the NBs were involved in H-bonding interactions. Last but not least, molecular networks of **T21** were obtained in the presence of Cu(II) and Cd(II). These networks revealed the coordination interactions of the terpyridine site to the metal center and the H-bonds between the thymine moieties.

II. Perspectives

One of the main objectives of this project, which is the generation of networks assembled *via* H-bonds of complementary tectons, was not reached for all the 16 tectons. Therefore, future work will focus on designing new networks by launching more crystallization to obtain suitable crystals. Multiple combinations are possible: either based on one tecton with different metallic salts or by mixing two complementary tectons of the same category such as: two complementary porphyrins (for example **T4** and **T5**) or two complementary dipyrrins (for example **T13** and **T15**) . Moreover, combining porphyrin based tectons with dipyrrin, pyridine or terpyridine based tectons in order to design heteroleptic and/or heterobimetallic networks is the second perspective of this work.

In addition, future work should focus on studies in solution, in order to determine the association constants between complementary and self-complementary tectons, in addition to luminescence studies of dipyrrins and terpyridine metal complexes.

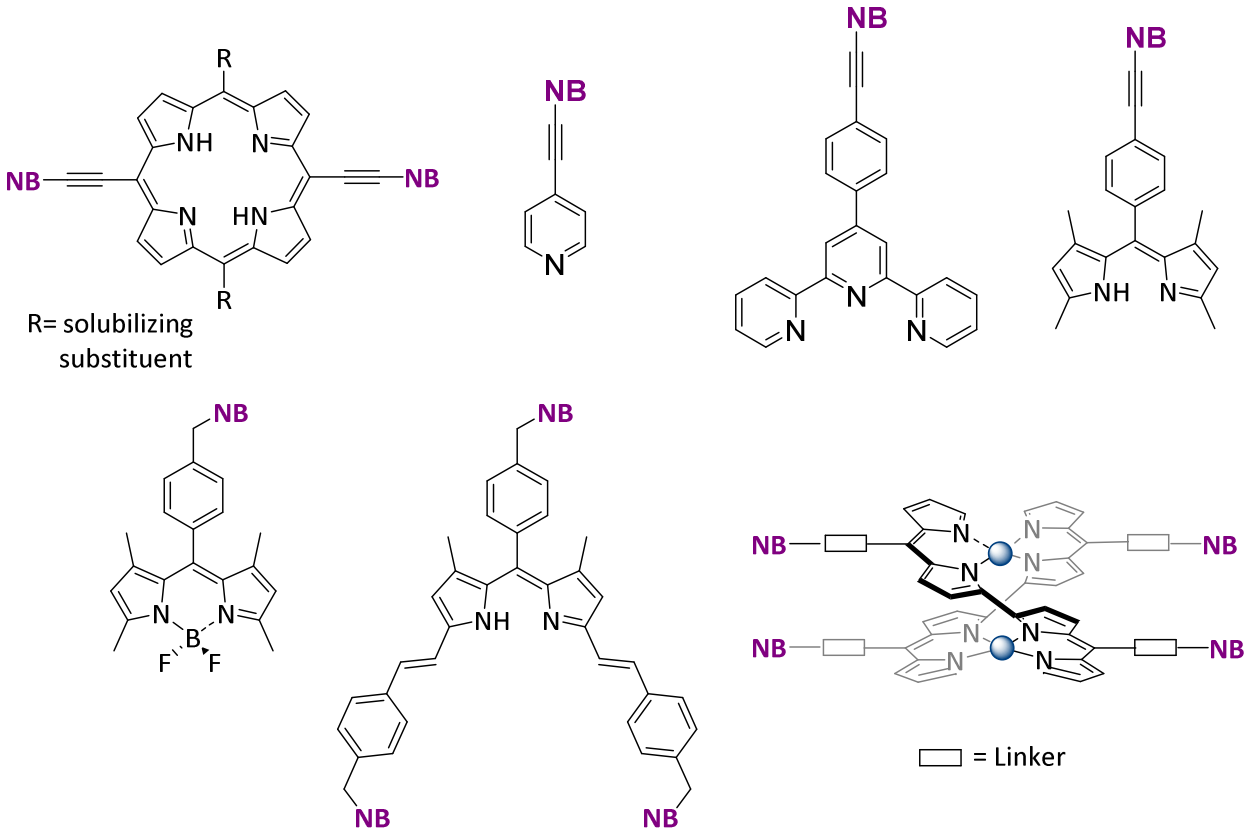

Figure 2: The chemical structure of possible future tectons.

Experimental Part

1) Dipyrromethane[1]

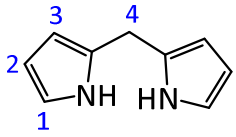

Chemical Formula: $C_9H_{10}N_2$
Molecular Weight: 146.19 g/mol

A mixture of pyrrole (96.6 g, 1.44 mol, 100 mL, 40 eq) and *para*formaldehyde (1.7 g, 0.036 mol, 1 eq) was treated with methanol (55 mL) and acetic acid (150 mL). The mixture was stirred at room temperature for 20 hours under argon and protected from light. After 20 hours, the mixture was diluted with chloroform (300 mL), then washed with water (2 x 400 mL) and 1 M KOH aqueous solution (2 x 400 mL). The organic phase was concentrated under reduced pressure. The crude product was purified by column chromatography (silica gel, cyclohexane/dichloromethane (2:1)) to give 2.3 g of a white solid (44 %).

^{1}H NMR (300 MHz, $CDCl_3$) δ: 3.95 (2H, s, H4), 6.06 (2H, m, H2), 6.17 (2H, dd, H3, ^3J = 5.7 Hz, ^4J = 2.6 Hz), 6.62 (2H, m, H1), 7.71 (2H, s, br, NH).

2) 5,15-dipentylporphyrin[2]

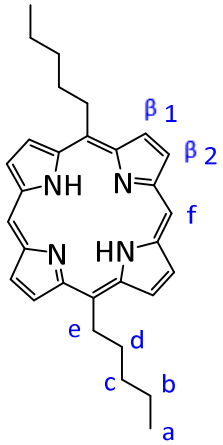

Chemical Formula: $C_{30}H_{12}N_4$
Molecular Weight: 428.45 g/mol

Montmorillonite K 10 (7 g) was activated under vacuum at 100 ºC for 2 hours and then cooled to room temperature under argon. To the same flask, a solution of hexanal (0.411 mL, 3.4 mmol, 1

eq) in degassed dichloromethane (35 mL) and a solution of dipyrromethane (0.5g, 3.4 mmol, 1 eq) in degassed dichloromethane (500 mL) were added. The mixture was degassed and stirred at room temperature under argon. The disappearance of dipyrromethane was followed by TLC. After 24 hours, the dipyrromethane disappeared and *p*-chloranil (1.25 g, 5 mmol, 1.5 eq) was added, then stirred under reflux. After 2 hours, the mixture was filtered through a celite pad and washed with chloroform. The filtrate was concentrated under reduced pressure and the crude product was purified by column chromatography (silica gel, DCM/ petroleum ether (7:3)) to give 0.21 g of a dark purple solid (27 %).

^{1}H NMR (300 MHz, $CDCl_3$) δ: -2.92 (2H, s, br, NH), 0.99 (6 H, t, ^{3}J=7.3 Hz, Ha), 1.54-1.62 (4H, m, Hb), 1.75-1.85 (4H, m, Hc), 2.50-2.60 (4H, m, Hd), 4.99 (4H, t, ^{3}J = 7.4 Hz, He), 9.39 (4H, d, ^{3}J = 4.6 Hz, Hβ), 9.56 (4H, d, ^{3}J = 4.6 Hz, Hβ), 10.15 (2 H, s, Hf).

3) 5,15-dibromo-10,20-dipentylporphyrin

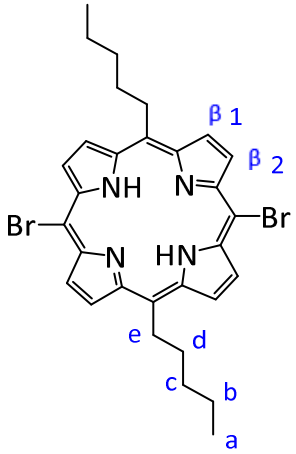

Chemical Formula: $C_{30}H_{32}Br_2N_4$
Molecular Weight: 608.41 g/mol

5,15-dipentylporphyrin (200 mg, 0.44 mmol, 1 eq) and pyridine (0.2 mL) were dissolved in 150 mL of dichloromethane. The mixture was cooled to 0 ºC in an ice bath and NBS (166 mg, 0.933 mmol, 2.2 eq) was added. The reaction was stirred for 2 hours, and then quenched with 5 mL of acetone. The solvent was evaporated and the crude product was washed with methanol several times (3 × 5ml) to give 190 mg of a dark purple solid (74 %).

^{1}H NMR (300 MHz, $CDCl_3$) δ: -2.76 (2H, s, br, NH), 0.97 (6H, t, ^{3}J = 7.4 Hz, Ha), 1.50-1.58 (4H, m, Hb) 1.75 (4H, tt, ^{3}J = 7.7 Hz, Hc), 2.55 (4H, tt, ^{3}J = 7.7 Hz, 7.4 Hz, Hd), 4.90 (4H, t, ^{3}J = 7.4 Hz, He), 9.39 (4H, d, ^{3}J = 4.6 Hz, Hβ), 9.65 (4H, d, ^{3}J = 4.6 Hz, Hβ).

4) 5,15-(4,4,5,5-tetramethyldioxaborane)-10,20-dipentylporphyrin[3]

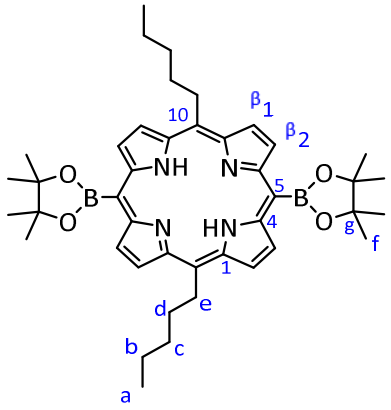

Chemical Formula: $C_{42}H_{56}B_2N_4O_4$
Molecular Weight: 702.45 g/mol

5,10-dipentyl-15,20-dibromoporphyrin (100 mg, 0.1644 mmol, 1 eq) was dissolved in 50 mL of degassed dry dichloroethane and 0.6 mL of triethylamine. To this solution, 4,4,5,5-tetramethyl-1,3,2-dioxaborolane (0.42 g, 3.28 mmol, 0.48 mL, 20 eq) and $PdCl_2(PPh_3)_2$ (11.5 mg, 0.0164 mmol, 0.1eq) were added. The reaction was stirred and heated overnight under reflux. The solution was concentrated under reduced pressure. The crude product was a mixture of de-brominated porphyrin, monoboronated poprphyrin and diboronated porphyrin. The products were separated and purified by column chromatography with a gradient eluent of dichloromethane/cyclohexane (silica gel, DCM/cyclohexane (1:2) then (1:1) (2:1)) to give 11 mg diboronated porphyrin (10 %), 55 mg monoboronated porphyrin (58 %) and 21 mg 5,15-dipentylporphyrin (30 %).

a) 5,15-(4,4,5,5-tetramethyldioxaborane)-10,20-dipentylporphyrin:

^{1}H NMR (300 MHz, $CDCl_3$) δ (ppm) : -3.00 (s, 2H, NH), 0.97 (6 H, t, ^{3}J = 7.4 Hz, Ha), 1.54 (4H m, Hb) 1.78 (4H, m, Hc), 1.87 ppm (24 H, s, Hf), 2.54 (4H, m, Hd), 4.68 (4H, t, ^{3}J = 7.4 Hz, He), 9.57 (4H, d, ^{3}J = 4.6 Hz, Hβ), 9.89 (4H, d, ^{3}J = 4.6Hz, Hβ).

^{13}C NMR (126 MHz, $CDCl_3$) δ: 14.32 (Ca), 22.95 (Cb), 29.86 (Cf), 32.87 (Cd), 34.75 (Cc), 38.48 (Ce), 66.06, 104.40, 118.98, 128.63, 128.63(Cβ), 132.16 (Cβ), 128.98, 131.07, 144.31, 147.60.

HRMS (ESI): m/z(M+): $[M+H]^+$ calculated = 703.4574, $[M+H]^+$ found = 703.4562.

b) 5-(4,4,5,5-tetramethyldioxaborane)-10,20-dipentylporphyrin

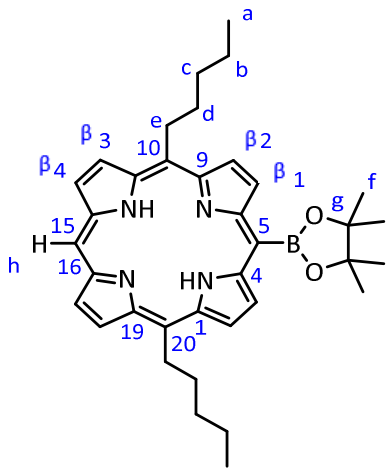

Chemical Formula: $C_{36}H_{45}BN_4O_2$
Molecular Weight: 576.59 g/mol

^{1}H NMR (300 MHz, $CDCl_3$) δ (ppm) : -3.02 (2H, s, NH), 0.98 (6 H, t, ^3J = 7.3 Hz, Ha), 1.58 (4H, m, Hb), 1.75 (4H, m, Hc), 1.89 (s, 12 H, Hf), 2.55 (4H, m, Hd), 5.01(4H, t, ^3J = 7 .4 Hz, He), 9.36 (2H d, ^3J = 4.6Hz, Hβ), 9.56 (2H d, ^3J = 4.6 Hz, Hβ), 9.61 (2H d, ^3J = 4.9 Hz, Hβ), 9.89 (2H d, ^3J = 4.9 Hz, Hβ), 10.12 (1H, s, Hh).

^{13}C NMR (126 MHz, $CDCl_3$) δ: 14.32 (Ca), 22.95 (Cb), 29.86 (Cf), 32.87 (Cd), 34.75 (Cc), 38.48 (Ce), 66.06, 104.40, 118.98, 128.63(Cβ), 128.63 (Cβ), 128.72 (Cβ), 132.16(Cβ), 133.07, 144.31, 147.60.

HRMS (ESI): m/z(M+): $[M+H]^+$ calculated = 577.3715, $[M+H]^+$ found = 577.3700.

5) Zn(II) [5-(4,4,5,5-tetramethyldioxaborane)-10,20-dipentylporphyrin]

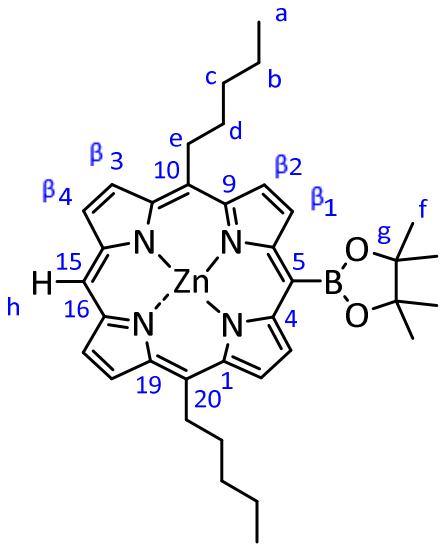

Chemical Formula: $C_{36}H_{43}BN_4O_2Zn$
Molecular Weight: 617.78 g/mol

10-(4,4,5,5-tetramethyldioxaborane)-5,15-dipentylporphyrin (50 mg, 0.087 mmol, 1 eq) was dissolved in 50 mL of chloroform. A solution of $Zn(OAc)_2.2H_2O$ (35 mg, 0.173 mmol, 2 eq) in methanol (5 mL) was added. The reaction mixture was stirred at room temperature for 4 hours, and followed by TLC. When the reaction was completed, the solvent was removed under reduced pressure. The crude product was dissolved with 100 ml of dichloromethane, then washed with water (2x50 mL). The organic phase was collected and dried over $MgSO_4$, then filtered and dried under reduced pressure to give 47 mg of a purple solid (89 %).

^{1}H NMR (300 MHz, $CDCl_3$) δ (ppm): 0.99 (6 H, t, ^3J = 7.3 Hz, Ha), 1.58-1.61 (4H, m, Hb), 1.83 (4H, m, Hc), 1.90 (s, 12 H, Hf), 2.58 (4H, m, Hd), 5.02 (4H, t, ^3J = 7.4 Hz, He), 9.39 (2H d, ^3J = 4.6 Hz, Hβ), 9.62 (2H d, ^3J = 4.6 Hz, , Hβ), 9.71 (2H, d, ^3J = 4.9 Hz, Hβ), 9.95 (2H, d, ^3J = 4.9 Hz, , Hβ), 10.09 (1H, s, Ha).

^{13}C NMR (126 MHz, $CDCl_3$) δ: 14.33 (Ca), 22.86 (Cb), 29.86 (Cf), 32.85 (Cd), 35.70 (Cc), 38.60 (Ce), 66.34, 119.52, 128.60 (Cβ), 129.88-129.90(Cβ), 132.10 (Cβ), 136.82, 145.28, 147.75.

6) N_1-benzylhydryl-5-iodouracil and N_1-benzylhydryl-5-bromouracil [4]

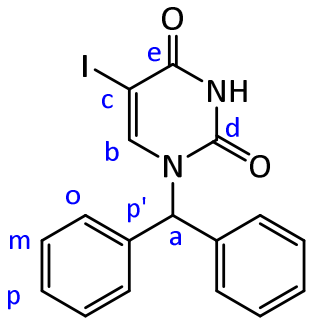

Chemical Formula: $C_{17}H_{13}IN_2O_2$
Molecular Weight: 404.21 g/mol

5-iodouracil (1g, 4.20 mmol, 1 eq) in 16 ml of acetonitrile was treated bis(trimethylsily)acetamide (2.6 mL, 10.51 mmol, 2.5 eq). The suspension was stirred until the bromouracil dissolved and a clear solution was obtained. Benzylhydrylbromide (2.02 g, 8.19 mmol, 2 eq) and a catalytic amount (10 mg) of iodine I_2 were added to the mixture and heated under reflux overnight. The reaction was followed by TLC. When the disappearance of 5-iodouracil was observed (*ca.* 12 hours), the reaction was evaporated under reduced pressure then diluted with dichloromethane (100 mL) and extracted with water (50 mL x 2). The organic phase was dried over $MgSO_4$, filtered and dried under reduced pressure. The crude product was washed with ethylacetate several times (4 × 7 mL), filtered and dried to give 1 g of a white precipitate (55 %).

^{1}H NMR (126 MHz, $CDCl_3$) δ: 7.03 ppm (1H, s, Ha), 7.16-7.19 ppm (4 H, m, Ho), 7.37 ppm (1 H, s, Hb), 7.38-7.46 (6 H, m, Hm and Hp), 8.59 ppm (1H, s, brd, NH).

^{13}C NMR (126 MHz, $CDCl_3$) δ: 63.09 (Ca), 37.92 (Cc), 128.53, 128.89 (Co), 129.43 (Cm), 137.06, 146.90 (Cb), 150.51 (Cd), 159.72 (Ce).

7) Pentyl-dipyrromethane [5]

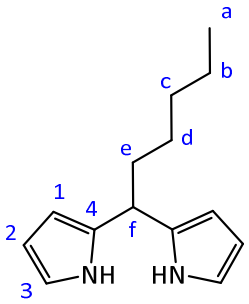

Chemical Formula: $C_{14}H_{20}N$
Molecular Weight: 216.33 g/mol

A mixture of pyrrole (68 mL, 984 mmol, 40 eq) and hexanal (3 mL, 24.6 mmol, 1eq) was treated with TFA (0.18 mL, 2.35 mmol, 0.1 eq) and stirred under argon at room temperature. After 4 hours, the reaction was quenched by adding 0.1 M NaOH solution until the medium became neutral (*ca* 5 mL). The mixture was extracted with dichloromethane (2x100 mL) and washed with water (2x50 mL). The organic phase was dried over $MgSO_4$, filtered and concentrated under reduced pressure. The crude product was purified with column chromatography (silica gel, cyclohexane: ethylacetate: triethylamine (8:2:0.1) to give 2.5 g of a yellowish viscous oil (47 %).

^{1}H NMR (400 MHz, $CDCl_3$) δ (ppm): 0.89 (3H, t, ^3J = 6.8 Hz, Ha), 1.32 (6H, m, Hb & Hc & Hd), 1.94 (2H, m, He), 3.94 (1H, t, ^3J = 7.6 Hz, Hf), 6.11 (2H, m, H2), 6.18 (2H, dd, ^3J = 5.8 Hz, ^4J = 2.7 Hz, H1), 6.58 (2H, dd, ^3J = 5.7 Hz, ^4J = 2.6 Hz, H_3), 7.57 ppm (2H, s, br, NH).

^{13}C NMR (126 MHz, $CDCl_3$) δ (ppm): 14.20(Ca), 22.66 (Cb), 27.03 (Cc), 27.30 (Cd), 31.79 (Ce), 34.39 (Cf), 105.65 (C1), 107.83 (C2), 117.23(C3), 133.78 (C4).

8) 5,15-di(trimethylsilylethynyl)-10,20-dipentylporphyrin (**Po1**) [6]

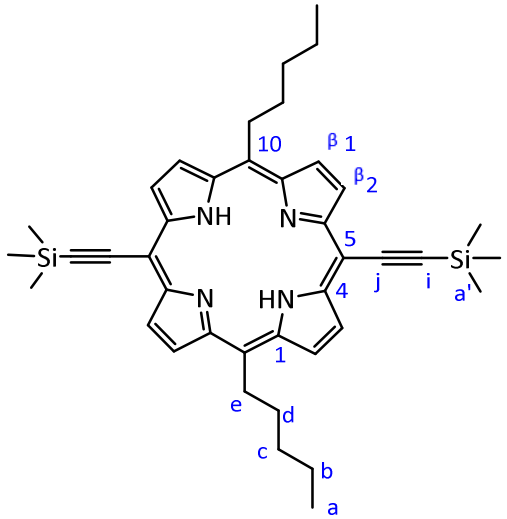

Chemical Formula: $C_{40}H_{28}N_4Si_2$
Molecular Weight: 642.36 g/mol

Pentyl-dipyrromethane (300 mg, 1.39 mmol, 1 eq) was dissolved in degassed dichloromethane (200 mL) and cooled to 0 °C in an ice bath. Then trimethylsilylethynylaldehyde (216 µL, 1.46 mmol, 1.05 eq) was slowly added to the flask. The reaction was stirred at 0 °C and borontrifluoride etherate ($BF_3.Et_2O$) (34 µL, 0.28 mmol, 0.2 eq) was added drop wise to the mixture. The reaction was stirred for 10 to 15 minutes and followed by TLC. When all the pentyl-dipyrromethane disappeared, the ice bath was removed and DDQ (334 mg, 1.06 eq) was added. The mixture was stirred at room temperature for 30 minutes, and then quenched by adding 0.56 mL of pyridine. The solvent was evaporated under reduced pressure. The crude was purified by column chromatography (silica gel, DCM: Cyclohexane (3:7)) to give 446 mg of a dark purple powder (38 %).

^{1}H NMR (300 MHz, $CDCl_3$) δ (ppm): -2.39 (2H, s, NH), 0.65 (18H , s, Ha'), 0.96 (6H t, ^3J = 7.30 Hz, Ha), 1.53 (4H, m, Hb), 1.73 (4H, tt, ^3J = 7.6 Hz, 5.79 Hz, Hc), 2.44 (4H, tt, ^3J = 7.9 Hz, 7.6 Hz, Hd), 4.79 (4H, t, ^3J = 8.0 Hz, He), 9.30 (4H, d, ^3J = 4.8 Hz, Hβ), 9.60(4H d, ^3J = 4.8 Hz, Hβ).

^{13}C NMR (126 MHz, $CDCl_3$) δ (ppm): 0.54 (Ca'), 14.28 (Ca), 22.89 (Cb), 27.07 (Cd), 32.75 (Cc), 35.04 (Ce), 99.60, 101.87, 107.51, 121.60, 128.24 (Cβ), 131.17 (Cβ).

9) Zn(II) [5,15-di(trimethylsilylethynyl)-10,20-dipentylporphyrin] (**Zn-Po1**)

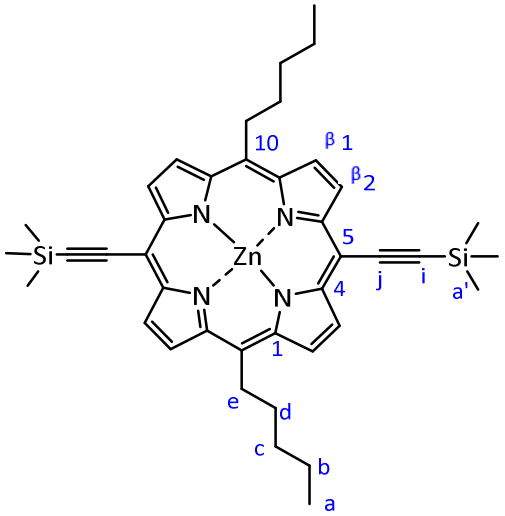

Chemical Formula: $C_{40}H_{26}N_4Si_2Zn$
Molecular Weight: 704.40 g/mol

A solution of $Zn(OAc)_2.2H_2O$ (58 mg, 0.29 mmol, 2 eq) in 5 mL methanol was added to a solution of 5,15-di(trimethylsilylethynyl)-10,20-dipentylporphyrin (90 mg, 0.145 mmol, 1 eq) in 150 mL chloroform. The mixture was stirred at room temperature for 3 hours. The disappearance of the starting material was followed by TLC. When the reaction was completed, the solvent was removed under reduced pressure. The crude product was washed with water (2x50 mL) to remove the excess of zinc(II). The organic phase was dried over $MgSO_4$, filtered and evaporated under reduced pressure. The crude was purified by column chromatography (silica gel, DCM: cyclohexane (3:7)) to give 90 mg of a greenish solid (90 %).

^{1}H NMR (300 MHz, $CDCl_3$) δ (ppm): 0.65 (18 H, s, Ha'), 0.97 (6H, t, ^3J = 7.3 Hz, Ha), 1.53 (4H, m, Hb), 1.72 (4H, tt, ^3J = 7.6 Hz, 6.7 Hz, Hc), 2.24 (4H, tt, ^3J = 7.8 Hz, 7.7 Hz, Hd), 4.52 (4H, t, ^3J = 7.8 Hz, He), 9.00 (4H d, ^3J = 4.6 Hz, Hβ), 9.30 (4H d, ^3J = 4.6 Hz, Hβ).

^{13}C NMR (126 MHz, $CDCl_3$) δ (ppm): 0.68 (Ca'), 14.33 (Ca), 22.89 (Cb), 27.06 (Cd), 32.95 (Cc), 35.49 (Ce), 99.66, 100.99, 107.94, 122.12, 128.92(Cβ), 130.99 (Cβ), 149.58, 150.62.

HRMS (ESI): m/z(M+): $[M+H]^+$ calculated = 705.27, $[M+H]^+$ found = 705.2704.

UV-VIS (CH_2Cl_2, λ_{max}(nm) (Ɛ x 10^3 ($mol^{-1}Lcm^{-1}$)) : 433 (134.91), 591 (12.25), 694 (4.40).

10) Zn(II) [5,15 -di(N_1-(benzylhydry)uracil)- 10,20-dipentylporphyrin] (**T1**)[7]

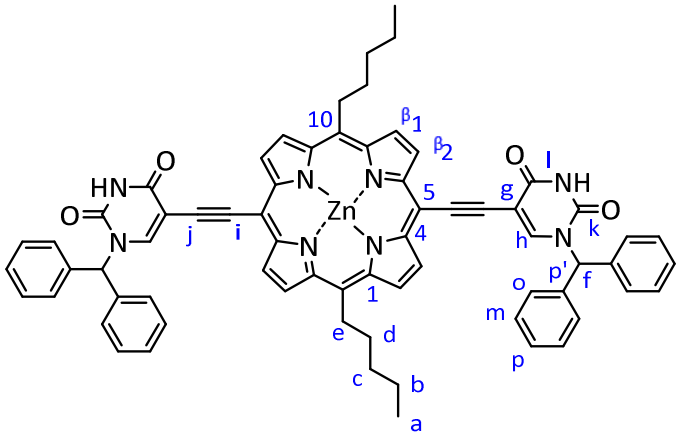

Chemical Formula: $C_{70}H_{60}N_8O_4Zn$
Molecular Weight: 1112.37g/mol

Zn(II)[5,15-di(trimethylsilylethynyl)-10,20-dipentylporphyrin] (120 mg, 0.169 mmol, 1eq), 4N-benzylhydryl-5-iodouracil (150 mg, 0.3718 mmol, 2.2 eq), $AsPh_3$ (61.39 mg, 0.2 mmol, 1.2 eq) and $Pd(PPh_3)_2Cl_2$ (34.8 mg, 0.0495 mmol, 0.25 eq) were treated with 33 mL of a TBAF solution (1M in THF). The reaction was stirred under argon for 3 hours under reflux at 75 °C. The disappearance of the starting materials was followed by TLC. When **Zn-Po1** disappeared, the reaction was concentrated under reduced pressure, extracted by DCM (50 mL) and washed with water (50 mL). The organic phase was dried over $MgSO_4$, filtered and dried under reduced pressure. The crude was purified by column chromatography (silica gel, 2% methanol in DCM) followed by a bio beads separation using a mixture of 20 % methanol in DCM as eluent (88 %).

^{1}H NMR (300 MHz, $CDCl_3$ + MeOD) δ (ppm): 0.93 (6H, t, ^3J = 8.3 Hz, Ha,), 1.48 (4 H, m, Hb), 1.71 (4H, tt, ^3J = 8.3 Hz, 7.2 Hz, Hc), 2.43 (4 H, tt, ^3J = 8.4 Hz, 7.5 Hz, Hd), 4.81 (4H, t, ^3J = 7.5 Hz, He), 7.20 (2H, s, Hf), 7.34 (8 H, m, Ho), 7.36 (2H, s, Hh), 7.48 (12 H, m, Hp & Hm), 9.34 (4H d, ^3J = 4.7 Hz, Hβ), 9.61(4H d, ^3J = 4.7 Hz, Hβ).

^{13}C NMR (126 MHz, $CDCl_3$ + MeOD) δ (ppm): 14.10 (Ca), 22.74 (Cb), 29.68 (Cd), 32.79 (Cc), 38.64 (Ce), 63.05 (Cf), 98.61, 98.66, 101.07 (Cg), 101.49, 122.59, 128.69 (Co), 128.83, 129.42 (Cm), 131.02, 137.23-137.25 (Cβ), 143.09, 149.05 (Ch), 150.18 (Ck) 150.71 (Cl).

HRMS (ESI): m/z(M+): $[M+H]^+$ calculated = 1113.3789, $[M+H]^+$ found= 1113.3721.

UV-VIS (CH_2Cl_2, λ_{max}(nm) (Ɛ x 10^3 ($mol^{-1}Lcm^{-1}$)) : 452 (123.79), 625 (14.87), 699 (5.08).
IR v(cm^{-1}): 3060.7, 2921.6, 2851.9, 1692.5, 1441.2, 1260.9, 1238.2, 1075.9, 1010.2, 790.8, 709.8, 565.7, 432.7.

11) 5,15-di(uracil)- 10,20-dipentylporphyrin (**T2**) [4]

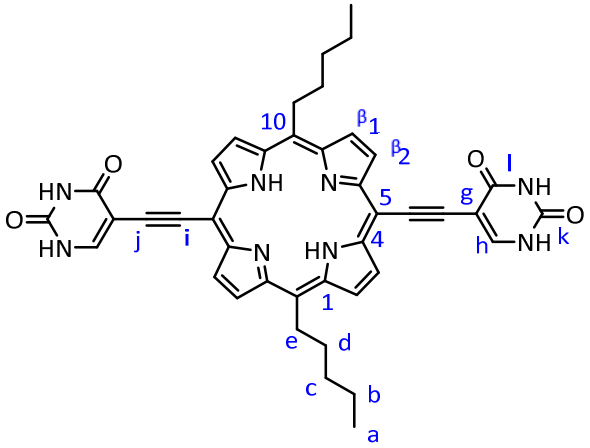

Chemical Formula: $C_{42}H_{36}N_8O_4$
Molecular Weight: 718.30 g/mol

Zn(II) [5,15-di((N_1-benzylhydry)uracil)-10,20-dipentylporphyrin], **T1**, (40 mg, 0.035 mmol, 1 eq) was treated with TFA (5 mL) and triflic acid (0.5 mL) at 0 ºC. The reaction was stirred at 0 ºC for 2 hours then the reaction was poured slowly on 50 g of ice. The green precipitate formed was filtered and collected to give 20 mg of an insoluble dark green solid (80 %).

HRMS (ESI): m/z(M+): $[M+H]^+$ calculated = 719.3089, $[M+H]^+$ found = 719.3063.

UV-VIS (DMSO, λ_{max}(nm) (Ɛ x 10^3 ($mol^{-1}Lcm^{-1}$)) : 431 (165.25), 557 (17.20), 658 (2.7).

12) N_1-hexyl-5-iodouracil [8]

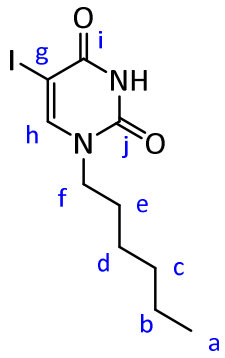

Chemical Formula: $C_{10}H_{15}IN_2O_2$
Molecular Weight: 322.15 g/mol.

5-iodouracil (0.5g, 2.1 mol, 3 eq) and Cs_2CO_3 (0.3 g, 0.91 mmol, 1.3 eq) were dissolved in 60 mL of dry DMF. To the suspension, 1-bromohexane (0.1 mL, 0.7 mmol, 1 eq) was added drop wise. The reaction was stirred at 40 °C under argon. After 24 hours, the mixture was evaporated under reduced pressure and then diluted with DCM (100 mL) and washed with water (50 mL x 2). The organic phase was dried over $MgSO_4$, filtered, and dried under reduced pressure. The crude product was purified by column chromatography (silica gel, DCM: MeOH (200:1)) to yield 210 mg of 1- hexyl-5-iodouracil as a white solid. (94 %)

^{1}H NMR (500 MHz, $CDCl_3$) δ (ppm): 0.89 (3H, t, ^3J = 6.7 Hz, Ha), 1.32 (6 H, m, Hb & Hc & Hd), 1.68 (2H, tt, ^3J = 7.5 Hz, 7.4 Hz, He), 3.73 (2H, t, ^3J = 7.5 Hz, Hf), 7.60 (1H, s, Hh), 8.39 (1H, s, br, NH).

^{13}C NMR (126 MHz, $CDCl_3$) δ (ppm): 14.12 (Ca), 22.60 (Cb), 26.15 (Cd), 29.30 (Ce), 31.40 (Cc), 49.41 (Cf), 67.51 (Cg), 149.03 (Ch), 150.25 (Cj), 160.32 (Ci).

13) Zn(II) [5, 15-di(N_1-hexyluracil)-10,20-dipentylporphyrin] [7] (**T3**)

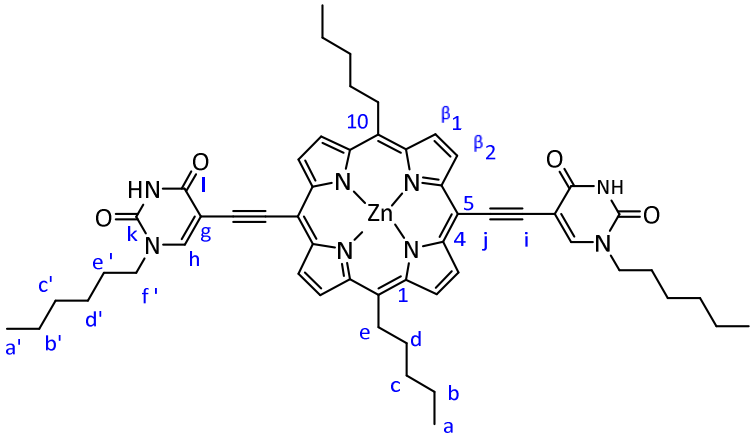

Chemical Formula: $C_{55}H_{63}N_8O_4Zn$
Molecular Weight: 965.54 g/mol

Zn(II)[5,15-di(trimethylsilylethynyl)-10,20-dipentylporphyrin] (100 mg, 0.141 mmol, 1eq), N_1-hexyl-6-iodouracil (96 mg, 0.311 mmol, 2.2 eq), $AsPh_3$ (51.81 mg, 0.169 mmol, 1.2 eq) and $Pd(PPh_3)_2Cl_2$ (24 mg, 0.035 mmol, 0.25 eq) were treated with 27 mL of a TBAF solution (1M in THF) under argon. The reaction was stirred for 3 hours under reflux and followed by TLC. When all starting porphyrin material disappeared, the reaction was concentrated under reduced pressure then extracted with DCM (50 mL) and washed twice with water (20 mL). The organic phase was dried over $MgSO_4$, filtered, and dried under reduced pressure. The crude was purified by column chromatography (silica gel, 2% methanol in DCM) followed by bio beads separation for further purification to give 136 mg of a green solid (80 %).

^{1}H NMR (300 MHz, $CDCl_3$) δ (ppm): 1.19 (12 H, t, ^3J = 7.2 Hz, Ha & Ha'), 1.41-152 (20 H, m, Hb & Hc & Hb' & Hc' & Hd'), 1.77 (4H, m, tt, ^3J = 7.4 Hz, 4.7 Hz, He'), 2.50 (4 H, t, ^3J = 8.3 Hz, Hd), 4.24 (4H, t, ^3J = 7.5 Hz, Hf'), 4.93 (4H, m, t, ^3J = 8.4 Hz, He), 8.14 (2H, s ,brd, Hh), 9.01 (4H, d, ^3J = 4.7 Hz, Hβ), 9.49 (4H, d, ^3J = 4.7 Hz, Hβ).

^{13}C NMR (126 MHz, $CDCl_3$) δ (ppm): 14.1 (Ca & Ca'), 20.9 (Cb & Cb'), 22.7- 26.4- 27.7- 30.8-31.9 (Cc, Cc', Cd, Cd', Ce, Ce'), 49.6 (Cf'), 88.4, 99.09, 100.9 (Cg), 117.5, 122.05, 130.39 (Cβ), 131.45 (Cβ), 142.7, 142.8 (Ch), 150.8 (Ck), 161.6 (Cl).

HRMS (ESI): m/z(M+): $[M+H]^+$ calculated = 965.5432, $[M+H]^+$found = 965.54325.

UV-VIS (CH_2Cl_2, λ_{max}(nm) (Ɛ x 10^3 ($mol^{-1}Lcm^{-1}$)) : 455 (237.60), 591 (12.71), 663 (7.42).

14) 5-iodocytosine [8]

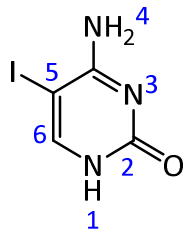

Chemical Formula: $C_4H_4IN_3O$
Molecular Weight: 237 g/mol

Cytosine (1g, 9.0 mmol, 1 eq), Iodine (3.4 g, 13.5 mmol, 1.5 eq) and Iodic Acid (2.2 g, 12.6 mmol, 1.4 eq) were treated with 33 mL of acetic acid. The mixture was stirred at 40 ºC. After 24 hours, the mixture was treated with 200 mL of a saturated aqueous solution of $Na_2S_2O_3$, resulting in a color change from black to white and the formation of white precipitate. If necessary, a 1 M aqueous NaOH solution was added to the filtrate to reach a final pH of 7. The precipitate was filtered and dried under reduced pressure to give 2g of a white solid (94 %).

^{1}H NMR (300 MHz, DMSO-d_6) δ (ppm): 6.96 (2 H, s, br, H4), 7.78 (1H, s, H6), 10.36 (1H, s, br, H1).

^{13}C NMR (126 MHz, MeOD-d_4) δ: 54.45 (C5), 139.47 (C6) 149.40 (C2) 178.95 (C4).

15) N_1-hexyl-5-iodocytosine [8]

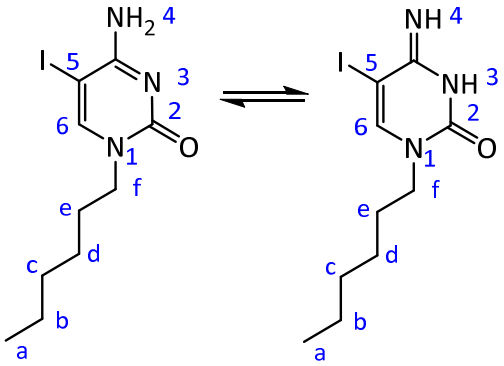

Chemical Formula: $C_{10}H_{16}IN_3O$
Molecular Weight: 321.16 g/mol

5-iodocytosine (0.5 g, 2.1 mmol, 1 eq) and K_2CO_3 (0.3455 g, 2.5 mmol, 1.2 eq) were dissolved in 10 mL of dry DMF. Iodohexane (0.5 mL, 0.53 g, 2.5 mmol, 1.2 eq) was added drop wise to the suspension. The reaction was stirred for 12 hours at 40 ºC under argon. After the reaction was completed, the mixture was evaporated and then diluted with DCM (100 mL) and washed with water (2x50 mL). The organic phase was dried over $MgSO_4$, filtered and evaporated under reduced pressure. The crude was purified by washing with ethyl acetate and petroleum ether to give 270 mg of a white solid (40 %).

^{1}H NMR (300 MHz, $CDCl_3$) δ (ppm): 0.88 (3H, t, ^3J = 6.9 Hz, Ha), 1.30 (6H, m, Hb & Hc & Hd), 1.69 (2H, tt, ^3J = 7.60 Hz, 7.5 Hz, He), 3.75 (2H, t, ^3J = 7.5 Hz, Hf), 5.44 (1H, s, br, H4), 7.48 (1H, s, br H3), 7.56 (1H, s, H6).

^{13}C NMR (126 MHz, $CDCl_3$) δ (ppm): 14.30 (Ca), 22.51 (Cb), 26.51 (Cd), 29.28 (Ce), 31.38 (Cc), 50.55 (Cf), 54.87 (C2), 151.01 (C1), 155.42 (C3), 163.70 (C4).

16) 5-((4-methoxyphenyl)ethynyl)-N_1-hexylcytosine

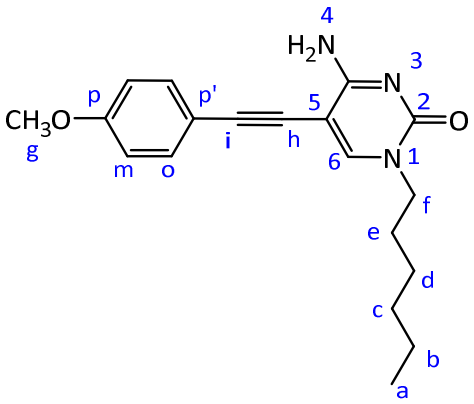

Chemical Formula: $C_{19}H_{23}N_3O_2$
Molecular Weight: 325.419 g/mol

[(4-methoxyphenyl)ethynyl](trimethyl)silane (0.247 mL, 237 mg, 1.16 mmol, 1 eq) and a 1 M TBAF solution in THF (1.16 mL, 1.16 mmol, 1 eq) were reacted for 2 hours at RT under argon. The solvent was evaporated under vacuum and the crude was extracted with diethylether several times until all the product was extracted. The deprotected (4-methoxyphenyl)ethynyl was dried

under vacuum and diluted with 20 mL THF:Et_3N 1:1 solution. To this solution, iodo-hexyl cytosine (247 mg, 0.77 mmol, 1 eq) was added and the solution was degassed for 10 minutes. PPh_3 (0.044 g, 0.2 eq) and $Pd(OAc)_2$ (0.025 g, 0.15 eq) were added to the solution. The mixture was stirred under argon and under reflux at 80 °C for 12 hours. The mixture was extracted by 50 mL DCM and washed with 50 mL of water. The organic phase was dried over $MgSO_4$, filtered and dried under reduced pressure. The crude was purified by column chromatography (silica gel, 2% methanol in DCM) to give 113 mg of a white solid (30 %).

^{1}H NMR (500 MHz, $CDCl_3$) δ: 0.87 (3H, t, ^3J = 6.9 Hz, Ha), 1.31 (6 H, m, Hb & Hc & Hd), 1.81 (2H, tt, ^3J = 7.6 Hz, 7.5 Hz, He), 3.84 (3H, s, Hg), 4.01 (2H, t, ^3J = 7.4 Hz, Hf), 6.32 (1H, s, br, NH, H4), 6.97 (2H, d, ^3J = 8.8 Hz, Ho), 7.73 (2H, d, ^3J = 8.7 Hz, Hm), 8.07 (1H, s, br, NH, H3).

^{13}C NMR (126 MHz, $CDCl_3$) δ: 14.13 (Ca), 22.63 (Cb), 26.43 (Cd), 29.55 (Ce), 31.60 (Cc), 52.46 (Cf), 55.51 (Cg), 94.49, 110.55, 114.60, 122.94, 127.06, 129.83, 138.79 (C6), 140.56, 155.43 (C2), 160.58 (C4).

17) N_9-hexyladenin [8]

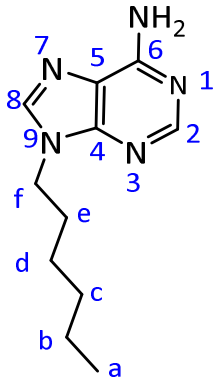

Chemical Formula: $C_{11}H_{17}N_5$
Molecular Weight: 219.29 g/mol

Adenine (100 mg, 0.74-mmol, 1 eq) and K_2CO_3 (121 mg, 0.88 mmol, 1.2 eq) were dissolved in 20 mL of degassed DMF. Bromohexane (146 mg, 0.12 mmol, 0.88 mmol, 1 eq) was added drop wise to the suspension. The mixture was stirred for 12 hours at 40 °C under argon, and was followed by TLC. When all adenine disappeared, the mixture was concentrated then diluted with 50 mL of DCM and washed with 20 mL of water and then with 20 mL of brine solution. The organic phase

was dried over $MgSO_4$, filtered and dried under reduced pressure. The crude product was purified by column chromatography (silica gel, 2% MeOH in DCM) to give 250 mg of a white solid (90 %).

^{1}H NMR (300 MHz, $CDCl_3$+ MeOD) δ (ppm): 0.87 (3H, t, ^3J = 7.0 Hz Ha), 1.33 (6H, m, Hb &Hc & Hd), 2.00 (2H, tt, ^3J = 7.5 Hz, 7.3 Hz, He), 4.38 (2H, t, ^3J = 7.3 Hz, Hf), 7.99 (1H, s, H8) 8.06 (1H, s, H2).

^{13}C NMR (126 MHz, $CDCl_3$) δ (ppm): 14.24 (Ca), 22.74 (Cb), 26.61 (Cd), 30.35(Ce), 31.50(Cc), 44.25(Cf), 120.03 (C5), 140.62 (C8), 150.35 (C4), 153.20 (C2), 156.06 (C6).

18) 8-iodo-N_9-hexyladenin [8]

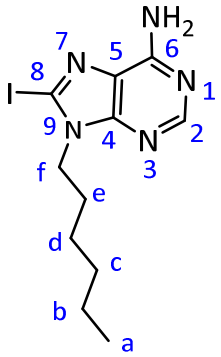

Chemical Formula: $C_{11}H_{16}N_5I$
Molecular Weight: 345.19 g/mol

N_9-hexyladenin (220 mg, 1.00 mmol, 1 eq), Iodine (67 mg, 0.38 mmol, 0.38 eq) and periodic acid H_5IO_6 (227 mg, 1.00 mmol, 1 eq) were dissolved in 10 mL of dry DMF and stirred at 70 °C for 12 hours. The reaction was followed by TLC. When all starting material disappeared, the mixture was evaporated and then diluted with 50 mL of DCM, washed with a 20 mL of a saturated aqueous solution of $Na_2S_2O_5$, then with 20 mL of water and 20 mL of brine solution. The organic phase was dried over $MgSO_4$, filtered and evaporated under reduced pressure. The crude was purified by column chromatography (silica gel, 5 % Methanol in DCM) to give 200 mg of a white solid (60 %).

^{1}H NMR (500 MHz, $CDCl_3$) δ (ppm): 0.88 (3H, t, ^{3}J = 6.80 Hz, Ha) 1.33 (6H, m, Hb & Hc & Hd), 1.83 (2H, tt, ^{3}J = 7.8 Hz, 7.2 Hz, He), 4.14 (2H, t, ^{3}J = 7.3 Hz, Hf), 8.29 (1H, s, H2).

^{13}C NMR (126 MHz, $CDCl_3$) δ (ppm): 14.10 (Ca), 22.60 (Cb), 26.46 (Cd), 30.19 (Ce), 31.34 (Cc), 44.12 (Cf), 119.77 (C5), 140.58 (C8), 150.21 (C4), 153.06 (C2), 16.61 (C6).

19) N_1-methylphenylthymine

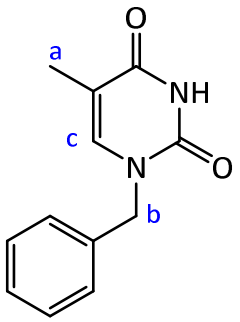

Chemical Formula: $C_{12}H_{12}N_2O_2$
Molecular Weight: 216.24 g/mol

Thymine (200 mg, 1.58 mmol, 2 eq), K_2CO_3 (120 mg, 0.87 mmol, 1. eq) and 4-(bromomethyl) benzene (135 mg, 0.79 mmol, 1 eq) were mixed in 15 mL of dry degassed DMF. The reaction was stirred at 40 ºC for 24 hours. The crude was dried under vacuum, and then washed with a minimum amount of water (5 mL). The product was purified by column chromatography (SiO_2, 5 % MeOH in DCM) to yield 100 mg of the targeted product as a white solid (60 %).

^{1}H NMR (500 MHz, $CDCl_3$) δ (ppm): 1.87 (3H, d, ^{4}J = 1.2 Hz, Ha), 4.89 (2H, s, Hb), 6.99 (1H, q, ^{4}J = 1.1 Hz, Hc), 7.33 (5H, m, H_{Phenyl}), 9.87 (1H, s, brd, NH).

20) 4-(bromomethyl)benzaldehyde (**Br-Ald**)[9]

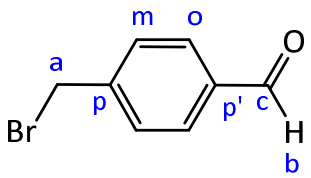

Chemical Formula: C_8H_7BrO
Molecular Weight: 199.05 g/mol

4-bromomethylbenzonitrile (1.0 g, 5.0 mmol, 1 eq) was dissolved in 20 mL of dry toluene. 1 M H-DIBAL solution in cyclohexane (1.023 g, 7.2 mmol, 7.2 mL, 1.4 eq) was added *via* an additional funnel over 20 minutes. The reaction was stirred at 0 °C and followed by TLC. After 2.5 hours, all starting material disappeared, and 25 mL of chloroform and 33.3 mL of 10 % HCl aqueous solution were added to the mixture and stirred for 1 hr at RT. The organic phase was separated and the aqueous phase was extracted twice with 100 mL of chloroform. The organic phases were combined, dried over $MgSO_4$, and evaporated. The crude was re-crystalized from hexane to give 0.94 g of white crystals (94 %).

^{1}H NMR (300 MHz, $CDCl_3$) δ (ppm): 4.51(2H, s, Ha), 7.54 (2H, d, ^3J = 8.2 Hz, Hm), 7.85 (2H, d, ^3J = 8.2 Hz, Ho), 10.01 (s, 1H, Hb).

^{13}C NMR (126 MHz, $CDCl_3$) δ (ppm): 32.13 (Ca), 129.82 (Cm), 130.31 (Co), 136.22 (Cp), 144.38 (Cp'), 191.69 (Cc).

21) Phenyl-dipyrromethane [10]

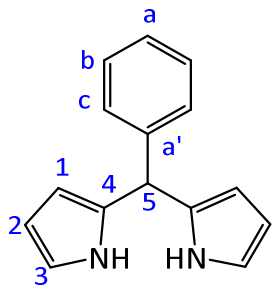

Chemical Formula: $C_{15}H_{14}N_2$
Molecular Weight: 220.10 g/mol

Pyrrole (97 mL, 1.4 mol, 100 eq) was filtered on an Alumina pad and then transferred to a round bottom flask and degassed. Benzaldehyde (1.5 mL, 1.53 g, 14 mmol, 1 eq) and $InCl_3$ (0.32 g, 1.4 mmol, 0.1 eq) were added to pyrrole. The mixture was protected from light and stirred under argon at RT for 2 hours. The reaction was quenched by adding NaOH (56 mg, 1.4 mmol, 0.1 eq) and stirred for 45 minutes. The mixture was filtered on a Büchner funnel and the filtrate was dried under vacuum. To remove the excess of pyrrole, petroleum ether and cyclohexane were added to

the flask and then evaporated under vacuum to give a yellowish solid. The solid was washed with a solution of ethanol: water (2:1) to give 2.2 g of a shiny white solid (72 %).

^{1}H NMR (300 MHz, $CDCl_3$) δ (ppm): 5.48 (1H, m, Ha), 5.93 (2H, m, H1), 6.17 (2H, m, H2), 6.70 (2H, m, H3), 7.31 (4H, m, Hb & Hc), 7.90 (2H, s, brd, NH).

22) 5,15-bis(4-(bromomethyl)phenyl)-10,20-diphenylporphyrin (**Po2**)

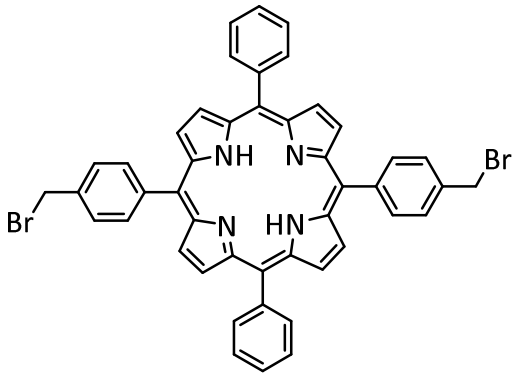

Chemical Formula: $C_{46}H_{32}Br_2N_4$
Molecular Weight: 800.60 g/mol

Phenyl-dipyrromethane (289 mg, 1.316 mmol, 1 eq) and 4-(bromomethyl)benzaldehyde (262 mg, 1.316 mmol, 1 eq) were dissolved in 150 mL of degassed chloroform. The solution was degassed with argon for 15 minutes, then $BF_3.Et_2O$ (4.65 µL, 53.55 mg, 0.7896 mmol, 0.6 eq) was added slowly, and the solution was stirred at RT under argon for 2 hours. *p*-chloranil (480 mg, 1.95 mmol, 1.5 eq) and triethylamine (0.163 mL, 0.12 mmol, 0.09 eq) were added to the mixture and stirred for another 2 hours under reflux at 65 °C. The crude was evaporated under vacuum then diluted with 50 ml of a solution of DCM: cyclohexane (1:1) and filtered twice over a pad of silica. The filtrate was evaporated under vacuum to give a purple solid that consisted of a mixture of 6 different porphyrins. Scrambling could be proved by MS and NMR. (Total mass: 310 mg, 34 %) The different porphyrins could not be clearly differentiated by NMR but they could be identified by MS.

MS (ES): m/z(HRM+): $[M+H]^+$ calculated = 801.62, $[M+H]^+$ found= 895.03, 801.11, 709.18, 615.26.

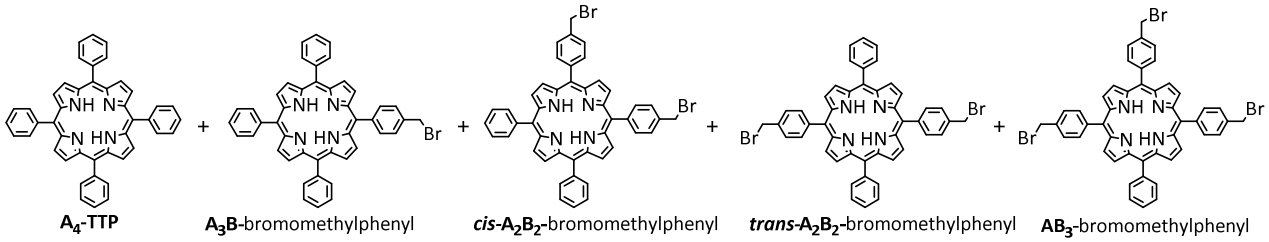

23) 5-(N_1-methylphenylthymine)10,15,20-triphenylporphyrin (**T4**)

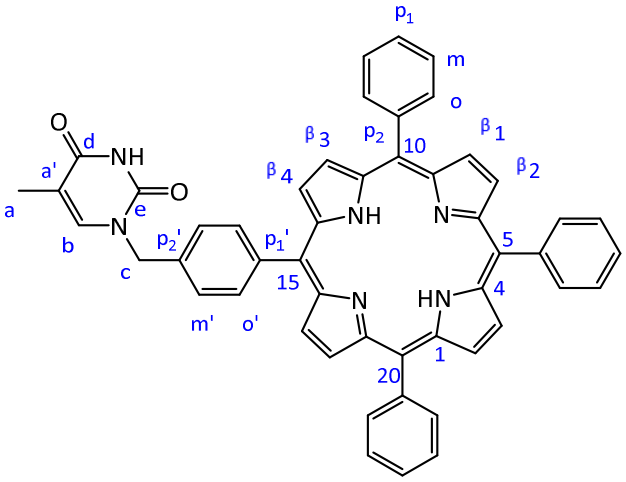

Chemical Formula: $C_{50}H_{36}N_6O_2$
Molecular Weight: 752.88 g/mol

The crude mixture containing 6 different porphyrins (174 mg, *ca* 0.217 mmol based on the major product : the 5,15-diphenyl-10,20-dibromoporphyrin) 1 eq), thymine (137 mg, 0.1086 mmol, 5 eq) and K_2CO_3 (89 mg, 0.651 mmol, 3 eq) were dissolved in 10 mL of degassed DMF and stirred at 40 °C. After 24 hours, the solvent was evaporated under vacuum. The crude was purified by column chromatography using gradient eluent. DCM: Cyclohexane 2:1 was used to elute H_2TTP, 1% MeOH in DCM to elute the 5-(N_1-methylphenylthymine)-10,15,20-triphenylpoprhyrin (**T4**) while further factions did not contain pure products. The fraction containing **T4** was evaporated under reduced pressure to give 30 mg of a purple solid (18 % with respect to the mixture of starting material).

^{1}H NMR (500 MHz, $CDCl_3$) δ (ppm): - 2.79 (2H, s, NH), 2.04 (3 H, s, Ha), 5.24 (2H, s, CH_2), 7.31 (1H, s, Hb), 7.66(2H, d, ^{3}J = 7.9 Hz, Hm'), 7.75 (9H, m, Hm & Hp_1), 8.21-8.24 (8H, m, Hβ), 8.29 (1H, s, brd, NHthymine), 8.85 (8H, m, Ho & Ho'), 8.90 (8H, m, Hβ).

^{13}C NMR (126 MHz, $CDCl_3$) δ (ppm): 12.70 (Ca), 51.33 (Cc), 111.69 (Ca'), 119.05, 120.41 (Cβ), 120.54, 126.26 (Cm'), 126.85 (Cβ), 127.91 (Cm), 134.70, 135.05 (Cb), 135.31 (Co), 140.20 (Co'), 142.22, 142.63, 151.18 (Cd), 163.88 (Ce).

HRMS (ESI): m/z(M+): $[M+H]^+$ calculated = 753.2982, $[M+H]^+$ found = 753.2984.
UV-VIS (DMF, λ_{max}(nm) (Ɛ x 10^3 ($mol^{-1}Lcm^{-1}$)) : 418 (298.76), 515 (11.72), 549 (5.18), 589 (3.68), 645 (3.58).
IR ν(cm^{-1}): 2924.43, 2849.8, 1696.1, 1679.5, 1596.9, 1475.4, 1439.1, 1349.9, 1249.5, 1176.2, 1071.9, 965.6, 727.0, 417.2.

24) Mesityl-dipyrromethane

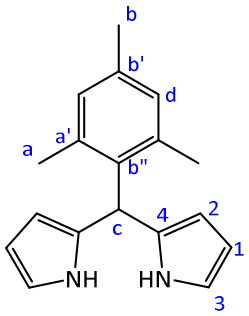

Chemical Formula: $C_{18}H_{20}N_2$
Molecular Weight: 264.37g/mol

Mesitylaldehyde (2.5 g, 16.85 mmol, 1 eq) was dissolved in pyrrole (118 mL, 1.18 mol, 70 eq) and degassed with argon for 30 minutes. $BF_3.Et_2O$ (1.726 mL, 1.985 g, 13.95 mmol, 0.8 eq) was added drop wise to the mixture and stirred for 3 hours at RT under argon. NaOH (0.55 g, 13.95 mmol,0.8 eq) was added to the mixture and stirred for 1 hour. The mixture was filtered on a frit and the filtrate evaporated under vacuum. Cyclohexane was used to help remove all the excess of pyrrole. The crude was purified by column chromatography (SiO_2, 5% ethylacetate in cyclohexane). The obtained solid was washed with diethylether to give 1.3 g of a white solid (30%).

^{1}H NMR (400 MHz, $CDCl_3$) δ (ppm): 2.06 (s, 6H, Ha), 2.28 (s, 3H, Hb), 5.93 (s, 1H, Hc), 6.00 (m, 2H, H1), 6.20 (m, 2H, H2), 6.68 (2H, m, H3), 6.90 (2H, s, Hd), 7.96 (s, brd, 2H, NH).

^{13}C NMR (126 MHz, $CDCl_3$) δ (ppm): 20.68 (Ca), 20.71 (Cb), 38.45 (Cc), 106.68 (C1). 108.78 (C2), 116.26 (C3), 130.47 (Cd), 131.37 (C4), 134.66 (Cb"), 136.69 (Cb'), 137.73 (Ca').

25) 5,15-bis(4-(bromomethyl)phenyl)-10,20-dimesitylporphyrin (**Po3**)[11]

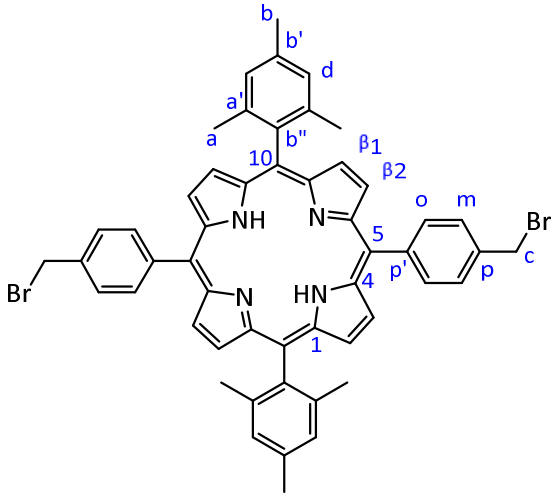

Chemical Formula: $C_{52}H_{44}Br_2N_4$
Molecular Weight: 884.76 g/mol

Mesityl-dipyrromethane (0.5 g, 1.89 mmol, 1 eq) and 4-(bromomethyl)benzaldehyde (0.376 g, 1.89 mmol, 1 eq) were dissolved in 189 mL of dichloromethane and degassed for 15 minutes. Then TFA (0.259 mL, 3.36 mmol, 0.3839 g, 1.78 eq) was added drop wise over 30 seconds to the mixture. The latter was stirred for 45 minutes at RT under argon in the dark. The reaction was followed by TLC, and when all DPM was consumed (*ca* 1 hour) DDQ (0.429 g, 1 eq) was added to the reaction and stirred for *ca* 30 minutes at RT. Then the mixture was poured on a silica pad and eluted by DCM. The filtrate was evaporated and purified by column chromatography (Silica gel, DCM: cyclohexane 1:1 then DCM to give 250 mg of a purple solid (15 %).

^{1}H NMR (400 MHz, $CDCl_3$) δ (ppm): -2.63 (2H, s, brd, NH), 1.85 (12 H, s, Ha), 2.64 (6 H, s, Hb), 4.85 (4H, s, Hc), 7.30 (4H, s, Hd), 7.78 (4H, d, ^{3}J = 7.8 Hz, Hm), 8.21 (4H, d, ^{3}J = 7.8 Hz, Ho) 8.71(4H, d, ^{3}J = 4.5 Hz, Hβ), 8.81 (4H, d, ^{3}J = 4.5 Hz, Hβ).

^{13}C NMR (126 MHz, $CDCl_3$) δ (ppm): 21.64 (Cb), 21.71 (Ca), 33.74 (Cc), 118.62, 118.68, 127.58(Cβ), 127.91 (Cm & Co), 134.99(Cd), 137.33, 137.92, 138.47, 139.50, 142.29.

HRMS (ESI): m/z(M+): $[M+H]^+$ calculated = 885.1992, $[M+H]^+$ found = 885.1914.
UV-VIS (DMF, λ_{max} (nm) (Ɛ x 10^3 ($mol^{-1}Lcm^{-1}$)): 419 (253.63), 515 (10.75), 549 (4.49), 591 (3.33), 646 (2.45).

26) 5,15-bis(N_1-methylphenylthymine)-10,20-dimesitylporphyrin (**T5**) [12]

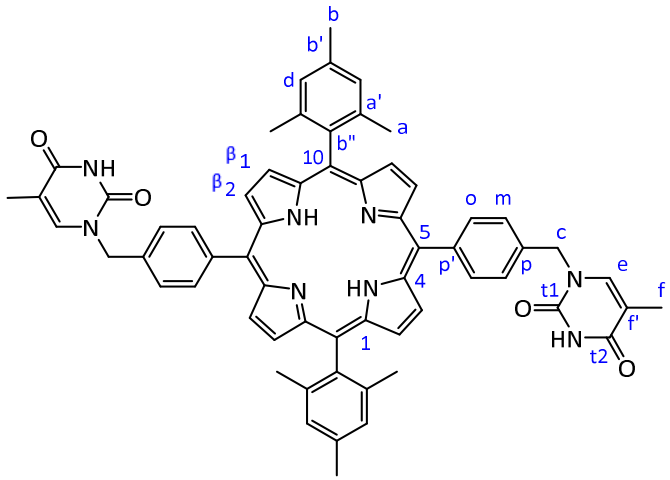

Chemical Formula: $C_{62}H_{54}N_8O_4$
Molecular Weight: 974.43 g/mol

5,15-bis(4-(bromomethyl)phenyl)-10,20-dimesitylporphyrin (132 mg, 0.1497 mmol, 1 eq) and excess of thymine (94 mg, 0.748 mmol, 5 eq) were dissolved in dry degassed DMF (8 mL). K_2CO_3 (62 mg, 0.449 mmol, 3 eq) was added to the suspension and stirred for 24 hours at 40 °C. The reaction was followed by TLC and stopped when all starting porphyrin was consumed. The solvent was evaporated and the resulting solid was washed with water (10 mL) to remove the excess of thymine and salt. The crude product was purified by Column Chromatography (Silica gel, 5% methanol in DCM) to give 106 mg of a purple solid (72 %).

^{1}H NMR (400 MHz, DMSO-d_6) δ (ppm): -2.77 (2H, s, NH), 1.76 (12 H, s, Ha), 1.87 (6H, s, Hf), 2.59 (6 H, s, Hb), 5.21 (4H, s, Hc), 7.35 (4H, s, brd, Hd), 7.70 (4H, d, ^3J = 7.8 Hz, Hm), 7.94 (2H, s, He), 8.24 (4H, d, ^3J = 8.0 Hz, Ho), 8.64 (4H, d, ^3J = 4.8 Hz, Hβ), 8.77 (4H,d, ^3J = 4.9 Hz, Hβ).

^{13}C NMR (126 MHZ, $CDCl_3$ + MeOD) δ (ppm): 12.44 (Cf), 21.44 (Cb), 21.59 (Ca), 51.15 (Cc), 111.5, 118.55, 123.81, 126.15 (Cβ), 127.79 (Cm & Co), 135.01, 135.08 (Cd), 137.88, 138.26, 139.36, 140.40(Ce), 142.14, 151.64 (Ct1), 164.89 (Ct2).

HRMS (ESI): m/z: $[M+H]^+$ calculated = 975.4323, $[M+H]^+$ found = 975.4322

UV-VIS (DMF, λ_{max}(nm) (Ɛ x 10^3 ($mol^{-1}Lcm^{-1}$)): 419 (227.97), 515 (9.69), 549 (3.85), 589 (2.99), 644 (2.38).

IR ν(cm^{-1}): 3028.3, 2928.8, 1715.8, 1666.6, 1477.9, 1445.3, 1423.7, 1380.4, 1243.2, 1201.1, 1027.6, 981.9, 933.7, 830.2, 810.5, 756.5, 738.4, 558.2, 470.9, 419.3.

27) 5,15-bis(N_9-methylphenyladenine)-10,20-dimesitylporphyrin (**T6**)[12]

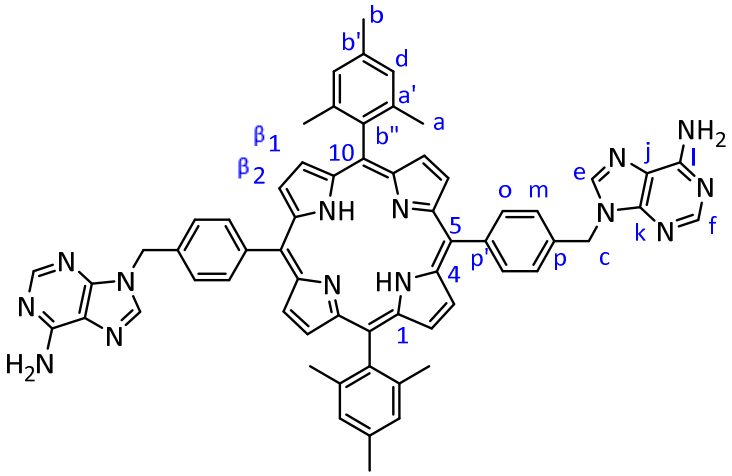

Chemical Formula: $C_{62}H_{52}N_{14}$
Molecular Weight: 992.45 g/mol

5,15-bis(4-(bromomethyl)phenyl)-10,20-dimesitylporphyrin (150 mg, 0.170 mmol, 1 eq) and excess of adenine (114.5 mg, 0.848 mmol, 5 eq) were dissolved in dry degassed DMF (10 mL). K_2CO_3 (70.1 mg, 0.508 mmol, 3 eq) was added to the suspension and stirred for 24 hours at 40 ºC. The reaction was followed by TLC and stopped when all starting porphyrin was consumed. The mixture was dried under vacuum, then washed with water (10 mL) to remove the excess of salt and adenine. The crude was purified by column chromatography (Silica gel, 5% Methanol in DCM) to give 90 mg of purple solid (54 %).

^{1}H NMR (500 MHz, $CDCl_3$ + MeOD) δ (ppm): -2.74 (2 H, s, brd, NH), 1.76 (12H, s, Ha), 2.58 (6 H, s, Hb), 5.69 (4H, s, Hc), 7.23 (4H, s, Hd), 7.60 (4H, d, ^{3}J = 7.9 Hz, Hm), 8.07 (2H, s, He), 8.16 (4H, d, ^{3}J = 7.9 Hz, Ho), 8.40 (2H, s, Hf), 8.63 (8 H, m, Hβ).

^{13}C NMR (126MHz, $CDCl_3$ + MeOD) δ (ppm): 21.49 (Cb), 21.63 (Ca), 47.39 (Cc), 118.34, 118.85, 119.11 (Cj), 126.08 (Cβ), 127.82 (Cm & Co), 134.89, 135.11 (Cd), 137.89, 138.27, 139.38, 140.59 (Ce), 142.30, 150.03 (Ck), 153.29 (Cf), 155.70 (Cl).

HRMS (ESI): m/z (M+): $[M+H]^+$ calculated = 993.4575, $[M+H]^+$ found = 993.4516.

UV-VIS (DMF, λ_{max} (nm) (Ɛ x 10^3 ($mol^{-1}Lcm^{-1}$)): 418 (283.28), 516 (3.19), 551 (2.68), 591 (2.30), 648 (2.22).

IR ν (cm^{-1}): 3076.5, 2922.1, 2851.8, 1681.2, 1603.7, 1580.9, 1468.4, 1431.3, 1332.1, 1308.8, 1245.9, 1076.1, 1076.1, 1021.5, 967.5, 825.1, 791.6, 771.8, 745.1, 727.7, 544.1, 407.7.

In addition to the target molecule, a minor fraction was also obtained with a yield of 5 %. This fraction is more soluble and less polar than the previous one.

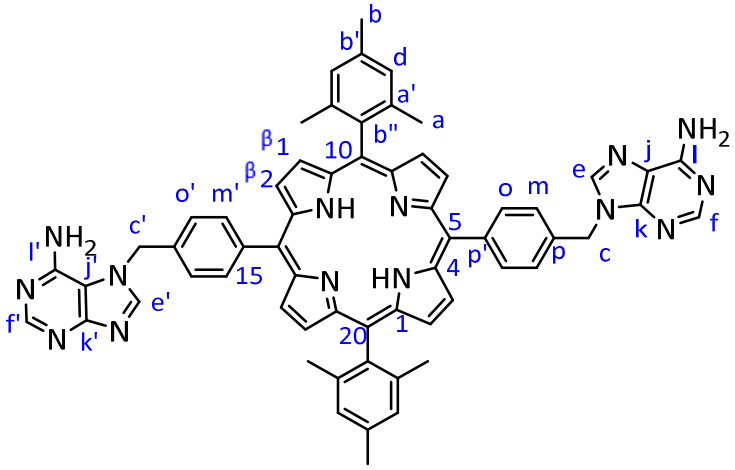

^{1}H NMR (500 MHz, $CDCl_3$ + MeOD) δ (ppm): -2.67 (2 H, s, NH), 1.81 (12H, s, Ha), 2.61 (6 H, s, Hb), 5.73 (2H, s, Hc), 5.84 (4H, s, brd, NH_2), 5.93 (2H, s, Hc'), 7.27 (4H, s, Hd), 7.63 (2H, d, ^{3}J = 7.9 Hz, Hm), 7.74 (2H, d, ^{3}J = 7.9 Hz, Hm'), 8.09 (1H, s, He), 8.10 (1H, s, He'), 8.20 (4H, m, Ho+o') 8.37 (1H, s, Hf) 8.52 (1H, s, Hf'), 8.66-8.74 (8 H, m, Hβ).

HRMS (MALDI-TOF): m/z (M+): $[M+H]^+$calculated = 993.4575, $[M+H]^+$ found = 993.4586.

28) 5,15-bis(N_1-methylphenylcytosine)-10,20-dimesitylporphyrin (**T7**) [12]

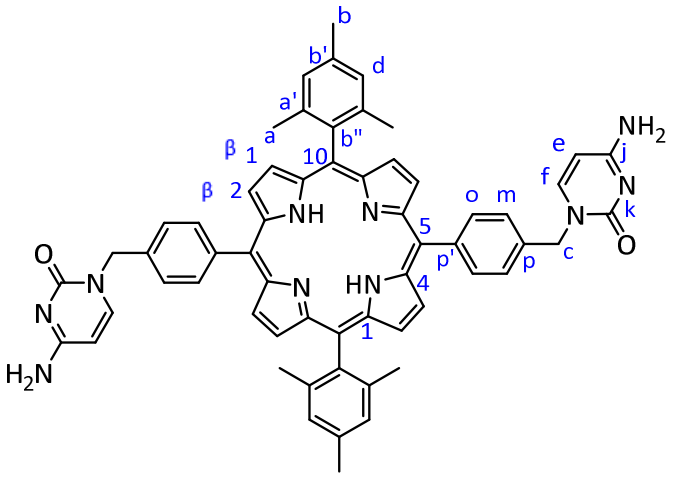

Chemical Formula: $C_{60}H_{52}N_{10}O_2$
Molecular Weight: 944.43 g/mol

5,15-bis(4-(bromomethyl)phenyl)-10,20-dimesitylporphyrin (130 mg, 0.156 mmol, 1 eq) and excess of cytosine (86 mg, 0.779 mmol, 5 eq) were dissolved in dry degassed DMF (12 mL). NaH (11.20 mg, 0.467 mmol, 3 eq) was added to the suspension and stirred for 24 hours at 40 ºC. The reaction was followed by TLC and stopped when all starting porphyrin were consumed. The reaction was dried under vacuum then washed with water to remove the excess of salt and cytosine. The crude was purified by Column Chromatography (Silica gel, 5% Methanol in DCM) to give 55 mg of a purple solid (37 %).

^{1}H NMR (400 MHz, DMSO-d_6) δ (ppm): -2.76 (2 H, s, NH), 1.75 (12H, s, Ha), 2.58 (6 H, s, Hb), 5.21 (4H, s, Hc), 5.82(2H, d, ^3J = 7.3 Hz, He), 7.09 (2H,s, brd, NHcytosine) 7.19 (2H,s, brd, NHcytosine), 7.34 (4H, s, Hd), 7.66 (4H, d, ^3J = 7.9 Hz, Hm), 7.96 (2H, d, ^3J = 7.2 Hz, Hf), 8.19 (4H, d, ^3J = 7.9 Hz, Ho), 8.62 (4 H, d, ^3J = 4.6 Hz, Hβ), 8.78 (4 H, d, ^3J = 4.7 Hz, Hβ).

^{13}C NMR (126 MHz, DMSO-d_6) δ (ppm): 21.12 (Cb), 21.27 (Ca), 51.48 (Cc), 93.99 (Ce), 113.49, 117.84, 119.16, 126.01 (Cβ), 127.98 (Cm & Co), 134.45 (Cd), 137.11, 137.75, 137.83, 138.48, 139.96, 140.50 (Cf), 156.17 (Ck), 166.24 (Cj).

HRMS (ESI): m/z: $[M+H]^+$ calculated = 945.4347, $[M+H]^+$ found = 945.4354.
UV-VIS (DMF, λ_{max}(nm) (Ɛ x 10^3 ($mol^{-1}Lcm^{-1}$)): 418 (190.49), 514 (9.50), 548 (4.87), 591 (3.21), 647 (2.85).
IR ν(cm^{-1}): 3320.8, 1644.5, 1489.3, 1384.9, 1264.7, 1077.7, 787.3, 726.3, 606.2, 410.7.

29) 5,15-bis(N_9-methylphenyl-2-amino-6-chloropurine)-10,20-dimesitylporphyrin (**T8**) [12]

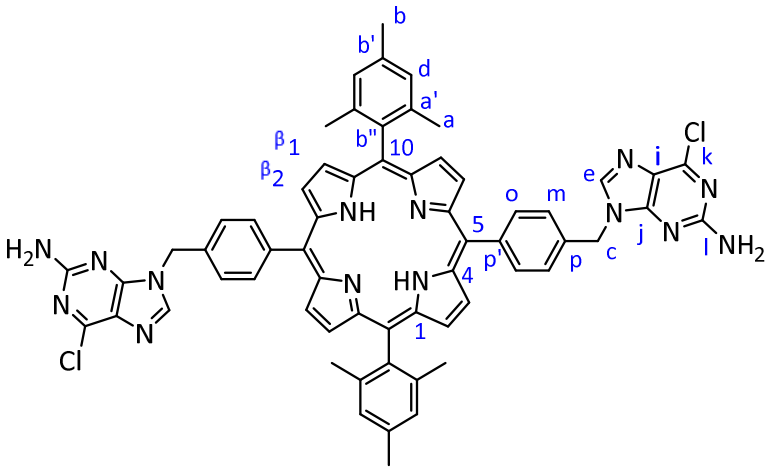

Chemical Formula: $C_{62}H_{50}Cl_2N_{14}$
Molecular Weight: 1062.08 g/mol

5,15-bis(4-(bromomethyl)phenyl)-10,20-dimesitylporphyrin (100 mg, 0.113 mmol, 1 eq) and excess of 2-amino-6-chloropurine (95.81 mg, 0.565 mmol, 5 eq) were dissolved in dry degassed DMF (15 mL). K_2CO_3 (46.85 mg, 0.339 mmol, 3 eq) was added to the suspension and stirred for 24 hours at 50 °C. The reaction was followed by TLC and stopped when all starting porphyrin was consumed. The reaction was dried under vacuum then washed with water (5 mL) to remove the excess of 4-chloro-1-aminopurine and salt. The crude product was purified by Column Chromatography (Silica gel, 5% Methanol in DCM) to give two fractions F1 (96 mg) and F2 (*ca.* 10 mg) of purple solids (80 % for F1, 8 % F2).

For F1:

^{1}H NMR (500 MHz, $CDCl_3$) δ (ppm): -2.68 (2 H, s, NH), 1.81 (12H, s, Ha), 2.63 (6 H, s, Hb), 5.21 (4H, s, NH_2), 5.61 (4H, s, Hc), 7.28 (4H, s, Hd), 7.63 (4H, d, ^3J = 7.9 Hz, Hm), 8.05 (2H, s, He), 8.20 (4H, d, ^3J = 8.0 Hz, Ho), 8.62 (4 H, d, ^3J = 4.7 Hz, Hβ), 8.78 (4 H, d, ^3J = 4.7 Hz, Hβ).

^{13}C NMR (126 MHz, $CDCl_3$ + MeOD) δ (ppm): 21.63 (Cb), 21.77 (Ca), 47.31 (Cc), 118.39, 118.72, 125.51 (Ci), 126.17 ($C\beta_1$ & $C\beta_2$), 127.92 (Cm& Co), 135.21 (Cd), 137.97, 138.37, 139.46, 142.47 (Ce), 142.53, 151.80 (Cj), 154.23 (Ck), 159.44 (Cl).

HRMS (ESI): m/z: $[M+H]^+$calculated = 1061.3793, $[M+H]^+$ found = 1061.3782.

UV-VIS (DMF, λ_{max} (nm) (ε x 10^3 ($mol^{-1}Lcm^{-1}$)): 418 (348.60), 514 (16.15), 548 (7.33), 591 (5.07), 647 (4.43).

IR $\nu(cm^{-1})$: 3458.8, 33313.1, 3073.9, 1699.9, 1628.7, 1559.1, 1518.0, 1469.1, 1407.6, 1391.8, 1348.0, 1210.9, 1165.8, 1119.3, 991.9, 914.2, 819.2, 782.7, 755.9, 734.1, 638.8, 605.9, 528.4, 496.2, 437.9.

For F2:

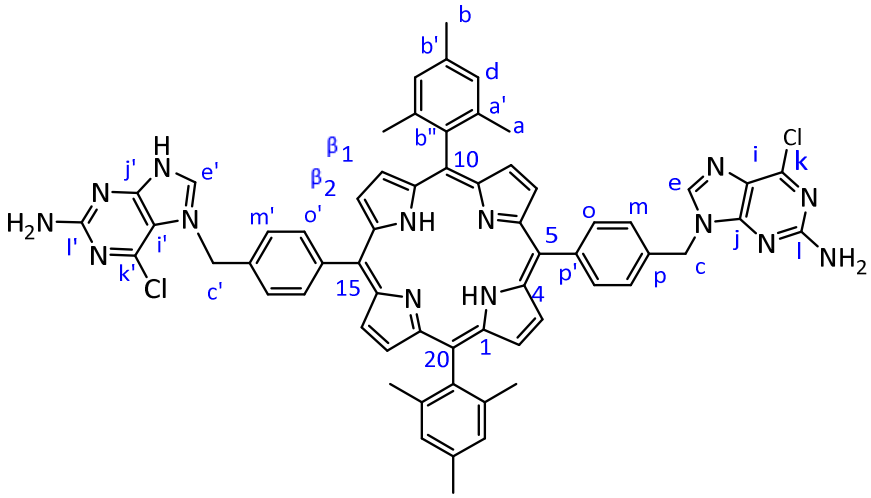

^{1}H NMR (500 MHz, $CDCl_3$) δ (ppm): -2.67 (2 H, s, NH), 1.82 (12H, s, Ha), 2.63 (6 H, s, Hb), 5.21 (2H, s, NH_2), 5.26 (2H, s, NH_2'), 5.60 (2H, s, Hc), 5.88 (2H, s, Hc'), 7.28 (4H, s, Hd), 7.50 (2H, d, ^3J = 7.9 Hz, Hm'), 7.63 (2H, d, ^3J = 7.9 Hz, Hm), 8.05 (1H, s, He), 8.20 (4H, m, Ho+o'), 8.50 (1H, s, He'), 8.69 (8 H, m, Hβ).

^{13}C NMR (126 MHz, $CDCl_3$ + MeOD) δ (ppm): 21.62 (Cb), 21.76 (Ca), 47.30 (Cc), 50.74 (Cc'), 116.82, 118.22, 118.42, 118.75, 125.51 (Ci), 125.147 ($C\beta_1$), 126.16 (Cβ), 127.92 (Cm & Co), 134.79-134.89 (Ci'), 135.20 (Cd), 137.96, 138.34, 139.45, 142.47 (Ce), 144.53, 144.08, 149.01 (Ce'), 151.78 (Cj), 154.22 (Ck), 159.69 (Cl), 159.69 (Cj') 164.58 (Ck').

MS (ESI): m/z: $[M+H]^+$calculated = 1061.37, $[M+H]^+$ found = 1061.38.

30) 5,15-bis(N_9-methylphenylguanine)-10,20-dimesitylporphyrin (**T9**) [12]

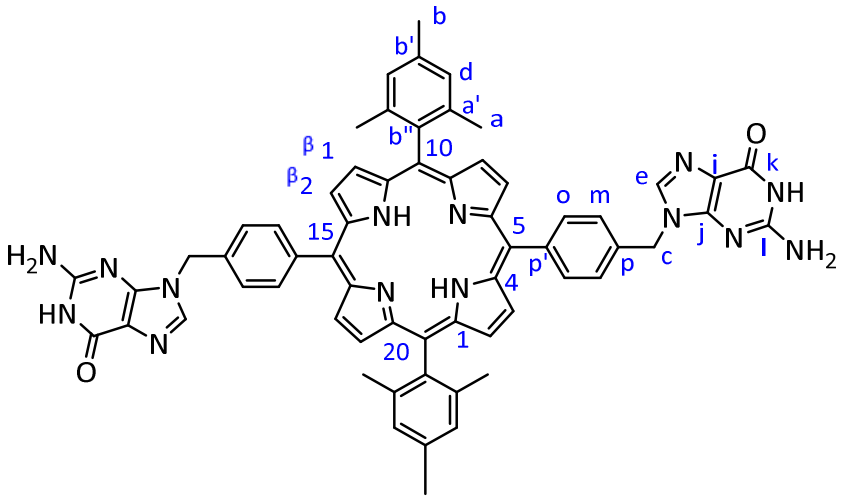

Chemical Formula: $C_{62}H_{52}N_{14}O_2$
Molecular Weight: 1024.44 g/mol

5,15-bis(N_9-methylphenyl-2-amino-6-chloropurine)-10,20-dimesitylporphyrin (60 mg, 0.0565 mmol, 1 eq) was dissolved in 20 mL of MeOH. 0.1 M of HCl aqueous solution was added to the mixture (4 mL, 0.4 mmol, 7 eq). Upon addition of HCl, the color of the solution changed from purple to green. The mixture was stirred overnight under reflux and the reaction was followed by TLC. When all starting material was consumed, 0.1 M NaOH solution was added drop wise to neutralize the solution (*ca*. 3 mL). The resulting purple precipitate was filtered, washed with water (10 mL) and acetone (10 mL) and dried under reduced pressure to give 56 mg of the final product (98 %).

^{1}H NMR (500 MHz, DMSO-d_6) δ (ppm): -2.80 (2 H, s, NH porph), 1.74 (12H, s, Ha), 2.58(6 H, s, Hb), 5.55 (4H, s, Hc), 6.77 (4H, s, brd, NH_2 guanine), 7.34 (4H, s, Hd), 7.62 (4H, d, ^3J = 7.8 Hz, Hm), 8.04 (2H, s, He), 8.21 (4H, d, ^3J = 8.0 Hz, Ho), 8.63 (4H, d, ^3J = 4.2 Hz, Hβ), 8.75 (4H, d, ^3J = 4.2 Hz, Hβ), 10.87 (2H, s, brd, NH Guanine).

^{13}C NMR (126 MHz, d_6-DMSO) δ (ppm): porphyrin is not soluble. ^{13}C NMR was dilute and could not be attributed. Even with 1,1,3,3-Hexafluoro-2-propanol-d2 (HFIP-d2) the ^{13}C NMR was not clear.

HRMS (ESI): m/z: $[M+H]^+$ calculated = 1025.4478, $[M+H]^+$ found = 1025.4489.

UV-VIS (DMF, λ_{max}(nm) (ε x 10^3 ($mol^{-1}Lcm^{-1}$)) : 418 (76.94), 514 (4.00), 548 (2.09), 591 (1.44), 647 (1.34).

IR v(cm^{-1}): 3113.9, 2923.1, 2852.0, 1682.8, 1606.8, 153.5, 1480.3, 1409.3, 1260.0, 1213.1, 1167.7, 1093.7, 1017.1, 797.8, 757.1, 688.9, 477.9.

31) 5,10,15,20-tetrakis[4-(bromomethyl)phenyl]porphyrin (**Po4**) [13]

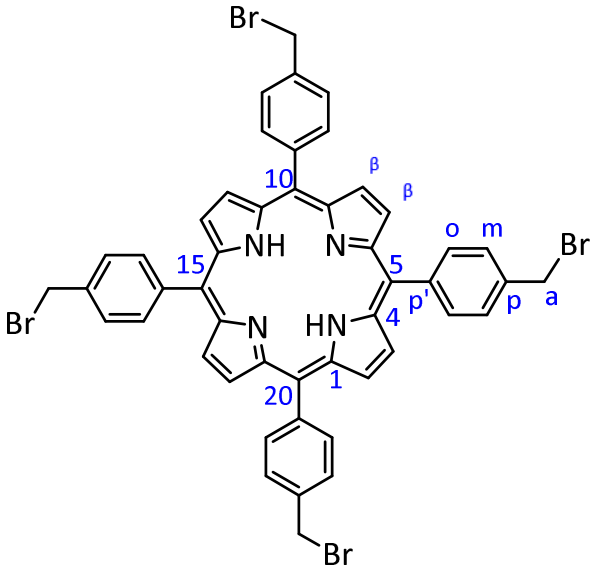

Chemical Formula: $C_{48}H_{34}Br_4N_4$
Molecular Weight: 986.95 g/mol

Pyrrole (0.168g, 2.5 mmol, 0.17 mL, 1 eq) and 4-(bromomethyl)benzaldehyde (0.5g, 2.5 mmol, 1 eq) were dissolved in 250 mL of degassed chloroform. A solution of $BF_3.Et_2O$ (55.95 mg, 0.825 mmol, 0.05mL, 1 eq) in 0.33 mL chloroform was added to the solution. The solution was stirred under argon at RT for 2 hours. Then Et_3N (0.142 mL, 1.02 mmol, 0.4 eq) and *p*-chloranil (0.4616 g, 1.88 mmol, 0.75 eq) were added to the mixture and heated under reflux at 65 °C for 1 hour. The mixture was evaporated under vacuum and then dissolved in DCM and filtered over a pad of Silica. The filtrate was dried under vacuum to give 0.6 g of a purple solid (70 %).

^{1}H NMR (400 MHz, $CDCl_3$) δ (ppm): -2.73 (2H, s, NH), 4.86 (8H, s, Ha), 7.78 (8 H, d, ^3J = 7.9 Hz, Hm), 8.19 (8H, d, ^3J = 7.9Hz, Ho), 8.84 (8H, s, Hβ).

^{13}C NMR (126 MHz, $CDCl_3$) δ: 33.65 (Ca), 118.95(Cβ), 119.67, 127.62 (Cm), 135.06 (Co), 137.51, 140.71, 142.32, 143.32.

HRMS (ESI): m/z(M+): $[M+H]^+$ calculated = 985.9831, $[M+H]^+$ found = 986.9532.

UV-VIS (DMF, λ_{max}(nm) (ε x 10^3 ($mol^{-1}Lcm^{-1}$)) : 418 (263.32), 515(38.7), 550 (24.63), 593 (6.75), 646 (6.43).

32) 5,10,15,20-tetrakis(N_1-methylphenylthymine)porphyrin (**T10**)

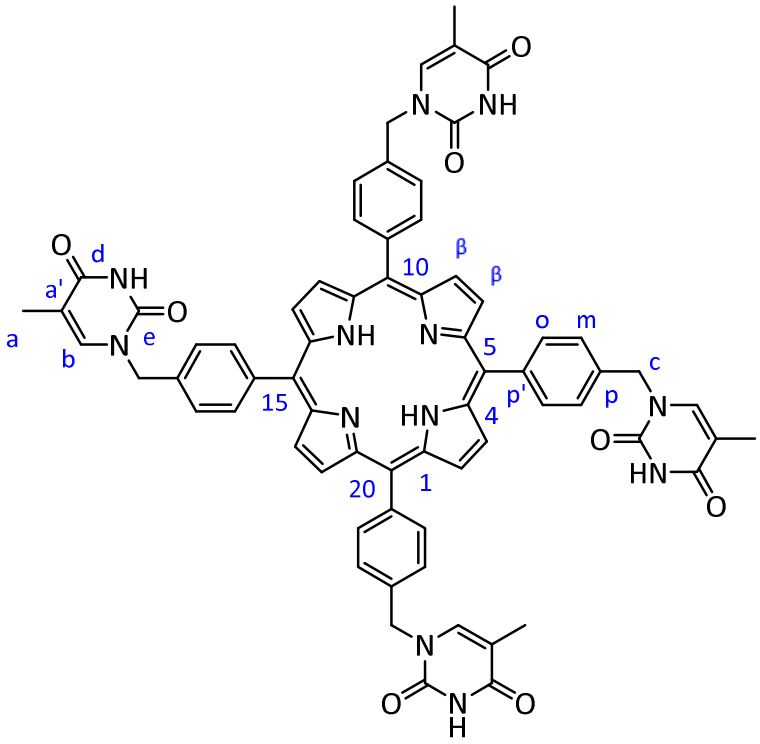

Chemical Formula: $C_{68}H_{54}N_{12}O_8$
Molecular Weight: 1167.26 g/mol

5,10,15,20-tetrakis(4-(bromomethyl)phenyl)porphyrin (200 mg, 0.203 mmol, 1 eq), excess of thymine (255 mg, 2.03 mmol, 10 eq) and K_2CO_3 (141 mg, 1.02 mmol, 5 eq) were dissolved in 10 mL of degassed DMF. The mixture was stirred overnight at 40 °C under argon. The reaction was followed by TLC. After the disappearance of the starting porphyrin, the reaction was dried under vacuum and then triturated with water (10 mL). The purple precipitate was filtered over a frit and washed with water (20 mL), then dried under vacuum to give 220 mg of a purple solid. (93 %)

^{1}H NMR (400 MHz, $CDCl_3$) δ (ppm): -2.80 (2H, s, brd, NH), 1.88 (12H, s, Ha), 5.22 (8H, s, Hc), 7.73 (8H, d, ^3J = 7.7 Hz, Hm), 7.96 (4H, s, Hb), 8.22 (8H, d, ^3J = 7.7 Hz, Ho), 8.84(8H, s, Hβ), 11.50 (4H, s, brd, NHthymine).

^{13}C NMR (126 MHz, DMF-d_7) δ (ppm): 11.74 (Ca), 50.73 (Cc), 73.38, 108.32 (Ca'), 110.05 (Cβ), 126.74 (Cm), 135.22 (Co), 137.57(Cb), 138.11, 141.79, 152.02 (Cd), 164.84 (Ce).

HRMS (ESI): m/z(HRM+): $[M+H]^+$ calculated = 1167.4260, $[M+H]^+$ found = 1167.4257.

UV-VIS (DMF, λ_{max}(nm) (ε x 10^3 ($mol^{-1}Lcm^{-1}$)) : 419 (231.96), 515(11.20), 550 (6.69), 593 (4.42), 646 (4.08).

IR ν(cm^{-1}): 2925.5, 1661.0, 1382.2, 1349.1, 1212.8, 982.2, 966.1, 798.8, 558.6, 477.6, 411.8.

33) 4-(N_1-methylthymine)benzylaldehyde (**T-Ald**)

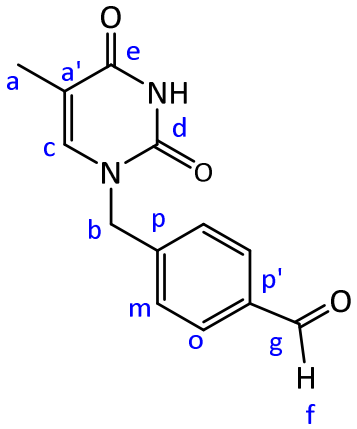

Chemical Formula: $C_{13}H_{12}N_2O_3$
Molecular Weight: 244.25 g/mol

Thymine (507 mg, 4.0 mmol, 2 eq) and K_2CO_3 (414 mg, 3.0 mmol, 1.5 eq) were dissolved in 10 mL of dry DMF under argon. In a separate flask, 4-(bromomethyl)benzaldehyde (400 mg, 2.0 mmol, 1 eq) was dissolved in 10 mL of dry and degassed DMF and added dropwise to the mixture, after which the clear mixture was brought to 50 °C and left to stir for 12h. Then, the mixture was dried under vacuum and washed with a minimum amount of water (5 mL) to remove the excess of salt. The crude product was purified by column chromatography (silica gel, 1% Methanol in DCM then 3% MeOH in DCM) to give 278 mg of a white solid (57 %).

^{1}H NMR (500 MHz, DMSO-d_6) δ (ppm): 1.76 (3H, s, Ha), 4.94 (2H, s, Hb), 7.48 (2H, d, ^3J = 8.0 Hz, Hm), 7.66 (1H, s, Hc), 7.90 (2H, d, ^3J = 8.0 Hz, Ho), 9.99 (1H, s, Hf), 11.39 (1H, s, NHthymine).

^{13}C NMR (126 MHz, DMSO-d6) δ (ppm): 12.04 (Ca), 50.08 (Cb), 109.28 (Ca'), 127.88 (Cm), 129.94 (Co), 135.52, 141.39 (Cc), 143.90, 151.07 (Cd), 164.35 (Ce), 192.81 (Cg).
HRMS (ESI): m/z: $[M+H]^+$ calculated = 245.0921, $[M+H]^+$ found = 245.0926.

34) 1,3,7,9-tetramethyl-5-(N_1-methylphenylthymine)-dipyrrin (**T-dipyrrin**) (**T11**)

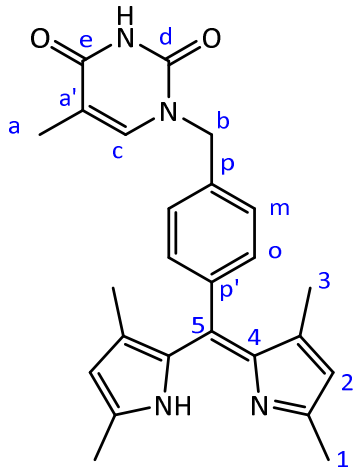

Chemical Formula: $C_{25}H_{26}N_4O_2$
Molecular Weight: 414.21 g/mol

T-Ald (180 mg, 0.737 mmol, 1 eq) was dissolved in 5 mL of degassed DCM. The flask was protected from light and 2,4-dimethylpyrrole (0.152 mL, 1.47 mmol, 2 eq) was added. Subsequently, two drops of TFA were added, and the reaction mixture was stirred at RT for 12h under argon and protected from light. When the disappearance of the aldehyde was confirmed by TLC, the reaction was stopped and the mixture dried under vacuum. The crude product was dissolved in 5 mL of dry THF. In a separate flask, DDQ (152 mg, 0.668 mmol, 0.9 eq) was dissolved in 5 mL of dry THF and added drop wise to the reaction mixture. The mixture was stirred overnight and followed by TLC. When all the dipyrromethane was oxidized, the reaction was stopped, the solvent was evaporated and the product purified by column chromatography (silica gel, 1% 7N ammonia in MeOH in DCM) to give 160 mg of pure **T-dipyrrin** (**T11**) as brown red solid (53 %).

^{1}H NMR (500 MHz, $CDCl_3$) δ (ppm): 1.26 (6H, s, H3), 1.88 (3H, d, ^4J = 1.1 Hz, Ha), 2.34 (6H, s, H1), 4.97 (2H, s, Hb), 5.89 (2H, s, H2), 6.95 (1H, q, ^4J = 1.1 Hz, Hc), 7.33-7.36 (4H, m, Hm & Ho).

^{13}C NMR (126 MHz, $CDCl_3$) δ (ppm): 12.55 (C3), 14.72 (Ca), 16.19 (C1), 50.76 (Cb), 111.48 (Ca'), 119.86 (C2), 128.40 (Cm), 130.20 (Co), 135.52, 136.25, 137.73, 138.50, 139.50 (Cc), 140.12, 151.19 (Cd), 152.01, 164.06 (Ce).

HRMS (ESI): m/z(M+): $[M+H]^+$ calculated = 415.2129, $[M+H]^+$ found = 415.2102.
UV-VIS ($CHCl_3$, λ_{max}(nm) (Ɛ x 10^3 ($mol^{-1}Lcm^{-1}$)): 272 (13.33), 307 (6.78), 447 (5.91).
IR ν(cm^{-1}): 2925.9, 1681.9, 1575.5, 1536.6, 1435.2, 1348.5, 1281.9, 1100.4, 942.4, 805.8, 712.8, 556.6, 473.1.

35) Zn(II)[1,3,7,9-tetramethyl-5-(N_1-methylphenylthymine)-dipyrrin] (**Zn-T-dipyrrin**)

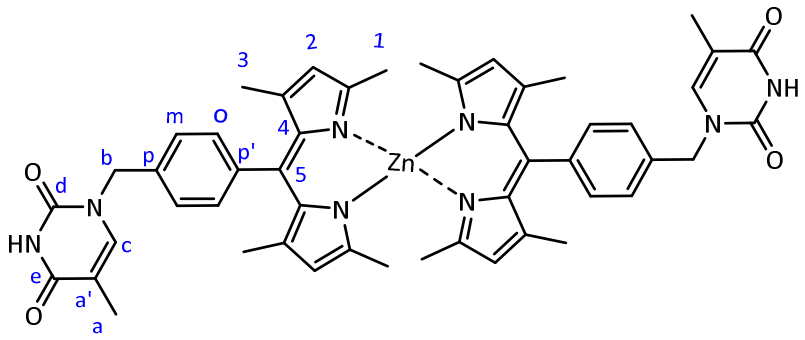

Chemical Formula: $C_{50}H_{50}N_8O_4Zn$
Molecular Weight: 890.32g/mol

T-dipyrrin (30 mg, 0.077 mmol, 1 eq) was dissolved in a 15 mL of a mixture of $CHCl_3$/MeOH (70/30). In a separate flask, $Zn(OAc)_2.2H_2O$ (22 mg, 0.100 mmol, 1.3 eq) was dissolved in 5 mL of MeOH. The zinc solution was added to the reaction mixture that was left to stir for 12h. The solvent was evaporated and the crude was washed with water (10 mL) and subsequently dried over $MgSO_4$, to afford 60 mg of **Zn-T-dipyrrin** as a yellow solid (87 %).

^{1}H NMR (400 MHz, Methanol-d_4) δ (ppm): 1.24 (24H ,s, H3), 1.86 (6H d, ^4J = 1.1 Hz, Ha), 2.34 (6H, s, H1), 4.26 (24H, s, H1), 4.96 (4H s, Hb) 7.33-7.30 (2H d, ^4J = 1.1 Hz, Hc), 7.39 (4H d, ^3J = 8.3 Hz, Hm), 7.58 (4H d, ^3J = 8.2 Hz, Ho).

^{13}C NMR (126 MHz, DMSO-d_6) δ (ppm): 13.81 (C3), 14.73 (Ca), 17.24 (C1), 53.30 (Cb), 110.57 (Ca'), 115.67 (C2), 127.34 (Cm), 129.60 (Co), 136.87, 136.95, 137.87, 138.50, 139.25 (Cc), 141.10, 150.80 (Cd), 152.01, 164.36 (Ce).

UV-VIS ($CHCl_3$, λ_{max}(nm) (Ɛ x 10^3 ($mol^{-1}Lcm^{-1}$)): 267 (17.32), 355 (6.75), 491 (3.10).

36) 4-(N_9-methylphenyladenine)benzylaldehyde (**A-Ald**)

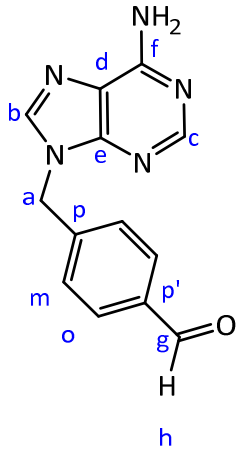

Chemical Formula: $C_{13}H_{11}N_5O$
Molecular Weight: 253.27 g/mol

Adenine (407 mg, 3.01 mmol, 2 eq) and K_2CO_3 (312.4 mg, 2.26 mmol, 1.5 eq) were added to 5 mL of dry degassed DMF. To the suspension, a 4-(bromomethyl)benzaldehyde solution (300 mg, 1.57 mmol, 1 eq) in 10 mL of dry DMF was added drop wise. The reaction mixture was stirred under argon at 50 °C overnight and followed by TLC. When all the aldehyde was consumed, the mixture was dried under vacuum and purified by column chromatography (silica gel, 3% MeOH in DCM) to give 170 mg of **A-Ald** as a white solid (45 %).

^{1}H NMR (500 MHz, $CDCl_3$ + MeOD-d_4) δ (ppm): 5.52 (s, 2H, Ha), 7.46 (2H, d, ^3J = 8.2 Hz, Hm), 7.87 (2H, d, ^3J = 8.2 Hz, Ho), 8.13 (1H, s, Hb), 8.22 (1H, s, Hc), 9.95 (1H, s, Hh).
^{13}C NMR (126 MHz, $CDCl_3$ + MeOD-d_4) δ (ppm): 46.96 (Ca), 118.9 (Cd), 128.16 (Cm), 130.53 (Co), 136.25, 140.27 (Cb), 142.03, 149.71 (Ce), 153.12 (Cc), 155.58 (Cf), 191.95 (Cg).

HRMS (ESI): m/z (H^+): $[M+H]^+$ calculated = 254.10 $[M+H]^+$ found = 254.10.

37) 1,3,7,9-tetramethyl-5-(N_9-methylphenyladenine)-dipyrrin (**A-dipyrrin**) (**T12**)

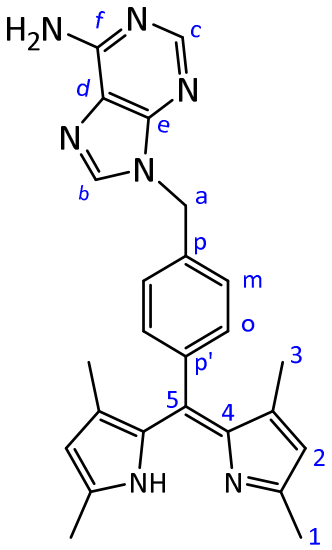

Chemical Formula: $C_{25}H_{25}N_7$
Molecular Weight: 423.52 g/mol

A-Ald (160 mg, 0.632 mmol, 1 eq) was dissolved in 5 mL of degassed DCM protected from light, then 2,4-dimethylpyrrole (0.130 mL, 1.26 mmol, 2 eq) was added followed by two drops of TFA. The reaction mixture was stirred at RT overnight. The disappearance of the aldehyde was confirmed by TLC. When all the starting material was consumed, the reaction was stopped and the mixture was dried under vacuum protected from light. Then the mixture was dissolved in 5 mL of dry THF and a solution of DDQ (0.9 eq., 129 mg, 0.569 mmol) in 5 mL of dry THF was added. The mixture was stirred at RT and followed by TLC. After 24 hours, the reaction was stopped and purified by column chromatography (silica gel, 1% 7N ammonia and 2 % MeOH in DCM, then 1% 7N ammonia and 5 % MeOH in DCM) to give 70 mg **A-dipyrrin** (**T12**) as a brown/orange solid (26 %).

^{1}H NMR (500 MHz, $CDCl_3$) δ (ppm): 1.25 (6H, s, H3), 2.33 (6H, s, H1), 5.44 (2H, s, Ha), 5.88 (2H, s, brd, $NH_{2\ adenine}$), 5.90 (2H, s, H2), 7.41-7.27 (4H, m, Hm & Ho), 7.75 (1H, s, Hb), 8.39 (1H, s, Hc).

^{13}C NMR (126 MHz, $CDCl_3$) δ (ppm): 14.76 (C3), 16.14 (C1), 47.21 (Ca), 119.62 (C2), 119.87 (Cd), 128.20 (Cm), 129.25, 130.23 (Co), 135.72, 136.22, 138.52, 140.24, 140.34 (Cb), 150.40 (Ce), 151.99, 153.40 (Cc), 155.60 (Cf).

HRMS (ESI): m/z(H^+) : $[M+H]^+$calculated = 424.2244, $[M+H]^+$ found = 424.2258.

UV-VIS (4% MeOH in $CHCl_3$, λ_{max}(nm) (ε x 10^3 ($mol^{-1}Lcm^{-1}$)) : 269 (91.23), 312 (18.7), 460 (9.2).

IR v(cm^{-1}): 3146.5, 2923.9, 2850.8, 1645.6, 1597.6, 1574.5, 1533.7, 1513.2, 1414.7, 1387.6, 1279.1, 1213.8, 1151.2, 1097.9, 941.2, 798.0, 712.8, 644.6, 588.1, 492.6.

38) 4-(N_1-methylcytosine)benzylaldehyde (**C-Ald**)

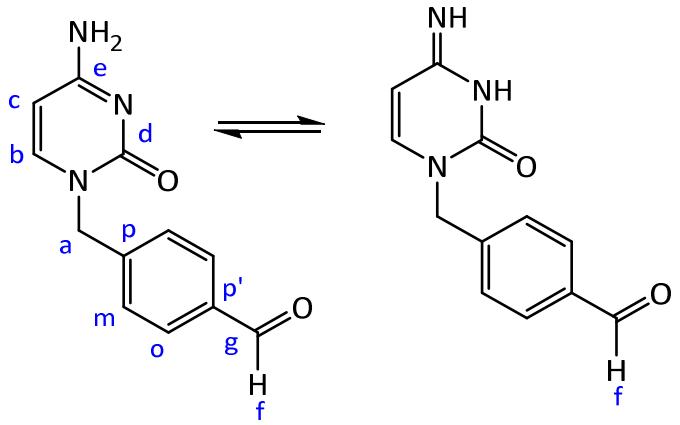

Chemical Formula: $C_{12}H_{11}N_3O_2$
Molecular Weight: 229.24 g/mol

Cytosine (446 mg, 4.02 mmol, 2 eq) was suspended in 15 mL of dry DMF under argon. NaH (72 mg, 3.01 mmol, 1.5 eq) was added to the suspension, which was stirred for 30 min. A solution of 4-(bromomethyl)benzaldehyde (400 mg, 2.01 mmol, 1 eq) in 5 mL of dry DMF was added dropwise to the reaction mixture, and it was left to stir for 12h at 40 °C. The disappearance of the aldehyde was followed by TLC. When all the aldehyde was consumed, the mixture was dried under vacuum and purified by column chromatography (silica gel, 3% MeOH in DCM) to give 207 mg of **C-Ald** as a white solid (45 %).

^{1}H NMR (500 MHz, DMSO-d_6) δ (ppm): 4.94 (2H, s, Ha), 5.69 (1H, d, ^3J = 7.2 Hz, Hc), 7.12 (1H, s, brd, NH cytosine), 7.18 (1H, s, brd, NH cytosine), 7.43 (2H, d, ^3J = 8.0 Hz, Hm), 7.73 (1H, d, ^3J = 7.2 Hz, Hb), 7.88 (2H, d, ^3J = 8.1 Hz, Ho), 9.98 (1H, s, Hf).

^{13}C NMR (126 MHz, DMSO-d_6) δ (ppm): 51.41 (Ca), 93.93 (Cc), 127.91 (Cm), 129.86 (Co), 135.31 (Cp), 145.09 (Cp'), 146.23 (Cd), 155.85 (Ce), 166.17 (Cf), 192.90 (Cg).

HRMS (ESI): m/z (H^+): $[M+H]^+$ calculated = 230.0924, $[M+H]^+$ found = 230.0935.

39) 1,3,7,9-tetramethyl-5-(N_1-methylphenylcytosine)-dipyrrin (**C-dipyrrin**) (**T13**)

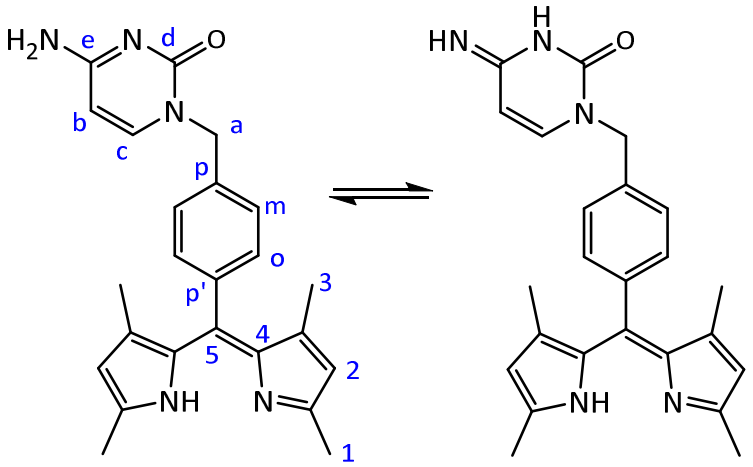

Chemical Formula: $C_{24}H_{25}N_5O$
Molecular Weight: 399.50 g/mol

C-Ald (200 mg, 0.872 mmol, 1 eq) and 2,4-dimethylpyrrole (0.180 mL, 1.74 mmol, 2 eq) were dissolved in 5 mL of degassed DCM protected from light, then two drops of TFA were added to the suspension. The reaction mixture was stirred at RT overnight and followed by TLC. When all starting material was consumed, the reaction was stopped and the mixture dried under vacuum protected from light. The crude was dissolved in 5 mL of dry THF and a solution of DDQ (179 mg, 0.785 mmol, 0.9 eq) in 5 mL of dry THF was added to the reaction mixture. The mixture was stirred at RT and followed by TLC. After 24 hours, the reaction was stopped and purified by column chromatography (silica gel, 5% 7N ammonia and 5 % MeOH in DCM) to give 70 mg of **C-dipyrrin** (**T13**) as a brown-red solid (20 %).

^{1}H NMR (300 MHz, DMSO-d_6) δ (ppm): 1.23 (6H, s, H3), 2.29 (6H, s, H1), 4.94 (2H, s, Ha), 5.69 (1H, d, ^3J = 7.2 Hz, Hb), 5.97 (2H, s, H2), 7.02 (1H, s, brd, NH cytosine), 7.10 (1H, s, brd, NH cytosine), 7.24 (2H, d, ^3J = 7.9 Hz, Hm), 7.37 (2H, d, ^3J = 7.9 Hz, Ho), 7.69 (1H, d, ^3J = 7.2 Hz, Hc).

^{13}C NMR (500 MHz, $CDCl_3$ + MeOD-d_4) δ (ppm): 14.20 (C3), 17.00 (C1), 51.45 (Ca), 94.98 (Cb), 119.87 (C2), 126.95 (Cm), 127.53 (Co), 128.20, 132.64, 135.42, 142.88, 144.87, 145.41 (Cc), 152.83, 157.12 (Cd), 166.09 (Ce).

HRMS (ESI): m/z (H^+): $[M+H]^+$calculated = 400.2129, $[M+H]^+$ found = 400.2130.
UV-VIS (4% MeOH in $CHCl_3$, λ_{max}(nm) (Ɛ x 10^3 ($mol^{-1}Lcm^{-1}$)): 280(22.02). 340 (12.66), 505(9.8).
IR ν(cm^{-1}): 3175.8, 1644.0, 1488.6, 1434.7, 1384.6, 1286.5, 1138.3, 962.6, 798.4, 691.9, 610.3.

40) 4-(N_9-methyl-2-amino-6-chloropurine)benzylaldehyde (**P-Ald**)

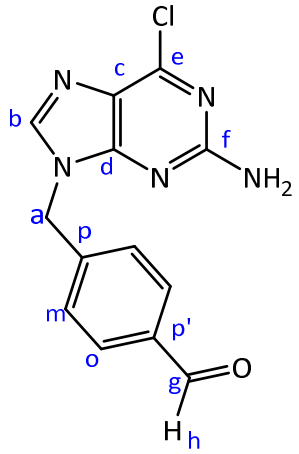

Chemical Formula: $C_{13}H_{10}N_5ClO$
Molecular Weight: 287.71 g/mol

2-amino-6-chloropurine (1 g, 6.03 mmol, 2 eq) and K_2CO_3 (624 mg, 4.52 mmol, 1.5 eq) were dissolved in 15 mL of dry degassed DMF. A solution of 4-(bromomethyl)benzaldehyde (600 mg, 3.014 mmol, 1 eq) in 5 mL of dry DMF was added dropwise, and the mixture was left to stir for 12h at 50 °C. The reaction was followed by TLC. When all the aldehyde was consumed, the mixture was dried under vacuum and purified by column chromatography (silica gel, 2% MeOH in DCM) to yield 380 mg of **P-Ald** as a white solid (43 %).

^{1}H NMR (400 MHz, MeOD-d_4) δ (ppm): 5.43 (2H, s, Ha), 7.50 (2H, d, ^3J = 8.0 Hz, Hm), 7.89 (2H, d, ^3J = 8.0 Hz, Ho), 8.11 (1H, s, Hb), 9.96 (1H, s, Hh).

^{13}C NMR (126 MHz, DMSO-d_6) δ (ppm): 45.60 (Ca), 116.59 (Cc), 127.49 (Cm), 129.65 (Co), 135.46, 137.52 (Cb), 144.02, 149.71 (Cd), 153.12 (Ce), 156.85 (Cf), 192.73 (Cg).

HRMS (ESI): m/z (H^+): $[M+H]^+$ calculated = 288.0647, $[M+H]^+$ found = 288.0650.

41) 1,3,7,9-tetramethyl-5-(N_9-methylphenyl-2-amino-6-chloropurine)dipyrrin (**P-dipyrrin**) (**T14**)

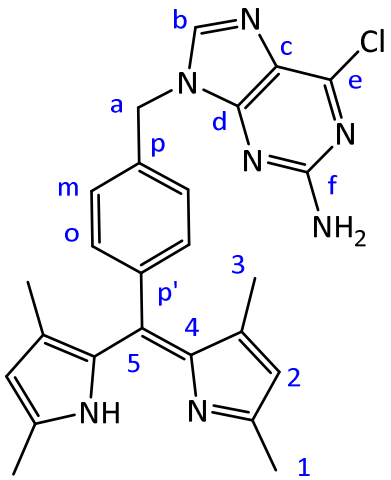

Chemical Formula: $C_{25}H_{24}N_7Cl$
Molecular Weight: 457.97 g/mol

P-Ald (300 mg, 1.04 mmol, 1 eq) and 2,4-dimethylpyrrole (0.213 mL, 2.07 mmol, 2 eq) were dissolved in 5 mL of degassed DCM protected from light, then two drops of TFA were added to the mixture. The reaction mixture was stirred at RT overnight and followed by TLC. When all starting materials were consumed, the reaction was stopped and the mixture dried under vacuum, protected from light. The crude was dissolved in 5 mL of dry THF. A solution of DDQ (222 mg, 0.931 mmol, 0.9 eq) in 5 mL of dry DMF was added to the reaction mixture and stirred at RT. After 24 hours, the reaction was stopped and purified by column chromatography (silica gel, 1% 7N ammonia and 1% MeOH in DCM) to give 105 mg of **P-dipyrrin** (**T14**) as a brown/yellow solid (33 %).

^{1}H NMR (500 MHz, $CDCl_3$) δ (ppm): 1.25 (6H, s, H3), 2.33 (6H, s, H1), 5.17 (2H, s, brd, NH_2), 5.31 (2H, s, Ha), 5.87 (s, 2H, H2), 7.36-7.29 (m, 4H, Hm & Ho), 7.70 (s, 1H, Hb)

^{13}C NMR (500 MHz, $CDCl_3$) δ (ppm): 14.72 (C3), 16.16 (C1), 47.19 (Ca), 119.88 (C2), 125.31 (Cc) , 128.28 (Cm), 130.25 (Co), 135.16, 136.27, 137.59, 138.70, 140.08, 141.85 (Cb), 151.59, 151.59, 154.01 (Ce), 159.32 (Cf).

HRMS (ESI): m/z (H^+): $[M+H]^+$ calculated = 458.1854, $[M+H]^+$ found = 458.1853.
UV-VIS (4% MeOH in $CHCl_3$, λ_{max}(nm) (Ɛ x 10^3 ($mol^{-1}Lcm^{-1}$)): 280(19.37). 360 (12.55), 504(5.8).

IR ν(cm^{-1}): 3322.2, 2924.5, 1609.2 (C=N stretching), 1561.4, 1514.3, 1462.6, 1406.3, 1368.9, 1281.6, 1216.3, 1139.2, 1099.1, 998.3, 942.2, 807.8, 911.5, 785.2, 720.7, 696.1, 644.1, 606.1, 460.0.

42) 1,3,7,9-tetramethyl-5-(N_9-methylphenylguanine)dipyrrin (**G-dipyrrin**) (**T15**)

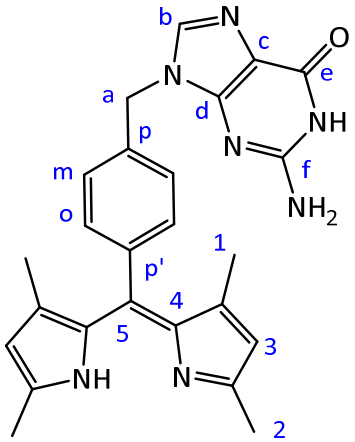

Chemical Formula: $C_{25}H_{25}N_7O$
Molecular Weight: 439.52 g/mol

P-dipyrrin (30 mg, 0.0655 mmol, 1 eq) was dissolved in 15 mL of MeOH, and 10 mL of 0.1 M HCl (aq) was added to the solution. The reaction mixture was brought to reflux and left to stir. After 12 hours, 0.1 M NaOH (aq) solution was added drop wise to the reaction mixture until precipitate started to form. The pH was then checked and the NaOH (aq) addition process was continued until a neutral pH was reached (*ca.* 10 mL of 0.1M NaOH (aq)). The mixture was filtered and the precipitate was collected, washed with 5 mL of water and then dried under vacuum to give 23 mg of **G-dipyrrin** (**T15**) as a low soluble bright red solid (80 %).

HRMS (ESI): m/z (H^+): $[M+H]^+$ calculated = 440.2193, $[M+H]^+$ found = 440.2203.

IR ν(cm^{-1}): 2924.7, 1682,7 (C=O stretching), 1586.6, 1507.5, 1439.3, 1349.7, 1269.9, 1137.8, 1034.8, 957.1, 807.7, 740.4, 680.6, 484.3.

43) 4-(N_1-methylthymine)pyridine (**T-Py**) (**T16**)[14]

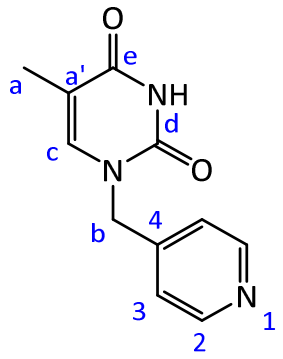

Chemical Formula: $C_{11}H_{11}N_3O_2$
Molecular Weight: 217 g/mol

Thymine (0.75 g, 5.94 mmol, 3 eq), K_2CO_3 (0.68 g, 4.95 mmol, 2.5 eq) and KI (10 mg, catalytic amount) were mixed in 17 mL of dry degassed DMF. The suspension was degassed for 15 minutes. A solution of 4-(bromomethyl)pyridine (0.5 g, 1.98 mmol, 1 eq) in 4 mL of dry degassed DMF was added slowly to the suspension. The reaction was stirred at 40 ºC overnight and followed by TLC. The crude was dried under vacuum and then washed with a minimum amount of water (7 mL). The product was purified by column chromatography (SiO_2, MeOH: Et_3N: DCM 1:0.2:20) to yield 190 mg of **T-Py** as a white solid (45 %).

^{1}H NMR (500 MHz, $CDCl_3$) δ (ppm): 1.92 (3H, d, ^4J = 1.1 Hz, Ha), 4.90 (2H, s, Hb), 6.96 (1H, q, ^4J = 1.1 Hz, Hc), 7.19 (2H, d, ^3J = 6.0 Hz, H3), 8.62 (2H, d, ^3J = 6.0 Hz, H2).

^{13}C NMR (126 MHz, $CDCl_3$) δ: 12.74 (Ca), 50.41 (Cb), 112.26 (Ca'), 122.47 (C3), 144.66 (Cc), 150.86 (C4), 151.16 (C2), 151.16 (Cd), 163.97 (Ce).

HRMS (ESI): m/z(H^+): $[M+H]^+$ calculated = 218.0924, $[M+H]^+$ found = 218.0926.
IR ν(cm^{-1}): 2996.5, 2927.8, 2748.2, 2680.7, 1600.6, 1444.9, 14717.5, 1382.3, 1345.8, 1314.9, 1226.6, 1214.9, 1065.2, 1006.6, 912.7, 799.5, 764.9, 540.1, 483.4, 465.9, 408.4.

44) 4-(1N$_9$-methyladenine)pyridine (**A-Py**) (**T17**)[14]

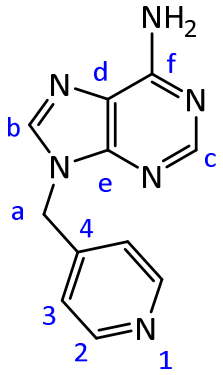

Chemical Formula: $C_{11}H_{10}N_6$
Molecular Weight: 226.24 g/mol

Adenine (0.39 g, 2.92 mmol, 2 eq), K_2CO_3 (0.51 g, 3.7 mmol, 2.5 eq) and KI (10 mg, catalytic amount) were mixed in 10 mL of dry degassed DMF. The suspension was degassed for 15 minutes. A solution of 4-(bromomethyl)pyridine (0.37 g, 1.46 mmol, 1 eq) in 2 mL of dry degassed DMF was added slowly to the suspension. The reaction mixture was stirred at 40 ºC overnight and followed by TLC. The crude was dried under vacuum, and then washed with a minimum amount of water (7 mL). The product was purified by column chromatography (SiO_2, MeOH: Et_3N: DCM 1:0.2:20) to give 177 mg of **A-Py** as a white solid (53 %).

^{1}H NMR (500 MHz, DMSO-d$_6$) δ (ppm): 5.43 (2H, s, Ha), 7.18 (2H, d, ^3J = 6.0 Hz, H3), 7.30 (2H, s, brd, NH_2 adenine), 8.12 (1H, s, Hb), 8.28 (1H, s, Hc), 8.51 (2H, d, ^3J = 6.0 Hz, H2).

^{13}C NMR (126 MHz, DMSO-d$_6$) δ: 45.14 (Ca), 118.67 (Cd), 122.05 (C3), 140.98 (Cb), 145.92 (Ce), 149.53 (C4), 149.96 (C2), 152.79 (Cc), 156.08 (Cf).

HRMS (ESI): m/z (H^+): $[M+H]^+$ calculated = 227.1040, $[M+H]^+$ found = 227.1025.

IR ν(cm^{-1}): 3309.0, 3086.8, 1647.0, 1571.6, 1596.0, 1484.8, 1415.5, 1389.0, 1356.1, 1326.5, 1246.5, 1155.32,1069.9, 1006.3, 970.5, 877.8, 796.0, 772.7, 726.0, 649.7, 852.7, 542.4, 464.8.

45) 4-(N_1-methylcytosine)pyridine (**C-Py**) (**T18**)[15]

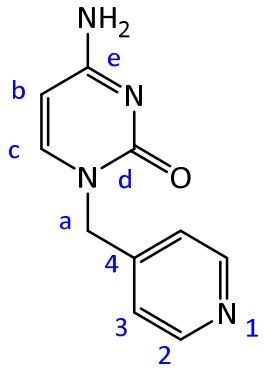

Chemical Formula: $C_{10}H_{10}N_6O$
Molecular Weight: 202.22 g/mol

Cytosine (0.65 g, 5.93 mmol, 3 eq) and KI (10 mg, catalytic amount) were mixed in 10 mL of dry DMF and degassed for 15 minutes. To the suspension, NaH (0.118 g, 4.9 mmol, 2.5 eq) was added and stirred for 30 minutes. A solution of 4-(bromomethyl)pyridine (0.5g, 1.97 mmol, 1 eq) in 2 mL of dry degassed DMF was added slowly to the mixture. The reaction mixture was stirred at 40 ^oC overnight and followed by TLC. The crude was dried under vacuum, and then washed with a minimum amount of water (10 mL). The product was purified by column chromatography (silica gel, MeOH: Et_3N: DCM 1:0.2:20) to yield 120 mg of **C-Py** as a white solid (30 %).

^1H NMR (500 MHZ, DMSO-d_6) δ (ppm): 4.87 (2H, s, Ha), 5.73 (1H, d, ^3J = 7.2 Hz, Hb), 7.08 (1H, s, brd, NH cytosine) 7.17 (2H, d, ^3J = 6.0 Hz, H3), 7.21 (1H, s, brd, NH cytosine), 7.69 (1H, d, ^3J = 7.2 Hz, Hc), 8.50 (2H, d, ^3J = 6.0 Hz, H2).

^{13}C NMR (126 MHZ, DMSO-d_6) δ (ppm): 50.61 (Ca), 93.90 (Cb), 122.01 (C3), 146.12 (Cc), 146.97 (C4), 149.67 (C2), 155.73 (Cd), 166.15 (Ce).

HRMS (ESI): m/z (H^+): $[M+H]^+$ calculated = 203.0927, $[M+H]^+$ found = 203.0934.
IR v(cm^{-1}): 3337.2, 3115.4, 1652.0, 1597.7, 1486.1, 1423.2, 1384.4, 1369.7, 1278.9, 1208.1, 1130.3, 965.3, 815.9, 781.6, 704.4, 682.8, 567.6, 521.4, 474.6, 405.4.

46) 4-(N_9-methyl-2-amino-6-chloropurine)pyridine (**P-Py**) (**T19**)[15]

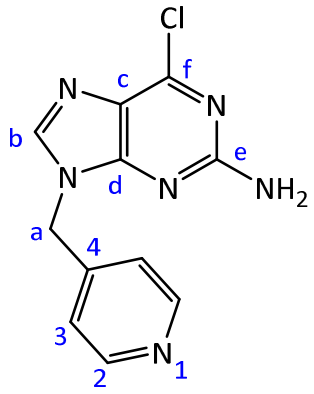

Chemical Formula: $C_{11}H_9N_6Cl$
Molecular Weight: 260.69 g/mol

2-amino-6-chloropurine (0.8 g, 4.74 mmol, 2 eq), K_2CO_3 (0.81 g, 5.90 mmol, 2.5 eq) and KI (10 mg, catalytic amount) were mixed in 10 mL of dry degassed DMF. The suspension was degassed for 15 minutes. A solution of 4-(bromomethyl)pyridine (0.6 g, 2.37 mmol, 1 eq) in 2 mL of dry degassed DMF was added slowly to the suspension. The reaction mixture was stirred at 40 ºC overnight and followed by TLC. The crude was dried under vacuum and then washed with a minimum amount of water (10 mL). The product was purified by column chromatography (silica gel, MeOH: Et_3N: DCM 1:0.2:20) to give 185 mg of **P-Py** a white pure solid (30 %).

^{1}H NMR (400 MHz, DMSO-d_6) δ (ppm): 5.36 (2H, s, Ha), 6.92 (2H, s, brd, NH_2 purine), 7.18 (2H, d, ^3J = 5.9 Hz, H3), 8.24 (1H, s, Hb), 8.51 (2H, d, ^3J = 6.0 Hz, H2).

^{13}C NMR (126 MHz, $CDCl_3$) δ: 45.97 (Ca), 121.93 (C3), 125.13 (Cd), 141.94 (Ce), 144.17(C4), 150.64 (C2), 151.88 (Cc), 153.93 (Ce), 159.46 (Cf).

MS (ESI): m/z (M+): $[M+H]^+$ calculated = 261.06, $[M+H]^+$ found = 261.07.

IR ν(cm^{-1}): 3314.9, 3196.5, 2920.7, 1613.8, 1563.8, 1524.5, 1408.7, 1282.4, 1176.0, 1024.2, 999.6, 913.6, 761.9, 720.1.

47) 4-(N_9-methylguanine)pyridine (**G-Py**) (**T20**) [15]

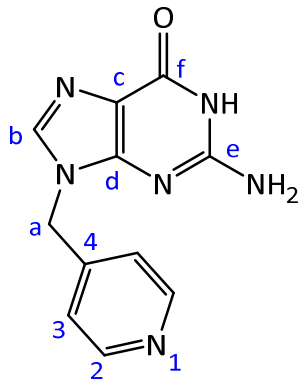

Chemical Formula: $C_{11}H_{10}N_6O$
Molecular Weight: 242.24 g/mol

P-Py (100 mg, 0.384 mmol, 1 eq) was dissolved in 20 mL of 0.1 M HCl aqueous solution. The reaction was stirred under reflux and followed by TLC. The reaction was left to stir for 5 hours until all 2-amino-6-chloropurine was oxidized into guanine. Then, 0.1 M NaOH solution was added dropwise to neutralize the solution (*ca.* 5 mL). The white precipitate was then filtered, washed with water (10 mL) and acetone (10 mL) and dried under reduced pressure to give 89 mg of **G-Py** as a white solid (96 %).

^{1}H NMR (500 MHz, DMSO-d_6) δ (ppm): 5.24 (2H, s, Ha), 6.74 (2H, s, brd, NH_2 guanine), 7.11 (2H, d, ^3J = 5.6 Hz, H2), 7.79 (1H, s, Hb), 8.51 (2H, d, ^3J = 5.6 Hz, H3), 10.94 (1H, s, brd, NH guanine).

^{13}C NMR (126 MHz, DMSO-d_6) δ: 44.79 (Ca), 116.59 (Cc), 121.66 (C3), 137.48 (Cb), 146.24 (C4), 149.93 (C3), 151.33 (Cd), 154.23 (Ce), 157.05 (Cf).

HRMS: m/z(M+): $[M+H]^+$ calculated = 243.0989, $[M+H]^+$ found = 243.0991.

IR ν(cm^{-1}): 3314.4, 1672.9, 1552.1, 1478.5, 1416.5, 1389.6, 1260.5, 1214.5, 1100.8, 775.9, 536.1.

48) 4'-(4-bromomethylphenyl)-2,2':6',2"-terpyridine (**Br-terPy**)[16]

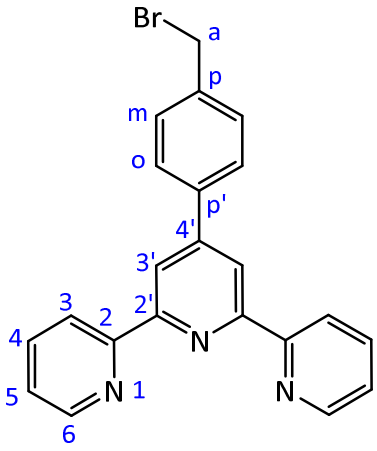

Chemical Formula: $C_{22}H_{16}BrN_3$
Molecular Weight: 402.30 g/mol

4'-p-tolyl-2,2':6',2"-terpyridine (0.5g, 1.55 mmol, 1 eq) and NBS (0.33g, 1.86 mmol, 1.2 eq) were dissolved in 24 mL of benzene. The reaction mixture was stirred for 3 hours under reflux and argon while illuminated by a 120 Watts lamp. The crude was evaporated under vacuum, diluted with 50 mL of DCM and then extracted twice with 50 mL of water. The organic phase was dried with $MgSO_4$, filtered and then evaporated under vacuum. The product was further washed with acetone to give 0.37 g of a white solid (60 %).

^{1}H NMR (400 MHz, $CDCl_3$) δ (ppm): 4.27 (2H, s, Ha), 7.36 (2H, ddd, ^3J = 7.4 Hz, 7.4 Hz, ^4J = 1.1 Hz, H5), 7.53 (2H, d, ^3J = 7.2 Hz, Hm), 7.88 (4H, m, Ho & H4), 8.66 (2H, d, ^3J = 7.4 Hz, H6), 8.74 (4H, m, H3 & H3').

49) 4'-(N_1-methylphenylthymine)-2,2':6',2''-terpyridine (**T-terPy**) (**T21**)[14]

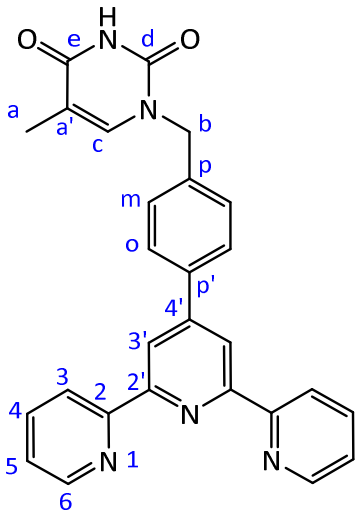

Chemical Formula: $C_{27}H_{21}N_5O_2$
Molecular Weight: 447.50 g/mol

Br-terPy (136 mg, 0.34 mmol, 1 eq), thymine (127 mg, 1.014 mmol, 3 eq) and K_2CO_3 (70.5 mg, 0.5 mmol, 1.5 eq) were mixed in 5 mL of dry DMF. The suspension was degassed for 15 minutes and stirred at 40 °C overnight. The crude was dried under vacuum and then diluted with 50 mL of DCM and extracted twice by 25 mL of water. The organic phase was dried over $MgSO_4$ then filtered and dried under vacuum. The product was purified by column chromatography (Al_2O_3, 2% MeOH in DCM) to yield 60 mg of **T-terPy** as a white solid (40 %).

^{1}H NMR (500 MHz, $CDCl_3$) δ (ppm): 1.91 (3H, d, ^4J = 1.1 Hz, Ha), 4.97 (2H, s, Hb), 7.01 (1H, q, ^4J = 1.1 Hz, Hc), 7.36 (2H, ddd, ^3J = 7.4 Hz, 7.4 Hz, ^4J = 1.1 Hz, H5), 7.44 (2H, d, ^3J = 8.2 Hz, Hm), 7.88 (2H, m, H4), 7.91 (2H, d, ^3J = 8.2 Hz, Ho), 8.28 (1H, s, brd, NH thymine), 8.67 (2H, d, ^3J = 7.4 Hz, H6), 8.72(4H, m, H3 & H3').

^{13}C NMR (126 MHZ, $CDCl_3$) δ(ppm): 12.57 (Ca), 50.81 (Cb), 111.55 (Ca'), 118.98 (C3'), 121.52 (C3), 124.08 (C5), 128.28 (Cm), 128.73 (Co), 137.07 (C4), 139.06, 139.72 (Cc), 149.30 (C6), 149.60, 151.01 (Cd), 156.20, 156.22, 163.76 (Ce).
HRMS: m/z(M+): $[M+H]^+$ calculated = 448.1752, $[M+H]^+$ found = 448.1759.

IR v(cm^{-1}): 2924.3, 2850.7, 1703.3, 1666.7, 1583.8, 1565.3, 1455.9, 1343.9, 1323.6, 1130.7, 1036.6, 1004.9, 936.0, 907.6, 732.5, 706.6, 602.0, 553.5, 404.3.

50) 4'-(N_9-methylphenyladenine)-2,2':6',2''-terpyridine (**A-terPy**) (**T22**)[14]

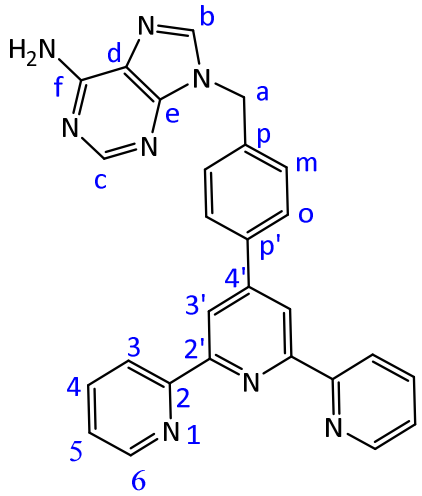

Chemical Formula: $C_{27}H_{20}N_8$
Molecular Weight: 456.51 g/mol

Br-terPy (140 mg, 0.348 mmol, 1 eq), adenine (94.5 mg, 0.70 mmol, 2 eq) and K_2CO_3 (72 mg, 0.522 mmol, 1.5 eq) were mixed in 5 mL of dry DMF. The suspension was degassed for 15 minutes and stirred at 40 °C overnight. The crude was dried under vacuum and then diluted with 50 mL of DCM and extracted twice with 25 mL of water. The organic phase was dried over $MgSO_4$ then filtered and dried under vacuum. The product was purified by column chromatography (Al_2O_3, 2% MeOH in DCM) to yield 86 mg of **A-terPy** as a white solid (54 %).

^{1}H NMR (400 MHz, $CDCl_3$) δ (ppm): 5.46 (2H, s, Ha), 5.60 (2H, s, brd, NH_2), 7.36 (2H, ddd, ^3J = 7.8 Hz, 7.5 Hz, ^4J = 1.1 Hz, H5), 7.44 (2H, d, ^3J = 8.2 Hz , Hm), 7.83 (1H, s, Hb), 7.89 (4H, m, Ho & H4), 8.43 (1H, s, Hc), 8.67 (2H, d, ^3J = 7.9 Hz, H6), 8.72 (4H, m, H3 & H3').

^{13}C NMR (126 MHz, $CDCl_3$) δ(ppm): 47.12 (Ca), 118.95 (C3'), 119.73 (Cd), 121.50 (C3), 124.06 (C5), 128.21 (Cm), 128.51 (Co), 136.40, 137.05 (C4), 137.05, 140.52 (Cb), 149.29 (C6), 149.57 (Ce), 150.44, 153.49 (Cc), 155.55 (Cf), 156.18, 156.23.

HRMS: m/z (M+): $[M+H]^+$ calculated = 457.1884, $[M+H]^+$ found = 457.1900.

IR v(cm^{-1}): 3092.3, 1649.3, 1600.4, 1584.8, 1567.7, 1479.3, 1467.6, 1438.4, 1410.1, 1390.2, 1353.0, 1323.6, 1302.4, 1245.6, 1114.9, 1077.9, 1039.4, 787.4, 770.0, 732.4, 688.7, 614.81, 551.6, 499.7.

51) 4'-(N_1-methylphenylcytosine)-2,2':6',2''-terpyridine (**C-terPy**) (**T23**)[15]

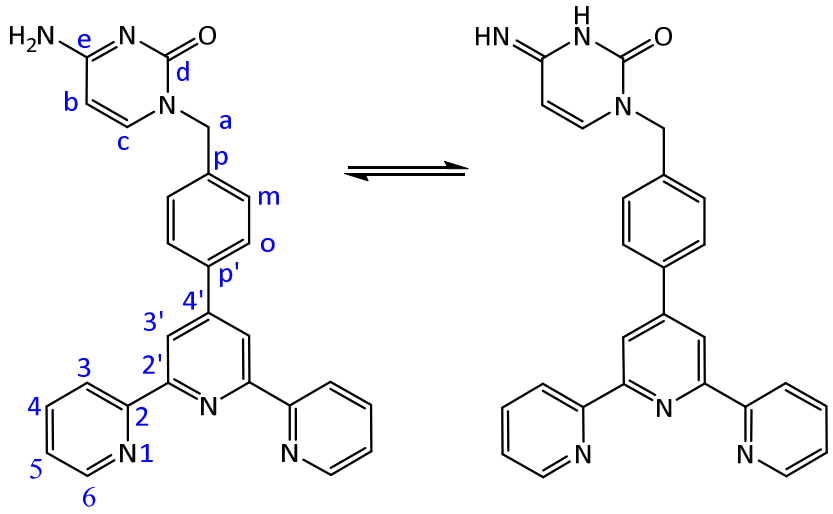

Chemical Formula: $C_{26}H_{20}N_6O$
Molecular Weight: 432.49 g/mol

Cytosine (329 mg, 2.97 mmol, 3 eq) and NaH (35 mg, 1.48 mmol, 1.5 eq) were dissolved in 10 mL of dry DMF, then degassed for 15 minutes. To the suspension, a solution of **Br-terPy** (400 mg, 0.99 mmol, 1 eq) in 2 ml of dry DMF was added drop wise. The reaction was stirred at 40 ºC overnight and followed by TLC. After the disappearance of **Br-terPy**, the mixture was dried under vacuum and then diluted with 50 mL DCM and extracted twice with 25 mL of water. The organic phase was dried over $MgSO_4$ then filtered and dried under vacuum. The product was purified by column chromatography (Al_2O_3, 2% MeOH in DCM) resulting in 330 mg of **C-terPy** as a white solid (79 %).

^{1}H NMR (400 MHz, DMSO-d_6) δ (ppm): 4.96 (2 H, s, Ha), 5.71 (1 H, d, ^3J = 7.2 Hz, Hb), 7.03 (1H, s, brd, NH cytosine), 7.10 (1H, s, brd, NH cytosine), 7.48 (2 H, d, ^3J = 8.1 Hz, Hm), 7.53 (2 H, ddd, ^3J = 7.2 Hz, 7.3 Hz, ^4J = 1.2 Hz, H5), 7.75 (1 H, d, ^3J = 7.2 Hz, Hc), 7.92 (2 H, d, ^3J = 8.1

Hz, Ho), 8.04 (2 H, ddd, ^{3}J = 7.9 Hz, 7.8 Hz, ^{4}J = 1.2 Hz, H4), 8.66 (2H, d, ^{3}J = 8.0 Hz, H6), 8.72 (4H, m, H3 & H3').

^{13}C NMR (126 MHZ, $CDCl_3$ + MeOD) δ(ppm): 52.01 (Ca), 95.07(Cb), 118.83 (C3'), 121.81 (C3), 124.12 (C5), 127.72 (Cm), 128.67 (Co), 137.25, 137.36 (C4), 138.07, 145.07 (Cc), 149.71, 155.87, 157.23 (C2), 157.23 (Cd), 165.86 (Ce).

HRMS: m/z (M+): $[M+H]^+$ calculated = 433.1771, $[M+H]^+$ found = 433.1733.
IR ν(cm^{-1}): 3133.2, 1610.3, 1583.9, 1567.1, 1516.9, 1488.9, 1466.1, 1358.5, 1265.8, 11863.8, 1038.5, 787.4, 729.2, 884.3, 689.6, 602.1, 538.9, 404.8.

52) 4'-(N_1-methylphenyl-2-amino-6-chloropurine)-2,2':6',2"-terpyridine (**P-terPy**)[15] (**T24**)

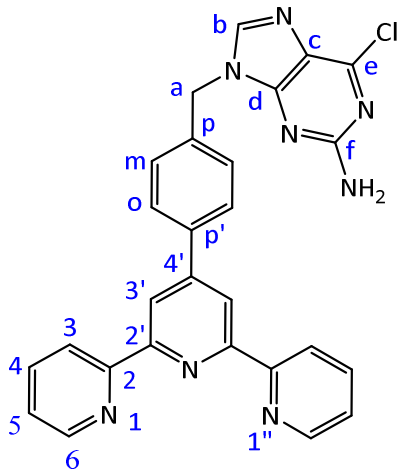

Chemical Formula: $C_{27}H_{19}N_8Cl$
Molecular Weight: 490.96 g/mol

2-amino-6-chloropurine (337.2 mg, 1.988 mmol, 2 eq) and K_2CO_3 (206 mg, 1.49 mmol, 1.5 eq) were dissolved in 15 mL of dry DMF and degassed for 15 minutes. To the suspension, a solution of **Br-terPy** (400 mg, 0.994 mmol, 1 eq) in 2 ml of dry DMF was added drop wise. The reaction was stirred at 50 °C overnight and followed by TLC. After the disappearance of **Br-terPy**, the crude was dried under vacuum and then washed with 10 mL of water. The product was then purified by column chromatography (Al_2O_3, 2% MeOH in DCM) to give 0.2 g of **G-terPy** as white solid (43 %).

^{1}H NMR (500 MHz, DMSO-d_6) δ (ppm): 5.41 (2H, s, Ha), 6.99 (2H, s, brd, NH_2 purine), 7.45 (2H, d, ^{3}J = 8.0 Hz, Hm), 7.46 (2H, ddd, ^{3}J = 7.1 Hz, 7.1 Hz, ^{4}J = 1.7 Hz, H5), 7.92 (2H, d, ^{3}J = 8.1 Hz, Ho), 8.04 (2H, ddd, ^{3}J = 7.2 Hz, 7.3 Hz, ^{4}J = 1.1 Hz, H4), 8.31 (1H, s, Hb), 8.66 (4H, d, ^{3}J = 8.05 Hz, H6), 8.67 (4H, m, H3 & H3').

^{13}C NMR (126 MHz, DMSO-d_6) δ(ppm): 45.87 (Ca), 117.95 (C3'), 21.02 (C3), 123.30 (Cc), 124.64 (C5), 127.42 (Cm), 128.15 (Co), 136.96, 137.56 (C4), 138.03, 143.35 (Cb), 149.05 (Cd), 149.41 (C6), 149.58, 154.19, 154.92 (C2), 155.74 (Ce), 160.01 (Cf).

HRMS (ESI): m/z (M+): $[M+H]^+$ calculated = 491.1494, $[M+H]^+$ found = 491.1495.

IR ν(cm^{-1}): 3478.0, 3306.3, 3178.3, 3086.0, 1629.0(C=N stretching), 160.6, 1584.6, 1562.1, 1515.0, 1460.4, 1406.1, 1389.5, 1345.5, 1277.2, 1218.2, 1137.9, 1115.7, 1036.4, 997.9, 939.1, 914.8, 879.5, 792.8, 784.1, 658.6, 594.6, 562.6, 529.2, 500.8, 409.2.

53) 4'-(N_1-methylphenylguanine)-2,2':6',2"-terpyridine (**G-terPy**)[15] (**T25**)

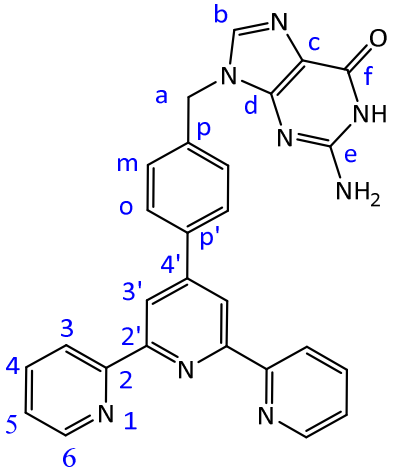

Chemical Formula: $C_{27}H_{20}N_8O$
Molecular Weight: 472.51 g/mol

P-terPy (0.1 g, 0.2 mmol, 1 eq) was dissolved in 20 mL of 0.1 M aqueous HCl solution and stirred at 100 °C under reflux overnight. The reaction was followed by TLC and then stopped when all the **P-terPy** was oxidized into **G-terPy**. To the reaction mixture, 0.1 M NaOH solution (3 mL) was added drop wise to neutralize the mixture. A white precipitate was formed, which was filtered and

washed with acetone (10 mL). The precipitate was dried under reduced pressure to give 90 mg of **G-terPy** as a white solid (96 %).

^{1}H NMR (500 MHz, DMSO-d_6) δ (ppm): 5.30 (2H, s, Ha), 6.56 (2H, s, brd, NH_2 guanine), 7.41 (2H, d, ^{3}J = 8.2 Hz, Hm,), 7.53 (2H, ddd, ^{3}J = 7.3 Hz, 7.3 Hz, ^{4}J = 1.0 Hz, H 5), 7.85 (1H, s, Hb), 7.91 (2H, d, ^{3}J = 8.2 Hz, Ho), 8.04 (2H, ddd, ^{3}J = 7.8 Hz, 7.7 Hz, ^{4}J = 1.7 Hz, H4), 8.66 (4H, d, ^{3}J = 7.95 Hz, H6), 8.72 (4H, m, H3 & H3'), 10.68 (1H, s, brd, NH guanine).

^{13}C NMR (126 MHz, $CDCl_3$) δ(ppm): 45.57 (Ca), 116.62 (Cc), 117.99 (C3') 121.07 (C3), 124.69 (C5), 127.39 (Cm), 128.08 (Co), 136.82, 137.62 (C4), 137.4 (Cb), 138.75, 149.16 (Cd), 149.45 (C6), 151.34, 153.86 (Ce), 154.96, 155.78 (C2), 156.91 (Cf).

HRMS (ESI): m/z (M+): $[M+H]^+$ calculated = 473.1833, $[M+H]^+$ found = 473.1830.

IR ν(cm^{-1}): 3177.7, 272.5, 1716.2 (C=O stretching), 1604.7, 1586.8, 1567.8, 1544.2, 1468.7, 1442.1, 1391.7, 1265.8, 1190.8, 1155.5, 1080.0, 1039.2, 864.2, 786.7, 764.7, 685.5, 680.4, 548.6, 503.0, 403.8.

References

1) Z. Fan, B. Liu, *Tetrahedron Lett.*, **2008**, *49*, 2311-2315.

2) D. Lahayde, K. Muthukumaran, C. H. Hung, D. Gryko, J. S. Reboucas, I. Spasojevic, I. Batinic-Haberle, J. S. Lindsey, *Bioorg. Med. Chem*, **2007**, *15*, 7066-7086.

3) (a) G. Hyslop, M. A. Kellett, P. M. Iovine, M. J. Therien, *J. Am. Chem. Soc*, **1998**, *120*, 1267-12677. (b) M. A. Bakar, N. N. Sergeeva, T. Juillard, M. O. Senge, *Organometallics*, **2011**, *30*, 3225-3228, (c) N. Aratani, A. Ouska, *Chem. Commun*., **2008**, 4067-4069.

4) F. Wu, M. G. Buhendwa, D. F. Weaver, *J. Org. Chem.* **2004**, *69*, 9307-9309.

5) C. H. Lee, J. S. Lindsey, *Tetrahedron*, **1994,** *50***,** 11427-11440.

6) G. Wilson, A. Scott, L. Harry, *Synlett*, **1996**, *11*, 1039-1040.

7) (a) A. Jiblaoui, C. Baudequin, V. Chaleix, G. Ducourthial, F. Louradour, Y. Ramondenc, V. Sol, S. L.-Lhez, *Tetrahedron*, **2013**, *69*, 5098-5103. (b) Y. Liang, Y. -X. Xie, J. -H. Li, *J. Org. Chem.* **2006**, *71*, 379-381. (c) Y. Liang, Y. -X. Xie, J.-H. Li, *J. Org. Chem.,* **2006**, *71*, 379-381. (d) A. Jiblaoui, C. Baudequin, V. Chaleix, G. Ducourthial, F. Louradour, Y. Ramondenc, V. Sol, S. Leroy-Lhez, *Tetrahedron*, **2013**, *69*, 5098-5103. (e) S. Rucareanu, O. Mongin, A. Schuwey, N. Hoyler, A. Gossauer, *J. Org. Chem.,* **2001,** *66,* 4973-4988.

8) N. Bilbao, V. Vazquez-Gonzalez, M. T. Aranda, D. Gonzalez-Rodriguez, *Eur. J. Org. Chem.,* **2015**, 7160-7175.

9) D. A. Roberts, T. W Schmidt, M. J. Crossley, S. Perrier, *Chem. Eur. J.,* **2013**, *19*, 12759-12770.

10) J. Laha, S. Dhanalekshmi, M. Taniguchi, A. Ambroise, J. Lindsey, *Org. Process Res. Dev.*, **2003***, 7*, 799-812.

11) (a) B. J. Littler, Y. Ciringh, J. S. Lindsey, *J. Org. Chem,* **1999**, *64*, 2864-2872. (b) G. R. Geier, B. J. Littler, J. S. Lindsey, *J. Chem. Soc., Perkin Trans. 2*, **2001**, 707-711.

12) (a) S. Ellipilli, K. N. Ganesh, *J. Org. Chem*., **2015**, *80*, 9185-9191. (b) A. Kiviniemi, M. Murtola, O. Ingman, P. Virta, *J. Org. Chem.*, **2013**, *78*, 5153-5159. (c) K. Pomeisl, A. Holy, R. Pohl, *Tetrahedron Letters*, **2007**, *48*, 3065-307.

13) (a) B. C. Brookser, T. C. Bruce*, J. Am. Chem. Soc.,* **1991**, *11,* 4208-4218. (b) D. A. Roberts, T. W. Schmidt, M. J. Crossley, S. Perrier, *Chem. Eur. J.,* **2013**, *19*, 12759-12770.

14) C. M. White, M. F. Gonzalez, D. A. Bardwell, L. H. Rees, J. C. Jeffery, M. D. Ward, N. Armaroli, G. Calogero, F. Barigelleti, *J. Chem. Soc, Dalton Trans*, **1997**, 727-735.

15) N. Armaroli, F. Barigelleti, G. Calogero, L. Flamigni, C. M. White, *Chem. Commun*., **1997**, 2181-2182.

16) J. P. Collin, A. Jouaiti, J. P. Sauvage, *J. Electroanal Chem.,* **1990**, *286*, 75-87.

Annex

Zn(II) [5,15 -di(N_1-(benzylhydry)uracil)- 10,20-dipentylporphyrin] (**T1**)

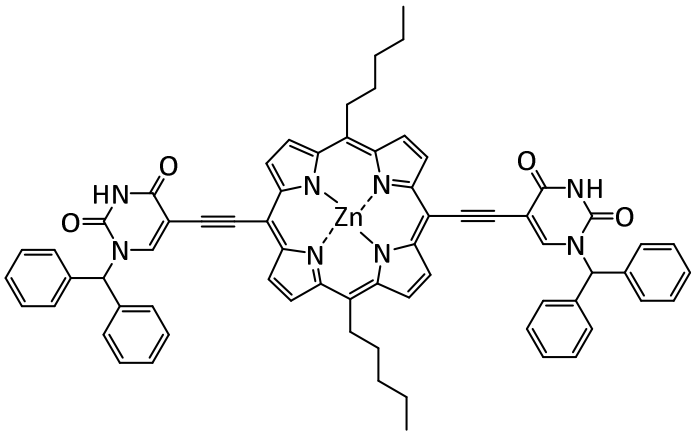

^{1}H NMR (300 MHz, $CDCl_3$ + MeOD)

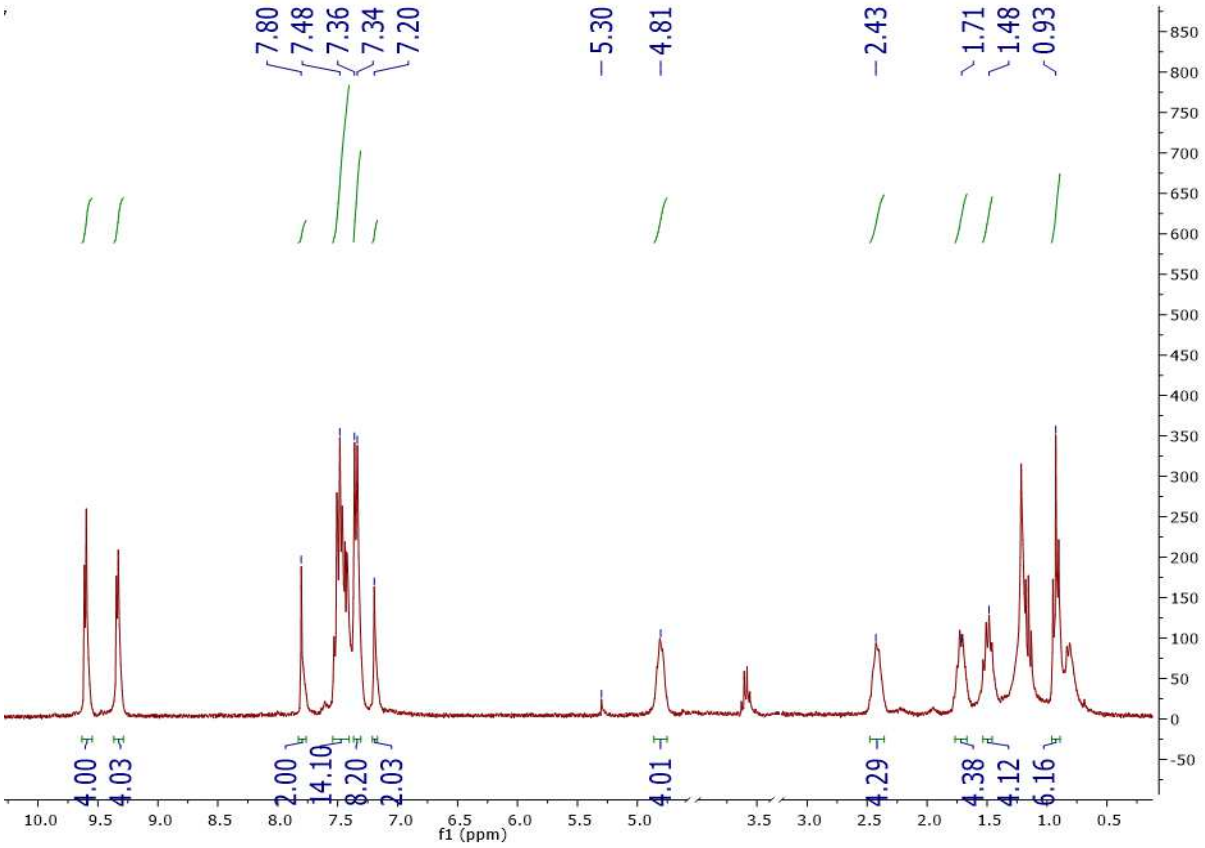

^{13}C NMR (126 MHz, $CDCl_3$ + MeOD)

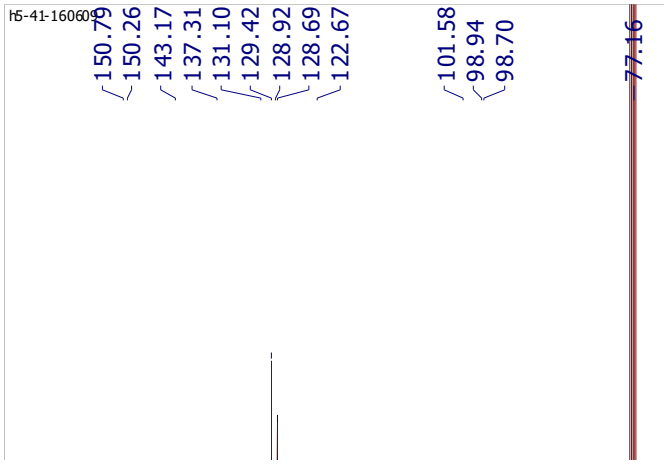

MS

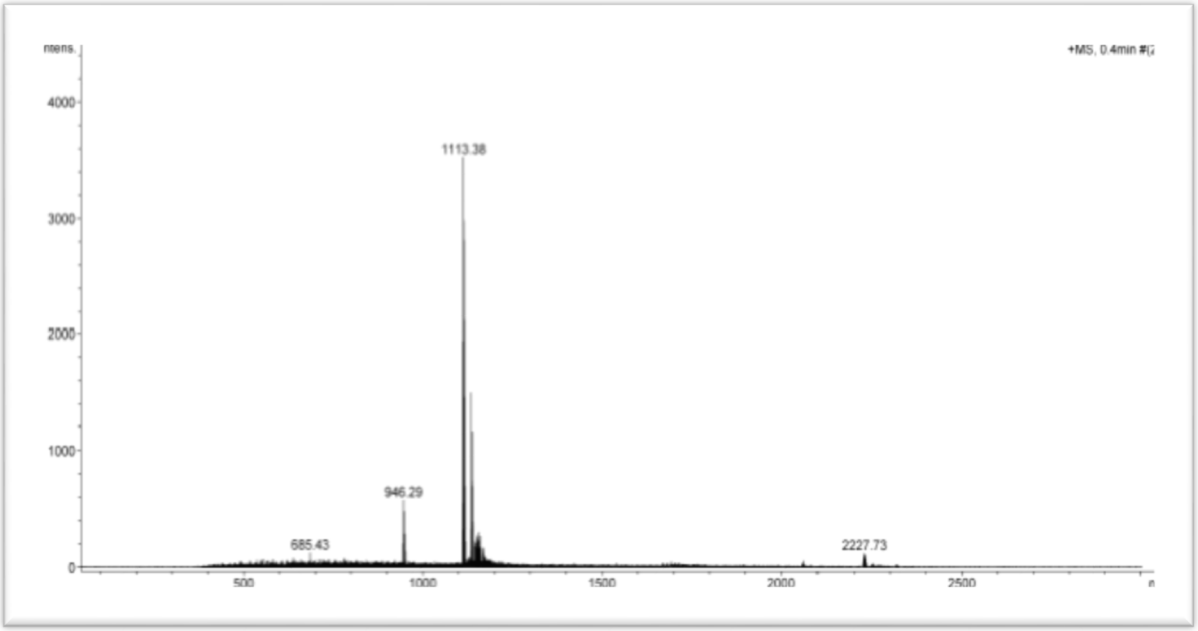

5,15-di(uracil)- 10,20-dipentylporphyrin (**T2**)

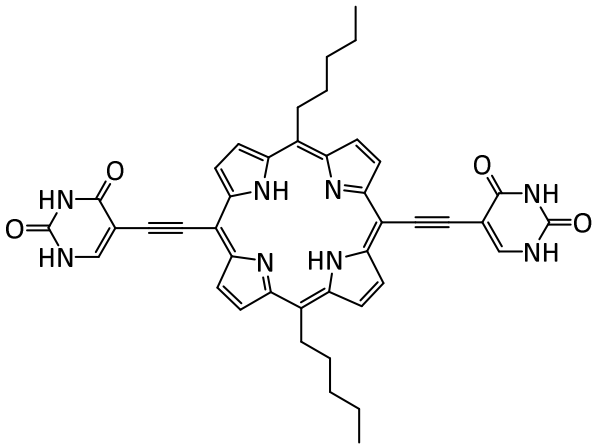

HRMS

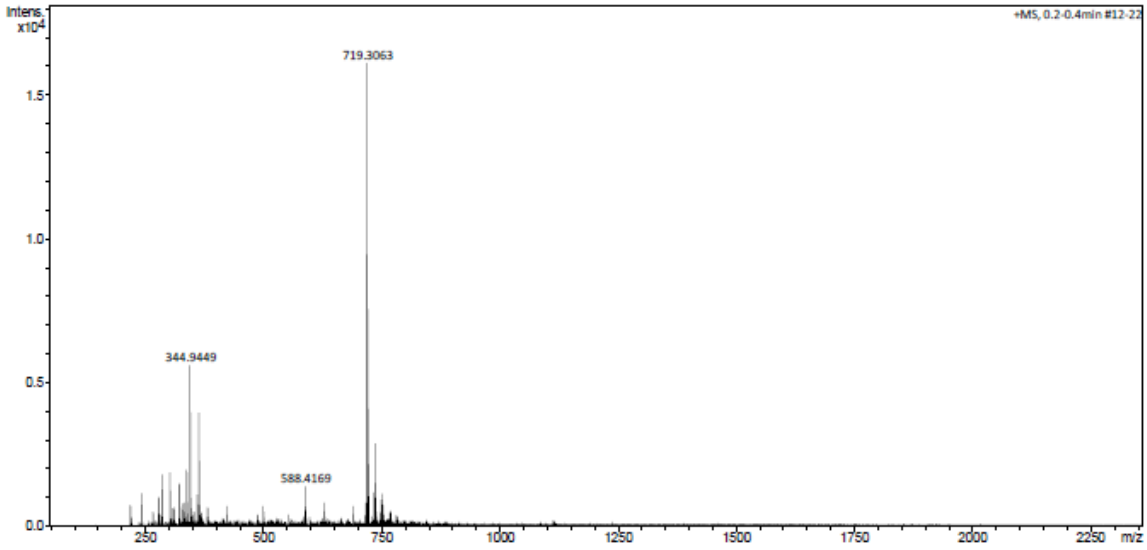

Zn(II) [5, 15-di(N_1-hexyluracil)-10,20-dipentylporphyrin] (**T3**)

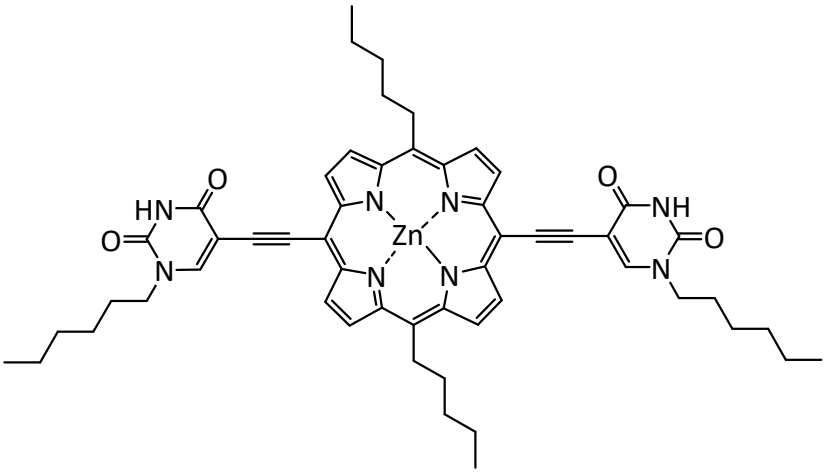

^{1}H NMR (300 MHz, $CDCl_3$)

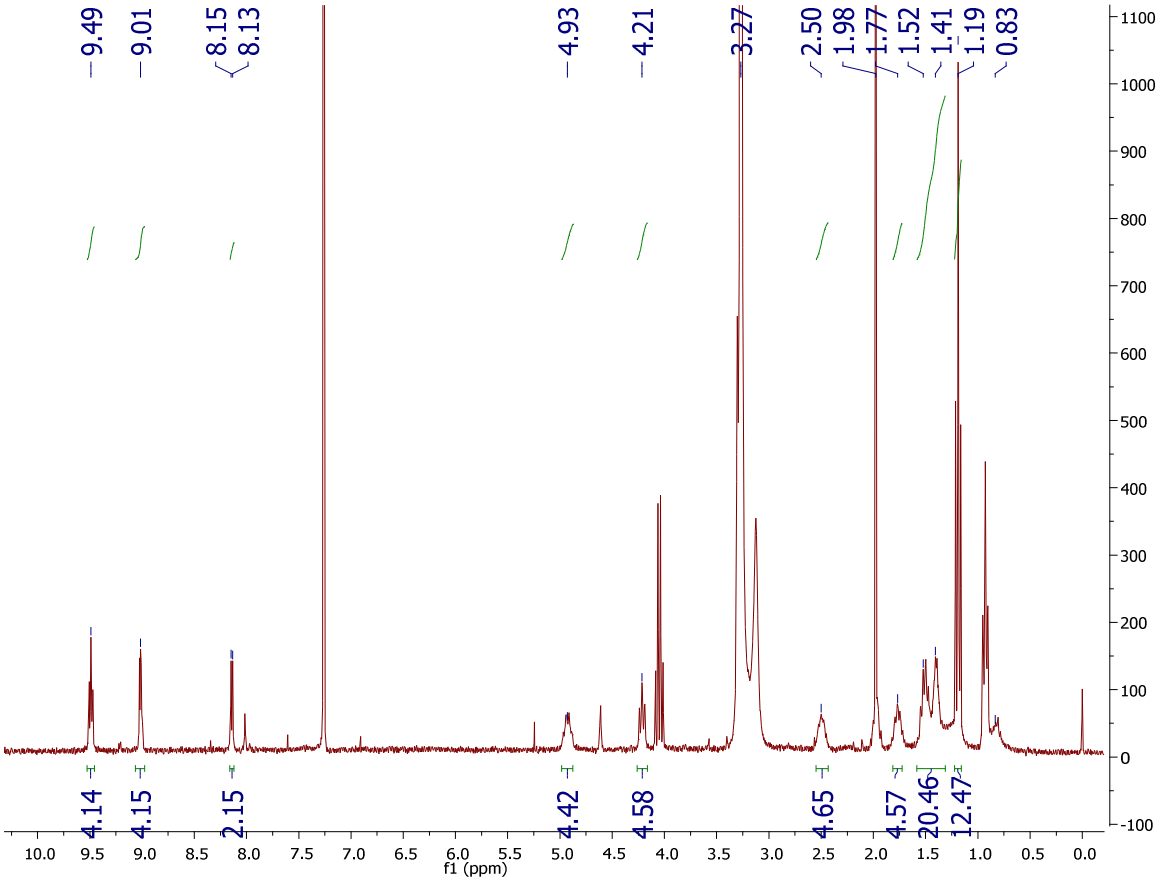

5-(N_1-methylphenylthymine)10,15,20-triphenylporphyrin (**T4**)

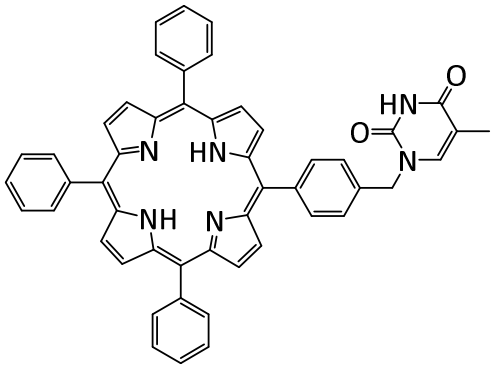

^{1}H NMR (500 MHz, $CDCl_3$)

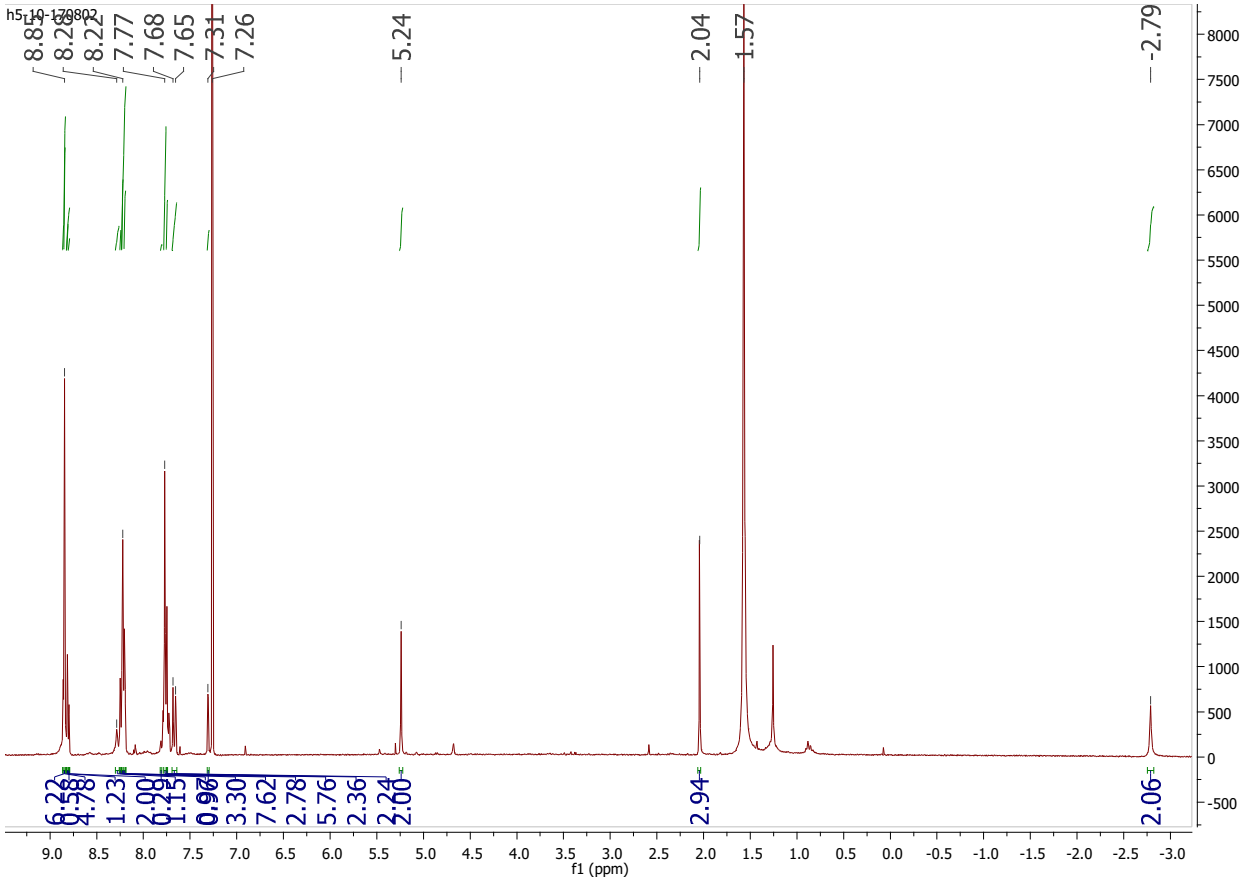

^{13}C NMR (126 MHz, $CDCl_3$)

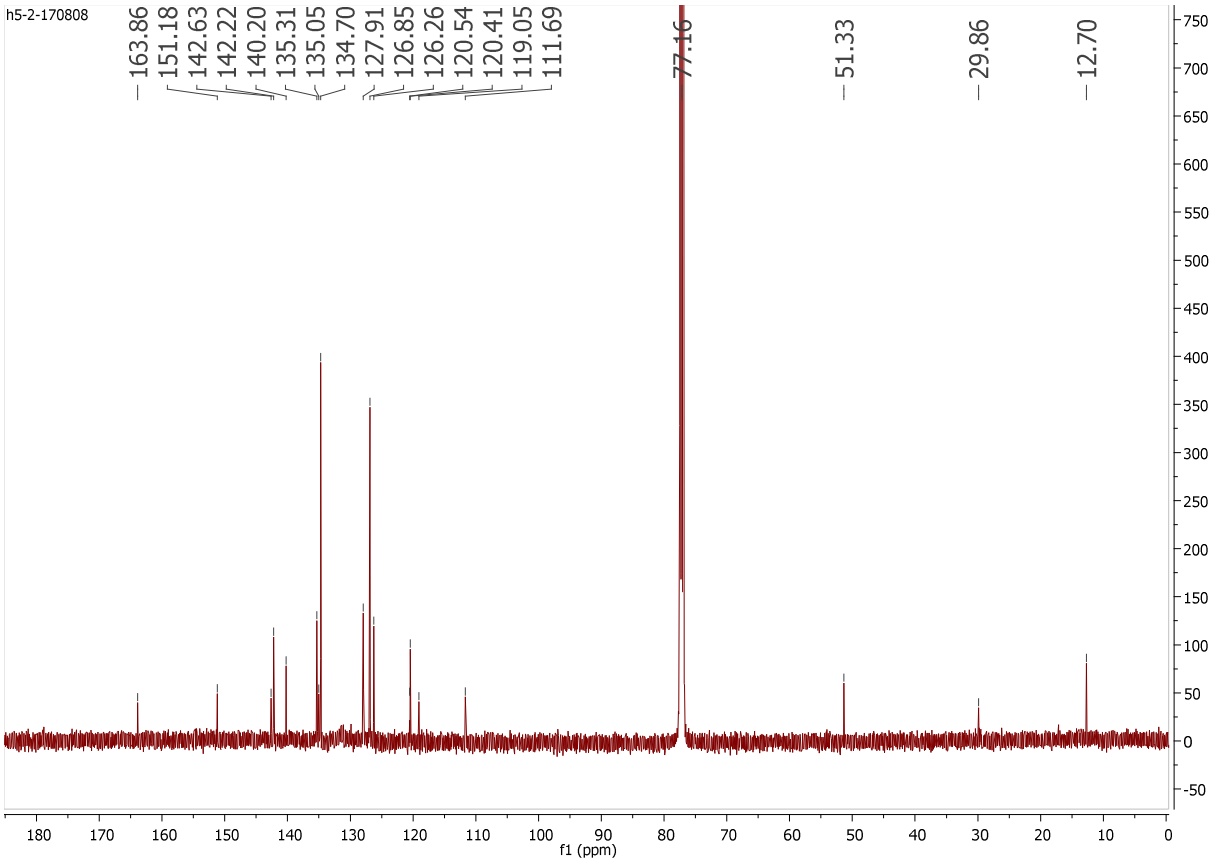

HRMS

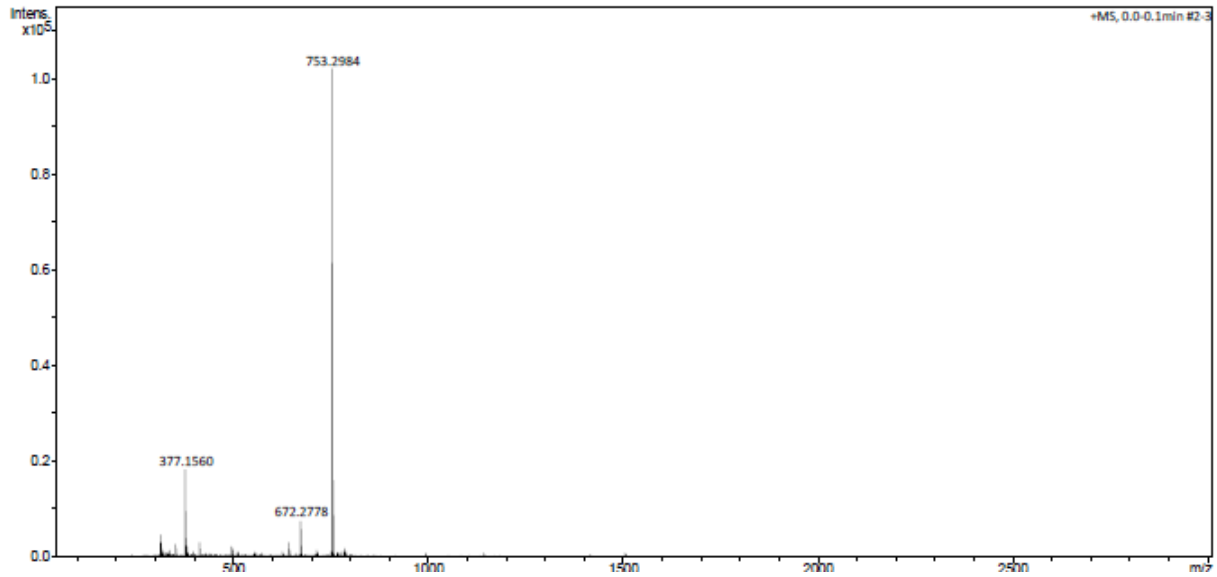

5,15-bis(N_1-methylphenylthymine)-10,20-dimesitylporphyrin (**T5**)

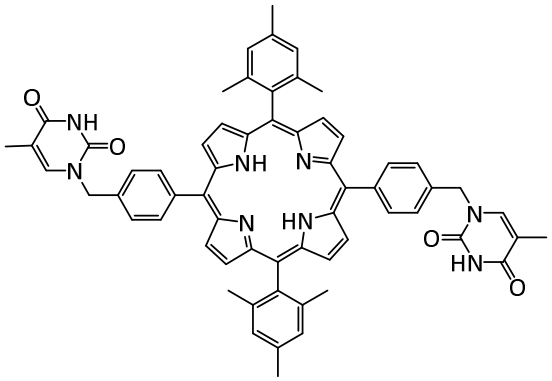

^{1}H NMR (400 MHz, DMSO-d_6)

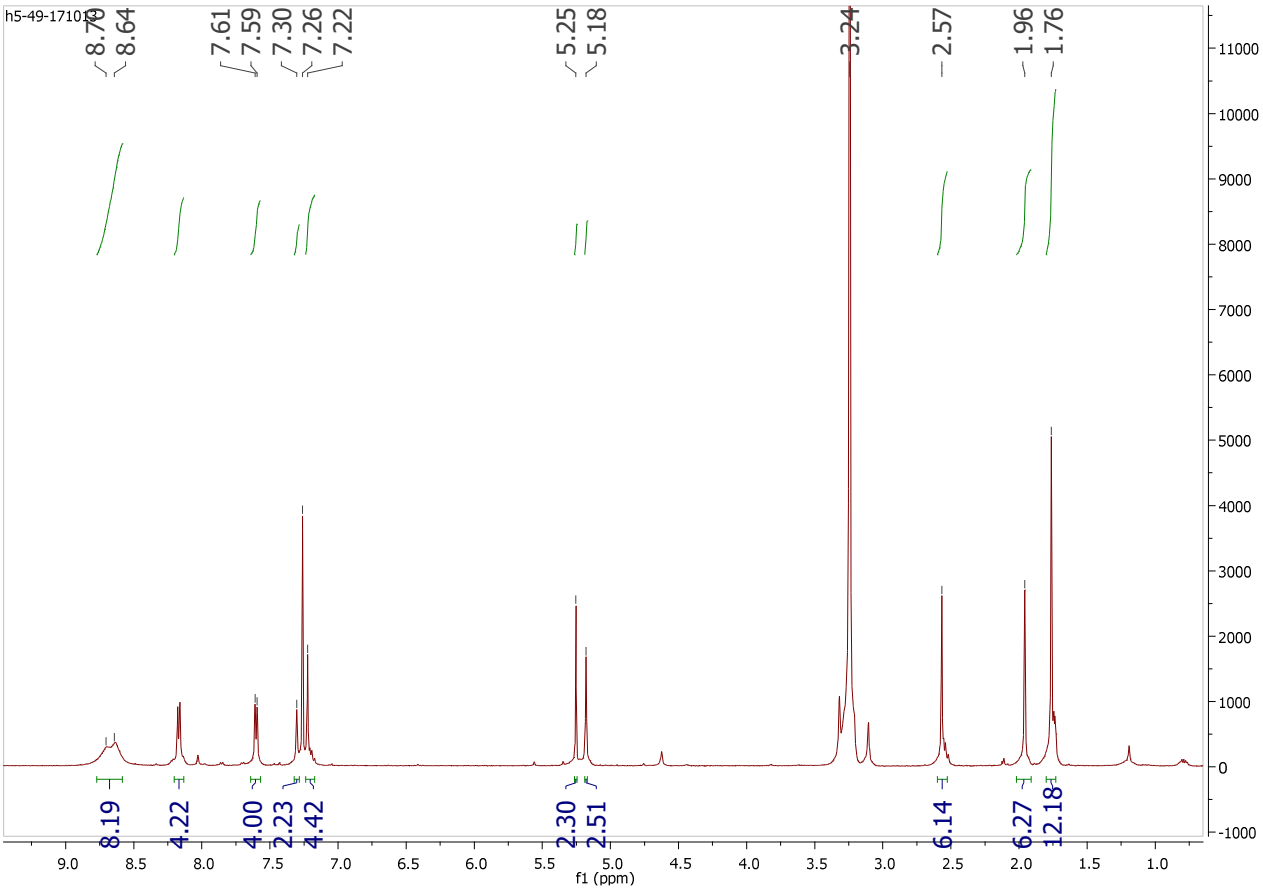

^{13}C NMR (126MHz, $CDCl_3$ + MeOD)

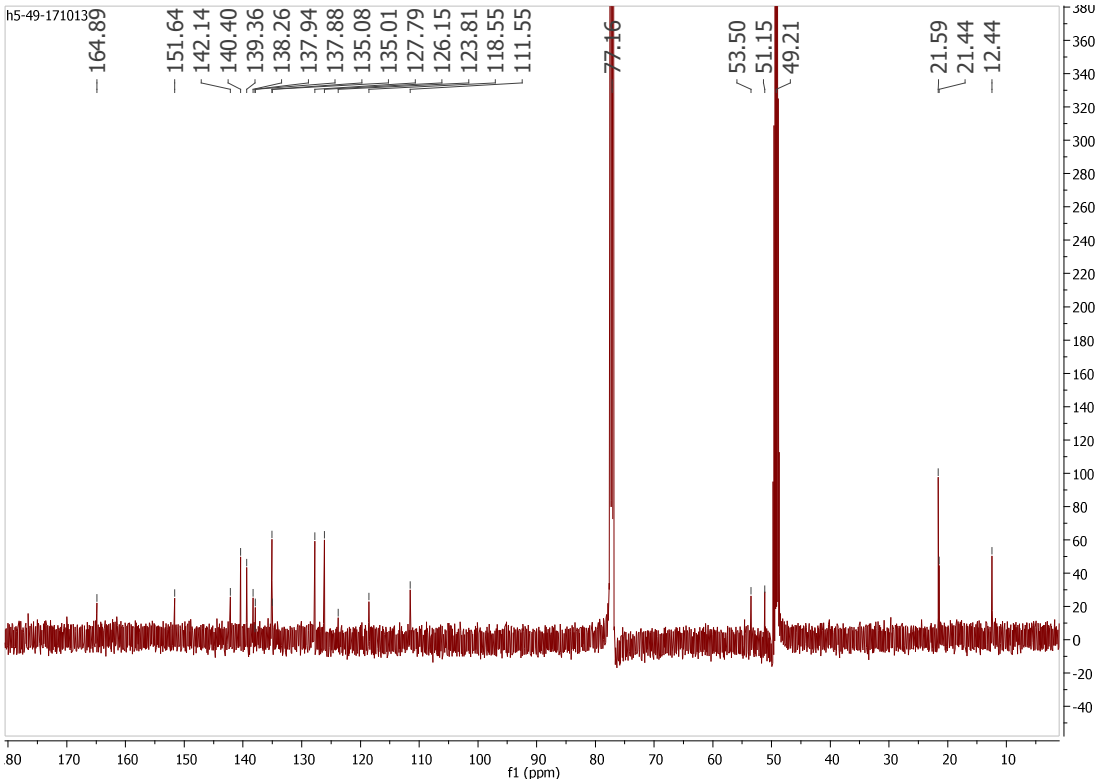

HRMS:

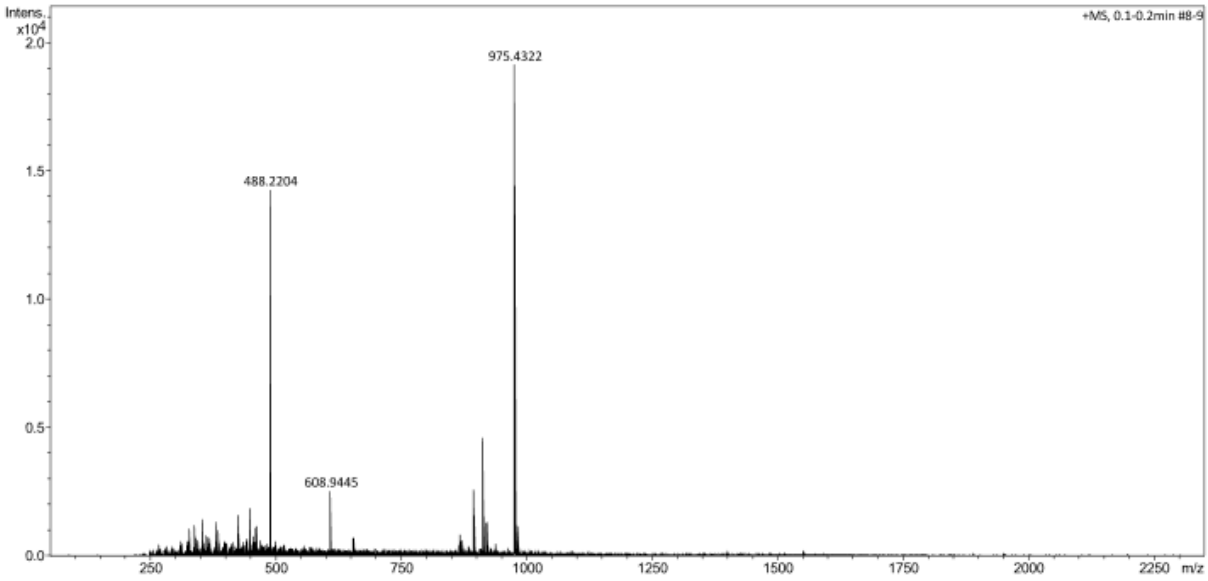

5,15-bis(N_9-methylphenyladenine)-10,20-dimesitylporphyrin (**T6**)

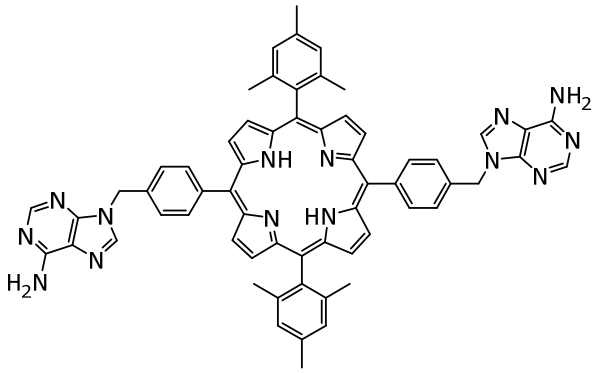

^{1}H NMR (500 MHz, $CDCl_3$ + MeOD)

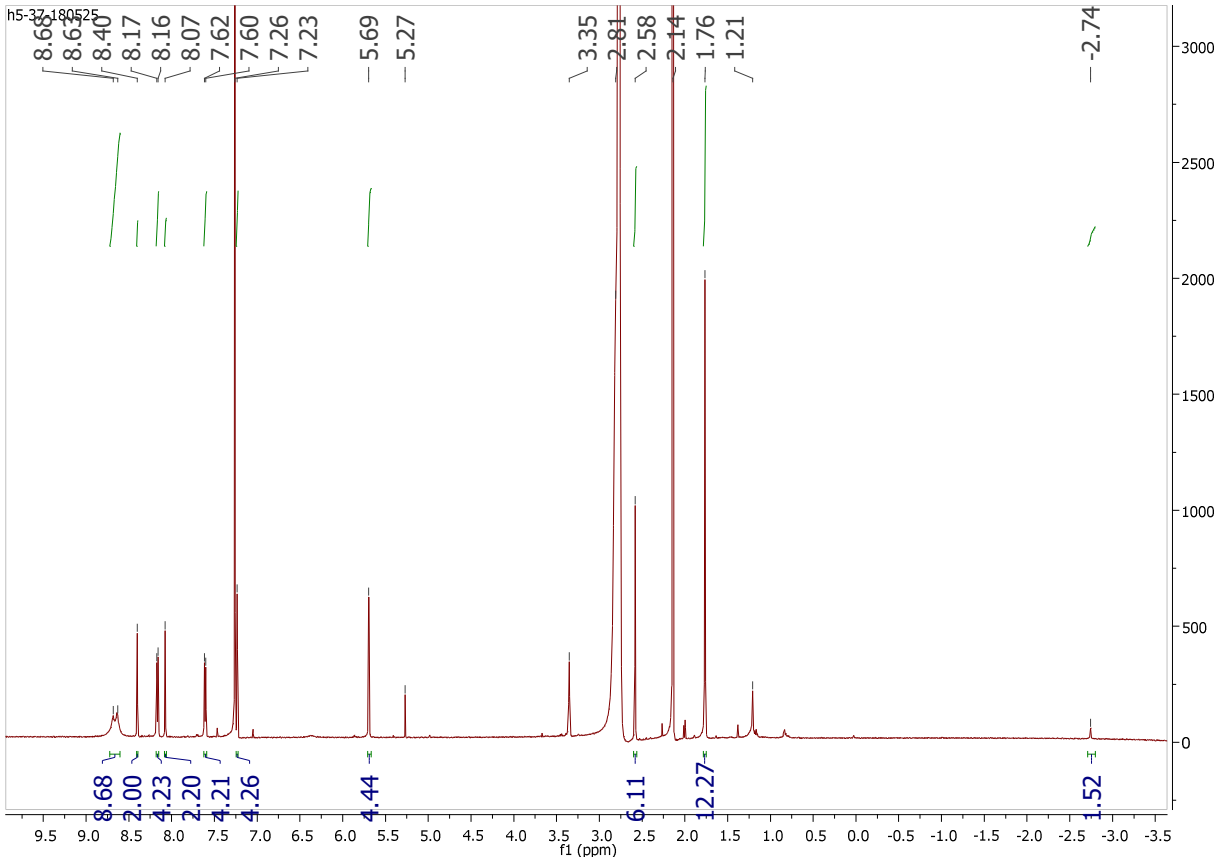

^{13}C NMR (126MHz, $CDCl_3$ + MeOD)

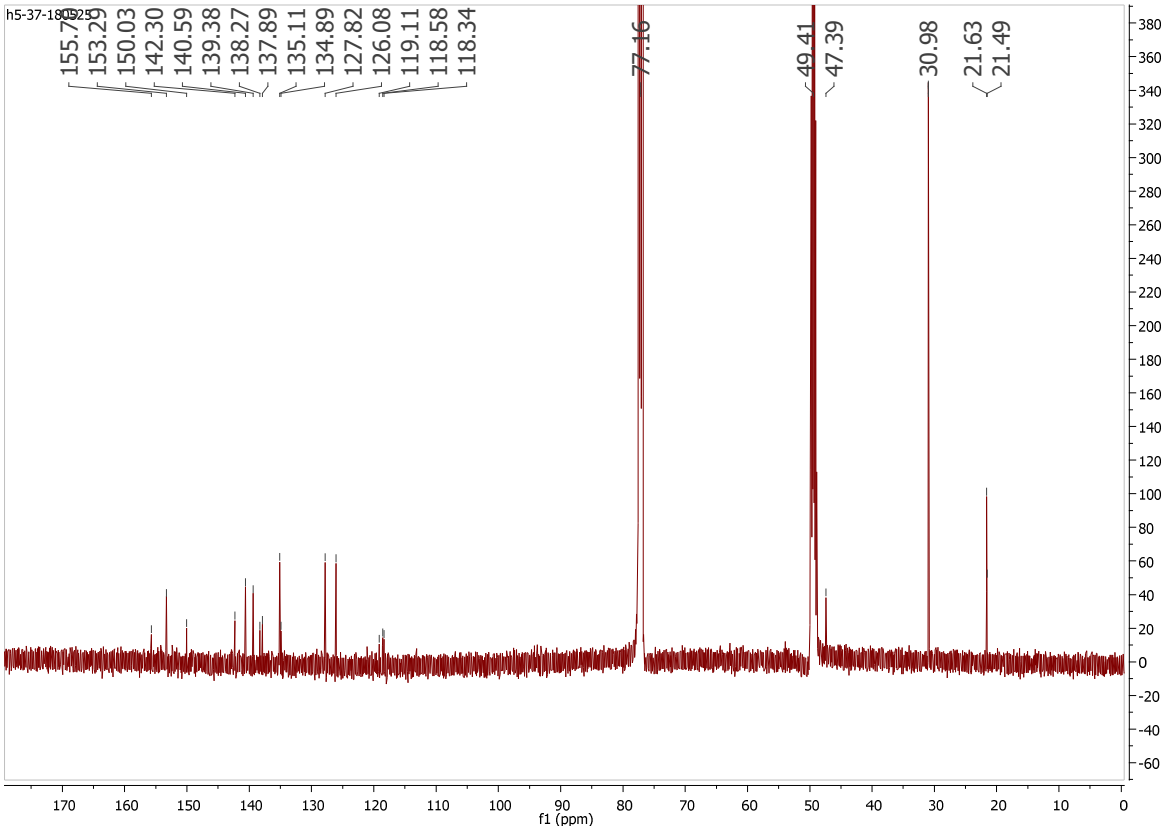

HRMS

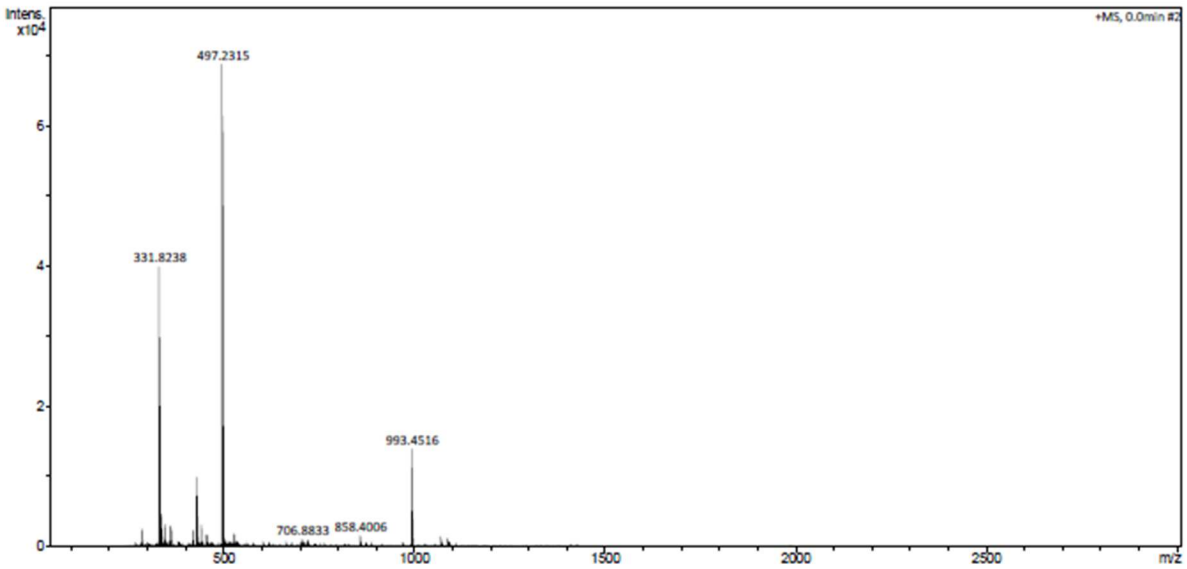

5,15-bis(N_1-methylphenylcytosine)-10,20-dimesitylporphyrin (**T7**)

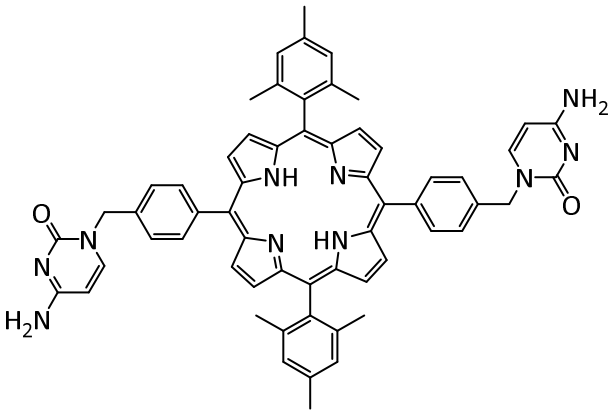

^{1}H NMR (400 MHz, DMSO-d_6)

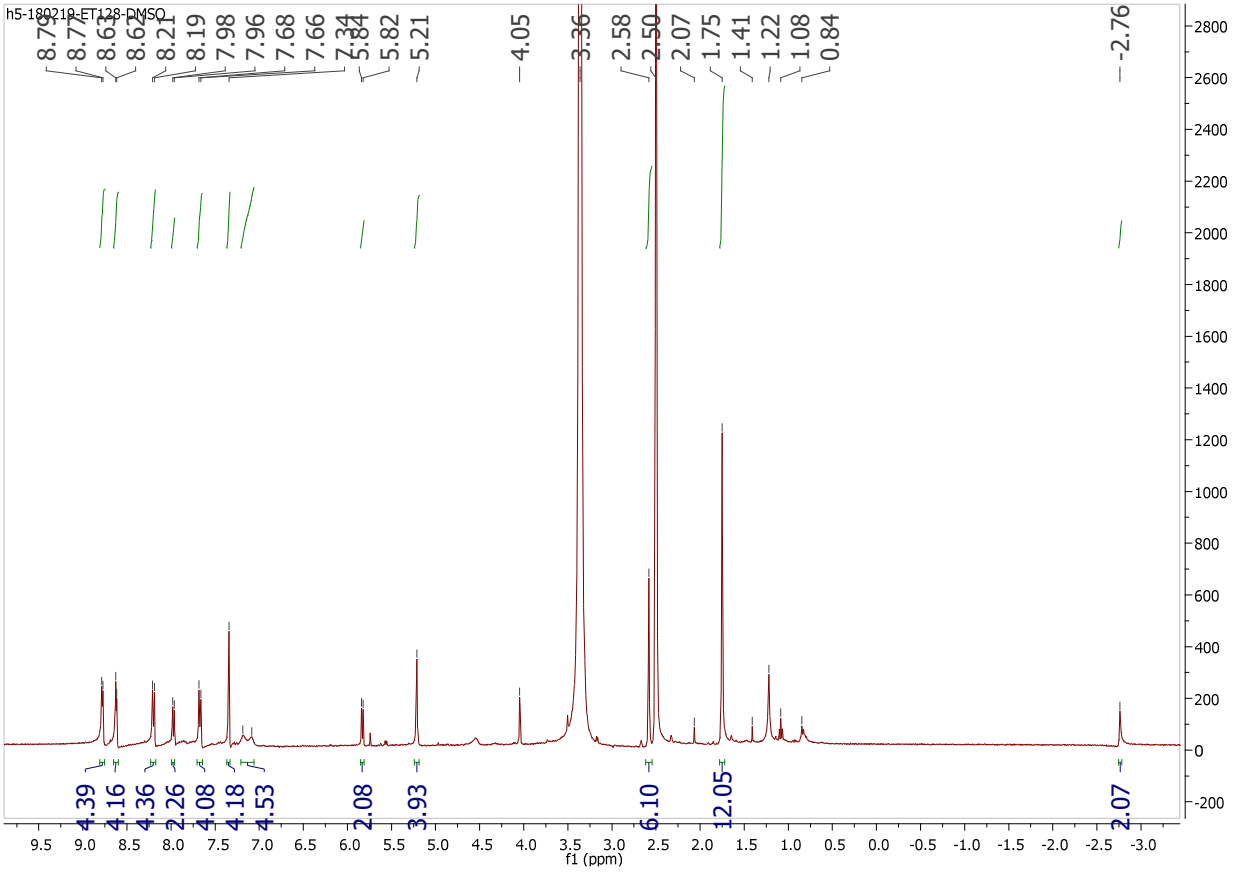

^{13}C NMR (126MHz, DMSO-d_6)

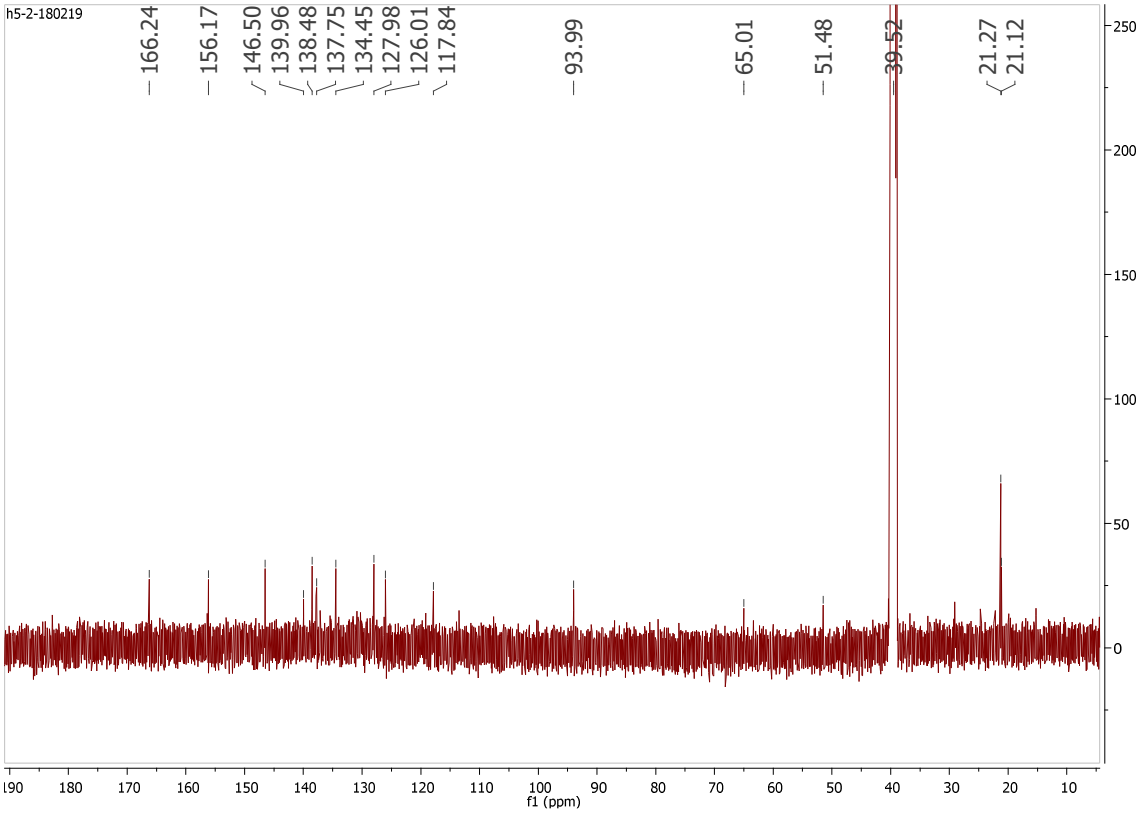

HRMS

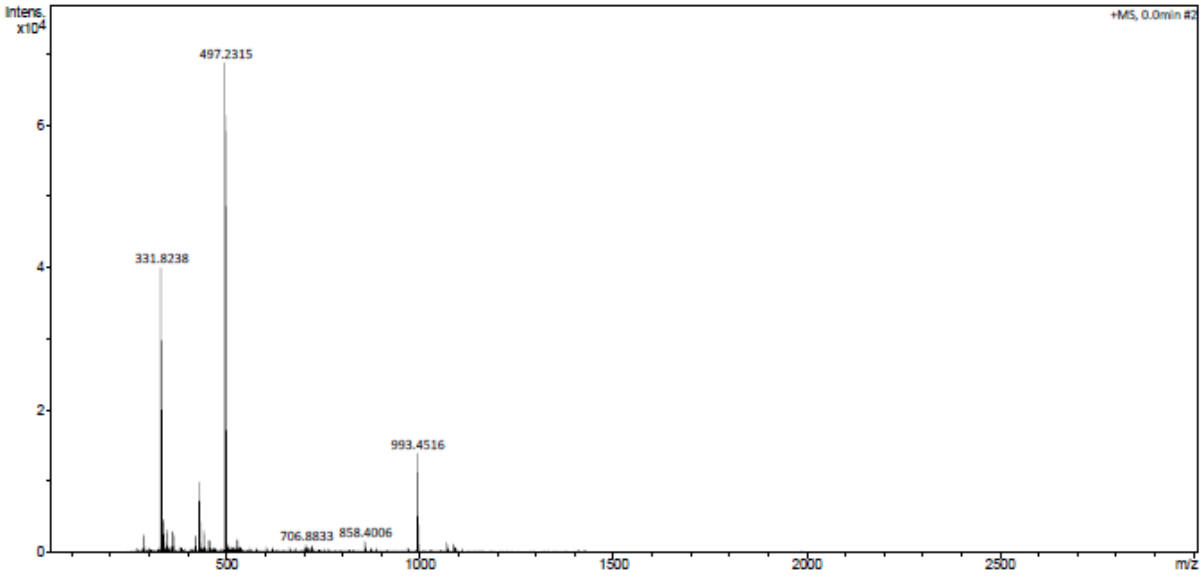

5,15-bis(N_9-methylphenyl-2-amino-6-chloropurine)-10,20-dimesitylporphyrin (**T8**)

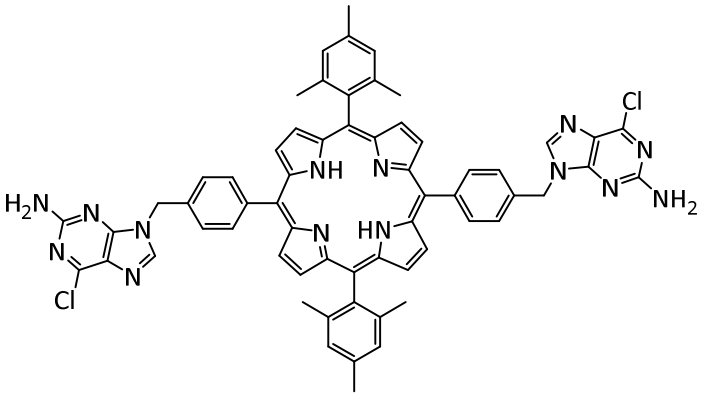

^{1}H NMR (500 MHz, $CDCl_3$)

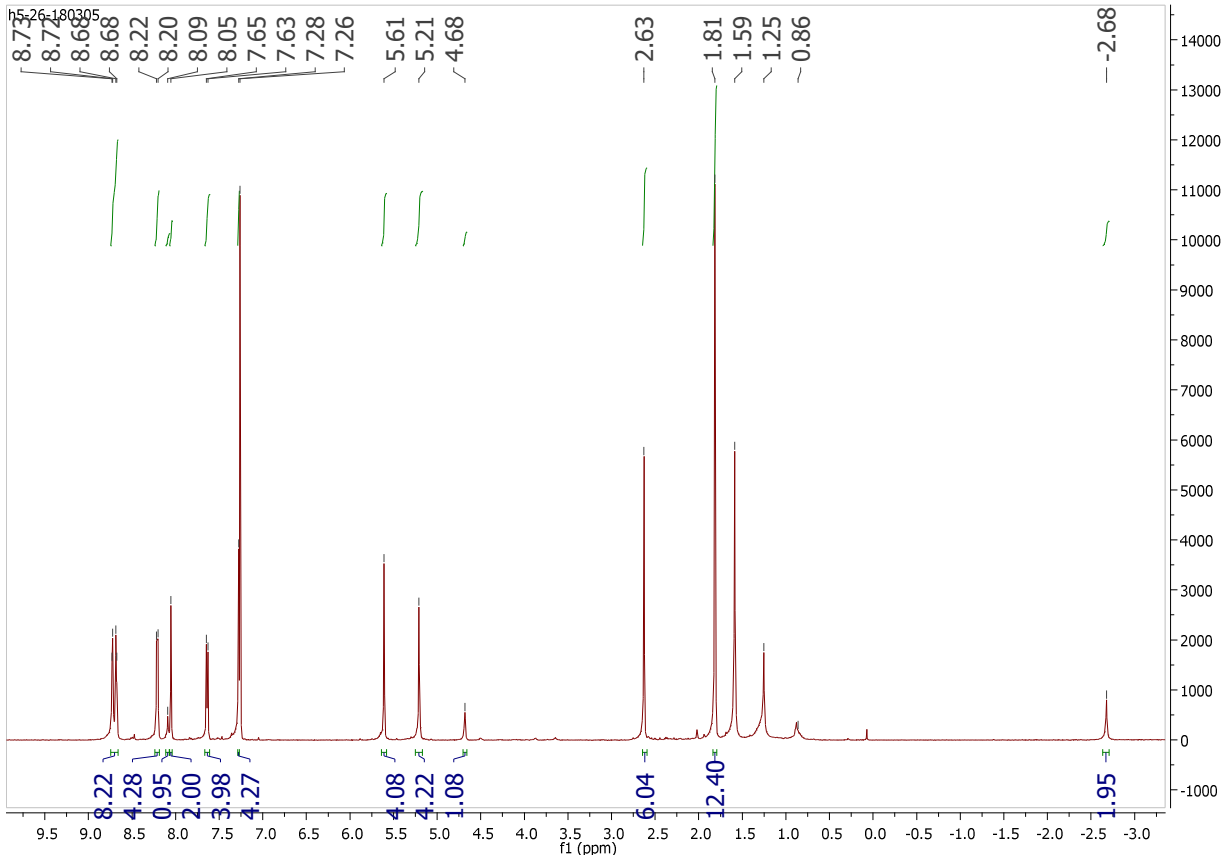

^{13}C NMR (126 MHz, $CDCl_3$ + MeOD)

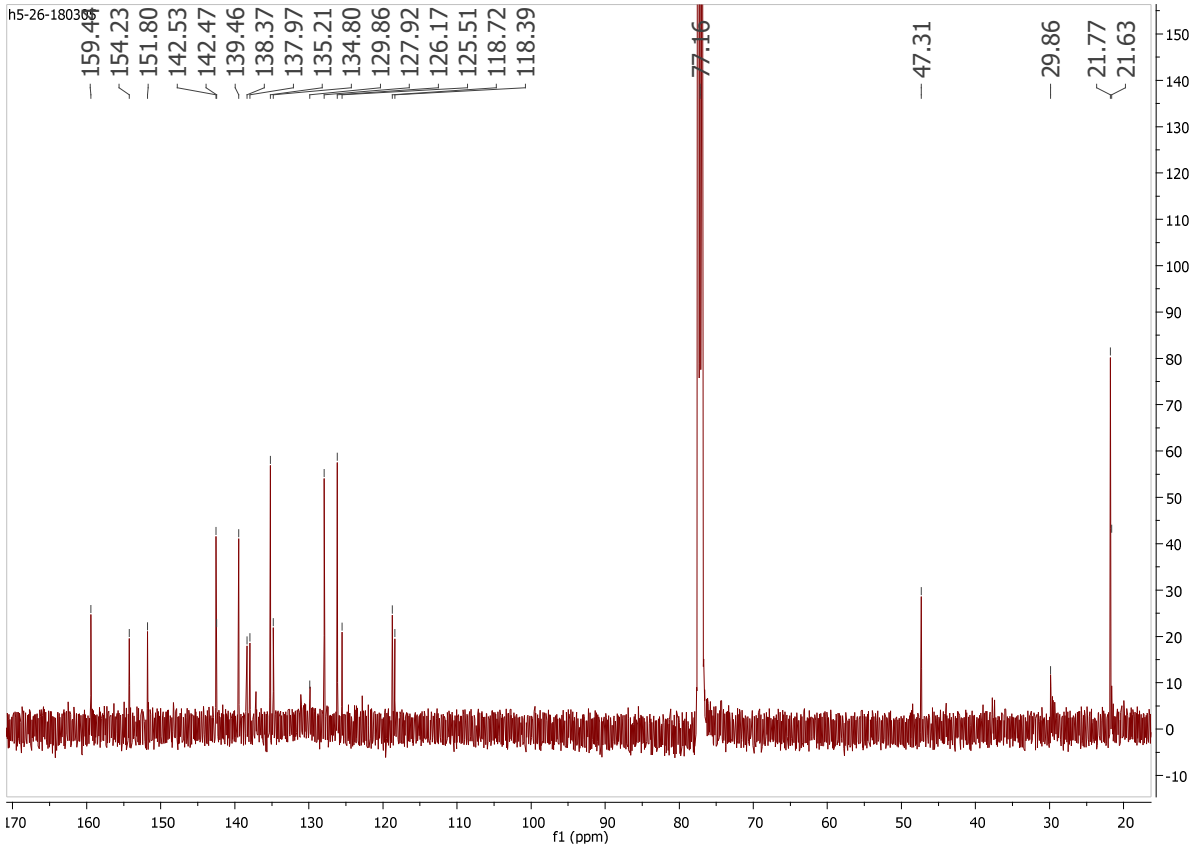

HRMS

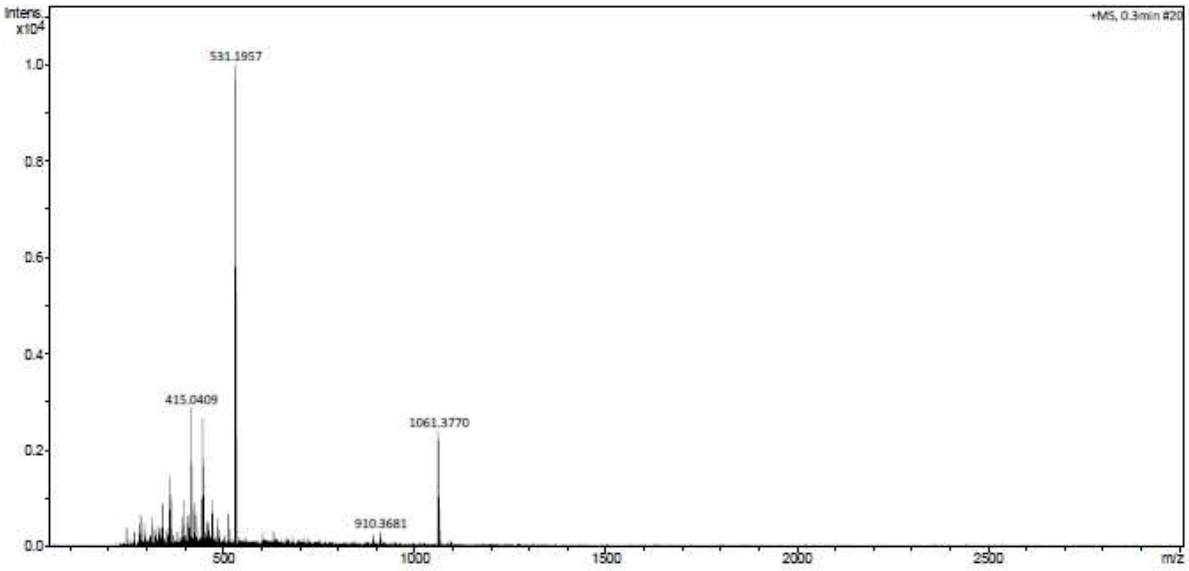

5,15-bis(N_9-methylphenylguanine)-10,20-dimesitylporphyrin (**T9**)

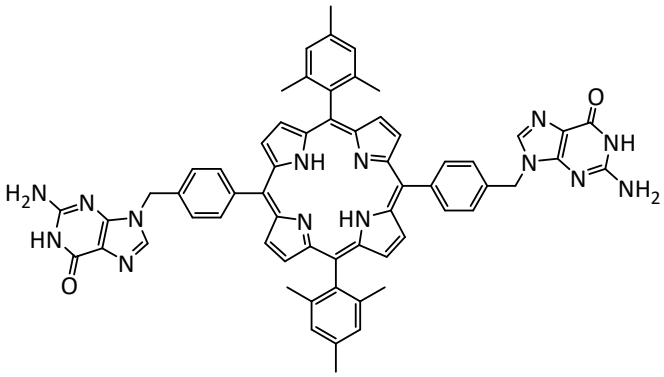

^{1}H NMR (500 MHz, DMSO-d_6)

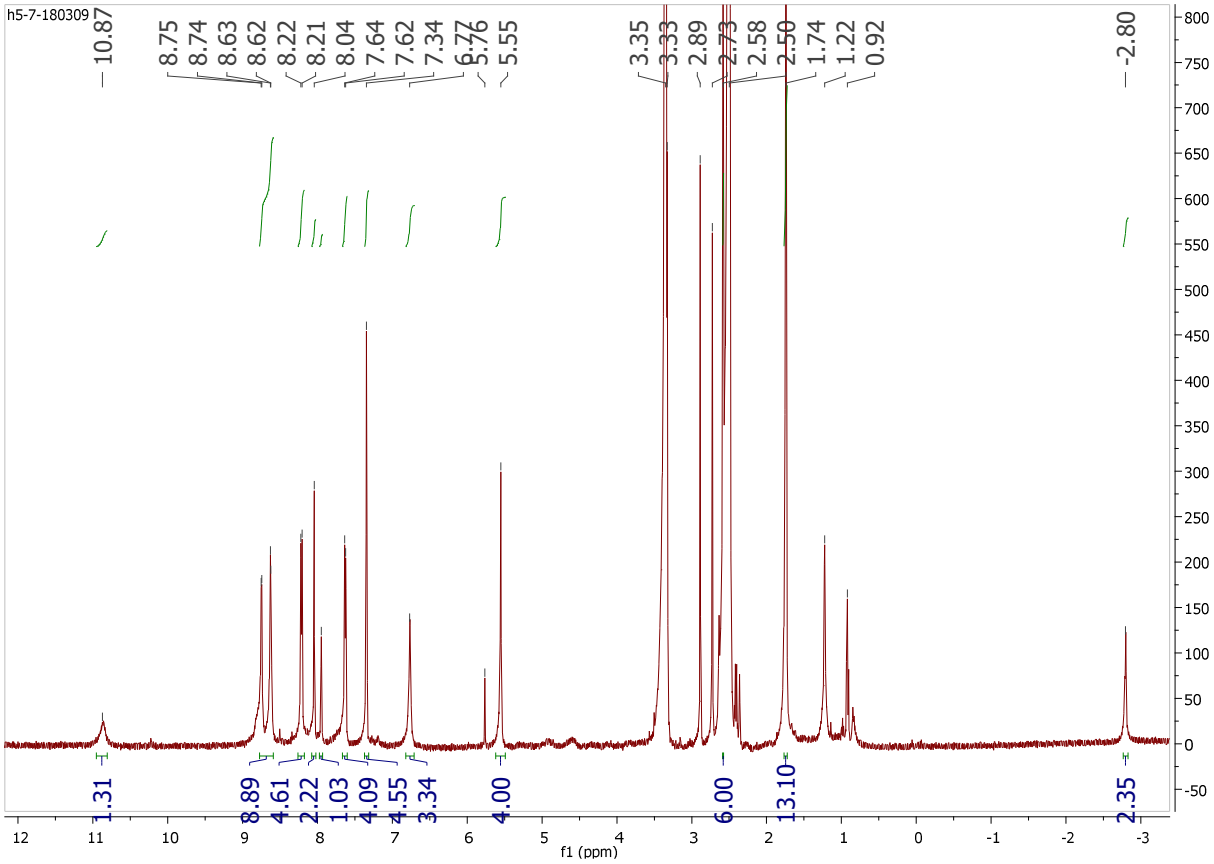

5,10,15,20-tetrakis(N_1-methylphenylthymine)porphyrin (**T10**)

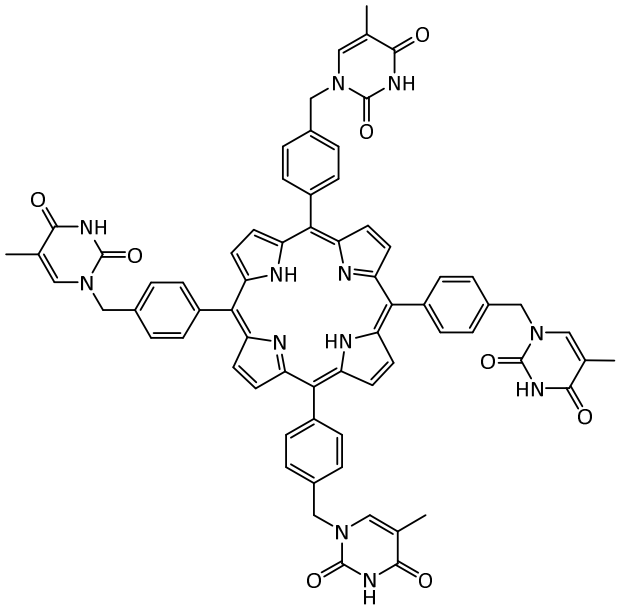

^{1}H NMR (400 MHz, $CDCl_3$)

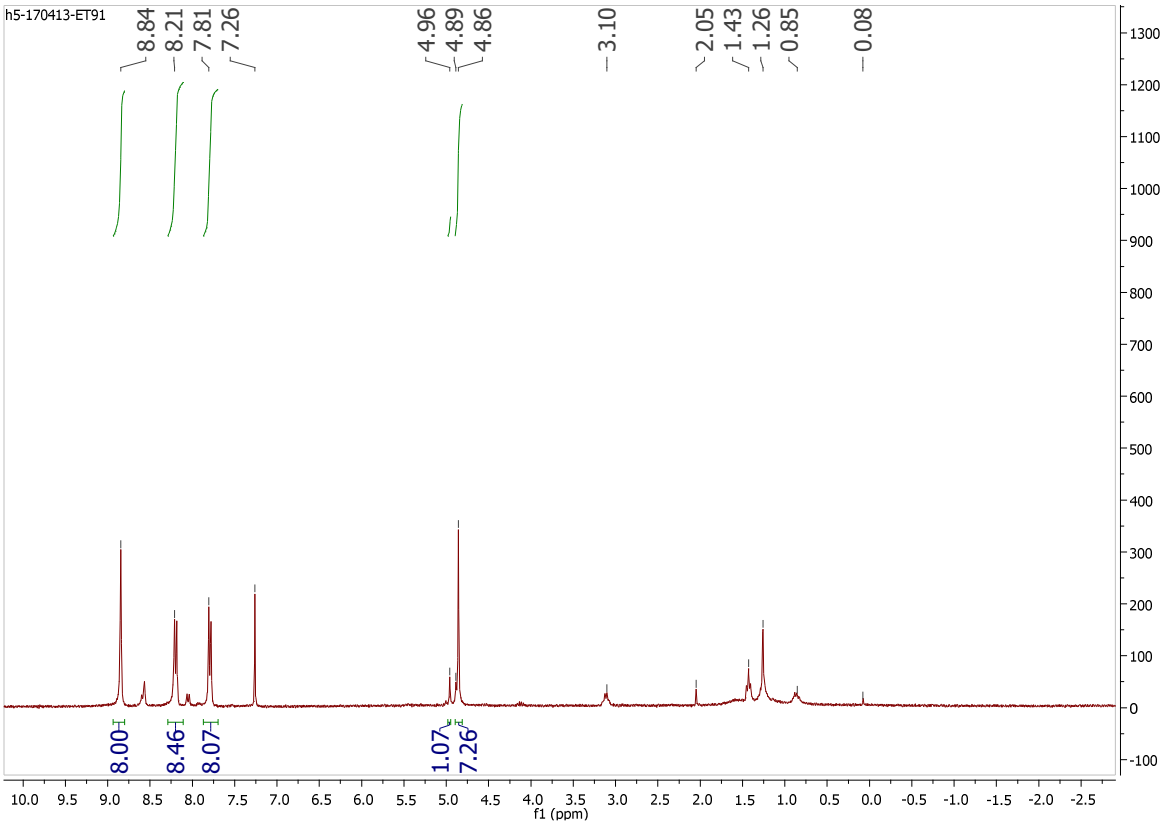

^{13}C NMR (126 MHz, $CDCl_3$)

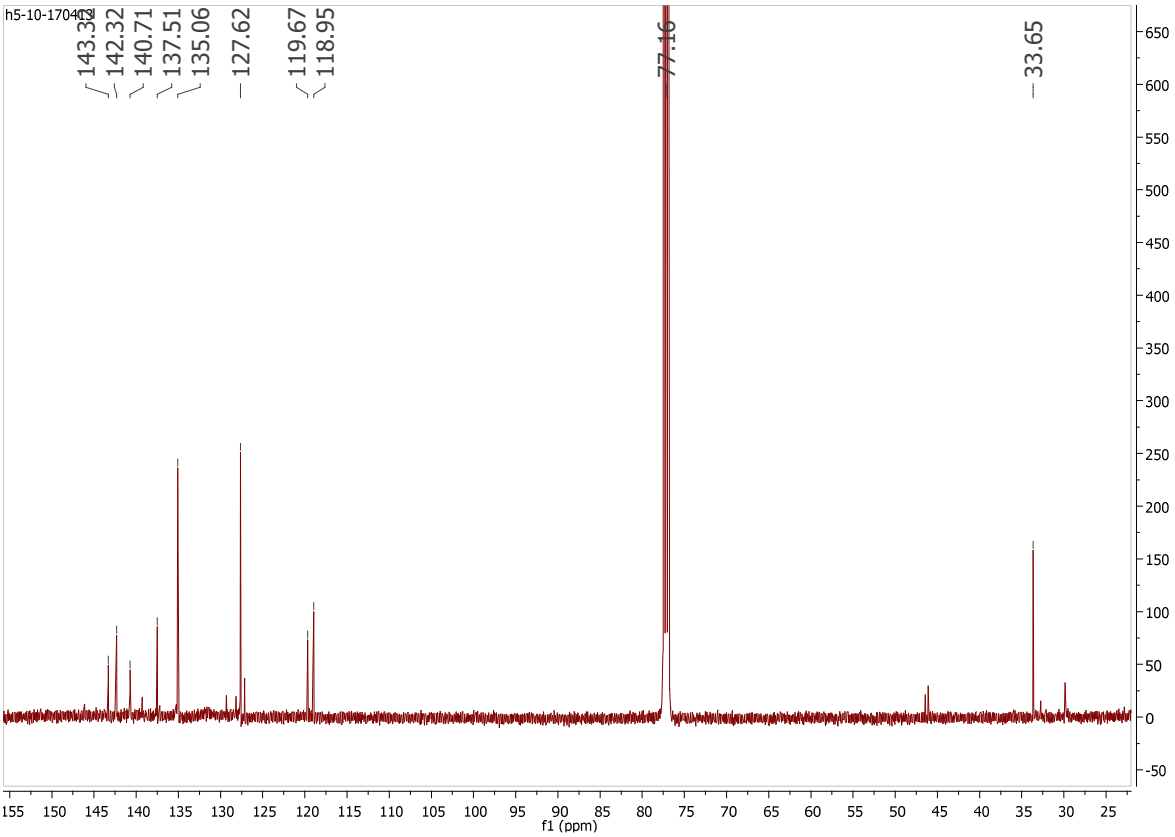

HRMS

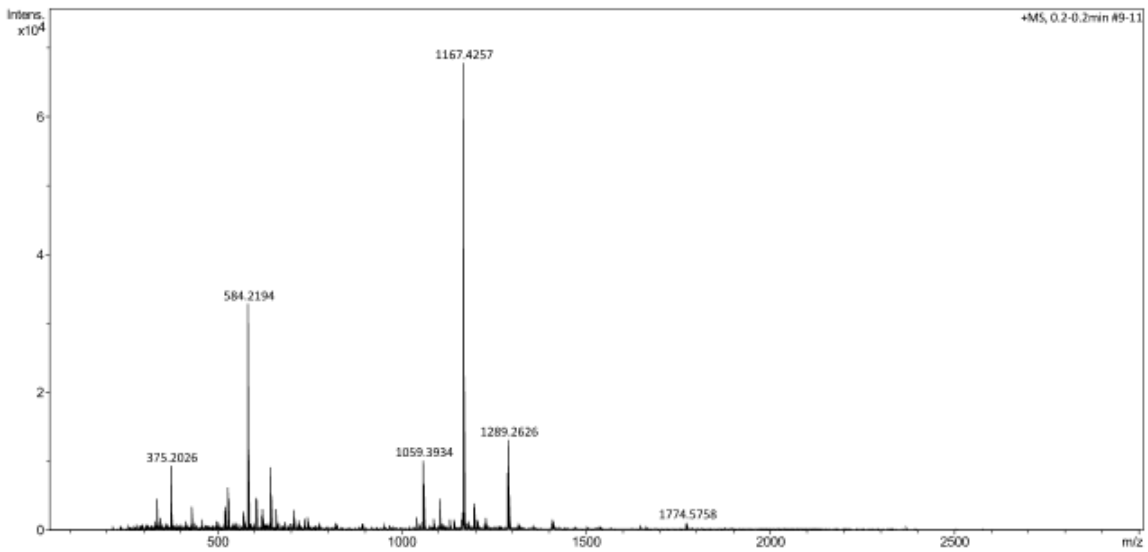

1,3,7,9-tetramethyl-5-(N_1-methylphenylthymine)-dipyrrin (**T-dipyrrin**) (**T11**)

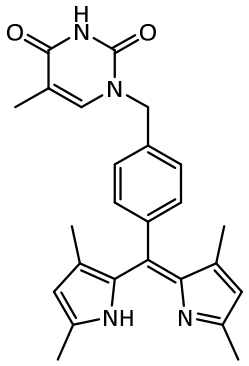

^{1}H NMR (500 MHz,$CDCl_3$)

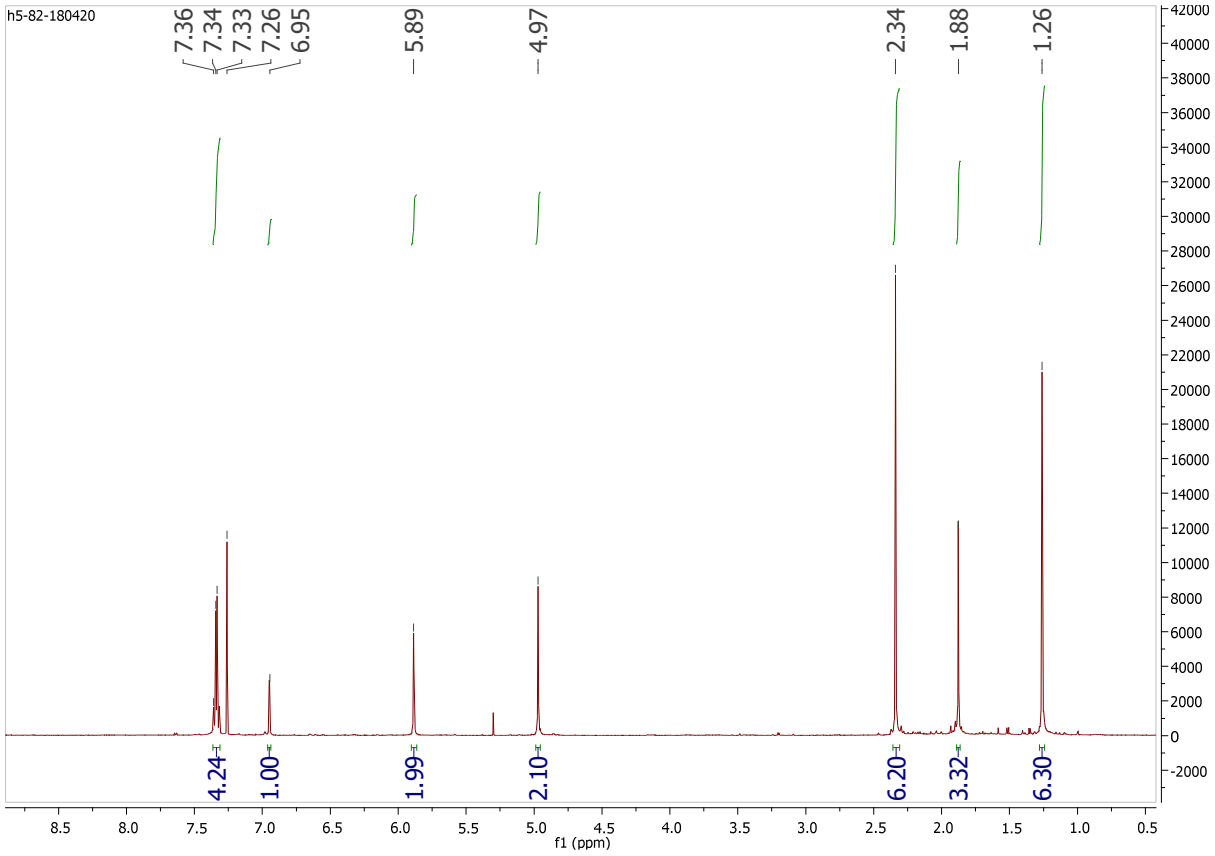

^{13}C NMR (126 MHz, $CDCl_3$)

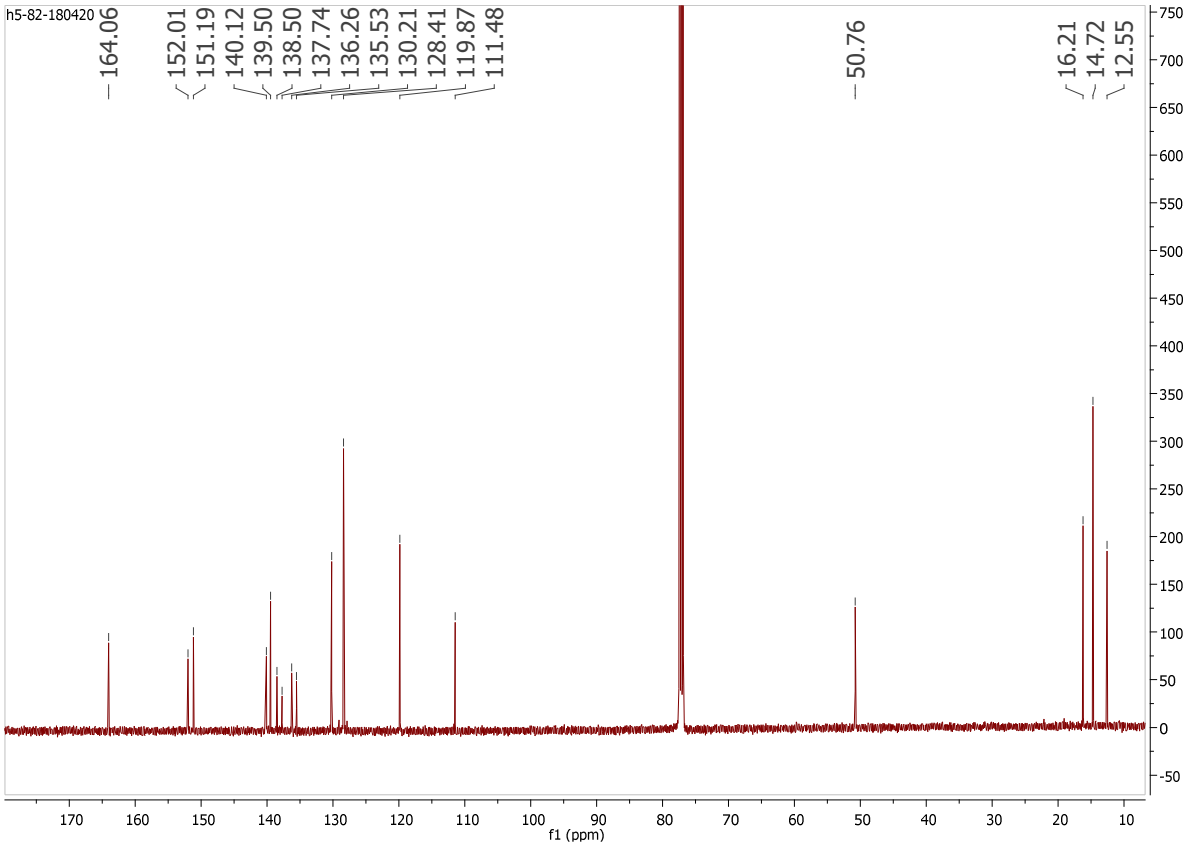

HRMS

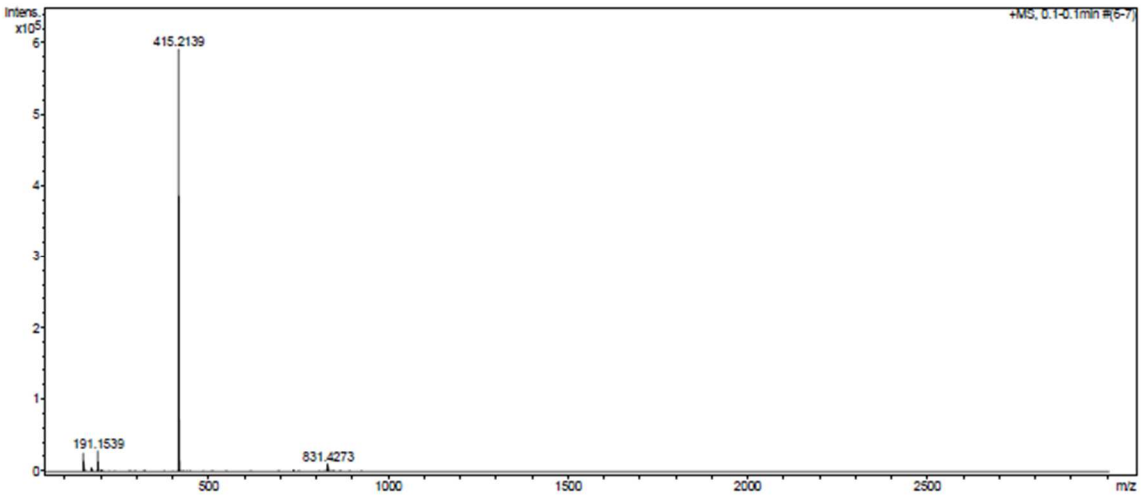

1,3,7,9-tetramethyl-5-(N_9-methylphenyladenine)-dipyrrin (**A-dipyrrin**) (**T12**)

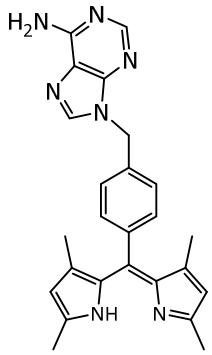

^{1}H NMR (500 MHz,$CDCl_3$)

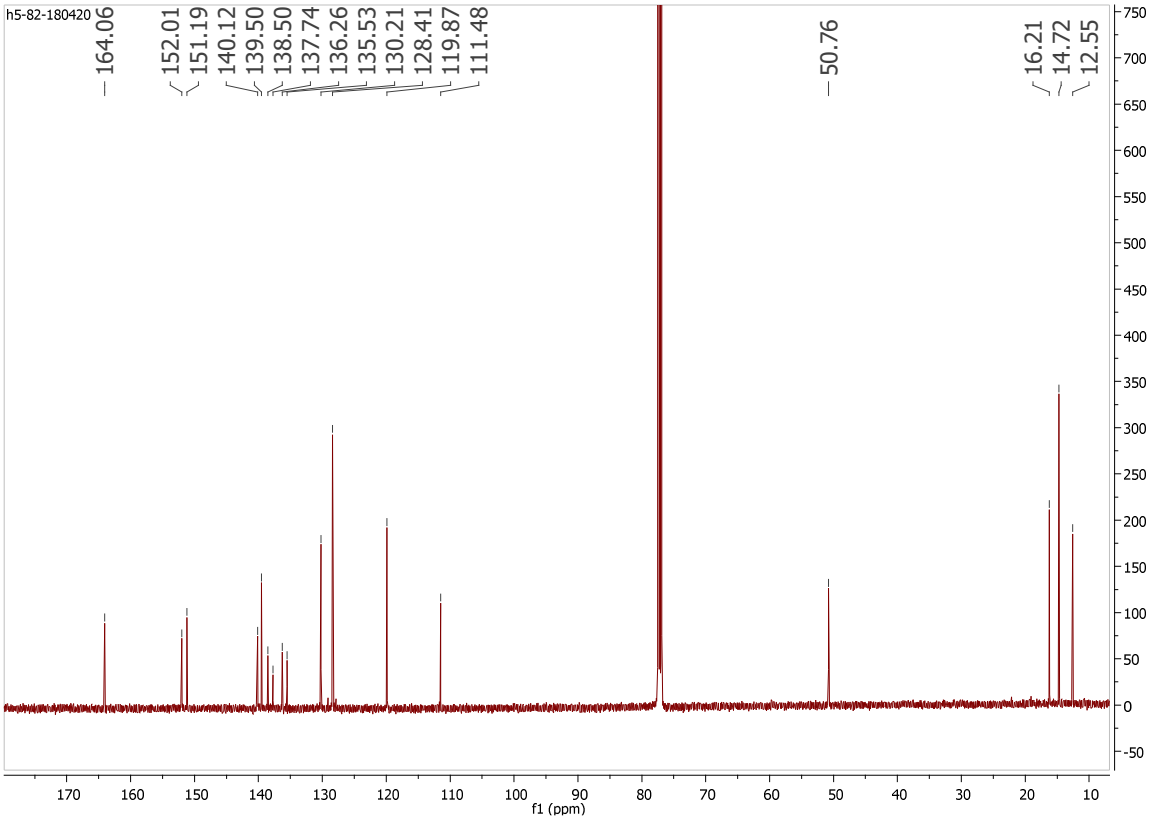

^{13}C NMR (126 MHz, $CDCl_3$)

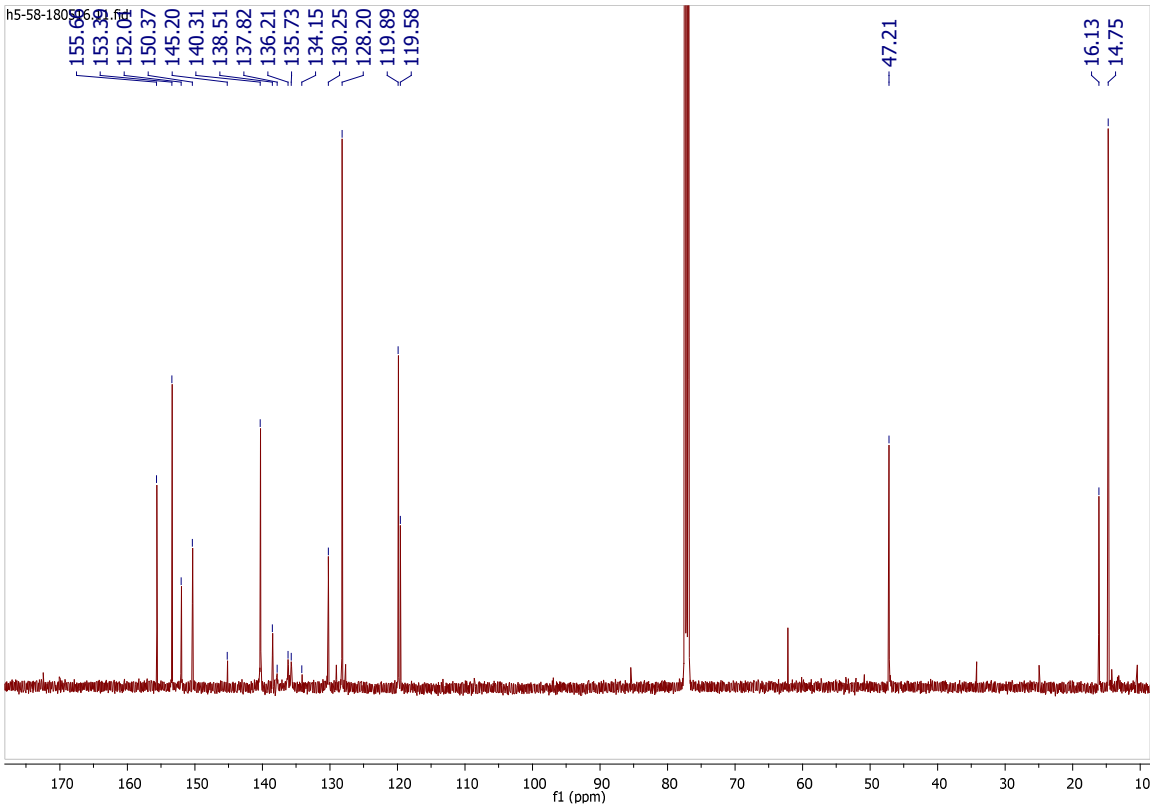

HRMS

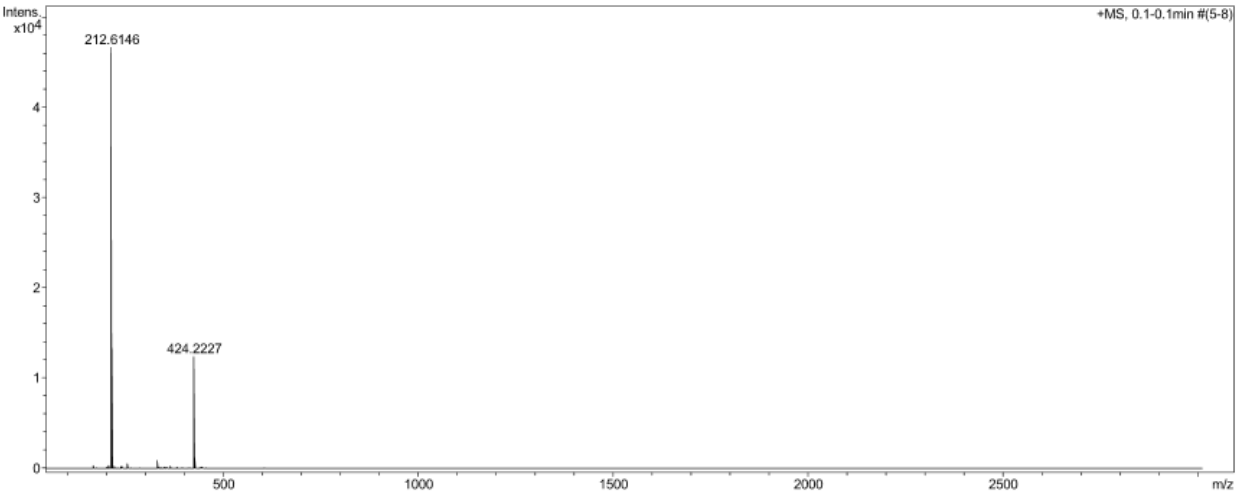

1,3,7,9-tetramethyl-5-(N_1-methylphenylcytosine)-dipyrrin (**C-dipyrrin**) (**T13)**

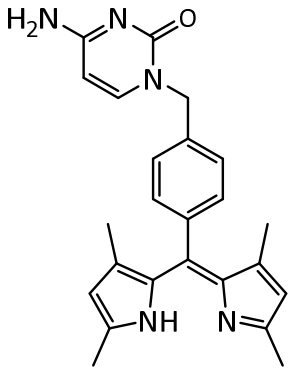

^{1}H NMR (300 MHz,DMSO-d_6)

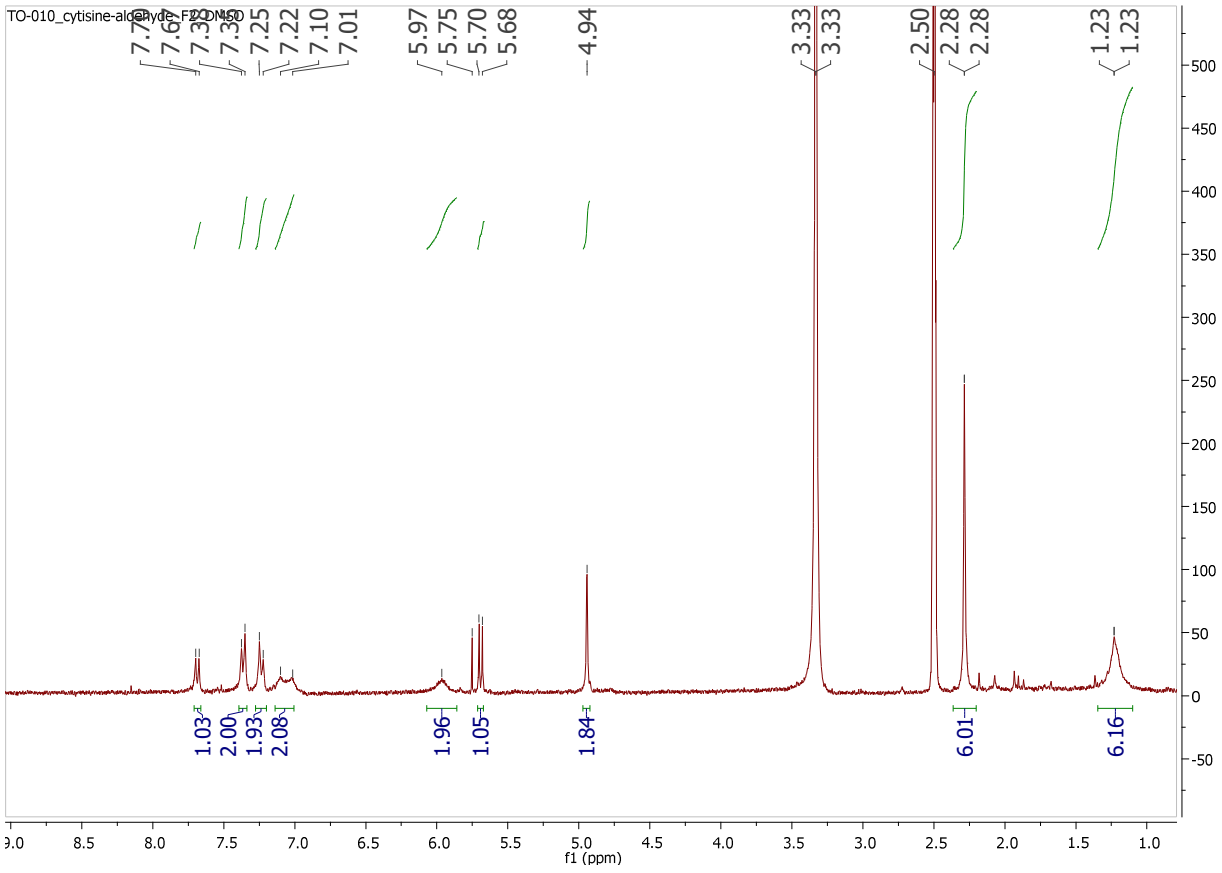

^{13}C NMR (500 MHz, DMSO-d_6)

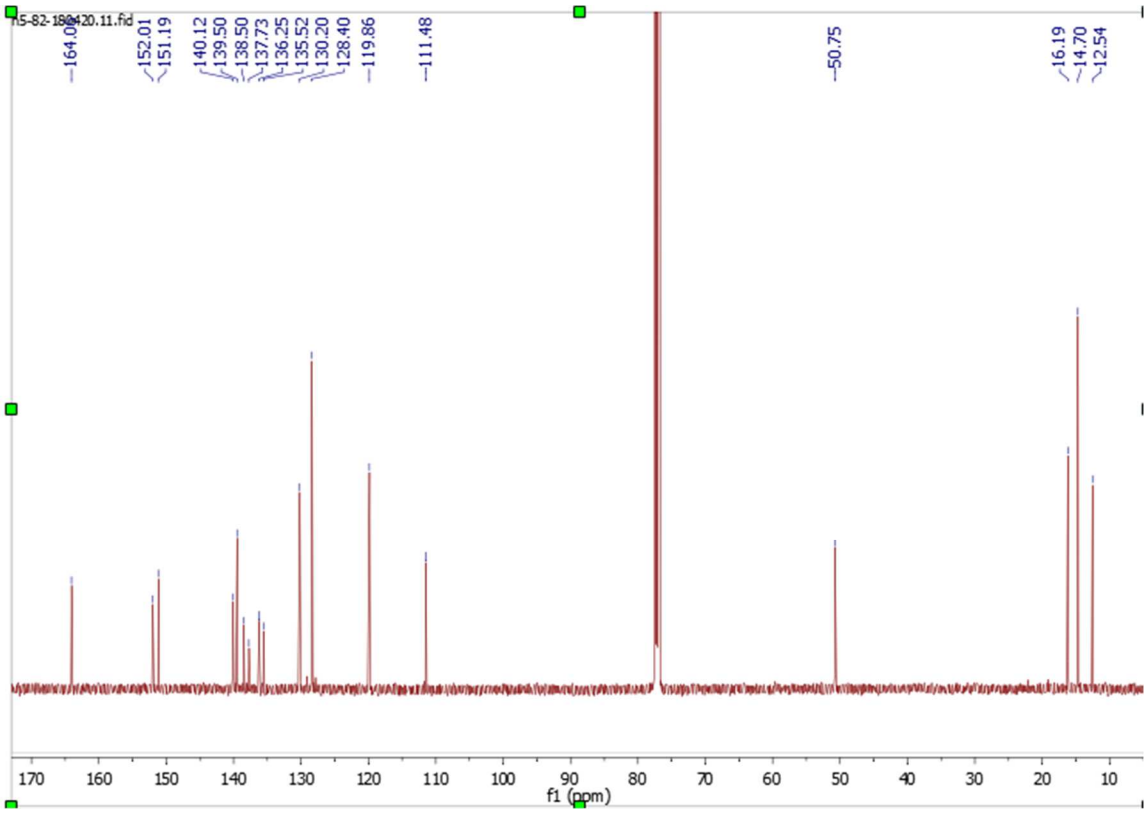

HRMS

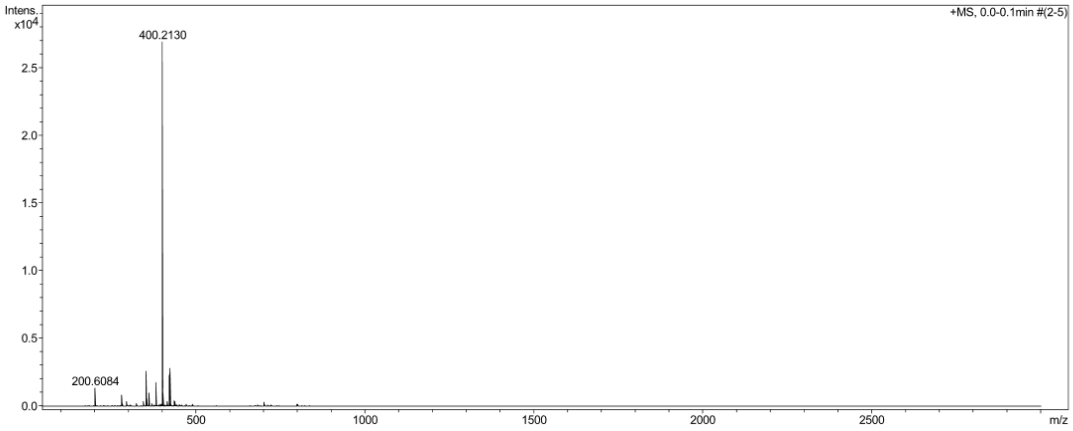

1,3,7,9-tetramethyl-5-(N_9-methylphenyl-2-amino-6-chloropurine)dipyrrin

(**P-dipyrrin**) (**T14**)

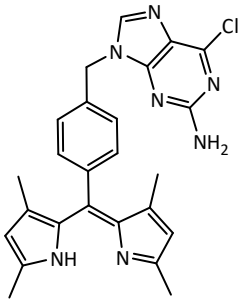

^{1}H NMR (500 MHz,$CDCl_3$)

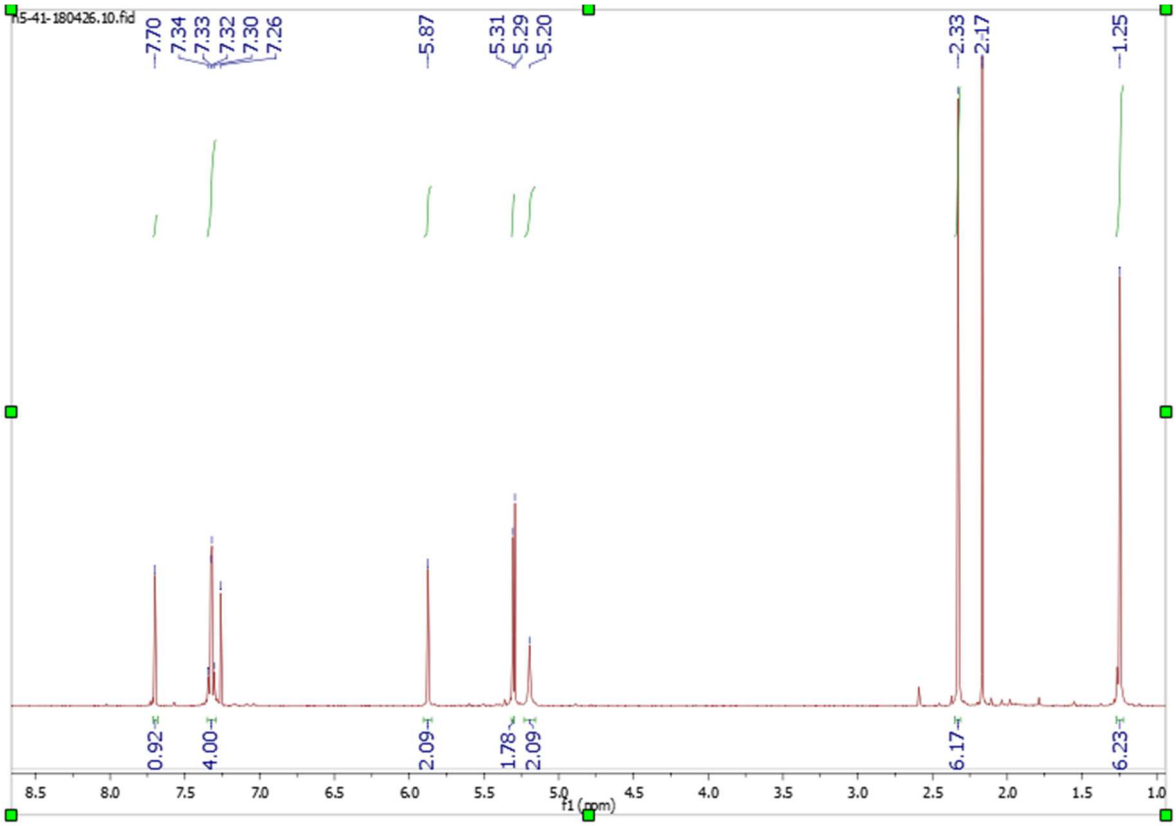

^{13}C NMR (126 MHz, $CDCl_3$)

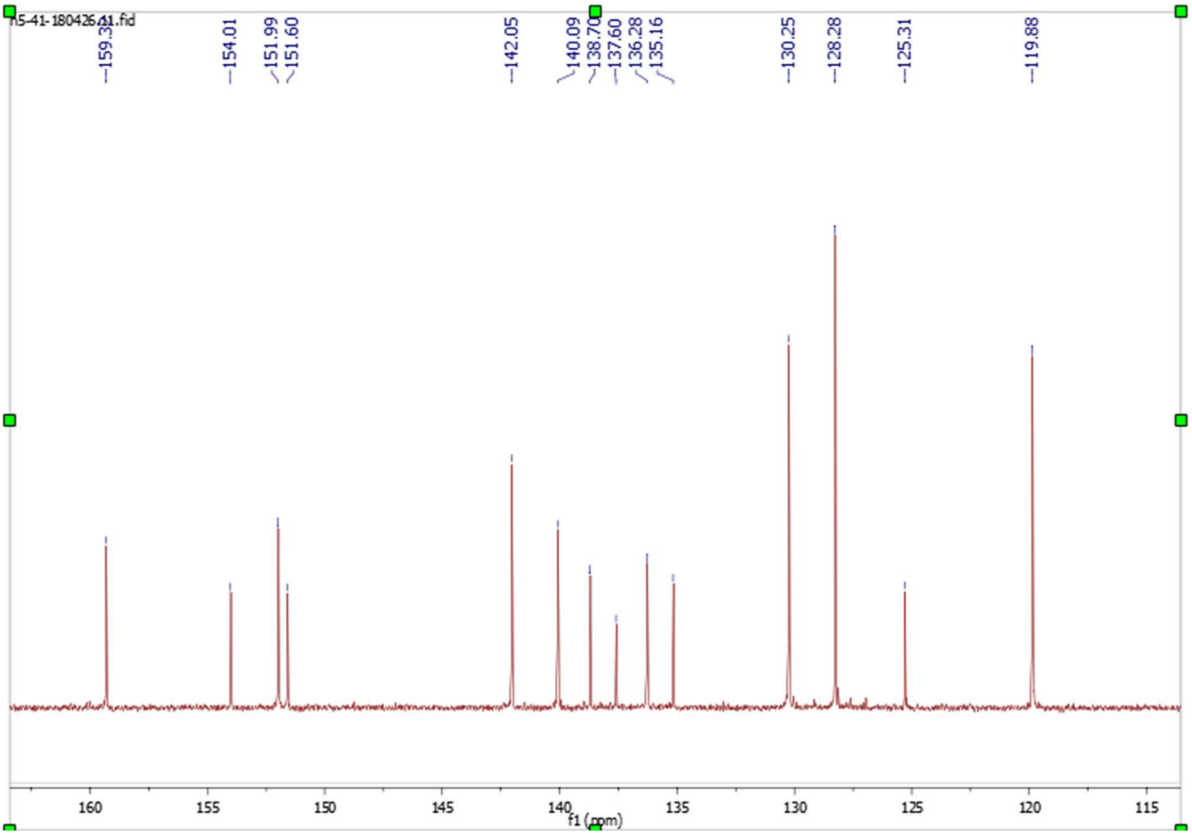

HRMS

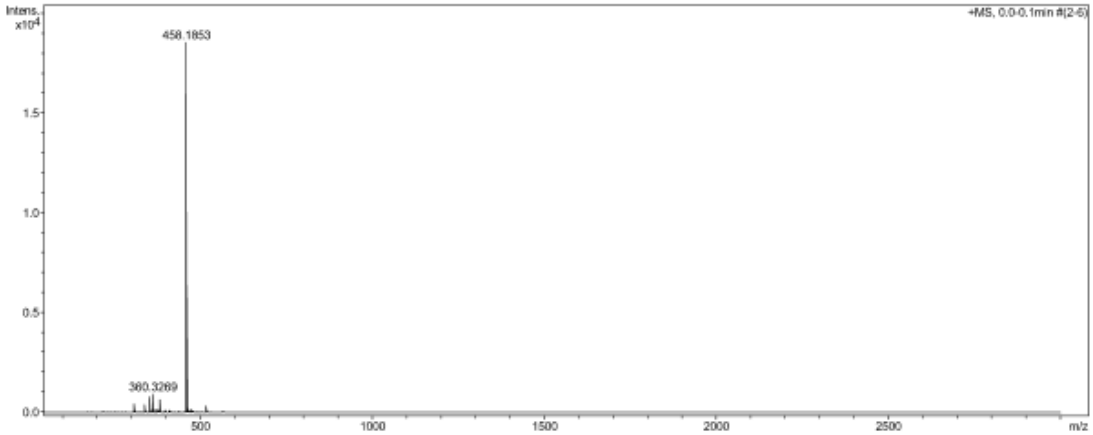

1,3,7,9-tetramethyl-5-(N_9-methylphenylguanine)dipyrrin (**G-dipyrrin**) (**T15)**

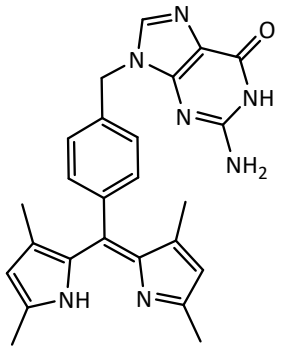

HRMS

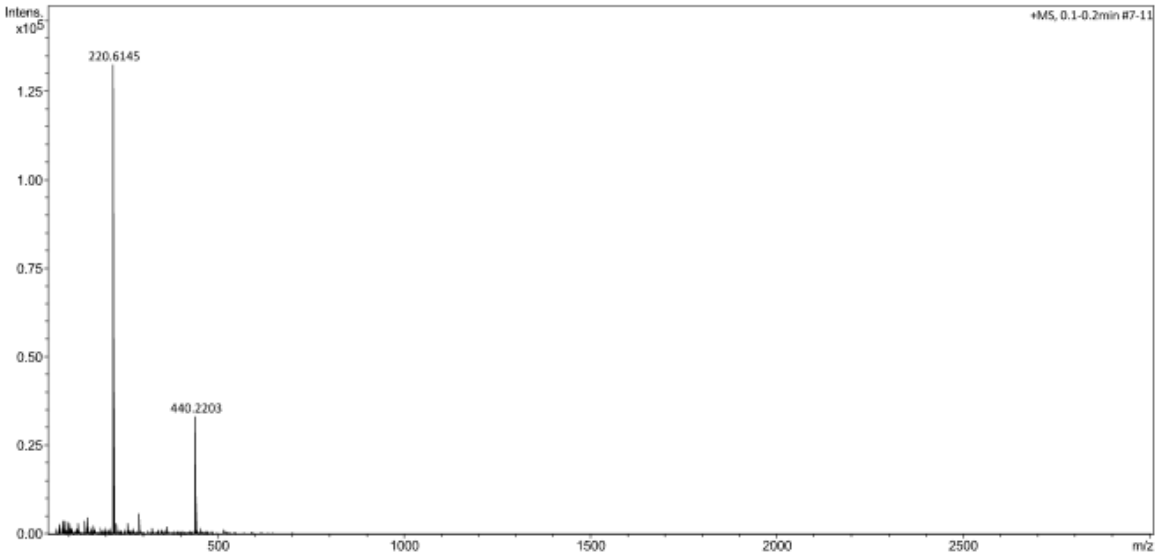

4-(N_1-methylthymine)pyridine (**T-Py**) (**T16**)

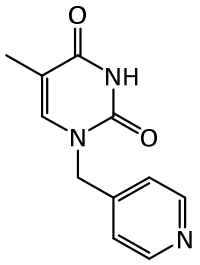

^{1}H NMR (500 MHz, $CDCl_3$)

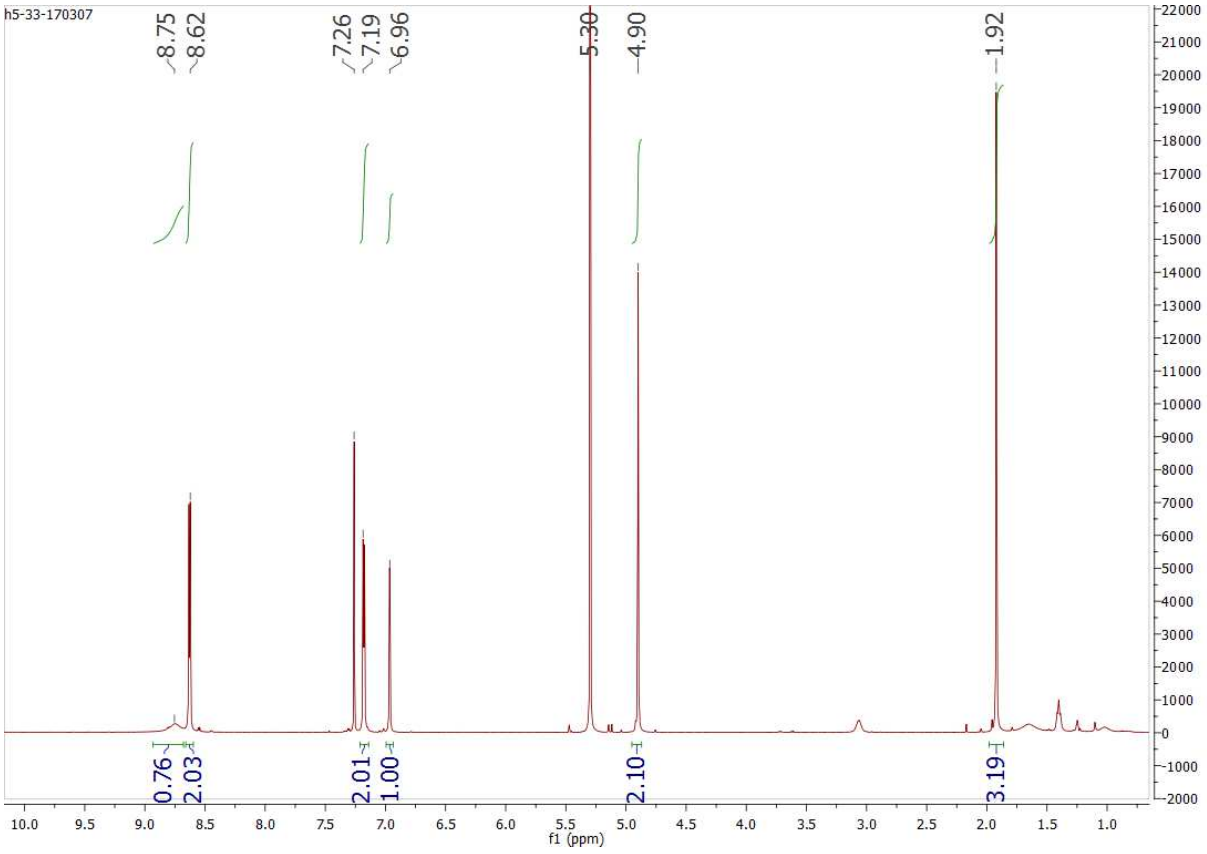

^{13}C NMR (126 MHz, $CDCl_3$)

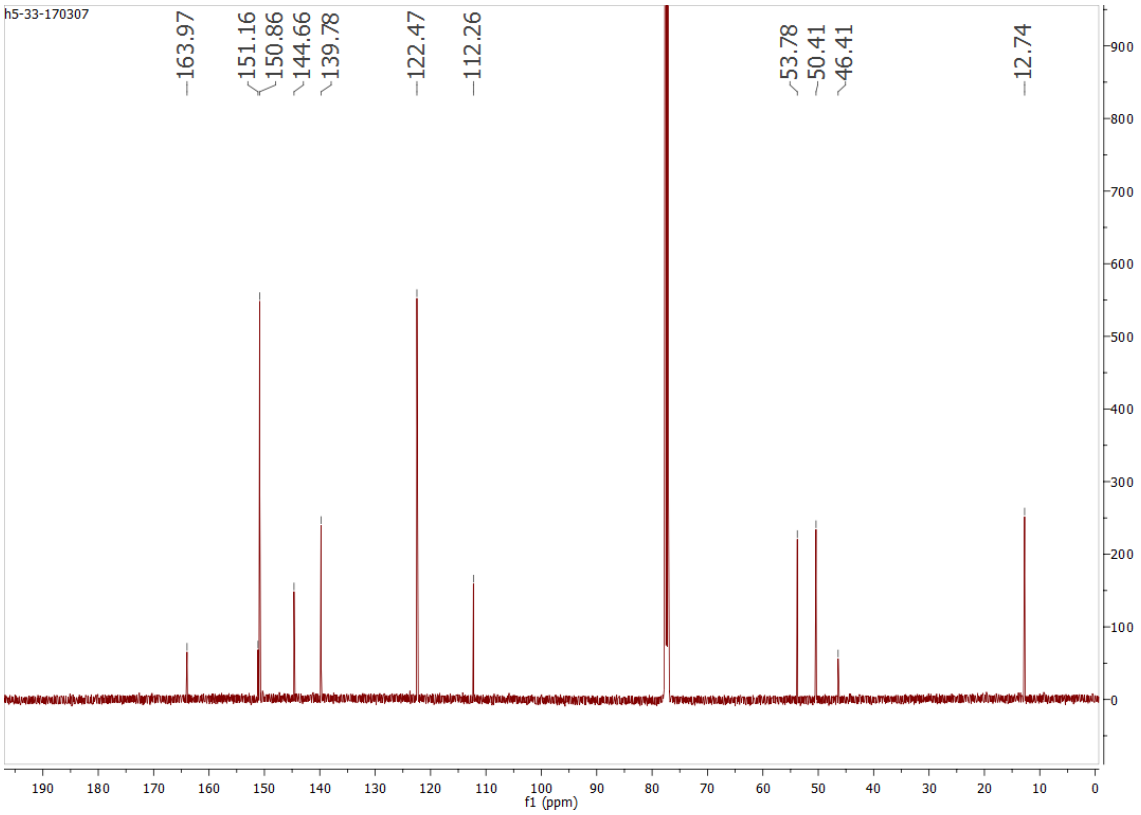

HRMS

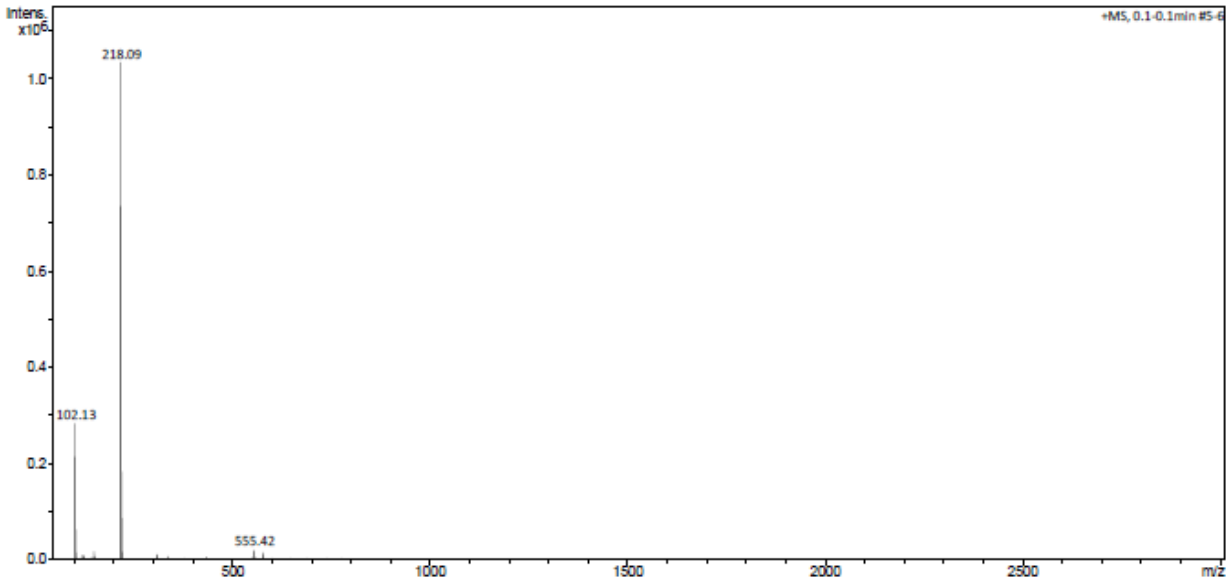

4-(N_9-methyladenine)pyridine (**A-Py**) (**T17**)

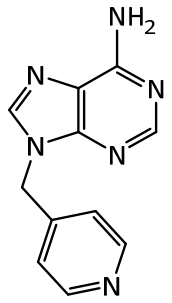

^{1}H NMR (500 MHz, DMSO-d_6)

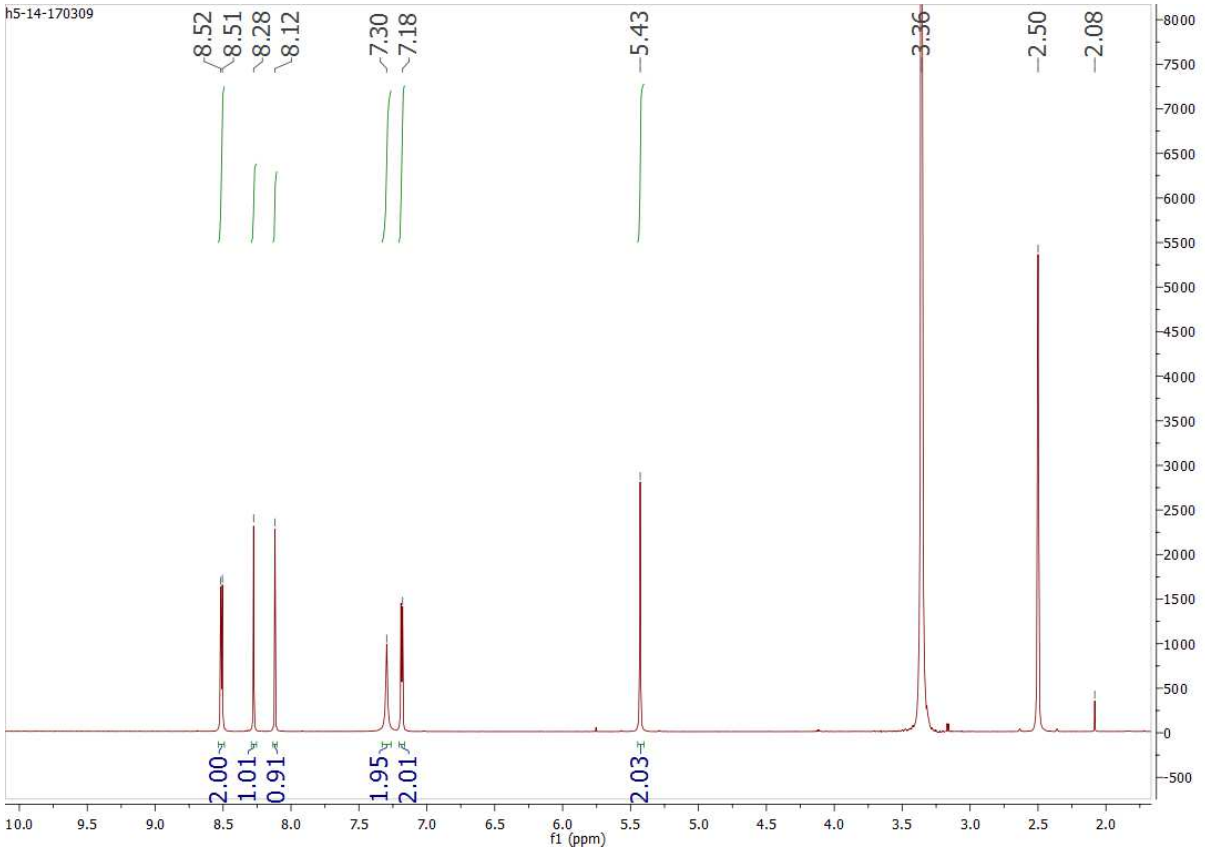

^{13}C NMR (126 MHz, DMSO-d_6)

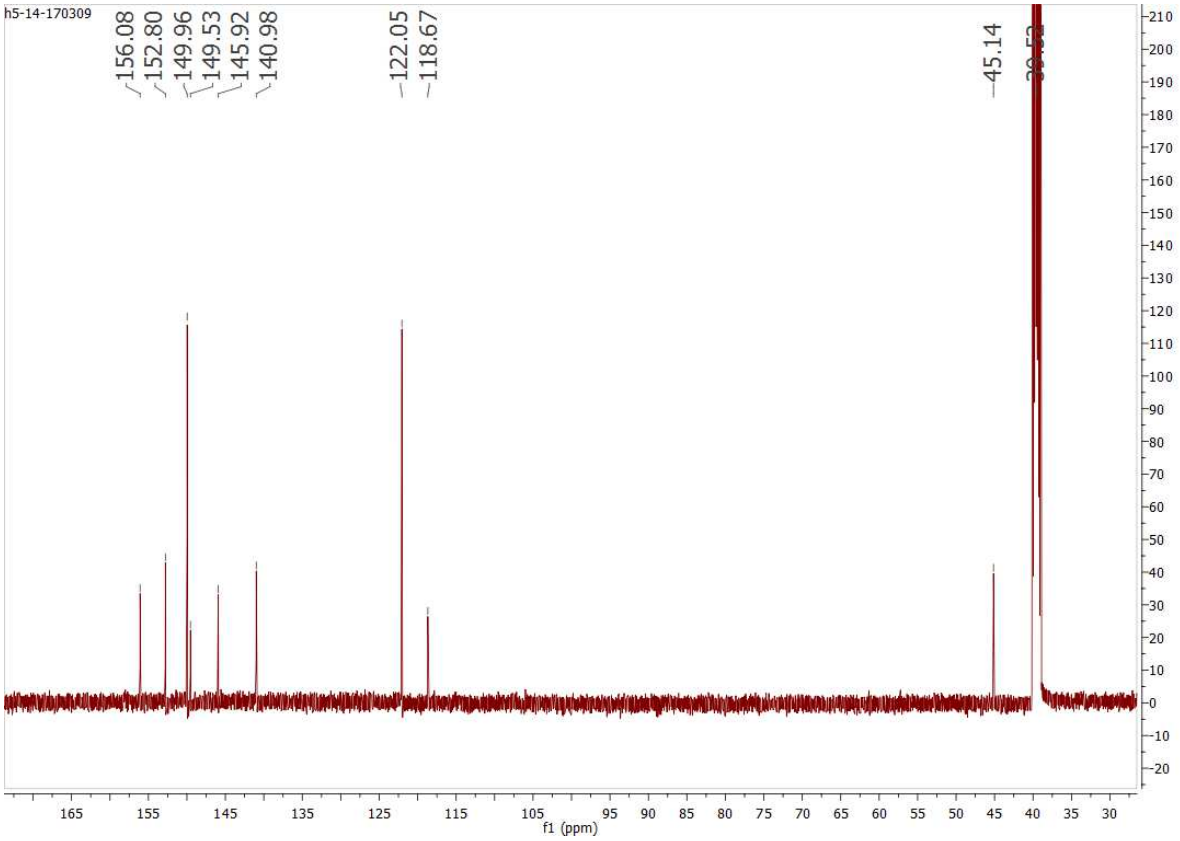

HRMS

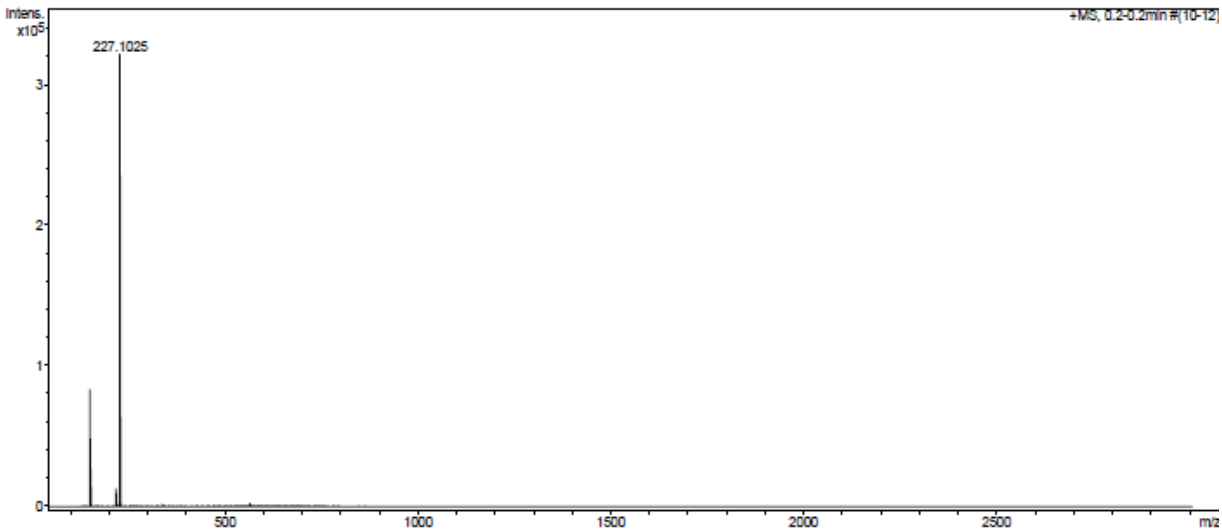

4-(N_1-methylcytosine)pyridine (**C-Py**) (**T18**)

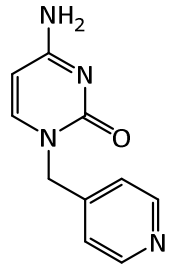

^{1}H NMR (500 MHz, DMSO-d_6)

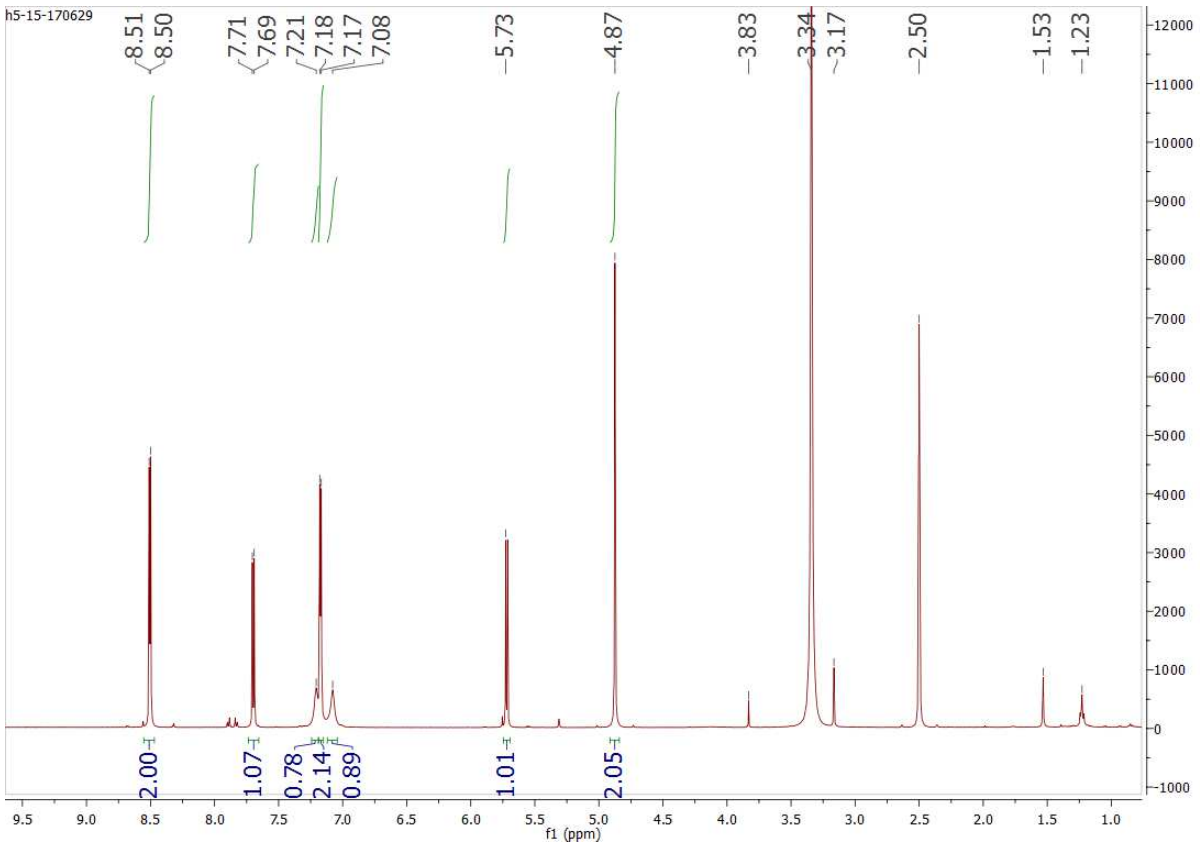

^{13}C NMR (126 MHz, DMSO-d_6)

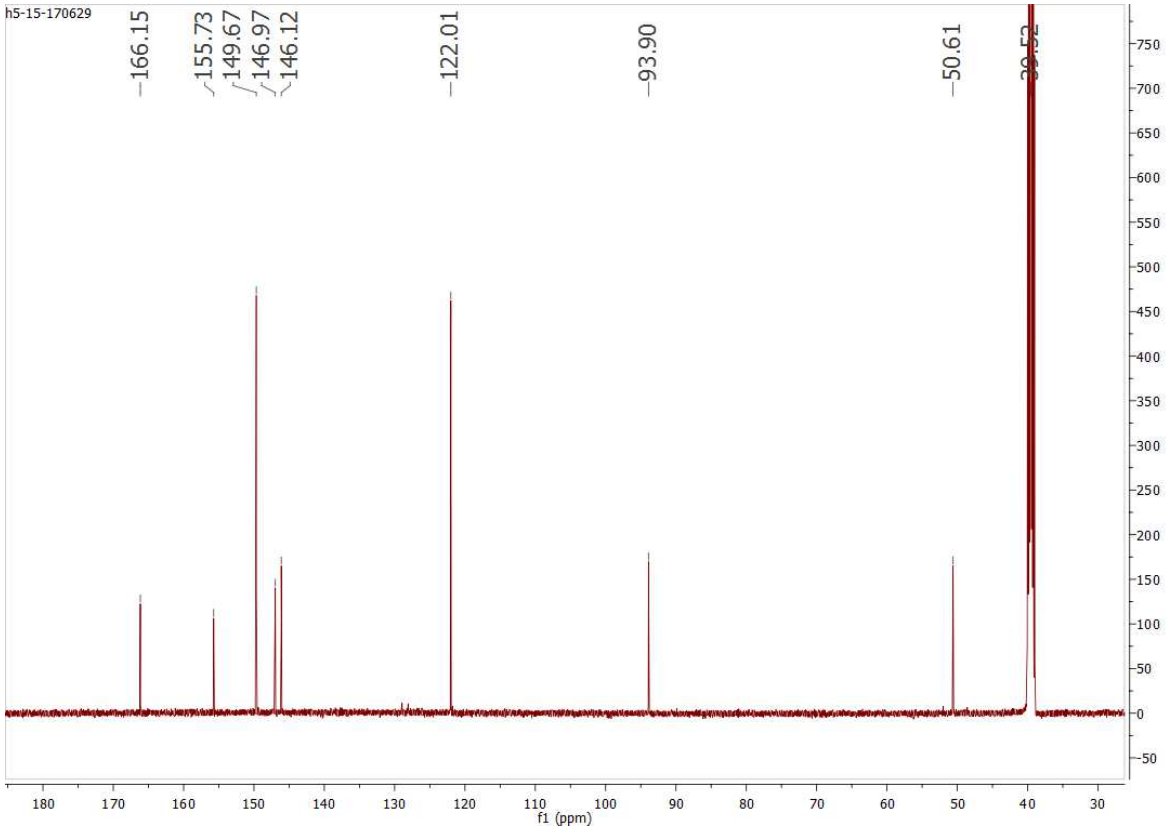

HRMS

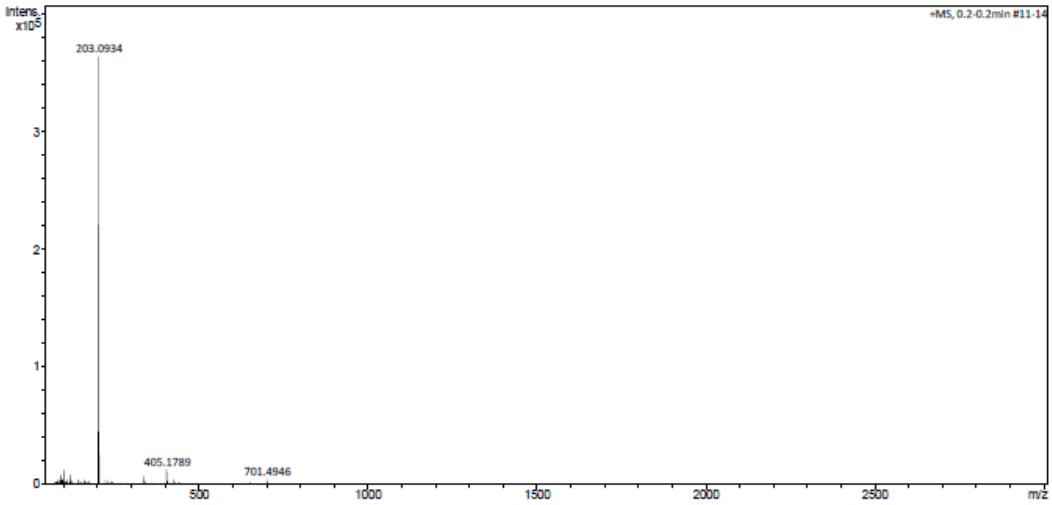

4-(N_9-methyl-2-amino-6-chloropurine)pyridine (**P-Py**) (**T19**)

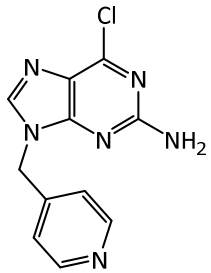

^{1}H NMR (500 MHz, DMSO-d_6)

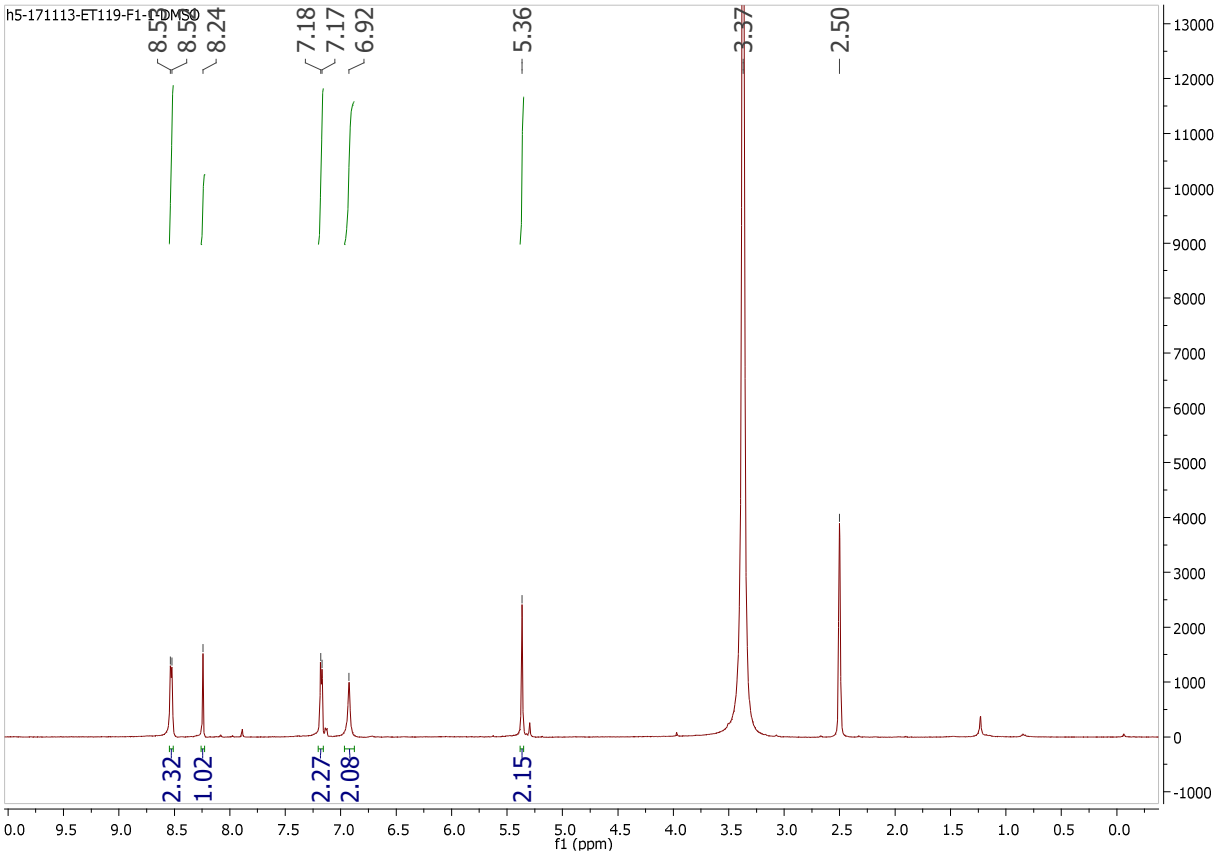

^{13}C NMR (126 MHz, DMSO-d_6)

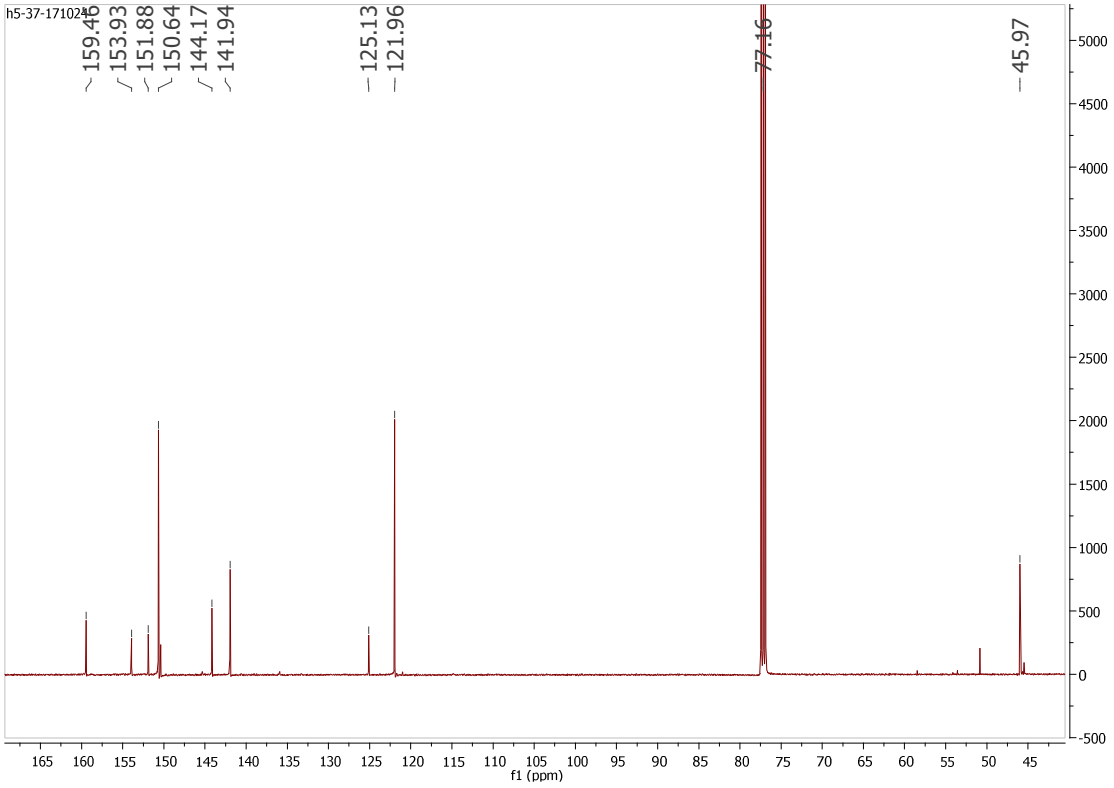

MS

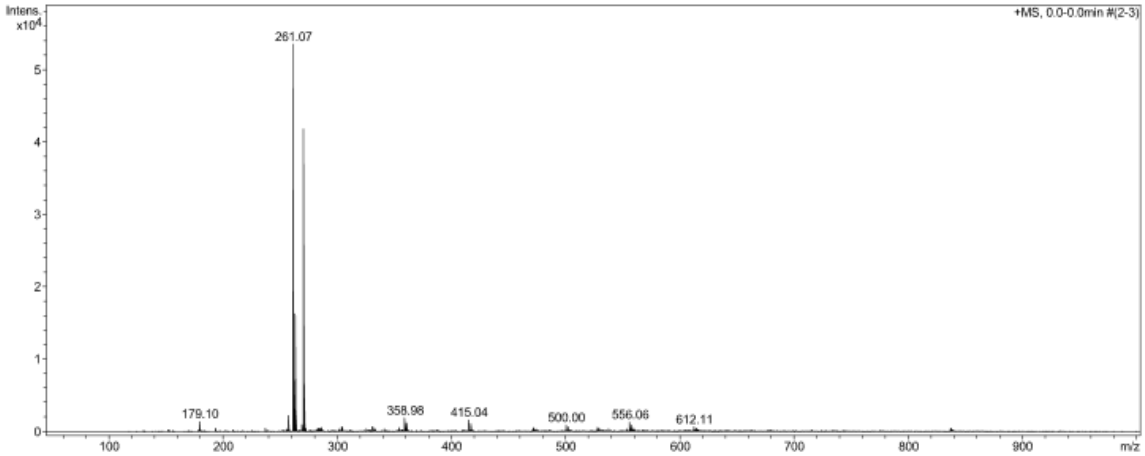

4-(N_9-methylguanine)pyridine (**G-Py**) (**T20**)

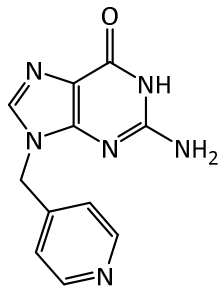

^{1}H NMR (500 MHz, DMSO-d_6)

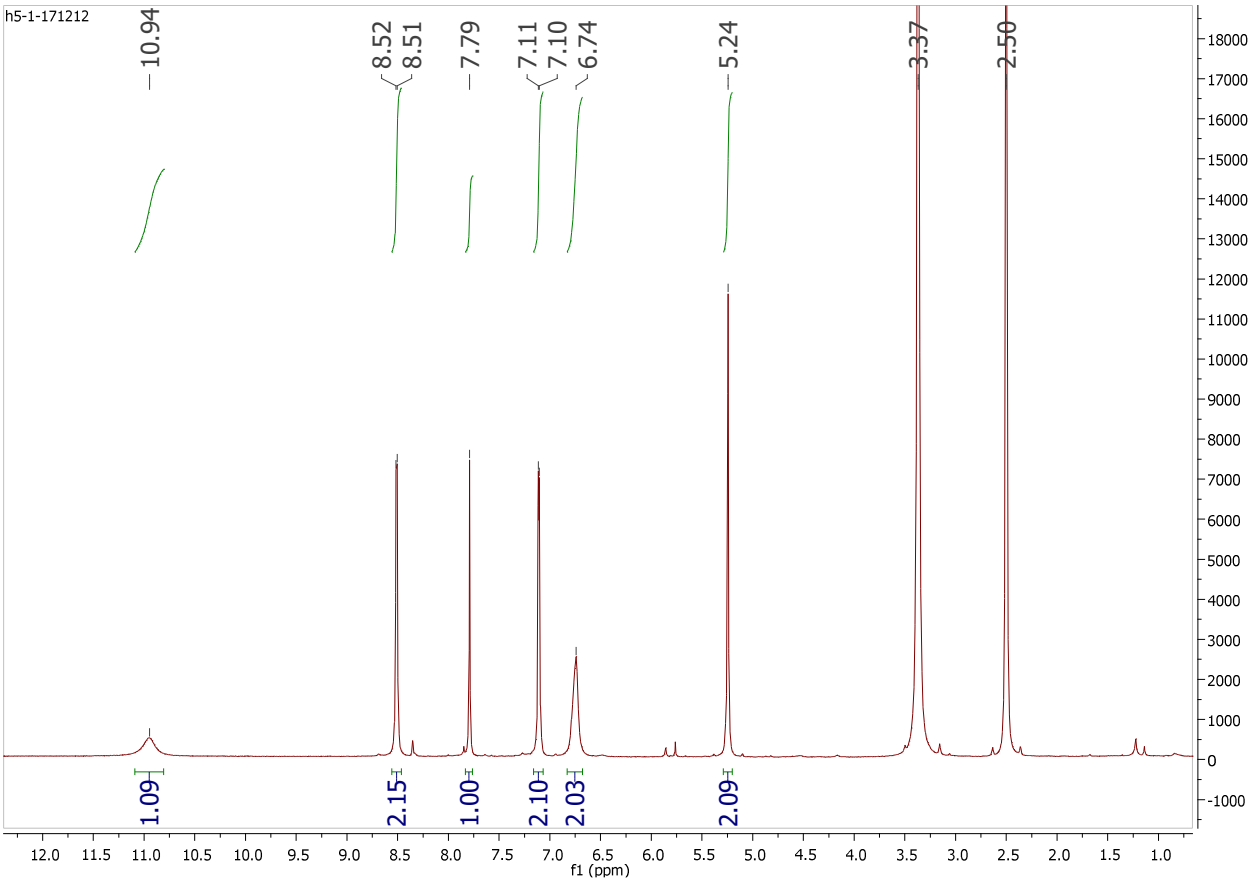

^{13}C NMR (126 MHz, DMSO-d_6)

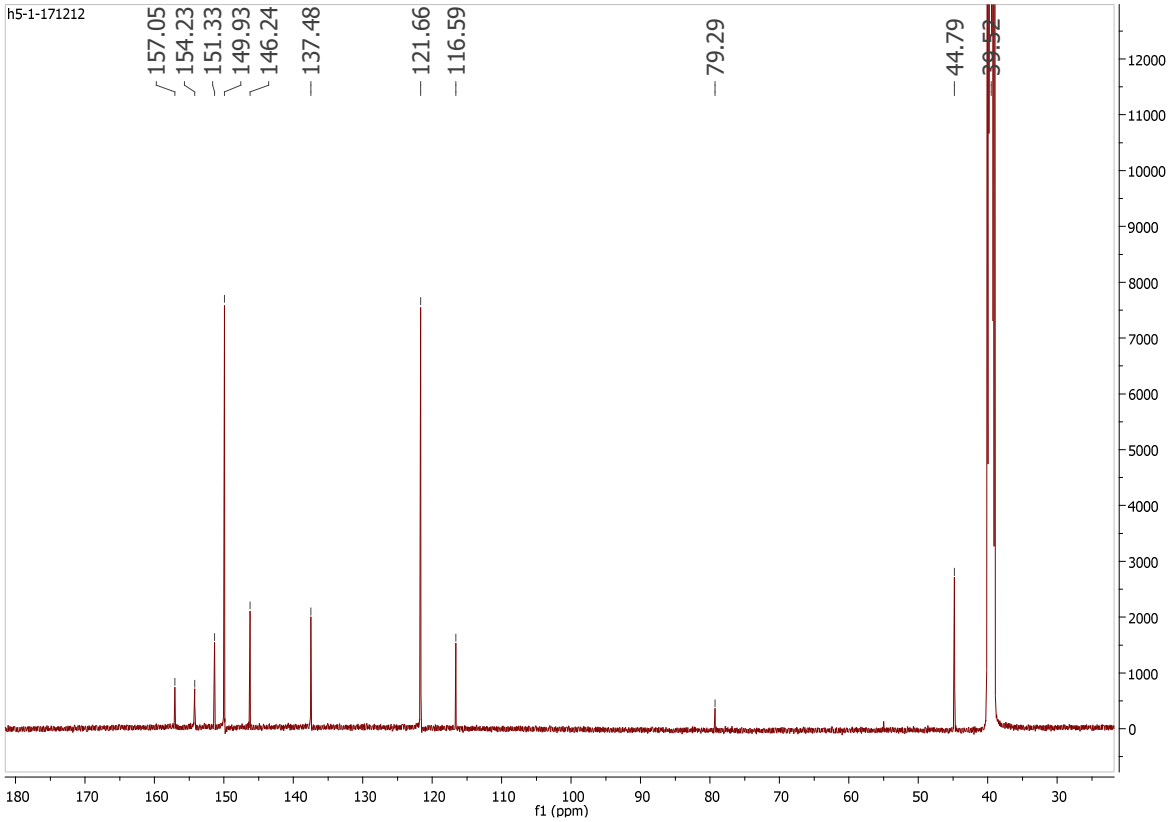

HRMS

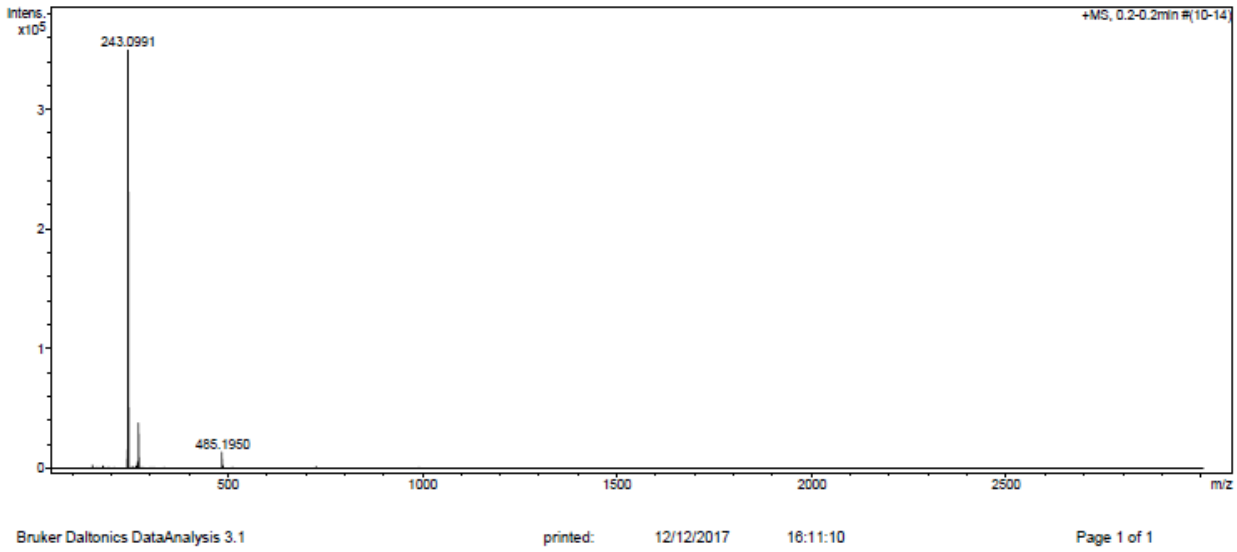

4'-(N_1-methylphenylthymine)-2,2':6',2"-terpyridine (**T-terPy**) (**T21**)

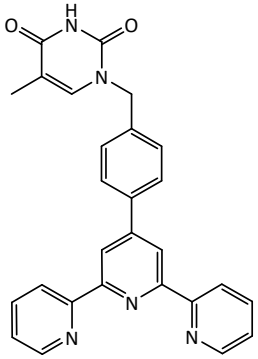

^{1}H NMR (500 MHz, $CDCl_3$)

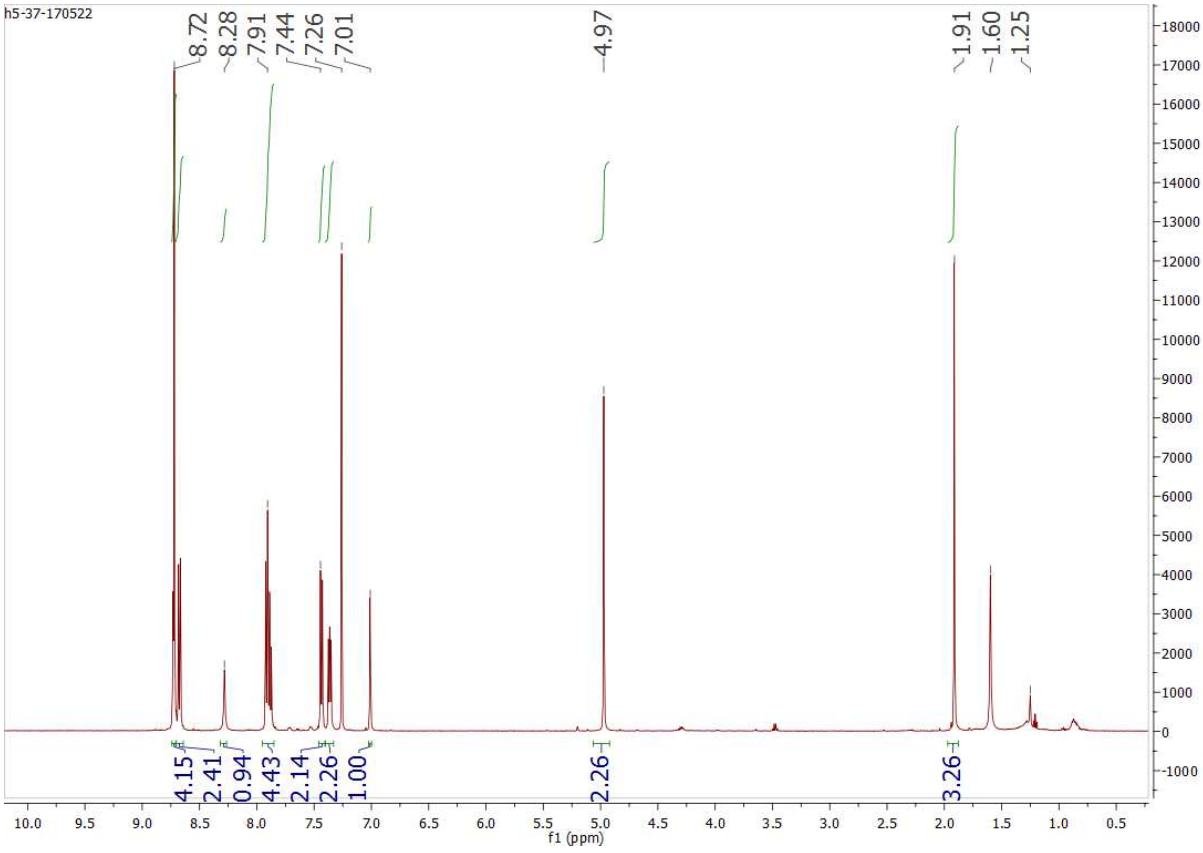

^{13}C NMR (126 MHz, $CDCl_3$)

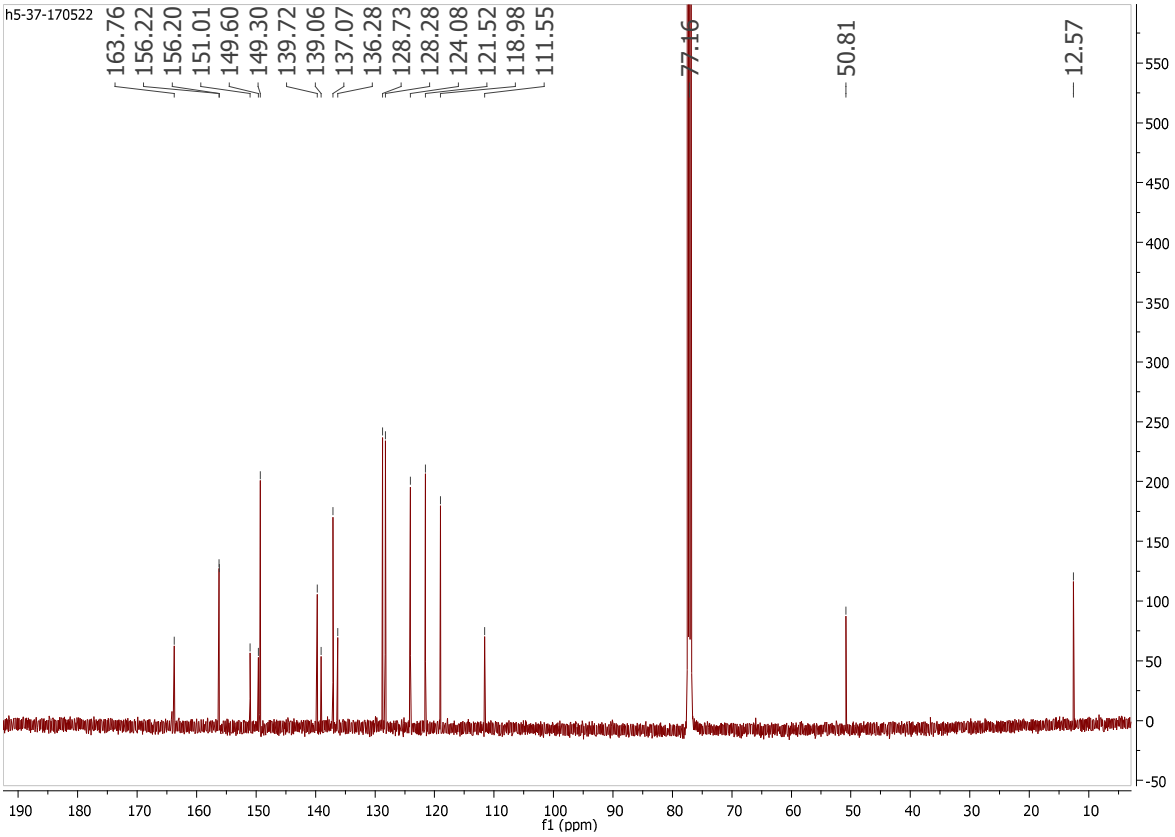

HRMS

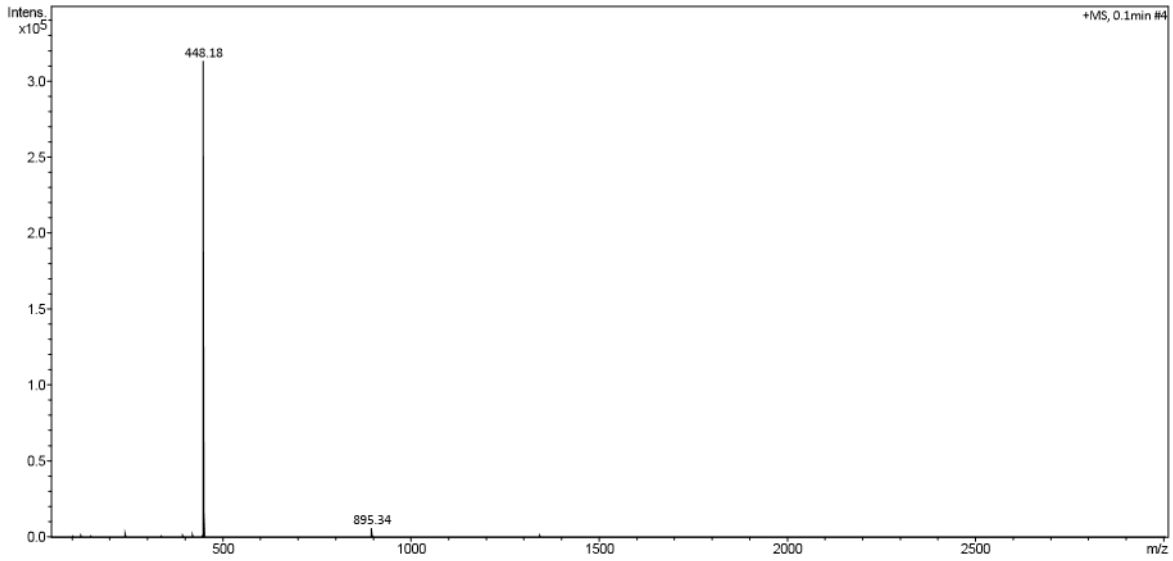

4’-(N_9-methylphenyladenine)-2,2’:6’,2”-terpyridine (**A-terPy**) (**T22**)

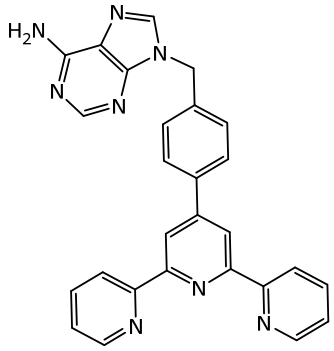

^{1}H NMR (500 MHz, $CDCl_3$)

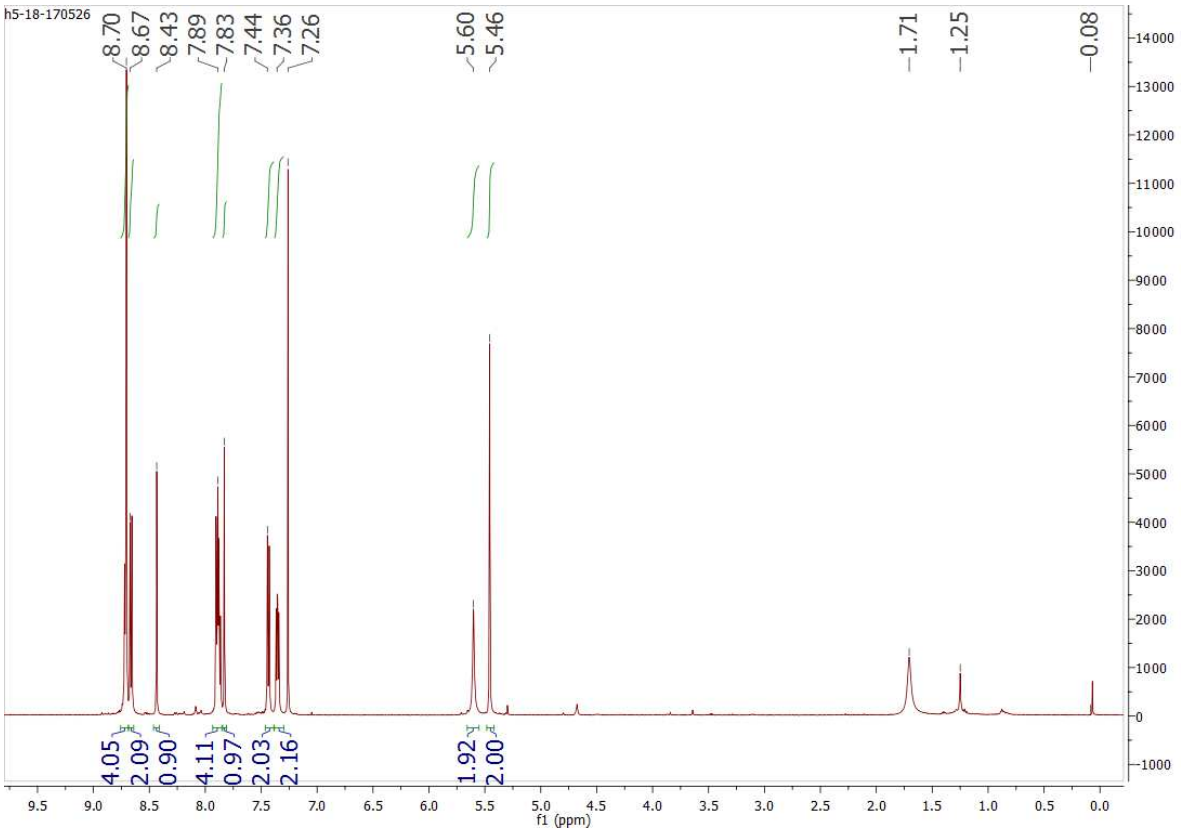

^{13}C NMR (126 MHz, $CDCl_3$)

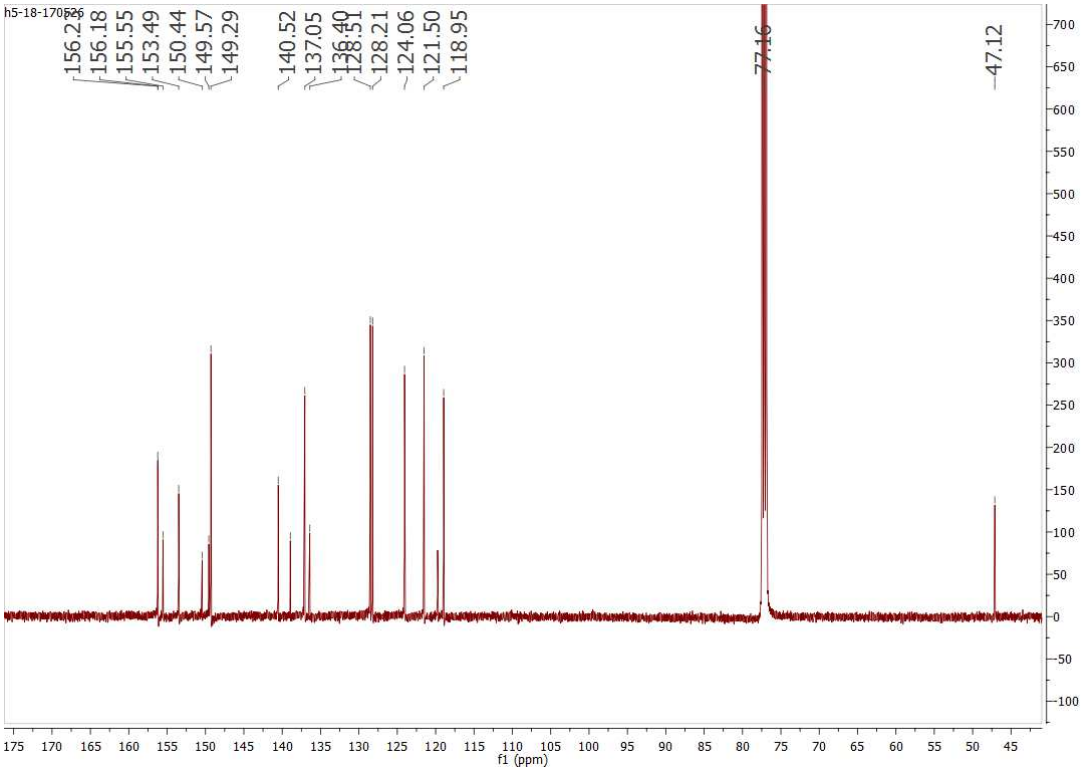

HRMS

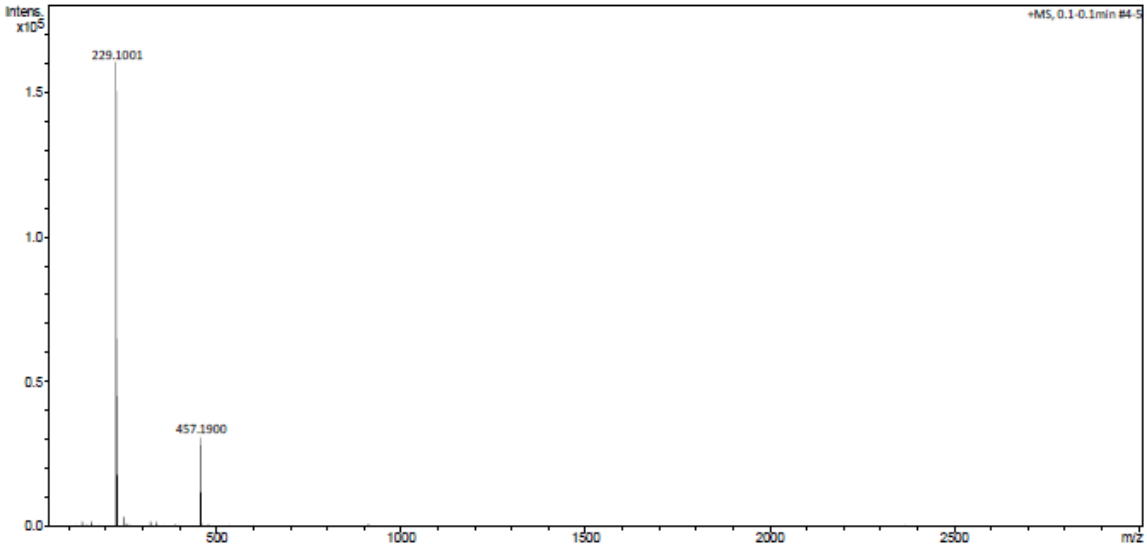

4'-(N_1-methylphenylcytosine)-2,2':6',2''-terpyridine (**C-terPy**) (**T23**)

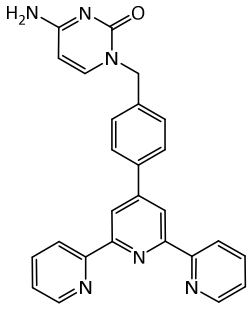

^{1}H NMR (400 MHz, DMSO-d_6)

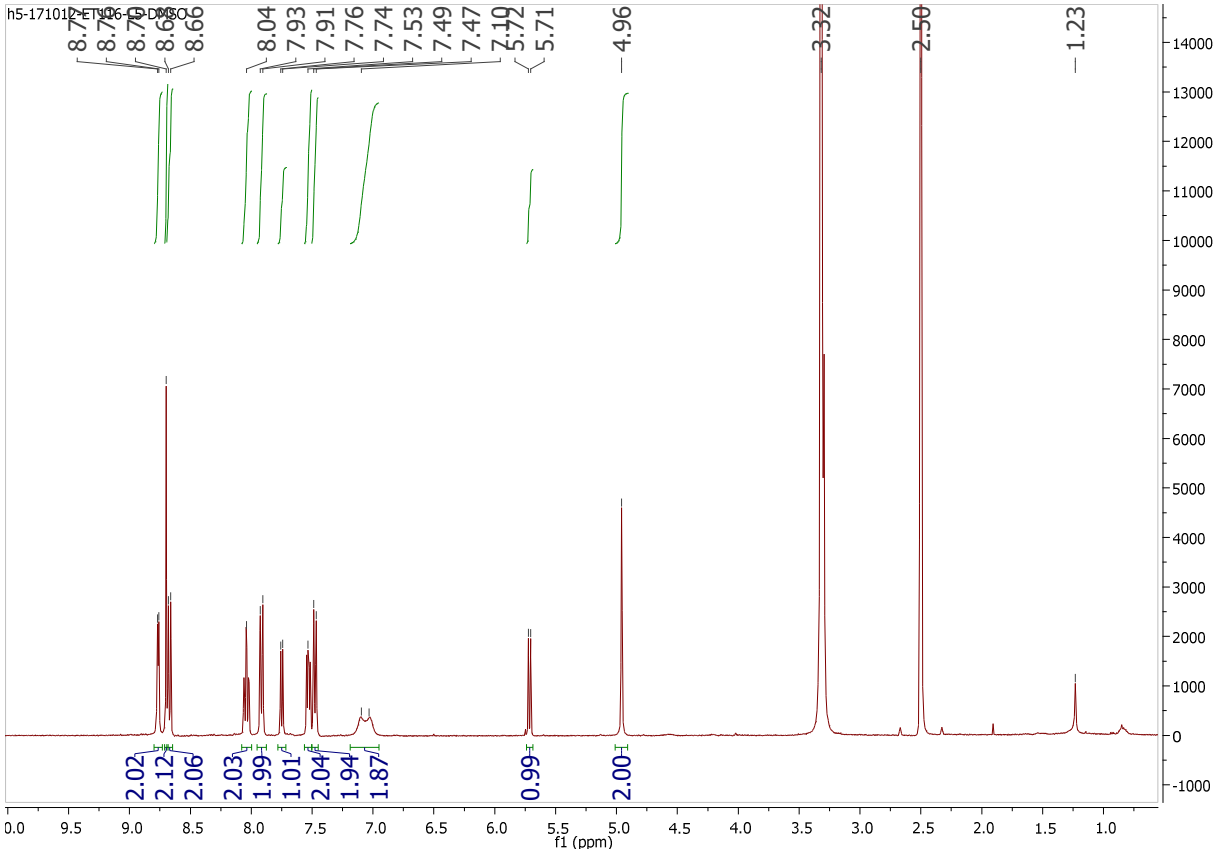

^{13}C NMR (126 MHz, $CDCl_3$ + MeOD)

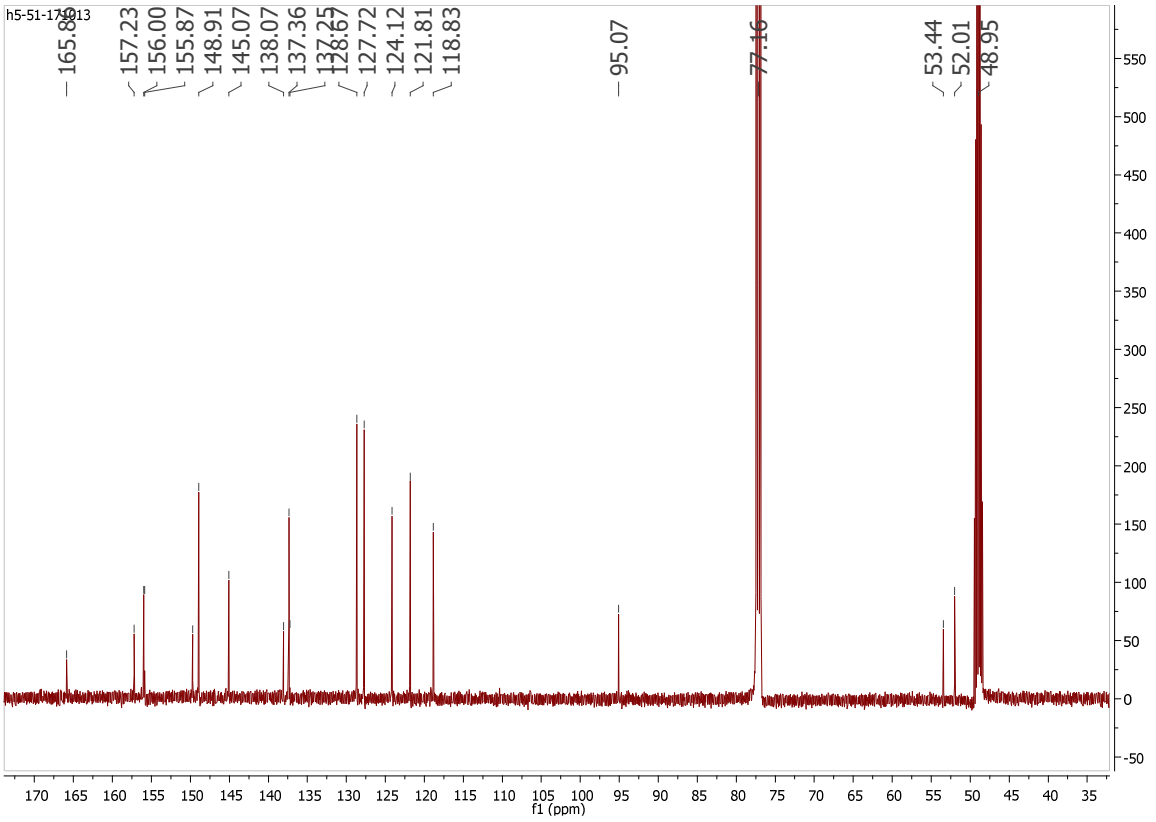

HRMS

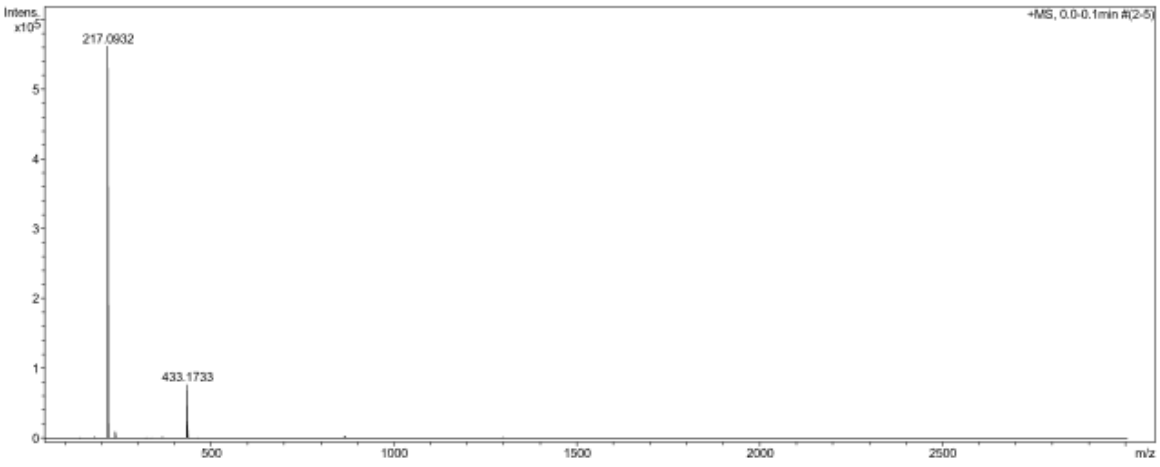

4’-(N_1-methylphenyl-2-amino-6-chloropurine)-2,2’:6’,2”-terpyridine

(P-terPy) (T24)

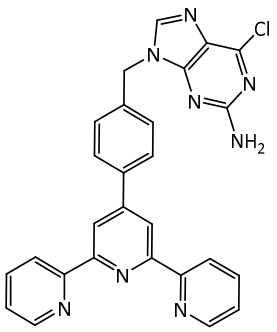

^{1}H NMR (500 MHz, DMSO-d_6)

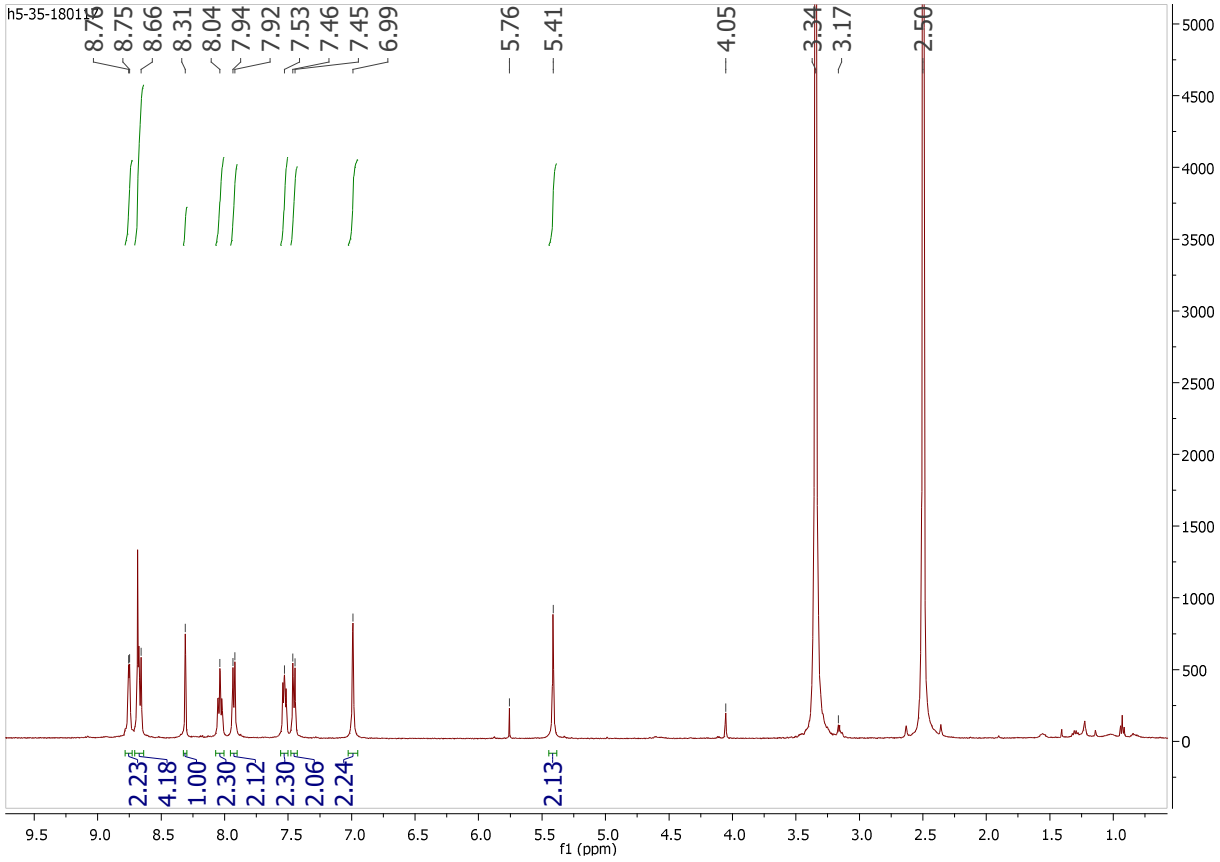

^{13}C NMR (126 MHz, DMSO-d_6)

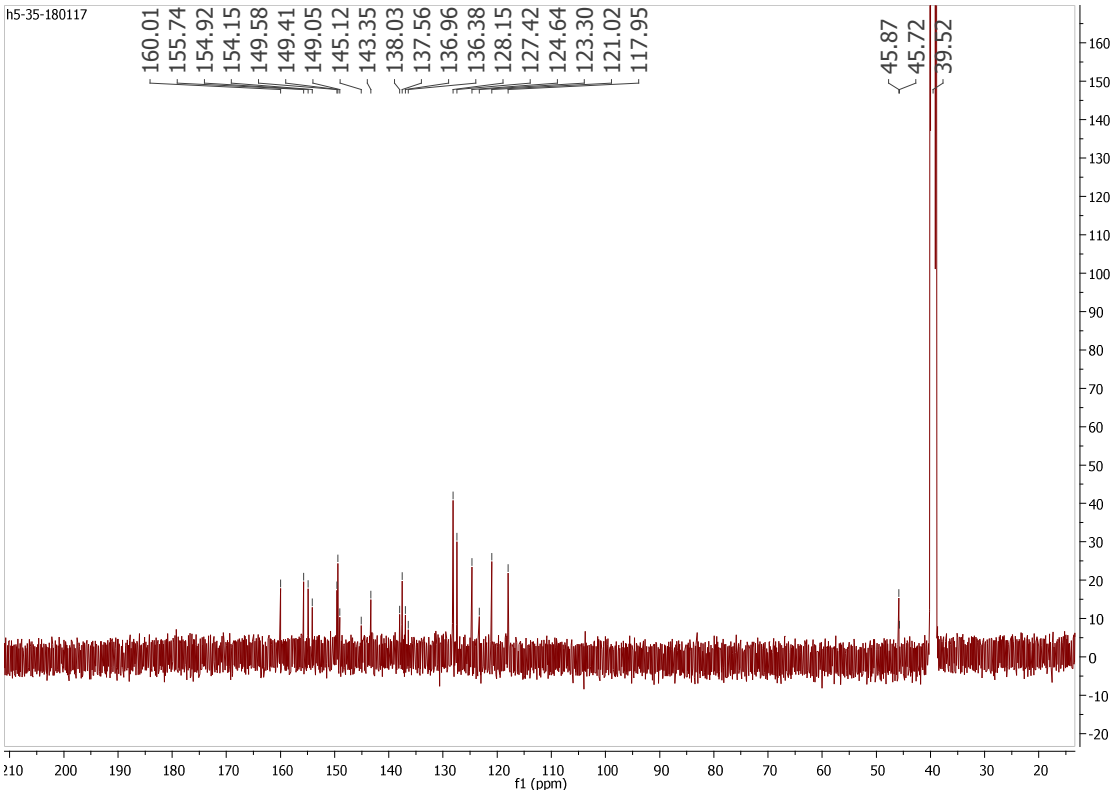

HRMS

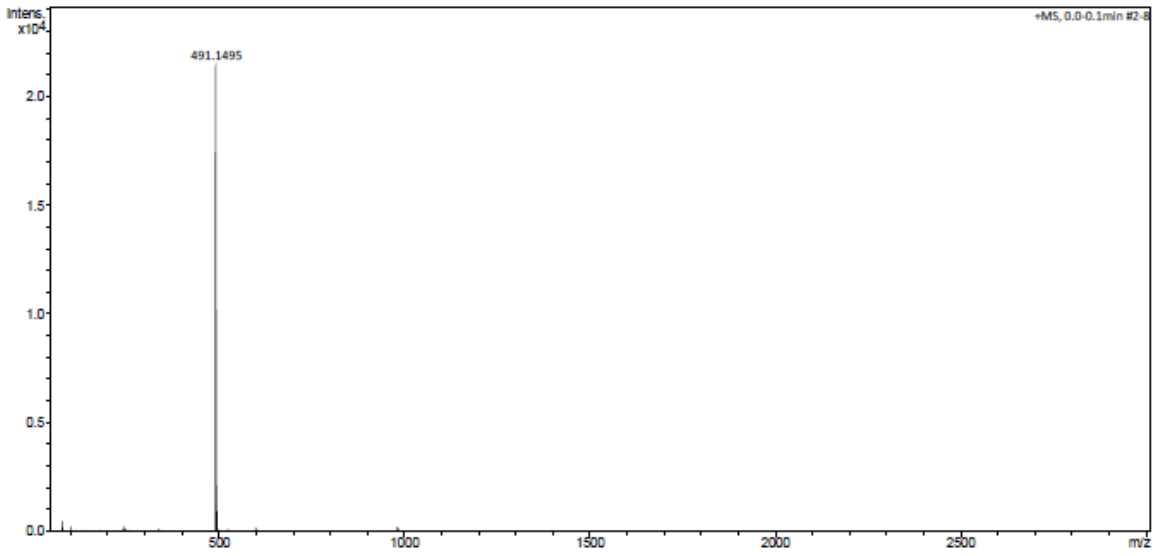

4’-(N_1-methylphenylguanine)-2,2’:6’,2”-terpyridine (**G-terPy**) (**T25**)

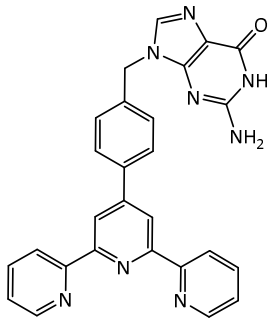

^{1}H NMR (500 MHz, DMSO-d_6)

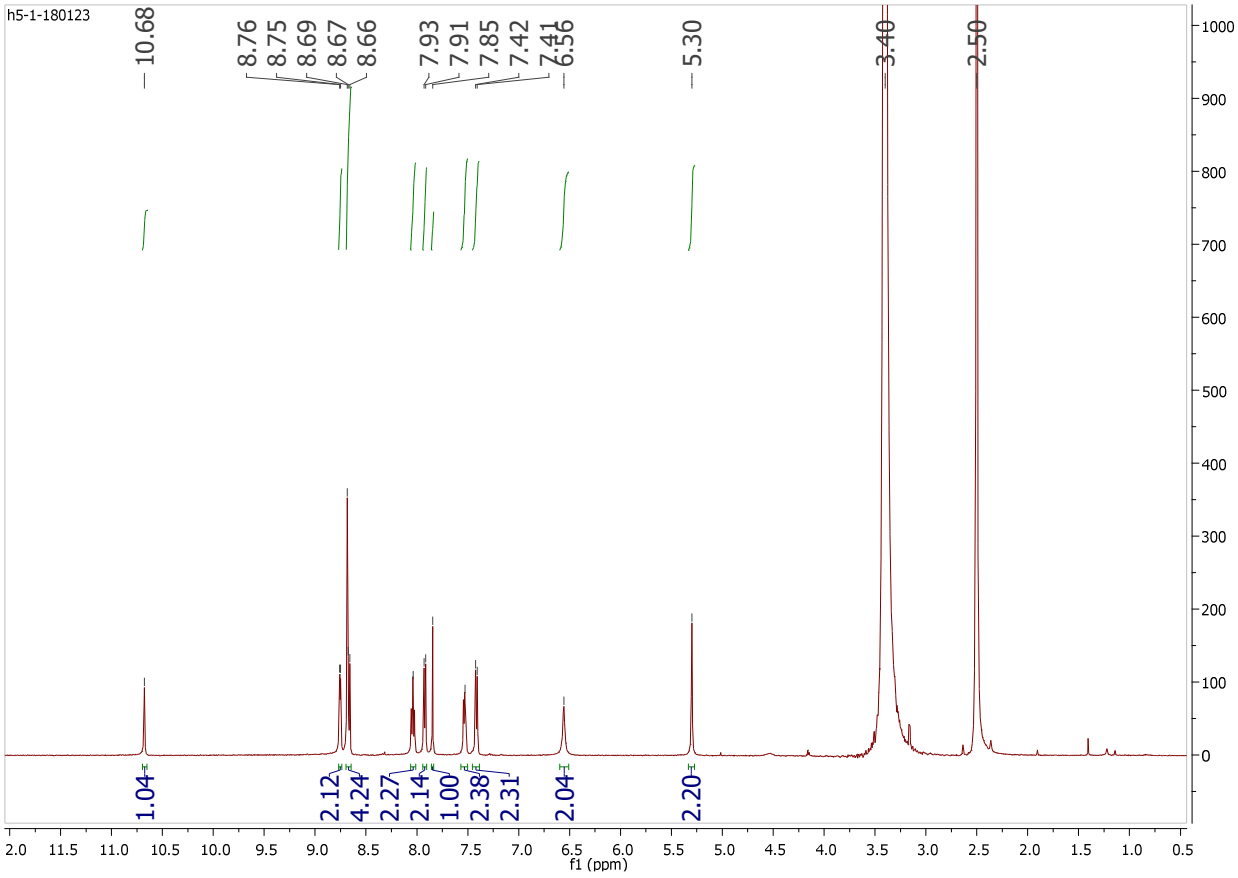

^{13}C NMR (126 MHz, DMSO-d_6)

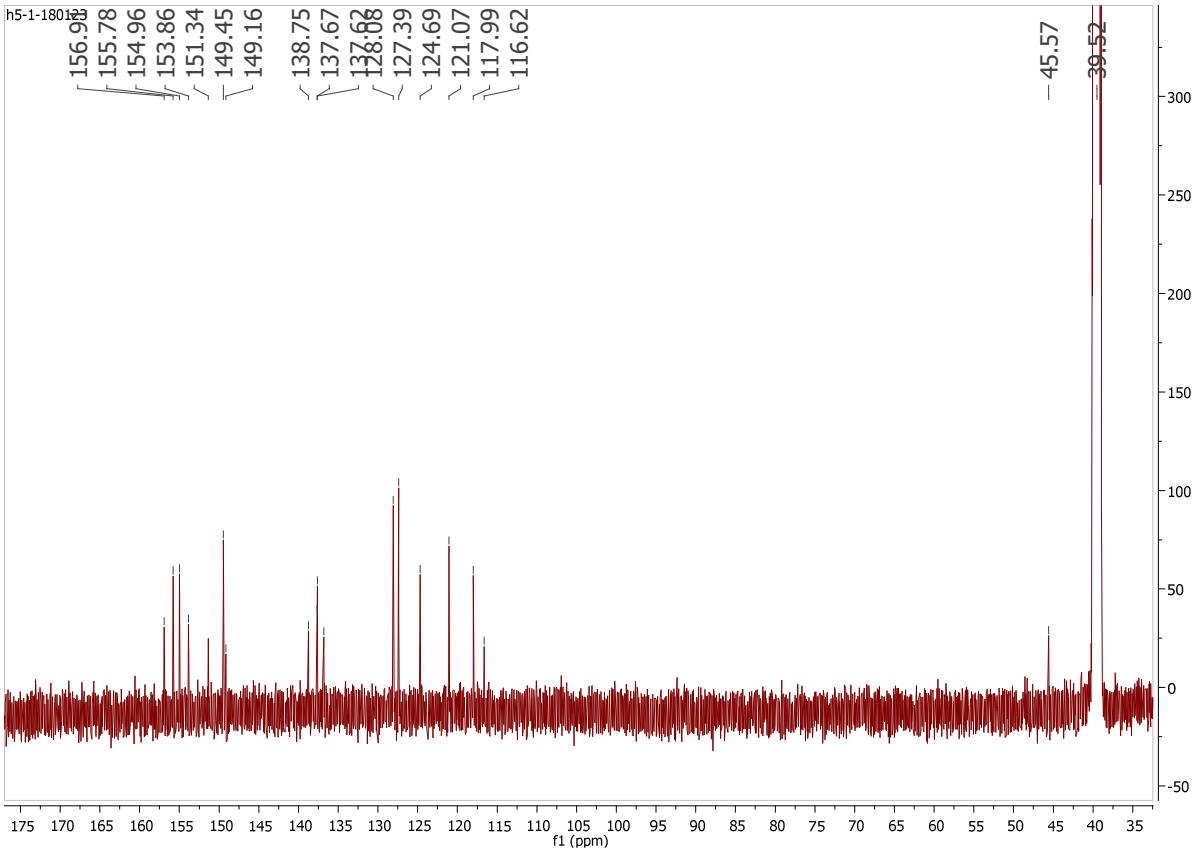

HRMS

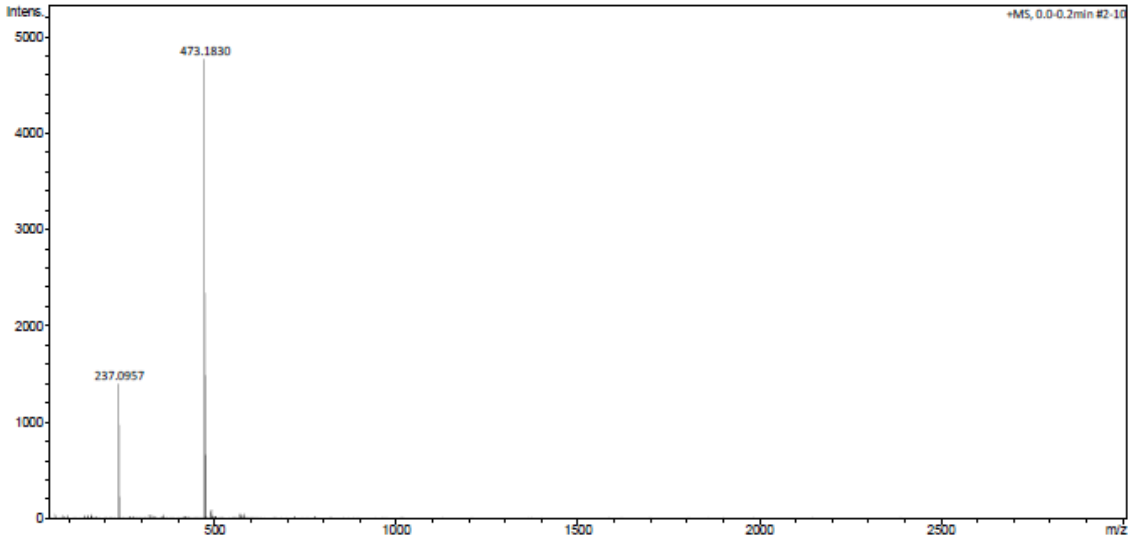

List of Tectons

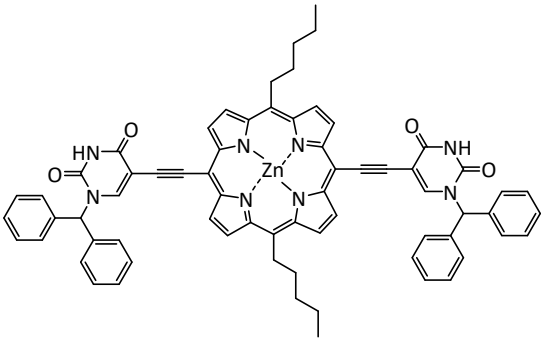

T1

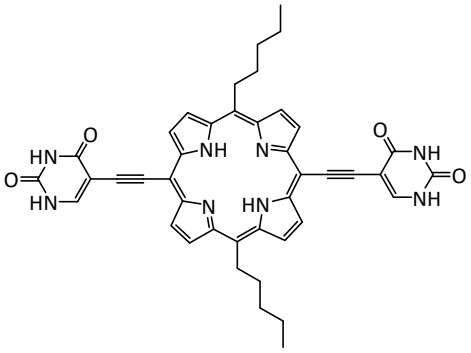

T2

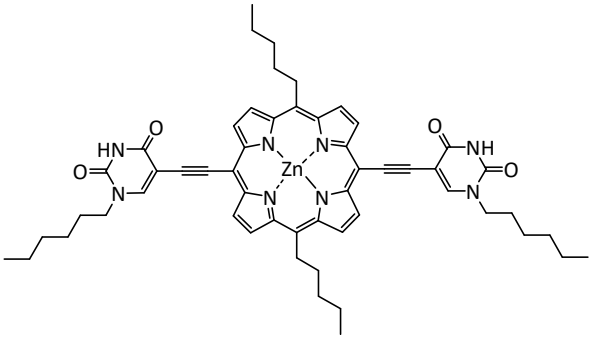

T3

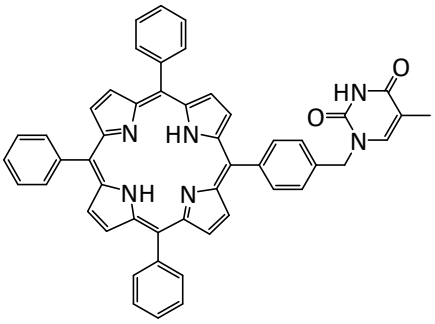

T4

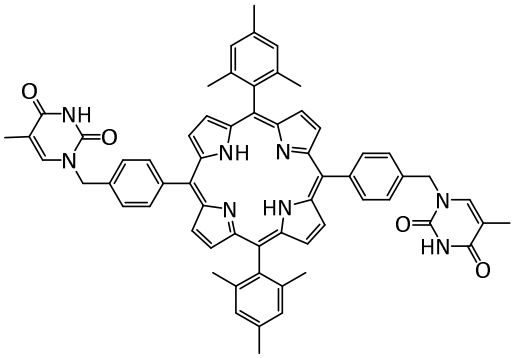

T5

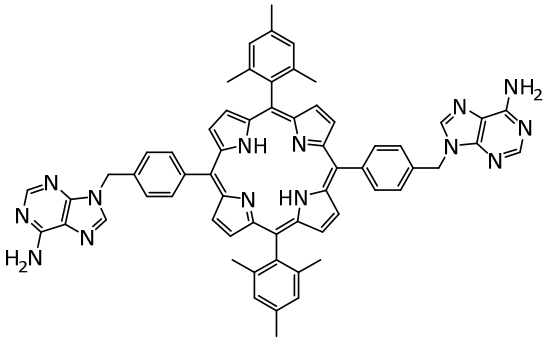

T6

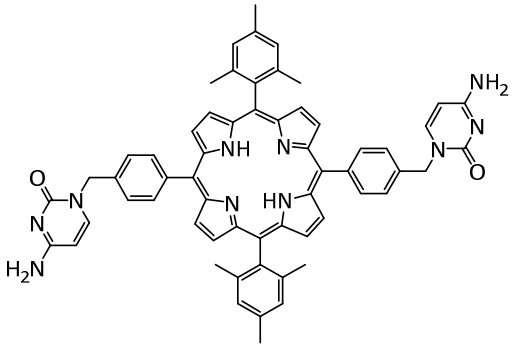

T7

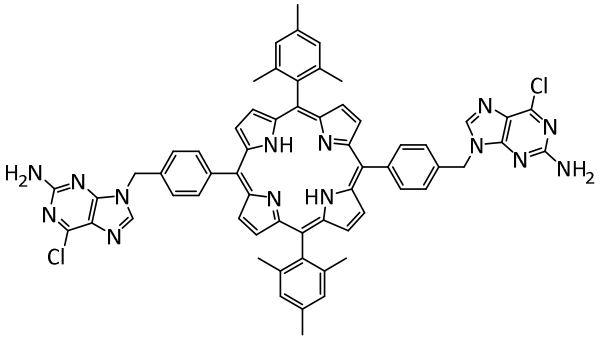

T8

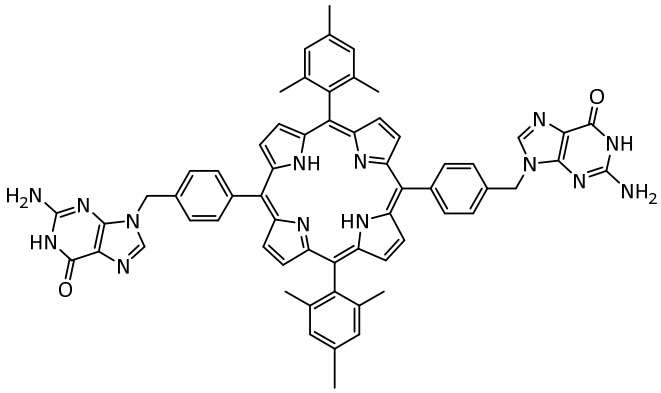

T9

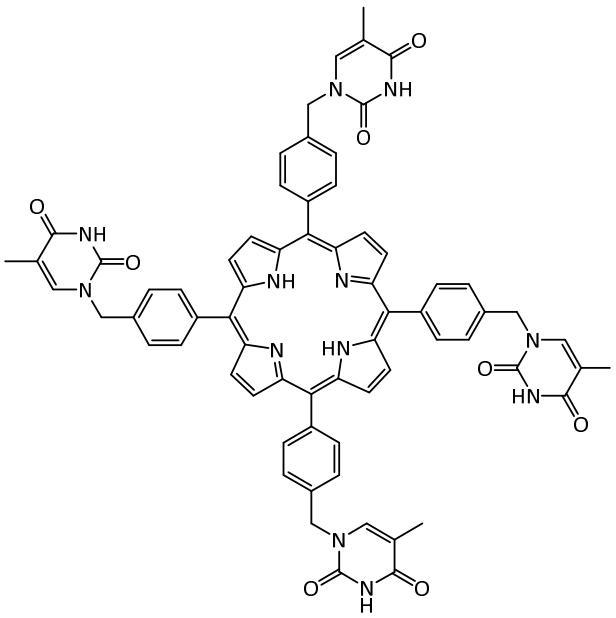

T10

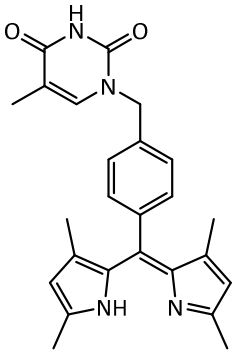

T11

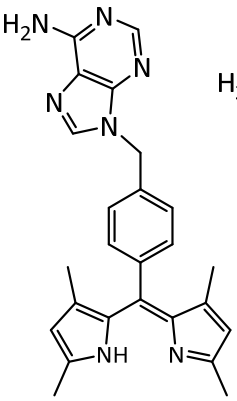

T12

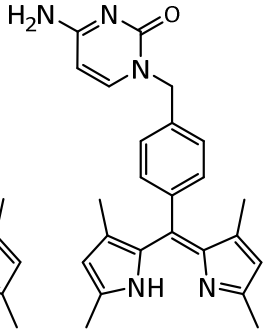

T13

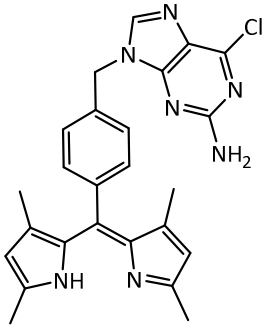

T14

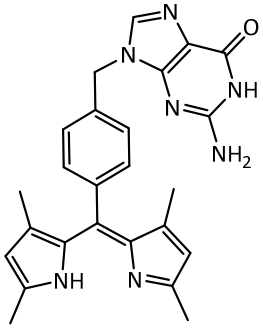

T15

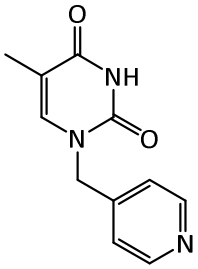

T16

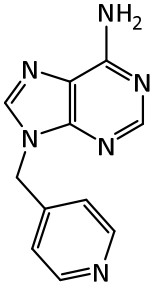

T17

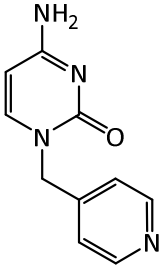

T18

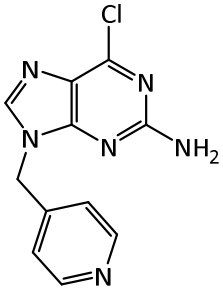

T19

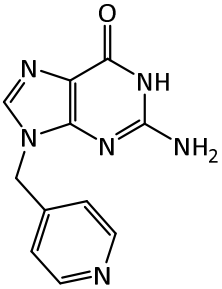

T20

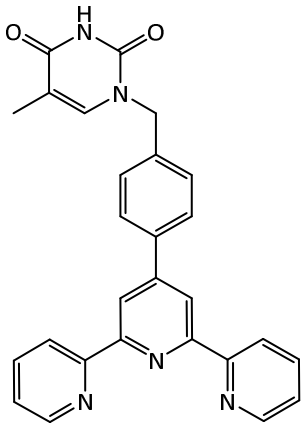

T21

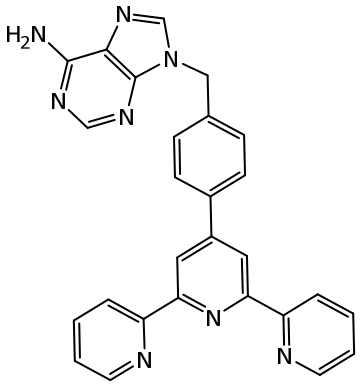

T22

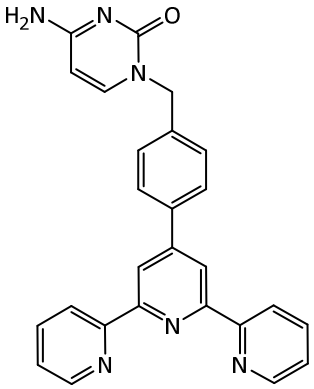

T23

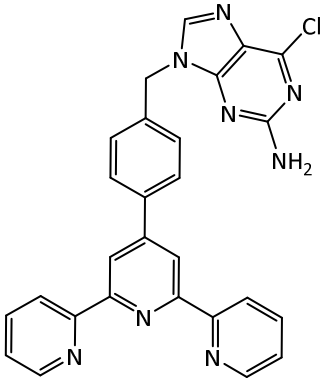

T24

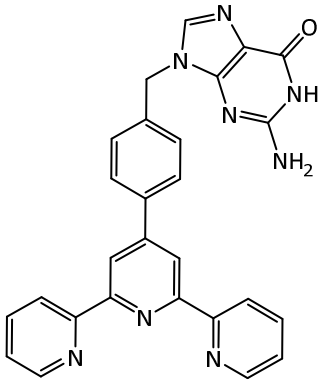

T25